



Arsenic inertization through alunite-type phases: Application to copper pyrometallurgy

Alba Sunyer i Borrell

ADVERTIMENT. La consulta d'aquesta tesi queda condicionada a l'acceptació de les següents condicions d'ús: La difusió d'aquesta tesi per mitjà del servei TDX (www.tdx.cat) i a través del Dipòsit Digital de la UB (diposit.ub.edu) ha estat autoritzada pels titulars dels drets de propietat intel·lectual únicament per a usos privats emmarcats en activitats d'investigació i docència. No s'autoritza la seva reproducció amb finalitats de lucre ni la seva difusió i posada a disposició des d'un lloc aliè al servei TDX ni al Dipòsit Digital de la UB. No s'autoritza la presentació del seu contingut en una finestra o marc aliè a TDX o al Dipòsit Digital de la UB (framing). Aquesta reserva de drets afecta tant al resum de presentació de la tesi com als seus continguts. En la utilització o cita de parts de la tesi és obligat indicar el nom de la persona autora.

ADVERTENCIA. La consulta de esta tesis queda condicionada a la aceptación de las siguientes condiciones de uso: La difusión de esta tesis por medio del servicio TDR (www.tdx.cat) y a través del Repositorio Digital de la UB (diposit.ub.edu) ha sido autorizada por los titulares de los derechos de propiedad intelectual únicamente para usos privados enmarcados en actividades de investigación y docencia. No se autoriza su reproducción con finalidades de lucro ni su difusión y puesta a disposición desde un sitio ajeno al servicio TDR o al Repositorio Digital de la UB. No se autoriza la presentación de su contenido en una ventana o marco ajeno a TDR o al Repositorio Digital de la UB (framing). Esta reserva de derechos afecta tanto al resumen de presentación de la tesis como a sus contenidos. En la utilización o cita de partes de la tesis es obligado indicar el nombre de la persona autora.

WARNING. On having consulted this thesis you're accepting the following use conditions: Spreading this thesis by the TDX (www.tdx.cat) service and by the UB Digital Repository (diposit.ub.edu) has been authorized by the titular of the intellectual property rights only for private uses placed in investigation and teaching activities. Reproduction with lucrative aims is not authorized nor its spreading and availability from a site foreign to the TDX service or to the UB Digital Repository. Introducing its content in a window or frame foreign to the TDX service or to the UB Digital Repository is not authorized (framing). Those rights affect to the presentation summary of the thesis as well as to its contents. In the using or citation of parts of the thesis it's obliged to indicate the name of the author.

PROGRAMA DE DOCTORAT
CIÈNCIA I TECNOLOGIA DE MATERIALS

**Arsenic inertization through
alunite-type phases: Application to
copper pyrometallurgy**

Alba SUNYER I BORRELL

Director de tesi
Dr. Joan VIÑALS I OLIÀ
Universitat de Barcelona

Agraïments

En primer lloc voldria agrair a en Joan Viñals per la direcció i l'ajut que m'ha donat tots aquests anys, des de que vaig entrar d'alumne intern un juliol en el departament fins ara.

També agraeixo al departament i especialment al grup de CPCM, a la Montserrat Cruells, a la Núria Llorca, al Toni Roca, al Pere Molera, al Pep Carrasco l'acull que m'han donat des del primer moment. Així com a l'Esther Vilalta pel seu ajut i els seus consells.

Agraeixo al Ministeri d'educació i ciència, per la beca de col·laboració que em va permetre començar a treballar en aquest projecte quan encara estava acabant la carrera, a la beca de la Fundació Bosch i Gimpera i a la beca APIF de la UB, que em van permetre acabar el màster i fer i acabar el doctorat. De la mateixa manera, agraeixo als projectes que han sortit i en què he pogut col·laborar, que m'han servit tan per completar la tesi com per aprendre de temes relacionats.

Als serveis científicotècnics de la UB, els agraeixo l'ajut i el suport que m'han donat durant tots aquests anys, especialment al Xavier Alcové de DRX, a la Maite Romero, al Toni Padró i a la Elionor Pelfort de ICP, i a l'Eva Prats, a l'Ana Dominguez, a l'Aranzazu Villuendas i al Javier García de Microscòpia electrònica.

Agraïr també a en John Dutrizac, per l'estada que em va permetre fer a Ottawa, al Canadà, per la direcció rebuda i tot el que em va ensenyar allà. De la mateixa manera voldria fer extensiu l'agraïment al CANMET, per la rebuda que em van fer des del primer moment.

Agraeixo també a la Marta el suport i l'ajuda que m'ha donat tot aquest temps que hem estat juntes des de que va començar el màster, i també a la Gemma tot el temps que vam compartir mentre feiem el màster, i a la Glòria, a l'Elisabet, el Jordi i l'Òscar, que en un període o altre del doctorat vam coincidir.

Finalment, agrair el suport rebut per part de la meva família, en especial al meu pare i a la meva mare, que em van donar bons consells quan els necessitava i em van donar suport des del primer moment, i que van ser els que des de ben petita em van encaminar cap a descobrir noves coses, a inventar i fer-me preguntes i a cercar les respostes. Al mateix temps agraeixo al meu germà Raimon i a la seva dona, la Núria, tots els consells que m'han donat. Finalment, també agraeixo al Ferran tot el suport que m'ha donat aquests últims mesos.

*Als meus pares,
al meu germà*

I	Introduction	1
1	The arsenic	3
2	Arsenic precipitation methods	5
2.1	Calcium arsenate	5
2.2	Co-precipitation of arsenic with ferric ions	6
2.3	Scorodite	7
2.3.1	Hydrothermal synthesis	7
2.3.2	Synthesis at less than 100°C	8
2.3.3	Biochemical synthesis	10
2.3.4	Advantages and disadvantages of scorodite	11
3	Alunite-type phases	13
3.1	Synthetic jarosites	15
3.2	Hematite formation from jarosites	16
3.3	Synthetic alunite	19
4	Thesis aim and objectives	21
II	Results and discussion	23
5	Thesis structure	25
6	Synthetic As-natroalunite	27
6.1	Effect of synthesis temperature	27
6.2	Effect of retention time	28
6.3	Effect of arsenic concentration	30
6.4	Synthesis with calcium in the medium	34
6.4.1	Synthesis of As-natroalunite	34
6.4.2	Synthesis in absence of sodium in the medium	38
7	Synthetic As-alunite	39
7.1	Alunites synthesized at 200°C	39
7.2	Alunites synthesized at 100°C	43

7.2.1	Effect of retention time and synthesis temperature	44
7.2.2	Effect of $\text{Al}_2(\text{SO}_4)_3 \cdot 18\text{H}_2\text{O}$ and K_2SO_4 concentration	44
7.2.3	Effect of arsenic (III) and arsenic (V)	45
8	Hydronium-alunite synthesis	47
9	Barium and lead alunites synthesis	51
9.1	Barium alunite	51
9.2	Lead alunites	55
10	As-natroalunites generated from industrial wastes	59
10.1	Calcium arsenate	61
10.2	Flash smelting dust	68
10.3	Ferric-arsenate intermediate	68
11	Stability tests	71
11.1	Short term tests	71
11.1.1	Stability at different pHs	71
11.2	Long-term/medium-term tests	75
11.2.1	Arsenical-natroalunite	76
11.2.2	Arsenical-alunite	76
11.2.3	Natural and synthetic scorodite	77
12	Crystal structure study	79
III	Conclusions	83
13	Conclusions	85
IV	References	89
14	References	91
V	Annex	95
A	Articles for compendium	97
A.1	Hematite formation from jarosite type compounds by hydrothermal conversion	98
A.2	Arsenate substitution in natroalunite: A potential medium for arsenic immobilization. Part 1: Synthesis and compositions	112
A.3	Arsenate substitution in natroalunite: A potential medium for arsenic immobilization. Part 2: Cell parameters and stability tests	124
A.4	The behaviour of As(III) and As(V) during the precipitation of alunite at 98°C	135
A.5	Arsenic inertization from copper pyrometallurgy through phases of the alunite supergroup (Copper 2010)	158
A.6	Arsenic inertization from copper pyrometallurgy through phases of the alunite supergroup (Erzmetall)	175

A.7	Arsenic stabilization of calcium arsenate waste by hydrothermal precipitation of arsenical natroalunite	186
A.8	Arsenic stabilization by hydrothermal synthesis of alunite-type phases. application to the copper metallurgy.	200
B	Article in review	211
B.1	Arsenic immobilization as alunite-type phases: The arsenate substitution in alunite and hydronium alunite.	211
C	Other published articles	239
C.1	Copper and zinc recoveries and arsenic stabilization from copper smelter flue dusts	239
C.2	New process for treating slag furnace (SCF) flue dust at Atlantic Copper	250
D	Database petitions	265
D.1	ICSD database	265
E	Resum en català	267

LIST OF TABLES

6.1	Bulk composition (ICP) and phases (Rietveld) of hydrothermal precipitated (na: natroalunite; am: amorphous phase; ma: mansfieldite; al: alarsite; ph: natropharmacoalumite).	29
6.2	Formula coefficients in natroalunite phase (normalized to S+As=2) (BCA: from bulk chemical analysis ICP. EDS: from mean spot analyses by EDS).	33
6.3	Formula coefficients in arsenical-natroalunites obtained in a medium with presence of calcium.	36
6.4	Reagents used and synthesis conditions in the synthesis of arsenical-natroalunites in presence of calcium in the medium.	36
6.5	Chemical composition and phases obtained in presence of calcium in the medium.	37
7.1	Initial conditions and final results of the arsenical-alunite experiments.	42
7.2	Formula coefficient by ICP and EDS of arsenical-alunites	42
8.1	Initial conditions and synthesis results of the hydronium-alunite experiments.	48
8.2	Formula coefficients by ICP and EDS of hydronium-alunites. . .	48
9.1	Initial condition and results of barium alunites.	53
9.2	Initial conditions and results of lead-alunite experiments.	56
10.1	Composition of wastes.	60
10.2	Composition and lixiviation of the calcium arsenate.	62
10.3	Initial conditions, bulk compositions and phases compositions. .	65
10.4	Formula coefficients from precipitated arsenical-natroalunite and mansfieldite.	66
E.1	Composició bulk (ICP) i fases (Rietveld) del precipitat hidrotermal (na: natroalunita; am: fase amorfa; ma: mansfieldita; al: alarsita; ph: natrofarmacoalunita).	274
E.2	Composició química i fases obtingudes en presència de calci. . . .	275
E.3	Condicions inicials i resultats de síntesis de les hidroni-alunites. .	278

- E.4 Condicions inicials, composicions bulk i composició de fases de la síntesis de natroalunites arsenicals a partir de residus industrials. 278

LIST OF FIGURES

2.1	Natural scorodite from Ojuela mine (SEM micrography).	8
2.2	SEM micrography of synthetic scorodite [Fujita et al., 2011].	9
2.3	Final concentration equilibrium solubility tests of different short-term (24 h) performed on scorodite [Bluteau and Demopoulos, 2007].	12
3.1	Natural Alunite from Vall d’Uxó.	13
3.2	Alunite-type structure [Sunyer i Viñals, 2011].	14
3.3	Cell parameters a and c in jarosites with different Na, K and H_3O substitutions [Basciano and Peterson, 2008].	17
3.4	Distances of the polyhedron A-O3 and A-O2 and the octahedrons Fe-O3 and Fe-O2 in jarosites with different Na, K and H_3O substitutions [Basciano and Peterson, 2008].	18
6.1	Precipitation of Al and As vs the retention time at $(AsO_4/(SO_4 + AsO_4))_{aq}=0.185$ (na: natroalunite; am: amorphous phase; ma: mansfieldite).	30
6.2	SEM images obtained at 160°C, 180°C and 200°C at different retention times and a molar ratio $(AsO_4/(SO_4 + AsO_4))_{aq}=0.185$ (na: natroalunite; am: amorphous phase; ma: mansfieldite).	31
6.3	Arsenate phases formed at high $AsO_4/(SO_4 + AsO_4)_{aq}$. A: Mansfieldite. B: Alarsite. C: Mansfieldite (ma) on corroded alarsite (al). D: Natropharmacoalumite.	32
6.4	X-ray patterns showing the effect of $(AsO_4/TO_4)_{aq}$ on phase composition at 200 °C (1: natroalunite; 2: mansfieldite; 3: alarsite; 4: natropharmacoalumite).	34
6.5	A-C: precipitates obtained in $Na^+/Ca^{2+}/Al^{3+}/SO_4^{2-}/AsO_4^{3-}$ medium. D: in $Ca^{2+}/Al^{3+}/SO_4^{2-}/AsO_4^{3-}$ medium (na: natroalunite; am: amorphous; ma: mansfieldite; an: anhydrite; hy: hydronium alunite).	35
7.1	SEM images of the arsenical-alunites at different $AsO_4/(SO_4 + AsO_4)$ molar ratio.	40
7.2	X-ray patterns obtained from arsenical-alunite precipitates at different $AsO_4/(SO_4 + AsO_4)$. n: alunite; m: mansfieldite.	41

7.3	Comparison between As-natroalunite and As-alunites at different $\text{AsO}_4/(\text{SO}_4 + \text{AsO}_4)_s$ (in bulk and in the As-alunite/As-natroalunite) and $\text{AsO}_4/(\text{SO}_4 + \text{AsO}_4)_{aq}$	43
7.4	Variation of the product yield when 0.3 M $\text{Al}(\text{SO}_4)_{1.5}$ - 0.2 M K_2SO_4 solutions at pH 3.00 were reacted for 24 h at various temperatures.	44
7.5	SEM images: Top) Backscattered electron image from alunite synthesized at 100°C. Bottom) Secondary electron image from alunite synthesized at 200°C.	45
8.1	XRD from precipitates with different $\text{AsO}_4/(\text{SO}_4 + \text{AsO}_4)$ molar ratio. n: hydroniumalunite; m: mansfieldite.	49
8.2	Hydronium-alunites at different $\text{AsO}_4/(\text{SO}_4 + \text{AsO}_4)_s$ (in bulk and in the hydronium-alunite) and $\text{AsO}_4/(\text{SO}_4 + \text{AsO}_4)_{aq}$	49
8.3	SEM images from precipitates obtained at different $\text{AsO}_4/(\text{SO}_4 + \text{AsO}_4)$ molar ratio.	50
9.1	SEM images of barium-alunite experiments at different $\text{AsO}_4/(\text{SO}_4 + \text{AsO}_4)$ molar ratio.	52
9.2	XRD from different barium-alunite experiments. n: natroalunite; h: hydronium-alunite; m: mansfieldite; a: anhydrite.	54
9.3	XRD from lead-alunite experiments. n: natroalunite; h: hydronium-alunite; m: mansfieldite.	57
9.4	SEM image of lead-alunite experiments at different $\text{AsO}_4/(\text{SO}_4 + \text{AsO}_4)$ molar ratio and initial conditions. A) 200°C, 1 h, $\text{AsO}_4/(\text{SO}_4 + \text{AsO}_4) = 0$; B) 200°C, 1 h, $\text{AsO}_4/(\text{SO}_4 + \text{AsO}_4) = 0.15$; C) 240°C, 1 h, $\text{AsO}_4/(\text{SO}_4 + \text{AsO}_4) = 0.15$; D) 200°C, 1 h, $\text{AsO}_4/(\text{SO}_4 + \text{AsO}_4) = 0.15$ with Na.	58
10.1	Waste treatment scheme.	60
10.2	SEM images from calcium arsenate. A) gypsum crystal; B) amorphous calcium arsenate precipitate.	61
10.3	SEM image from hydrothermal treatment of calcium arsenate waste (2-h retention time). A) 200°C, $(\text{Al}/\text{As})_{aq}=1.5$, pH ₀ 2; B) 200°C, $(\text{Al}/\text{As})_{aq}=1.5$, pH ₀ 1; C) 200°C, $(\text{Al}/\text{As})_{aq}=3$, pH ₀ 1; D) 180°C, $(\text{Al}/\text{As})_{aq}=3$, pH ₀ 1.	62
10.4	XRD from the hydrothermal precipitates obtained from calcium arsenate waste at different $(\text{Al}/\text{As})_{aq}$ molar ratio, 200°C and pH ₀ 1.	63
10.5	Arsenical-natroalunite. A) From calcium arsenate with gypsum presence; B) From calcium arsenate in absence of gypsum; C) Synthesized from pure reagents.	64
10.6	Effect of $(\text{Al}/\text{As})_{aq}$ molar ratio in the precipitation of the elements presents in the calcium arsenate waste at 200°C and 2-h retention time.	67
10.7	Correlation with cadmium dissolution and hydrothermal calcium of hydrothermal precipitates which contained anhydrite. These results correspond to the solubilities between pH 1 to 10 in three consecutive tests.	68

10.8	SEM image from the phases found in flash smelting dust (section 10.2). A) General view (f: ferrite); B) Tenorite particles; C) Delafossite particles; D) Arsenic-lead-sulfate aggregate (white).	69
10.9	SEM image from ferric-arsenate intermediate.	69
10.10	XRD from hydrothermal precipitates from ferric-arsenate intermediate at different $(Al/As)_{aq}$ molar ratio.	70
10.11	SEM image from hydrothermal precipitate obtained from ferric-arsenate intermediate.	70
11.1	Arsenic release at synthetic arsenical-natroalunites and mixtures of arsenical-natroalunite and mansfieldite.	72
11.2	Arsenic release at mansfieldite, arsenical-natroalunite mansfieldite mixtures and, arsenical-natroalunite from calcium-arsenate waste.	73
11.3	Arsenic release from arsenical-alunite (24 h).	74
11.4	Top) XRD of original natropharmacoalumite sample and after the lixiviation tests at different pHs. Bottom) SEM-EDS analyses from natropharmacoalumite: original and after lixiviation tests at different pHs.	75
11.5	SEM images from natroalunite and natropharmacoalumite lixiviated at different pHs.	76
11.6	Long-term test from arsenical-natroalunite, arsenical-natroalunite plus mansfieldite, and arsenical-natroalunite from calcium-arsenate waste.	76
11.7	Medium-term test of synthetic arsenical-alunite, synthetic scorodite and natural scorodite.	77
12.1	c cell parameter vs $AsO_4/(SO_4 + AsO_4)$ molar ratio in arsenical-natroalunite (from synthetic reagents and from industrial wastes), arsenical-alunites and arsenical-jarosites.	80
12.2	Optimized structure of the hydronium cation within the alunite structure as computed at the AM05/TZ2P level of theory. Here the orientation of the figure is the same as shown in Figure 1, with the c axis being vertical as shown. The hydronium cation now forms two hydrogen bonds to O atoms of hydroxyl groups that bridge aluminum atoms (on left-hand side of figure) and one hydrogen bond to an O atom of a sulfate group coordinated to another aluminum atom (right-hand side). [Gale et al., 2010].	81
E.1	Micrografia SEM d'escorodita sintètica [Fujita et al., 2011].	269
E.2	Estructura tipus alunita [Sunyer i Viñals, 2011].	270
E.3	Comparació entre natroalunites arsenical i alunites arsenicals a diferents $AsO_4/(SO_4 + AsO_4)_s$ (en el bulk in en As-alunita/As-natroalunita) i $AsO_4/(SO_4 + AsO_4)_{aq}$	276
E.4	Arsènic solubilitzat en alunita arsenical (24 h).	279
E.5	Arsènic solubilitzat en natroalunites arsenicals sintètiques i mescles de natroalunita arsenical i mansfieldita.	280

E.6	A dalt) DRX de la mostra original i de les mostres després dels tests de lixiviació a diferents pH's de natrofarmacoalunita. A sota) Anàlisi SEM-EDS de la natrofarmacoalunita: mostra original i de les mostres després dels tests de lixiviació a diferents pH's	281
E.7	Tests de llarg termini de natroalunita arsenical, natroalunita arsenical més mansfieldita, i natroalunita arsenical del residu d'arseniat càlcic.	282
E.8	Tests a mitjà termini de alunita arsenical, escorodita sintètica i escorodita natural.	282
E.9	El paràmetre de cel·la c vs la relació molar $\text{AsO}_4/(\text{SO}_4 + \text{AsO}_4)$ en natroalunita arsenical (de reactius sintètics i de residus industrials), alunita arsenical i jarosita arsenical.	283

PART I

Introduction

CHAPTER 1

THE ARSENIC

Today, one of the major problems of water pollution is the arsenic. Arsenic is a toxic element, especially in its inorganic forms, which ingested can cause important health problems (diarrhea, skin effects, cancer, etc.), and in high levels can cause death. Despite health problems resulted in high doses, Greeks and Arabs used it as a drug. Arsenic was used in small doses because its associated properties against cough, dyspnea and voice problems.

The abundance of arsenic in the crust makes it present in many of the ores used in metallurgy. Currently, the advance of technology has led to a high demand of some metals such as copper. Copper has been used for millennia to create objects and coins. In recent centuries, its main use has been the transport of electrical energy. Nowadays, the richest copper mines with low arsenic concentration have been depleted, and the ores being exploited contain high concentrations of arsenic. Thus, arsenic residues from copper metallurgy has increased in recent years and it becomes to be a problem in some countries, where arsenic pollution in groundwater is due to the presence of unstable arsenic wastes which are dissolved and reached groundwater. Although WHO has established maximum levels of 0.01 mg/L arsenic in drinking water -the minimum detectable concentration-. In South and Central America, as well as in Asia several areas have health problems due to the high arsenic content in the water they consume.

Aside health problems, the increase of arsenic in ores can produce arsenic pollution in groundwater, generating environmental problems. For many years, arsenic pollution problem drove to researches for new methods of precipitation or adsorption of arsenic present in solution. But, precipitation of arsenic does not mean that it has been immobilized. Then, it did not remain stable over time and can be dissolved by the effect of the rain. These techniques, described in the following sections, have a low stability in water, and some of them do not pass the toxicity tests of different countries. For this reason, they must be dump in controlled sites. Another important aspect is the toxicity tests do not test the behaviour in a long-term period. Arsenic wastes -as the produced in metallurgy- decomposes due to rain water and air. Thus, the atmospheric effects produce the release of arsenic to the groundwater and cause a pollution of water [Riveros et al, 2001].

CHAPTER 2

ARSENIC PRECIPITATION METHODS

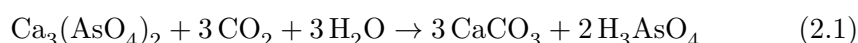
For years, various methods are being used for the precipitation of arsenic. Basically, three methods of precipitation are used: Calcium arsenates, ferric arsenates and scorodite. All these methods are considered valid for the precipitation of arsenic, because they pass the toxicity tests that have a duration of 24 h. Thus, they do not determine the long-term toxicity. All these methods require economic reagents, and are widely used in metallurgical industry.

Other methods are adsorption, ion exchange resins, reverse osmosis and cementation processes, but none of these methods are as used as the commented above.

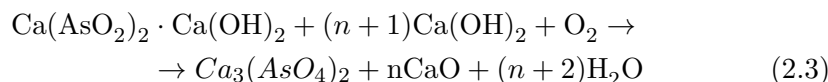
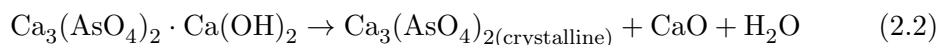
2.1 Calcium arsenate

Calcium arsenate is the most widely used method because lime is a very economic reagent and it can be performed at room temperature. This method is used to precipitate all metals remaining in the final solution of the process increasing the pH up to 12 with lime. Arsenic (V) precipitates easily and creates various types of calcium such as arsenates: $\text{Ca}_4(\text{OH})_2(\text{AsO}_4)_2 \cdot 4 \text{H}_2\text{O}$, $\text{Ca}_5(\text{AsO}_4)_3$, $\text{Ca}_3(\text{AsO}_4)_2 \cdot 3\frac{2}{3} \text{H}_2\text{O}$, $\text{CaHAsO}_4 \cdot x\text{H}_2\text{O}$ or $\text{Ca}_5\text{H}_2(\text{AsO}_4)_4$. The arsenates precipitates depend on the temperature, the pH and the ratio Ca:As [Riveros et al., 2001].

The stability of these calcium arsenates is really low. Some studies confirm that they did not pass the toxicity tests giving values between 900 and 4400 mg/L. These high values are due to the contact of CO_2 and water with calcium arsenate, which caused the carbonation of this precipitate and the consequent arsenic release in water. (Eq. 2.1) [Riveros et al., 2001].



To increase the stability of calcium arsenates, a calcination at 700°C is used to convert the amorphous calcium arsenate and calcium arsenite with excess of lime to a crystalline calcium arsenate (Eq. 2.2 and 2.3). However, some studies suggest that in the case of calcium arsenite this transformation would be incomplete at temperatures below 800°C .

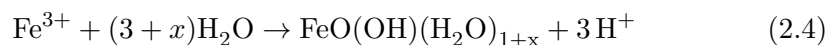


Some other studies suggested that with excess lime, calcium arsenites and arsenates have a lower stability because the pH remains high, exceeding 10, however, over time, the reduction of the buffer effect due to carbonation of lime, can result in the arsenic release in water. Calcination is used in Chile's metallurgy, where dry weather helps in the stability of this phase [Riveros et al., 2001].

2.2 Co-precipitation of arsenic with ferric ions

The co-precipitation of arsenic ions with Fe(III) has been very studied for some authors. Initially, was believed that an amorphous ferric arsenate was formed. But later, it was demonstrated that at temperatures under 100°C was formed ferrihydrite, except in case of high concentrations of Fe(III) and As(V) and a gradual increase of pH. In these conditions, intermediate ferric arsenate phases formed prior to the formation of ferrihydrite, can reach saturation and precipitate. Ferrihydrite precipitation takes place in 3 steps [Riveros et al., 2001]:

1. At 80°C, adding Fe(III) in the As(V) solution.
2. The basification to pH between 2 and 3, which causes the precipitation of ions Fe(III) as a ferrihydrite (Eq. 2.4) and, a quimioadsorption of arsenates on ferrihydrite (Eq. 2.5).
3. The solution is neutralized with lime. Thus, in case of do not have added the minimum iron needed to precipitate all the arsenic, the rest of it precipitates as calcium arsenates at pH 3-4.



This precipitation can be affected by many factors. The presence of sulfates and some cations in the medium can modify the efficiency of arsenic adsorption and the optimum pH -between 4 and 7- for the co-precipitation. The lack of efficiency in the presence of sulfates is due to the adsorption of these ferrihydrite and, consequently affect the arsenates adsorption.

Moreover, it has been demonstrated that the co-precipitation Fe(III)-As(III) is not as effective as co-precipitation Fe(III)-As(V). For this reason, a previous oxidation of As(III) (very common in metallurgical wastes) to As(V) is important. This oxidation is difficult to perform because the effluents of arsenic in such industries generally are acidic pHs and temperature. Oxidants like oxygen are totally ineffective except at high pHs and with copper ions as a catalyst. A

similar problem is in hydrogen peroxide, which is unable to oxidize the arsenic except in alkaline medium or in the case of acidic medium, at high temperature. Other oxidants, such as chlorine, potassium permanganate, ammonium persulfate or sodium hypochlorite, can only oxidize arsenic (III) to arsenic (V) under specific conditions. Thus, the only effective oxidant for the oxidation of arsenic is ozone, which can perform this oxidation under the conditions in which is normally found the arsenic in the effluent, ie in acid medium and ambient temperature. Then, some oxidizing economic systems are being search, such as mixtures SO_2/O_2 catalyzed with iron or, simply O_2 catalyzed with UV and iron, although the latter is more effective in the case of low initial concentrations of arsenic [Riveros et al., 2001].

Furthermore, the difficulties that represents the oxidation of arsenic in plants, arsenical-ferrihydrite precipitates form a voluminous waste that is difficult to filtrate because it is not enough crystalline. Despite these problems, this method is used in many Canadian metallurgies [Riveros et al., 2001].

Despite being used in many industries, as happens with calcium arsenates, the long-term stability is not good because ferrihydrite decomposes to goethite and hematite in contact with water, and the arsenate adsorbed on ferrihydrite is released [Riveros et al., 2001]. Moreover, it could have been formed calcium arsenates if in first stage was not added enough iron, which may result in a poor stability in a short-term period.

2.3 Scorodite

Scorodite ($\text{FeAsO}_4 \cdot 2\text{H}_2\text{O}$) (Figure 2.1) can be easily synthesized at temperatures between 95 and 150°C. However, in recent years numerous synthesis methods have been studied, in both, chemical and biochemical pathway. Crystalline scorodite can be synthesized easily by chemical pathways at 150°C. At less than 100°C scorodite can be formed with enough reagents to saturate the solution. With these high concentrations in the synthesis medium, scorodite can precipitate easily and without high temperatures. Another chemical pathway to obtain scorodite precipitation at less than 100°C is the slow oxidation of Fe^{2+} to Fe^{3+} (Figure 2.2). The biochemical pathway does not differ too much from the latter and also use the slow oxidation of Fe^{2+} to Fe^{3+} . The main difference is that this oxidation is done using the bacterium *Thiobacillus ferrooxidans*, which allows the oxidation of Fe^{2+} to Fe^{3+} . The latter pathway obtains good results and has a higher stability than the chemically synthesized.

2.3.1 Hydrothermal synthesis

Hydrothermal scorodite synthesis is the less studied pathway, since most studies have been conducted with the aim of low synthesis temperatures (<100°C). Nevertheless, some authors have studied the precipitation of scorodite at temperatures above 100°C. Dutrizac and Jambor (1988) studied the precipitation of crystalline scorodite with and without the presence of sulfate in the medium at temperatures above 100°C. The solutions used for the synthesis were 0.3 M As(V) and 0.3 M Fe(III), in order to complete the reaction according to Eq. 2.6. The results obtained at temperatures above 125°C gave a well-crystallized scorodite. However, to ensure a good crystallization as a standard tempera-

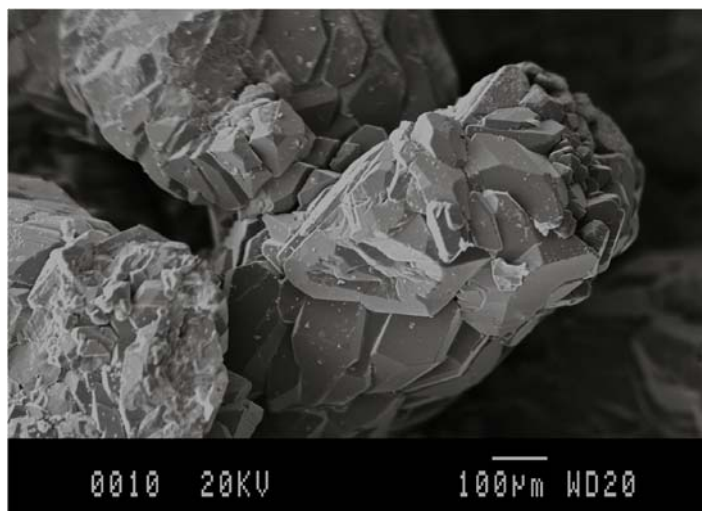


Figure 2.1: Natural scorodite from Ojuela mine (SEM micrography).

ture was used 160°C and a retention time of 24 h. The influence of pH on scorodite had little effect on its composition, except in presence of sulfate in the medium when it can reach up to 1 % of that of the structure. Bluteau and Demopoulos (2007) also studied hydrothermal scorodite in order to make stability studies. When the stability test were performed, they need to wash very well the scorodite due to the presence of an amorphous phase which released arsenic very easily.



2.3.2 Synthesis at less than 100°C

As scorodite synthesis in autoclaves at temperatures above 125°C is expensive, the synthesis at less than 100°C at atmospheric pressure resulted very attractive. Two different forms of scorodite synthesis at this temperature are described in this subsection: a) synthesis with Fe(III), and b) synthesis with the oxidation of Fe(II) to Fe(III).

The scorodite synthesis from Fe(III) is controlled by the saturation of the reagents in the medium. Demopoulos et al. (1995) achieved the synthesis of crystalline scorodite in concentrated chloride media from 1 to 6 M Cl^- at ambient pressure and a temperature between 80 and 95°C. At these temperatures crystalline scorodite can be achieved by over saturation control of Fe(III) and As(V) in the medium. They have different steps for the neutralization of the solutions at a constant temperature. The steps depended on the supersaturation line chosen from scorodite synthesized at 160°C. It should be noted that the line of supersaturation change with the working temperature, ie when the temperature is lower, less concentration of As(V) and Fe(III) will be needed. The same will happen at the stage of neutralization, in which will be needed a lower amount of NaOH. Control of supersaturation is important to avoid the formation of amorphous ferric arsenates. Paktunc et al. (2008), based on the same technique of supersaturation, performed the scorodite synthesis at 70°C

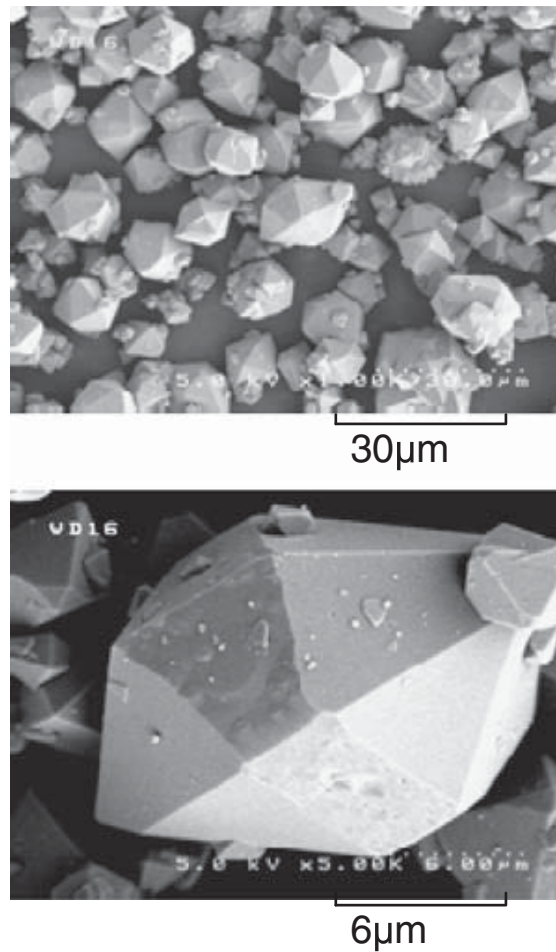


Figure 2.2: SEM micrography of synthetic scorodite [Fujita et al., 2011].

and different pH, but unlike Demopoulos et al. (1995) used in a medium with sulfate instead of chloride. The solutions used were 0.2 M $\text{Fe}(\text{SO}_4)_{1.5}$ and 0.2 M Na_2HAsO_4 with a retention time of 24 h. The synthesis at sulfate medium is important because most of the metallurgical effluents that contain arsenic and are also sulfate-rich.

Demopoulos et al. (1995) introduced some improvement to the process with the use of scorodite seed. The seed allows to synthesize scorodite at 80°C. Otherwise, at this temperature but within seed amorphous phases were formed. No seed is needed to synthesize scorodite at 95°C, but it is formed on the walls of the vessel. In case of use seed, the crystallization is easier and is not formed on the walls of the vessel. One of the advantages of scorodite precipitation at low temperatures, is that it is the first phase formed and, until the final stages no other iron phases are precipitated. Otherwise, one of the disadvantages of

this synthesis is that sulfates have an inhibitory effect, and its presence slow the precipitation kinetics of the scorodite or completely inhibits its formation.

The synthesis at 70°C and pH 1 was described by Paktunc et al. (2008). The scorodite precipitation began after 13-h retention time, but the precipitate was not seen before 21-h retention time. At pH 1 the chemical analyzes indicated some incorporation of sulfates in scorodite. However, this incorporation was not found in the synthesis at pHs 2 and 3. Moreover, the latter synthesis -at pHs 2 and 3- began to precipitate as soon as the base (NaOH) was added in order to neutralize the medium at the desired pH. Although the initial precipitate was amorphous, after 16-h retention time at pH 2 and after 37-h retention time at pH 3 scorodite start to precipitate. This indicates a high pH control.

Other authors have described synthesis processes for scorodite by Fe(II). Fujita et al. (2008a, 2008b) performed a process to obtain well crystallized scorodite at temperatures between 70 and 95°C and a short retention time, between 1 and 7 h, enough time to oxidize Fe(II) ions with the air or oxygen in presence of As(V). The experiments were done with different concentrations of As(V) and Fe(II) heated up to 95°C. The Fe(II) was oxidized using pure oxygen and, as it was oxidized, it reacted with As(V) forming scorodite. The molar ratio used was Fe/As=1.5. The retention time was short, especially compared to those found Paktunc et al. (2008), and in 7 h, 97 % of arsenic present in the solution had been precipitated. Furthermore, the results showed that after 5 min scorodite was moderately crystalline and, after 1 h it was completely crystalline (Figure 2.2).

2.3.3 Biochemical synthesis

Scorodite biosynthesis is possible with various microorganisms. These microorganisms always need to be adapted to mediums with extreme conditions, as it could be a medium for the scorodite synthesis. Scorodite production can be carried out, among others, by thermophilic bacteria, as long as temperatures are over 60°C and pH below 1.3 [Gonzalez-Contreras et al., 2010]. Many studies have been conducted with scorodite biosynthesis Archeobacteries, specifically from the order of Sulfolobales. These bacteria are able to oxidize simultaneously large amounts of Fe²⁺ and sulfide in thermophilic conditions (60-80°C) through the co-oxidation of sulfide and iron [Gonzalez-Contreras et al., 2012]. The Acidianus Sulfidivorans and Acidithiobacillus Ferrooxidans are examples of bacteria able to oxidize Fe²⁺ to Fe³⁺, and can therefore make possible the synthesis of scorodite. Furthermore, the second has a high tolerance to metals, which is a great advantage if it is considered that waste from metallurgical industries contain high metal concentrations [Gonzalez-Contreras et al ., 2010; Chandraprabha and Natarajan, 2011].

Acidianus Sulfidivorans was studied by Gonzalez-Contreras et al. (2010). This bacterium had a high tolerance with the presence of arsenic in the medium. In conditions of 80°C of temperature and a molar ratio of Fe(II)/As(V) = 1.1 was obtained scorodite. However, this precipitation was slow, and were needed 16 days to precipitate the 80±2 % of arsenic.

Acidithiobacillus ferrooxidans also tolerate the presence of arsenic in the medium in both forms, as As(III) and as As(V) [Chandraprabha and Natarajan, 2011]. Chandraprabha and Natarajan (2011) made experiments with bacteria prepared in arsenate, arsenite and sulfate media, as well as in bacteria that had

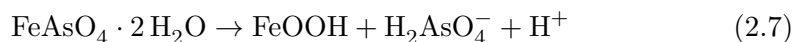
not been in contact with any of these media. The results made with industrial waste from these bacteria get different answers depending on the environment in which they had previously grown. So those that had not grown in any medium, only formed jarosite, while those bacteria grown in arsenate medium precipitated jarosite and scorodite, and bacteria grown in arsenite medium formed jarosite and tooeleite ($\text{Fe}_6(\text{AsO}_3)_4(\text{SO}_4)(\text{OH})_4 \cdot 4 \text{H}_2\text{O}$).

2.3.4 Advantages and disadvantages of scorodite

The advantage of scorodite in comparison with ferrihydrite is that scorodite is crystalline and therefore, easier to filter. In addition, the volume of scorodite is smaller compared to other forms of arsenic precipitation. Otherwise allows to precipitate large amounts of arsenic with a low amount of iron as this has a ratio of Fe:As 1:1, while other phases such as arsenic ferrihydrite needs a ratio of Fe:As 3:1 [Bluteau and Demopoulos, 2007; Paktunc et al., 2008]. Moreover, the stability of the scorodite is also better than the obtained in arsenical ferrihydrite [Riveros et al., 2001].

Although compared with arsenic precipitation methods described in sections 2.1 and 2.2, scorodite's stability is greater and it passed toxicity tests satisfactorily [Riveros et al. 2001], scorodite tends to amorphous arsenic phases in the surface of the scorodite crystals that increases the leaching of arsenic. Thus, authors such Bluteau and Demopoulos (2007) need to make an important wash before perform the stability tests to obtain scorodite's values and not the high leaching of arsenic obtained with only a regular wash. Consequently, the results of arsenic leaching in scorodites varies a lot between the publications due to the dependence on the previous wash (Figure 2.3).

Furthermore, it has been demonstrated that scorodite is metastable under normal atmospheric conditions over time. The transformation reaction of scorodite to goethite is slow, but is produced over time, and allows the dissolution of arsenic in water (Eq. 2.7) [Welham et al., 2000; Bluteau and Demopoulos, 2007]. The reaction kinetics is slow, nevertheless should be considered when a arsenic bearing stable phase is searched.



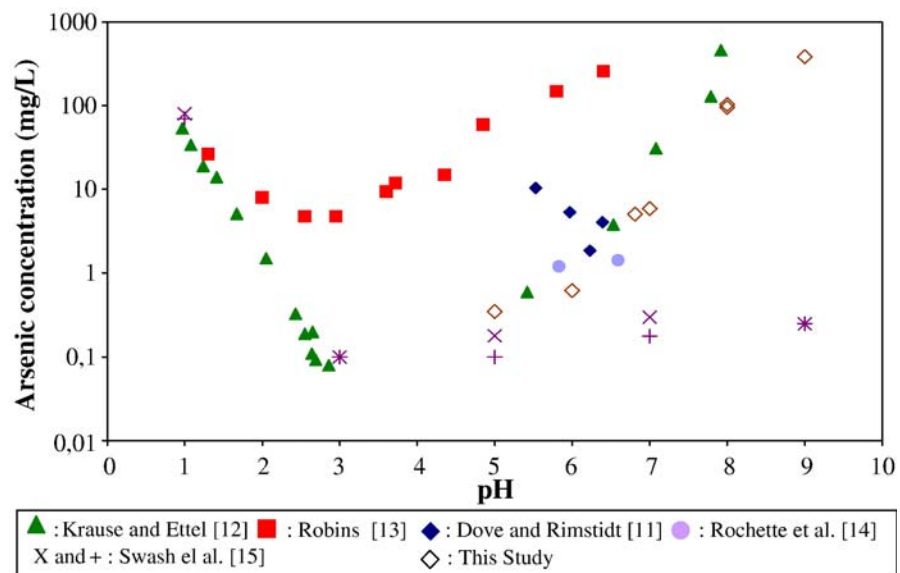


Figure 2.3: Final concentration equilibrium solubility tests of different short-term (24 h) performed on scorodite [Bluteau and Demopoulos, 2007].

CHAPTER 3

ALUNITE-TYPE PHASES

Alunites are a supergroup of minerals type $AB_3(TO_4)_2(OH)_6$, where A is a monovalent or divalent (Na, K, Ba, etc.), B is a trivalent (Fe, Al, etc.) and TO_4 can be SO_4 , PO_4 , or AsO_4 (Figure 3.2). This supergroup of minerals comprise more than 40 species, some of them very rare. In nature, the most common species of this supergroup are alunite (Figure 3.1) and natroalunite ($KAl_3(SO_4)_2(OH)_6$ and $NaAl_3(SO_4)_2(OH)_6$, respectively) and, jarosite and natrojarosite ($KFe_3(SO_4)_2(OH)_6$ and $NaFe_3(SO_4)_2(OH)_6$, respectively). In this alunite-type structure the partial substitution in TO_4 of SO_4 -for- AsO_4 exist, and is the base of lots of studies about removal of arsenic by alunite-type phases [Baron and Palmer, 1995; Jambor, 1999; Dutrizac and Jambor, 2000; Stoffregen et al., 2000; Rudolph et al., 2003].

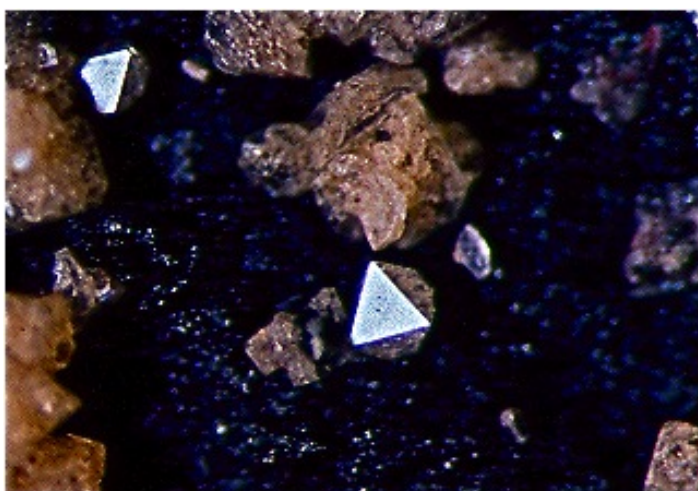


Figure 3.1: Natural Alunite from Vall d'Uxó.

In alunites, the structure consists of icosahedra ($AO_6(OH)_6$), octahedra ($B(OH)_4O_2$), and tetrahedra (TO_4). The octahedra shares oxygens O2 and O3 with the icosahedra, while O3 from tetrahedra shares oxygens with the octahedra and also has oxygen O1 forming hydrogen bonds with H and the O3 [Stoffregen et al., 2000; Rudolph et al., 2003].

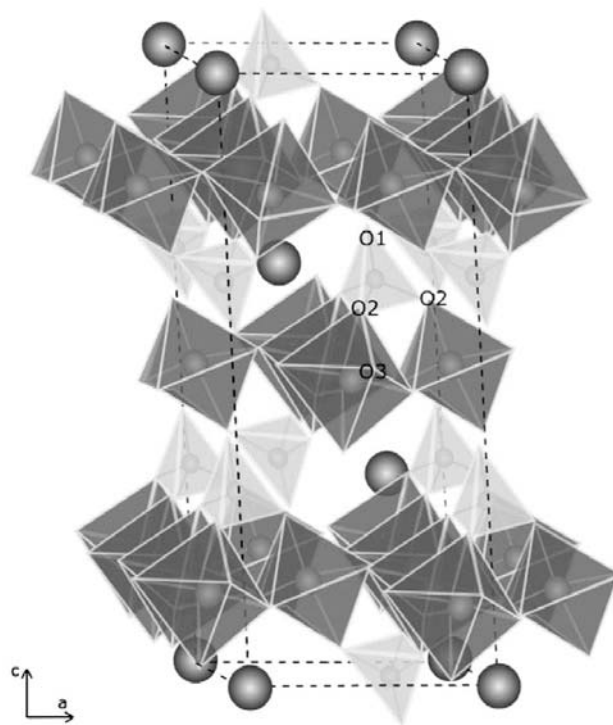


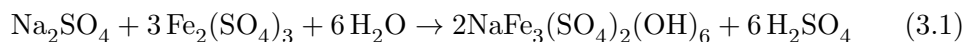
Figure 3.2: Alunite-type structure [Sunyer i Viñals, 2011].

The lattice parameters of the structure vary with A, B and T elements. In all cases, depend on the ionic radius of the element, the cell parameters can vary significantly. At A position, the higher the ionic radius of the element is, the higher the cell parameter c is. e.g. K and Na: Potassium has an ionic radius of 1.64 Å, higher than sodium (1.39 Å [Shannon, 1976]). Therefore, the cell parameter a in the alunite ($\text{KAl}_3(\text{SO}_4)_2(\text{OH})_6$) is 6.9833 Å, similar to that found in natroalunite ($\text{NaAl}_3(\text{SO}_4)_2(\text{OH})_6$) of 6.9729 Å, whereas the c parameter is greater in alunite than in natroalunite (17.197 Å and 16.877 Å, respectively). If the change is in position B, the affected parameter is a . As in the previous case, parameter a will increase if the ionic radius of B increases. An example is found with alunite and jarosite ($\text{KFe}_3(\text{SO}_4)_2(\text{OH})_6$). As previously mentioned, alunite has a cell parameter a of 6.9833 Å, however, jarosite has a cell parameter a of 7.2768 Å [Sato et al. 2009]. This change is due to the difference in ionic radius between Al (0.535 Å) and Fe (0.645 Å) [Shannon, 1976]. A change in the TO_4 also affect the cell parameters. In this case, c cell parameter increase when increases the ionic radius of TO_4 . e.g. when SO_4 is replaced by AsO_4 . This case has been studied in jarosites and, as will be seen, in this thesis. Sulfur has an ionic radius of 0.12 Å smaller than that of arsenic, which has an ionic radius of 0.335 Å [Shannon, 1976]. In studies on jarosite, parameter c clearly tend to increase from 8.17 Å of jarosite synthesized without arsenic at almost 17.15 Å of jarosite synthesized with an arsenic partial substitution structure [Paktunc and Dutrizac, 2003].

The incorporation of arsenic in alunite-type structures has been studied previously in jarosites ($\text{KFe}_3(\text{SO}_4)_2(\text{OH})_6$) that gave good results in arsenic incorporation, up to 0.16 moles per formula unit. However, iron can be a problem some environmental conditions, as in reducing soil could easily produce the reduction of iron, releasing the arsenic presented in the structure. Unlike jarosite, incorporation of arsenic into phases as natroalunite or alunite has not ever been studied. The advantage of alunite or natroalunite in respect to jarosite stability is that they contain aluminum instead of iron in B position. The advantage of aluminum is that is not reducible in anaerobic conditions.

3.1 Synthetic jarosites

Jarosites are especially important in hydrometallurgy industry, especially in zinc, where are used to control impurities as iron and alkali sulfates among others, present on the process, and with the property that divalent metal ion such as Cu, Zn or Ni practically do not precipitate. The use of jarosite in hydrometallurgical industry is very extensive, because the precipitate is easily filterable and, all the precipitation can be done in acidic conditions avoiding neutralization steps. At industrial level jarosite synthesized are usually of sodium or ammonium, because these alkalis are the most economic [Dutrizac and Kaiman, 1976; Dutrizac and Jambor, 2000]. The reagents used in the synthesis are the alkali desired sulfates and iron sulfate, so that the reaction occurs is Eq. 3.1 [Dutrizac and Jambor, 2000].

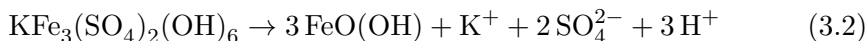


Synthesis of jarosite can be carried out from a temperature of 25°C, although the rate of precipitation is very low in these conditions. At higher temperatures, the product yield increases, and already at 80°C is quite high and, at 100°C can complete the reaction in some hours. The retention time is important if you want to obtain precipitation of jarosite, especially when working at low temperatures. In industrial practice, the working temperatures used are above 90°C [Dutrizac and Jambor, 2000].

Jarosites are also used to precipitate arsenic in metallurgical industries. In studies performed in hydrothermal conditions, at 150°C, it was found that jarosites could substitute only a 4 % of sulfur by arsenic in the structure before it began to precipitate scorodite. However, at 98°C was achieved the precipitation of jarosite with an arsenic incorporation up to 9.91 % before it began to precipitate scorodite, and reached a 14.83 % with co-precipitation of jarosite [Paktunc and Dutrizac, 2003]. Paktunc and Dutrizac (2003) also studied the effects of arsenic incorporation in the structure of jarosite, where they saw the substitution of sulfates by arsenates led to an increase in the *c* cell parameter that increased with the arsenate incorporation in the structure, while the *a* cell parameter remained constant.

As happened with scorodite, jarosite may also decompose to goethite in long term storage as shown in Eq. 3.2 [Welham et al., 2000, Stoffregen et al., 2000]. This decomposition could allow the releasing of arsenic contained in jarosites. A part of the solution in aerobic conditions, iron is a phase that could easily

react in anaerobic conditions, which certainly would lead to the dissolution of jarosite.

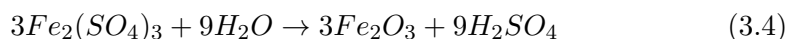
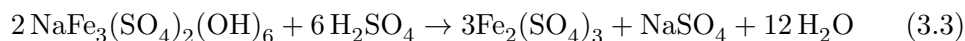


As explained in the previous section, one of the most interesting properties of jarosite are the structural changes that present depending on the ions. In particular, these changes have been extensively reported in jarosite-type phases. Drouet and Navrotsky (2003) found a linear decline in the c cell parameter as incorporated in the structure of sodium jarosite. Moreover, Basciano and Peterson (2008) presented an article showing that the sodium, potassium and hydronium jarosites c cell parameters varies depending on which A cation contained, and it changed linearly with the ionic radius of the cation that produced changes in the distance A-O3 (Figures 3.3 and 3.4). Sato et al. (2009) confirmed the change produced in the c cell parameter when there is a change in the alkali, and this change depends on the ionic radius of the alkali. So if the ionic radius of the alkali is minor, the cell parameter c decreases. The same happens when there is a change in the metal cation B, although in this case changed the parameters a and c .

3.2 Hematite formation from jarosites

Jarosite is an easily filterable precipitate. Unfortunately, this precipitate has a large volume and cannot be used as a byproduct. For this reason, hematite could be of interest as it is still an easily filtrable precipitate, which in addition has a high density. So, it has a smaller volume than jarosite. Besides, hematite can be used as a by-product, as it can be used in cement industry. However, the synthesis process of hematite is very expensive due to the high temperatures needed to reach for the oxidation of iron. The cost increases because very often the solutions are diluted and the iron is not in the optimal concentrations. This can be solved by a previous precipitation of iron as jarosite. Thus, it permits a process with the optimum concentration of iron in the solution. At the same time is used the oxidized iron from jarosites. Then, it is not needed to reach high temperatures for the iron oxidation. The hematite formation from jarosites is discussed in the article J.E. Dutrizac, A. Sunyer, 2012, Hematite formation from jarosite type compounds by hydrothermal conversion, Canadian Metallurgical Quarterly, 51, 1, 11-23 (annex A.1).

The conversion of jarosite to hematite happened according to the equations 3.3, 3.4 and 3.5.



Before this study, Dutrizac (1989) reflected the possibility to transform sodium jarosite to hematite at temperatures above 200°C. This study demonstrated that the most important variables in the transformation of sodium jarosite to hematite were temperature, retention time, acid concentration and,

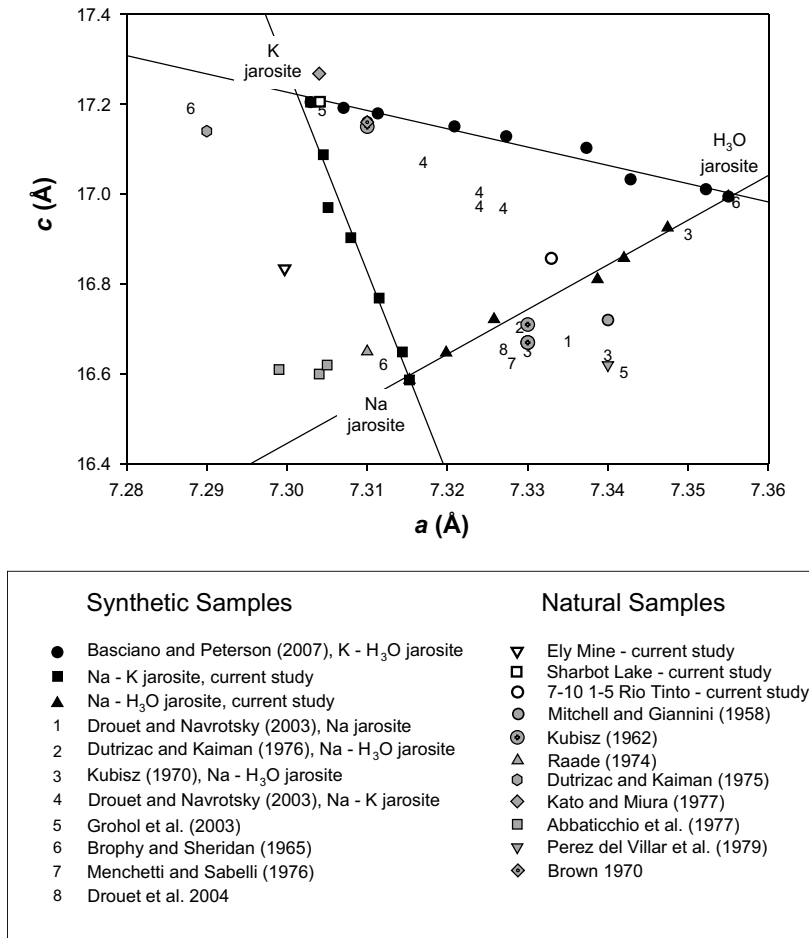


Figure 3.3: Cell parameters a and c in jarosites with different Na, K and H₃O substitutions [Basciano and Peterson, 2008].

addition of hematite seed. All these parameters were studied in the article Dutrizac and Sunyer (2012) (annex A.1) for potassium, lead and sodium-silver jarosites, sodium jarosite containing arsenic and, sodium jarosite made in situ and immediately transformed to hematite.

All jarosites were synthesized from iron sulphate and the sulphate of the corresponding alkali or alkaline. The synthesis temperature of potassium, sodium-silver jarosites was 97°C, while lead and sodium jarosite containing arsenic were synthesized at 150°C.

The results obtained were:

Potassium jarosite was transformed to hematite at temperatures above 240°C. Therefore, the stability of this phase is higher to that of sodium jarosite, which just needed temperatures above 200°C to be completely transformed to hematite. In presence of seed (Fe₂O₃) the temperature of the transformation diminish to 230°C, similar to what happened in sodium jarosite. Retention time was studied in all cases at 225°C. This is one of the most important variables. At a temperature of 225°C was chosen to compare the studies previously done with

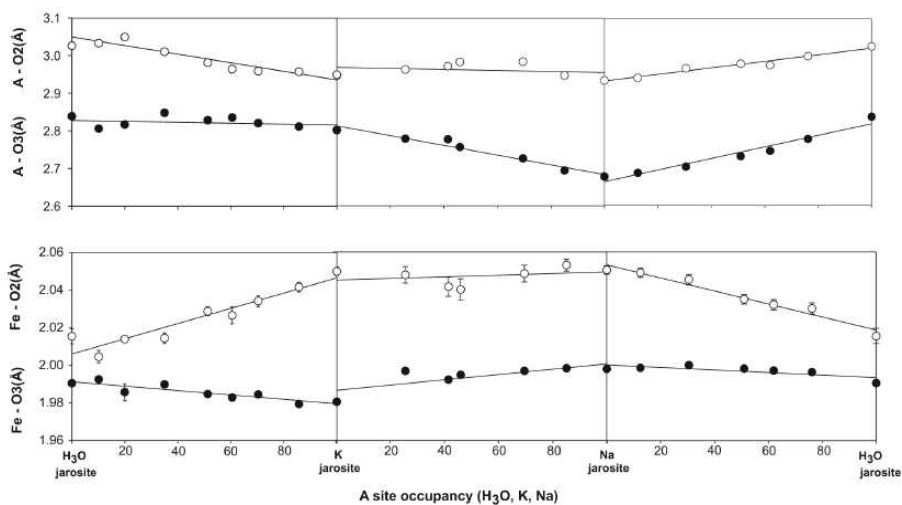


Figure 3.4: Distances of the polyhedron A-O3 and A-O2 and the octahedrons Fe-O3 and Fe-O2 in jarosites with different Na, K and H₃O substitutions [Basciano and Peterson, 2008].

sodium jarosite. Potassium jarosite required a minimum of 2 hours for a complete conversion to hematite. At this temperature, there is also a significant difference with sodium jarosite, which only needs 30 minutes to be completely transformed to hematite.

Lead jarosite and sodium-lead jarosite at temperatures of 225°C needed only 45 min of retention time, similar to that of sodium jarosite. The main difference of this reaction was that besides the hematite precipitated lead sulfate. In the case of sodium-silver jarosite, for a temperature of 225°C, the transformation to hematite was done within 30-min retention time.

Sodium jarosite containing arsenic were synthesized at 225°C and different concentrations of sulfuric acid. In these jarosites was found that at concentrations between 0 and 0.4 M H₂SO₄ precipitated hematite, which permitted to precipitate about 95 % of the arsenate contained in the initial jarosite. At concentrations >0.4 M of H₂SO₄, Fe(SO₄)(OH) co-precipitated with Fe₂O₃, and in some cases sodium jarosite was also detected, although in no case was detected scorodite. In addition, precipitation of arsenate decreased as the acid concentration increased.

Sodium jarosite synthesized in situ was formed within 45 min of retention time, after heating the pressure reactor. Sodium jarosite synthesized under these conditions was more stable than the not synthesized in situ and, until temperatures above 230°C hematite was not detected. At 250°C the transformation of jarosite to hematite was not complete. The transformation temperature of sodium jarosite synthesized in situ could be diminished to 210°C after the addition of the hematite seed before the synthesis of jarosite.

Thus, this study suggests that it would be possible to concentrate iron by two steps: 1) the precipitation of jarosite to concentrate the iron; 2) the trans-

formation of jarosites to hematite, which will be more economic than the direct synthesis of hematite. Furthermore, it indicates that the precipitation of arsenical jarosite would permit the transformation to hematite with the 95 % of arsenic precipitated in the same step. However, it has to be performed with a concentration of H_2SO_4 below 0.4 M in the medium.

3.3 Synthetic alunite

Unlike jarosites, alunites have been much less studied because these phases could not be directly applied in the industry. However, since 50's alunites had been synthesized. Basset (1950) explained the lead alunite synthesis from aluminum sulfate and lead nitrate. In the same article mentioned authors who had done research on potassium alunite in 1937.

Alunites are commonly synthesized with a stoichiometric solution of A_xSO_4 and $\text{Al}_2(\text{SO}_4)_3$ at temperatures between 190 and 205°C (Eq. 3.6). At these temperatures are obtained well-crystallized alunite phases. Depending on the type of alkali is obtained more or less product yield. Therefore, observed that the potassium alunite has the highest product yield (~ 3.8 g), higher than the obtained in the same conditions for natroalunite (~ 1.5 g). While hydronium alunite has the lowest product yield (~ 1.2 g) [Rudolph et al., 2003]. This is coherent with the frequency of the alunite-types found in the nature, where potassium alunite is the most common and, few specimens of hydronium alunite have been found.



Currently, most studies made about alunite-type phases are structural studies, which mainly analyse the effects of the different atoms on the cell parameters.

Different authors studied the effect of the substitution of different cations in the alunite-type phases' structure [Rudolph et al., 2003, Sato et al. 2009]. In these studies, linear changes on the cell parameters in the case of partial substitutions were observed. Depending on the position of the cation changed, the change occurs in a or c cell parameters. So Rudolph et al. (2003) found that changing the K for H_3O the c cell parameter increased with the addition of K. The change in this parameter is due to the differences in the atomic radii, so sodium alunite will has a c cell parameter smaller than potassium alunite, since the sodium atomic radius is smaller than that of potassium and, the position where the alkaline is located affects the cell parameter c . Sato et al. (2009) associated the structural changes with the distances between atoms of icosahedra $\text{AO}_6(\text{OH})_6$, octahedra $\text{M}(\text{OH})_4\text{O}_2$ and tetrahedra TO_4 , due to the change of A, M or T. According to their ionic radii, the distances in between them and O are affected. Thus, if the change was in A, it will affect the cell parameter c , while the cell parameter a will not be affected. Otherwise, if the change is in M the affected cell parameters will be both, a and c . Finally, in the case that the change occurs in T, c will be the only affected cell parameter, while the cell parameter a will not suffer any change.

CHAPTER 4

THESIS AIM AND OBJECTIVES

The aim of these thesis was the arsenic inertization through alunite-type phases with B site occupied by Al. The stability of these phases in neutral pHs and in long term storage, as well as the application of these phases in high sulfate/arsenate industrial wastes from copper pyrometallurgy.

This thesis consisted in the subsequent objectives:

1. Synthesis of arsenical-natroalunites, optimization of the process and ensure the arsenic stability. For these objectives arsenical-natroalunites were synthesized at different retention times, temperatures and concentrations of arsenic. The incorporation of arsenate in natroalunite's structure was proved by ICP, SEM-EDS and XRD. The As-natroalunites stability was checked by short (24 h) and long (6 months) term tests.
2. The application of arsenical-natroalunite in copper pyrometallurgical arsenical wastes was performed in two different residues from different companies. The first was the final effluent from the electrolytic section, while the second was a flash smelter dust. In both cases the steps were similar:
 - (a) Leaching and recovery of copper
 - (b) The precipitation of arsenic as arsenical-natroalunite. As in synthetic samples, arsenic stability tests were performed in all cases to ensure the stability.
3. To know the effect of the arsenic incorporation in the alunite-type structure, the cell parameters were calculate for arsenical natroalunites. Cell parameter c increases as the arsenate incorporation increased. This enlargement drove to think in a major incorporation of arsenic in other alunite-type phases with a higher c cell parameter, such as lead-alunite, barium-alunite, potassium-alunite and hydronium-alunite. These phases were studied as arsenical-natroalunite, at different retention times, temperatures and arsenic concentration, and were characterized by ICP, SEM-EDS and XRD.
4. Finally, a short and a medium-term (5 weeks) stability tests were performed on synthetic potassium alunites. This study was complemented with a medium-term stability test for natural and synthetic scorodite.

PART II

Results and discussion

CHAPTER 5

THESIS STRUCTURE

This thesis has been written as article compendium. All the articles that stand up for this thesis are in the annex A and B. All the chapters of this thesis discuss in a structured way the results found during the investigation. For an easy understanding, the chapters are not only referenced to one article, they make references to some and other parts of various articles, indicated with the complete reference at the beginning of each chapter.

The structure of this thesis is:

1. Synthesis of different alunite-type phases from pure reagents and the arsenate incorporation in the structure. Inside all chapters, the effects that affect the formation of these phases are also described.
2. Generation of arsenical-natroalunites from arsenical-wastes from two different pyrometallurgical copper plants.
3. Stability tests in short and long term from the successfully synthesized alunite-type phases.
4. A structure study and the effect in the alunite-type phases structure of the incorporation of arsenate.
5. Conclusions of the thesis.

For the synthesis of alunite-type phases was considerate the use of economic reagents, because one of the objectives is the application of this inertization process to copper pyrometallurgical arsenical wastes.

For economical reasons, the first alunite-type phase synthesized was natroalunite ($\text{NaAl}_3(\text{SO}_4)_2(\text{OH})_6$). The synthesis of this phase was performed using sodium sulfate and aluminum sulfate as a reagents, both of them a very economic reagents.

Natroalunite was successfully synthesized. After this exit, other alunite-type phases of this group were synthesized. The cations chosen were: K, Pb, Ba, H_3O . Furthermore, other phases like schlossmacherite or arsenocrandallite were synthesized with the objective to obtain a maximum incorporation of arsenic in the structure.

All synthesized phases were characterized by XRD, SEM-EDS and ICP. In addition, stability tests in short, medium and long term, as well as structural studies with Rietveld method to determine the effect of the arsenic in alunite structure were performed in the phases synthesized successfully.

CHAPTER 6

SYNTHETIC AS-NATROALUNITE

Precipitation of arsenical-natroalunite analyzed different variables: retention time, temperature and arsenate concentration. The latter is referred as $\text{AsO}_4/(\text{SO}_4 + \text{AsO}_4)$ molar ratio. This ratio was also used in Paktunc and Dutrizac (2003) for the arsenate-for-sulfate substitution in jarosites. This molar ratio also considers the concentration of SO_4 in the medium. If SO_4 increases in the medium but AsO_4 do not increase, the ratio $\text{AsO}_4/(\text{SO}_4 + \text{AsO}_4)$ will decrease, then, less arsenate can be incorporated in the structure, because arsenate is incorporated substituting part of natroalunite's sulfate. So, arsenate concentration effect must be analyzed as the molar ratio $\text{AsO}_4/(\text{SO}_4 + \text{AsO}_4)$.

This chapter is based on the subsequent article:

- A. Sunyer, J. Viñals, 2011, Arsenate substitution in natroalunite: A potential medium for arsenic immobilization. Part 1: synthesis and compositions, *Hydrometallurgy*, 109, 54-64. (Annex A.2).

6.1 Effect of synthesis temperature

Experiments without arsenic were done at temperatures between 100°C and 200°C. Whereas experiments with arsenic were performed at temperatures of 100°C and between 160°C and 200°C.

Synthesis without arsenic showed that at 100°C and 200°C and a short retention time (2 h), natroalunite was not precipitated. Despite at 100°C and 72-h retention time natroalunite precipitated. Without seed 16 % of natroalunite precipitated, while with seed precipitated a 29 % of natroalunite. At 140°C natroalunite precipitated within 2-h retention time. However, only a 1 % of natroalunite was precipitated. Between 140°C and 200°C natroalunite precipitation increased in a linear manner rising up to 55 % at 200°C.

In experiments in presence of arsenic, the effect of the temperature was performed with a molar ratio of $\text{AsO}_4/(\text{SO}_4 + \text{AsO}_4) = 0.185$ in the initial medium. With the addition of arsenic the formation of arsenical amorphous phases or mansfieldite ($\text{AlAsO}_4 \cdot 2\text{H}_2\text{O}$) was possible.

At 100°C and with the use of seed of arsenical-natroalunite, the precipitation rate was 22 %, however, the precipitation of arsenical-natroalunite was just 5 % calculated with sodium balance. In electronic microscopy was observed a large

amount of amorphous phase recovering the arsenical-natroalunite crystals used as seed. This amorphous phase was really soluble in water. Thus, the synthesis at 100°C was discarded and the subsequent working temperatures studied were above 160°C.

At 160°C and 180°C and a retention time of 2 h arsenical natroalunite and mansfieldite were precipitated. Both phases were well crystallized. However, at 200°C and 2-h retention time only arsenical natroalunite was precipitated. The absence of mansfieldite could be due for a very low final pH in this synthesis. This acidic condition in the medium could not permit the formation of mansfieldite.

6.2 Effect of retention time

The effect of retention time was studied at different temperatures. This procedure let to observe the different steps in the formation of arsenical natroalunites. This effect was evaluated in two different $\text{AsO}_4/(\text{SO}_4 + \text{AsO}_4)$ molar ratio: 0.185 and 0.083 (table 6.1, figures 6.1 and 6.2).

The general scheme obtained in arsenical-natroalunites formation between 160°C and 180°C, with a molar ratio of $\text{AsO}_4/(\text{SO}_4 + \text{AsO}_4)$ of 0.185 and retention times between 15 min and 4 h was:

1. Within 15 min, at 160°C and at 180°C, precipitated arsenical amorphous phases and natroalunites.
2. At 30 min and 160°C, still appeared amorphous phase, although the natroalunite precipitation increased. Otherwise, at 180°C did not precipitate amorphous phases and, natroalunite and mansfieldite were precipitated.
3. Within 2 h and 160°C, natroalunite was the only precipitated phase. But at 180°C natroalunite and mansfieldite precipitated.
4. At 4-h retention time, at both temperatures, 160°C and 180°C, natroalunite and mansfieldite precipitated.

At molar ratio $\text{AsO}_4/(\text{SO}_4 + \text{AsO}_4) = 0.083$, at 180°C and 2 h retention time, mansfieldite did not precipitate. Thus, the precipitation of mansfieldite needed more arsenate in the medium.

At 200°C, the formation of arsenical-natroalunite was independent of the retention time. In both $\text{AsO}_4/(\text{SO}_4 + \text{AsO}_4)$ molar ratio (0.083 and 0.185), arsenical-natroalunite was precipitated within 5 min (table 6.1, figures 6.1 and 6.2).

Table 6.1: Bulk composition (ICP) and phases (Rietveld) of hydrothermal precipitated (na: natroalunite; am: amorphous phase; ma: mansfieldite; al: alarsite; ph: natropharmacoalumite).

Temperature (°C)	Time (h)	(As/(S + As)) _{aq}	Chemical composition (%)				Phases (XRD and SEM/EDS)
			Na	Al	S	As	
<i>Na⁺/Al³⁺/SO₄²⁻</i>							
100	2	0	–	–	–	–	no precipitate
100	72	0	not det.	–	–	–	na (16% yield)
100	72	0	3.84	20.08	16.64	0.00	na (29% yield)
120	2	0	–	–	–	–	no precipitate
140	2	0	not det.	–	–	–	na (1% yield)
160	2	0	not det.	–	–	–	na (16% yield)
180	2	0	not det.	–	–	–	na (37% yield)
200	2	0	4.05	17.95	15.07	0.00	na (55% yield)
<i>Na⁺/Al³⁺/SO₄²⁻/AsO₄³⁻</i>							
100	72	0.185	3.49	18.48	11.91	7.22	na (74% ^a) + am (26% ^b)
160	0.083	0.185	1.63	15.45	6.14	14.72	na (33% ^a) + am (67% ^b)
160	0.5	0.185	3.77	17.43	11.77	7.26	na (75% ^a) + am (25% ^b)
160	2	0.185	5.10	20.02	15.12	2.95	na
160	4	0.185	4.16	18.25	12.52	8.51	na (85%) + ma (15%)
180	0.083	0.185	3.63	17.92	11.96	7.42	na (73% ^a) + am (27% ^b)
180	0.5	0.185	3.83	18.40	12.45	7.29	na (87%) + ma (13%)
180	2	0.185	4.98	18.97	13.67	7.53	na (91%) + ma (9%)
180	4	0.185	4.00	18.87	12.93	8.59	na (82%) + ma (18%)
200	0.083	0.185	5.18	19.13	15.07	3.43	na
200	0.5	0.185	4.57	18.40	14.87	3.00	na
160	0.083	0.083	1.75	19.05	7.74	8.46	na (35% ^a) + am (65% ^b)
160	2	0.083	5.08	18.92	14.99	1.45	na
160	4	0.083	4.73	18.38	17.62	3.09	na (95%) + ma (5%)
180	2	0.083	5.18	18.90	16.46	1.43	na
200	0.083	0.083	4.87	18.63	14.86	1.52	na
200	0.5	0.083	4.98	18.36	14.91	1.28	na
200	2	0.083	4.88	18.42	14.88	1.24	na
200	2	0.101	4.52	17.18	13.94	1.32	na
200	2	0.114	4.66	18.70	15.02	1.69	na
200	2	0.130	4.59	16.96	13.53	1.94	na
200	2	0.152	4.91	17.53	13.77	2.53	na
200	2	0.185	4.72	18.93	14.55	2.80	na
200	2	0.231	3.68	17.92	10.46	12.97	na (71%) + ma (29%)
200	2	0.270	5.26	19.27	12.91	5.98	na (95%) + ma (3%) + al (2%)
200	2	0.311	1.79	15.41	4.41	25.71	na (32%) + ma (68%)
200	2	0.359	0.87	14.24	2.00	30.09	na (16%) + ma (85%)
200	2	0.421	0.18	16.46	0.06	41.99	al (98%) + ma (2%)
200	2	0.474	2.17	14.96	0.08	32.52	ph (65% ^a) + (al + ma) (35% ^b)

^a Determined from the Na content in the bulk product.^b By difference.

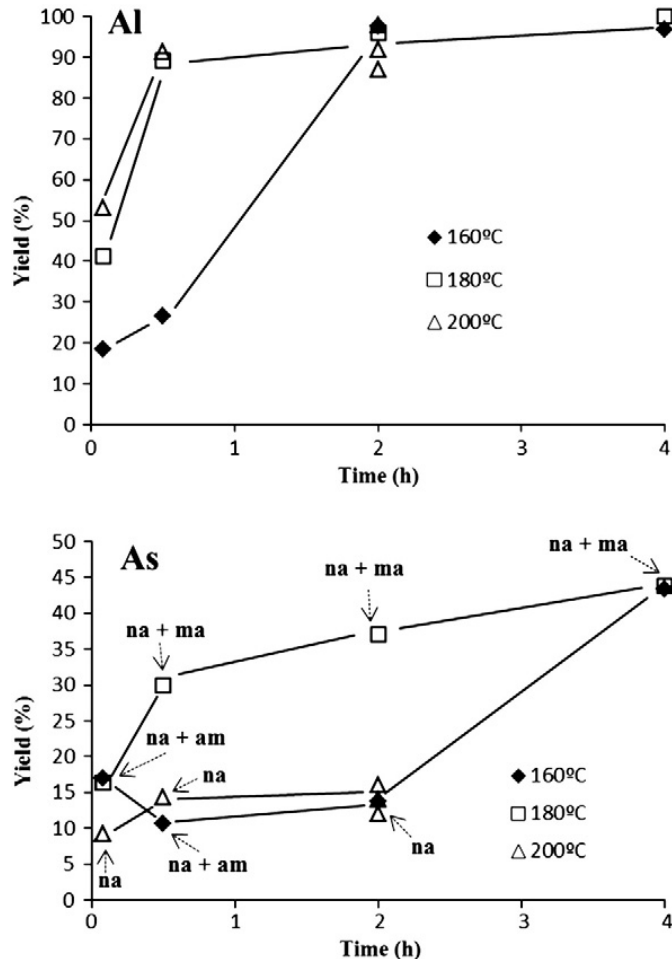


Figure 6.1: Precipitation of Al and As vs the retention time at $(\text{AsO}_4/(\text{SO}_4 + \text{AsO}_4))_{aq}=0.185$ (na: natroalunite; am: amorphous phase; ma: mansfieldite).

6.3 Effect of arsenic concentration

The experiments were performed at different $(\text{AsO}_4/(\text{SO}_4 + \text{AsO}_4))_{aq}$ molar ratio in the same synthesis conditions: 200°C and 2-h retention time.

This retention time and the temperature were chosen because no amorphous phases were formed with the presence of arsenic and, without arsenic presence, natroalunite presented a good precipitation yield (55%) compared with lower temperatures.

The $\text{AsO}_4/(\text{SO}_4 + \text{AsO}_4)$ molar ratio studied were between 0 and 0.474. Different phases were precipitated depending on the molar ratio (table 6.2 and figure 6.4). With the experiments could be determined different zones at different $\text{AsO}_4/(\text{SO}_4 + \text{AsO}_4)$ molar ratios (figure 6.3):

1. Between 0 and 0.2: Only natroalunite/As-natroalunite was precipitated.
2. Between 0.2 and 0.4: Co-precipitated natroalunite and mansfieldite.

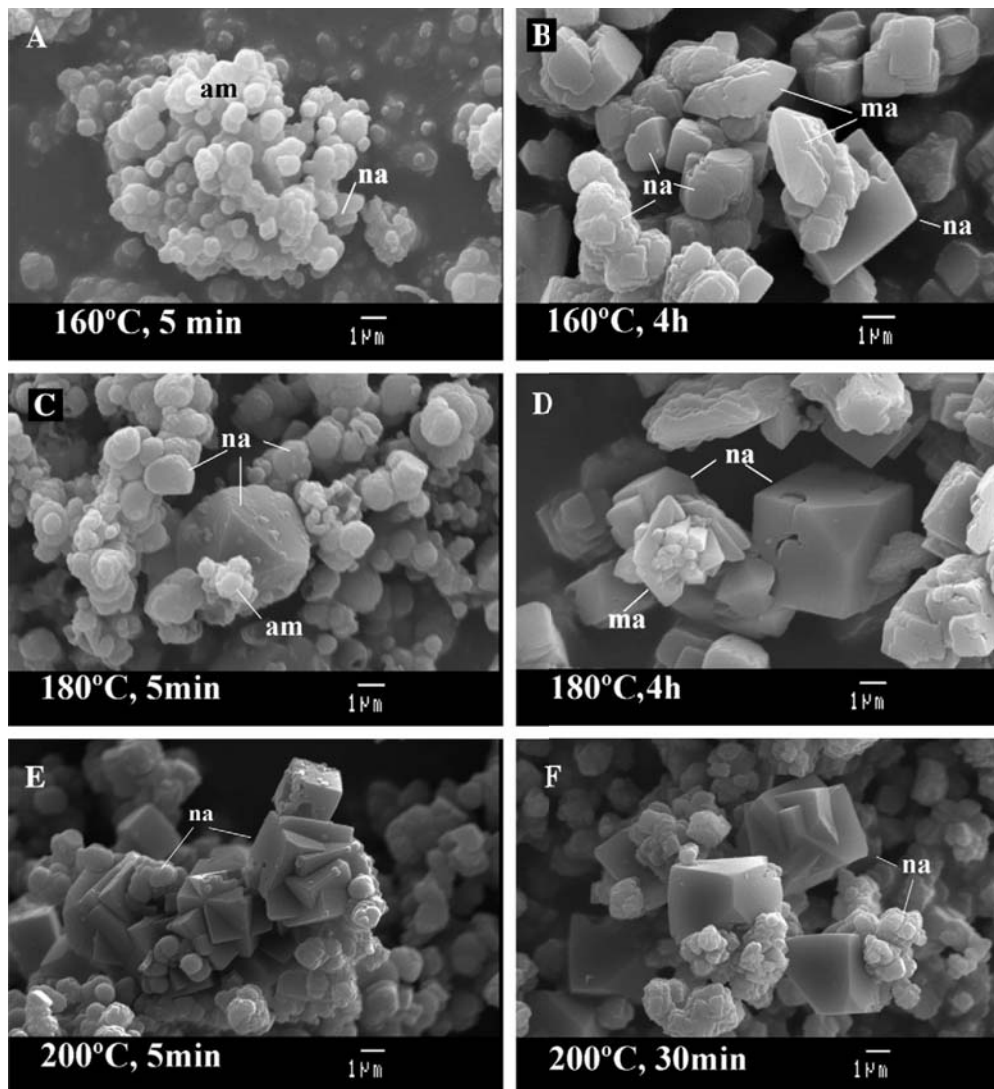


Figure 6.2: SEM images obtained at 160°C, 180°C and 200°C at different retention times and a molar ratio $(\text{AsO}_4/(\text{SO}_4 + \text{AsO}_4))_{aq}=0.185$ (na: natroalunite; am: amorphous phase; ma: mansfieldite).

3. Around 0.421: Alarsite (AlAsO_4) and some mansfieldite were precipitated.
4. Around 0.474: Natropharmacoalumite ($\text{NaAl}_4(\text{AsO}_4)_3(\text{OH})_4 \cdot 4\text{H}_2\text{O}$) and mansfieldite were precipitated.

The arsenate incorporation in natroalunite was evaluated with ICP and SEM/EDS. The latter permitted to determine the arsenate incorporation in multiple phase samples.

The incorporation of arsenate depended on the initial $\text{AsO}_4/(\text{SO}_4 + \text{AsO}_4)$ molar ratio. When the $\text{AsO}_4/(\text{SO}_4 + \text{AsO}_4)$ molar ratio increases, the incorporation of arsenate increased in a linear manner with a slope of 0.5 between the ratios $[\text{AsO}_4/(\text{SO}_4 + \text{AsO}_4)_{\text{nat}}]/[\text{AsO}_4/(\text{SO}_4 + \text{AsO}_4)_{\text{aq}}]$. The maximum arsenic incorporation without precipitation of mansfieldite was 0.15 in formula. However, the incorporation of arsenic increased with mansfieldite precipitation, rising up to 0.31 in formula (figure 6.3 and table 6.2).

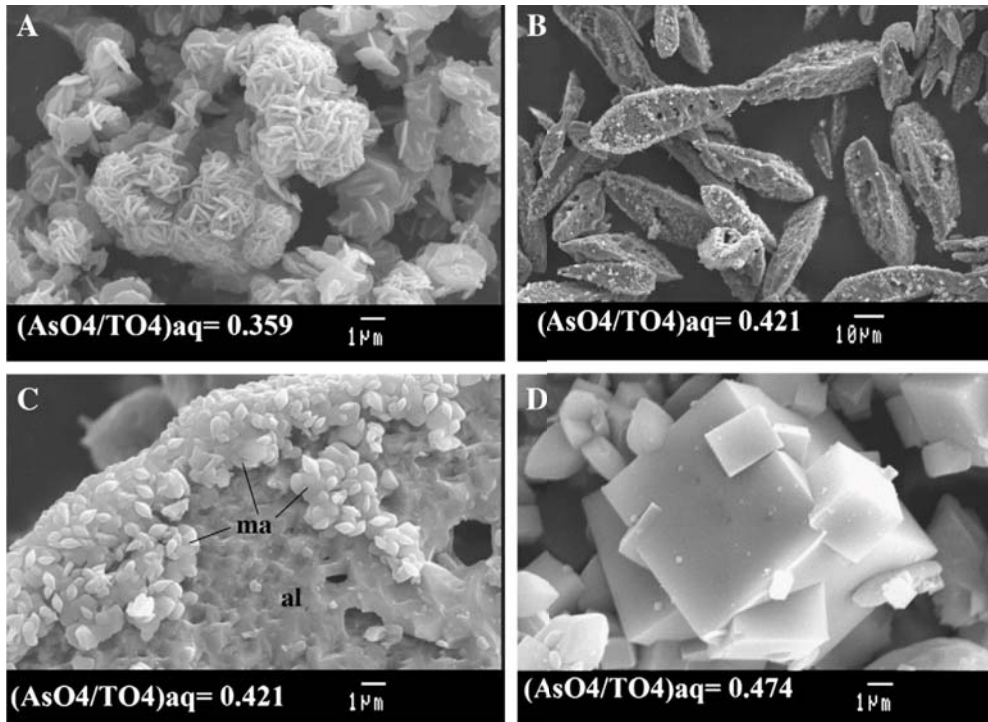


Figure 6.3: Arsenate phases formed at high $\text{AsO}_4/(\text{SO}_4 + \text{AsO}_4)_{\text{aq}}$. A: Mansfieldite. B: Alarsite. C: Mansfieldite (ma) on corroded alarsite (al). D: Natropharmacoalumite.

Table 6.2: Formula coefficients in natroalunite phase (normalized to S+As=2) (BCA: from bulk chemical analysis ICP. EDS: from mean spot analyses by EDS).

Temp. (°C)	Time (h)	(As/(S+As)) _{aq}	BCA				EDS			
			Na	Al	S	As	Na	Al	S	As
Na ⁺ /Al ³⁺ /SO ₄ ²⁻										
100	72	0	0.65	2.86	2.00	0.00	0.66±0.11	2.81±0.12	2.00	0.00
200	2	0	0.75	2.83	2.00	0.00	0.74±0.08	2.88±0.10	2.00	0.00
Na ⁺ /Al ³⁺ /SO ₄ ²⁻ /AsO ₄ ³⁻										
160	0.5	0.185		Not det. (phase mixture)			1.02±0.06	2.78±0.06	1.79±0.01	0.21±0.01
160	2	0.185	0.87	2.90	1.85	0.15	0.98±0.12	2.88±0.12	1.85±0.01	0.15±0.01
160	4	0.185		Not det. (phase mixture)			0.94±0.14	2.76±0.09	1.80±0.02	0.20±0.02
180	0.083	0.185		Not det. (phase mixture)			0.85±0.07	2.67±0.06	1.79±0.01	0.21±0.01
180	0.5	0.185		Not det. (phase mixture)			0.93±0.10	2.72±0.10	1.81±0.02	0.19±0.02
180	2	0.185		Not det. (phase mixture)			0.96±0.09	2.74±0.12	1.82±0.03	0.18±0.03
180	4	0.185		Not det. (phase mixture)			0.96±0.10	2.69±0.08	1.80±0.02	0.20±0.02
200	0.083	0.185	0.87	2.76	1.82	0.18	0.99±0.02	2.73±0.04	1.81±0.02	0.19±0.02
200	0.5	0.185	0.80	2.71	1.84	0.16	0.96±0.07	2.74±0.08	1.84±0.01	0.16±0.01
160	2	0.083	0.91	2.88	1.92	0.080			Not det.	
180	2	0.083	0.85	2.63	1.93	0.072			Not det.	
200	0.083	0.083	0.88	2.85	1.92	0.084			Not det.	
200	0.5	0.083	0.90	2.84	1.93	0.069			Not det.	
200	2	0.083	0.88	2.84	1.93	0.068	0.80±0.12	2.80±0.10	1.93±0.01	0.074±0.006
200	2	0.101	0.87	2.82	1.92	0.078	0.82±0.16	2.80±0.14	1.92±0.01	0.086±0.006
200	2	0.114	0.83	2.82	1.91	0.092	0.88±0.10	2.92±0.08	1.90±0.01	0.10±0.01
200	2	0.130	0.89	2.80	1.88	0.12	0.82±0.12	2.82±0.08	1.87±0.01	0.13±0.01
200	2	0.152	0.92	2.81	1.85	0.15	0.94±0.12	2.80±0.08	1.85±0.01	0.15±0.01
200	2	0.185	0.84	2.86	1.85	0.15	0.94±0.10	2.84±0.10	1.84±0.02	0.16±0.02
200	2	0.231		Not det. (phase mixture)			0.97±0.10	2.77±0.14	1.78±0.03	0.22±0.03
200	2	0.270		Not det. (phase mixture)			1.01±0.08	2.86±0.08	1.74±0.02	0.26±0.02
200	2	0.311		Not det. (phase mixture)			0.98±0.09	2.92±0.18	1.69±0.02	0.31±0.02

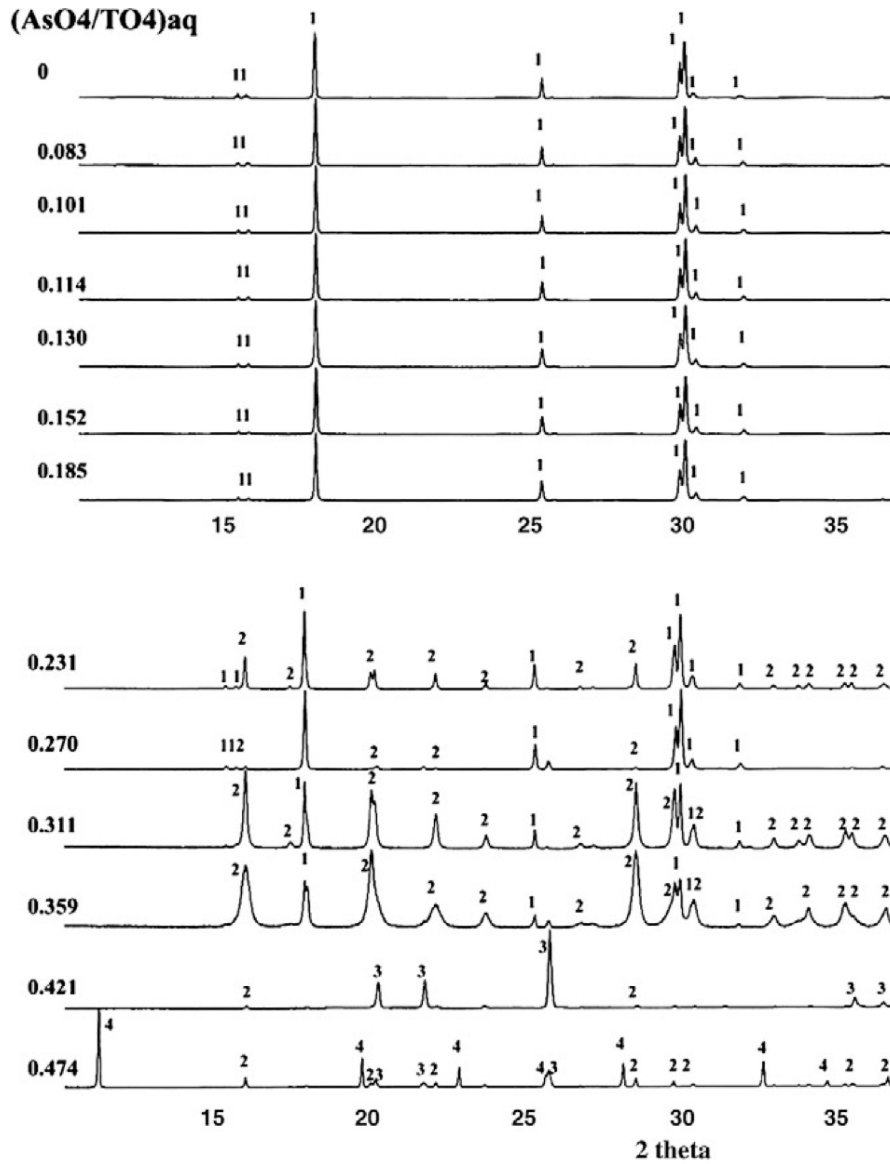


Figure 6.4: X-ray patterns showing the effect of $(\text{AsO}_4/\text{TO}_4)_{aq}$ on phase composition at 200 °C (1: natroalunite; 2: mansfieldite; 3: alarsite; 4: natropharmacoalumite).

6.4 Synthesis with calcium in the medium

6.4.1 Synthesis of As-natroalunite

Most of the wastes and industrial effluents that contain arsenic also contain calcium sulfate. This is due to the use of calcium hydroxide as a precipitation agent. Then, the effect of calcium present in the medium during the arsenical-natroalunite precipitation was of interest.

The obtained results gave a little incorporation of calcium in arsenical-natroalunite structure, up to 0.04 in formula (table 6.3). However, this in-

corporation was independent of the calcium concentration in the medium, the synthesis temperature and the retention time. The larger part of it precipitated as anhydrite (CaSO_4).

The effect of retention time and temperature was studied in this medium. The results are in tables 6.4 and 6.5. At 180°C and less than 30 min was formed natroalunite, amorphous phase and anhydrite. While in 2-h retention time no amorphous phase were formed and instead, mansfieldite was precipitated, as well as natroalunite and anhydrite. Otherwise, at 200°C and less than 30 min, natroalunite, mansfieldite and anhydrite were precipitated, whereas at 2-h retention time were only formed natroalunite and anhydrite.

Arsenic incorporation in arsenical natroalunites in presence of calcium was studied for molar ratios $\text{As}/(\text{S}-\text{Ca}+\text{As})$ between 0.100 and 0.309. The obtained values are similar to the obtained in absence of calcium in the medium (figure 6.5). Thus, the presence of calcium in the medium does not have any effect for arsenical-natroalunite synthesis.

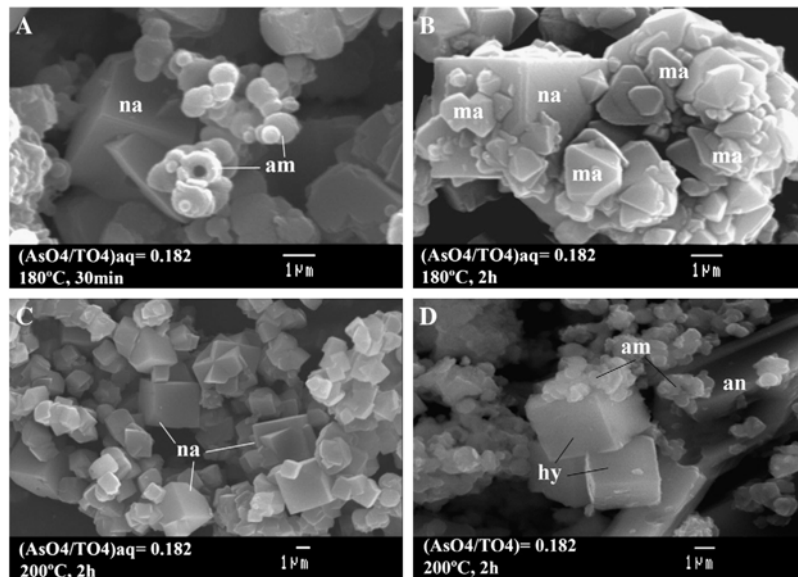


Figure 6.5: A-C: precipitates obtained in $\text{Na}^+/\text{Ca}^{2+}/\text{Al}^{3+}/\text{SO}_4^{2-}/\text{AsO}_4^{3-}$ medium. D: in $\text{Ca}^{2+}/\text{Al}^{3+}/\text{SO}_4^{2-}/\text{AsO}_4^{3-}$ medium (na: natroalunite; am: amorphous; ma: mansfieldite; an: anhydrite; hy: hydronium alunite).

Table 6.3: Formula coefficients in arsenical-natroalunites obtained in a medium with presence of calcium.

Temperature (°C)	Time (h)	(As/((S-Ca) + As)) _{aq}	Na	Ca	Al	S	As
<i>Na⁺/Ca²⁺/Al³⁺/SO₄²⁻/AsO₄³⁻</i>							
200	2	0.100	0.72 ± 0.08	0.04 ± 0.01	2.78 ± 0.07	1.93 ± 0.01	0.073 ± 0.008
200	2	0.182	0.79 ± 0.07	0.04 ± 0.01	2.99 ± 0.18	1.84 ± 0.01	0.16 ± 0.01
200	0.5	0.182	0.73 ± 0.04	0.06 ± 0.01	2.78 ± 0.12	1.82 ± 0.01	0.18 ± 0.01
200	0.25	0.182	0.76 ± 0.04	0.06 ± 0.01	2.78 ± 0.15	1.82 ± 0.02	0.18 ± 0.02
180	2	0.182	0.77 ± 0.06	0.06 ± 0.01	2.74 ± 0.08	1.80 ± 0.02	0.20 ± 0.02
180	0.5	0.182	0.73 ± 0.05	0.06 ± 0.01	2.70 ± 0.04	1.80 ± 0.02	0.20 ± 0.02
180	0.25	0.182	0.82 ± 0.05	0.06 ± 0.01	2.82 ± 0.12	1.80 ± 0.02	0.20 ± 0.02
200	2	0.309	0.87 ± 0.08	0.07 ± 0.02	2.76 ± 0.08	1.68 ± 0.03	0.32 ± 0.02
<i>Ca²⁺/Al³⁺/SO₄²⁻/AsO₄³⁻</i>							
200	2	0.182	0.00	0.12 ± 0.03	2.73 ± 0.02	1.73 ± 0.07	0.27 ± 0.07

Table 6.4: Reagents used and synthesis conditions in the synthesis of arsenical-natroalunites in presence of calcium in the medium.

<i>Fixed reagent addition: Al₂(SO₄)₃·18H₂O: 6.33 g</i>							
	<i>Na⁺/Ca²⁺/Al³⁺/SO₄²⁻/AsO₄³⁻</i>						
ASC1	0.99	0.564	200	2	0.100		1.0
ASC2	1.98	0.564	200	2	0.182		0.9
ASC3	1.98	0.564	200	0.5	0.182		0.9
ASC4	1.98	0.564	200	0.25	0.182		0.9
ASC5	1.98	0.564	180	2	0.182		0.9
ASC6	1.98	0.564	180	0.5	0.182		1.1
ASC7	1.98	0.564	180	0.25	0.182		1.7
ASC8	3.98	1.095	200	2	0.309		1.1
ASC9	3.98	2.187	200	2	0.309		1.2

Table 6.5: Chemical composition and phases obtained in presence of calcium in the medium.

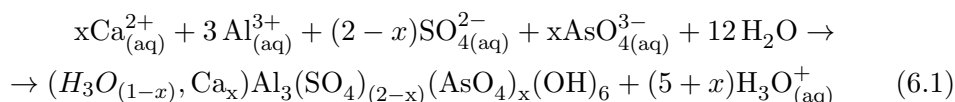
Temperature (°C)	Time (h)	(As/ ((S-Ca) + As)) _{aq}	Chemical composition (%)					Phases (XRD and SEM/EDS)
			Na	Ca	Al	S	As	
<i>Na⁺/Ca²⁺/Al³⁺/SO₄²⁻/AsO₄³⁻</i>								
200	2	0.100	4.20	1.03	21.00	17.91	1.35	na (98%) + an (2%)
200	2	0.182	4.75	1.07	20.37	16.14	2.60	na (98%) + an (2%)
200	0.5	0.182	4.26	1.55	18.44	14.93	3.46	na (97%) + ma (1%) + an (2%)
200	0.25	0.182	4.50	1.98	18.09	14.87	3.38	na (97%) + ma (1%) + an (2%)
180	2	0.182	4.11	1.53	17.34	13.03	6.62	na (89%) + ma (9%) + an (2%)
180	0.5	0.182	4.07	1.56	18.33	14.08	4.15	na (92%) + am (6%) + an (2%) ^a
180	0.25	0.182	4.42	1.49	17.24	14.24	3.60	na (94%) + am (4%) + an (2%) ^a
200	2	0.309	1.79	3.60	15.51	9.25	22.05	na (36%) + ma (51%) + an (11%)
200	2	0.309	1.57	7.90	13.52	10.33	18.69	na (31%) + ma (43%) + an (26%)
<i>Ca²⁺/Al³⁺/SO₄²⁻/AsO₄³⁻</i>								
200	2	0.182	0.00	17.97	9.71	14.88	9.33	hy (3%) + am (37%) + an (60%) ^b
200	2	0.309	0.00	1.20	15.20	3.55	34.40	ma (96%) + an (4%)
200	2	0.309	0.00	9.27	10.09	8.47	26.61	ma (68%) + an (32%)

^a Natroalunite and anhydrite from the Na and Ca contents. Amorphous by difference.

^b Anhydrite from Ca content. Hydronium alunite from the ratio hydronium alunite/anhydrite from Rietveld. Amorphous by difference.

6.4.2 Synthesis in absence of sodium in the medium

The effect of calcium in the medium was also done in absence of sodium with the objective of synthesizing schlossmacherite $((\text{H}_3\text{O}, \text{Ca})\text{Al}_3(\text{SO}_4, \text{AsO}_4)_2(\text{OH})_6)$ or arsenocrandellite $(\text{CaAl}_3(\text{AsO}_4)_2(\text{OH})_6(\text{H}_2\text{O}))$ or other intermediate members. The expected reaction was Eq. 6.1.



To compare the experiments, As/(S-Ca+As) molar ratios were the same as the used in presence of sodium and calcium in the medium (0.182 and 0.309).

At molar ratio 0.182, the only crystalline phase obtained with arsenic was the hydronium-calcium alunite with a grade of arsenate substitution up to 14%. This substitution grade was higher than the found in arsenical natroalunites, around 8-10 % at the same $\text{AsO}_4/(\text{SO}_4 + \text{AsO}_4)$ molar ratio. This moderate increment in the arsenate substitution could be due to a major substitution of calcium in the hydronium-alunite (12 %) than in natroalunite (4-6 %). Nevertheless, these substitutions of arsenate and calcium were lower than the found in natural schlossmacherite, in which calcium reached a substitution of 26 % and arsenate of 25 %. Moreover, precipitation of hydronium-alunite was practically insignificant (< 5 %) compared with the obtained in natroalunite (~ 95 %). Consequently, the generated acidity was lower than in As-natroalunite synthesis, and the pH only decreased up to 1.9. Then, the arsenic was extensively precipitated as an amorphous phase of $\text{Al}^{3+}/\text{AsO}_4^{3-}/\text{SO}_4^{2-}$. Lower precipitation rates, as well as the extensive co-precipitation of amorphous phases, did not make attractive this hydronium-alunite as arsenic-stabilization phase.

At molar ratio $\text{As}/(\text{S-Ca+As}) = 0.309$, the unique phase precipitated was mansfieldite. Thus, the increment of AsO_4^{3-} did not form alunite-type phases in $\text{Ca}^{2+}/\text{Al}^{3+}/\text{SO}_4^{2-}/\text{AsO}_4^{3-}$ medium. Then, arsenocrandallite cannot be precipitated in a medium in presence of sulfates.

Alunite ($\text{KAl}_3(\text{SO}_4)_2(\text{OH})_6$) has a c cell parameter higher than natroalunite's. This parameter increases with the arsenate incorporation (chapter 12). For this reason, the aim of arsenical-alunite synthesis was to investigate if a major c cell parameter permitted a higher arsenate incorporation in the structure at 200°C. Another objective was if arsenical-alunites could be synthesized at 100°C as can be done in As-jarosites [Paktunc and Dutrizac, 2003].

This chapter is based on the subsequent articles:

- A. Sunyer, J.E. Dutrizac, 2011, The Behaviour of As(III) and As(V) during the Precipitation of Alunite at 98°C, Waste Processing and Recycling in Mineral and Metallurgical Industries –VI Proceedings of the 50th Annual Conference of Metallurgists of CIM, Montreal, Canada, Edited by S.R. Rao, C.Q. Jia, C.A. Pickles, S. Brienne, V. Ramachandran, VI, 331-336. ISBN 978-1-926872-05-6. (Annex A.4)
- A. Sunyer, M. Currubí, J. Viñals, Arsenic immobilization as alunite-type phases: The arsenate substitution in alunite and hydronium alunite, Journal of Hazardous Materials, in review. (Annex B.1)

7.1 Alunites synthesized at 200°C

For arsenical alunites, at 200°C only the effect of arsenic concentration was studied. This effect was performed with the objectives to know the maximum arsenate incorporation in the structure and, to know the concentration in which a second phase was precipitated. The reagents used in these experiments were $\text{Al}_2(\text{SO}_4)_3 \cdot 18\text{H}_2\text{O}$, K_2SO_4 and arsenic acid. The latter was synthesized in the laboratory, oxidizing a solution of arsenic (III) oxide with ozone.

The temperature and the retention time were not studied. The experiments were performed at 200°C and 1-h retention time. The conditions were chosen based on arsenical-natroalunite experiments (chapter 6), which at this temperature the synthesis did not depend on the retention time.

X-ray diffraction patterns (figure 7.2) and SEM images (figure 7.1) of different arsenical-alunites showed that a second phase -in this case mansfieldite -did not appear until $\text{AsO}_4/(\text{SO}_4 + \text{AsO}_4) = 0.286$ molar ratio (K2 in X-ray

patterns). This ratio is higher than the one where mansfieldite appeared in arsenical-natroalunite synthesis, $\text{AsO}_4/(\text{SO}_4 + \text{AsO}_4) = 0.231$ (table 7.1).

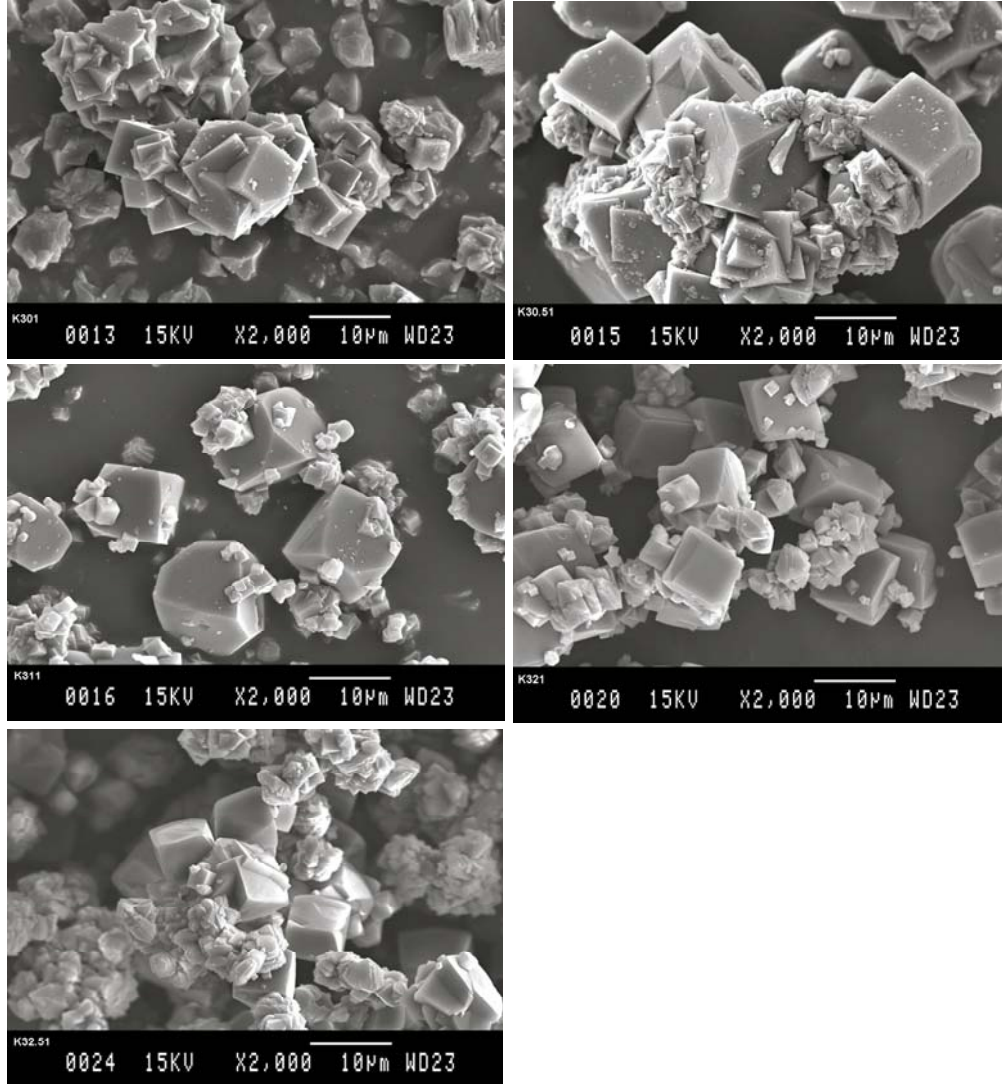


Figure 7.1: SEM images of the arsenical-alunites at different $\text{AsO}_4/(\text{SO}_4 + \text{AsO}_4)$ molar ratio.

As in arsenical-natroalunite samples, the incorporation of arsenate was analyzed through ICP and SEM-EDS spot analyses. The formula coefficients obtained are in the table 7.2. Figure 7.3 shows the comparison between arsenical-natroalunites and arsenical-alunites obtained at different $\text{AsO}_4/(\text{SO}_4 + \text{AsO}_4)$ molar ratios and their phase partition. At first glance, mansfieldite precipitated later in arsenical-alunites than in arsenical-natroalunites. Mansfieldite precipitation is consistent with an increase of the total arsenic in the bulk precipitate, and consequently with X-ray patterns and SEM images (figures 7.1 and 7.2). On the other hand, figure 7.3 also shows the arsenate incorporation in arsenical-alunites and arsenical-natroalunites. Incorporation of arsenate is represented by $(\text{AsO}_4/(\text{SO}_4 + \text{AsO}_4))_s$ molar ratio in the precipitate. As seen in the figure, in one-phase section the $(\text{AsO}_4/(\text{SO}_4 + \text{AsO}_4))_s$ molar ratio values

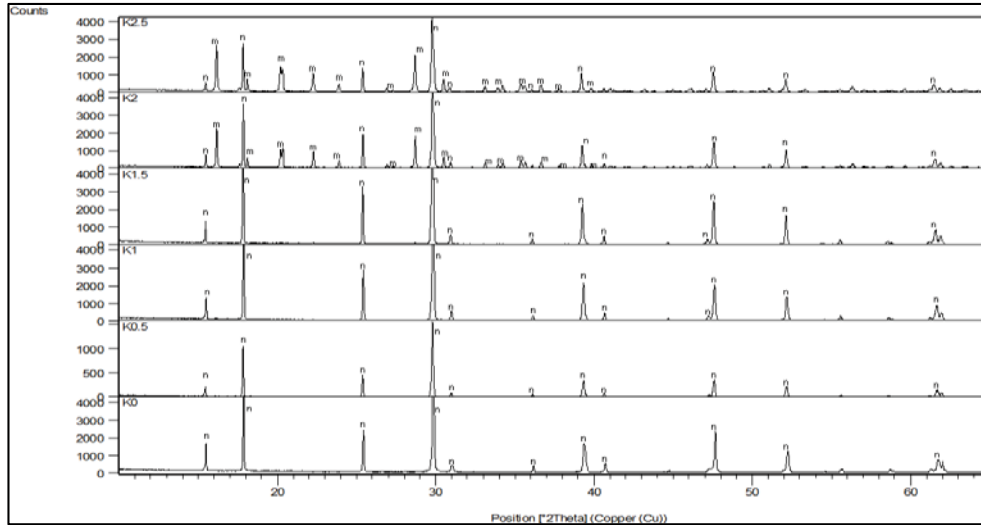


Figure 7.2: X-ray patterns obtained from arsenical-alunite precipitates at different $\text{AsO}_4/(\text{SO}_4 + \text{AsO}_4)$. n: alunite; m: mansfieldite.

obtained by ICP and obtained by SEM/EDS are coincident. However, when mansfieldite is precipitated ICP values for the bulk chemical analysis increased significantly the $(\text{AsO}_4/(\text{SO}_4 + \text{AsO}_4))_s$ molar ratio, due to the high arsenate content and the absence of sulfate in precipitated mansfieldite. Despite this, the $(\text{AsO}_4/(\text{SO}_4 + \text{AsO}_4))_s$ values obtained by SEM/EDS spot analyses increased in the same linear manner than the found in one-phase section. In both cases, As-alunite and As-natroalunite, the slope between $(\text{AsO}_4/(\text{SO}_4 + \text{AsO}_4))_s$ and $(\text{AsO}_4/(\text{SO}_4 + \text{AsO}_4))_{aq}$ is the same, ~ 0.5 . This means that the incorporation of arsenate in arsenical-natroalunite and arsenical-alunite is about 0.5 the arsenate present in the medium.

The arsenate incorporation in alunites was similar to the found in arsenical-natroalunites (table 7.2). However, before mansfieldite precipitation arsenical-alunites incorporated 0.24 moles arsenic in formula unit, while arsenical-natroalunites incorporated 0.15 moles arsenic in formula unit. Then, a higher c cell parameter did not effect in the arsenate incorporation in alunite-type phases (chapter 12).

Table 7.1: Initial conditions and final results of the arsenical-alunite experiments.

	$\text{Al}_2(\text{SO}_4)_3 \cdot 18\text{H}_2\text{O}$ (g)	K_2SO_4 (g)	As (g) as H_3AsO_4	$\text{AsO}_4/$ ($\text{SO}_4 + \text{AsO}_4$)	V (mL)	T (°C)	t (h)	pH ₀	pH _f	Wt (g)	XRD	SEM
K0	6.332	0.5519	0	0	150	200	1	3.1	0.2	2.0391	Alunite	Alunite
K0.5	6.3322	0.5518	0.2376	0.090	150	200	1	1.9	0.3	1.8571	Alunite	Alunite
K1	6.3322	0.5519	0.4752	0.167	150	200	1	1.6	0.2	2.3241	Alunite	Alunite
K1.5	6.3319	0.552	0.7128	0.23	150	200	1	1.3	0.4	1.7557	Alunite	Alunite
K2	6.3317	0.5516	0.952	0.286	150	200	1	1.3	0.4	2.2583	Alunite (65.88%) + Mansfieldite (34.12%)	Alunite + Mansfieldite
K2.5	6.3326	0.5511	1.184	0.333	150	200	1	1.2	0.2	2.1729	Alunite (51.01%) + Mansfieldite (48.99%)	Alunite + Mansfieldite

Table 7.2: Formula coefficient by ICP and EDS of arsenical-alunites

	EDS						ICP					
	K	H ₂ O	Al	S	As	OH	K	H ₂ O	Al	S	As	OH
K0	0.65	0.35	2.92	2.00	0.00	5.76	0.68	0.32	2.93	2.00	0.00	5.78
K0.5	0.63	0.37	2.93	1.88	0.12	5.68	0.66	0.34	2.98	1.91	0.09	5.84
K1	0.62	0.38	2.89	1.84	0.16	5.51	0.65	0.35	2.94	1.87	0.13	5.69
K1.5	0.63	0.37	2.92	1.76	0.24	5.53	0.63	0.37	2.93	1.78	0.22	5.56
K2	0.6	0.4	2.94	1.72	0.28	5.54						
K2.5	0.62	0.38	2.91	1.67	0.32	5.42						

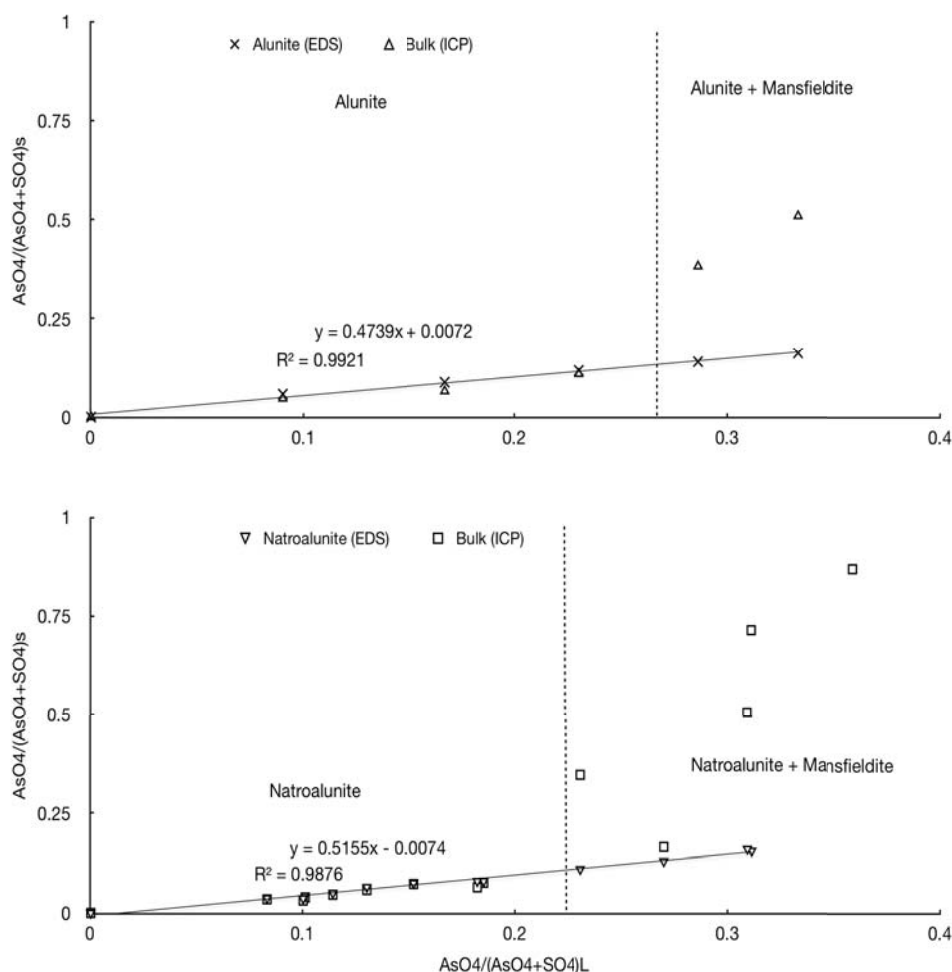


Figure 7.3: Comparison between As-natroalunite and As-alunites at different $\text{AsO}_4/(\text{SO}_4 + \text{AsO}_4)_s$ (in bulk and in the As-alunite/As-natroalunite) and $\text{AsO}_4/(\text{SO}_4 + \text{AsO}_4)_{aq}$.

7.2 Alunites synthesized at 100°C

Alunite-type phase like jarosites ($\text{KFe}_3(\text{SO}_4)_2(\text{OH})_6$) were easily synthesized at 100°C. The synthesis of this phase in presence of arsenate resulted in arsenical-jarosites with the incorporation of arsenic in the structure [Paktunc and Dutrizac, 2003]. With this background, it was decided to study the synthesis of alunite at 100°C with and without the presence of arsenic in the medium in similar conditions as previous studies of jarosites at 100°C.

The precipitation of alunites at 100°C was initially studied in a media without arsenic. At this media were studied the effect of retention time and synthesis temperature, the initial pH and, the concentration of $\text{Al}_2(\text{SO}_4)_3 \cdot 18\text{H}_2\text{O}$ and K_2SO_4 . Once determined the ideal conditions, the effect of arsenic (III) and arsenic (V) in the solution was studied.

To precipitate alunites at this temperature, supersaturated solutions of the

reagents were used. The reagents used in experiments without arsenic were $\text{Al}_2(\text{SO}_4)_3 \cdot 18\text{H}_2\text{O}$ and K_2SO_4 .

7.2.1 Effect of retention time and synthesis temperature

At low temperatures, the formation of alunite depended on the retention time and the synthesis temperature. An increase in the retention time or an increase in the temperature implied an increase in the product yield. However, these variations did not affect in precipitates chemical composition. Despite at high temperatures (200°C) the retention time did not affect the product yield, at lower temperatures alunite precipitation depended on it.

The temperature is also an important factor. At the same retention time, an increase in the temperature implied an increase in the product yield. Figure 7.4 shows the product yield obtained at different synthesis temperature. At 150°C alunite precipitation was much higher than at 100°C . Figure 7.5 is a comparison between SEM images obtained for alunites at 100°C and at 200°C . These images were taken at different conditions. The 100°C -alunites image was taken with backscattered electrons and, the 200°C -alunites image was taken with secondary electrons. Despite this differences, it is easy to compare the crystal size of both alunites, in which it can be appreciated a major alunite crystal size in the alunites synthesized at 200°C .

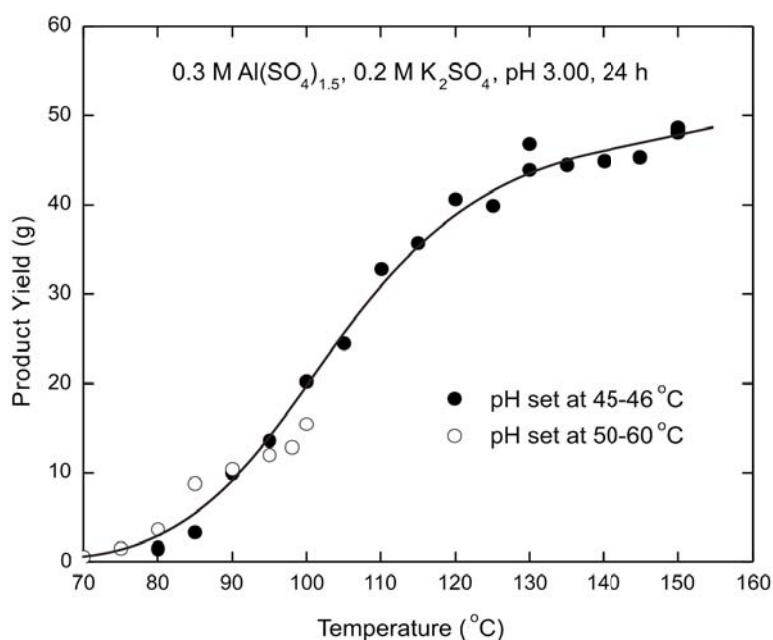


Figure 7.4: Variation of the product yield when $0.3 \text{ M Al}(\text{SO}_4)_{1.5} - 0.2 \text{ M K}_2\text{SO}_4$ solutions at pH 3.00 were reacted for 24 h at various temperatures.

7.2.2 Effect of $\text{Al}_2(\text{SO}_4)_3 \cdot 18\text{H}_2\text{O}$ and K_2SO_4 concentration

At a constant concentration of K_2SO_4 , an increasing concentration of $\text{Al}_2(\text{SO}_4)_3 \cdot 18\text{H}_2\text{O}$ increased the alunite precipitation.

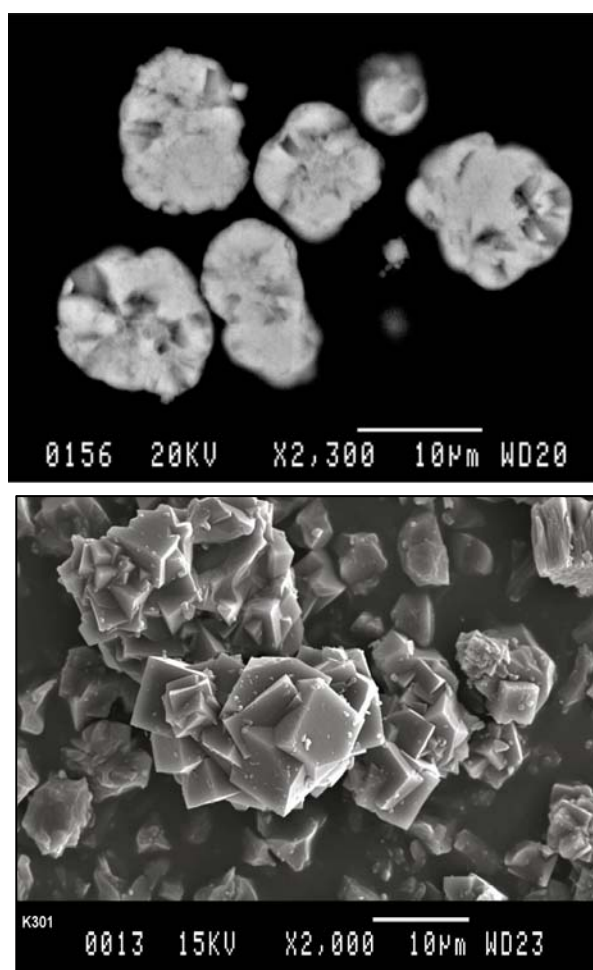


Figure 7.5: SEM images: Top) Backscattered electron image from alunite synthesized at 100°C. Bottom) Secondary electron image from alunite synthesized at 200°C.

At a constant concentration of $\text{Al}_2(\text{SO}_4)_3 \cdot 18\text{H}_2\text{O}$, when the concentration of K_2SO_4 increased, also increased the precipitation yield of alunite.

Thus, the concentration of both reagents affects the precipitation yield and are important to optimize the synthesis of alunite.

7.2.3 Effect of arsenic (III) and arsenic (V)

Arsenic (III) and arsenic (V) were added in the medium with the purpose to obtain arsenical-alunites. The experiments were performed with 0.3 M $\text{Al}(\text{SO}_4)_{1.5}$, 0.1 M K_2SO_4 and an increasing concentration of As_2O_3 or As_2O_5 .

The As_2O_3 experiments did not react and, the arsenic was not incorporated in alunite structure. Thus, the arsenic (III) cannot be incorporated in alunite. Then the oxidized form of arsenic is the only one that can be incorporated in alunite's structure, as it happened at 200°C experiments. Despite this, the presence of arsenic (III) increased the precipitation of alunite.

Otherwise, arsenic (V) was incorporated in alunite's structure and it had an important effect on the precipitation yield of the alunite. Alunite precipitation

increased with the addition of arsenic in the medium. Moreover, arsenic (V) was incorporated in the structure. The arsenic incorporation in the alunite was up to 20 %. This incorporation was reflected in the sulfate, which diminish as the arsenate increases.

TCLP (american toxicity test) was performed to two arsenical-alunites synthesized at 100°C and with an incorporation of arsenate of 8.5 % and 19.5 %. The former sample pass the toxicity test releasing 0.34 mg/L of arsenic, while the latter sample did not pass the test, releasing 7.8 mg/L of arsenic.

CHAPTER 8

HYDRONIUM-ALUNITE SYNTHESIS

Hydronium alunite, as alunite, presented a *c* cell parameter higher than natroalunite's. Thus, with the same aim as alunite, hydronium alunite was studied with the principal objective to find a phase that could incorporate more arsenic than arsenical natroalunite.

This chapter is based on the subsequent article:

- A. Sunyer, M. Currubí, J. Viñals, Arsenic immobilization as alunite-type phases: The arsenate substitution in alunite and hydronium alunite, Journal of Hazardous Materials, in review. (Annex B.1)

Hydronium-alunites were synthesized hydrothermally, in the same conditions than arsenical-alunite: at 200°C and 1-h retention time (table 8.1).

Hydronium alunites -without arsenic addition- give low precipitation yields [Rudolph et al., 2003]. Unfortunately, the addition of arsenic in the medium produces a decrease on the product yield and a fast precipitation of other phases:

- At molar ratios $\text{AsO}_4/(\text{SO}_4 + \text{AsO}_4)$ between 0.14 and 0.23 appeared an amorphous phase.
- At molar ratios $\text{AsO}_4/(\text{SO}_4 + \text{AsO}_4)$ higher than 0.23 mansfieldite precipitated.

In all cases the incorporation of arsenic in hydronium-alunite was practically null (figures 8.1, 8.2, 8.3 and table 8.2).

Thus, this phase was not suitable for arsenic precipitation due to its low product yields and the problems with the arsenic addition in the medium. The possible causes of this results are extensively discussed in chapter 12.

Table 8.1: Initial conditions and synthesis results of the hydronium-alunite experiments.

	$\text{Al}_2(\text{SO}_4)_3 \cdot 18\text{H}_2\text{O}$ (g)	As (g) as H_3AsO_4	$\text{AsO}_4/$ ($\text{SO}_4 + \text{AsO}_4$)	V (mL)	T (°C)	t (h)	pH ₀	pH _f	Wt (g)	XRD	SEM
H0	6.3329	0	0	150	200	1	3.2	1.0	0.6733	H ₃ O-alunite	H ₃ O-alunite
H0.25	6.3309	0.12	0.0413	150	200	1	0.95	0.5	0.4122	H ₃ O-alunite	H ₃ O-alunite
H0.5	6.331	0.24	0.0757	150	200	1	0.95	0.67	0.2349	H ₃ O-alunite	H ₃ O-alunite
H0.75	6.3311	0.352	0.1141	150	200	1	0.97	0.64	0.2509	H ₃ O-alunite	H ₃ O-alunite
H1	6.3300	0.472	0.1489	150	200	1	0.98	0.75	0.1455	H ₃ O-alunite	H ₃ O-alunite
H1.5	6.3301	0.712	0.1908	150	200	1	0.99	0.78	0.0339	Mansfieldite (48.13%) + H ₃ O- alunite (51.87%)	Mansfieldite + H ₃ O-alunite

Table 8.2: Formula coefficients by ICP and EDS of hydronium-alunites.

	EDS					ICP				
	H3O	Al	S	As	OH	H3O	Al	S	As	OH
H0	1	2.94	2.000	0.000	5.82	1	3.08	2.000	0.000	6.232
H0.25	1	2.91	1.989	0.011	5.73	1	2.99	1.991	0.009	5.951
H0.5	1	2.96	1.991	0.009	5.87	1	3.06	1.997	0.003	6.239
H0.75	1	2.90	1.992	0.008	5.68	1	3.08	1.998	0.002	6.173
H1	1	2.98	1.981	0.019	5.91	1	3.06	1.996	0	6.173
H1.5			Not det.					Not det.		

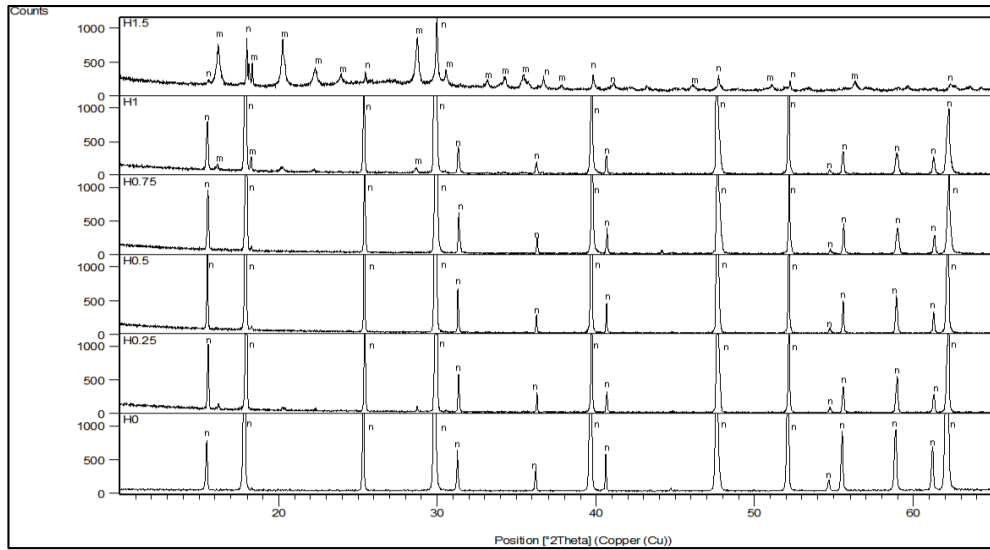


Figure 8.1: XRD from precipitates with different $\text{AsO}_4/(\text{SO}_4 + \text{AsO}_4)$ molar ratio. n: hydroniumalunite; m: mansfieldite.

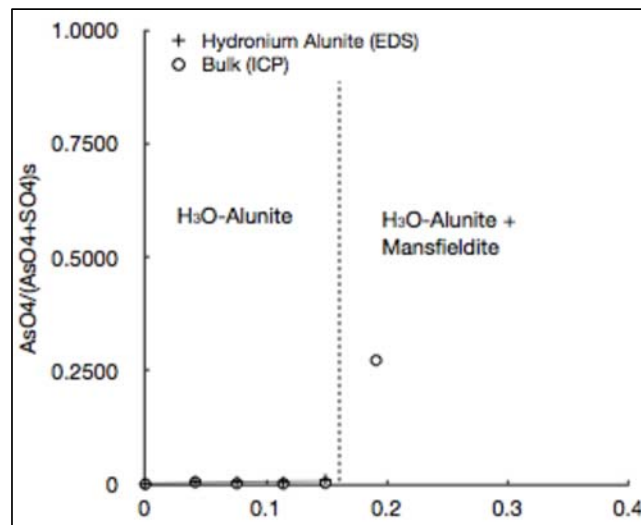


Figure 8.2: Hydronium-alunites at different $\text{AsO}_4/(\text{SO}_4 + \text{AsO}_4)_s$ (in bulk and in the hydronium-alunite) and $\text{AsO}_4/(\text{SO}_4 + \text{AsO}_4)_{aq}$.

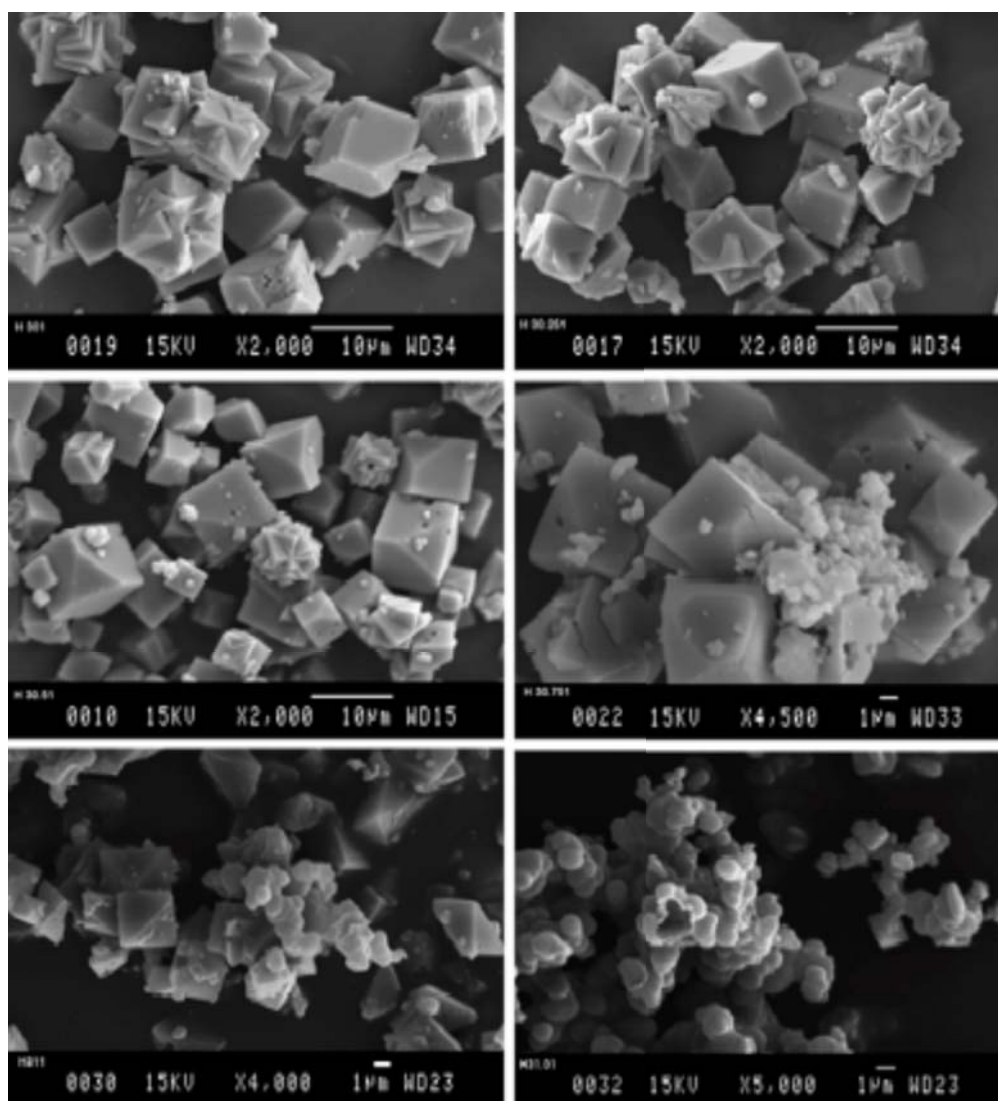


Figure 8.3: SEM images from precipitates obtained at different $\text{AsO}_4/(\text{SO}_4 + \text{AsO}_4)$ molar ratio.

CHAPTER 9

BARIUM AND LEAD ALUNITES SYNTHESIS

9.1 Barium alunite

The results in this chapter do not have been published.

Barium alunite was synthesized because it was economic (if barium sulfate was used as a reagent) and to try an increase of arsenate incorporation in the structure.

In the nature, barium-alunite is walthierite ($\text{Ba}_{0.5}\text{Al}_3(\text{SO}_4)_2(\text{OH})_6$). This phase has a c cell parameter of 34.443. The $Z=6$, double than natroalunite's ($Z=3$). Thus, to compare the c cell parameter of both phases is necessary to divide the c cell parameter of walthierite for 2. In this case, we can consider that walthierite would has a c cell parameter of 17.2215 for a $Z=3$, higher than natroalunite's.

The experiments were performed at the same conditions as hydrothermal arsenical-alunites: 200°C and 1-h retention time. Reagents used were barium sulfate, aluminum sulfate and arsenic acid (Table 9.1).

The experiments with absence of arsenic formed hydronium alunite, with no significant incorporation of barium. Thus, barite (barium sulfate) is not reactive in these conditions. On the other hand, the addition of arsenic in the medium diminish the hydronium-alunite precipitation and, the arsenate was practically not incorporated in hydronium-alunite structure, as explained in chapter 8 (figures 9.1 and 9.2, and Table 9.1).

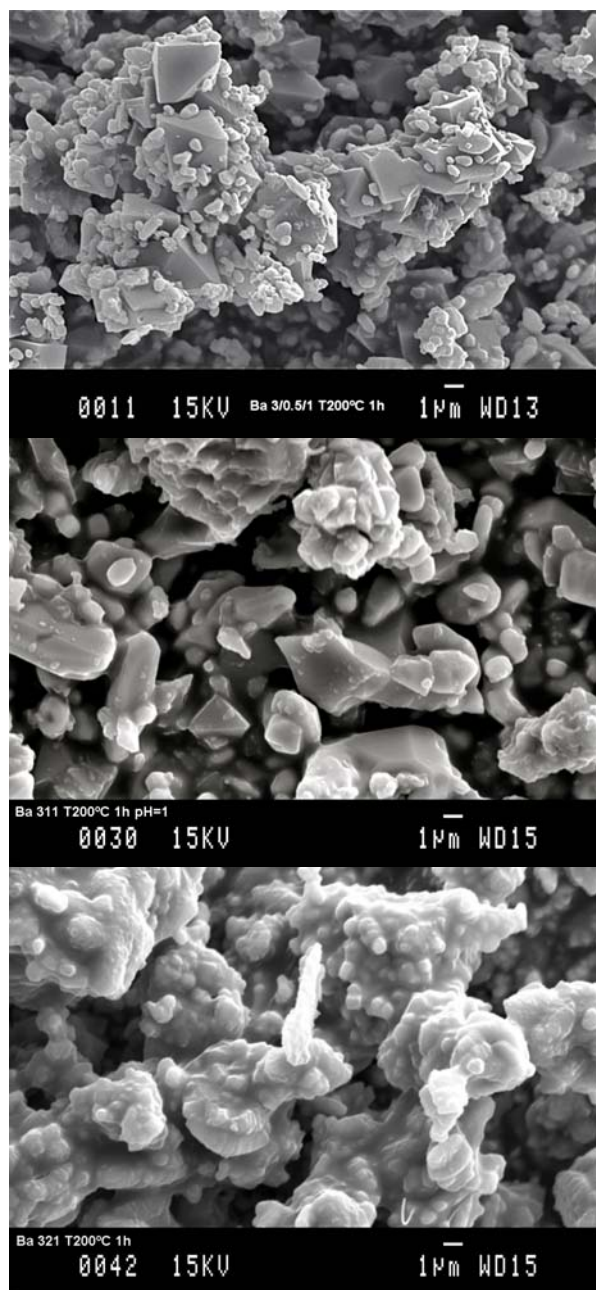


Figure 9.1: SEM images of barium-alunite experiments at different $\text{AsO}_4/(\text{SO}_4 + \text{AsO}_4)$ molar ratio.

Table 9.1: Initial condition and results of barium alunites.

	Al ₂ (SO ₄) ₃ ·18H ₂ O (g)	BaSO ₄ (g)	Ba(OH) ₂	Ca(OH) ₂	As (g) as H ₃ AsO ₄	As/(SO ₄ +AV) (mL)	T (°C)	t (h)	pH ₀	pH _f	Wt (g)	XRD	SEM	
Ba 601	6.3305	0.7406	0	0	0	0	150	200	1	3.06	1.04	2.1746	Barita + Hidroni-alunite	Barita + Hidroni-alunite
Ba 30.51	6.3314	1.4816	0	0	0.2411	0.0845	150	200	1	1.89	0.82	2.8884	Barita + Hidroni-alunite	Barita + Hidroni-alunite + mansfieldite
Ba 311	6.3311	1.4815	0	0	0.4748	0.1539	150	200	1	1.56	1.11	2.2056	Barita + Hidroni-alunite	Barita + Hidroni-alunite + mansfieldite
Ba 31.51	6.333	1.482	0	0	0.7159	0.2151	150	200	1	1.65	0.39	3.1741	Barita + Hidroni-alunite + Mansfieldite	Barita + Hidroni-alunite + Mansfieldite
Ba 321	6.3306	1.4814	0	0	0.9496	0.2667	150	200	1	1.61	0.83	3.5040	Barita +Mansfieldite	Barita +Mansfieldite
Na/Al/As/Ba 2311	6.3303	1.4818	0	0	0.4732	0.1534	150	200	1	2.92	0.46	4.1724	Barita + Hidroni-alunite	Barita + Hidroni-alunite
Ba Ca 311	6.3313	1.4819	0	1.2607	0.4748	0.1539	150	200	1	3.42	1.09	5.8005	Barita + Hidroni-alunite + Mansfieldite + Anhidrita	Barita + Hidroni-alunite + Mansfieldite + Anhidrita
Ba 311	6.3307	1.4816	0	0	0.4748	0.1539	150	240	1	1.36	0.30	3.0586	Barita + Hidroni-alunite	Barita + Hidroni-alunite
Ba 311	6.332	0	4.8720	0	0.4748	0.1889	150	200	1	2.92	0.96	6.0836	Barita + Hidroni-alunite + Mansfieldite	Barita + Hidroni-alunite + Mansfieldite

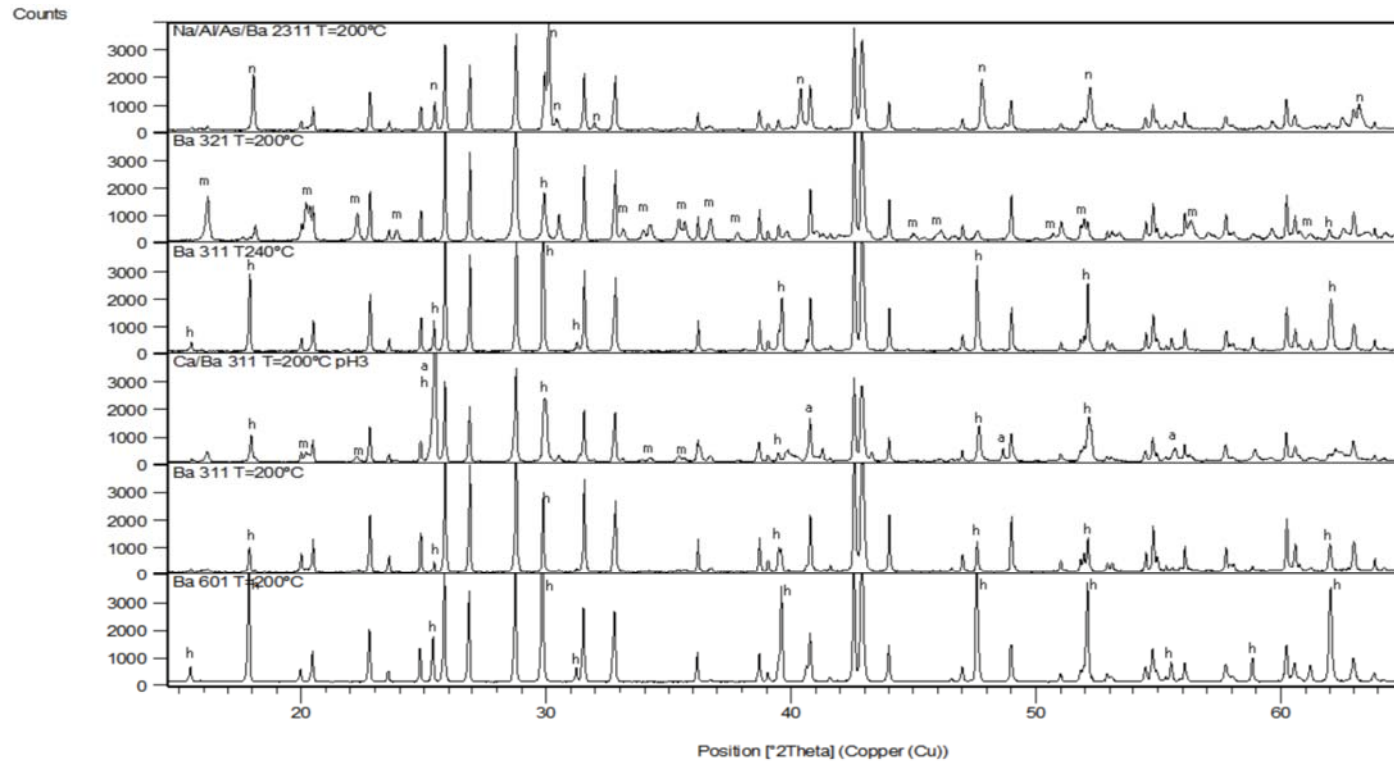


Figure 9.2: XRD from different barium-alunite experiments. n: natroalunite; h: hydronium-alunite; m: mansfieldite; a: anhydrite.

9.2 Lead alunites

Lead alunites were synthesized with the objective to get a coinertization lead-arsenic. Reagents used were lead sulfate (anglesite), aluminum sulfate and arsenic acid. Anglesite was used because it is present in some pyrometallurgical copper waste, for example the converter dust. Lead alunites are found in nature as arsenate bearing phases. e.g. hidalgoite $(\text{PbAl}_3(\text{AsO}_4)(\text{SO}_4)(\text{OH})_6)$, which contained sulfate and arsenate. This high arsenate content in this mineral is of interest because it can permit a high arsenate precipitation. Frost et al. (2011) affirmed that beudentite $(\text{PbFe}_3(\text{AsO}_4, \text{SO}_4)(\text{OH})_6)$, an analogous phase of hidalgoite, can be synthesized with the right quantities of Pb, Al, AsO_4 and SO_4 as indicated in Eq. 9.1.



Reagents used for the lead alunite synthesis were lead sulfate, aluminum sulfate and arsenic acid. Experiments were performed at different initial conditions (table 9.2) with the subsequent results (figures 9.3 and 9.4):

- Temperature: 200°C; retention time: 1 h: The insolubility of lead sulfate did not permit the formation of lead alunites. Instead, hydronium-alunites were formed. In case of arsenic addition in the medium, the phases formed were hydronium-alunite and mansfieldite.
- An increase in the retention time up to 2 h: Did not change the results obtained with 1-h retention time. Hydronium-alunite was formed again.
- An increase in the synthesis temperature and pressure to 240°C and 35 bar gave the same results as the obtained at 200°C: without arsenic hydronium-alunite was formed; with arsenic addition hydronium-alunite + mansfieldite were formed.
- Sodium added as $\text{Na}_2\text{HAsO}_4 \cdot 7\text{H}_2\text{O}$ drove to the formation of arsenical-natroalunite. But lead-alunite was not formed.

Changes with the retention time and the synthesis temperature did not affect the final results. This experiments show the impossibility of lead-alunite synthesis with lead sulfate as a reagent due to its insolubility.

Table 9.2: Initial conditions and results of lead-alunite experiments.

	$\text{Al}_2(\text{SO}_4)_3 \cdot 18\text{H}_2\text{O}$ (g)	PbSO_4 (g)	As (g) as H_3AsO_4	$\text{AsO}_4/(\text{SO}_4+\text{AsO}_4)$	V (mL)	T (°C)	t (h)	pH ₀	pH _f	Wt (g)	XRD	SEM
Pb 601	6.3323	0.9606	0	0	150	200	1	2.98	1.43	3.1731	Sulfat de plom + Hidroni-alunite	Sulfat de plom + Hidroni-alunite
Pb 311	6.3318	1.9218	0.4748	0.1539	150	200	1	1.99	1.15	3.9838	Sulfat de plom + Hidroni-alunite + Mansfieldita	Sulfat de plom + Hidroni-alunite + Mansfieldita
Na/Al/As/Pb 2311	6.331	1.9228	0.4749	0.1539	150	200	1	2.88	0.7	4.3998	Sulfat de plom + Natroalunite	Sulfat de plom + Natroalunite
Pb 601	6.3341	0.9611	0	0	150	240	1	3.02	1.08	1.9928	Sulfat de plom + Hidroni-alunite	Sulfat de plom + Hidroni-alunite
Pb 601	6.3333	0.9619	0	0	150	200	2	3.06	1.33	2.0719	Sulfat de plom + Hidroni-alunite	Sulfat de plom + Hidroni-alunite
Pb 311	6.3324	1.9216	0.4748	0.1539	150	240	1	1.68	0.93	3.2714	Sulfat de plom + Hidroni-alunite + Mansfieldita	Sulfat de plom + Hidroni-alunite + Mansfieldita
Pb 311	6.3312	1.9215	0.4748	0.1539	150	200	1	0.89	0.79	2.5164	Sulfat de plom + Hidroni-alunite + Mansfieldita	Sulfat de plom + Hidroni-alunite + Mansfieldita

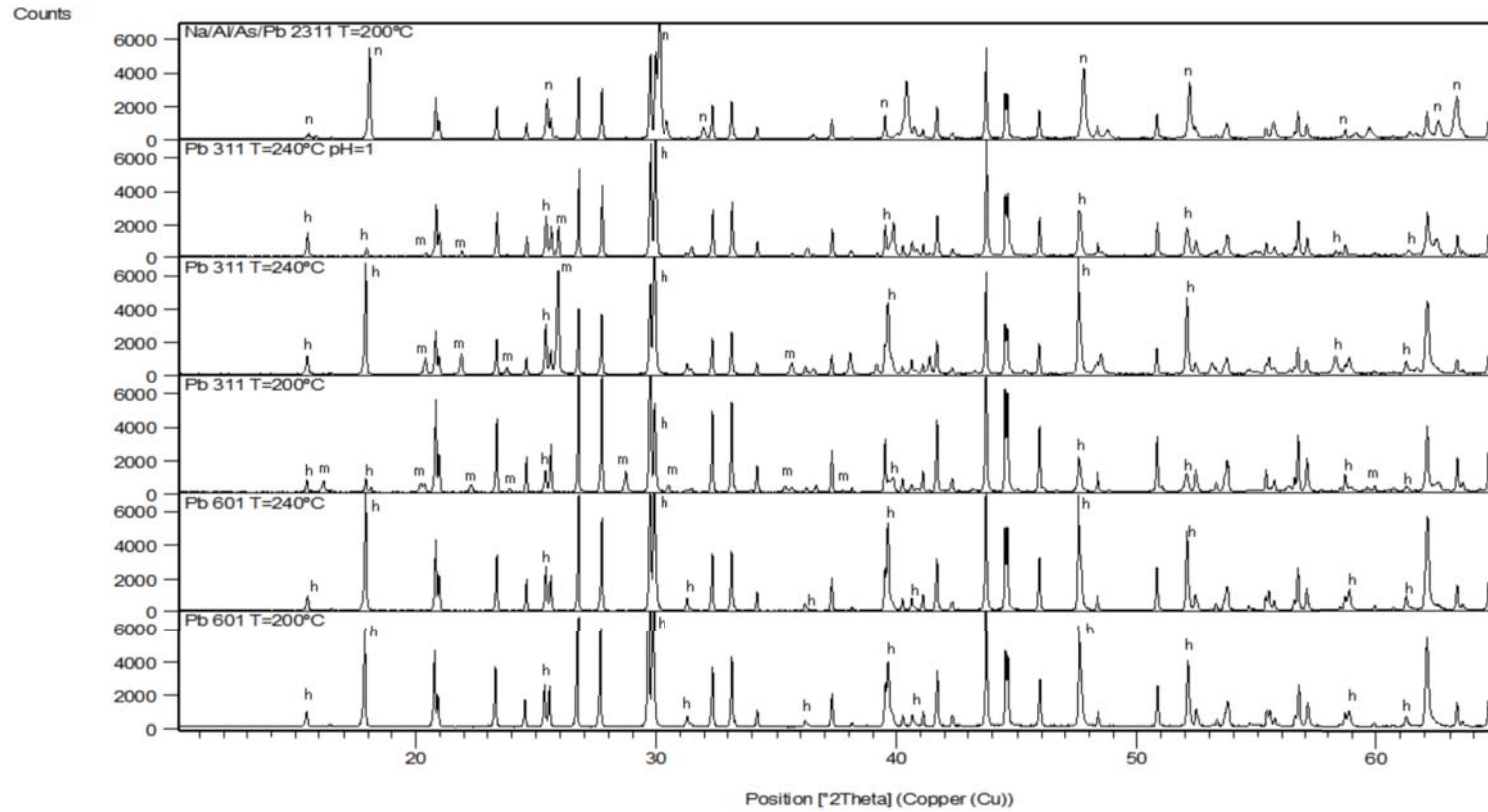


Figure 9.3: XRD from lead-alunite experiments. n: natroalunite; h: hydronium-alunite; m: mansfieldite.

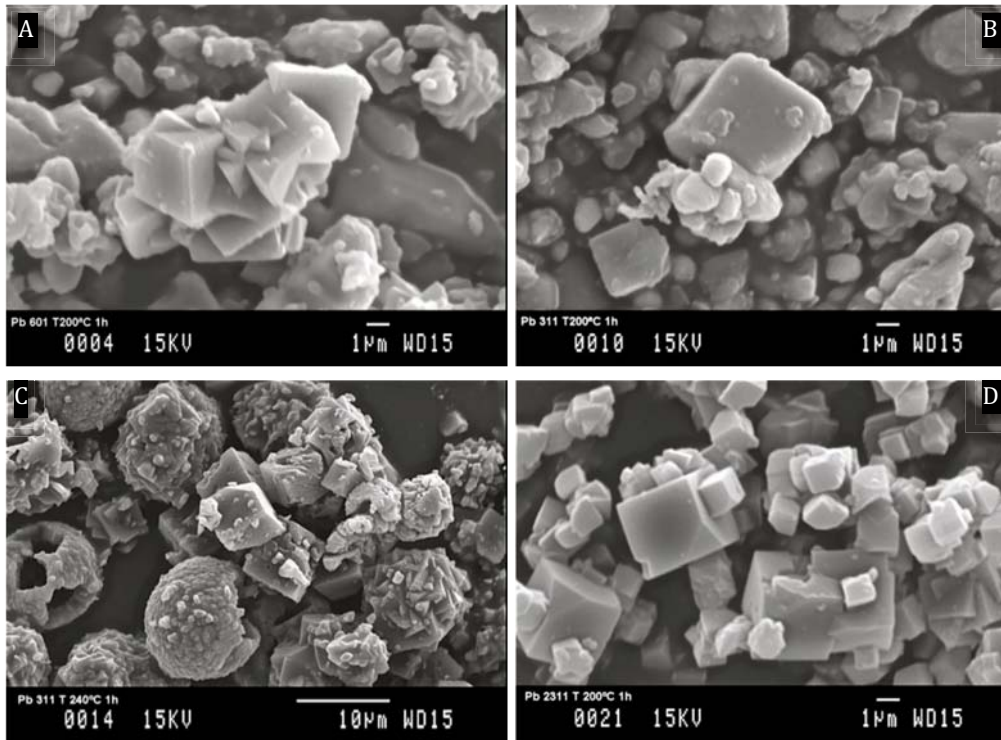


Figure 9.4: SEM image of lead-alunite experiments at different $\text{AsO}_4/(\text{SO}_4 + \text{AsO}_4)$ molar ratio and initial conditions. A) 200°C , 1 h, $\text{AsO}_4/(\text{SO}_4 + \text{AsO}_4) = 0$; B) 200°C , 1 h, $\text{AsO}_4/(\text{SO}_4 + \text{AsO}_4) = 0.15$; C) 240°C , 1 h, $\text{AsO}_4/(\text{SO}_4 + \text{AsO}_4) = 0.15$; D) 200°C , 1 h, $\text{AsO}_4/(\text{SO}_4 + \text{AsO}_4) = 0.15$ with Na.

CHAPTER 10

AS-NATROALUNITES GENERATED FROM INDUSTRIAL WASTES

This chapter is based on the subsequent articles:

- J. Viñals, A. Sunyer, E. Torres, V. Beltran, N. Llorca, 2010, Arsenic Inertization from Copper Pyrometallurgy through Phases of the Alunite Supergroup, In: Harre, J., (Ed), Copper 2010, GDMB, Clausthal-zellerfeld, Germany, 5, 2071-2086. ISBN 978-3-940276-29-2. (Annex A.5)
- J. Viñals, A. Sunyer, E. Torres, 2010, Arsenic Inertization from Copper Pyrometallurgy through Phases of the Alunite Supergroup, *Erzmetall*, 63, 6, 5-13. (Annex A.6)
- J. Viñals, A. Sunyer, P. Molera, M. Cruells, N. Llorca, 2010, Arsenic stabilization of calcium arsenate waste by hydrothermal precipitation of arsenical natroalunite, *Hydrometallurgy*, 104, 247- 259. (Annex A.7)
- J. Viñals, M. Cruells, A. Sunyer, L. Garcia, V. Beltrán, 2009, Arsenic Stabilization by Hydrothermal Synthesis of Alunite-type Phases. Application to the Copper Metallurgy. Proceedings of the HydroCopper 2009. P. 37-46. E. Domic & J. Casas Eds. Gecamin Ltd. Santiago, Chile. ISBN 978-956-8504-21-2. (Annex A.8)

Arsenic inertization from pyrometallurgical copper wastes was studied through two different wastes: calcium arsenate waste and flash smelting dust. The former was the calcium precipitate from the final effluent of the electrolytic section, while the latter was the dust from a flash smelter. In both wastes, the followed steps were the same:

1. Recovery of value metals.
2. Precipitation of arsenic through arsenical-natroalunite synthesis (figure 10.1).

In industrial wastes that contain value metals, its recovery is important. In some cases, recovery of value metals is more important than the arsenic inertization. For example, dust from an electric furnace from the copper pyrometallurgy,

which was rich in Zn, the recovery of the metals was more important than the arsenic inertization, because this last process would be the same as in calcic arsenate effluent from the plant [Rios et al., 2012 (Annex C.2) and Morales et al., 2011 (Annex C.1)].

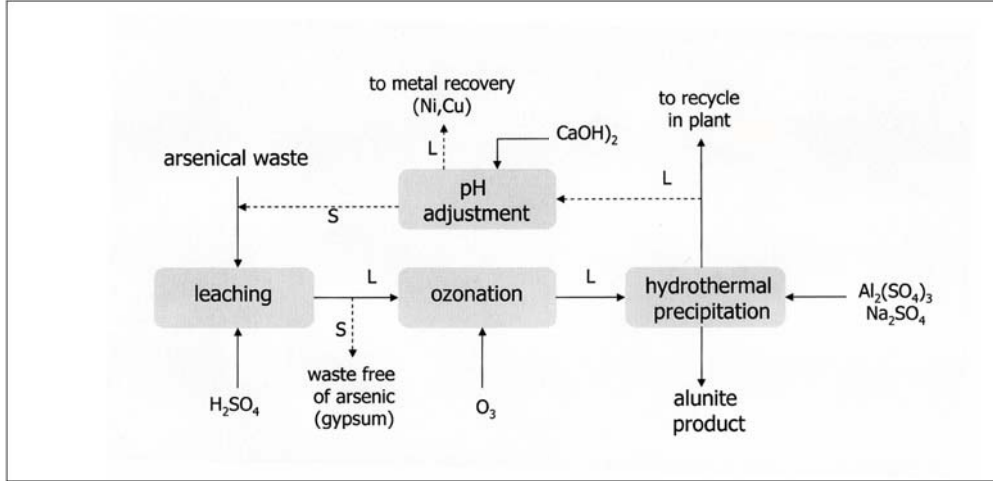


Figure 10.1: Waste treatment scheme.

The studied wastes had the composition show at table 10.1. Calcium arsenate waste (figure 10.2) contained little amounts of copper, and its main components were calcium (22.80 %), sulfur (11.37 %) and arsenic (5.23 %). Otherwise, flash smelting dust had substantial differences with the composition. In this waste, the main elements were copper (30.50 %) and iron (12.60 %), meanwhile arsenic was only 1.93 % .

Table 10.1: Composition of wastes.

	Calcium arsenate	Flash smelting dust	Intermediate ferric arsenate
As (%)	5.23	1.93	13.8
Ca (%)	22.80	0.24	0.07
Fe (%)	1.08	12.60	26.6
S (%)	11.37	6.50	2.30
Cu (%)	0.56	30.5	6.80
Zn (%)	0.95	3.66	0.04
Ni (%)	2.65	-	-
Mo (%)	-	0.18	1.80
Pb (%)	0.04	0.43	0.12
Bi (%)	0.02	0.13	-
SiO ₂ (%)	0.86	2.78	-

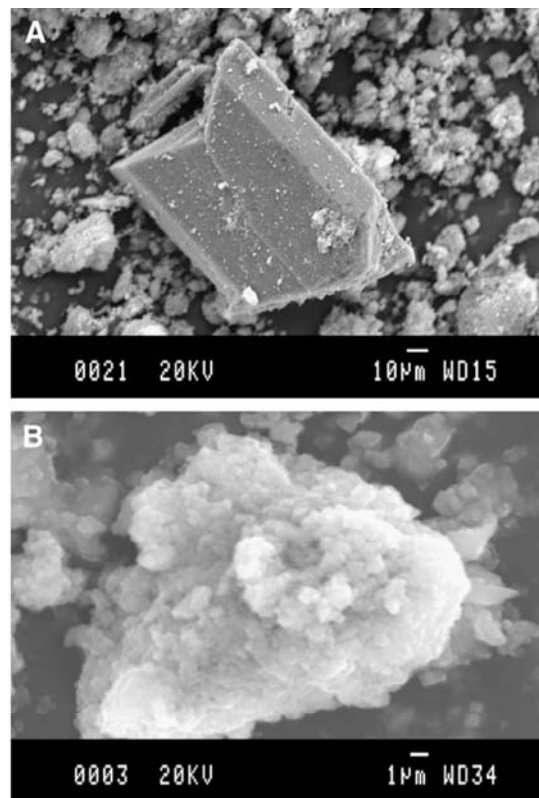


Figure 10.2: SEM images from calcium arsenate. A) gypsum crystal; B) amorphous calcium arsenate precipitate.

10.1 Calcium arsenate

Calcium arsenate was lixiviated with sulfuric acid to obtain the maximum dissolution of arsenic. At pH 1 the arsenic extraction was total, as well as iron, nickel, copper and zinc extractions (table 10.2). After this treatment, the liquid was ozonated to oxidize arsenic (III) to arsenic (V). This process was followed through the ORP.

Hydrothermal experiments were performed at 200°C and 2-h retention time. These experiments were done with the same quantity of waste, but the aluminum sulfate was modified. Previous lixiviation of waste with concentrate sulfuric acid, which produced an excess of sulfate in the medium, did not permit to evaluate the arsenic effect with the $\text{AsO}_4/(\text{SO}_4 + \text{AsO}_4)$ molar ratio. Thus, the effect of arsenic was evaluated through the Al/As molar ratio. At table 10.3 initial conditions and final pHs, as well as the obtained phases are shown.

As observed in figure 10.3, at pH₀ 2 was mainly formed an amorphous phase and mansfieldite. While at pH₀ 1 no amorphous phase was formed, instead arsenical-natroalunite and mansfieldite were formed (table 10.3 and figure 10.4). The formation of such phases depended on the Al/As molar ratio. This, at Al/As = 1.5, mansfieldite was practically the only phase precipitated, while at Al/As = 4.5 the only precipitated phase was arsenical-natroalunite. Arsenical-natroalunite formation increased as the initial aluminum sulfate increased in the medium.

Table 10.2: Composition and lixiviation of the calcium arsenate.

Composition (weight %)										
Ca	S	As	Ni	Fe	Zn	Cu	Cd	Pb	Bi	SiO ₂
22.80	11.37	5.23	2.65	1.08	0.95	0.56	0.17	0.04	0.02	0.86
pH		Solubility (mg/L)								
		As	Ni	Zn	Cu	Cd	Fe			
9 (as received)		34	<0.10	<0.10	0.12	0.14	<0.10			
7		150	3.5	<0.10	0.10	0.31	<0.10			
H ₂ SO ₄ leaching pH		Extraction (%)								
		As	Ni	Zn	Cu	Cd	Fe			
4		69	62	85	31	74	<1			
3		72	78	95	59	89	4			
2		75	94	99	87	96	10			
1.5		96	97	99	95	95	73			
1		99	99	99	99	>99	>99			

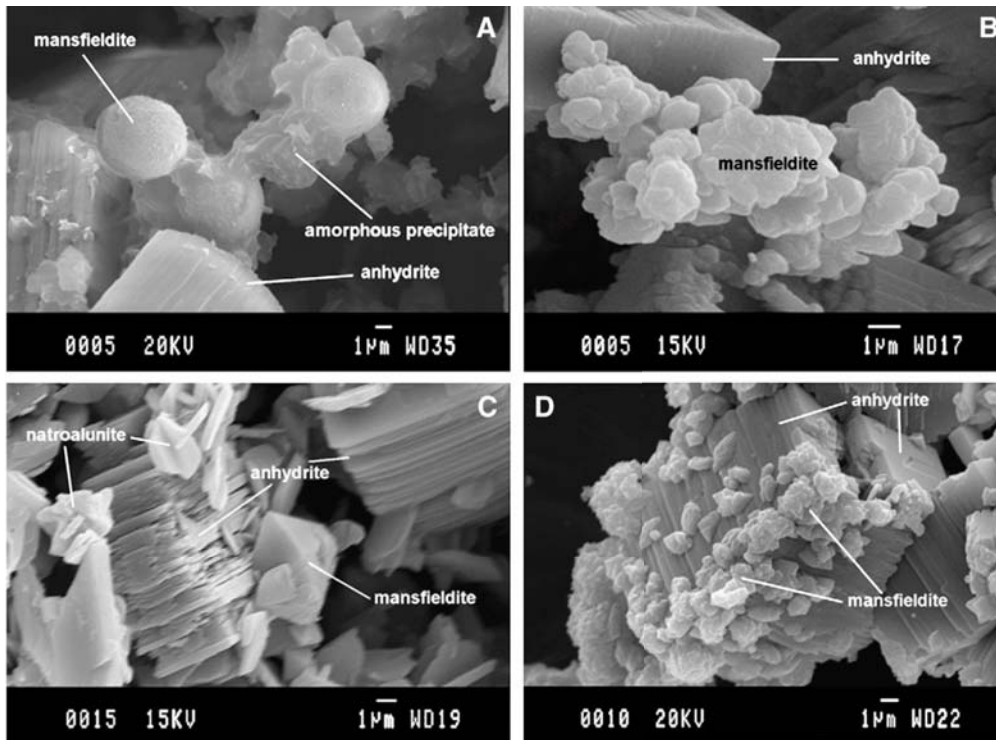


Figure 10.3: SEM image from hydrothermal treatment of calcium arsenate waste (2-h retention time). A) 200°C, $(Al/As)_{aq}=1.5$, pH_0 2; B) 200°C, $((Al/As)_{aq}=1.5$, pH_0 1; C) 200°C, $(Al/As)_{aq}=3$, pH_0 1; D) 180°C, $(Al/As)_{aq}=3$, pH_0 1.

Formula coefficients found for arsenical-natroalunites and mansfieldites are in table 10.4. Major arsenate incorporation is at low Al/As molar ratio. At $Al/As = 2.25$ arsenate in formula is 0.28, while at $Al/As = 4.5$ arsenate incorporation is 0.14 in formula. In both phases iron was incorporated in the

structure, in which substituted part of the aluminum. This substitution was minor in arsenical-natroalunite than in mansfieldite. In the latter, iron substitution was up to 0.31 in formula at $Al/As = 1.5$, this value decreased as arsenical-natroalunite formation increased. Phosphorus was also incorporated in arsenical-natroalunite structure in TO_4 site. Phosphate substituted little amounts of sulfate in arsenical-natroalunite, and its maximum incorporation was 0.04 in formula. Mansfieldite also incorporated phosphorous in the structure, in this case as a substitution of arsenate. As in arsenical-natroalunites, the phosphorous substitution was very little, up to 0.05 moles per formula.

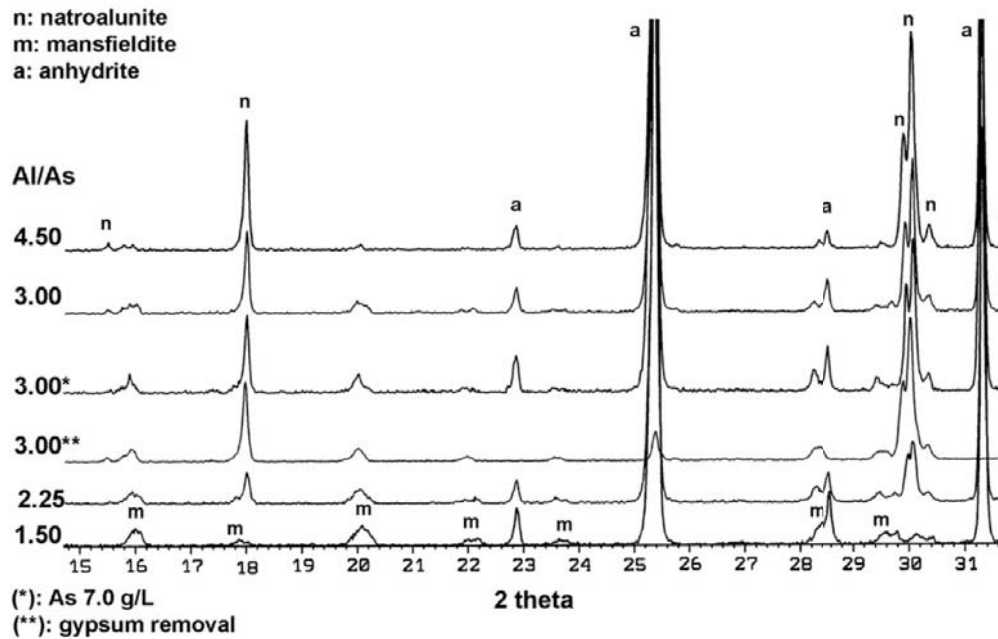


Figure 10.4: XRD from the hydrothermal precipitates obtained from calcium arsenate waste at different $(Al/As)_{aq}$ molar ratio, $200^{\circ}C$ and pH_0 1.

Gypsum initially present in the waste in hydrothermal conditions precipitated as anhydrite (figure 10.5), except a little part of Ca that was incorporated in arsenical-natroalunite (0.04-0.08 in formula) (table 10.4). A previous separation of gypsum before the hydrothermal experiment did not have any significant effect in formed phases ratio, except for the absence of anhydrite in the final precipitate.

As in synthetic arsenical-natroalunite experiments, the reaction is fast, less than 15 min are needed for the formation of arsenical-natroalunite. At this retention time, the composition is similar to the found in higher retention times. The effect of the synthesis temperature was significant. Thus, in temperatures lower than $200^{\circ}C$ was formed more mansfieldite than arsenical-natroalunite at the same $(Al/As)_{aq}$ molar ratio (tables 10.3 and 10.4).

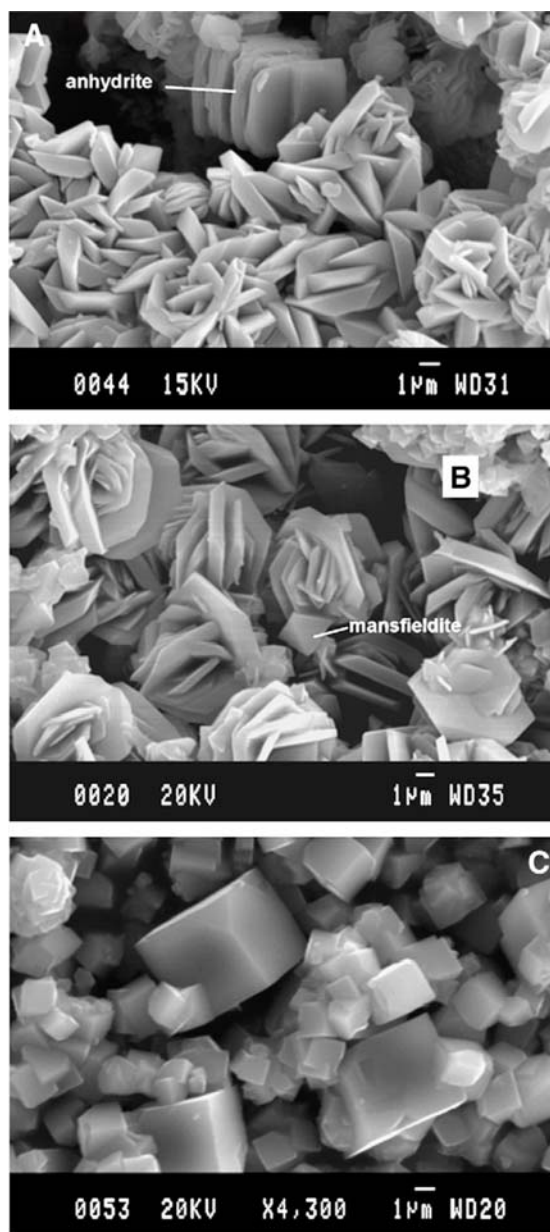


Figure 10.5: Arsenical-natroalunite. A) From calcium arsenate with gypsum presence; B) From calcium arsenate in absence of gypsum; C) Synthesized from pure reagents.

Table 10.3: Initial conditions, bulk compositions and phases compositions.

(Al/As) _{aq}	Temp (°C)	Time (min)	pH _i	pH _f	Bulk composition (weight %)										Phase composition (%)		
					S	As	Al	Fe	Ca	Na	Cd	Ni	Zn	Cu	n	m	a
1.50	200	120	2.0	1.6	19.0	3.77	2.66	1.34	22.5	0.26	0.15	0.22	0.18	0.24	-	~23*	~77
1.50	200	120	1.0	0.8	20.0	3.34	0.88	1.12	24.5	0.07	0.13	0.006	0.03	0.06	~1	~10	~85
2.25	200	120	1.0	0.7	19.2	3.41	2.64	1.23	21.6	0.65	0.13	0.01	0.03	0.02	~8	~12	~75
3.00	180	15	1.0	0.9	20.5	2.60	3.73	1.01	22.8	1.00	0.13	0.03	0.03	0.05	~18	~5	~77
3.00	180	30	1.0	0.8	20.4	3.05	3.85	1.05	21.7	1.09	0.12	0.05	0.04	0.04	~19	~6	~75
3.00	180	120	1.0	0.8	19.7	3.60	3.83	1.05	21.8	0.96	0.12	0.06	0.03	0.04	~17	~8	~75
3.00	200	15	1.0	0.7	21.0	2.41	4.04	1.10	22.1	1.10	0.13	0.008	0.02	0.02	~20	~5	~75
3.00	200	30	1.0	0.7	20.4	2.50	4.01	1.15	21.6	1.05	0.12	0.01	0.02	0.04	~20	~5	~75
3.00	200	120	1.0	0.7	19.7	2.67	4.20	1.16	20.6	1.15	0.12	0.008	0.02	0.04	~20	~5	~70
3.00**	200	120	1.0	0.5	19.3	2.45	3.69	1.07	22.4	1.11	0.12	0.009	0.03	0.03	~19	~5	~75
3.00***	200	120	1.0	0.5	11.5	9.85	16.2	4.22	0.13	4.49	0.004	0.008	0.02	0.04	~80	~20	-
4.50	200	120	1.0	0.7	19.4	1.10	5.98	0.94	18.4	1.60	0.09	<0.001	0.008	0.05	~30	~2	~65

* : mansfieldite + amorphous phase.

** : As concentration (7.0 g/L) double than in the rest of experiments.

*** : with prior gypsum removal.

Table 10.4: Formula coefficients from precipitated arsenical-natroalunite and mansfieldite.

(Al/As) _{aq}	Temp (°C)	Time (min)	Natroalunite (based on S + As + P = 2)							Mansfieldite (based on As + P = 1)			
			As	S	P	Al	Fe	Na	Ca	As	P	Al	Fe
1.50	200	120	Not determined (trace)							0.95	0.05	0.69	0.31
2.25	200	120	0.28	1.68	0.04	2.70	0.08	0.90	0.04	0.99	0.01	0.76	0.24
3.00	180	15	0.26	1.70	0.04	2.78	0.10	0.94	0.07	Not determined (small grains)			
3.00	180	30	0.28	1.68	0.04	2.70	0.08	0.98	0.08	Not determined (small grains)			
3.00	180	120	0.28	1.70	0.02	2.74	0.08	0.98	0.07	Not determined (small grains)			
3.00	200	15	0.28	1.70	0.02	2.67	0.12	0.98	0.08	Not determined (small grains)			
3.00	200	30	0.24	1.72	0.04	2.63	0.09	0.96	0.07	Not determined (small grains)			
3.00	200	120	0.22	1.76	0.02	2.69	0.12	0.96	0.08	0.97	0.03	0.78	0.28
3.00*	200	120	0.22	1.74	0.04	2.65	0.09	1.00	0.08	0.98	0.02	0.66	0.34
3.00**	200	120	0.20	1.80	0.00	2.82	0.15	1.00	0.00	0.96	0.04	0.76	0.24
4.50	200	120	0.14	1.84	0.02	2.70	0.12	0.98	0.08	Not determined (trace)			

* As concentration (7.0 g/L) double that in the rest of experiments.

** With prior gypsum removal.

Arsenic precipitation in one step was up to 20% when only arsenical-natroalunite was precipitated. However, an important precipitation of about 40 % can be achieved with approximately a 5 % of mansfieldite precipitation (figure 10.6).

Elements such as nickel, zinc and copper did not precipitate significantly. That will permit a post-recuperation of these value metals. Otherwise, cadmium precipitated with anhydrite, in which partially substituted calcium in the structure. This cadmium incorporation in anhydrite can become a serious environmental problem, due to the easy dissolution of this phase in water and the high cadmium toxicity (figure 10.7). The easiest solution to this problem is the previous separation of gypsum after the metals lixiviation at pH 1 and before the hydrothermal treatment.

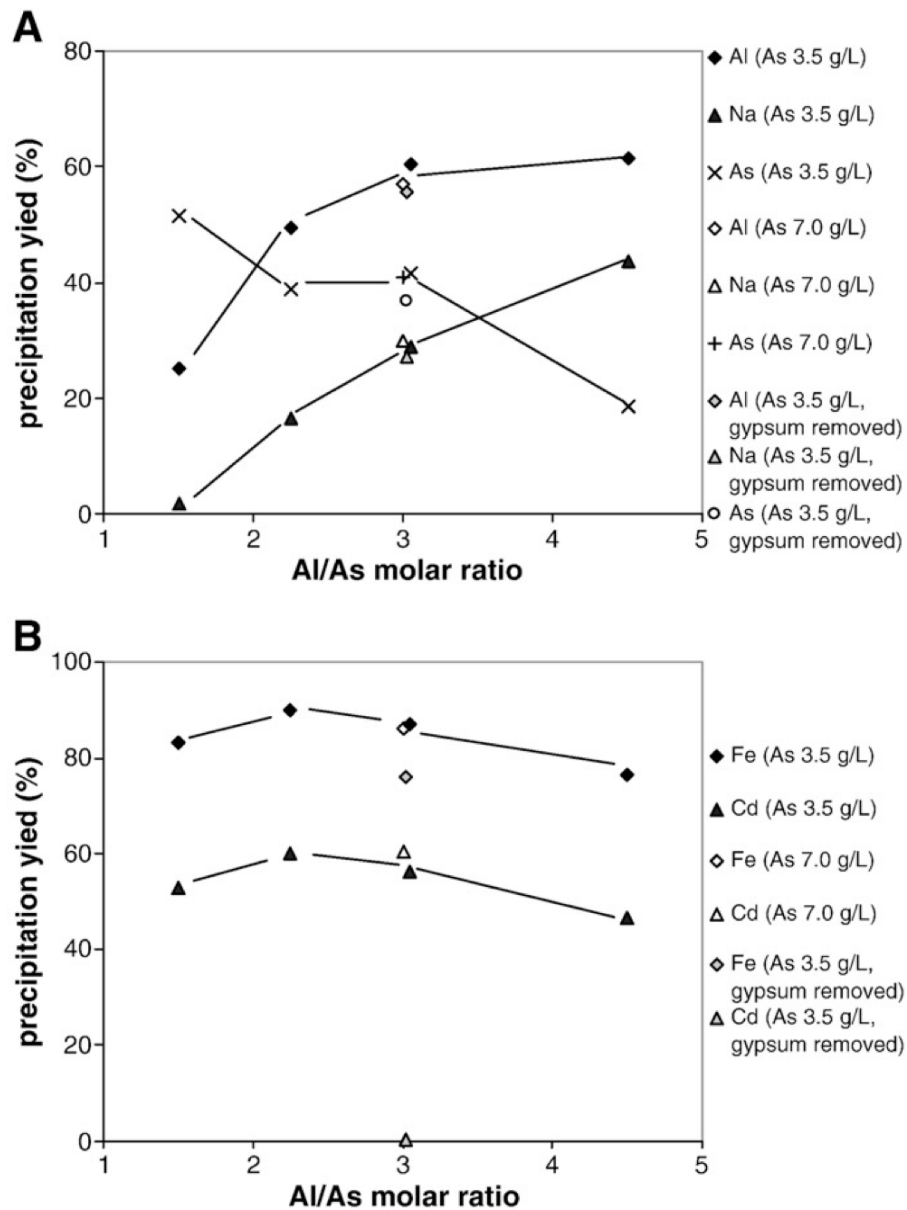


Figure 10.6: Effect of $(Al/As)_{aq}$ molar ratio in the precipitation of the elements presents in the calcium arsenate waste at 200°C and 2-h retention time.

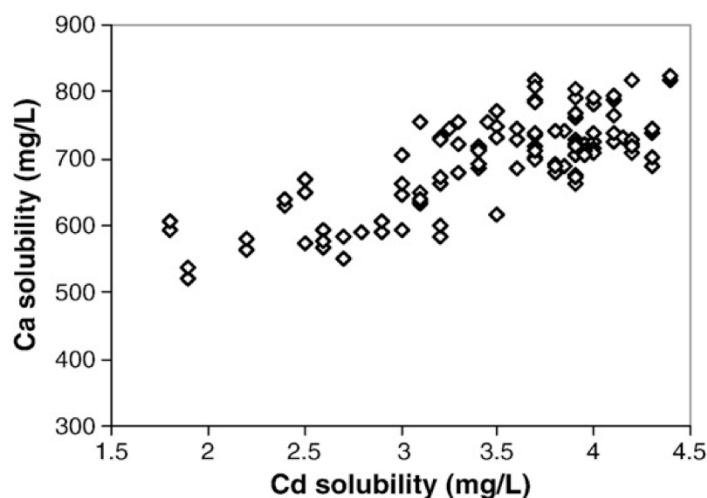


Figure 10.7: Correlation with cadmium dissolution and hydrothermal calcium of hydrothermal precipitates which contained anhydrite. These results correspond to the solubilities between pH 1 to 10 in three consecutive tests.

10.2 Flash smelting dust

XRD and SEM-EDS analyses performed on the flash smelting dust give soluble copper phases as tenorite and delafossite (figure 10.8). Then, the most important consideration was the recovery of this high copper content. This recovery was done with the addition of concentrate sulfuric acid up to pH 1 and a temperature of 80°C. This work temperature and pH permitted the dissolution of tenorite and delafossite, and so, the post-recovery of copper.

Once the dust was lixiviated, it was ozonated to be sure to have the iron and the arsenic in their oxidized forms. The high content of iron present in the dust permitted its co-precipitation with arsenic only with the basification of the medium with the addition of NaOH up to pH 3.5-4. This co-precipitation results in a ferric-arsenate intermediate (table 10.1), which can be used as a previous step before arsenical-natroalunite precipitation.

10.3 Ferric-arsenate intermediate

This intermediate was used for arsenical-natroalunite synthesis (figure 10.9). It was treated as the synthesis of arsenical-natroalunite from calcium arsenate waste, 200°C, pH 1 and 2-h retention time. But the Al/As molar ratio used was between 4.5 and 9. As the quantity of iron in the medium was really important, the formed arsenical-natroalunite was rich in iron. At lower Al/As molar ratio (4.5 and 6) were detected scorodite traces (figures 10.10 and 10.11).

As in calcium arsenate waste, copper did not precipitate during the arsenical-natroalunite synthesis. However, molybdenum precipitated. Arsenic incorporation in arsenical-natroalunite structure was similar in both wastes and, in ferric-arsenate intermediate it was up to 0.07 moles arsenic in formula unit.

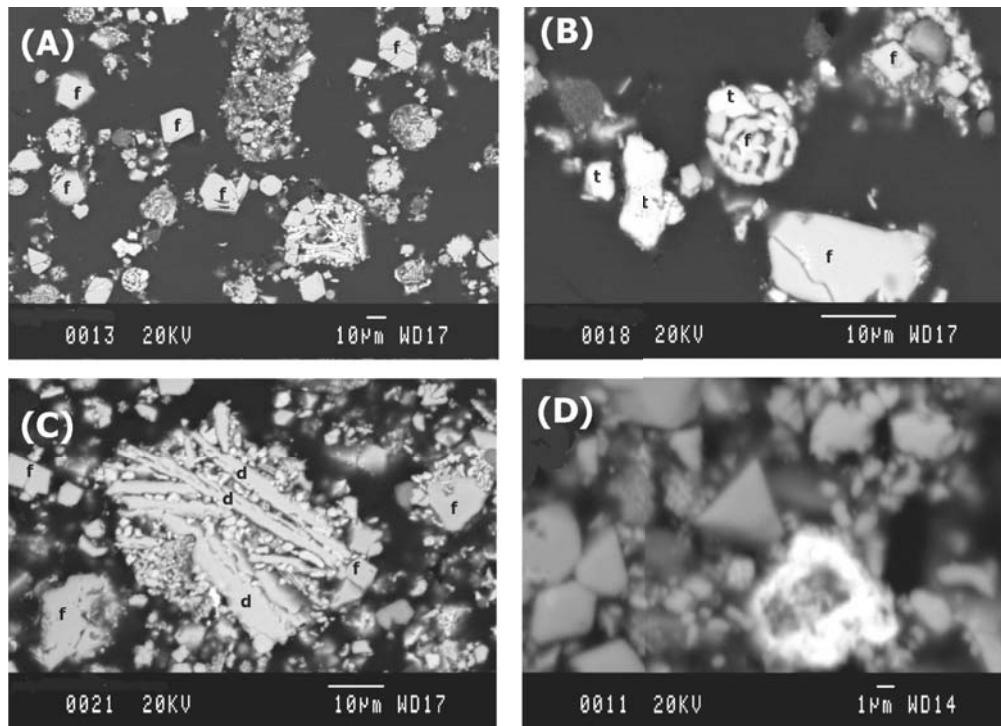


Figure 10.8: SEM image from the phases found in flash smelting dust (section 10.2). A) General view (f: ferrite); B) Tenorite particles; C) Delafossite particles; D) Arsenic-lead-sulfate aggregate (white).

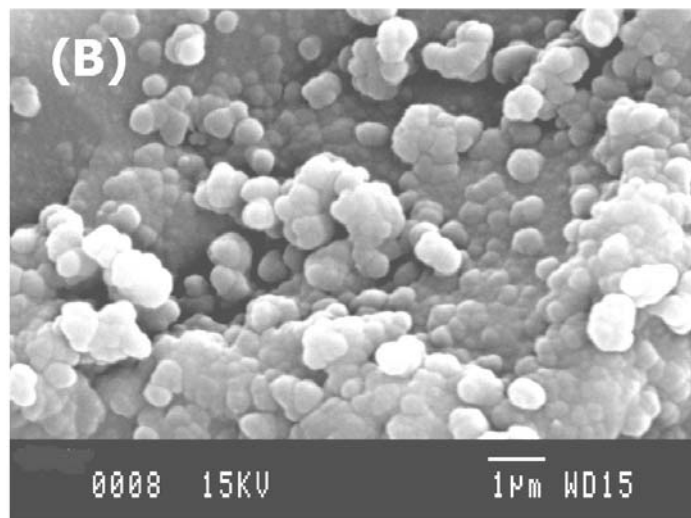


Figure 10.9: SEM image from ferric-arsenate intermediate.

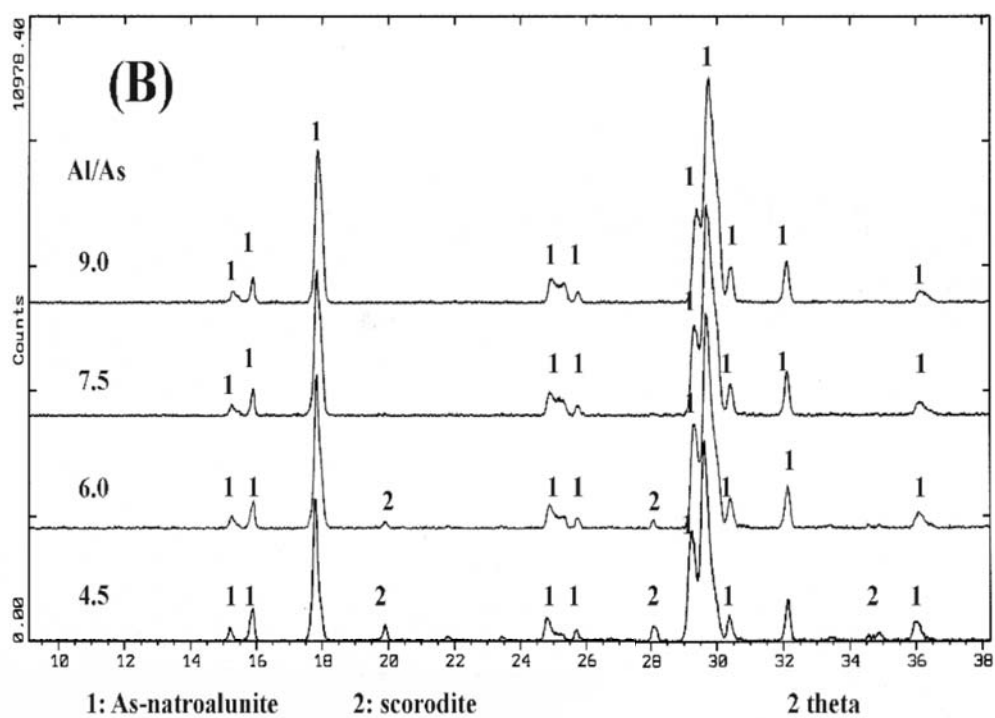


Figure 10.10: XRD from hydrothermal precipitates from ferric-arsenate intermediate at different $(\text{Al/As})_{aq}$ molar ratio.

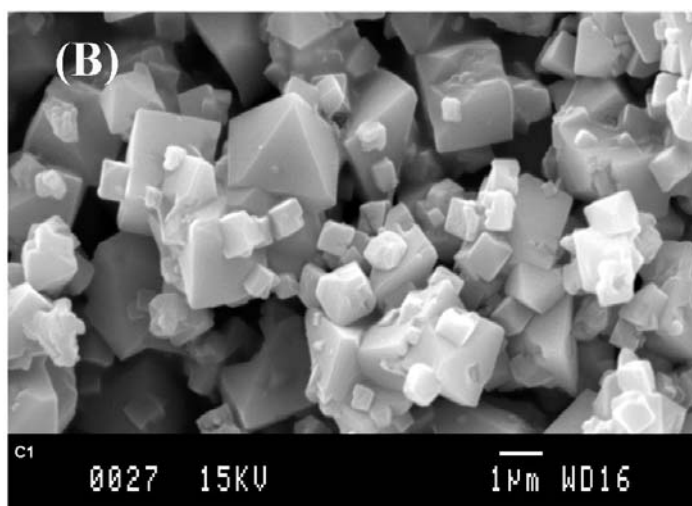


Figure 10.11: SEM image from hydrothermal precipitate obtained from ferric-arsenate intermediate.

This chapter is based on the subsequent articles:

- A. Sunyer, M. Currubí, J. Viñals, Arsenic immobilization as alunite-type phases: The arsenate substitution in alunite and hydronium alunite, *Journal of Hazardous Materials*, in review. (Annex B.1)
- A. Sunyer, J. Viñals, 2011, Arsenate substitution in natroalunite: A potential medium for arsenic immobilization. Part 2: cell parameters and stability tests, *Hydrometallurgy*, 109, 106-115. (Annex A.3).
- J. Viñals, A. Sunyer, P. Molera, M. Cruells, N. Llorca, 2010, Arsenic stabilization of calcium arsenate waste by hydrothermal precipitation of arsenical natroalunite, *Hydrometallurgy*, 104, 247- 259. (Annex A.7)
- J. Viñals, M. Cruells, A. Sunyer, L. Garcia, V. Beltrán, 2009, Arsenic Stabilization by Hydrothermal Synthesis of Alunite-type Phases. Application to the Copper Metallurgy. *Proceedings of the HydroCopper 2009*. P. 37-46. E. Domic & J. Casas Eds. .Gecamin Ltd. Santiago, Chile. ISBN 978-956-8504-21-2. (Annex A.8)

11.1 Short term tests

11.1.1 Stability at different pHs

The solubilities were performed at samples obtained from synthetic reagents and samples obtained from industrial wastes. These solubilities were done and compared with bibliographic stability results found in scorodite's.

Arsenical-natroalunites and mixtures of arsenical-natroalunite and mansfieldite

The behaviour of synthetic arsenical-natroalunites and mixtures of arsenical-natroalunite and mansfieldite was studied at a pH range 1-12. This study gave a good stability of both. The minimum values of arsenic were found at the range of pH between 5 and 8, with a arsenic releasing between 0.01 and 0.05 mg/L. These values are lower than the found in scorodites [Langmuir et al., 2006; Bluteau

and Demopoulos, 2007], and indicate a good stability of arsenical-natroalunites and mixtures of arsenical-natroalunite and mansfieldite. Moreover, the samples showed a good stability at pH 1, despite at pH 12 were dissolved completely, indicating a high instability at very basic pHs (figure 11.1).

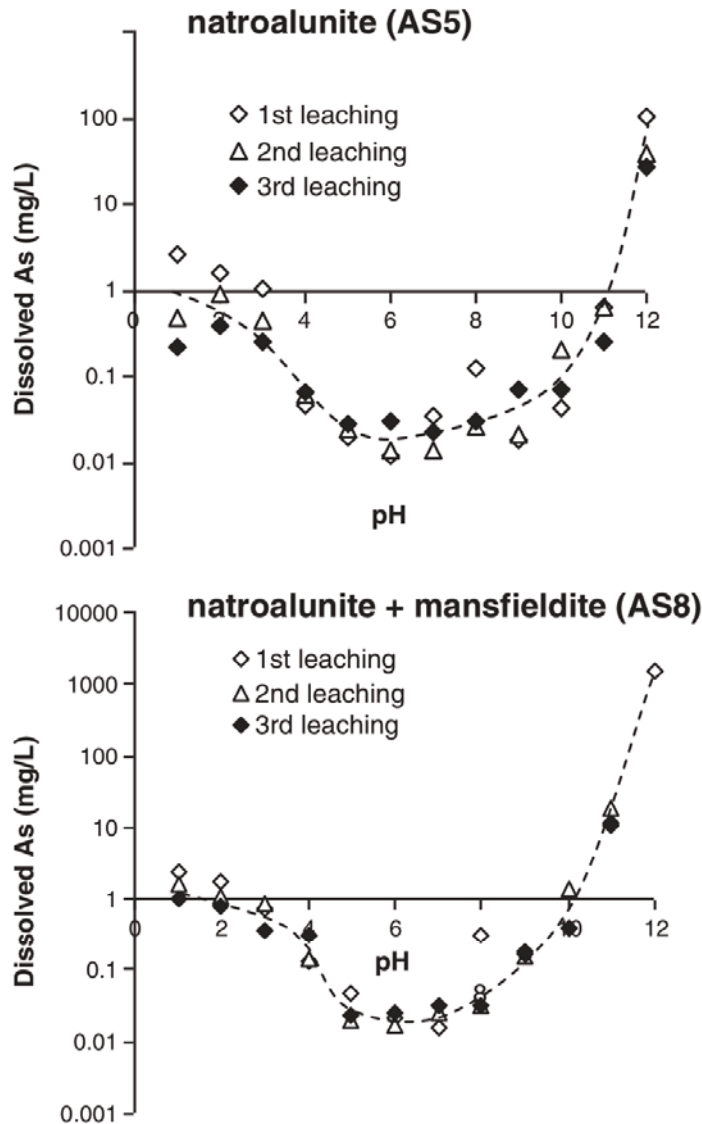


Figure 11.1: Arsenic release at synthetic arsenical-natroalunites and mixtures of arsenical-natroalunite and mansfieldite.

Arsenical-natroalunite had a congruent dissolution at pHs between 1 and 3, where the dissolution was very little, between 0.1 and 1 % in 24 h. The congruent behaviour was also found at pH 12, where arsenical-natroalunite was completely dissolved. At pHs between 4 and 11, the dissolution was incongruent and the extraction of arsenic was higher than the aluminum (figure 11.1).

These tests were also performed at arsenical-natroalunite and mixtures of arsenical-natroalunite and mansfieldite synthesized from calcium-arsenate waste. The results were the same as the commented above for synthetic arsenical natroalunites' samples (figures 11.2).

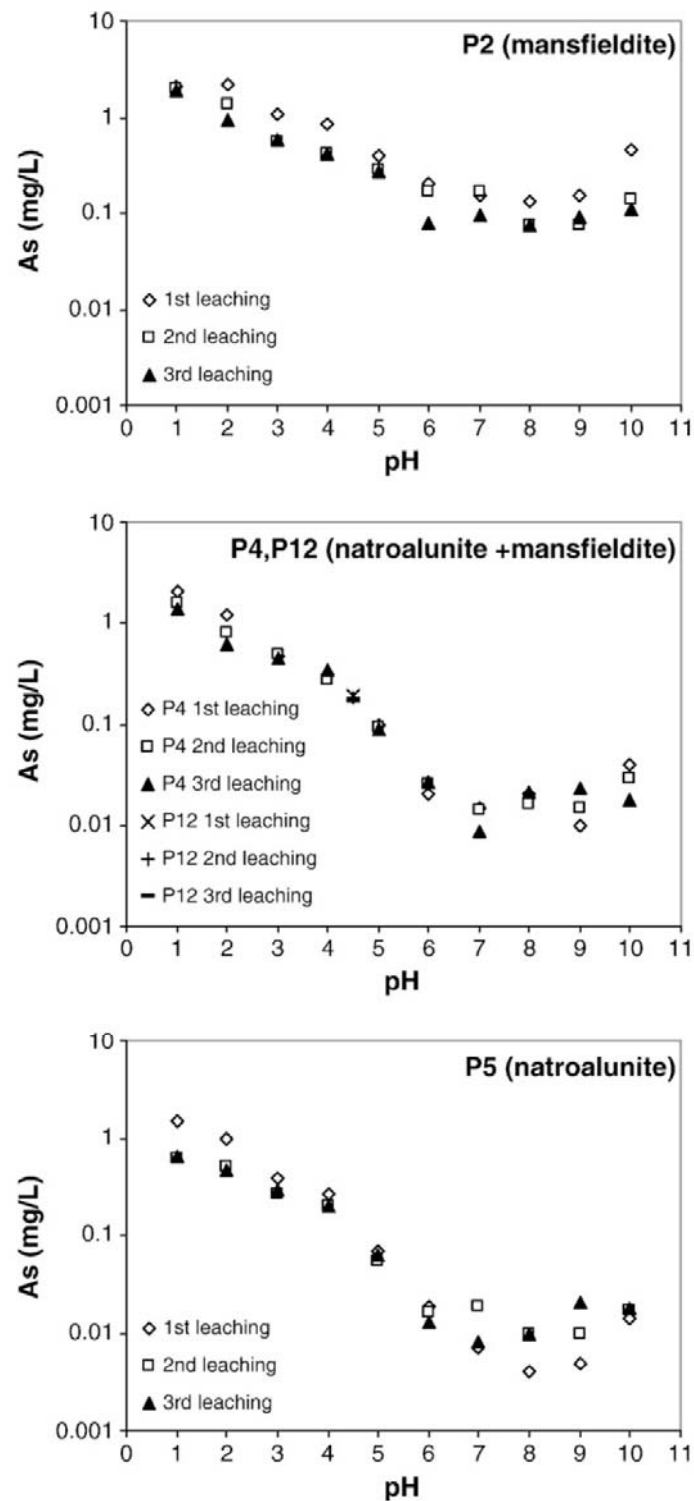


Figure 11.2: Arsenic release at mansfieldite, arsenical-natroalunite mansfieldite mixtures and, arsenical-natroalunite from calcium-arsenate waste.

Arsenical-alunite

Arsenical-alunite also gave good stability results, it were also better than the found for scorodites [Langmuir et al., 2006; Bluteau and Demopoulos, 2007].

These tests were performed between pHs 1 to 12 and, the results were similar to the found in arsenical natroalunites. The minimum arsenic release was found at neutral pHs (4 to 8) (figure 11.3). At these pHs were only dissolved between 0.01 and 0.03 mg/L of arsenic.

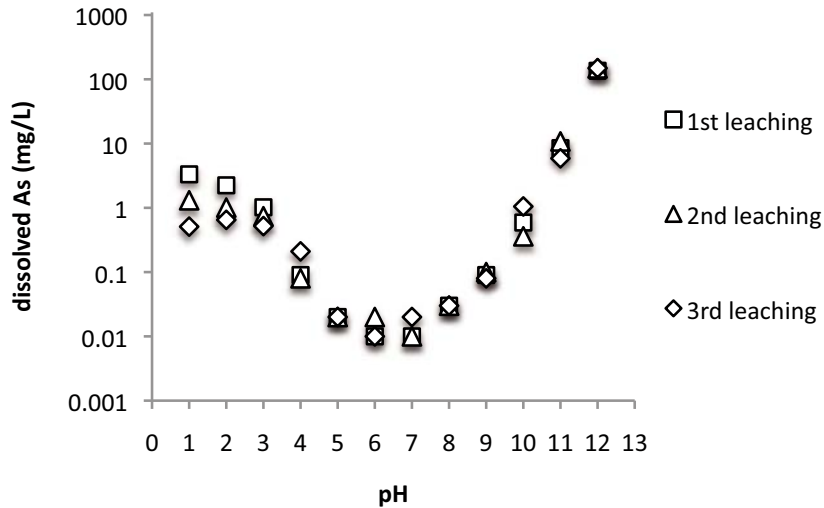


Figure 11.3: Arsenic release from arsenical-alunite (24 h).

Mansfieldite

Arsenic release from mansfieldite was studied in samples obtained from calcium-arsenate industrial waste (figure 11.2). The stability of this phase was very low in comparison to the found in alunite-type phases. The minimum arsenic release was 0.1 mg/L, 10 times higher than the found in arsenical-natroalunites, but similar to that found in scorodites [Langmuir et al., 2006; Bluteau and Demopoulos, 2007].

The high arsenic releasing of mansfieldite, make this phase unsuitable for arsenic inertization. Despite this, little amounts of mansfieldite precipitated with arsenical-natroalunite did not increase significantly the release of arsenic, as it was seen above.

Natropharmacoalumite

Natropharmacoalumite samples tested contained also alarsite and mansfieldite. As seen, in successive lixiviations at different pHs, alarsite and mansfieldite were unstable (figure 11.4). Alarsite was completely dissolved at pH 1 and at pH 12, while mansfieldite was completely dissolved at pH 12. On the other hand, natropharmacoalumite did not suffer any dissolution process in all pH range between 1 and 12 (figure 11.5). The final precipitates of these samples were analysed through SEM-EDS. The analyses from the precipitates lixiviated at pH 12 and the original precipitate before the lixiviation, show a presence of sodium in natropharmacoalumite crystals, while the precipitates from the

lixiviate at pH 1 did not show sodium, possibly due to an exchange of sodium-to-hydronium in the structure that results in a formation of an analogous phase (figure 11.4).

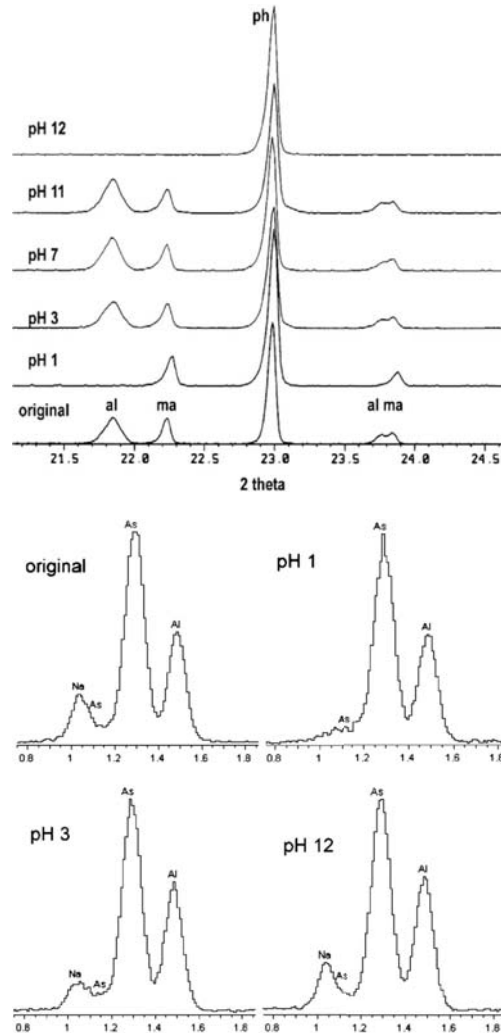


Figure 11.4: Top) XRD of original natropharmacoalumite sample and after the lixiviation tests at different pHs. Bottom) SEM-EDS analyses from natropharmacoalumite: original and after lixiviation tests at different pHs.

11.2 Long-term/medium-term tests

These tests were performed in arsenical-natroalumite (synthetic and from industrial wastes), mixtures arsenical-natroalumite plus mansfieldite, arsenical-alunite and scorodite (synthetic and natural) samples. All of them were performed at its natural pH with continued magnetic stirring and between 5 weeks (medium term) or 6 months (long term). These tests tried to imitate the conditions in which the residues would be once they were dump to evaluate possible environmental arsenic contamination. pH was measured over these months and samples of these tests were periodically taken to analyse the arsenic release.

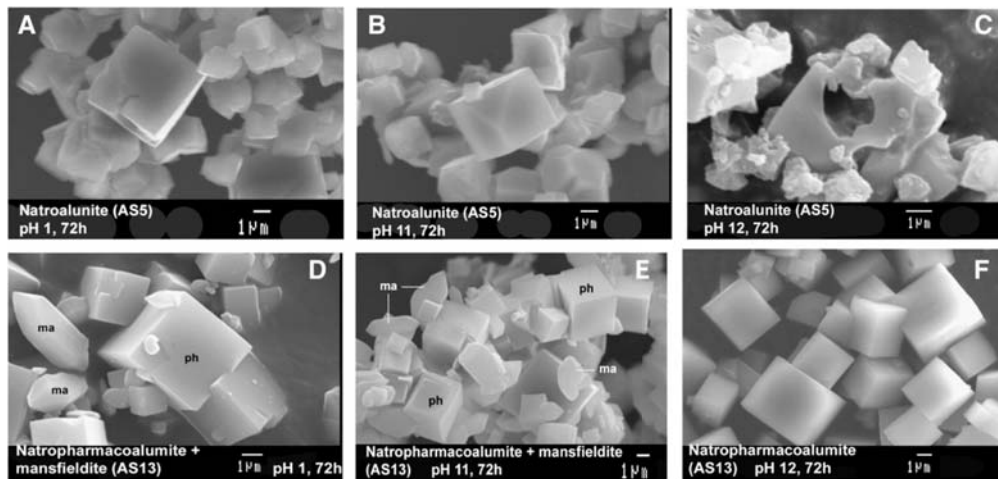


Figure 11.5: SEM images from natroalunite and natropharmacoalunite lixiviated at different pHs.

11.2.1 Arsenical-natroalunite

The long-term stability was good (figure 11.6). Tests were performed at arsenical-natroalunite samples at its natural pH, between 4 and 5. In these conditions, the arsenic release was stabilized at 0.1 mg/L in solution. This stability contrasts with the found in arsenical-natroalunite plus mansfieldite mixtures, in which the arsenic release was between 5 and 10 mg/L.

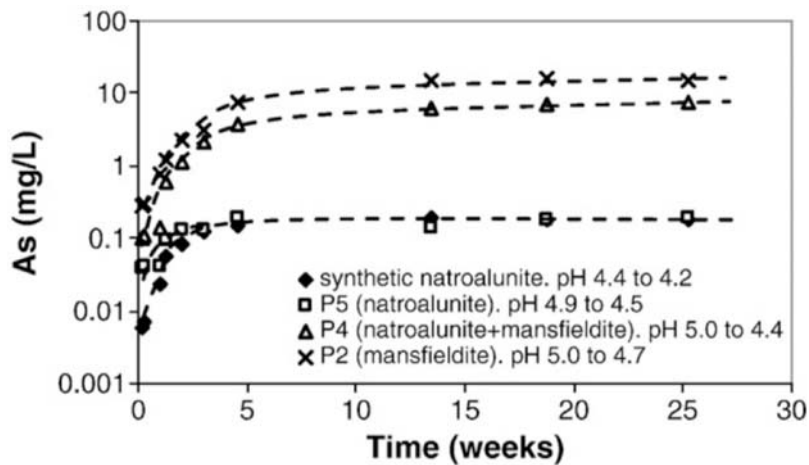


Figure 11.6: Long-term test from arsenical-natroalunite, arsenical-natroalunite plus mansfieldite, and arsenical-natroalunite from calcium-arsenate waste.

11.2.2 Arsenical-alunite

Arsenical-alunites also presented a good stability in medium-term tests. The natural pH of these samples was between 6.6 and 5.2. Arsenic release was constant after 2.5 weeks, and it was about 0.3 mg/L. Figure 11.7 shows the arsenic release of the arsenical-alunite, indicated in gray and black round circles.

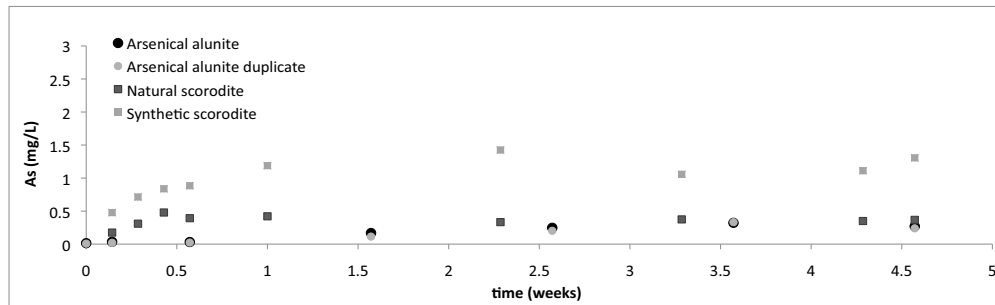


Figure 11.7: Medium-term test of synthetic arsenical-alunite, synthetic scorodite and natural scorodite.

11.2.3 Natural and synthetic scorodite

Natural scorodite was selected from a museum grade sample of the Ojuela mine. The selected sample was previously observed in SEM and after that it was molturated. XRD was performed to ensure the purity of this sample. Medium-term tests were performed at pH between 5.8 and 5.6.

Synthetic scorodite was synthesized hydrothermally by the method used in the majority of the studies and published for first time by Dutrizac and Jambor (1988). The medium-term tests were performed in parallel with natural scorodite's test. In synthetic scorodite, the natural pH was between 4.8 and 4.5.

Natural scorodite was stabilized at 0.4 mg/L of arsenic, very similar results as the found in arsenical-alunites' test. However, synthetic scorodite gave higher arsenic release result, which was stabilized at 1.3 mg/L of arsenic after 1 week (figure 11.7).

As explain Bluteau and Demopoulos (2007) and Fujita et al. (2012), the dissolution of scorodite is a complex phenomena. The crystal size is one of the factors that can effect the scorodite dissolution. Then, different values obtained in natural scorodite (large crystal) and synthetic scorodite (small crystal) could be due to the crystal size.

This chapter is based on the subsequent articles:

- A. Sunyer, J. Viñals, 2011, Arsenate substitution in natroalunite: A potential medium for arsenic immobilization. Part 2: cell parameters and stability tests, *Hydrometallurgy*, 109, 106-115. (Annex A.3)
- A. Sunyer, M. Currubí, J. Viñals, Arsenic immobilization as alunite-type phases: The arsenate substitution in alunite and hydronium alunite, *Journal of Hazardous Materials*, in review. (Annex B.1)

Arsenical-natroalunite, arsenical-alunite and hydronium-alunite structures were studied by XRD through Rietveld method for structure analysis. The aim of this study was to determine the effect of the arsenate incorporation in alunite-type structure.

Results obtained in the studied samples gave good fitting values in all cases. Arsenate incorporation in alunite-type phases produced a cell expansion proportional to the arsenic atomic radius. Concretely, the arsenate incorporation produced an increase in the c cell parameter. This increase was produced in all alunite-type phases studied. Arsenical-alunites and arsenical-natroalunites, from industrial waste and from synthetic reagents, presented a very similar increase in the c cell parameter, which presented an slope of 0.58 with the arsenate incorporation in all cases (figure 12.1).

Hydronium incorporation in arsenical-natroalunites and arsenical-alunites affected the c cell parameter. This effect was easily found and eliminated in arsenical-natroalunites from synthetic reagents, and in arsenical-alunites was eliminated with the data obtained by Rudolph et al. (2003), who studied the effect of hydronium in alunite structure. As the effect in the structure of this cation is really important, it is important to correct it to find the effect of arsenate in the structure.

Arsenical-natroalunite presents a c cell parameter lower than arsenical-alunite, due to the sodium cation, which has an atomic radius inferior to potassium. Arsenical-natroalunites from industrial waste contained iron in the structure. Iron produced an increase in the c cell parameter, which is seen in figure 12.1. The obtained parameters for natroalunites and alunites synthesized in absence of arsenic coincide to those found in the bibliography.

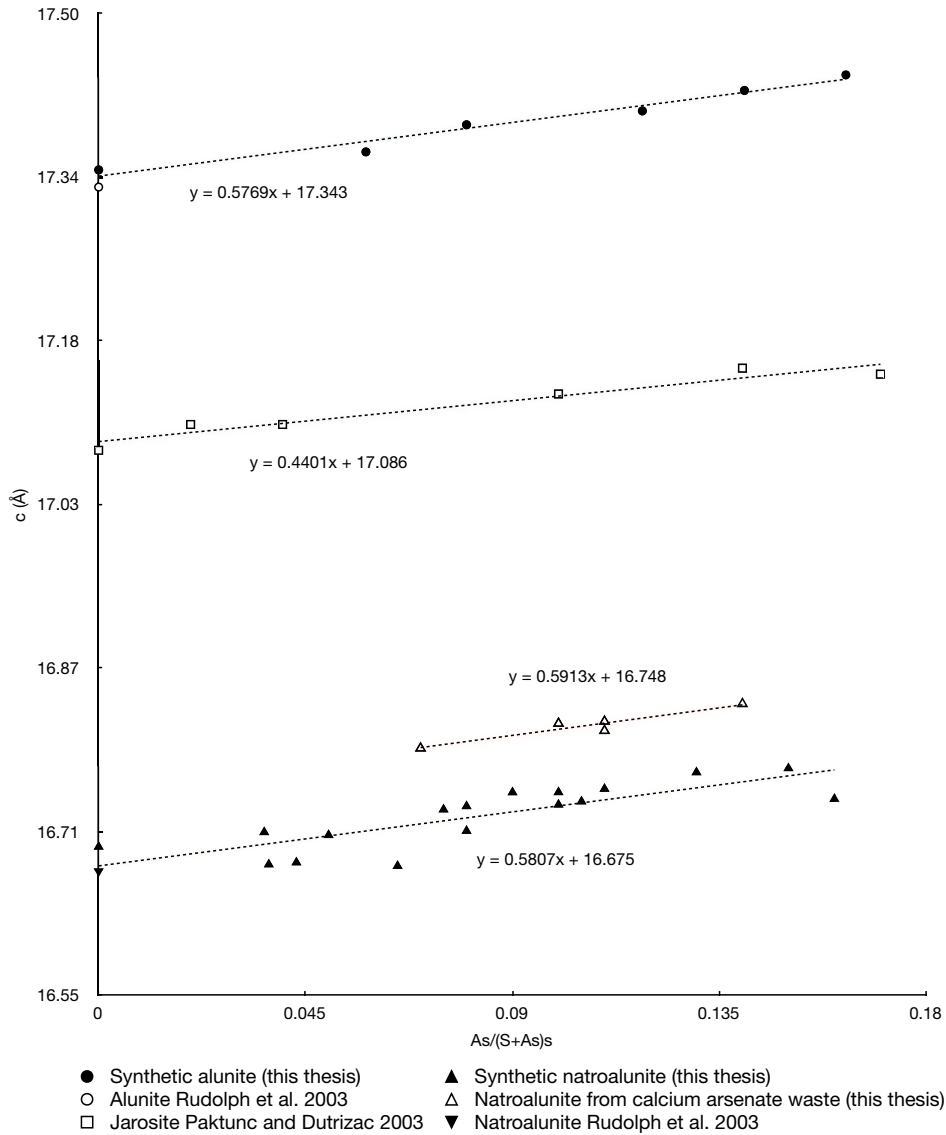


Figure 12.1: c cell parameter vs $\text{AsO}_4/(\text{SO}_4 + \text{AsO}_4)$ molar ratio in arsenical-natroalunite (from synthetic reagents and from industrial wastes), arsenical-alunites and arsenical-jarosites.

A small increase in the c cell parameter (max. $\sim 0.1\text{Å}$) is due to the AsO_4 incorporation in alunite and natroalunite structure. This increase is obviously limited for the maximum observed substitution ($\sim 15\%$). However, if a 100% substitution was possible, the extrapolated expansion would be 0.58-0.59 Å in the c axis of the cell. This expansion is very similar to the found theoretically. If a value of 0.12 Å is taken considering the differences between apical distances (T-O1) between As-O and S-O in alunites structure [Sato et al., 2009] and, for each unit cell is considered to have three layers of tetrahedra TO_4 , the theoretical cell expansion would be of 0.54 Å.

On the other hand, the total substitution of AsO_4 -for- SO_4 exists in alunite supergroup with divalent cations such as Ca^{2+} , represented for its extreme members: huangite and arsenocrandellite ($\text{Ca}_{0.5}\square_{0.5}\text{Al}_3(\text{SO}_4)_2(\text{OH})_6$ and $\text{CaAl}_3(\text{AsO}_4)_2(\text{OH})_4(\text{H}_2\text{O})$, respectively). Small differences between the atomic radii of Na^+ (1.39 Å) and Ca^{2+} (1.34 Å) permits the comparison between this calcium-alunite phases and natroalunites [Shannon, 1976]. These phases also present similar cell parameters: huangite subcell parameters are $a=6.9830$ Å; $c/2=16.7585$ Å [Li et al., 1992]; natroalunite cell parameters are $a=6.9711$ Å; $c=16.6700$ Å [Rudolph et al., 2003]; and arsenocrandellite are $a=7.0810$ Å i $c=17.2700$ Å [Scwab et al., 1991]. According to these cell parameters, the expansion of Ca^{2+} alunite series is 0.51 Å. This value is similar to those observed in arsenical-natroalunite and arsenical-alunite. Then, these results corroborate the substitution of SO_4 -for- AsO_4 in alunites and natroalunites.

The substitution of SO_4^{2-} -for- AsO_4^{3-} in alunite structures required a charge compensation. In alunites of divalent metals (Ca, Pb), this compensation can be verified for coupled substitution, ie for each substituted arsenate, one monovalent cation is substituted for a divalent cation in the structure. In alunites, monovalent cation (Na, K, H_3O) the substitution of SO_4^{2-} -for- AsO_4^{3-} require the protonation of AsO_4^{3-} as HAsO_4^{2-} or OH^- as H_2O . In alunites and natroalunites these protonations do not produce significant changes at structural level, because these protonations did not change significantly the size of the TO_4 tetrahedron or the OH^- . Despite this, hydronium-alunite can be affected for these protonations. H_3O position in the structure is very specific (figure 12.2) [Gale et al., 2010]. H_3O do hydrogen bonds with two O of the $\text{Al-O}_2(\text{OH})_4$ and one O of the SO_4 group. These hydrogen bonds permit to compensate the charge balance in the structure and to be locally stable. However, these hydrogen bonds could not permit an additional protonation in the TO_4 group, necessary for the incorporation of HAsO_4^{2-} or the protonation of OH^- to H_2O . This could explain the null incorporation of arsenic in hydronium-alunite structure.

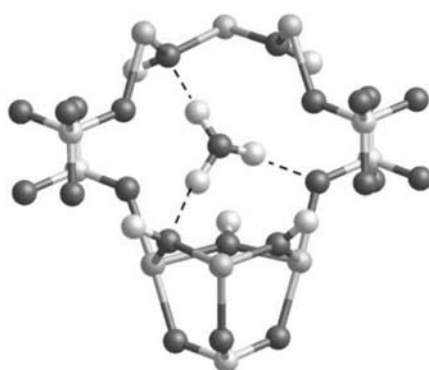


Figure 12.2: Optimized structure of the hydronium cation within the alunite structure as computed at the AM05/TZ2P level of theory. Here the orientation of the figure is the same as shown in Figure 1, with the c axis being vertical as shown. The hydronium cation now forms two hydrogen bonds to O atoms of hydroxyl groups that bridge aluminum atoms (on left-hand side of figure) and one hydrogen bond to an O atom of a sulfate group coordinated to another aluminum atom (right-hand side). [Gale et al., 2010].

PART III

Conclusions

Synthetic arsenical natroalunites:

The precipitation yield of synthetic arsenical natroalunites increases with the synthesis temperature and the arsenic concentration. The precipitation of this phase is practically completed at a synthesis temperature of 180°C and a retention time of 30 min. In a medium $\text{Na}^+/\text{Al}^{3+}/\text{SO}_4^{2-}/\text{AsO}_4^{3-}$ natroalunite precipitation is preferred in respect to mansfieldite precipitation. Moreover, the arsenical-natroalunite precipitation is very fast.

At 200°C, depending on the $(\text{AsO}_4/(\text{SO}_4 + \text{AsO}_4))_{aq}$ ratio are produced the following phases:

- For $(\text{AsO}_4/(\text{SO}_4 + \text{AsO}_4))_{aq} < 0.2$: Arsenate precipitates as arsenical-natroalunite.
- For $0.2 < (\text{AsO}_4/(\text{SO}_4 + \text{AsO}_4))_{aq} < 0.4$: Arsenical-natroalunite and mansfieldite are formed.
- For $(\text{AsO}_4/(\text{SO}_4 + \text{AsO}_4))_{aq} > 0.4$: Arsenical-natroalunite is not formed, and other phases such as alarsite, mansfieldite or natropharmacolumite are precipitated.

Arsenic incorporation in natroalunite between 160°C and 200°C did not depend on the synthesis temperature nor in the retention time. However, it depends on the $(\text{AsO}_4/(\text{SO}_4 + \text{AsO}_4))_{aq}$ molar ratio. When this ratio increased, the incorporation of arsenic in natroalunite increased in a linear manner. The arsenate-for-sulfate substitution was determined in natroalunites at 200°C to be: $(\text{AsO}_4/(\text{SO}_4 + \text{AsO}_4))_{nat} \approx 0.5 (\text{AsO}_4/(\text{SO}_4 + \text{AsO}_4))_{aq}$. And this arsenate substitution can raise up to 0.15 moles per formula unit. Moreover, the calcium presence did not alter the mechanism nor the reaction yield nor the grade of arsenate incorporation in natroalunite structure. Although calcium presents a little incorporation in arsenical-natroalunite (4-6 % molar) and essentially forms anhydrite.

In absence of sodium cation in the medium $(\text{Ca}_2^+/\text{Al}_3^+/\text{SO}_4^{2-}/\text{AsO}_4^{3-})$, no alunite-type phases rich in Ca/As were formed. Then, the suitable application of phases such as arsenocrandellite for arsenate inertization is questionable for high and moderate contain of SO_4^{2-} in wastes.

Synthetic arsenical-alunites:

Alunite precipitation increases with the synthesis temperature. In synthesis at low temperature (98°C), the precipitation increased with the retention time and the initial pH. Arsenic (III) was practically not incorporated in the structure, and the morphology of the alunites is very similar to the alunites without arsenic. Arsenic (V) was incorporated in the structure, approximately 20 % of AsO_4 in formula. Precipitates with less arsenic (8.5 %) did not present morphologic differences with arsenical alunites, while precipitates with more arsenic presented two different phases: an arsenic-rich phase enclosed in a arsenic-poor phase. The latter arsenical-alunites did not pass the TCLP test. At 200°C synthetic arsenical-alunites incorporates a similar amount of arsenate as arsenical-natroalunites. However, before mansfieldite precipitation, arsenate substitution in arsenical-alunite was up to 0.24 moles per formula unit. Arsenical-alunites synthesized at 200°C are more stable than the synthesized at 100°C.

Synthetic hydronium-alunites:

Hydronium-alunite presents a very low precipitation in absence of arsenic. In media with arsenic this phase is practically not formed, and the little amounts formed did not incorporate arsenic. Moreover, at molar ratios $\text{AsO}_4/(\text{SO}_4+\text{AsO}_4)$ between 0.14 and 0.23 amorphous phase are formed, and at higher molar ratios mansfieldite is formed.

Arsenical-natroalunites generated from industrial wastes:

Arsenical-natroalunites were generated from pyrometallurgical copper wastes as calcium arsenate and flash smelting dust. This procedure resolves the production of intermediate arsenical gypsum, because gypsum is transformed to free-arsenic anhydrite. Precipitation of arsenical-natroalunite at 200°C is very fast, less than 15 min. And the incorporation of arsenate was similar to those found in synthetic arsenical-natroalunites. The main disadvantage of the arsenic inertization is the low arsenic partition between solid and liquid phases: $(\text{AsO}_4/(\text{SO}_4+\text{AsO}_4)_{\text{nat}} \approx 0.5 \text{AsO}_4/(\text{SO}_4+\text{AsO}_4)_{\text{aq}})$. However, technically, the precipitation speed and the global precipitation yield could be increase through a semi-continuous addition of the reagents in a unique hydrothermal operation.

The precipitated arsenical-natroalunite from both wastes was a complex phase with little amounts of Fe, Ca and P in the structure. Other elements present in the initial media like Ni, Cu or Zn, were not precipitated and could be recovered from final solution. However, in flash smelting dust waste is recommended a previous recovery of the copper due to the high content of this metal in the initial solution and, a final inertization of arsenic through arsenical-natroalunite formed from an intermediate of ferric arsenate.

Short-term tests:

All arsenical-natroalunites and arsenical-alunites in absence and with minor amounts of mansfieldite presented a low arsenic release in 24-h test (0.01-0.03 mg/L) at pHs between 5 and 8. These values are one order of magnitude lower than in conventional scorodite-type precipitates.

Other phases, as mansfieldite, alarsite and amorphous phases presented high arsenic releasing values, 2 and 3 orders of magnitude higher than arsenical natroalunites and alunites. Despite this, natropharmacoalumite phase did not present any damage at pHs between 1 to 12. This phase had ion exchange at acid pHs, substituting Na^+ for H_3O^+ . This solubility characteristics and the buffer effect make this phase attractive for arsenic inertization, mainly in acid

soils. Nevertheless, this phase seems difficult to be produced in the studied media.

Long-term/medium-term tests:

Arsenical-natroalunite gave good arsenic stability at long term (6 months), and it remains stable at 0.1 mg/L arsenic. Arsenical-alunite did not give as good results as arsenical-natroalunite in medium-term tests (5 weeks). However it gave a low value (0.3 mg/L As). The values found for arsenical natroalunites and alunites were similar to than found for natural scorodite (0.4 mg/L), and better to than found in synthetic scorodite (1.3 mg/L).

Crystal structure study:

Arsenical natroalunites and alunites structures were R-3m and Z=3 confirmed by Rietveld analysis. Both phases presented an expansion of the cell with the arsenate incorporation. In arsenical-natroalunite as well as in arsenical-alunite the expansion was equal: *a* cell parameter was constant while *c* cell parameter increased with an slope of ~ 0.58 . This increment is consistent with the expected cell expansion deduced from the difference between As-O1 and S-O1 distances in the tetrahedral sites of the alunite-type structure.

Despite alunite and natroalunite phases, hydronium-alunite did not incorporate significant amounts of arsenic. This may be related by the difficulty of substituting protonated HAsO_4^{2-} -for- SO_4^{2-} or H_2O -for- OH^- groups, due to the location of the H-bridges of the H_3O in the structure. These characteristics make hydronium alunite unsuitable for arsenic immobilization.

PART IV

References

CHAPTER 14

REFERENCES

Baron, D., & Palmer, C. D. (1996). Solubility of jarosite at 4-35 C. *Geochimica et Cosmochimica Acta*, 60(2), 185–195.

Basciano, L. C., & Peterson, R. C. (2008). Crystal chemistry of the natrojarosite-jarosite and natrojarosite-hydronium jarosite solid-solution series: A synthetic study with full Fe site occupancy. *American Mineralogist*, 93(5-6), 853–862.

Bassett, H. (1950). 300. Lead alunite. *Journal of the Chemical Society*, 1460–1461. The Royal Society of Chemistry.

Bluteau, M.-C., & Demopoulos, G. P. (2007). The incongruent dissolution of scorodite-Solubility, kinetics and mechanism. *Hydrometallurgy*, 87(3-4), 163–177.

Chandraprabha M N & Natarajan K A (2012). Mechanism of arsenic tolerance and bioremoval of arsenic by *Acidithiobacillus ferrooxidans*. *Journal of Biochemical Technology*, 3(2), 257–265.

Demopoulos, G., Droppert, D., & Van Weert, G. (1995). Precipitation of crystalline scorodite ($\text{FeAsO}_4 \cdot 2\text{H}_2\text{O}$) from chloride solutions. *Hydrometallurgy*, 38(3), 245–261.

Drouet, C., & Navrotsky, A. (2003). Synthesis, characterization, and thermochemistry of K-Na-H₃O jarosites. *Geochimica et Cosmochimica Acta*, 67(11), 2063–2076.

Dutrizac, J E (1989). The Hydrothermal Conversion of Jarosite-Type Compounds to Hematite. *Productivity and Technology in the Metallurgical Industries*; Cologne; FRG; 17(22), 587-612.

Dutrizac, J. E., & Jambor, J. L. (1988). The synthesis of crystalline scorodite, $\text{FeAsO}_4 \cdot 2\text{H}_2\text{O}$. *Hydrometallurgy*, 19(3), 377–384.

Dutrizac, J. E., & Jambor, J. L. (2000). Jarosites and Their Application in *Hydrometallurgy*. *Reviews in Mineralogy and Geochemistry*, 40(1), 405–452.

Dutrizac, J., & Kaiman, S. (1976). Synthesis and properties of jarosite-type compounds. *The Canadian Mineralogist*, 14(2), 151–158.

Fujita, T., Taguchi, R., Abumiya, M., Matsumoto, M., Shibata, E., & Nakamura, T. (2008). Novel atmospheric scorodite synthesis by oxidation of ferrous sulfate solution. Part I. *Hydrometallurgy*, 90(2-4), 92–102.

Fujita, T., Taguchi, R., Abumiya, M., Matsumoto, M., Shibata, E., & Nakamura, T. (2008). Novel atmospheric scorodite synthesis by oxidation of ferrous

sulfate solution. Part II. Effect of temperature and air. *Hydrometallurgy*, 90(2-4), 85–91.

Fujita T., Fujieda S., Shinoda K., Suzuki S. (2012). Environmental leaching characteristics of scorodite synthesized with Fe(II) ions. *Hydrometallurgy*, 111-112, 87-102.

J.D. Gale, K.Wright, K.A. Hudson-Edward (2010), A first-principles determination of the orientation of H₃O⁺ in hydronium alunite, *American Mineralogist*, 95, 1109-1112. Gonzalez-Contreras, P., Weijma, J., Weijden, R. V. D., & Buisman, C. J. N. (2010). Biogenic Scorodite Crystallization by Acidianus sulfidivorans for Arsenic Removal. *Environmental Science & Technology*, 44(2), 675–680.

Gonzalez-Contreras, P., Weijma, J., & Buisman, C. J. N. (2011). Kinetics of ferrous iron oxidation by batch and continuous cultures of thermoacidophilic Archaea at extremely low pH of 1.1–1.3. *Applied Microbiology and Biotechnology*, 93(3), 1295–1303.

Jambor, J. L. (1999). Nomenclature of the alunite supergroup. *The Canadian Mineralogist*, 37(6), 1323–1341. Mineralogical Association of Canada.

Morales, A., Cruells, M., Roca, A., Sunyer, A., Viñals, J., (2011). Copper and Zinc Recoveries and Arsenic Stabilization from Copper Smelter Flue Dusts, *Proceedings of the 6th International Seminar on Copper Hydrometallurgy*, Viña del Mar, Chile, Edited by Jesús M. Casas, Cleve Lightfoot, Gustavo Tapia, 38-39. ISBN 978-956-8504-49-6. (Annex C.1)

Paktunc, D., & Dutrizac, J. E. (2003). Characterization of arsenate-for-sulfate substitution in synthetic jarosite using X-ray diffraction and X-ray absorption spectroscopy. *The Canadian Mineralogist*, 41(4), 905–919. Mineralogical Association of Canada.

Paktunc, D., Dutrizac, J., & Gertsman, V. (2008). Synthesis and phase transformations involving scorodite, ferric arsenate and arsenical ferrihydrite: Implications for arsenic mobility. *Geochimica et Cosmochimica Acta*, 72(11), 2649–2672.

Rios, G., Arbizu, C., Sunyer, A., Viñals, J., (2012). New Process for Treating Slag Furnace (SCF) Flue Dust at Atlantic Copper, *Proceedings of T.T. Chen Honorary Symposium*. Edited by S. Wang, J.E. Dutrizac, M.L. Free, J.Y. Hwang and D. Kim, 177-190. John Wiley & Sons, Hoboken, New Jersey, USA. ISBN 978-1-11829-123-8. (Annex C.2)

Riveros, P., Dutrizac, J., & Spencer, P. (2001). Arsenic disposal practices in the metallurgical industry. *Canadian Metallurgical Quarterly*, 40(4), 395–420. Maney Publishing.

Rudolph, W. W., Mason, R., & Schmidt, P. (2003). Synthetic alunites of the potassium-oxonium solid solution series and some other members of the group: synthesis, thermal and X-ray characterization. *European Journal of Mineralogy*, 15(5), 913–924.

Sato, E., Nakai, I., Miyawaki, R., & Matsubara, S. (2009). Crystal structures of alunite family minerals: beaverite, corkite, alunite, natroalunite, jarosite, svanbergite, and woodhouseite. *Neues Jahrbuch für Mineralogie - Abhandlungen*, 185(3), 313–322.

Shannon, R. (1976). Revised effective ionic radii and systematic studies of interatomic distances in halides and chalcogenides. *Acta Crystallographica Section A: Crystal Physics, Diffraction, Theoretical and General Crystallography*,

32(5), 751–767. International Union of Crystallography.

Stoffregen, R. E., Alpers, C. N., & Jambor, J. L. (2000). Alunite-Jarosite Crystallography, Thermodynamics, and Geochronology. *Reviews in Mineralogy and Geochemistry*, 40(1), 453–479.

Welham, N., Malatt, K., & Vukcevic, S. (2000). The stability of iron phases presently used for disposal from metallurgical systems—A review. *Minerals Engineering*, 13(8-9), 911–931.

PART V

Annex

ANNEX A _____
_____ ARTICLES FOR COMPENDIUM

A.1 Hematite formation from jarosite type compounds by hydrothermal conversion

J.E. Dutrizac, A. Sunyer, 2012, Hematite formation from jarosite type compounds by hydrothermal conversion, Canadian Metallurgical Quarterly, 51, 1, 11-23.

Resum en català

La conversió hidrotermal a hematita de la jarosita de potassi, la jarosita de plom, la jarosita de sodi, la jarosita de plata-sodi, la jarosita de sodi amb AsO_4 i la jarosita de potassi i de sodi formades in situ van ser investigades. La jarosita de potassi és la més estable de les espècies de jarosites. La seva conversió a hematita en absència de llavor de Fe_2O_3 va ser parcial després de 5 h de reacció a $> 240^\circ\text{C}$. En presència de llavor de Fe_2O_3 , la conversió a hematita va ser parcialment completa en 2 h a 225°C i va ser completa a 240°C . La precipitació de jarosita de potassi, in situ a 225°C en presència de 50 g/L de llavor de Fe_2O_3 , és més ràpida que el seu grau de conversió hidrotermal a hematita. En canvi, la conversió completa de la jarosita de plom o la jarosita de sodi-plom a hematita i PbSO_4 insoluble va ser en 0.75h a 225°C en presència de 20 g/L de llavor de Fe_2O_3 . $\text{Fe}(\text{SO}_4)_{1.5}$ dissolt inhibeix la conversió de la jarosita de plom o forma jarosita de plom a partir del PbSO_4 generat. La conversió hidrotermal de la jarosita sodi-plata a hematita va ser completa en 0.75 h a 225°C en presència de 20 g/L de llavor d'hematita. La plata es va dissoldre durant la conversió hidrotermal i present a la dissolució final. No obstant, la presència de minerals de sofre o sulfurs van causar la reprecipitació de la plata. La conversió de les jarosites de sodi que contenen AsO_4 a 225°C i en presència de 20 g/L Fe_2O_3 com a llavor va ser completa en 2 h, per a concentracions d' $\text{H}_2\text{SO}_4 < 0.4\text{M}$. Increments en el contingut d' AsO_4 en la jarosita de sodi van resultar en un increment lineal del contingut AsO_4 en l'hematita, i $\sim 95\%$ de l' AsO_4 va romandre en el producte de conversió. Un increment en les temperatures i de l'addició de la llavor de Fe_2O_3 va augmentar significativament la conversió hidrotermal de la jarosita de sodi formada in situ a $200\text{-}240^\circ\text{C}$. Tanmateix, la conversió de la jarosita de sodi sintetitzada prèviament sembla arribar a un grau més elevat que la jarosita de sodi formada in situ.

Hematite formation from jarosite type compounds by hydrothermal conversion

J. E. Dutrizac*¹ and A. Sunyer²

The hydrothermal conversion of K jarosite, Pb jarosite, Na jarosite, Na–Ag jarosite, AsO₄ containing Na jarosite and *in situ* formed K jarosite and Na jarosite to hematite was investigated. Potassium jarosite is the most stable jarosite species. Its conversion to hematite in the absence of Fe₂O₃ seed occurred only partially after 5 h reaction at >240°C. In the presence of Fe₂O₃ seed, the conversion to hematite was nearly complete within 2 h at 225°C and was complete at 240°C. The rate of K jarosite precipitation, *in situ* at 225°C in the presence of 50 g L⁻¹ Fe₂O₃ seed, is faster than its rate of hydrothermal conversion to hematite. In contrast, complete conversion of either Pb jarosite or Na–Pb jarosite to hematite and insoluble PbSO₄ occurs within 0.75 h at 225°C in the presence of 20 g L⁻¹ Fe₂O₃ seed. Dissolved Fe(SO₄)_{1.5} either inhibits the conversion of Pb jarosite or forms Pb jarosite from any PbSO₄ generated. The hydrothermal conversion of Na–Ag jarosite to hematite was complete within 0.75 h at 225°C in the presence of 20 g L⁻¹ Fe₂O₃ seed. The Ag dissolved during hydrothermal conversion and reported to the final solution. However, the presence of sulphur or sulphide minerals caused the reprecipitation of the dissolved Ag. The conversion of AsO₄ containing Na jarosite at 225°C in the presence of 20 g L⁻¹ Fe₂O₃ seed was complete within 2 h, for H₂SO₄ concentrations <0.4M. Increasing AsO₄ contents in the Na jarosite resulted in a linear increase in the AsO₄ content of the hematite, and ~95% of the AsO₄ remained in the conversion product. Increasing temperatures and Fe₂O₃ seed additions significantly promote the hydrothermal conversion of *in situ* formed Na jarosite at 200–240°C. However, the conversion of previously synthesised Na jarosite seems to proceed to a greater degree than that of *in situ* formed Na jarosite.

On a examiné la conversion hydrothermale en hématite de la jarosite de K, de la jarosite de Pb, de la jarosite de Na, de la jarosite de Na-Ag, de la jarosite de Na contenant de l'AsO₄, et de la jarosite de K et de la jarosite de Na qui sont formées *in situ*. La jarosite de potassium est la plus stable des espèces de jarosite. Sa conversion en hématite ne se produisait que partiellement après 5 h de réaction à >240°C en l'absence d'amorce de Fe₂O₃. En présence d'amorce de Fe₂O₃, la conversion en hématite était presque complète à moins de 2 h à 225°C et était complète à 240°C. La vitesse de précipitation de la jarosite de K, *in situ* à 225°C en présence de 50 g L⁻¹ d'amorce de Fe₂O₃, est plus rapide que sa vitesse de conversion hydrothermale en hématite. Par contraste, la conversion complète soit de la jarosite de Pb ou de la jarosite de Na-Pb en hématite et en PbSO₄ insoluble se produit à moins de 0.75 h à 225°C en présence de 20 g L⁻¹ d'amorce de Fe₂O₃. Le Fe(SO₄)_{1.5} dissous soit inhibe la conversion de la jarosite de Pb ou forme de la jarosite de Pb à partir de tout PbSO₄ produit. La conversion hydrothermale de la

¹CANMET-MMSL, 555 Booth Street, Ottawa K1A 0G1, Canada

²Facultat de Física i Química, University of Barcelona, Barcelona 08028, Spain

*Corresponding author, email jdutrizac@nrcan.gc.ca

jarosite de Na-Ag en hématite était complète à moins de 0.75 h à 225°C en présence de 20 g L⁻¹ d'amorce de Fe₂O₃. L'Ag se dissolvait lors de la conversion hydrothermale et se rapportait dans la solution finale. Cependant, la présence de soufre ou de minéraux sulfurés avait pour résultat la re-précipitation de l'Ag dissous. La conversion de la jarosite de Na contenant de l'AsO₄ à 225°C en présence de 20 g L⁻¹ d'amorce de Fe₂O₃ était complète à moins de 2 h, avec des concentrations d'H₂SO₄ <0.4 M. L'augmentation de la teneur en AsO₄ de la jarosite de Na avait pour résultat une augmentation linéaire de la teneur en AsO₄ de l'hématite et ~95% de l'AsO₄ demeurait dans le produit de conversion. L'augmentation de la température et d'additions d'amorce de Fe₂O₃ favorisait significativement la conversion hydrothermale de la jarosite de Na qui est formée *in situ* à 220–240°C. Cependant, la conversion de la jarosite de Na synthétisée antérieurement semblait se produire à un plus grand degré que celle de la jarosite de Na qui est formée *in situ*.

Keywords: jarosite-type compound, hematite, hydrothermal conversion, potassium jarosite, arsenate jarosite, lead jarosite

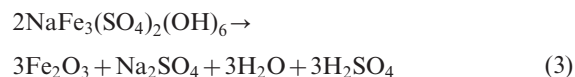
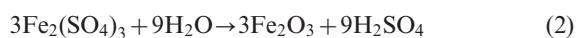
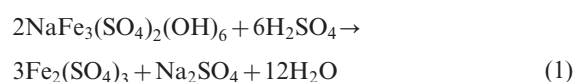
Introduction

Iron is a common impurity in most hydrometallurgical processing circuits and the dissolved iron creates significant difficulties for the recovery of divalent base metals such as Zn, Ni, Co, Cu, etc. For this reason, the dissolved iron must be eliminated from the processing circuit before the metal recovery operations. However, simple neutralisation of concentrated processing solutions generates iron hydroxide precipitates which cannot be easily filtered or washed. To address this widespread iron control problem, the zinc industry has developed the jarosite, goethite, paragoethite and hematite processes. Among these technologies, the jarosite process is the most economical and is the most commonly used. The process is easily integrated into existing hydrometallurgical circuits; furthermore, it can be carried out at <100°C and at atmospheric pressure.^{1–3} Most importantly, jarosite precipitates are relatively easy to filter and wash. Jarosite type compounds [MFe₃(SO₄)₂(OH)₆, where M is Na⁺, K⁺, Rb⁺, Ag⁺, Tl⁺, NH₄⁺, H₃O⁺, ½Pb²⁺ and ½Hg²⁺] also have the advantage that they do not incorporate most divalent base metals in their structure, but they do eliminate various impurities such as sulphate, arsenate, the alkali metals, etc.^{2,4} On the other hand, jarosite precipitates have a high residue volume and the residues are unstable under certain impoundment conditions. It is generally accepted that jarosite precipitates have no commercial applications. Similar observations apply to the goethite and paragoethite (FeO.OH) processes although these latter processes generate somewhat more compact residues.

In contrast, the hematite (Fe₂O₃) process generates high density precipitates which have high iron contents.^{5,6} The precipitates are filterable, and the precipitated hematite is commercially used for cement manufacture and has some potential for iron production.⁷ In addition, hematite precipitates offer many potential advantages with respect to residue disposal and impoundment. Although hematite can be precipitated at 145–155°C, in most industrial processes, the hematite is precipitated at

temperatures >180°C to ensure a high degree of iron removal. The direct precipitation of hematite in high temperature autoclaves presents a significant processing cost, which increases if the feed solutions are relatively dilute in iron as a result of processing constraints.⁸ The cost of the hematite process is further increased because of the need to first reduce the iron to the ferrous state and then to reoxidise it in the autoclave. Within this framework, the conversion of jarosite type compounds to hematite would have the potential advantages of avoiding the reduction–oxidation step and operating under ideal autoclave conditions with a high pulp density. That is, the approach would combine the benefits of low cost jarosite precipitation at <100°C to eliminate dissolved iron from the processing solution with the advantages of hematite generation for subsequent use or disposal.

The overall reactions for the hydrothermal conversion of jarosite type compounds to hematite are presented below, using sodium jarosite as an example⁹



A previous paper demonstrated that a high degree of hydrothermal conversion of sodium jarosite to hematite (equation (3)) could be achieved at temperatures >200°C.⁹ The principal factors affecting the conversion of sodium jarosite to hematite were shown to be temperature, retention time, acid concentration, and especially, the presence of hematite seed. The present paper extends the reported studies on the hydrothermal conversion of sodium jarosite to a number of other jarosite species of relevance to hydrometallurgical processing. Specifically, the hydrothermal conversion of potassium jarosite, lead jarosite, sodium–silver jarosite,

arsenate containing sodium jarosite and *in situ* formed sodium jarosite to hematite was investigated for a range of parameters of relevance to hydrometallurgical processing. Furthermore, the experiments presented in this paper are of an exploratory and research nature and are not intended to closely replicate a possible industrial process operating continuously with high pulp densities.

Experimental

Reagent grade chemicals were used for all the experiments. Potassium jarosite was synthesised by reacting 0.3M $\text{Fe}(\text{SO}_4)_{1.5}$ and 0.3M K_2SO_4 solutions at pH 1.6 for 24 h at 97°C.¹⁰ As was the situation for all the syntheses, the pH was adjusted at room temperature and was not controlled during the reaction. Solid MgCO_3 or Li_2CO_3 were used to adjust the pH because the carbonates dissolved slowly enough to avoid the massive, and undesirable, precipitation of ferric hydroxide species. Also, the use of the solid resulted in a minimum change in the solution volume and reagent concentrations, and neither Mg nor Li formed end member jarosite type compounds. The precipitates were thoroughly washed with water and were dried at 110°C. Several lots were prepared and the various dried lots were blended to provide feed material for the hydrothermal conversion experiments. X-ray diffraction analysis of the blended material detected only potassium jarosite which had the following composition: 6.86%K, 33.28%Fe and 39.21% SO_4 . End member potassium jarosite contains 7.80%K, 33.46%Fe and 38.25% SO_4 . Thus, the synthesised product is potassium jarosite having a minor amount of hydronium ion substituting for potassium in the jarosite structure.¹⁰

Lead jarosite was synthesised by reacting 0.3M $\text{Fe}(\text{SO}_4)_{1.5}$ and 0.03M H_2SO_4 solutions for 24 h at 150°C in the presence of 30 g L^{-1} of PbSO_4 . Excess PbSO_4 was removed by slurry washing the product three times in 1 L lots of 30% ammonium acetate solution.¹¹ The final acetate washed products were water washed and then dried at 110°C. Several lots were prepared and the various dried lots were blended to provide feed material for the hydrothermal conversion experiments. X-ray diffraction analysis of the blended product detected lead jarosite with a trace amount of PbSO_4 . The chemical composition suggested the formation of a $\text{Pb-H}_3\text{O}$ jarosite species containing 9.87%Pb, 30.1%Fe and 37.17% SO_4 . End member lead jarosite contains 18.32%Pb, 29.6%Fe and 33.98% SO_4 . A sodium-lead jarosite was prepared from chloride media by reacting 0.5M FeCl_3 , 3M NaCl and 0.2M Li_2SO_4 solutions containing 20 g L^{-1} PbCl_2 at 97°C for 24 h.¹² Several lots were prepared and each was washed in hot water to remove any excess PbCl_2 . The various lots were dried and then blended to provide feed material for the hydrothermal conversion experiments. X-ray diffraction analysis of the blended product detected 'sodium jarosite' which had the following composition: 2.99%Na, 0.81%Pb, 33%Fe and 40% SO_4 .

Sodium-silver jarosite was synthesised by reacting 0.2M $\text{Fe}(\text{SO}_4)_{1.5}$, 0.025M Na_2SO_4 and 0.005M Ag_2SO_4 solutions at pH 1.6 for 24 h using the procedures of

Dutrizac and Jambor.^{13,14} The individual precipitates were extensively washed with warm water to remove any unreacted silver sulphate, and were then dried at 110°C. Several lots of the dried precipitate were blended to give sufficient material for the hydrothermal decomposition experiments. X-ray diffraction analysis of the blended material yielded a pattern similar to that of sodium jarosite; the blended material had the following composition: 2.13%Na, 4.74%Ag, 31.6%Fe and 39.0% SO_4 .

Arsenate containing sodium jarosite was synthesised by reacting 1 L volumes of 0.3M $\text{Fe}(\text{SO}_4)_{1.5}$ and 0.2M Na_2SO_4 solutions, containing 0.33, 0.66 or 1.00 g L^{-1} of As(V), added as Na_2HAsO_4 , at pH 1.0 for 24 h at 150°C in a Parr 2-L autoclave. The procedures were essentially the same as those described previously.¹⁵ The precipitates were thoroughly washed with water to remove any residual synthesis solution, especially any sodium arsenate. The washed precipitates were then dried at 110°C. For each of the jarosite species produced using the different As(V) concentrations, several lots were prepared and the dried lots were blended to provide feed materials for the hydrothermal conversion experiments. X-ray diffraction analysis of the various blended lots of arsenate containing sodium jarosite detected only sodium jarosite. The composition of the blended product made from 0.33 g L^{-1} As(V) as Na_2HAsO_4 solutions contained 4.15%Na, 33.54%Fe, 39.11% SO_4 and 0.35% AsO_4 . The analogous product made from the 0.66 g L^{-1} As(V) solutions analysed 4.28%Na, 33.8%Fe, 41.0% SO_4 and 0.96% AsO_4 ; the product from the 1.00 g L^{-1} As(V) solutions contained 4.05%Na, 33.8%Fe, 38.3% SO_4 and 2.59% AsO_4 . End member sodium jarosite contains 4.74%Na, 34.57%Fe and 39.64% SO_4 .

In a previous investigation, solid sodium jarosite was added to the autoclave, and its conversion to hematite was monitored as a function of several experimental parameters.⁹ To complement those findings, experiments were also carried out wherein sodium jarosite was formed *in situ*, during the ~45 min required to heat the autoclave to the reaction temperature. In these experiments, 0.3M $\text{Fe}(\text{SO}_4)_{1.5}$ solutions containing 0.1 or 0.3M Na_2SO_4 , at pH 1.5, were reacted for various times at 200 or 240°C in the presence and absence of 20 g L^{-1} of hematite seed. The results were compared with those obtained previously when solid sodium jarosite was initially added to the autoclave.

The hydrothermal conversion experiments were carried out in a Parr 2-L autoclave fitted with a glass liner and titanium internal components. Generally, 40 g of the different jarosites were slurried in 1 L of 0.2M H_2SO_4 solution, and reagent grade hematite (Fe_2O_3) was commonly added as a seed material. The hematite seed analysed 69.62%Fe and 0.76% SO_4 and was shown by X-ray diffraction analysis to consist of hematite only. Its Brunauer-Emmett-Teller surface area was 8.4 $\text{m}^2 \text{g}^{-1}$. The experiments were generally done at 225°C and using a 2 or 5 h retention time at temperature. All the experiments were done in a batch mode, although a possible commercial process would likely operate continuously. During the heat-up stage of the batch

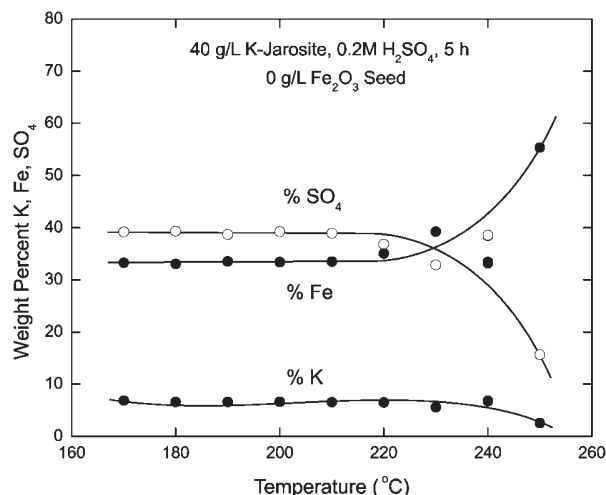
experiments, various reactions, such as the precipitation of hydronium jarosite, might occur and any products formed must then dissolve at the 225°C reaction temperature. Thus, a continuous process would likely yield more rapid and complete conversion of the added jarosite type compounds to hematite. Elevated temperatures promote the hydrolysis of ferric ions, and as a consequence, it was found that the hematite formed at elevated temperatures partly dissolved at room temperature in the hydrolysis acid formed during the reaction.¹⁶ This problem exists in both batch and continuous modes of operation. To address the problem in the present batch experiments, the autoclaves were rapidly cooled (~15 min) at the completion of the experiments by the use of an internal water cooling coil, and the slurries were immediately filtered on a Buchner vacuum filter using No. 3 Whatman paper. The precipitates were thoroughly water washed and subsequently dried at 110°C before analysis.

The precipitates were characterised by chemical analysis and X-ray diffraction analysis. For the chemical analyses, the precipitates were dissolved in HCl or in aqua regia, when necessary. Microwave digestion in sealed vessels was employed when potentially volatile elements, such as As, were present. The chemical analyses were done using inductively coupled plasma spectroscopy or atomic absorption analysis with matrix matched standards. The X-ray diffraction analyses were performed using a Rigaku rotating anode diffractometer with Cu $K_{\alpha 1}$ radiation at 50 kV and 180 mA in a step scan of 0.02° and a scan rate of 4° min⁻¹ in 2 θ . Because the confident detection limit of crystalline phases on the diffractometer is 1–2%, some samples were also analysed using Guinier–deWolff precision X-ray diffraction analysis that can detect 0.25–0.5% of such phases. Some of the precipitates were also examined by scanning electron microscopy (SEM) with energy dispersive X-ray analysis (EDX) to characterise the phases present and to detect possible impurities.

Results and discussion

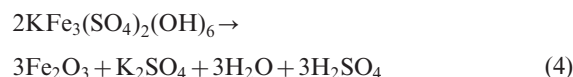
Potassium jarosite

The hydrothermal conversion of 40 g L⁻¹ of K jarosite after 5 h of reaction in 0.2M H₂SO₄ solutions was studied at temperatures between 170 and 250°C; the overall conversion reaction is given by equation (4). Figure 1 presents the compositions of the products made in the absence of hematite seed. In these experiments, the product yield remained essentially constant at 35 g at temperatures <210°C, but decreased progressively to 10 g as the temperature increased from 210 to 250°C. The composition of the products remained nearly constant as the temperature increased up to 210°C, and X-ray diffraction analysis of these products detected only K jarosite. At 220, 230 and 240°C, the composition changed, and X-ray diffraction analysis of these products detected major amounts of both K jarosite and hematite. X-ray diffraction analysis of the 250°C conversion product detected dominant hematite with lesser amounts of K jarosite. These results follow

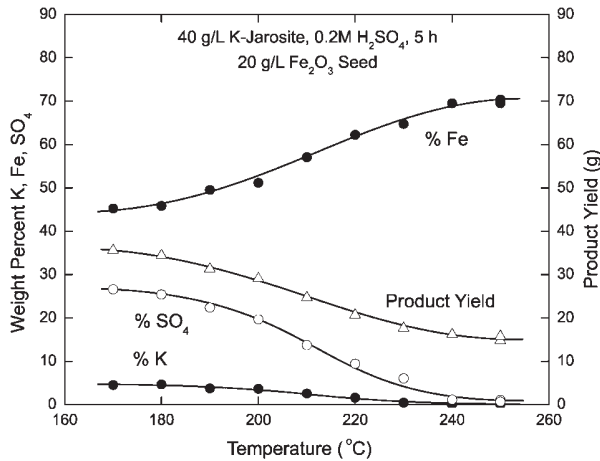


1 Effect of reaction temperature on composition of products made during hydrothermal conversion of K jarosite (6.86%K, 33.28%Fe and 39.21%SO₄) after 5 h of reaction in 0.2M H₂SO₄ solutions, in absence of Fe₂O₃ seed

the same trends as those obtained previously for the hydrothermal conversion of Na jarosite,⁹ with the notable difference that significant hydrothermal conversion of Na jarosite occurred at temperatures >190°C. In the potassium jarosite system, in the absence of Fe₂O₃ seed, hematite was not produced in dominant amounts except at temperatures >240°C, and this observation is consistent with the greater thermodynamic stability of K jarosite.³ Thus, the hydrothermal conversion of K jarosite to hematite, in the absence of Fe₂O₃ seed, occurs at higher temperatures than the conversion of Na jarosite.



The effect of the temperature on the hydrothermal conversion of 40 g L⁻¹ of K jarosite after 5 h of reaction in 0.2M H₂SO₄ solutions, but in the presence of 20 g L⁻¹ Fe₂O₃ seed, was also investigated. Figure 2 shows the effect of reaction temperatures between 170 and 250°C on the product yield (weight of the precipitate obtained minus the weight of Fe₂O₃ seed added) and product composition when 40 g L⁻¹ of K jarosite was heated in the presence of 20 g L⁻¹ of Fe₂O₃ seed. The product yield decreased progressively as the temperature increased, and nearly constant product yields are noted at temperatures >240°C, suggesting the nearly complete conversion of K jarosite to hematite at these temperatures. X-ray diffraction analyses of the products made in the 170–220°C temperature range detected major amounts of both K jarosite and hematite. At 230°C, the product consisted of major hematite with minor K jarosite. Finally, only hematite was detected at 240 and 250°C, and the terminal compositions of ~70%Fe, ~1%SO₄ and <0.04%K are consistent with

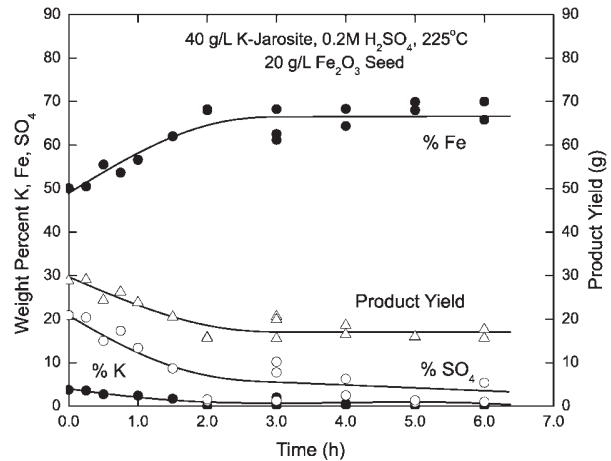


2 Effect of reaction temperature on amount and composition of products made during hydrothermal conversion of K jarosite (6.86%K, 33.28%Fe and 39.21%SO₄) after 5 h of reaction in 0.2M H₂SO₄ solutions, but in presence of 20 g L⁻¹ of Fe₂O₃ seed

that of hematite. The comparison of the data of Fig. 2 with those of Fig. 1 indicates the significant beneficial effect of hematite seed additions on the hydrothermal conversion of K jarosite to hematite. Relative to the results obtained for the hydrothermal conversion of Na jarosite in the presence of 20 g L⁻¹ Fe₂O₃ seed, K jarosite is more stable and persists under conditions where Na jarosite is extensively converted to hematite.⁹ For example, Na jarosite was entirely converted to hematite at 200°C, whereas K jarosite did not react completely until 240–250°C.

The SEM–EDX analysis of several of the products generated during the hydrothermal conversion of the K jarosite in the presence of Fe₂O₃ seed showed the hematite to consist of spheroidal or subspheroidal masses 10–100 μm in diameter. The spheroidal masses likely are composed very small individual particles (nanoparticles?). The morphology is similar to that observed when hematite was precipitated directly from homogeneous solutions at 225°C.¹⁶ The EDX analysis of the hematite products detected dominant amounts of Fe, and commonly, trace amounts of S, which seems to be present as adsorbed SO₄. Similar SEM–EDX analyses were carried out on several of the other hematite products produced in this study, and all had similar morphologies and compositions.

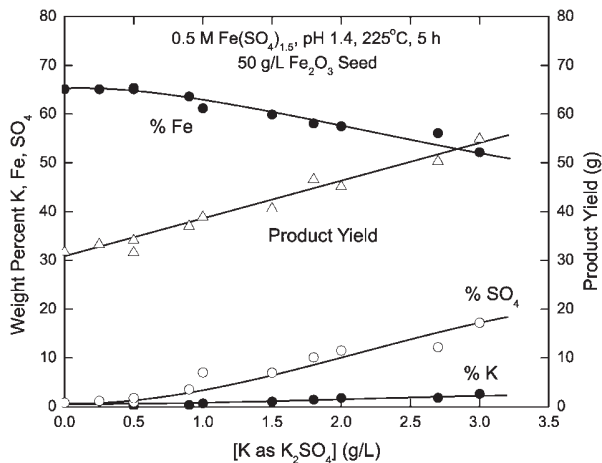
The effect of retention time at temperature on the hydrothermal conversion of 40 g L⁻¹ of K jarosite at 225°C in 0.2M H₂SO₄ solutions, in the presence of 20 g L⁻¹ Fe₂O₃ seed, was also studied. The retention times ranged between 0 and 6 h, and zero time was taken to be the moment when the temperature reached 225°C, ~45 min after heating of the autoclave began. As shown in Fig. 3, the product yields and the K, Fe and SO₄ contents vary constantly over the first 2 h of reaction, but remain essentially constant for retention times between 2 and 6 h. Guinier X-ray diffraction analysis of the products made at retention times between 0 and



3 Variation in product yield and product composition with increasing retention time at temperature when 40 g L⁻¹ of K jarosite (6.86%K, 33.28%Fe and 39.21%SO₄) was reacted at 225°C in 0.2M H₂SO₄ solutions in presence of 20 g L⁻¹ of Fe₂O₃ seed

1.5 h, detected major amounts of both K jarosite and hematite. The products made at retention times between 2 and 6 h were shown to consist mainly of hematite with trace amounts of K jarosite. The results indicate that the hydrothermal conversion of K jarosite to hematite, in the presence of 20 g L⁻¹ Fe₂O₃ seed, is practically complete within 2 h at 225°C, and that longer retention times have little effect on the reaction. A retention time of only ~0.5 h was adequate for the complete hydrothermal conversion of Na jarosite at 225°C in the presence of 20 g L⁻¹ of Fe₂O₃ seed,⁹ and the difference is consistent with the greater stability of K jarosite and the need for more aggressive conditions to effect hydrothermal conversion of K jarosite to hematite.

Complementary experiments were also carried out wherein potassium jarosite was formed *in situ* in the autoclave, during the ~45 min heat-up period and the 5 h retention time at 225°C. The experiments were intended to assess the rate of K jarosite precipitation relative to the rate of K jarosite conversion to hematite. In these experiments, 0.5M Fe(SO₄)_{1.5} solutions at pH 1.4 and containing various concentrations of K as K₂SO₄ were heated to 225°C in the presence of 50 g L⁻¹ of Fe₂O₃ seed. Previous studies, done in the absence of Fe₂O₃ seed,¹⁰ indicated that extensive potassium jarosite precipitation would occur rapidly under these conditions. Figure 4 shows that increasing K concentrations (added as K₂SO₄) systematically increase the product yield, and the K, Fe and SO₄ contents of the various products. Such dependences are expected given the elevated 0.5M Fe(SO₄)_{1.5} concentration and the moderate K concentrations involved. That is, there is always an initial excess of ferric ions to potassium for the precipitation of K jarosite. For K concentrations up to 0.5 g L⁻¹, the K, Fe and SO₄ contents remain nearly constant. This observation is consistent with the Guinier X-ray diffraction analyses which detected only hematite in the products formed from solutions containing 0 and

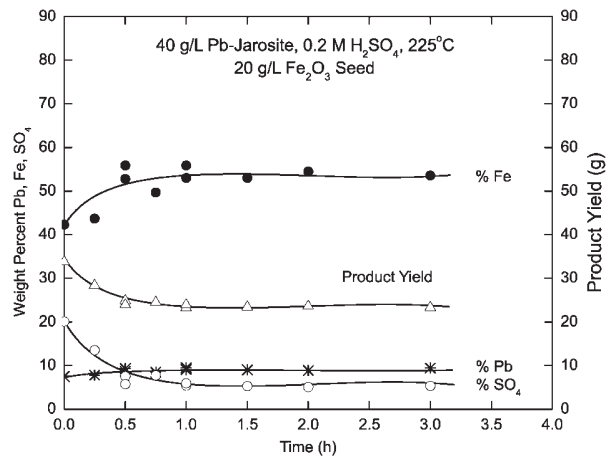


4 Influence of concentration of K, added as K₂SO₄, on amount and composition of products formed after 5 h of reaction at 225°C from 0.5M Fe(SO₄)_{1.5} solutions at pH 1.5, and in presence of 50 g L⁻¹ of Fe₂O₃ seed

0.25 g L⁻¹ K, and hematite with a trace amount of K jarosite in the product formed from the 0.5 g L⁻¹ K solution. The Guinier X-ray diffraction analyses also indicated the progressive abundance of K jarosite in the products made as the K concentration of the solution increased. Extensive precipitation of K jarosite certainly occurred during the ~45 min autoclave heat-up period.¹⁰ When only small amounts of K jarosite formed, the jarosite was extensively converted to hematite, and part of the initial 0.5M Fe(SO₄)_{1.5} concentration precipitated as hematite. As the concentration of K increased >0.5 g L⁻¹, more K jarosite precipitated, and much of this jarosite persisted (or repeatedly reprecipitated) during the 5 h retention period, despite the 225°C reaction temperature and the presence of Fe₂O₃ seed. As a result, the products consist of major amounts of K jarosite and hematite, some of which was initially added as seed. The implication is that the rate of K jarosite precipitation is faster than the rate of hydrothermal conversion of K jarosite to hematite. As a consequence, K jarosite is reprecipitated continuously from the K₂SO₄ liberated by the hydrothermal conversion reaction (equation (4)) and the elevated ferric ion concentration present in these experiments.

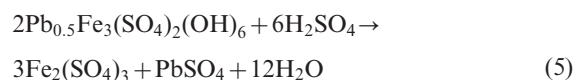
Lead jarosite

The effect of retention time on the conversion of 40 g L⁻¹ of Pb jarosite at 225°C in 0.2M H₂SO₄ solutions, in the presence of 20 g L⁻¹ Fe₂O₃ seed, was also studied. Figure 5 shows the product yield and the Pb, Fe and SO₄ contents of the solids generated. The Pb content of the zero time sample was ~8% but it increased gradually to ~9.8%Pb after 0.75 h at temperature. The SO₄ contents decreased from 20% in the zero time product to ~5% after 0.75 h of reaction. These results are consistent with the precipitation of insoluble PbSO₄ during the hydrothermal conversion of Pb jarosite to hematite. In this regard, X-ray diffraction analysis of the products generated for retention times

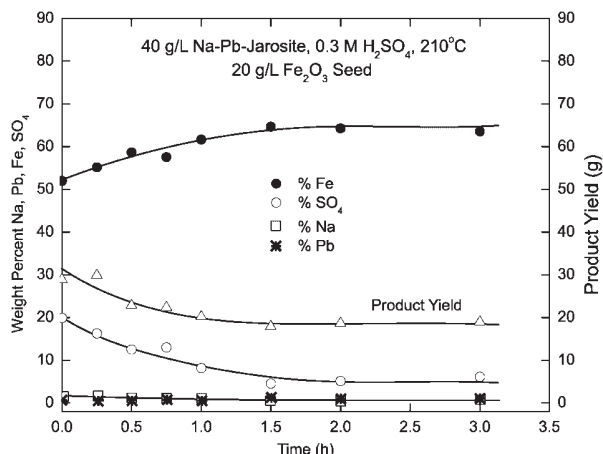


5 Effect of retention time on product yield and product composition when 40 g L⁻¹ of Pb jarosite (9.87%Pb, 30.1%Fe and 37.17%SO₄) was subjected to hydrothermal conversion at 225°C in 0.2M H₂SO₄ solutions, in presence of 20 g L⁻¹ Fe₂O₃ seed

between 0 and 0.75 h showed the presence of Fe₂O₃, PbSO₄ and Pb jarosite. X-ray diffraction analysis of a product made after 1 h of reaction at temperature detected Fe₂O₃, PbSO₄ and a trace amount of Pb jarosite, but only Fe₂O₃ and PbSO₄ were observed in a replicate experiment. Finally, only Fe₂O₃ and PbSO₄ were detected in the products generated using retention times between 1.5 and 3 h. These observations indicate that Pb jarosite is rapidly converted to hematite and insoluble PbSO₄ when heated to 225°C in moderately acidic media and in the presence of Fe₂O₃ seed. The comparison with Fig. 3 indicates that the hydrothermal conversion of Pb jarosite to hematite in the presence of 20 g L⁻¹ Fe₂O₃ seed is faster than the analogous reaction of K jarosite, which required ~2 h for the essentially complete conversion. In contrast, the time required for the complete conversion of Pb jarosite is similar to that reported previously for the complete conversion of Na jarosite to hematite at 225°C in the presence of 20 g L⁻¹ of Fe₂O₃ seed.⁹ However, unlike soluble K₂SO₄ and Na₂SO₄ which are generated during the hydrothermal conversion of K jarosite and Na jarosite (equations (3) and (4)), PbSO₄ is essentially insoluble and accumulates in the product along with any residual Pb jarosite (equation (5)). To confirm this assumption, 10 mass balances for Pb were carried out. Between 95 and 103% of the Pb initially present in the Pb jarosite was calculated to remain in the solid products, and the modest differences are likely due to various experimental errors and analytical imprecision.



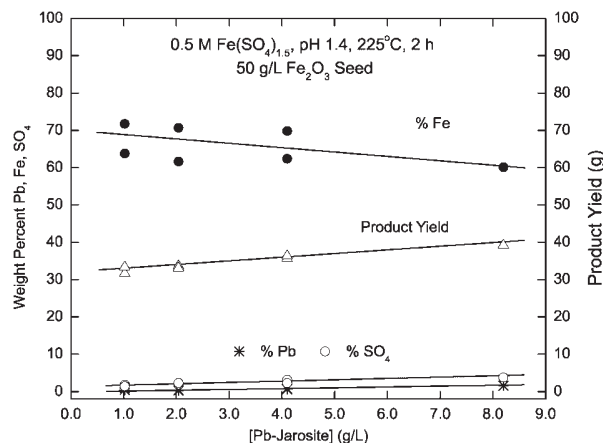
The effect of the retention time at temperature on the conversion of 40 g L⁻¹ of Na-Pb jarosite, together with 20 g L⁻¹ of Fe₂O₃ seed, at 210°C in 0.3M H₂SO₄ solutions was also studied. Figure 6 illustrates the



6 Variation in product yield and product composition when 40 g L^{-1} of Na-Pb jarosite (2.99%Na, 0.81%Pb, 33%Fe and 40%SO₄) was subjected to hydrothermal conversion for various times at 210°C in 0.3M H₂SO₄ solutions, and in presence of 20 g L^{-1} Fe₂O₃ seed

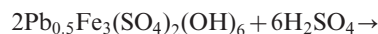
product yields and product compositions realised for retention times ranging from 0 to 3 h. The compositional data given in Fig. 6 are consistent with the X-ray diffraction analyses. X-ray diffraction analysis of the products made at retention times of 0, 0.25, 0.5 and 0.75 h indicated Fe₂O₃, Na jarosite and a trace amount of PbSO₄. The presence of PbSO₄ in the zero time product indicates that the hydrothermal conversion of Na-Pb jarosite to hematite and PbSO₄ begins during the heat-up period. X-ray diffraction analysis of the products made after 1, 1.5, 2 and 3 h detected Fe₂O₃, a minor amount of Na jarosite and a trace of PbSO₄. The trace amount of PbSO₄ detected in all the X-ray diffraction analyses is consistent with the relatively low 0.7–0.9%Pb contents of all the conversion products. Mass balance calculations for Pb indicated that between 96 and 105% of the Pb initially present in the Na-Pb jarosite reported to the conversion products, and the minor differences are likely due to various experimental and analytical errors. Overall, these results indicate that the hydrothermal conversion of the Na-Pb jarosite to hematite and PbSO₄ occurs at 210°C in the presence of hematite seed. Because of the 210°C temperature used for these experiments, the extent of Na-Pb jarosite conversion at a given time is not as great as that observed for the hydrothermal conversion of Pb jarosite at 225°C and also in the presence 20 g L^{-1} Fe₂O₃ seed. However, the hydrothermal conversion of either Na-Pb jarosite or Pb jarosite proceeds more rapidly than the hydrothermal conversion of K jarosite which, for example, requires at least 2 h at 225°C and the presence of Fe₂O₃ seed to proceed to completion.

A few experiments were also carried out wherein various concentrations of lead jarosite, together with 50 g L^{-1} of hematite seed, were heated to 225°C in 0.5M Fe(SO₄)_{1.5} solutions at pH 1.4. The slurries were then held at 225°C for 2 h to assess the hydrothermal conversion of Pb jarosite in moderately concentrated ferric ion solutions. Figure 7 illustrates the product



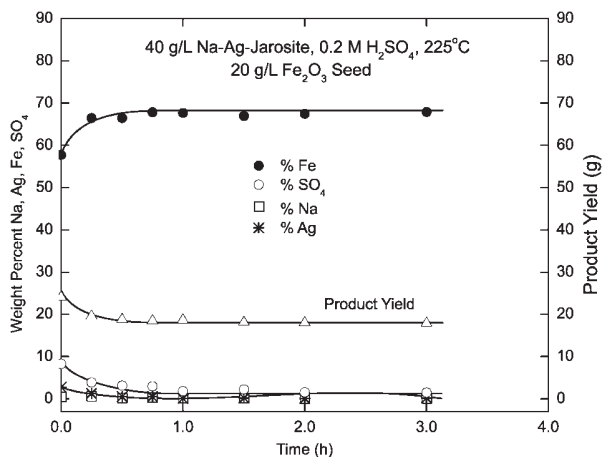
7 Variation in product yield and product composition when various concentrations of Pb jarosite, together with 50 g L^{-1} of Fe₂O₃ seed, were reacted for 2 h at 225°C in 0.5M Fe(SO₄)_{1.5} solutions at pH 1.4

yields and product compositions obtained in these experiments. As would be expected, the Pb contents increase in an essentially linear manner, from 0.15 to 1.6%Pb as the concentration of Pb jarosite rises from 1.0 to 8.0 g L⁻¹. Guinier X-ray diffraction analysis showed the products made in the presence of 1.0 and 2.0 g L⁻¹ of Pb jarosite to consist of hematite, Pb jarosite and a trace amount of PbSO₄. The products formed in the presence of 4.0 or 8.0 g L⁻¹ Pb jarosite contained hematite, Pb jarosite and a minor quantity of PbSO₄. The comparison with the data of Fig. 5 seems to indicate that the presence of dissolved Fe(SO₄)_{1.5} inhibits the hydrothermal conversion of Pb jarosite, and likely other jarosite species as well. Although part of the initial 0.5M Fe(SO₄)_{1.5} precipitates as hematite at the 225°C reaction temperature, with the generation of hydrolysis acid (equation (6)), the remaining solution still contains a sufficiently high Fe(SO₄)_{1.5} concentration to inhibit the decomposition of the Pb jarosite and/or to form Pb jarosite from any PbSO₄ which is generated (equation (7)). This hypothesis is supported by the observation that the addition of 2.0 g L^{-1} of PbSO₄ to the 0.5M Fe(SO₄)_{1.5} solution, in the absence of any initially added Pb jarosite, resulted in significant Pb jarosite formation during the ~45 min heat-up period of the autoclave and the persistence of that Pb jarosite during the 2 h retention time at 225°C.



Sodium-silver jarosite

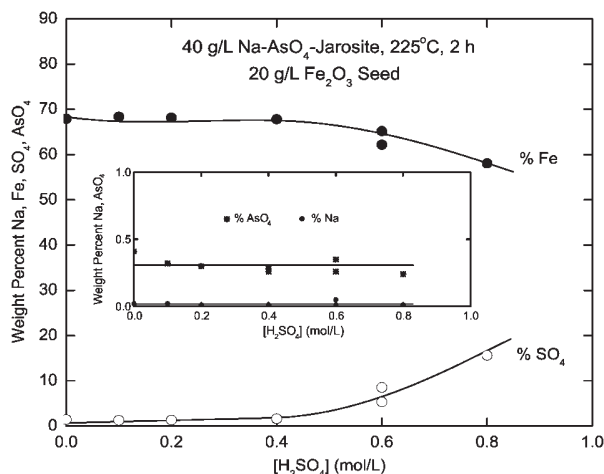
The effect of retention times between 0 and 3 h on the hydrothermal conversion of 40 g L^{-1} of Na-Ag jarosite, with 20 g L^{-1} of Fe₂O₃ seed, at 225°C in 0.2M H₂SO₄ solutions was also studied. Figure 8 shows the product yields and product compositions realised in these



8 Effect of retention time on product yield and product composition when 40 g L⁻¹ of Na-Ag jarosite (2.13%Na, 4.74%Ag, 31.6%Fe and 39.0%SO₄) was subjected to hydrothermal conversion at 225°C in 0.2M H₂SO₄ solutions, and in presence of 20 g L⁻¹ Fe₂O₃ seed

experiments, which are essentially constant for retention times between 0.5 and 3 h. The Ag content of the zero time sample was 2.8%, but the Ag content fell to 0.09% in the 0.25 h product and to 0.02–0.03%Ag in the products generated after 2 or 3 h of reaction at 225°C. These results indicate that the Ag content of the Na–Ag jarosite dissolves during hydrothermal conversion and collects in the final solution. In fact, a mass balance for Ag was carried out for an experiment done for 2 h at 225°C in the presence of 20 g L⁻¹ of Fe₂O₃ seed. It was calculated that 95% of the Ag initially present in the Na–Ag jarosite reported to the final solution and only 4% of the initial Ag remained in the final product. However, the dissolved Ag is readily precipitated, and it was demonstrated that the addition of 10 g L⁻¹ of either elemental sulphur or sphalerite (ZnS) to the autoclave resulted in the nearly total precipitation of all the dissolved Ag. In both those experiments, the concentration of Ag in the final solution was <0.1 mg L⁻¹.

The Guinier X-ray diffraction analyses showed the products made after 0, 0.25 and 0.5 h to consist of major Fe₂O₃ and a very minor amount of Na jarosite. X-ray diffraction analysis of the products generated for retention times of 0.75–3 h detected Fe₂O₃ and a trace quantity of Na jarosite. The compositional data and the X-ray diffraction results indicate that part of the Na–Ag jarosite was converted to hematite during the ~45 min heat-up period. For example, the Ag contained in the 0 h reaction product (2.8%Ag) was 64% of that present in the initial Na–Ag jarosite. After 0.25 h of reaction, the value was 26%, after 0.75 h of reaction it was 10% and after 1 h of reaction it was only 3% of the amount of Ag initially present in the Na–Ag jarosite. The hydrothermal conversion of Na–Ag jarosite at 225°C in the presence of 20 g L⁻¹ Fe₂O₃ seed is as fast as the conversion of Pb jarosite under the same conditions. Both jarosite species react extensively during the heat-up period and both are largely converted to hematite within

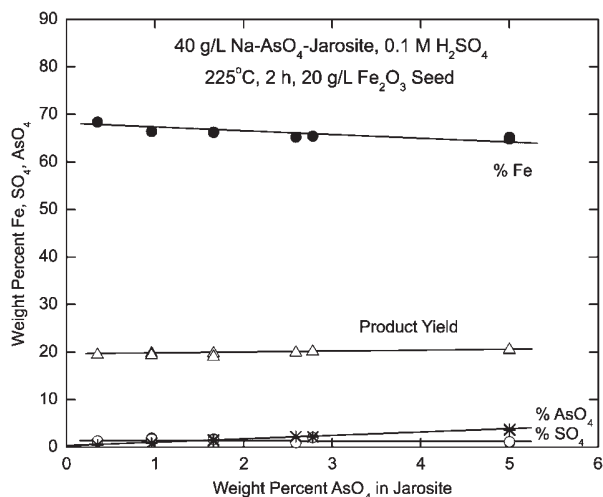


9 Effect of H₂SO₄ concentration on amount and composition of products formed when 40 g L⁻¹ of AsO₄ bearing Na jarosite (4.14%Na, 33.54%Fe, 39.1%SO₄ and 0.35%AsO₄) was reacted for 2 h at 225°C in presence of 20 g L⁻¹ of reagent Fe₂O₃ seed

0.75 h at temperature. A similar retention time (~0.5 h) is required for the hydrothermal conversion of Na jarosite at 225°C in the presence of 20 g L⁻¹ of Fe₂O₃ seed.⁹ Moreover, the hydrothermal conversion of all of these jarosite type compounds proceeds more rapidly than the conversion of K jarosite to hematite which requires a 2 h retention time at 225°C.

Arsenate containing sodium jarosite

Several batches of AsO₄ containing sodium jarosite were prepared using the conditions described in the section on 'Experimental'. The various batches were blended to yield a product which analysed 4.14%Na, 33.54%Fe, 39.1%SO₄ and 0.35%AsO₄, and was shown by X-ray diffraction analysis to consist of Na jarosite only. Figure 9 illustrates the effect of the H₂SO₄ concentration on the amount and composition of the products formed when 40 g L⁻¹ of the AsO₄ bearing Na jarosite was reacted for 2 h at 225°C in the presence of 20 g L⁻¹ of reagent Fe₂O₃ seed. In these experiments, the product yield decreased slightly from 20 to 17 g as the acid concentration increased from 0.0 to 0.8M H₂SO₄. As shown in the inserted figure, the Na contents remained essentially constant at 0.02%, and the AsO₄ contents varied randomly from 0.26 to 0.41% as the H₂SO₄ concentration increased from 0.0 to 0.8M. X-ray diffraction analysis of the products made from solutions containing 0.0–0.4M H₂SO₄ detected only hematite whereas the products made from the more acidic solutions consisted of hematite together with increasing amounts of Fe(SO₄)(OH) and occasional trace quantities of sodium jarosite. Scorodite was not detected in any of the products. Mass balances for AsO₄ were carried out, and the amounts of AsO₄ in the solid plus solution phases were within ±5% of the initially added quantity. It was calculated that the percentage of the initially added AsO₄ retained in the solid product decreased from 95 to 68% as the H₂SO₄ concentration increased from

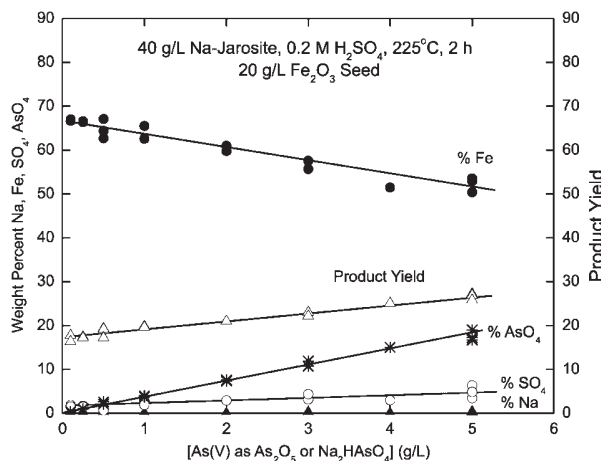


10 Variation in product yield and product composition when 40 g L^{-1} of AsO_4 bearing Na jarosite, having AsO_4 contents ranging from 0.35 to 5.00%, was reacted for 2 h at 225°C in $0.1\text{M H}_2\text{SO}_4$ media and in presence of 20 g L^{-1} of reagent Fe_2O_3 seed

0.0 to 0.8M . Thus, it appears that small amounts of arsenate can be incorporated in the hematite structure or that arsenate can be strongly adsorbed on the hematite nanocrystals. It is also evident from the X-ray diffraction results and the consistently low Na contents that the elevated SO_4 contents of some of these products are mostly due to the presence of $\text{Fe}(\text{SO}_4)(\text{OH})$.

Similar blended batches of Na jarosite containing 0.35, 0.96, 1.66, 2.59, 2.78 and 5.00% AsO_4 were prepared at 150°C from $0.3\text{M Fe}(\text{SO}_4)_{1.5}$ and $0.2\text{M Na}_2\text{SO}_4$ solutions containing from 0.33 to 1.5 g L^{-1} of As(V) , added as Na_2HAsO_4 . X-ray diffraction analysis showed all the blended products to consist only of Na jarosite, and this finding is consistent with a previous study of AsO_4 containing Na jarosite.¹⁵ To assess the effect of the AsO_4 content on the conversion of sodium jarosite to hematite, 40 g L^{-1} of the each blended batch of the AsO_4 bearing Na jarosite were reacted for 2 h at 225°C in $0.1\text{M H}_2\text{SO}_4$ media and in the presence of 20 g L^{-1} of reagent Fe_2O_3 seed. As shown in Fig. 10, the AsO_4 contents of the products increased linearly from 0.41 to 3.70% as the initial AsO_4 content of the blended Na jarosite increased from 0.35 to 5.00% , whereas the Na contents were $<0.06\%$. In all instances, X-ray diffraction analysis of the products detected only hematite, again suggesting that arsenate is either strongly adsorbed on the hematite nanocrystals or is incorporated in the hematite structure.

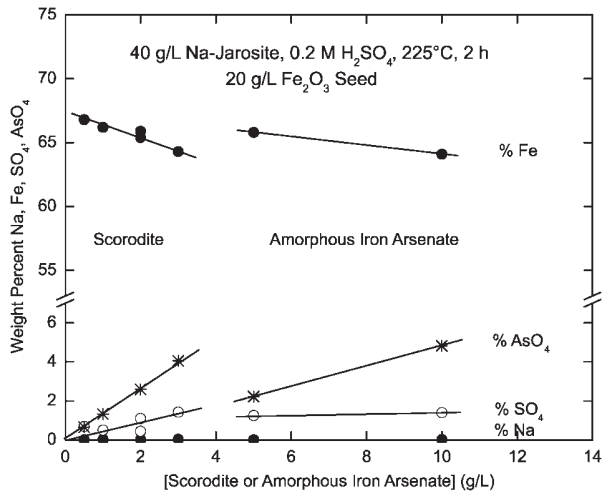
A related series of experiments were carried out wherein AsO_4 free sodium jarosite, containing 4.21% Na, 33.37% Fe and 39.39% SO_4 was reacted in the presence of various concentrations of dissolved As(V) . Figure 11 illustrates the effect of the dissolved As(V) concentration on the product yields and compositions realised when 40 g L^{-1} of AsO_4 free sodium jarosite was reacted for 2 h at 225°C in $0.2\text{M H}_2\text{SO}_4$ solutions also containing 20 g L^{-1} of reagent Fe_2O_3 seed. As the concentration



11 Effect of dissolved As(V) concentration on product yields and product compositions realised when 40 g L^{-1} of AsO_4 free sodium jarosite (4.21% Na, 33.37% Fe and 39.39% SO_4) was reacted for 2 h at 225°C in $0.2\text{M H}_2\text{SO}_4$ solutions, also containing 20 g L^{-1} of reagent Fe_2O_3 seed

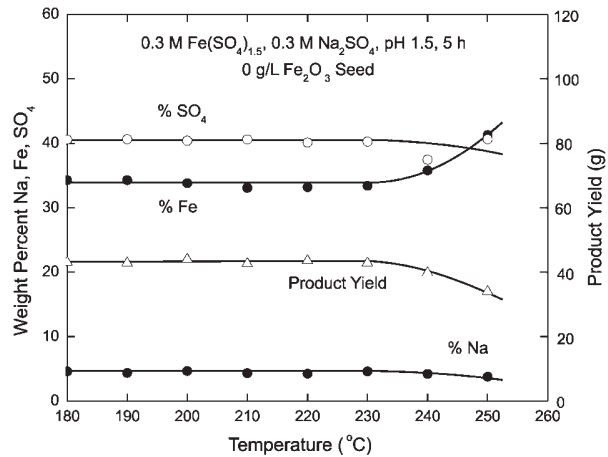
of As(V) increased from 0.1 to 5.0 g L^{-1} , the AsO_4 contents of the products increased in a linear manner to almost 20% . The Na contents are 0.02 – 0.37% , indicating the extensive conversion of the Na jarosite to other phases. X-ray diffraction analysis detected only hematite in the products made from solutions containing $<0.5 \text{ g L}^{-1}$ As(V) . The products made from 1.0 g L^{-1} As(V) solutions consisted of hematite with trace amounts of sodium jarosite. The products made from the more concentrated As(V) solutions contained progressively increasing amounts of scorodite in addition to trace or minor amounts of Na jarosite, and it is known that scorodite can incorporate several per cent SO_4 in its structure.¹⁷ This behaviour is different from that observed when the As(V) was initially present in the structure of the Na jarosite (Fig. 10), but the reasons for the differences are not well understood. Mass balances for As were also carried out, but the mass balances only closed to within -7 to $+14\%$ of the initially present As(V) . Nevertheless, the mass balances suggested that $\sim 88\%$ of the initially added As(V) reported to the solid product regardless of the As(V) concentration involved. In contrast, the percentage of As(V) remaining in the final solution seemed to decrease progressively from 18% to 7 – 8% as the As(V) concentration increased from 0.1 to 5.0 g L^{-1} .

In addition to As containing jarosite, commercial jarosite precipitates could also contain minor amounts of scorodite ($\text{FeAsO}_4 \cdot 2\text{H}_2\text{O}$) and/or amorphous iron arsenate. It is desirable to determine the behaviour of these species during the conversion of jarosite type compounds to hematite, and accordingly, some preliminary experiments were carried out using these species. In the first series of experiments, various amounts of synthetic scorodite¹⁸ were mixed with 40 g L^{-1} of As free sodium jarosite in $0.2\text{M H}_2\text{SO}_4$ solution, and the mixture was reacted for 2 h at 225°C in the presence of 20 g L^{-1} of reagent Fe_2O_3 seed. In the second set of



12 Effect of concentration of scorodite and amorphous iron arsenate on Na, Fe, SO₄ and AsO₄ contents of products made when 40 g L⁻¹ of AsO₄ free Na jarosite was reacted for 2 h at 225°C in 0.2M H₂SO₄ media and in presence of 20 g L⁻¹ of reagent Fe₂O₃ seed

experiments, various amounts of amorphous iron arsenate (prepared at 60°C from 0.5M Fe(SO₄)_{1.5} and 0.1M Na₂HAsO₄ solutions and containing 43.3%Fe, 23.7%AsO₄ and 4.19%SO₄) were also mixed with 40 g L⁻¹ of As free sodium jarosite and reacted under the same conditions. The product yield increased in an essentially linear manner from 19 to 22 g as the scorodite addition increased from 0.0 to 3.0 g L⁻¹, and Fig. 12 illustrates the compositions of the various products. X-ray diffraction analysis of these products detected hematite together with trace amounts of sodium jarosite, and these observations are consistent with the <0.06%Na contents. Significantly, no scorodite was detected in any of these products, and this indicates the complete dissolution of the scorodite and the subsequent reprecipitation of the dissolved iron and most of the initially present arsenate as hematite. In fact, mass balances for arsenic indicated that 86–95% of the initially present AsO₄ remained in the final products. However, the addition of greater amounts of scorodite (results not shown) resulted in significant increases in the Na and SO₄ contents, and X-ray diffraction analysis of those products detected major amounts of sodium jarosite and traces of scorodite. Clearly, the presence of significant amounts of scorodite somehow inhibits the hydrothermal conversion of Na jarosite to hematite, but this aspect requires more detailed investigation. Figure 12 also illustrates the composition of the products generated in the presence of 5 or 10 g L⁻¹ of the amorphous iron arsenate. As the amount of added amorphous iron arsenate increases, the Fe content decreases slightly and the SO₄ content increases to a moderate degree. There is a relatively significant increase in the AsO₄ content that is consistent with the increase in the product yield from 23 to 27 g. Guinier X-ray diffraction analysis of these products detected hematite, with a very faint trace of sodium jarosite that is consistent with the <0.02%Na contents. Increasing the amount of amorphous iron arsenate



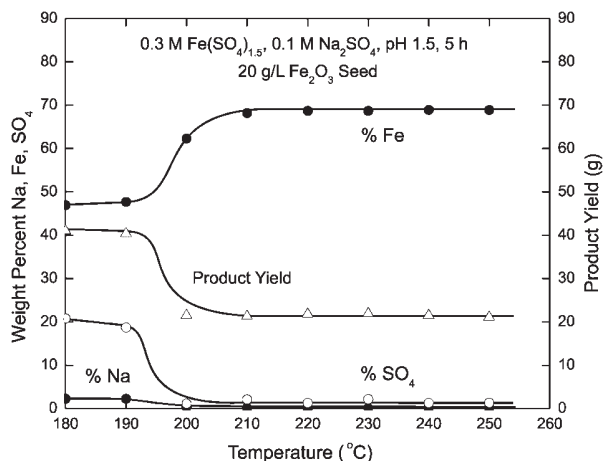
13 Product yields and compositions of products made when 0.3M Fe(SO₄)_{1.5} and 0.3M Na₂SO₄ solutions at pH 1.5 were reacted for 5 h in absence of Fe₂O₃ seed

to 20 g L⁻¹ generated a product containing 1.23%Na, 54.1%Fe, 12.5%SO₄ and 6.67%AsO₄ that was shown by X-ray diffraction analysis to consist of major amounts of both hematite and sodium jarosite. In all instances, however, ~90% of the AsO₄ initially present in the amorphous iron arsenate remained in the solid phase, and this indicates that the amorphous iron arsenate dissolves completely during reaction but that the arsenate reprecipitates with the hematite.

In situ formed sodium jarosite

An earlier study discussed the hydrothermal conversion of previously precipitated Na jarosite at elevated temperatures.⁹ To extend those observations, complementary experiments were carried out wherein sodium jarosite was formed *in situ* in the autoclave, during the ~45 min heat-up period and retention time at temperature. The experiments were intended to shed additional light on rate of Na jarosite precipitation relative to the rate of conversion of the Na jarosite to hematite. Figure 13 shows the effect of increasing temperature on the yield and composition of the products formed when 0.3M Fe(SO₄)_{1.5} and 0.3M Na₂SO₄ solutions at pH 1.5 were reacted for 5 h and in the absence of initially added Fe₂O₃ seed. Guinier X-ray diffraction analysis detected dominant amounts of *in situ* formed Na jarosite in the products made at temperatures between 180 and 230°C. Although trace amounts of hematite were sometimes detected in the products made at temperatures <230°C, the precipitates formed at 240 and 250°C consisted of Na jarosite together with minor amounts of hematite. The presence of minor quantities of hematite explains the decreasing product yields at temperatures of 240 and 250°C, and also the changes in the Na, Fe and SO₄ contents of the precipitates formed at the highest temperatures.

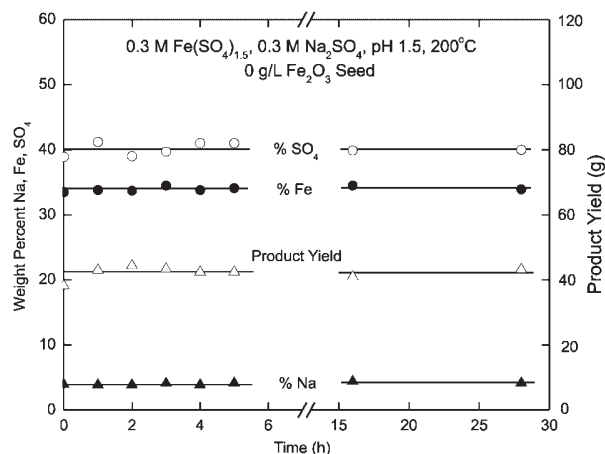
Similar experiments were also carried out to investigate the effect of increasing temperature on the yield and composition of the products formed when 0.3M Fe(SO₄)_{1.5} and 0.1M Na₂SO₄ solutions at pH 1.5 were



14 Product yields and compositions of products made when 0.3M $\text{Fe}(\text{SO}_4)_{1.5}$ and 0.1M Na_2SO_4 solutions at pH 1.5 were reacted for 5 h at various temperatures in presence of 20 g L^{-1} of Fe_2O_3 seed

reacted for 5 h at temperatures between 180 and 250°C, but in the presence of 20 g L^{-1} of initially added Fe_2O_3 seed. The product yields and compositions are shown in Fig. 14. X-ray diffraction analysis of the products made at 180 and 190°C detected major amounts of both hematite and Na jarosite, whereas hematite with minor Na jarosite was evident in the product generated at 200°C. However, only hematite was detected in the products made in the temperature range of 210–250°C, and this observation is consistent with the <0.14%Na content of these products. Figures 13 and 14 indicate that Na jarosite forms *in situ* during the ~45 min heat-up period and the retention time at temperature. In the absence of Fe_2O_3 seed, the *in situ* formed Na jarosite is relatively stable at temperatures up to 230°C, and only minor hydrothermal conversion to hematite takes place at 240 and 250°C. The addition of 20 g L^{-1} of Fe_2O_3 seed significantly accelerates the hydrothermal conversion of the *in situ* formed Na jarosite such that dominant hematite formation occurs after 5 h of reaction at temperatures >210°C. The above results are generally consistent with those obtained when previously synthesised Na jarosite was subjected to hydrothermal conversion reacted under approximately the same conditions, although the previously synthesised Na jarosite seems to react to a greater degree at temperatures <200°C, in both the presence and absence of Fe_2O_3 seed.⁹

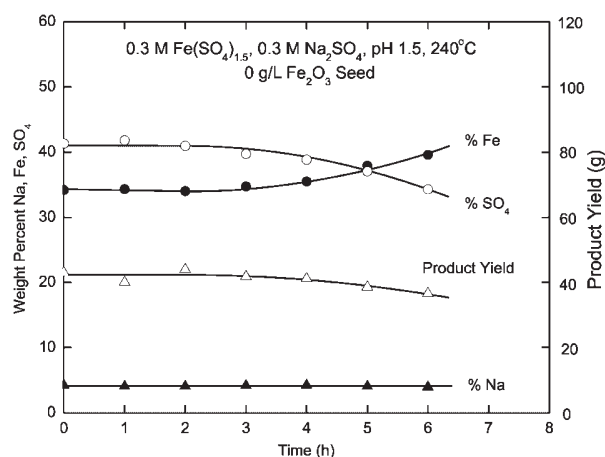
The above discussion suggests that the hydrothermal conversion of Na jarosite to hematite proceeds slowly in the absence of Fe_2O_3 seed. This point is further illustrated in Fig. 15 which presents the yields and compositions of the products made when 0.3M $\text{Fe}(\text{SO}_4)_{1.5}$ and 0.3M Na_2SO_4 solutions at pH 1.5 were reacted for various times at 200°C in the absence of Fe_2O_3 seed. The Na, Fe and SO_4 contents remained essentially constant for all the retention times, and the compositions are characteristic of that of Na jarosite. These observations are consistent with the Guinier X-ray diffraction analyses which detected only Na jarosite



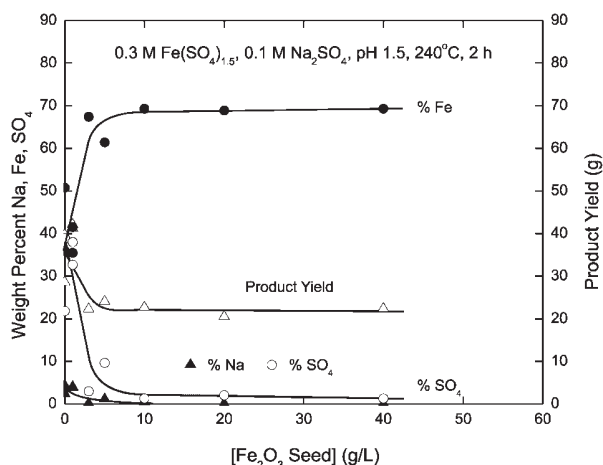
15 Product yields and composition of products made when 0.3M $\text{Fe}(\text{SO}_4)_{1.5}$ and 0.3M Na_2SO_4 solutions at pH 1.5 were reacted for various times at 200°C in absence of Fe_2O_3 seed

in the products made after 0, 1, 2 and 4 h of reaction, and Na jarosite with a very faint trace of hematite in the products made after 3 and 5 h of reaction. The products made after 16 and 28 h of reaction consisted of Na jarosite with a trace amount of hematite.

Somewhat more rapid reaction is achieved at 240°C, as illustrated in Fig. 16 which shows the product yield and composition of the products made when 0.3M $\text{Fe}(\text{SO}_4)_{1.5}$ and 0.3M Na_2SO_4 solutions at pH 1.5 were reacted for various times at 240°C in the absence of Fe_2O_3 seed. Guinier X-ray diffraction analyses showed that the products formed during the first 3 h of reaction to consist of Na jarosite with occasional faint trace amounts of Fe_2O_3 . The products formed after 4–6 h of reaction consisted of Na jarosite with minor amounts of Fe_2O_3 . The comparison of the above results with those generated when previously precipitated Na jarosite was reacted at 225–240°C⁹ indicates that previously



16 Effect of retention time on product yield and composition of products made when 0.3M $\text{Fe}(\text{SO}_4)_{1.5}$ and 0.3M Na_2SO_4 solutions at pH 1.5 were reacted for various times at 240°C in absence of Fe_2O_3 seed



17 Effect of amount of initially added Fe_2O_3 seed on yield and composition of products made when 0.3M $\text{Fe}(\text{SO}_4)_{1.5}$ and 0.1M Na_2SO_4 solutions at pH 1.5 were reacted for 2 h at 240°C

precipitated Na jarosite seems to react more rapidly than *in situ* generated Na jarosite, at least in the absence of Fe_2O_3 seed. As was the situation for the hydrothermal conversion of K jarosite, the implication is that the rate of Na jarosite precipitation is faster than the rate of hydrothermal conversion of Na jarosite to hematite. As a result, Na jarosite is reprecipitated continuously from the Na_2SO_4 liberated by the hydrothermal conversion reaction (equation (3)) and the Na jarosite tends to accumulate in the autoclave product.

The above results indicate that the presence of hematite seed significantly promotes the hydrothermal conversion of *in situ* formed Na jarosite, and this aspect was systematically investigated. In these experiments, 0.3M $\text{Fe}(\text{SO}_4)_{1.5}$ and 0.1M Na_2SO_4 solutions at pH 1.5 were reacted for 2 h at 240°C in the presence of different amounts of initially added Fe_2O_3 seed. As indicated in Fig. 17, the presence of even $\sim 5 \text{ g L}^{-1}$ of Fe_2O_3 seed results in significant variations in the product yield and product composition. For example, the Na contents decrease from 4.3% in the precipitate formed in the absence of seed to 1.2% Na in the product made in the presence of 5 g L^{-1} of Fe_2O_3 seed and to 0.1% Na in the product formed in the presence of 40 g L^{-1} of hematite seed. These observations are consistent with the Guinier X-ray diffraction analyses which showed the precipitate made in the absence of Fe_2O_3 seed to consist of Na jarosite with a trace amount of hematite. As the concentration of Fe_2O_3 seed increased, the relative amount of Na jarosite decreased whereas the amount of hematite increased. The products generated in the presence of 10 g L^{-1} or more of Fe_2O_3 seed consisted of hematite only. A few similar experiments were carried out to examine the effect of Fe_2O_3 seed additions on the hydrothermal conversion of *in situ* formed Na jarosite at 200°C. Although similar trends were noted, the extent of reaction was much less than that noted at 240°C. For example, the product formed after 2 h of hydrothermal conversion in the presence of even 40 g L^{-1} of Fe_2O_3

seed analysed 1.6%Na, 49.6%Fe and 9.0% SO_4 and was shown by X-ray diffraction analysis to consist of major amounts of both Na jarosite and hematite. Clearly, elevated reaction temperatures and the presence of adequate Fe_2O_3 seed are as important to the hydrothermal conversion of *in situ* formed Na jarosite as they are to the conversion of previously synthesised Na jarosite.⁹

Conclusions

The hydrothermal conversion of potassium jarosite, lead jarosite, sodium–silver jarosite, arsenate containing sodium jarosite and *in situ* formed sodium jarosite to hematite was investigated. Potassium jarosite is the thermodynamically most stable jarosite species and the hydrothermal conversion to hematite, in the absence of Fe_2O_3 seed, did not occur extensively within 5 h, except at temperatures $>240^\circ\text{C}$. However, in the presence of 20 g L^{-1} Fe_2O_3 seed, significant hydrothermal conversion took place at 220°C and complete conversion to hematite occurred at 240°C. In the presence of 20 g L^{-1} Fe_2O_3 seed, the hydrothermal conversion of K jarosite to hematite is practically complete within 2 h at 225°C, but shorter retention times result in products having significant residual K jarosite contents. Complementary experiments were carried out wherein potassium jarosite was formed *in situ* in the autoclave to establish the rate of K jarosite precipitation relative to the rate of K jarosite conversion to hematite. As the K concentration increased, more K jarosite precipitated, and much of this jarosite persisted during the 5 h retention period at 225°C in the presence of 50 g L^{-1} Fe_2O_3 seed. The implication is that the rate of K jarosite precipitation is faster than its rate of hydrothermal conversion to hematite.

In contrast, complete hydrothermal conversion of either Pb jarosite or Na–Pb jarosite to hematite and PbSO_4 occurs within 0.75 h at 225°C in the presence of 20 g L^{-1} of Fe_2O_3 seed. The presence of dissolved $\text{Fe}(\text{SO}_4)_{1.5}$ inhibits the hydrothermal conversion of Pb jarosite, and likely other jarosite species as well. Although part of the $\text{Fe}(\text{SO}_4)_{1.5}$ precipitates as hematite at 225°C, the remaining $\text{Fe}(\text{SO}_4)_{1.5}$ either directly inhibits the conversion of the Pb jarosite or forms Pb jarosite from any PbSO_4 which is present as a result of the reaction. The hydrothermal conversion of Na–Ag jarosite at 225°C in the presence of 20 g L^{-1} Fe_2O_3 seed proceeds about as rapidly as the conversion of Pb jarosite or Na–Pb jarosite. Both jarosite species react extensively during the heat-up period and both are largely converted to hematite within 0.75 h at temperature. Whereas the PbSO_4 conversion product is insoluble, the Ag content of the Na–Ag jarosite dissolves during hydrothermal conversion and collects in the final solution. However, the dissolved Ag is readily precipitated by either elemental sulphur or sphalerite (ZnS) to give a final Ag concentration of $<0.1 \text{ mg L}^{-1}$.

The hydrothermal conversion of AsO_4 containing sodium jarosite at 225°C in the presence of 20 g L^{-1} of reagent Fe_2O_3 seed was investigated as a function of the H_2SO_4 concentration. For H_2SO_4 concentrations

<0.4M, complete conversion to hematite occurred within 2 h, and ~95% of the AsO₄ remained in the conversion product. Furthermore, the AsO₄ contents of the hematite conversion products increased in a linear manner as the AsO₄ content of the Na jarosite increased to 5.00%. The hydrothermal conversion of Na jarosite, formed *in situ* during the heat-up period of the autoclave, was studied at 200 and 240°C. Increasing temperatures and Fe₂O₃ seed additions significantly promote the conversion of the *in situ* formed Na jarosite. The results are consistent with those obtained using previously synthesised Na jarosite, although the previously synthesised Na jarosite seems to react to a greater degree at temperatures <200°C, in both the presence and absence of Fe₂O₃ seed.

References

1. V. Arregui, A. R. Gordon and G. Steintveit: 'The jarosite process – past, present and future', In 'Lead-Zinc-Tin'80', (ed. J. M. Cigan *et al.*), 97–124; 1979, Warrendale, PA, The Metallurgical Society of AIME.
2. J. E. Dutrizac and J. L. Jambor: 'Jarosites and their application in hydrometallurgy', *Rev. Mineral. Geochem.*, 2000, **40**, 405–451.
3. C. Drouet and A. Navrotsky: 'Synthesis, characterization, and thermochemistry of K–Na–H₃O jarosites', *Geochim. Cosmochim. Acta*, 2003, **67**, (11), 2063–2076.
4. D. Paktunc and J. E. Dutrizac: 'Characterization of arsenate-for-sulphate substitution in synthetic jarosite using X-ray diffraction and X-ray absorption spectroscopy', *Can. Mineral.*, 2003, **41**, 905–919.
5. A. Onozaki, K. Sato and S. Kuramochi: 'Effect of some impurities on iron precipitation at the Iijima zinc refinery', in 'Iron control in hydrometallurgy', (ed. J. E. Dutrizac and A. J. Monhemius), 742–752; 1986, Chichester, Ellis Horwood Limited.
6. A. von Ropenack: 'Hematite – the solution to a disposal problem – an example from the zinc industry', in 'Iron control in hydrometallurgy', (ed. J. E. Dutrizac and A. J. Monhemius), 730–741; 1986, Chichester, Ellis Horwood Limited.
7. H. Arima, T. Aichi, Y. Kudo, K. Saruta, M. Kanno and R. Togashi: 'Recent improvements in the hematite precipitation process at the Akita Zinc Company', in 'Iron control technologies', (ed. J. E. Dutrizac and P. A. Riveros), 123–134; 2006, Montreal, The Metallurgical Society of CIM.
8. A. Ismay, R. W. Stanley, D. Shink and D. Daoust: 'The high temperature conversion process', in 'Iron control and disposal', (ed. J. E. Dutrizac and A. J. Monhemius), 618–639; 1986, Chichester, Ellis Horwood.
9. J. E. Dutrizac: 'The hydrothermal conversion of jarosite-type compounds', in 'Productivity and technology in the metallurgical industries', (ed. M. Koch and J. C. Taylor), 587–612; 1989, Warrendale, PA, The Minerals, Metals and Materials Society.
10. J. E. Dutrizac: 'Factors affecting the precipitation of potassium jarosite in sulfate and chloride media', *Metall. Mater. Trans. B*, 2008, **39B**, 771–783.
11. J. E. Dutrizac, O. Dinardo and S. Kaiman: 'Factors affecting lead jarosite formation', *Hydrometallurgy*, 1980, **5**, 305–324.
12. J. E. Dutrizac: 'The precipitation of lead jarosite from chloride media', *Hydrometallurgy*, 1991, **26**, 327–346.
13. J. E. Dutrizac and J. L. Jambor: 'Behaviour of silver during jarosite precipitation', *Trans. Inst. Min. Metall. Sect. C*, 1987, **96**, C206–C218.
14. J. E. Dutrizac and J. L. Jambor: 'Formation and characterization of argentojarosite and plumbojarosite and their relevance to metallurgical processing', in 'Applied mineralogy', (ed. W. C. Park *et al.*), 507–530; 1984, Warrendale, PA, The Metallurgical Society of AIME.
15. J. E. Dutrizac, J. L. Jambor and T. T. Chen: 'The behaviour of arsenic during jarosite precipitation: reactions at 150°C and the mechanism of arsenic precipitation', *Can. Metall. Q.*, 1987, **26**, (2), 103–115.
16. J. E. Dutrizac and T. T. Chen: 'Hematite precipitation from ferric sulphate solutions at 225 and 100°C', *World Metall. – ERZMETALL*, 2011, **64**, 5–21.
17. J. E. Dutrizac and J. L. Jambor: 'Characterization of the iron arsenate-sulphate compounds precipitated at elevated temperatures', *Hydrometallurgy*, 2007, **86**, 147–163.
18. J. E. Dutrizac and J. L. Jambor: 'The synthesis of crystalline scorodite, FeAsO₄·2H₂O', *Hydrometallurgy*, 1988, **19**, 377–384.

A.2 Arsenate substitution in natroalunite: A potential medium for arsenic immobilization. Part 1: Synthesis and compositions

A. Sunyer, J. Viñals, 2011, Arsenate substitution in natroalunite: A potential medium for arsenic immobilization. Part 1: synthesis and compositions, Hydrometallurgy, 109, 54-64.

Resum en català

La substitució d'arseniat per sulfat en natroalunites s'ha investigat com a base d'un mètode potencial per a la immobilització d'arsènic. Els efectes de temperatura, temps de reacció i de la relació molar $\text{AsO}_4/(\text{SO}_4+\text{AsO}_4)$ en el medi inicial s'han estudiat. La precipitació s'ha incrementat amb l'augment de temperatura i la concentració d' AsO_4^{3-} , i va ser pràcticament completa en <30 min a $>180^\circ\text{C}$. La formació de natroalunite va ser ràpida i va ser preferent a la precipitació de mansfieldita; Aquesta última va créixer amb l'augment de temperatura i la disminució de la relació $(\text{AsO}_4/\text{TO}_4)_{aq}$ ($\text{TO}_4 \equiv \text{SO}_4 + \text{AsO}_4$). Per $(\text{AsO}_4/\text{TO}_4)_{aq} < 0.2$ a 200°C , la precipitació d'arsènic va ser quasi exclusivament com a natroalunite. Per $(\text{AsO}_4/\text{TO}_4)_{aq}$ entre 0.2 i 0.4 a 200°C , es va formar una mescla de natroalunite i mansfieldita. Per $(\text{AsO}_4/\text{TO}_4)_{aq} > 0.4$, no va precipitar natroalunite, i altres fases d'arseniat com l'alarsita, la mansfieldita i la natrofarmacolaumite van aparèixer.

La substitució d' AsO_4 en la natroalunite en l'interval de $160\text{-}200^\circ\text{C}$ va ser pràcticament independent a la temperatura i al temps de reacció però va incrementar amb l'augment d' $(\text{AsO}_4/\text{TO}_4)_{aq}$. A 200°C la substitució va ser $(\text{AsO}_4/\text{TO}_4)_{nat} \cong 0.5(\text{AsO}_4/\text{TO}_4)_{aq}$. La màxima substitució d'arseniat observada a l'estructura de la natroalunite va ser del 15% molar. La introducció del guix en el medi inicial va donar lloc a la precipitació d'anhidrita i natroalunite amb una substitució de Ca per Na de 4-6% molar i un grau de substitució similar d'arseniat per sulfat. En absència de Na^+ , fases tipus alunites riques en Ca/As com ara la schlossmacherite o l'arsenocrandallite no van tenir rendiments de precipitació raonables en medis $\text{Ca}^{2+}/\text{Al}^{3+}/\text{SO}_4^{2-}/\text{AsO}_4^{3-}$.



Arsenate substitution in natroalunite: A potential medium for arsenic immobilization. Part 1: Synthesis and compositions

Alba Sunyer, Joan Viñals*

Department of Materials Science and Metallurgical Engineering, University of Barcelona, Martí i Franqués 1, 08028 Barcelona, Spain

ARTICLE INFO

Article history:

Received 24 February 2011

Received in revised form 11 May 2011

Accepted 19 May 2011

Available online 27 May 2011

Keywords:

Arsenic
Immobilization
Alunite
Natroalunite
Mansfieldite
Alarsite
Natropharmacoalumite

ABSTRACT

Arsenate-for-sulfate substitution in natroalunite has been investigated as the basis of a potential method for arsenic immobilization. The effects of temperature, reaction time and $\text{AsO}_4/(\text{SO}_4 + \text{AsO}_4)$ molar ratio in the initial aqueous medium were studied. The rate of precipitation increased with increasing temperature and AsO_4^{3-} concentration, and it was practically complete in <30 min at >180 °C. Natroalunite formation was faster and preferential than mansfieldite precipitation; the latter decreased when the temperature increased and the $(\text{AsO}_4/\text{TO}_4)_{\text{aq}}$ ratio ($\text{TO}_4 \equiv \text{SO}_4 + \text{AsO}_4$) decreased. For $(\text{AsO}_4/\text{TO}_4)_{\text{aq}} < 0.2$ at 200 °C, arsenic precipitated almost exclusively as natroalunite. For $(\text{AsO}_4/\text{TO}_4)_{\text{aq}}$ between 0.2 and 0.4 at 200 °C, a mixture of natroalunite and mansfieldite was formed. For $(\text{AsO}_4/\text{TO}_4)_{\text{aq}} > 0.4$, natroalunite was not precipitated, and other arsenate phases such as alarsite, mansfieldite and natropharmacoalumite appeared.

AsO_4 substitution in natroalunite in the interval 160–200 °C was practically independent of temperature and reaction time but it increased when increased $(\text{AsO}_4/\text{TO}_4)_{\text{aq}}$. At 200 °C the substitution type was $(\text{AsO}_4/\text{TO}_4)_{\text{nat}} \approx 0.5 (\text{AsO}_4/\text{TO}_4)_{\text{aq}}$. The maximum arsenate substitution observed in the natroalunite structure was ~15% molar.

The introduction of gypsum in the initial medium ends with the precipitation of anhydrite and natroalunite with a Ca-for-Na substitution about 4–6% molar and a similar degree of arsenate-for-sulfate substitution. In absence of Na^+ , Ca/As-rich alunite-type phases such as schlossmacherite or arsenocrandallite were not precipitated at reasonable rates in $\text{Ca}^{2+}/\text{Al}^{3+}/\text{SO}_4^{2-}/\text{AsO}_4^{3-}$ media.

© 2011 Elsevier B.V. All rights reserved.

1. Introduction

Arsenic immobilization from solid wastes or liquid effluents remains as a significant problem, especially for primary base metal industries (Riveros et al., 2001). Among the most studied stabilization methods is the precipitation of scorodite ($\text{FeAsO}_4 \cdot 2\text{H}_2\text{O}$) (Caetano et al., 2009; Demopoulos et al., 1995; Ichimura et al., 2007; Monhemius and Swash, 1999). Scorodite has a high As content, a reasonable stability (Bluteau et al., 2009; Bluteau and Demopoulos, 2007; Krause and Ettel, 1989) and it can be precipitated in atmospheric conditions through controlled supersaturation processes (Demopoulos et al., 2003; Fujita et al., 2008a,b, 2009). Mansfieldite ($\text{AlAsO}_4 \cdot 2\text{H}_2\text{O}$), the aluminum analog of scorodite, has also been investigated but it seems ineffective for long-term storage, due to its slow but significant arsenic leaching at neutral or near neutral pHs (Le Berre et al., 2007a,b; Viñals et al., 2010a).

However, many metallurgical wastes contain small or moderate concentrations of arsenic in sulfate-rich media. For these wastes, precipitation of arsenic as sulfate-type compounds with arsenate in diluted solid solution could also be of potential interest. The phases of the alunite supergroup are well known as natural and synthetic products

(Jambor, 1999). Their general formula can be written as $\text{AB}_3(\text{TO}_4)_2(\text{OH}, \text{H}_2\text{O})_6$, in which the A site is a monovalent (Na, K, H_3O , etc.) or a large divalent or trivalent (Ca, Ba, Pb, Bi, rare earth, etc.). The B site is occupied principally by Al and Fe(III), and TO_4 is principally SO_4^{2-} , AsO_4^{3-} or PO_4^{3-} . Multiple substitutions of A, B or T are possible because charge balance can be achieved by coupled substitutions at the different sites, cationic vacancies or protonation of OH or TO_4 groups. Moreover, these compounds exhibit good stability in a wide range of environmental conditions and for this reason they have been proposed for long-term storage of toxic metals (Alcobé et al., 2001; Kolitsch and Pring, 2001). Along similar lines, the precipitation of arsenical natroalunite (ideally $\text{NaAl}_3(\text{SO}_4)_2(\text{OH})_6$) has recently been tested for the stabilization of a complex calcium arsenate waste from the copper pyrometallurgy (Viñals et al., 2010a, 2010b). Arsenical natroalunite could be an effective means of arsenic immobilization since the As solubility at its natural pH (4–5) remains stable at ~0.1 mg/l in 6 months leaching tests. However, few basic studies of arsenate-for-sulfate substitution in simple alunites have been developed.

Arsenate-for-sulfate substitution in jarosite ($\text{KFe}_3(\text{SO}_4)_2(\text{OH})_6$) has been studied by Dutrizac et al. (1987), Paktunc and Dutrizac (2003) and Savage et al. (2005). Jarosite obtained in hydrothermal conditions (150 °C) incorporated up to 4 wt.% AsO_4 (Dutrizac et al., 1987). Results of the maximum arsenate substitution in jarosites obtained at ~100 °C were between 17% molar (Paktunc and Dutrizac, 2003) and about 30% molar at

* Corresponding author. Tel.: +34 934021317; fax: +34 934039621.
E-mail address: jvinalsvinals@ub.edu (J. Viñals).

TO₄ site (Savage et al., 2005). Attempts to increase arsenic substitution by increasing the AsO₄³⁻ concentration in the aqueous medium result in the formation of amorphous iron arsenate phases and scorodite. These studies also reported that jarosite structure expanded slightly due to the larger As–O distance (1.66–1.68 Å) than S–O distance (1.47 Å). Moreover, the extent of As substitution may be limited by charge-balance mechanism, such as the H₂O-for-OH⁻ and HAsO₄²⁻-for-SO₄²⁻.

The present paper is the Part 1 of a basic research on arsenical natroalunite generation. It principally includes hydrothermal precipitation at 160–200 °C. The effects of temperature, reaction time, solution composition and presence of gypsum on precipitation yields, phase composition and degree of arsenate-for-sulfate substitution in natroalunite are reported.

Structural analysis and the As solubility for selected precipitates in a wide range of pH have been included in the Part 2 of this research (Sunyer and Viñals, 2011–this issue).

2. Experimental methods

The composition of the initial solutions and molar ratios for the synthesis experiments are reported in Table 1. Four media were used: (a) Na⁺/Al³⁺/SO₄²⁻ for preliminary tests of natroalunite (As-free) precipitation, (b) Na⁺/Al³⁺/SO₄²⁻/AsO₄³⁻ for the study of AsO₄ substitution in natroalunite, (c) Na⁺/Ca²⁺/Al³⁺/SO₄²⁻/AsO₄³⁻ for the study of precipitation in presence of gypsum and (d) Ca²⁺/Al³⁺/SO₄²⁻/AsO₄³⁻ for the

Table 1

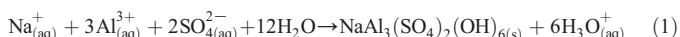
Experimental conditions and reagents for natroalunite synthesis (150 ml; pH_{initial}: 2.8–2.9; stirring speed: 750 rpm).

Test	Na ₂ HAsO ₄ ·7H ₂ O (g)	CaSO ₄ ·2H ₂ O (g)	Temperature (°C)	Time (h)	Initial solution molar ratio		pH _{final}
					As/((S–Ca) + As)		
Fixed reagent addition: Al ₂ (SO ₄) ₃ ·18H ₂ O: 6.33 g; Na ₂ SO ₄ : 0.45 g							
	Na ⁺ /Al ³⁺ /SO ₄ ²⁻						
N1	0	0	100	2	0		2.8
N2	0	0	100	72	0		1.4
N3 ^a	0	0	100	72	0		1.2
N4	0	0	120	2	0		2.8
N5	0	0	140	2	0		1.8
N6	0	0	160	2	0		1.2
N7	0	0	180	2	0		1.1
N8	0	0	200	2	0		1.0
	Na ⁺ /Al ³⁺ /SO ₄ ²⁻ /AsO ₄ ³⁻						
TAS0 ^b	2.23	0	100	72	0.185		2.2
TAS1	2.23	0	160	0.083	0.185		2.1
TAS2	2.23	0	160	0.5	0.185		1.9
TAS3	2.23	0	160	2	0.185		1.4
TAS4	2.23	0	160	4	0.185		0.9
TAS5	2.23	0	180	0.083	0.185		1.5
TAS6	2.23	0	180	0.5	0.185		1.0
TAS7	2.23	0	180	2	0.185		1.0
TAS8	2.23	0	180	4	0.185		1.0
TAS9	2.23	0	200	0.083	0.185		1.0
TAS10	2.23	0	200	0.5	0.185		0.9
TAS11	0.89	0	160	0.083	0.083		1.8
TAS12	0.89	0	160	2	0.083		1.5
TAS13	0.89	0	160	4	0.083		1.2
TAS14	0.89	0	180	2	0.083		1.1
TAS15	0.89	0	200	0.083	0.083		1.0
TAS16	0.89	0	200	0.5	0.083		1.1
AS1	0.89	0	200	2	0.083		1.1
AS2	1.11	0	200	2	0.101		1.1
AS3	1.27	0	200	2	0.114		1.1
AS4	1.48	0	200	2	0.130		1.1
AS5	1.78	0	200	2	0.152		1.1
AS7	2.23	0	200	2	0.185		1.0
AS8	2.97	0	200	2	0.231		1.0
AS9	3.65	0	200	2	0.270		1.1
AS10	4.45	0	200	2	0.311		1.1
AS11	5.54	0	200	2	0.359		1.1
AS12	7.16	0	200	2	0.421		1.6
AS13	8.89	0	200	2	0.474		1.1
Fixed reagent addition: Al ₂ (SO ₄) ₃ ·18H ₂ O: 6.33 g							
	Na ⁺ /Ca ²⁺ /Al ³⁺ /SO ₄ ²⁻ /AsO ₄ ³⁻						
ASC1	0.99	0.564	200	2	0.100		1.0
ASC2	1.98	0.564	200	2	0.182		0.9
ASC3	1.98	0.564	200	0.5	0.182		0.9
ASC4	1.98	0.564	200	0.25	0.182		0.9
ASC5	1.98	0.564	180	2	0.182		0.9
ASC6	1.98	0.564	180	0.5	0.182		1.1
ASC7	1.98	0.564	180	0.25	0.182		1.7
ASC8	3.98	1.095	200	2	0.309		1.1
ASC9	3.98	2.187	200	2	0.309		1.2
	Ca ²⁺ /Al ³⁺ /SO ₄ ²⁻ /AsO ₄ ³⁻ (As added as H ₃ AsO ₄)						
ASC10	0	1.095	200	2	0.182		1.9
ASC11	0	1.095	200	2	0.309		0.9
ASC12	0	2.187	200	2	0.309		1.2

^a Seeding with 1.5 g of natroalunite from N8.

^b Seeding with 1.5 g of natroalunite from AS7.

possible generation of alunite-type phases in the absence of Na^+ . Arsenic was added as $\text{Na}_2\text{HAsO}_4 \cdot 7\text{H}_2\text{O}$, except for the $\text{Ca}^{2+}/\text{Al}^{3+}/\text{SO}_4^{2-}/\text{AsO}_4^{3-}$ medium in which arsenic acid solution was used. Calcium was added as freshly precipitated gypsum, which was obtained by neutralization of $\text{Ca}(\text{OH})_2$ with diluted H_2SO_4 . Experiments for As-free natroalunite were designed with a stoichiometric ratio $\text{Na}^+/\text{Al}^{3+}$ (1:3). Experiments involving arsenical natroalunite were performed with an excess of Na^+ (Table 1) and, consequently, Al^{3+} was the limiting reagent for natroalunite precipitation:



Synthesis experiments were performed in a Parr 4563 autoclave reactor with temperature, pressure and stirring controls. The solutions (or slurries) containing the reactants were heated at $5^\circ\text{C}/\text{min}$, then maintained at the selected temperature for a fixed, nominal time, and finally cooled at $5^\circ\text{C}/\text{min}$. After treatment, the precipitates were filtered and washed five times with 50 ml of distilled water (each time) and dried for 5 days at ambient temperature. The precipitates were characterized by bulk chemical analysis, XRD and SEM/EDS, as described in a previous paper (Viñals et al., 2010a). Bulk chemical composition was determined by dissolving 0.1 g of the sample in 6 M HCl at 80°C for 3–4 days and analyzing the resulting solution by ICP-OES. XRD patterns were obtained in Bragg–Brentano geometry in a Panalytical X'pert PRO MDP Alpha 1.

Phase percentages were determined through the Rietveld refinement as described in the Part 2 of this research (Sunyer and Viñals, 2011-this issue). When the precipitates contained amorphous phases, the natroalunite percentage was evaluated from the total Na content obtained by bulk chemical analysis and the Na content in the natroalunite phase determined by EDS.

SEM/EDS examinations were performed in a JEOL JSM-840 instrument with INCA-250 analytical software and calibrated with the following standards: quartz (O K_{α}), albite (Na K_{α}), orthoclase (Al K_{α}), pyrite (S K_{α}), wollastonite (Ca K_{α}) and InAs (As L_{α}). Analyses were conducted from carbon coated mounts using a beam current of 0.6 nA at 20 kV for 30 s (spot size ~50 nm). The results were normalized to 100% atomic sum of all elements (except C). Formula coefficients for natroalunite were obtained from the mean atomic percentage of about ten punctual analyses and assuming the structural basis of $\text{S} + \text{As} = 2$.

3. Results and discussion

3.1. As-free natroalunite

The precipitation yield in the synthesis of natroalunite was strongly dependent on the temperature (Table 2). In atmospheric conditions (100°C), the yield was negligible in 2 h, and it was only

Table 2
Bulk chemical composition (ICP) and phase content (Rietveld) of hydrothermal precipitates (na: natroalunite; am: amorphous; ma: mansfieldite; al: alarsite; ph: natropharmacoalunite).

Temperature ($^\circ\text{C}$)	Time (h)	(As/S + As) _{aq}	Chemical composition (%)				Phases (XRD and SEM/EDS)
			Na	Al	S	As	
<i>$\text{Na}^+/\text{Al}^{3+}/\text{SO}_4^{2-}$</i>							
100	2	0	–	–	–	–	no precipitate
100	72	0	not det.	–	–	–	na (16% yield)
100	72	0	3.84	20.08	16.64	0.00	na (29% yield)
120	2	0	–	–	–	–	no precipitate
140	2	0	not det.	–	–	–	na (1% yield)
160	2	0	not det.	–	–	–	na (16% yield)
180	2	0	not det.	–	–	–	na (37% yield)
200	2	0	4.05	17.95	15.07	0.00	na (55% yield)
<i>$\text{Na}^+/\text{Al}^{3+}/\text{SO}_4^{2-}/\text{AsO}_4^{3-}$</i>							
100	72	0.185	3.49	18.48	11.91	7.22	na (74% ^a) + am (26% ^b)
160	0.083	0.185	1.63	15.45	6.14	14.72	na (33% ^a) + am (67% ^b)
160	0.5	0.185	3.77	17.43	11.77	7.26	na (75% ^a) + am (25% ^b)
160	2	0.185	5.10	20.02	15.12	2.95	na
160	4	0.185	4.16	18.25	12.52	8.51	na (85%) + ma (15%)
180	0.083	0.185	3.63	17.92	11.96	7.42	na (73% ^a) + am (27% ^b)
180	0.5	0.185	3.83	18.40	12.45	7.29	na (87%) + ma (13%)
180	2	0.185	4.98	18.97	13.67	7.53	na (91%) + ma (9%)
180	4	0.185	4.00	18.87	12.93	8.59	na (82%) + ma (18%)
200	0.083	0.185	5.18	19.13	15.07	3.43	na
200	0.5	0.185	4.57	18.40	14.87	3.00	na
160	0.083	0.083	1.75	19.05	7.74	8.46	na (35% ^a) + am (65% ^b)
160	2	0.083	5.08	18.92	14.99	1.45	na
160	4	0.083	4.73	18.38	17.62	3.09	na (95%) + ma (5%)
180	2	0.083	5.18	18.90	16.46	1.43	na
200	0.083	0.083	4.87	18.63	14.86	1.52	na
200	0.5	0.083	4.98	18.36	14.91	1.28	na
200	2	0.083	4.88	18.42	14.88	1.24	na
200	2	0.101	4.52	17.18	13.94	1.32	na
200	2	0.114	4.66	18.70	15.02	1.69	na
200	2	0.130	4.59	16.96	13.53	1.94	na
200	2	0.152	4.91	17.53	13.77	2.53	na
200	2	0.185	4.72	18.93	14.55	2.80	na
200	2	0.231	3.68	17.92	10.46	12.97	na (71%) + ma (29%)
200	2	0.270	5.26	19.27	12.91	5.98	na (95%) + ma (3%) + al (2%)
200	2	0.311	1.79	15.41	4.41	25.71	na (32%) + ma (68%)
200	2	0.359	0.87	14.24	2.00	30.09	na (16%) + ma (85%)
200	2	0.421	0.18	16.46	0.06	41.99	al (98%) + ma (2%)
200	2	0.474	2.17	14.96	0.08	32.52	ph (65% ^a) + (al + ma) (35% ^b)

^a Determined from the Na content in the bulk product.

^b By difference.

16% in 72 h. The effect of seeding was also studied at 100 °C, using 10 g/l of hydrothermally obtained natroalunite at 200 °C. The precipitation rate increased but only to 29% in 72 h.

Increasing the temperature increased the precipitation rate, reaching a 55% yield in 2 h at 200 °C. The crystal size also increased with temperature. The maximum crystal size, about 10 µm, was observed at 180 °C and 200 °C; it decreased to 4 µm at 160 °C, to 3 µm at 140 °C and to <1 µm at 100 °C. XRD patterns and EDS spectra showed only the natroalunite phase at all temperatures. The chemical composition (Table 2) was studied for samples obtained at 100 °C (test N3) and 200 °C (test N8), because the EDS spectra from samples obtained at intermediate temperatures were essentially identical. Formula coefficients for natroalunite (Table 3) showed a significant Na⁺ deficit at the alkali site (26–36%) and also a small (4–6%) deficit of Al³⁺ at the trivalent site. The Na⁺ deficit can be attributed to H₃O⁺-for-Na⁺ substitution. These effects are common in the synthesis of alunites (Rudolph et al., 2003) and jarosites (Drouet and Navrotsky, 2003; Paktunc and Dutrizac, 2003).

3.2. Arsenical natroalunite

3.2.1. Temperature effect

3.2.1.1. Atmospheric precipitation at 100 °C with seeding. Precipitation of arsenical natroalunite at 100 °C (test TASO) was studied using a seeding (10 g/l) of arsenical natroalunite obtained at 200 °C (test AS7). The initial (AsO₄/TO₄)_{aq} molar ratio was 0.185 (TO₄≡SO₄+AsO₄), the same composition used in the synthesis of seeding crystals. After 72 h, the As precipitation yield was 22%, but the natroalunite precipitation yield computed from the Na balance was less than 5%. On the other hand, the sample examined by SEM showed large amounts of a spheroidal amorphous phase (~1 µm), which precipitated over the seeding crystals (Fig. 1A). EDS microanalysis of the amorphous phase (Fig. 1B) indicated that it consisted of an aluminum/arsenate/sulfate with atomic ratios of Al³⁺/AsO₄³⁻~2 and AsO₄³⁻/SO₄²⁻~2. The formation of this amorphous phase was also detected in the XRD pattern which showed a broad hump centered at about 26° 2θ, in the baseline signal. Solubility test (2 g/20 ml H₂O, 24 h) performed on this precipitate at its natural pH (~4) give 7 mg/l of As, a value clearly

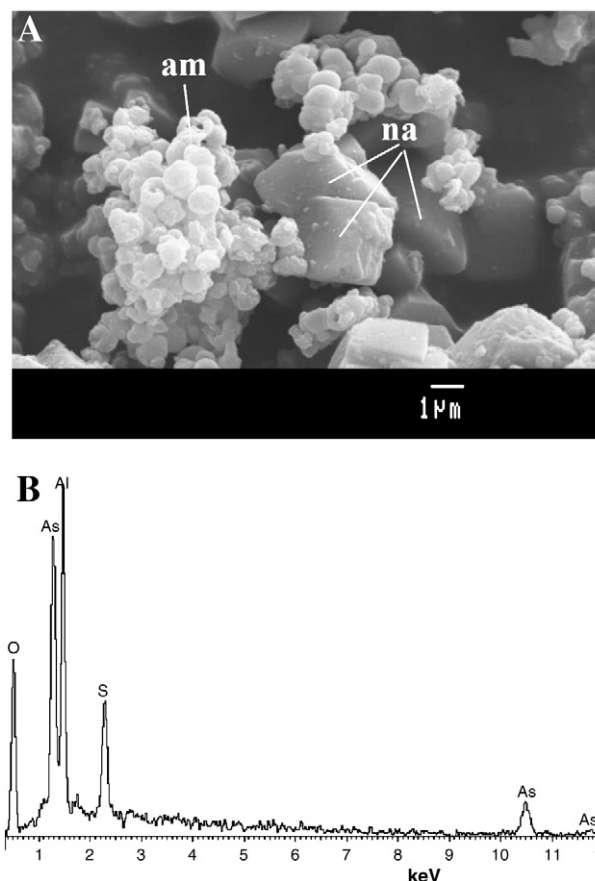


Fig. 1. Test with seeding at 100 °C, 72 h. A: amorphous Al³⁺/AsO₄³⁻/SO₄²⁻ phase (am) on natroalunite seed (na). B: EDS spectrum of the amorphous phase.

unacceptable for waste disposal. For this reason, the subsequent research on the synthesis of arsenical natroalunite was conducted hydrothermally at ≥ 160 °C.

Table 3

Formula coefficients in natroalunite phase (normalized to S+As=2) (BCA: from bulk chemical analysis ICP. EDS: from mean punctual analysis by EDS).

Temp. (°C)	Time (h)	(As/(S+As)) _{aq}	BCA				EDS			
			Na	Al	S	As	Na	Al	S	As
Na ⁺ /Al ³⁺ /SO ₄ ²⁻										
100	72	0	0.65	2.86	2.00	0.00	0.66±0.11	2.81±0.12	2.00	0.00
200	2	0	0.75	2.83	2.00	0.00	0.74±0.08	2.88±0.10	2.00	0.00
Na ⁺ /Al ³⁺ /SO ₄ ²⁻ /AsO ₄ ³⁻										
160	0.5	0.185	Not det. (phase mixture)				1.02±0.06	2.78±0.06	1.79±0.01	0.21±0.01
160	2	0.185	0.87	2.90	1.85	0.15	0.98±0.12	2.88±0.12	1.85±0.01	0.15±0.01
160	4	0.185	Not det. (phase mixture)				0.94±0.14	2.76±0.09	1.80±0.02	0.20±0.02
180	0.083	0.185	Not det. (phase mixture)				0.85±0.07	2.67±0.06	1.79±0.01	0.21±0.01
180	0.5	0.185	Not det. (phase mixture)				0.93±0.10	2.72±0.10	1.81±0.02	0.19±0.02
180	2	0.185	Not det. (phase mixture)				0.96±0.09	2.74±0.12	1.82±0.03	0.18±0.03
180	4	0.185	Not det. (phase mixture)				0.96±0.10	2.69±0.08	1.80±0.02	0.20±0.02
200	0.083	0.185	0.87	2.76	1.82	0.18	0.99±0.02	2.73±0.04	1.81±0.02	0.19±0.02
200	0.5	0.185	0.80	2.71	1.84	0.16	0.96±0.07	2.74±0.08	1.84±0.01	0.16±0.01
160	2	0.083	0.91	2.88	1.92	0.080	Not det.			
180	2	0.083	0.85	2.63	1.93	0.072	Not det.			
200	0.083	0.083	0.88	2.85	1.92	0.084	Not det.			
200	0.5	0.083	0.90	2.84	1.93	0.069	Not det.			
200	2	0.083	0.88	2.84	1.93	0.068	0.80±0.12	2.80±0.10	1.93±0.01	0.074±0.006
200	2	0.101	0.87	2.82	1.92	0.078	0.82±0.16	2.80±0.14	1.92±0.01	0.086±0.006
200	2	0.114	0.83	2.82	1.91	0.092	0.88±0.10	2.92±0.08	1.90±0.01	0.10±0.01
200	2	0.130	0.89	2.80	1.88	0.12	0.82±0.12	2.82±0.08	1.87±0.01	0.13±0.01
200	2	0.152	0.92	2.81	1.85	0.15	0.94±0.12	2.80±0.08	1.85±0.01	0.15±0.01
200	2	0.185	0.84	2.86	1.85	0.15	0.94±0.10	2.84±0.10	1.84±0.02	0.16±0.02
200	2	0.231	Not det. (phase mixture)				0.97±0.10	2.77±0.14	1.78±0.03	0.22±0.03
200	2	0.270	Not det. (phase mixture)				1.01±0.08	2.86±0.08	1.74±0.02	0.26±0.02
200	2	0.311	Not det. (phase mixture)				0.98±0.09	2.92±0.18	1.69±0.02	0.31±0.02

3.2.1.2. Precipitation at 160–200 °C. Precipitation at 160–200 °C was basically studied for an initial $(AsO_4/TO_4)_{aq} = 0.185$, which is near the maximum value for the production of natroalunite precipitates free of mansfieldite at 200 °C (see Section 3.2.2). Figs. 2 and 3 show the precipitation yields of Al and As at different times and the phase morphology, respectively. Table 2 shows the bulk chemical composition and phase content of the precipitates and Table 3 the natroalunite formula coefficients.

The rate of natroalunite precipitation increased with increasing temperature. The precipitation was practically complete in 30 min at 180–200 °C, whereas at 160 °C it required about 2 h. However, the behavior of As during natroalunite precipitation was complex (Fig. 2). At 160 °C in 5 min, arsenic mainly precipitated as an amorphous $Al^{3+}/AsO_4^{3-}/SO_4^{2-}$ phase with fine natroalunite intergrown (Fig. 3A). The composition and morphology of this amorphous phase was similar to those obtained at 100 °C (Fig. 1). At 160 °C in 30 min, the natroalunite precipitation yield increased, but the As precipitation yield diminished slightly as a consequence of the partial re-dissolution of the amorphous phase. At 160 °C in 120 min, the precipitation of arsenical natroalunite was practically complete. Under these conditions the As precipitation yield was ~15%, the maximum As precipitation yield when As substitutes in natroalunite, and the degree of AsO_4 substitution in natroalunite was about 9% (Fig. 4), which was also the maximum AsO_4 substitution in natroalunite for $(AsO_4/TO_4)_{aq} = 0.185$ (see Section 3.2.2). Finally, at 160 °C in 240 min the As precipitation yield increased dramatically as a consequence of mansfieldite co-precipitation (Fig. 3B).

The sequence was similar at 180 °C but at a higher reaction rate. At 180 °C 5 min, the precipitate contained natroalunite + amorphous phase (Fig. 3C). At 180 °C 30 min the precipitation of natroalunite was practically complete; the amorphous phase was re-dissolved and the precipitation of mansfieldite had already initiated. Increasing the reaction

time at 180 °C, the results indicated an increment in mansfieldite precipitation (Fig. 3D). Meanwhile, at 200 °C the amorphous phase and mansfieldite were not observed at $(AsO_4/TO_4)_{aq} = 0.185$ (Fig. 3E, F). Natroalunite precipitation was very fast, and it was practically completed in 30 min. Also the As yield was about 15% and the degree of AsO_4 substitution in natroalunite $((AsO_4/TO_4)_{nat})$ was about 9% molar (Fig. 4).

Additional experiments were performed with initial solutions containing considerably less arsenic, $(AsO_4/TO_4)_{aq} = 0.083$. At 160 °C, the sequence was similar to that obtained at $(AsO_4/TO_4)_{aq} = 0.185$: amorphous + natroalunite → natroalunite → natroalunite + mansfieldite (Table 2). However, the AsO_4 -for- SO_4 substitution in natroalunite was reduced to about 4%. At 180 °C and 120 min, and at 200 °C in the interval 5–240 min, only the natroalunite phase was obtained with similar AsO_4 substitution to that at 160 °C (Fig. 4).

These results indicated that the amorphous $Al^{3+}/AsO_4^{3-}/SO_4^{2-}$ phase was formed during the heating process at pH 2–3. Nevertheless, this amorphous arsenate re-dissolved in the strong acid media (pH ≤ 1) generated by the extensive natroalunite precipitation (Eq. 1), increasing its dissolution rate with increasing time and temperature. On the other hand, this intermediate amorphous phase might favor the nucleation of natroalunite, because the precipitation rate of arsenical natroalunite (Fig. 2) was significantly greater than for As-free natroalunite (Table 2). Savage et al. (2005) also reported the formation of amorphous $Fe^{3+}/AsO_4^{3-}/SO_4^{2-}$ phases during the synthesis of arsenical jarosites. They were formed for $(AsO_4/TO_4)_{aq} > 0.04$, being apparently stable at 95 °C, pH 1.5.

In the conditions studied, an important effect was that the precipitation of arsenic as arsenical natroalunite was faster and preferential than mansfieldite generation. Accordingly, mansfieldite only appeared on previously formed natroalunite clusters (Fig. 3B, C). Moreover, other significant effects were that mansfieldite formation decreased when decreased the $(AsO_4/TO_4)_{aq}$ ratio and, especially, when increased temperature (Table 2).

The degree of AsO_4 -for- SO_4 substitution in natroalunite was almost independent of temperature and reaction time (Fig. 4), but it depended strongly on the solution composition, increasing when increase $(AsO_4/TO_4)_{aq}$ ratio.

3.2.2. Arsenic partition at 200 °C

The effect of $(AsO_4/TO_4)_{aq}$ in the initial solution on the precipitation yields, phase composition, AsO_4 incorporation in the bulk precipitate $((AsO_4/TO_4)_{bulk})$ and in natroalunite phase $((AsO_4/TO_4)_{nat})$ was studied at 200 °C. The range extended from 0 to 0.474 (Table 1). Fig. 5 shows the Al and As precipitation yields and Fig. 6 the phase composition obtained by XRD.

In the region of $(AsO_4/TO_4)_{aq}$ from 0 to about 0.2, the unique phase was natroalunite. The Al precipitation raised when the $(AsO_4/TO_4)_{aq}$ ratio was increased and was >90% at $(AsO_4/TO_4)_{aq} \sim 0.2$. However, in a single precipitation step, the As precipitation yield in this region was very moderate (12–15%).

In the region of $(AsO_4/TO_4)_{aq}$ from 0.2 to about 0.4, a mixture of natroalunite + mansfieldite was obtained, increasing the mansfieldite/natroalunite ratio when increased $(AsO_4/TO_4)_{aq}$. Consequently, the As precipitation yield showed an abrupt increment (Fig. 5) and the Al yield decreased. Finally, for $(AsO_4/TO_4)_{aq} > 0.4$, natroalunite was not formed, and only “arsenate” phases precipitated: alarsite ($AlAsO_4$), mansfieldite and natropharmacoalunite ($NaAl_4(AsO_4)_3(OH)_4 \cdot 4H_2O$) (Fig. 6).

The arsenic distribution in the bulk precipitate $((AsO_4/TO_4)_{bulk})$ and in the natroalunite phase $((AsO_4/TO_4)_{nat})$ vs. $(AsO_4/TO_4)_{aq}$ at 200 °C is shown in Fig. 7. Vertical bars show the approximate phase domains. The $(AsO_4/TO_4)_{bulk}$ lineally increased with $(AsO_4/TO_4)_{aq}$ up to 0.2. The results from punctual EDS analyses of natroalunite crystals $((AsO_4/TO_4)_{nat})$ are practically identical, confirming the formation of a single natroalunite phase. In this region, the maximum AsO_4 substitution was 9%. For $(AsO_4/TO_4)_{aq} > 0.2$, the $(AsO_4/TO_4)_{bulk}$ showed a strong increment due to the

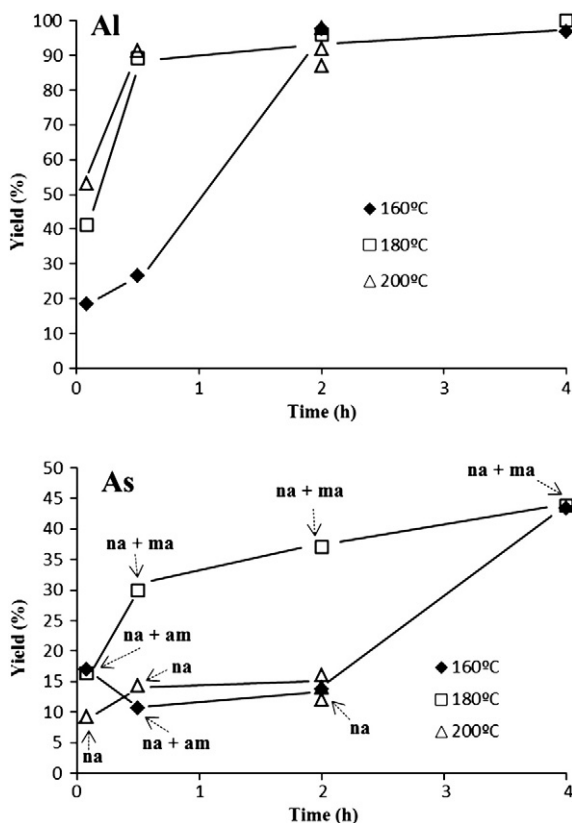


Fig. 2. Al and As precipitation yields vs. time at different temperatures for $(AsO_4/TO_4)_{aq} = 0.185$ (na: natroalunite; am: amorphous; ma: mansfieldite).

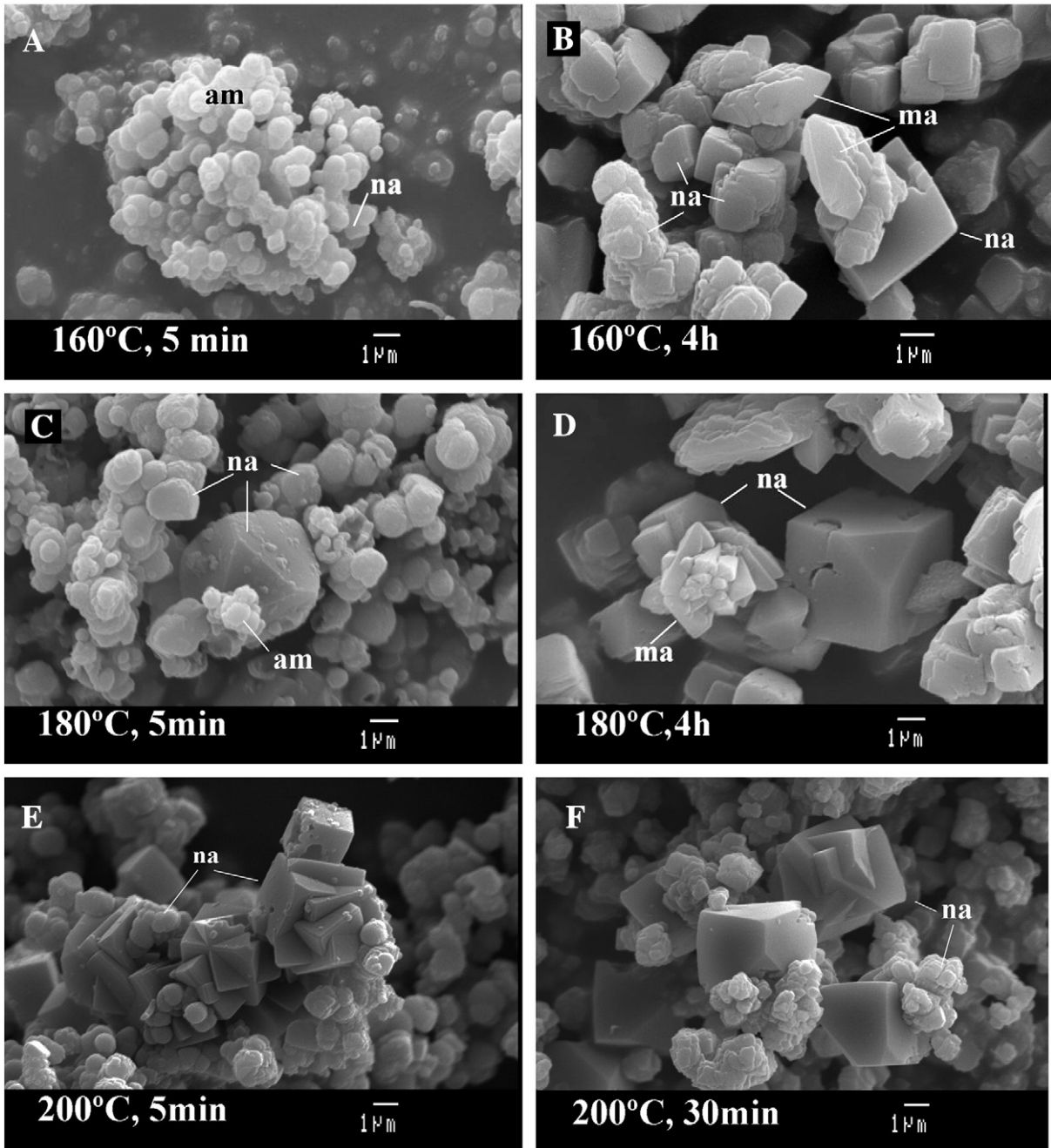


Fig. 3. Morphology of the arsenical natroalunite precipitates obtained at different times and temperatures. ($(AsO_4/TO_4)_{aq} = 0.185$) (na: natroalunite; am: amorphous; ma: mansfieldite).

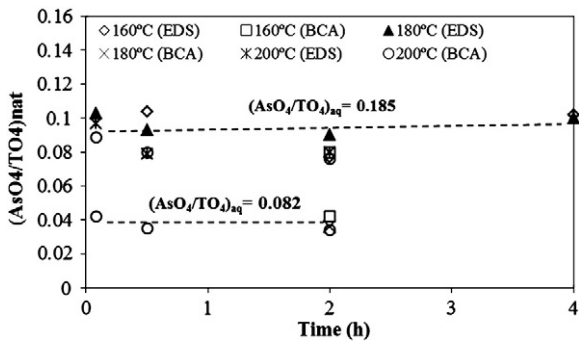


Fig. 4. Effect of time and temperature on arsenate substitution in natroalunite (BCA: from bulk ICP chemical analysis; EDS: from mean punctual EDS analysis).

precipitation of mansfieldite, but the arsenic incorporation in natroalunite showed the same tendency as observed before:

$$(AsO_4/TO_4)_{nat} \cong 0.50 (AsO_4/TO_4)_{aq} \quad (2)$$

The maximum AsO_4 -for- TO_4 substitution detected in this second region was 15% for $(AsO_4/TO_4)_{aq} = 0.31$. These values are very close to those obtained in a previous study of arsenical natroalunite precipitation from an industrial calcium arsenate waste (Viñals et al., 2010a): maximum 8% in the absence of mansfieldite and up to 14% when mansfieldite co-precipitated. Paktunc and Dutrizac (2003) reported similar values, up to 17% molar, for arsenic substitution in jarosite.

XRD patterns showed narrow natroalunite peaks in all samples (Fig. 6). The patterns were well indexed with rhombohedral cell (space group R-3m) and the structural model of natroalunite was

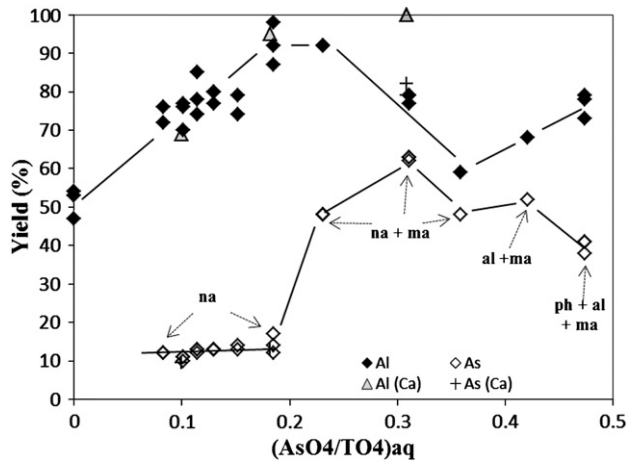


Fig. 5. Al and As precipitation yields as a function of $(AsO_4/TO_4)_{aq}$ at 200 °C (Ca: precipitation in presence of gypsum; na: natroalunite; ma: mansfieldite; al: alarsite; ph: natropharmacoalumite).

satisfactory (Sunyer and Viñals, 2011-this issue) and consistent with AsO_4 -for- SO_4 substitution in the alunite structure.

The substitution of arsenic in natroalunite did not change the morphology observed in the As-free crystals, which were rhombohedral (pseudo-cubic) with (012) dominant and (001) subordinate faces. However, by increasing $(AsO_4)_{aq}$ the natroalunite nucleation was favored and consequently the crystal growth decreased. The

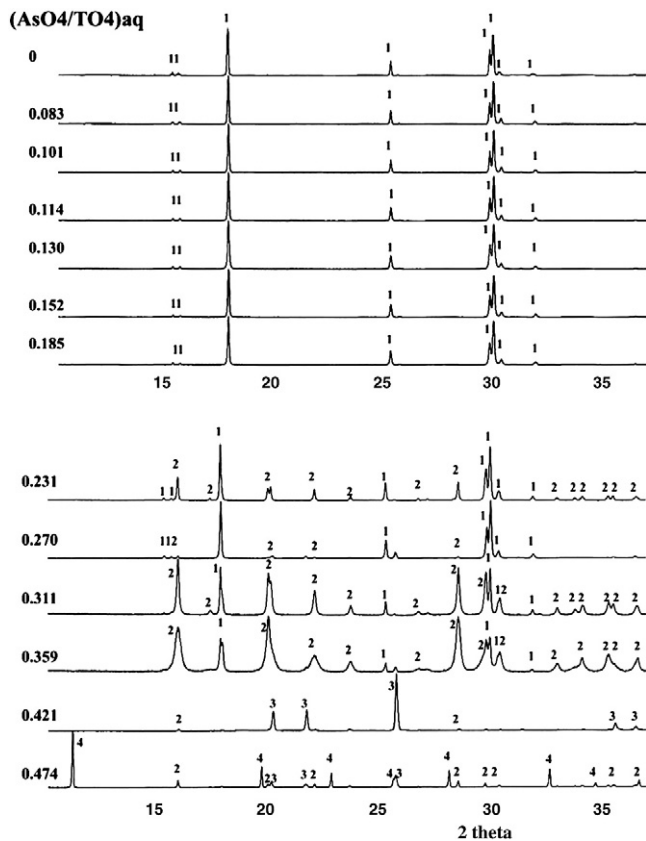


Fig. 6. X-ray patterns showing the effect of $(AsO_4/TO_4)_{aq}$ on phase composition at 200 °C (1: natroalunite; 2: mansfieldite; 3: alarsite; 4: natropharmacoalumite).

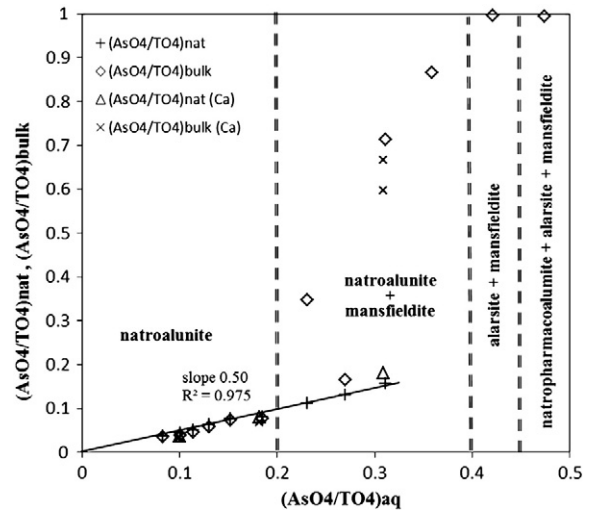


Fig. 7. Effect of $(AsO_4/TO_4)_{aq}$ on the arsenic distribution in the bulk precipitate ($(AsO_4/TO_4)_{bulk}$) and in the natroalunite phase ($(AsO_4/TO_4)_{nat}$) at 200 °C (2 h) (Ca: in presence of gypsum).

maximum crystal sizes were $\sim 10 \mu m$ at $(AsO_4/TO_4)_{aq} = 0.1$, $\sim 5 \mu m$ at $(AsO_4/TO_4)_{aq} = 0.18$ and $\sim 2.5 \mu m$ at $(AsO_4/TO_4)_{aq} = 0.27$.

3.2.3. Other arsenate phases

3.2.3.1. Mansfieldite. At 200 °C, mansfieldite was formed from ratios $(AsO_4/TO_4)_{aq} > 0.2$. Up to $(AsO_4/TO_4)_{aq} 0.31$, mansfieldite precipitated on previously crystallized natroalunite, as described in Section 3.2.1.2 (Fig. 3B,D). Under these conditions, mansfieldite occurs as small but well developed orthorhombic crystals (up to $\sim 5 \mu m$), with (111) and (001) dominant faces. The XRD spectra showed neat peaks at standard positions (Fig. 6). However, the composition determined by EDS showed a small SO_4 content, which presumably substituted AsO_4 in the mansfieldite structure. Nevertheless, the possible mechanism for charge balance was unknown. The atomic ratios obtained (mean of 10 punctual analyses) were $Al/(S + As) = 1.04 \pm 0.04$ and $S/(As + S) = 0.06 \pm 0.01$.

For $(AsO_4/TO_4)_{aq} = 0.359$, mansfieldite formed extensively (85%) but as a poorly crystalline product with very broad lines in the XRD pattern (Fig. 6). The morphology was also clearly different (Fig. 8A). Mansfieldite resembled platy natroalunite crystals (dominant form (001)), but the composition indicated mainly mansfieldite. These platy forms were probably a pseudomorphic (partial) replacement of mansfieldite over previously formed natroalunite crystals.

3.2.3.2. Alarsite. Alarsite was extensively precipitated at $(AsO_4/TO_4)_{aq} = 0.42$, jointly with small amounts of mansfieldite (2%). Alarsite formed relatively large, strongly corroded crystals (Fig. 8B) up to $60 \mu m$ in size, partially covered by small mansfieldite crystals (Fig. 8C). The formation of anhydrous $AlAsO_4$ instead of the mansfieldite common hydrate could be related with the high salt concentration of the medium at $(AsO_4/TO_4)_{aq} = 0.42$ (Table 1) which reduced the water activity. The composition determined by EDS (mean of eight punctual analyses) and normalized to $AsO_4 = 1$, showed practically the ideal formula, $Al_{1.04 \pm 0.06}(AsO_4)_{1.00}$ and the XRD pattern showed neat peaks located at the standard positions (Fig. 6). Alarsite is a well-known inorganic compound that is isostructural with quartz, which was synthesized by hydrothermal reaction between Al_2O_3 and As_2O_5 at 260 °C (Kosten, 1978). To our knowledge, however, the conditions reported in the present paper represents the first synthesis at a lower temperature and in an $Al^{3+}/Na^+/AsO_4^{3-}/SO_4^{2-}$ medium. On the other hand, alarsite is a very rare arsenate and unstable at the Earth's surface; it was only identified

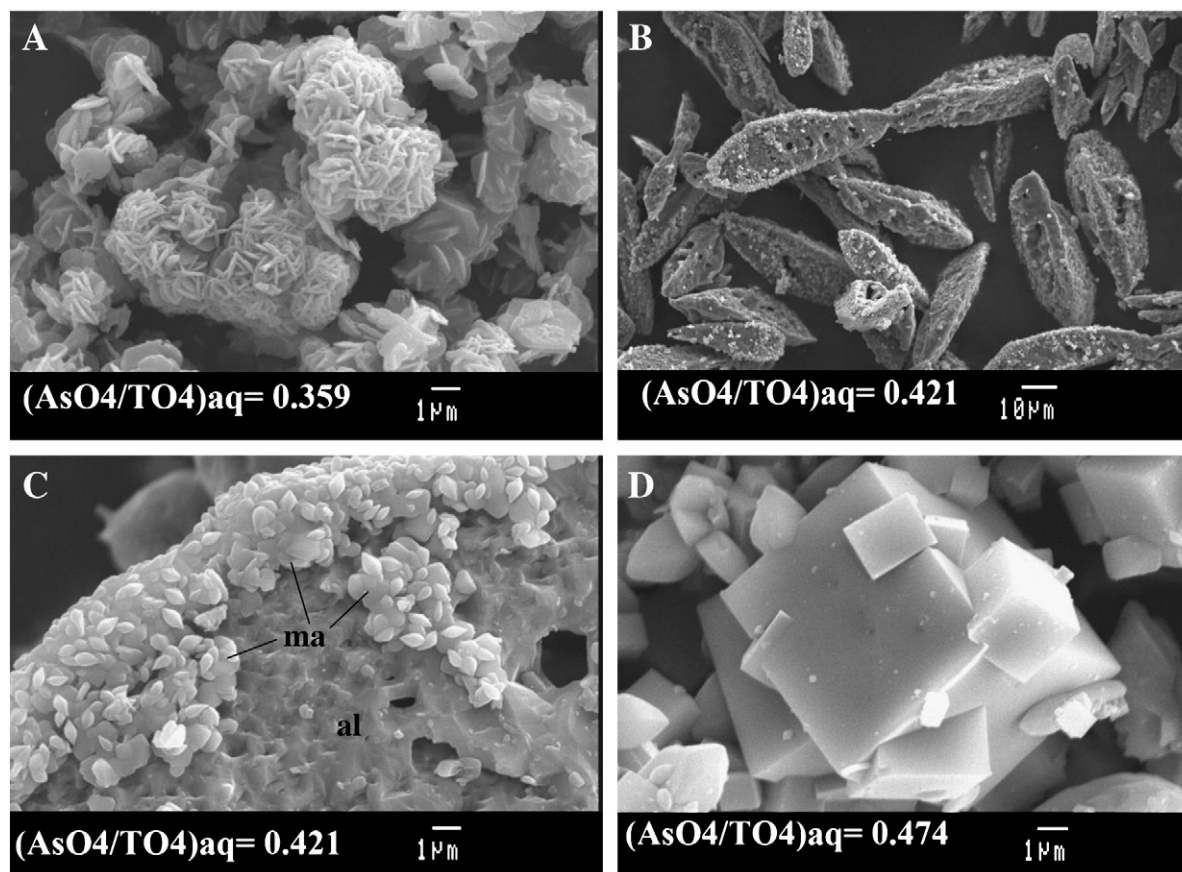


Fig. 8. Arsenate phases formed at high $(AsO_4/TO_4)_{aq}$. A: Mansfieldite. B: Alarsite. C: Mansfieldite (ma) on corroded alarsite (al). D: Natropharmacoalumite.

from a unique volcanic exhalation (Semenova et al., 1994). Thus, this phase seems clearly ineffective as a host for arsenic immobilization, as is also shown in Part 2 of this research (Sunyer and Viñals, 2011-this issue).

3.2.3.3. Natropharmacoalumite. Natropharmacoalumite precipitated at the highest $(AsO_4/TO_4)_{aq}$ studied (0.47) and in the presence of a large $(Na/Al)_{aq}$ ratio (3.34). It formed perfect cubic crystals up to 6 μm in size

(Fig. 8D) and the composition determined by EDS (mean of 10 punctual analyses) gave close to the ideal formula, $Na_{0.99 \pm 0.19}Al_{4.03 \pm 0.13}(AsO_4)_{3.00}(OH)_{4.08} \sim 5H_2O$. The formula was obtained by normalizing to $AsO_4 = 3$, OH by charge balance and H_2O was an approach given from the balance of total oxygen. Natropharmacoalumite was recently discovered as a natural phase (Rumsey et al., 2010) in close association with stable supergenetic phases such as minerals of the alunite family and

Table 4

Bulk chemical composition (ICP) and phase content (Rietveld) of hydrothermal precipitates in presence of gypsum (na: natroalunite; am: amorphous; an: anhydrite; ma: mansfieldite; hy: hydronium alunite).

Temperature (°C)	Time (h)	$(As/(S-Ca+As))_{aq}$	Chemical composition (%)					Phases (XRD and SEM/EDS)
			Na	Ca	Al	S	As	
$Na^+/Ca^{2+}/Al^{3+}/SO_4^{2-}/AsO_4^{3-}$								
200	2	0.100	4.20	1.03	21.00	17.91	1.35	na (98%) + an (2%)
200	2	0.182	4.75	1.07	20.37	16.14	2.60	na (98%) + an (2%)
200	0.5	0.182	4.26	1.55	18.44	14.93	3.46	na (97%) + ma (1%) + an (2%)
200	0.25	0.182	4.50	1.98	18.09	14.87	3.38	na (97%) + ma (1%) + an (2%)
180	2	0.182	4.11	1.53	17.34	13.03	6.62	na (89%) + ma (9%) + an (2%)
180	0.5	0.182	4.07	1.56	18.33	14.08	4.15	na (92%) + am (6%) + an (2%) ^a
180	0.25	0.182	4.42	1.49	17.24	14.24	3.60	na (94%) + am (4%) + an (2%) ^a
200	2	0.309	1.79	3.60	15.51	9.25	22.05	na (36%) + ma (51%) + an (11%)
200	2	0.309	1.57	7.90	13.52	10.33	18.69	na (31%) + ma (43%) + an (26%)
$Ca^{2+}/Al^{3+}/SO_4^{2-}/AsO_4^{3-}$								
200	2	0.182	0.00	17.97	9.71	14.88	9.33	hy (3%) + am (37%) + an (60%) ^b
200	2	0.309	0.00	1.20	15.20	3.55	34.40	ma (96%) + an (4%)
200	2	0.309	0.00	9.27	10.09	8.47	26.61	ma (68%) + an (32%)

^a Natroalunite and anhydrite from the Na and Ca contents. Amorphous by difference.

^b Anhydrite from Ca content. Hydronium alunite from the ratio hydronium alunite/anhydrite from Rietveld. Amorphous by difference.

Table 5
Formula coefficients in alunite phase obtained in presence of gypsum (EDS. Normalized to S + As = 2).

Temperature (°C)	Time (h)	(As/((S-Ca) + As)) _{aq}	Na	Ca	Al	S	As
<i>Na⁺/Ca²⁺/Al³⁺/SO₄²⁻/AsO₄³⁻</i>							
200	2	0.100	0.72 ± 0.08	0.04 ± 0.01	2.78 ± 0.07	1.93 ± 0.01	0.073 ± 0.008
200	2	0.182	0.79 ± 0.07	0.04 ± 0.01	2.99 ± 0.18	1.84 ± 0.01	0.16 ± 0.01
200	0.5	0.182	0.73 ± 0.04	0.06 ± 0.01	2.78 ± 0.12	1.82 ± 0.01	0.18 ± 0.01
200	0.25	0.182	0.76 ± 0.04	0.06 ± 0.01	2.78 ± 0.15	1.82 ± 0.02	0.18 ± 0.02
180	2	0.182	0.77 ± 0.06	0.06 ± 0.01	2.74 ± 0.08	1.80 ± 0.02	0.20 ± 0.02
180	0.5	0.182	0.73 ± 0.05	0.06 ± 0.01	2.70 ± 0.04	1.80 ± 0.02	0.20 ± 0.02
180	0.25	0.182	0.82 ± 0.05	0.06 ± 0.01	2.82 ± 0.12	1.80 ± 0.02	0.20 ± 0.02
200	2	0.309	0.87 ± 0.08	0.07 ± 0.02	2.76 ± 0.08	1.68 ± 0.03	0.32 ± 0.02
<i>Ca²⁺/Al³⁺/SO₄²⁻/AsO₄³⁻</i>							
200	2	0.182	0.00	0.12 ± 0.03	2.73 ± 0.02	1.73 ± 0.07	0.27 ± 0.07

clays (kaolinite). For this reason, natropharmacalumite could be investigated as a potential carrier for arsenic stabilization. However, the product synthesized in the present study was not especially suitable, due to the co-precipitation of alarsite and mansfieldite.

3.3. Precipitation in the presence of gypsum

Precipitation in the presence of gypsum was studied because many arsenical wastes contain large amounts of this product (Viñals et al. 2010a). Moreover, it was thought that a significant incorporation of Ca²⁺ in the “alkali” site could increase the AsO₄³⁻ substitution in the alunite structure through a charge balance mechanism.

3.3.1. Precipitation in Na⁺/Ca²⁺/Al³⁺/SO₄²⁻/AsO₄³⁻ media

The precipitation was studied from Al/Ca/As molar ratios of 6:1:1 to 3:2:2, changing the amounts of gypsum and Na₂HAsO₄·7H₂O added (Table 1). In all conditions, calcium appeared in the final product mainly as anhydrite, which obviously increased as the amount of gypsum added increased (Table 4). Furthermore, in the presence of an excess of Na⁺, the Ca²⁺ substitution in the alkali site of the alunite phase was very small (4–6%) and practically independent of gypsum addition, temperature, reaction time and other reagent ratios (Table 5).

The effect of the reaction time was studied for (AsO₄/TO₄)_{aq} = 0.182, at 180 °C and 200 °C. The effective (TO₄)_{aq} was taken as ((S-Ca)_{tot} + As)_{aq}, reflecting an approximation to the real SO₄²⁻_{aq}. Fig. 9A shows the Al & As precipitation yields. Precipitation at 180 °C followed the sequence natroalunite + amorphous → natroalunite + mansfieldite (Fig. 10A, B) observed previously in the absence of gypsum. Precipitation at 200 °C was faster than at 180 °C and the precipitates practically contained only natroalunite (Fig. 10C). However, the precipitates obtained at 180 °C and 200 °C presented an AsO₄-for-SO₄ substitution in natroalunite that was practically independent of the reaction time (Fig. 9B). These results are virtually identical to those observed for the precipitation in the absence of gypsum; the phase morphology and the crystal sizes were also similar.

The arsenic partition was studied for (AsO₄/TO₄)_{aq} from 0.100 to 0.309 at 200 °C. Results for the precipitation yields and AsO₄³⁻ distribution in solids are plotted in the Figs. 5 and 7, with the results obtained in the absence of gypsum. Like in the absence of gypsum, up to (AsO₄/TO₄)_{aq} = 0.182, the precipitates practically contained only natroalunite, but at (AsO₄/TO₄)_{aq} = 0.309 a large amount of mansfieldite was also formed. Furthermore, the ratios (AsO₄/TO₄)_{nat} and (AsO₄/TO₄)_{bulk} were also similar to those obtained in the absence of gypsum. Thus, the effect of gypsum addition during natroalunite precipitation was only a small Ca substitution in the alunite phase and the formation of anhydrite. Anhydrite occurred as large prismatic crystals (up to ~100 μm), which were formed before the natroalunite or mansfieldite, as these last phases usually grew on it.

3.3.2. Precipitation in Ca²⁺/Al³⁺/SO₄²⁻/AsO₄³⁻ media

Precipitation in the absence of Na⁺ was studied with the objective of forming alunite phases with high Ca and As content, such as schlossmacherite ((H₃O,Ca)Al₃(SO₄,AsO₄)₂(OH)₆), arsenocrandallite (CaAl₃(AsO₄)₂(OH)₆(H₂O)), or intermediate members:

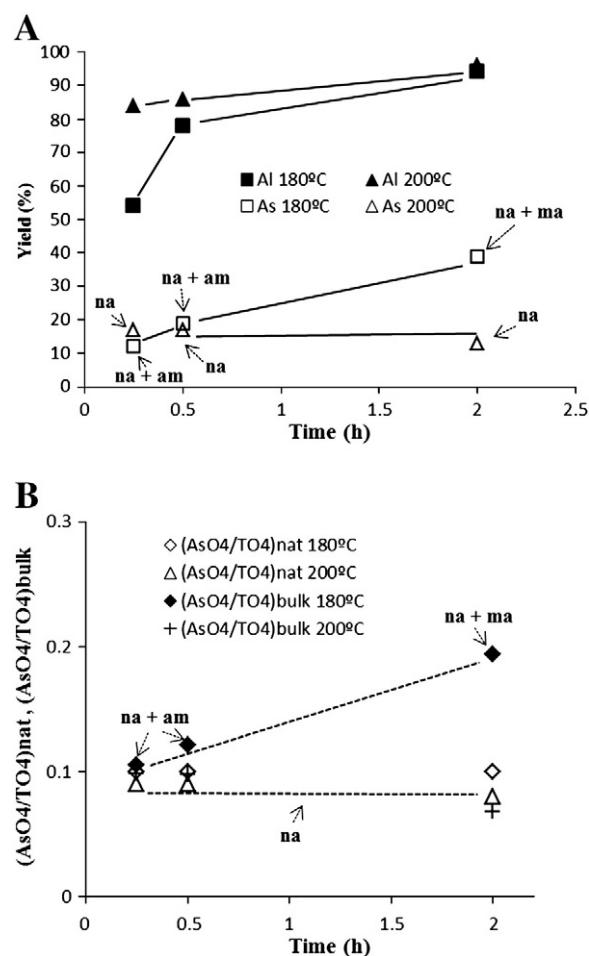
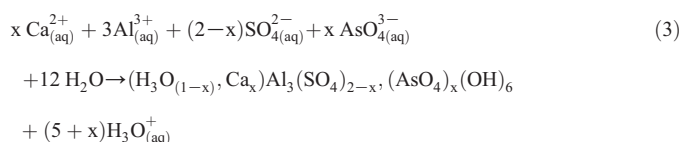


Fig. 9. Precipitation in presence of gypsum at (AsO₄/TO₄)_{aq} = 0.182. A: Al and As precipitation yields. B: Effect of time on arsenic incorporation.

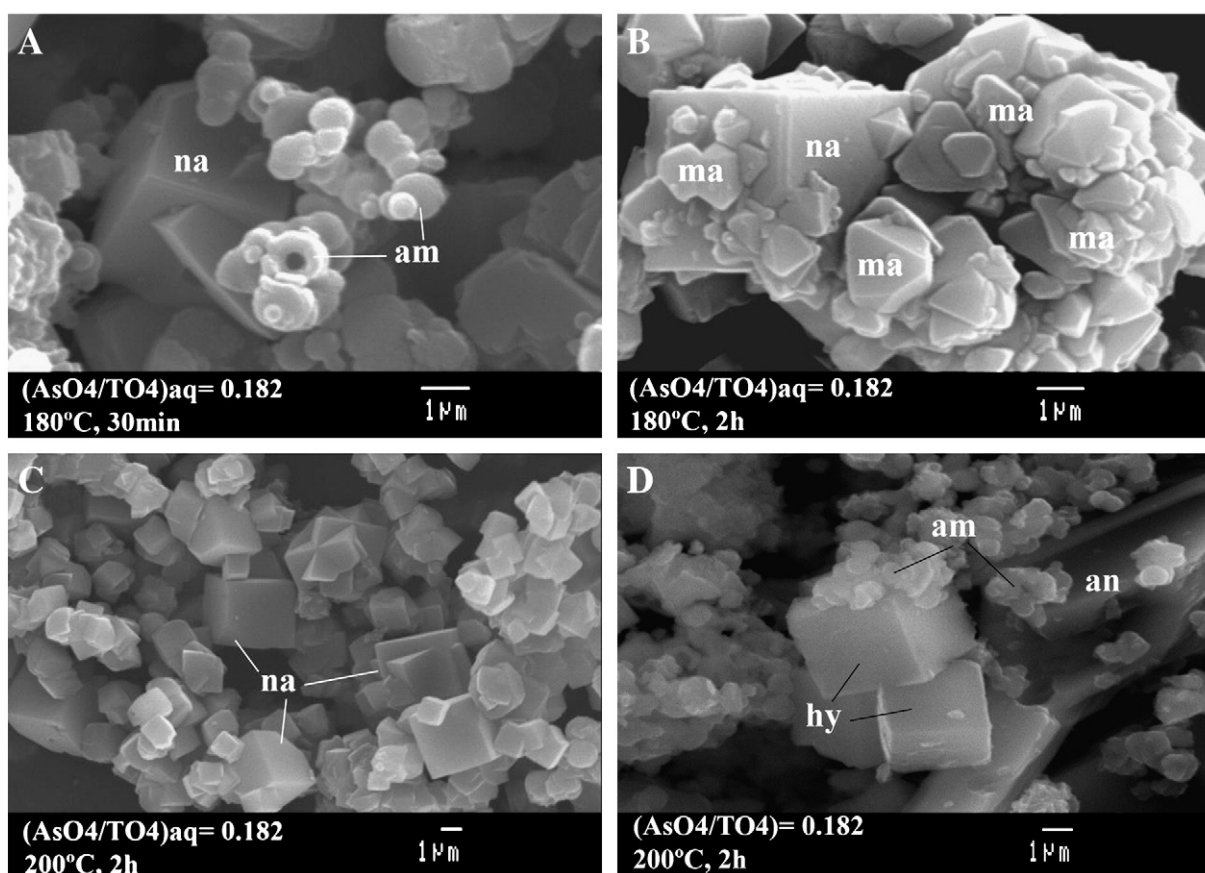


Fig. 10. A–C: precipitates obtained in $\text{Na}^+/\text{Ca}^{2+}/\text{Al}^{3+}/\text{SO}_4^{2-}/\text{AsO}_4^{3-}$ medium. D: in $\text{Ca}^{2+}/\text{Al}^{3+}/\text{SO}_4^{2-}/\text{AsO}_4^{3-}$ medium (na: natroalunite; am: amorphous; ma: mansfieldite; an: anhydrite; hy: hydronium alunite).

For comparison purposes, the experiments were performed at the same $(\text{AsO}_4/\text{TO}_4)_{\text{aq}}$ ratio that as those given in the preceding Section (0.182 and 0.309). For $(\text{AsO}_4/\text{TO}_4)_{\text{aq}} = 0.182$, the unique crystalline phase containing arsenic was a calcian hydronium alunite (Fig. 10D), with a degree of AsO_4 -for- SO_4 substitution of 14%. This substitution was higher than that observed for natroalunite (8–10%) at the same $(\text{AsO}_4/\text{TO}_4)_{\text{aq}}$ ratio. This moderate increase is probably related to a higher Ca^{2+} substitution in hydronium alunite (12%) than in natroalunite (4–6%). Nevertheless, these As and Ca substitution levels were smaller than those reported for the natural phase schlossmacherite, in which Ca substitution reached 26% and AsO_4 25% (Schmetzer et al., 1980). Meanwhile, the precipitation yield of hydronium alunite was almost insignificant (<5%) compared to the yield obtained in natroalunite precipitation (~95%). Consequently, the acidity generated was also low (final pH 1.9) and arsenic precipitated extensively as the amorphous $\text{Al}^{3+}/\text{AsO}_4^{3-}/\text{SO}_4^{2-}$ phase (Fig. 10D). These low precipitation yields as well as the extensive co-precipitation of the amorphous phase make hydronium alunite few attractive for arsenic immobilization. Rudolph et al. (2003) also reported that hydronium alunite was more difficult to synthesize, obtaining lower yields than for its potassium or sodium analogs.

For $(\text{AsO}_4/\text{TO}_4)_{\text{aq}} = 0.309$, the unique arsenical phase was mansfieldite (Table 4). So, an increase in $(\text{AsO}_4)_{\text{aq}}$ did not form alunite-type phases in the $\text{Ca}^{2+}/\text{Al}^{3+}/\text{SO}_4^{2-}/\text{AsO}_4^{3-}$ medium. The reported synthesis for arsenocrandallite (Schwab et al., 1991) was without SO_4^{2-} in the medium, and it was precipitated by the reaction of stoichiometric amounts of $\text{Ca}(\text{OH})_2 + \text{Al}(\text{OH})_3 + \text{H}_3\text{AsO}_4$ at 200 °C in 3 months. These conditions for arsenocrandallite synthesis, done in absence of SO_4^{2-} in the medium and long reaction times, limits this phase

as a suitable for arsenic immobilization of many arsenical wastes, in spite of its high arsenic content (20%) and probable good stability.

4. Conclusions

The rate of arsenical natroalunite precipitation increased with increasing temperature and AsO_4^{3-} concentration, being practically complete in <30 min at >180 °C. In $\text{Na}^+/\text{Al}^{3+}/\text{SO}_4^{2-}/\text{AsO}_4^{3-}$ aqueous media, natroalunite formation was faster and preferential than mansfieldite precipitation. The mansfieldite content in the precipitates decreased when increase the temperature, decrease the reaction time and, especially, when decreased the $(\text{AsO}_4/\text{TO}_4)_{\text{aq}}$ ratio. For $(\text{AsO}_4/\text{TO}_4)_{\text{aq}} < 0.2$ arsenic precipitated almost exclusively as natroalunite at 200 °C. For $(\text{AsO}_4/\text{TO}_4)_{\text{aq}}$ between 0.2 and 0.4 at 200 °C, a mixture of natroalunite + mansfieldite was formed and for $(\text{AsO}_4/\text{TO}_4)_{\text{aq}} > 0.4$, natroalunite was not precipitated, and other arsenate phases such as alarsite, mansfieldite and natropharmacoalunite appeared.

AsO_4 -for- SO_4 substitution in natroalunite between 160 and 200 °C was practically independent of the temperature and the reaction time, but it increased when the $(\text{AsO}_4/\text{TO}_4)_{\text{aq}}$ ratio increased. At 200 °C the degree of substitution can be expressed as $(\text{AsO}_4/\text{TO}_4)_{\text{nat}} \cong 0.5(\text{AsO}_4/\text{TO}_4)_{\text{aq}}$. The maximum arsenate substitution was ~15% molar.

Precipitation in the presence of gypsum conducted to the formation of anhydrite and to slight Ca substitution (4–6% molar) in the natroalunite structure. The effect of gypsum addition does not significantly change the arsenic precipitation pathway and the degree of arsenate-for-sulfate substitution in natroalunite.

In the absence of Na^+ , Ca/As rich alunite-type phases were not precipitated in $\text{Ca}^{2+}/\text{Al}^{3+}/\text{SO}_4^{2-}/\text{AsO}_4^{3-}$ media at reasonable rates.

Thus, the potential application of arsenocrandallite as a carrier for arsenic immobilization appears questionable, especially for wastes with high or moderate $\text{SO}_4^{2-}/\text{AsO}_4^{3-}$ ratios.

Acknowledgements

We acknowledge financial support from the *Spanish Ministerio de Ciencia e Innovación (DGI) (Programa de Materiales, MAT 2007-61466)* and the support of the *Serveis Científicotècnics de la Universitat de Barcelona* with the instrumentation for the characterization studies.

References

- Alcobé, X., Bassas, J., Tarruella, I., Roca, A., Viñals, J., 2001. Structural characterization of beudantite-type phases by Rietveld refinements. *Materials Science Forum* 378, 671–676.
- Bluteau, M.C., Demopoulos, G.P., 2007. The incongruent dissolution of scorodite—solubility, kinetics and mechanism. *Hydrometallurgy* 87, 163–177.
- Bluteau, M.C., Becze, L., Demopoulos, G.P., 2009. The dissolution of scorodite in gypsum-saturated waters: evidence of Ca-Fe-AsO₄ mineral formation and its impact on arsenic retention. *Hydrometallurgy* 97, 221–227.
- Caetano, M., Ciminelli, V., Rocha, S., Spitale, M., Caldeira, C., 2009. Batch and continuous precipitation of scorodite from dilute industrial solutions. *Hydrometallurgy* 95, 44–52.
- Demopoulos, G., Droppert, D., Van Weert, G., 1995. Precipitation of crystalline scorodite from chloride solutions. *Hydrometallurgy* 38, 245–261.
- Demopoulos, G.P., Lagno, F., Wang, Q., Singhana, S., 2003. The atmospheric scorodite process. In: Riveros, P., Dicon, D., Dreisinger, D., Menacho, J. (Eds.), *Copper 2003, IIMCH-MET SOC Canada, Santiago, Chile, TMS, VI(2)*, pp. 597–616.
- Drouet, C., Navrotsky, A., 2003. Synthesis, characterization, and thermochemistry of K–Na–H₂O jarosites. *Geochimica et Cosmochimica Acta* 67 (11), 2063–2076.
- Dutrizac, J.E., Jambor, J.L., Chen, T.T., 1987. Behaviour of arsenic during jarosite precipitation: reactions at 150 °C and the mechanism of arsenic precipitation. *Canadian Metallurgical Quarterly* 26 (2), 103–115.
- Fujita, T., Taguchi, R., Abumiya, M., Matsumoto, M., Shibata, E., Nakamura, T., 2008a. Novel atmospheric scorodite synthesis by oxidation of ferrous sulfate solution: Part I. *Hydrometallurgy* 90, 92–102.
- Fujita, T., Taguchi, R., Abumiya, M., Matsumoto, M., Shibata, E., Nakamura, T., 2008b. Novel atmospheric scorodite synthesis by oxidation of ferrous sulfate solution: Part II. Effect of temperature and air. *Hydrometallurgy* 90, 85–91.
- Fujita, T., Taguchi, R., Abumiya, M., Matsumoto, M., Shibata, E., Nakamura, T., 2009. Effect of pH on atmospheric scorodite synthesis by oxidation of ferrous ions: Physical properties and stability of scorodite. *Hydrometallurgy* 96, 189–198.
- Ichimura, R., Tateiwa, H., Almendares, C., Sanchez, G., 2007. Arsenic immobilization and metal recovery from El Teniente smelter dust. In: Riveros, P.A., Dixon, D.G., Dreisinger, D.B., Collins, M.J. (Eds.), *Copper 2007, CIM, Toronto, Canada, IV(2)*, pp. 191–203.
- Jambor, J.L., 1999. Nomenclature of the alunite supergroup. *Canadian Mineralogist* 37, 1323–1341.
- Kolitsch, U., Pring, A., 2001. Crystal chemistry of the crandallite, beudantite and alunite groups: a review and evaluation of the suitability storage materials for toxic products. *Journal of Mineralogical and Petrological Sciences* 96, 67–78.
- Kosten, A., 1978. ICDD Grant-in-Aid. Institut für Kristallographie, Technische Hochschule, Aachen, Germany.
- Krause, E., Ettl, V.A., 1989. Solubilities and stabilities of ferric arsenate compounds. *Hydrometallurgy* 22, 311–337.
- Le Berre, J.F., Cheng, T.C., Gauvin, R., Demopoulos, G.P., 2007a. Hydrothermal synthesis and stability evaluation of mansfieldite in comparison to scorodite. *Canadian Mineralogist Quarterly* 46, 1–9.
- Le Berre, J.F., Cheng, T.C., Gauvin, R., Demopoulos, G.P., 2007b. Hydrothermal synthesis and stability evaluation of iron (III)-aluminum (III) arsenate solid solutions. *Metallurgical and Materials Transactions B* 38, 159–166.
- Monhemius, A.J., Swash, P.M., 1999. Removal and stabilizing As from copper refining circuits by hydrothermal processing. *JOM* 51, 30–33.
- Paktunc, D., Dutrizac, J.E., 2003. Characterization of arsenate-for sulfate substitution in synthetic jarosite using X-ray diffraction and X-ray absorption spectroscopy. *Canadian mineralogist* 41, 419–905.
- Riveros, P.A., Dutrizac, J.E., Spencer, P., 2001. Arsenic disposal practices in the metallurgical industry. *Canadian Metallurgical Quarterly* 40, 395–420.
- Rudolph, W.W., Mason, R., Schmidt, P., 2003. Synthetic alunites of the potassium-oxonium solid solution series and some other members of the group: synthesis, thermal and X-ray characterization. *European Journal of Mineralogy*, 15, 913–924.
- Rumsey, M.S., Mills, M.S., Spratt, J., 2010. Natropharmacalumite, NaAl₄(OH)₄(AsO₄)₃·4H₂O, a new mineral of the pharmacosiderite supergroup and the renaming of aluminopharmacosiderite to pharmacalumite. *Mineralogical Magazine* 74 (5), 929–936.
- Savage, K.S., Bird, D.K., O'Day, P.A., 2005. Arsenic speciation in synthetic jarosite. *Chemical Geology* 215 (81–4), 473–498.
- Schmetzer, K., Ottemann, J., Bank, H., 1980. Schlosstmacherit, (H₂O,Ca)Al₃[(OH)₆](S,AsO₄)₂, ein neues Mineral der Alunit-Jarosit-Reihe. *Neues Jahrbuch für Mineralogie-Monatshefte* 215–220 (in German).
- Schwab, R.G., Götz, C., Harold, H., De Oliveira, N.P., 1991. Compounds of the crandallite type: synthesis and properties of pure (Ca, Sr, Ba, Pb, La, Ce, to Eu)-arsenocrandallites. *Neues Jahrbuch für Mineralogie-Monatshefte* 3, 97–112.
- Semenova, T.F., Vergasova, L.P., Filatov, S.K., Ananov, V.V., 1994. Alarsite AlAsO₄: a new mineral from volcanic exhalations. *Doklady Acad. Nauk SSSR* 338, 501–505 (In Russian).
- Sunyer, A., Viñals, J., 2011. Arsenate substitution in natroalunite: A potential medium for arsenic immobilization. Part 2: cell parameters and stability tests. *Hydrometallurgy* 109, 106–115 (this issue).
- Viñals, J., Sunyer, A., Molera, P., Cruells, M., Llorca, N., 2010a. Arsenic stabilization of calcium arsenate waste by hydrothermal precipitation of arsenical natroalunite. *Hydrometallurgy* 104, 247–259.
- Viñals, J., Sunyer, A., Torres, 2010b. Arsenic inertization from copper pyrometallurgy through phases of the alunite supergroup. *World of Metallurgy-Erzmetall* 63 (6), 301–309.

A.3 Arsenate substitution in natroalunite: A potential medium for arsenic immobilization. Part 2: Cell parameters and stability tests

A. Sunyer, J. Viñals, 2011, Arsenate substitution in natroalunite: A potential medium for arsenic immobilization. Part 2: cell parameters and stability tests, Hydrometallurgy, 109, 106-115.

Resum en català

L'efecte de la substitució d'AsO₄ en natroalunite ((Na, H₃O)Al₃(SO₄)_{2-x}(AsO₄)_x(OH)_{6-x}, x≤0.3) ha estat investigat a través de refinament dels DRX per Rietveld. Els refinaments han confirmat una estructura dels tipus R-3m amb Z=3 característica de les fases tipus alunite. La substitució AsO₄/(SO₄+AsO₄) va fer augmentar lleugerament el paràmetre de cel·la *c*, consistent amb l'expansió de cel·la degut a les diferències entre les distàncies As-O1 i S-O1 en l'estructura cristal·lina. El paràmetre de cel·la *a* va ser pràcticament independent a la substitució d'AsO₄.

La lixiviació i l'estabilitat de l'arsènic a les natroalunites arsenicals comparades amb altres fases relacionades (mansfieldita, alarsita, natrofarmacoalunite i arseniats d'alumini amorfs) van ser estudiades en un interval de pH's entre 1 i 12. La dissolució de la natroalunite arsenical va ser congruent a pH<3 i pH 12 i incongruent a pH's entre 4 i 11, mostrant una estabilitat màxima en pH's entre 5 i 8, en la que la solubilització de l'arsènic (24 h) va ser 0.01-0.05 mg/L. Aquests valors poden ser considerats bons per a la inertització d'arsènic en residus que contenen relacions SO₄²⁻/AsO₄³⁻ elevades. En els tests de lixiviació a curt termini (24 h), la mescla de natroalunite arsenical i mansfieldita va donar un comportament similar a la natroalunite arsenical. Tanmateix, els precipitats que contenien alarsita o arseniats d'alumini amorfs van donar valors de solubilitat d'arsènic de dos a tres ordres de magnitud majors. La natrofarmacoalunite va ser estable durant les 72 h de lixiviació a tot el rang de pH's d'entre 1 i 12. En medi àcid, aquesta fase intercanvia H₃O⁺ per Na⁺. L'estabilitat i les propietats d'intercanvi en àcid de la natrofarmacoalunite poden fer-la potencialment atractiva per l'eliminació d'arsènic, especialment quan pot existir contacte amb medi àcid o altres residus.



Arsenate substitution in natroalunite: A potential medium for arsenic immobilization. Part 2: Cell parameters and stability tests

Alba Sunyer, Joan Viñals*

Department of Materials Science and Metallurgical Engineering, University of Barcelona, Martí i Franqués 1, 08028 Barcelona, Spain

ARTICLE INFO

Article history:

Received 24 February 2011

Received in revised form 2 June 2011

Accepted 2 June 2011

Available online 13 June 2011

Keywords:

Arsenic
Immobilization
Inertization
Sodium alunite
Mansfieldite
Alarsite
Natropharmacoalumite

ABSTRACT

The effect of AsO_4 substitution in natroalunite $((\text{Na},\text{H}_3\text{O})\text{Al}_3(\text{SO}_4)_{2-x}(\text{AsO}_4)_x(\text{OH})_{6-x}, x \leq 0.3)$ has been investigated by Rietveld refinement of the XRD patterns. Cell refinements confirmed a structural type R-3 m $Z=3$, characteristic of alunite-type phases. AsO_4 -for- SO_4 substitution slightly increased the c unit-cell parameter, in consistency with the cell expansion due to the differences between As-O1 and S-O1 distances in the crystal structure. The a cell parameter was practically independent of the AsO_4 substitution.

The arsenic leaching and stability of arsenical natroalunite compared with other related phases (mansfieldite, alarsite, natropharmacoalumite and amorphous Al-arsenate) was studied in the pH interval 1 to 12. The dissolution of arsenical natroalunite was congruent at $\text{pH} < 3$ and $\text{pH} 12$ and incongruent at pH between 4 and 11, showing the maximum stability at pH 5 to 8, in which the As solubilization (24 h) were 0.01–0.05 mg/L. These values can be considered suitable for the inertization of wastes containing large $\text{SO}_4^{2-}/\text{AsO}_4^{3-}$ ratios. In short term leaching tests (24 h), the mixture of arsenical natroalunite and mansfieldite showed a similar behavior to arsenical natroalunite. However, precipitates containing alarsite or amorphous Al-arsenate showed As solubilization two or three orders of magnitude greater. Natropharmacoalumite was very stable for 72 h of leaching in pH range 1 to 12. In acid medium, this phase exchanged H_3O^+ for Na^+ . The stability and acid-exchange properties of natropharmacoalumite could make it potentially attractive for arsenic disposal, especially when it can exist in contact with acidic soils or wastes.

© 2011 Elsevier B.V. All rights reserved.

1. Introduction

The effects of temperature, reaction time and solution composition on precipitation yields, phase composition and degree of arsenate-for-sulfate substitution in natroalunite (ideally $\text{NaAl}_3(\text{SO}_4)_2(\text{OH})_6$) have been reported in the Part 1 of this research (Sunyer and Viñals, 2011-this issue). The previous study showed that for $(\text{AsO}_4/\text{TO}_4)_{\text{aq}} < 0.2$ ($\text{TO}_4 \equiv \text{SO}_4 + \text{AsO}_4$), arsenic precipitated almost exclusively as natroalunite at 200 °C. For $(\text{AsO}_4/\text{TO}_4)_{\text{aq}}$ between 0.2 and 0.4 at 200 °C, a mixture of natroalunite + mansfieldite ($\text{AlAsO}_4 \cdot 2\text{H}_2\text{O}$) was formed and for $(\text{AsO}_4/\text{TO}_4)_{\text{aq}} > 0.4$, natroalunite was not precipitated, appearing arsenate phases such as mansfieldite, alarsite (AlAsO_4) and natropharmacoalumite ($\text{NaAl}_4(\text{AsO}_4)_3(\text{OH})_4 \cdot 4\text{H}_2\text{O}$). Precipitation in the presence of gypsum ends with the precipitation of anhydrite and produced a small Ca substitution (4–6% molar) in the natroalunite structure. However, the effect of gypsum addition did not significantly change the arsenic precipitation pathway and the degree of arsenate-for-sulfate substitution. In the interval 160–200 °C, AsO_4 -for- SO_4 substitution in natroalunite was practically independent of temperature and reaction time but increased when $(\text{AsO}_4/\text{TO}_4)_{\text{aq}}$ increased.

The maximum arsenate substitution observed was ~15% molar. However, the effect of this substitution in the natroalunite structure was unknown.

Phases of the alunite supergroup ($\text{AB}_3(\text{TO}_4)_2(\text{OH},\text{H}_2\text{O})_6$) are hexagonal and generally belong to the space group R-3 m (Menchetti and Sabelly, 1976; Sato et al., 2009; Szymanski, 1985). Most of the members of this group have unit cells with $Z=3$ and cell parameters: $a \sim 7 \text{ \AA}$ and $c \sim 17 \text{ \AA}$. However, sulfates of the alunite ($B = \text{Al}$) or jarosite ($B = \text{Fe}$) families containing $\text{Ca}_{0.5}$, $\text{Ba}_{0.5}$ and $\text{Pb}_{0.5}$ have supercells with $Z=6$ and double c parameter ($\sim 34 \text{ \AA}$) as a consequence of the ordering of the A atom and associated vacancy (Basciano and Peterson, 2010; Li et al., 1992). The structure of most of these phases, and particularly natroalunite, has been extensively studied (Okada et al., 1982; Sato et al., 2009). It consists of a TO_4 tetrahedra and $\text{BO}_2(\text{OH})_4$ octahedra, linked as schematized in Fig. 1. The alkali site is coordinated with six O atoms and six OH groups as a $\text{AO}_6(\text{OH})_6$ icosahedra. According to the structure arrangement, the c parameter should basically depends on the A and T atom size and the a parameter on the B atom size (Sato et al., 2009; Schwab et al., 2005).

Structural researches on partial or complete substitutions in alunite-type compounds are also known. Rudolph et al. (2003) investigated the K–Na– H_3O alunite solid solution series and Drouet and Navrotsky (2003) and Basciano and Peterson (2010) the K–Na– H_3O jarosites. These studies corroborate that substitution in the A site

* Corresponding author. Tel.: +34 934021317; fax: +34 934039621.
E-mail address: jvinalsvinals@ub.edu (J. Viñals).

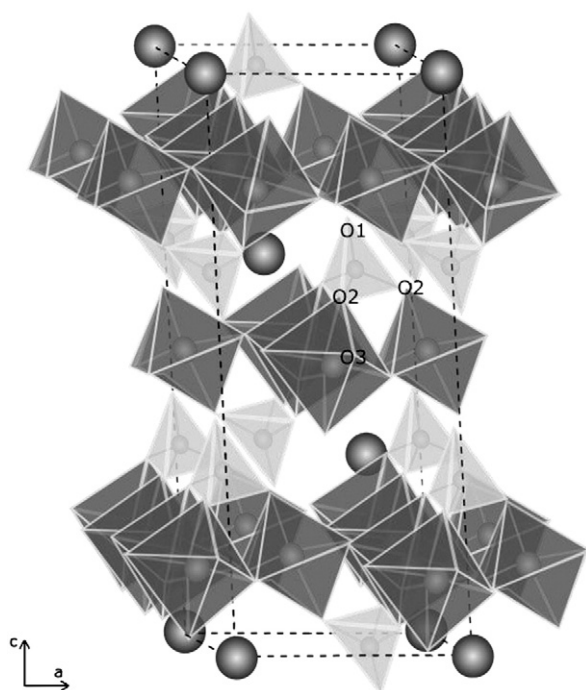


Fig. 1. Schema of the natroalunite structure. The dashed lines show the unit cell. SO_4 groups are the light colored tetrahedra, $\text{Al-O}_2(\text{OH})_4$ octahedra are dark grey and the large spheres represent Na. The SO_4 group is triply coordinated with $\text{Al-O}_2(\text{OH})_4$ octahedra through the O2 atom, whereas the O1 (apical) atom is not coordinated. The O3 atom is linked as OH group (H atoms are not shown).

affects mainly the c parameter, increasing lineally when increases K or H_3O substitution in Na-alunites or Na-jarosités, whereas the a parameter is scarcely affected. Nevertheless, few studies have focused the studies on partial As substitution in simple alunites or jarosités. Paktunc and Dutrizac (2003) reported up to 17% molar As substitution in potassium jarosite and Savage et al. (2005) up to 30%. The effect of this substitution was reflected in an increase in the c parameter on increasing As-substitution, whereas the a parameter remained practically constant (Paktunc and Dutrizac, 2003). However, the stability of these arsenical jarosités and particularly the arsenic solubilization was not reported.

The objectives of this paper are a structural study by the Rietveld method of the As substitution in natroalunite and a comparative leaching study to evaluate the As solubilization and phase stability in a wide pH interval (1–12).

2. Experimental methods

2.1. Rietveld study

Rietveld refinement was done basically to corroborate the alunite-type structure, the variation in cell parameters and the phase quantification. Two types of arsenical natroalunites were studied (Table 1): a) selected samples obtained from pure reagents and b) selected samples obtained from the stabilization process of a real waste (Viñals et al., 2010). Most of the arsenical natroalunites from pure reagents contained significant hydronium substitution. The arsenical natroalunites from waste inertization did not have a significant hydronium but contained small amounts of iron and calcium and trace of phosphorous as a result of the complex composition of the original waste. In addition, some samples were mixtures of arsenical natroalunite with mansfieldite and/or anhydrite (CaSO_4).

Powder diffraction data were collected using PANalytical X'Pert PRO MDP Alpha'1 equipment with Bragg-Brentano geometry and

Table 1

Samples studied by Rietveld refinement. Phase content and natroalunite formula (H_3O by difference) (na: natroalunite; ma: mansfieldite; an: anhydrite).

Sample	Phases (%)			Natroalunite formula (EDS)						
	na	ma	an	S	As	Al	Fe	Na	H_3O	Ca
<i>From pure reagents</i>										
N8	100	–	–	2.00	0.00	2.88	–	0.74	0.26	–
TAS4	85	15	–	1.80	0.20	2.76	–	0.94	0.06	–
TAS6	87	13	–	1.79	0.21	2.72	–	0.93	0.07	–
TAS7	91	9	–	1.82	0.18	2.74	–	0.96	0.04	–
TAS8	82	18	–	1.80	0.20	2.69	–	0.96	0.04	–
AS1	100	–	–	1.93	0.074	2.80	–	0.80	0.20	–
AS2	100	–	–	1.92	0.086	2.80	–	0.82	0.18	–
AS3	100	–	–	1.90	0.10	2.92	–	0.88	0.12	–
AS4	100	–	–	1.87	0.13	2.82	–	0.82	0.18	–
AS5	100	–	–	1.85	0.15	2.80	–	0.94	0.06	–
AS7	100	–	–	1.84	0.16	2.84	–	0.94	0.06	–
AS8	71	29	–	1.78	0.22	2.77	–	0.97	0.03	–
AS9 ^a	95	3	–	1.74	0.26	2.86	–	1.01	–	–
AS10	32	68	–	1.69	0.31	2.92	–	0.98	0.02	–
ASC1	98	–	2	1.93	0.073	2.78	–	0.72	0.20	0.04
ASC2	98	–	2	1.84	0.16	2.99	–	0.79	0.13	0.04
ASC8	36	51	11	1.68	0.32	2.76	–	0.87	–	0.07
<i>From calcium arsenate waste^b</i>										
W1	38	2	60	1.84	0.14	2.70	0.12	0.98	–	0.08
W2	23	6	71	1.76	0.22	2.69	0.12	0.96	–	0.08
W3	13	10	77	1.68	0.28	2.70	0.08	0.90	0.02	0.04
W4	20	9	71	1.74	0.22	2.64	0.09	1.00	–	0.08
W5	81	19	–	1.80	0.20	2.82	0.15	1.00	–	0.00

^a Contained 2% alarsite. ^b Contained 0.00–0.04 P.

240 mm radius. Data were collected from 10° to 120° 2θ with a monochromatic radiation Cu-K α 1 1.5406, with a step size of 0.017 using a step counting time of 200 s. The Rietveld method (Rietveld, 1967, 1969) was used for the profile refinements using the FullProf program (Rodríguez-Carvajal, 1990, 1997). The modified Thomson-Cox-Hasting pseudo-Voigt function for the calculated profile was used in the refinements. The starting atomic parameters for natroalunite, mansfieldite, anhydrite, and alarsite were taken from Okada et al. (1982), Harrison (2000), Hawthorne and Ferguson (1975) and Sowa (1991), respectively. The starting site occupancies for natroalunite were changed using the formulas obtained by EDS analysis (Table 1). The refined parameters were the background, the scale factors, the unit cell parameters, the profile and the asymmetry. All the parameters were adjusted to minimum values.

2.2. Leaching experiments

Leaching experiments to determine the As solubilization and the comparative phase stability were performed on four selected samples containing natroalunite, natroalunite + mansfieldite, alarsite + natropharmacoalumite + mansfieldite and amorphous Al-arsenate (Table 2). Experiments were performed as described in Viñals et al. (2010) as follows: 0.5 g sample was treated with a 50 mL solution of desired pH in a plastic erlenmeyer with magnetic stirring (250 rpm). The

Table 2

Samples studied in leaching tests. Bulk chemical composition and phase content (na: natroalunite; ma: mansfieldite; al: alarsite; ph: natropharmacoalumite; am: amorphous; hy: hydronium alunite; an: anhydrite).

Sample	Bulk chemical composition (ICP)					Phases (%)						
	S	As	Al	Na	Ca	na	ma	al	ph	am	hy	an
AS5	13.77	2.53	17.53	4.91	–	100	–	–	–	–	–	–
AS8	10.46	12.97	17.92	3.68	–	71	29	–	–	–	–	–
AS13	0.08	32.52	14.96	2.17	–	–	11	24	65	–	–	–
ASC10	14.88	9.33	9.71	–	17.97	–	–	–	–	37	3	60

Table 3
Data collection and structure refinement details.

Sample	X_{As}	X_{H_3O}	a(Å)	c(Å)	V(Å ³)	R_p	R_{wp}	R_{exp}	S	R_f
<i>From pure reagents</i>										
N8	0.000	0.26	6.9972(8)	16.8149(2)	712.99(1)	14.0	18.7	7.87	2.38	5.59
AS1	0.037	0.20	7.0010(2)	16.7698(4)	711.84(0)	9.71	13.2	7.74	1.71	6.06
AS2	0.043	0.18	7.0006(5)	16.7624(7)	711.45(1)	14.3	14.8	8.86	1.67	5.93
AS3	0.050	0.12	6.9998(9)	16.7609(6)	711.23(4)	9.80	13.2	8.82	1.50	5.35
AS4	0.065	0.18	6.9988(0)	16.7590(7)	710.93(1)	9.72	13.2	9.11	1.45	4.70
AS5	0.075	0.06	7.0016(9)	16.7577(7)	711.46(4)	8.69	11.8	7.64	1.54	4.94
AS7	0.080	0.06	7.0028(6)	16.7609(6)	711.83(6)	9.09	12.2	7.62	1.60	5.21
TAS7	0.090	0.04	7.0052(6)	16.7650(1)	712.49(6)	13.4	18.8	16.4	1.15	6.43
TAS4	0.10	0.06	7.0054(9)	16.7624(7)	712.43(5)	12.1	16.7	14.4	1.16	4.74
TAS8	0.10	0.04	7.0040(7)	16.7651(9)	712.26(3)	12.4	17.4	15.5	1.13	5.05
TAS6	0.11	0.07	7.0058(1)	16.7701(5)	712.82(8)	13.9	19.4	14.5	1.34	5.10
AS8	0.11	0.03	7.0028(7)	16.7637(2)	711.95(7)	7.68	10.1	7.14	1.41	3.96
AS9	0.13	–	7.0025(7)	16.7657(7)	711.98(2)	14.5	18.9	11.4	1.67	6.93
AS10	0.15	0.02	7.0055(5)	16.779(0)	713.15(2)	6.85	9.07	6.65	1.36	3.88
ASC1	0.036	0.10	6.9964(8)	16.801(0)	712.24(0)	18.2	24.5	16.2	1.52	7.40
ASC2	0.080	0.07	6.9965(8)	16.765(2)	710.74(0)	16.7	23.3	17.1	1.36	7.05
ASC8	0.16	–	7.0019(0)	16.740(9)	710.79(2)	15.3	22.0	12.4	1.78	8.52
<i>From calcium arsenate waste</i>										
W1	0.07	–	6.9953(8)	16.789(0)	711.50(5)	26.6	28.5	19.1	1.49	6.31
W5	0.10	–	7.0021(4)	16.813(1)	713.90(8)	27.3	23.2	18.4	1.23	4.89
W2	0.11	–	6.9915(6)	16.806(9)	711.49(0)	31.0	32.8	20.2	1.62	6.13
W4	0.11	–	6.984(5)	16.815(6)	710.43(8)	40.8	47.6	19.3	2.47	7.84
W3	0.14	–	6.984(8)	16.832(9)	711.23(0)	32.3	34.0	21.0	1.62	7.61

X: Occupancies; R_p : R-pattern; R_{wp} : weighted pattern; R_{exp} : R-expected; $S = R_{wp}/R_{exp}$: goodness of fitting; R_f : crystallographic R-factor for natroalunite phase.

solutions of different pH were obtained from stock solutions of diluted H_2SO_4 and NaOH. During the experiments, the pH was monitored and the variations were corrected. For acidic to near neutral media, these corrections were sporadic but from neutral to strong alkaline media the system required more correction because of the tendency towards acidulation. However, variations in pH in these media were maintained to ± 0.3 pH units. Three consecutive leaching tests of 24 h were performed. After each leaching, the sample was filtered and the solid underwent the subsequent leaching. Solutions obtained after leaching were diluted 1:10 in 1% HCl to prevent possible re-precipitation during storage. Finally, the solutions and blanks were analyzed for As, Al and occasionally for Na and S, by ICP-MS in a Perkin Elmer Elan-6000 spectrometer. Selected residues from leaching experiments (72 h total leaching) were characterized by XRD and SEM/EDS.

3. Results and discussion

3.1. Structural study

3.1.1. Rietveld refinement

Results of the Rietveld refinement of arsenical natroalunite are given in Table 3. Fig. 2 shows Rietveld plots for three selected samples: a sample of natroalunite from pure reagents, a sample of natroalunite + mansfieldite from pure reagents and a sample of natroalunite + mansfieldite + anhydrite from calcium arsenate waste. Most of the samples containing natroalunite, and natroalunite + mansfieldite showed natroalunite crystallographic R_f parameters less than 6%. This indicated that the structural model taken from Okada et al. (1982) was accurate for our samples, independently of the AsO_4 -for- SO_4 substitution. Profile parameters (R_p , R_{wp}) were relatively large, probably due to the variations in the microstructural composition (zonation) of the crystallites, caused by the changing composition of the solution during the synthesis. However, the S factor (goodness of fitting) was satisfactory.

In samples containing anhydrite (ASC and W), the R_f of natroalunite was between 6 and 8.5%. This fact may be related to the difficulties to correct the preferred orientation of anhydrite when this phase overlaps with some major peaks of natroalunite.

On the other hand, the R_p and R_{wp} in samples from calcium arsenate waste (W) were higher than those obtained from samples from pure reagents. This can be attributed to the wider and more complex shapes of the peaks, as consequence of the more complex lattice substitutions, but the goodness of fitting was also relatively satisfactory.

3.1.2. Effect of AsO_4 substitution on cell parameters

According to the topology of the alunite structure (Fig. 1), each TO_4 tetrahedra in the unit cell is placed so that one of its basal planes is perpendicular to c axis. Consequently, the partial substitution of AsO_4 -for- SO_4 in natroalunite should increase especially the c parameter, because the As–O apical distances (As–O1 ~ 1.57 Å) in arsenates of alunite group are significantly greater than the S–O apical distances (S–O1 ~ 1.45 Å) (Sato et al., 2009). However, the c parameter also depends on the A cation size because it is positioned in a 12-fold coordination polyhedra ($(AO_6OH)_6$) between two sheets, which can also have strongly influence on the interlayer distance. Thus, when significant hydronium substitution was present jointly with arsenate substitution in natroalunite, these two effects overlapped. In the natroalunite-hydronium alunite series, the c parameter increased with hydronium substitution as: $c = 16.6700 + 0.466 X_{H_3O}$ (Å) (Rudolph et al., 2003), due to the difference between the H_3O^+ ionic radius (1.52 Å) and the Na^+ ionic radius (1.39 Å) (Basciano and Peterson, 2008; Shannon, 1976).

The variation of the c parameter as a function of As-substitution in natroalunite, including the reported values from arsenical jarosite (Paktunc and Dutrizac, 2003), is given in Fig. 3. For natroalunite samples from calcium arsenate waste –which were practically free of hydronium substitution– the c parameter increased, with a slope of 0.59 when AsO_4 substitution increased. For natroalunite from synthetic reagents –which showed up to ~25% molar hydronium substitution– the c values were corrected as: $c_{cor} = c - 0.466 X_{H_3O}$ (Å), according to the data reported by Basciano and Peterson (2008) on the effect of the H_3O occupancy (X_{H_3O}). These corrected values also showed a similar dependency on AsO_4 substitution. The c parameters for arsenical jarosite were greater than arsenical natroalunite because of the large difference in A ionic radius ($K^+ = 1.64$ Å; Shannon, 1976),

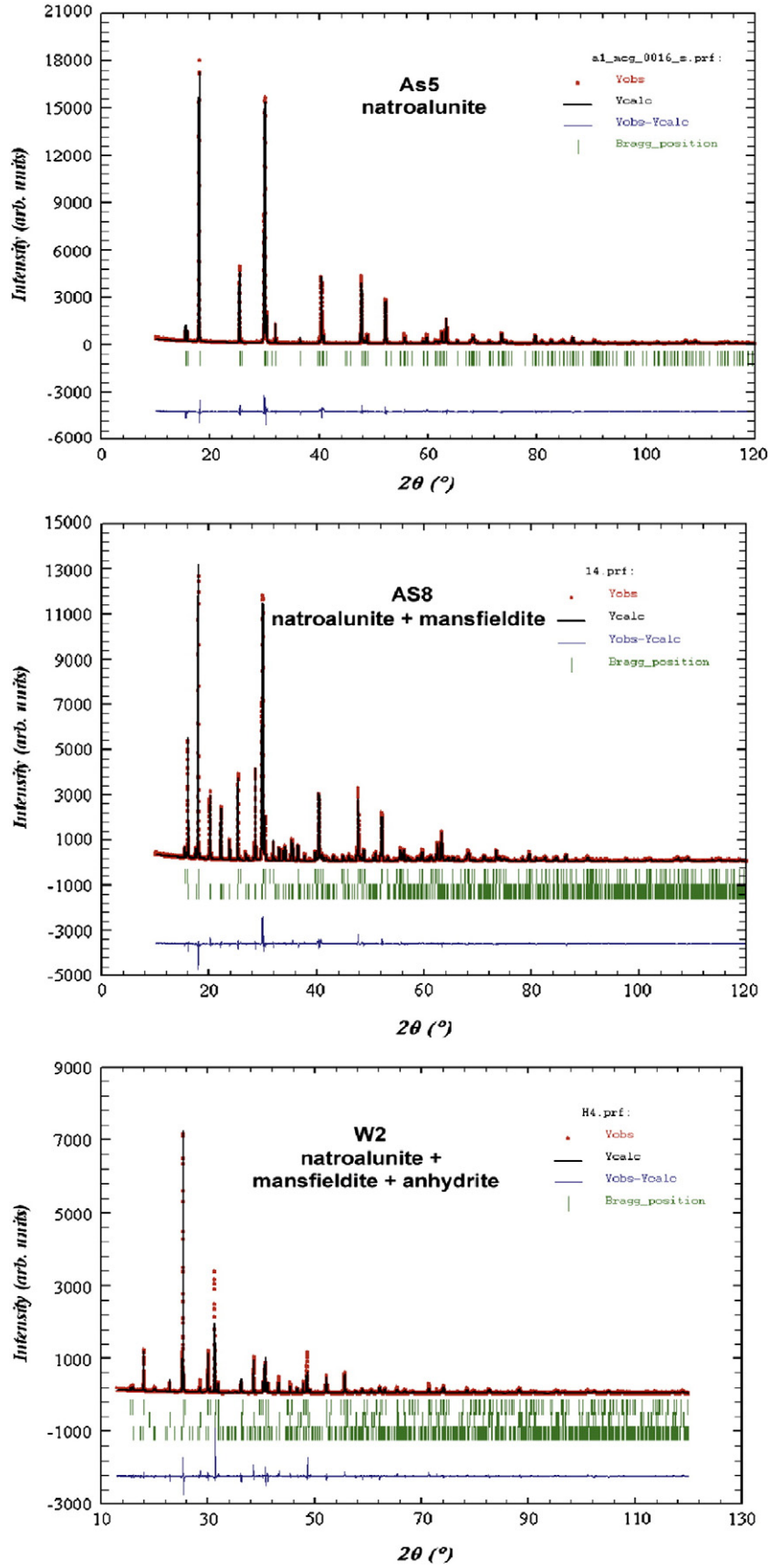


Fig. 2. Rietveld plots: arsenical natroalunite from pure reagents (AS5). Arsenical natroalunite + mansfieldite from pure reagents (AS8). Arsenical natroalunite + mansfieldite + anhydrite from calcium arsenate waste (W2).

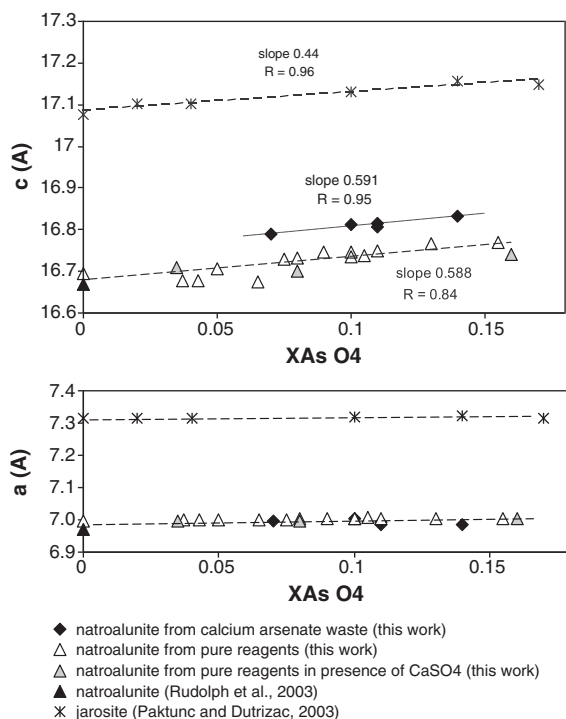


Fig. 3. Effect of AsO₄ substitution in cell parameters of natroalunite compared with jarosite (*c* parameter in natroalunite was corrected for H₃O⁺ substitution as: $c = 0.466 \cdot X_{\text{H}_3\text{O}}$).

but the reported increment with AsO₄ substitution was relatively similar (slope 0.44).

In contrast, the variation of the *a* parameter with AsO₄ substitution was insignificant (Fig. 3). The *a* parameter of arsenical jarosite was also greater than in arsenical natroalunite because of the difference in B–O distances in alunite-type structures (Al–O₂ ~2.81 Å, Fe–O₂ ~2.96 Å; Sato et al., 2009), but the effect of AsO₄ substitution on the *a* parameter was also negligible.

The increase in the *c* parameter due to the AsO₄ incorporation in natroalunite was relatively small (<0.1 Å) and was obviously limited by the maximum ~15% substitution observed. However, if 100% substitution was possible, the extrapolated expansion would be 0.58 Å on the *c* axis. Taking a value of 0.12 Å for the difference between As–O and S–O apical distances (T–O1) in the alunite structures (Sato et al., 2009) and given that the unit cell hold three layers of tetrahedra, the *c* expansion for complete substitution would be ~0.54 Å. On the other hand, complete AsO₄-for-SO₄ substitution is well known in the alunite supergroup for divalent cations such as Ca²⁺, in which the end members are represented by huangite (Ca_{0.5}□_{0.5}Al₃(SO₄)₂(OH)₆) and arsenocrandallite (CaAl₃(AsO₄)₂(OH)₆(H₂O)). Comparison of Ca and Na alunites was easier due to the small difference of Na⁺ (1.39 Å) and Ca²⁺ (1.34 Å) ionic radii (Shannon, 1976) and corroborated by the relatively similar subcell parameters of huangite (*a* = 6.9830 Å, *c*/2 = 16.7585 Å; Li et al., 1992) and the cell parameters of natroalunite (*a* = 6.9711 Å, *c* = 16.6700 Å, Rudolph et al., 2003). For arsenocrandallite, the reported parameters were *a* = 7.0810 Å and *c* = 17.2700 Å (Schwab et al., 1991). Consequently, the expansion in Ca-alunite series is 0.51 Å on the *c* axis, close to the extrapolated value for arsenical natroalunite. We recognize that the cell parameters in this study may also be slightly affected by the small variations in the Al occupancy and, in some samples, by small substitutions of Ca or Fe; however, these effects should be less significant. Thus, the results obtained supported the substitution of AsO₄-for-SO₄ in the tetrahedral sites of the alunite structure.

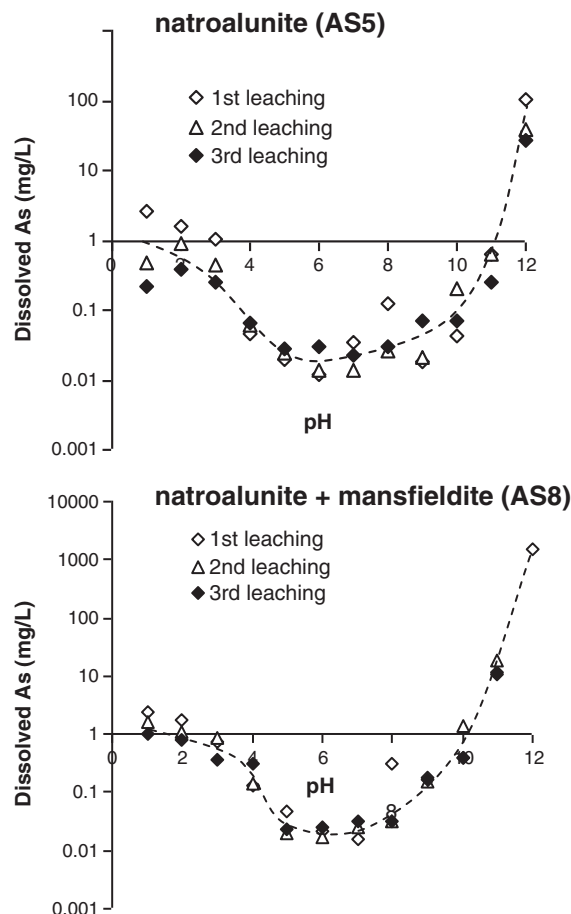


Fig. 4. Dissolved As as a function of pH for samples containing natroalunite and natroalunite + mansfieldite (24 h).

3.2. Leaching study

3.2.1. Arsenic leaching

3.2.1.1. Samples of natroalunite and natroalunite + mansfieldite. The dissolved arsenic as a function of pH for the samples of natroalunite, and natroalunite (71%) + mansfieldite (29%) was relatively similar in all pH range studied (Fig. 4). Generally, the values of the 1st leaching were slightly higher than those of the 2nd and the 3rd, which were practically identical. Natroalunite and mansfieldite were very stable at pH 1. The dissolved As at this pH was less than 1 mg/L in the 2nd and 3rd leaching in natroalunite, whereas mansfieldite showed values between 1 and 2 mg/L. These results are consistent with those obtained from natroalunite and mansfieldite from real wastes (Viñals et al., 2010). Compared with scorodite, arsenical natroalunite and mansfieldite were much more stable at pH 1. Scorodite reported values were 50–100 mg As/L at this pH (Krause and Ettel, 1989; Swash et al., 2000).

When the pH was increased, the As solubilization from the natroalunite and the natroalunite + mansfieldite mixture decreased, reaching minimum values about 0.01–0.05 mg/L in the interval of pH 5 to 8, similar as the found in natroalunite precipitates from real waste (Viñals et al., 2010). Few data from other synthetic alunites or jarosites with partial AsO₄-for-SO₄ substitution are available for comparison purposes. Smith et al. (2006) studied a sample of Pb–As-jarosite (15% molar AsO₄ substitution), which showed As solubilities of 3 mg/L at pH 2 and 0.15 mg/L at pH 8. For scorodite, the minimum solubilities reported by Krause and Ettel (1989), Bluteau and Demopoulos (2007), Fujita et al. (2009) at pH 5 were 0.1–1 mg/L.

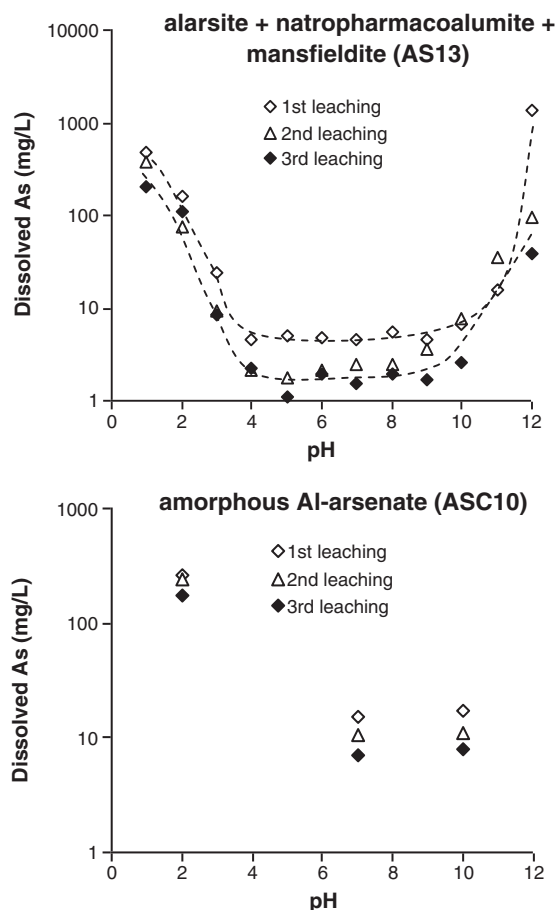


Fig. 5. Dissolved As as a function of pH for samples containing alarsite and amorphous Al-arsenate (25 °C, 24 h).

In the interval of pH 9 to 11, the As solubilization from natroalunite increased, this increment being more significant in the sample containing mansfieldite. Finally, at pH 12 the leached As increased dramatically as a result of the extensive or total decomposition of natroalunite and mansfieldite.

3.2.1.2. Samples containing alarsite and amorphous arsenate. The As leaching in sample AS13, which contained alarsite (24%), natropharmacoalumite (65%) and mansfieldite (11%), is shown in Fig. 5. The As concentrations were two or three orders of magnitude greater than in samples of natroalunite, and of natroalunite + mansfieldite. This was attributed to the unstable nature of the alarsite, which was shown in a previous study (Sunyer and Viñals, 2011-this issue) and is corroborated in the next section.

The results of the dissolved arsenic at pH 2, 7 and 10 for sample ASC10, which contained practically all the arsenic as amorphous Al-arsenate, are also reported in Fig. 5. Compared with natroalunite and mansfieldite, the dissolved arsenic was also more than two orders of magnitude greater. Thus, the presence of alarsite and/or amorphous arsenates even in amounts of <1%, which are very difficult to detect by SEM and spectroscopic techniques, may dramatically alter the As solubility data for some crystalline aluminium arsenate phases. An indicator of its potential presence after synthesis could be the results of the leaching tests, especially at strong acid pH's.

3.2.2. Stability considerations

3.2.2.1. Natroalunite and mansfieldite. The results of As and Al extraction in natroalunite as a function of pH are shown in Fig. 6.

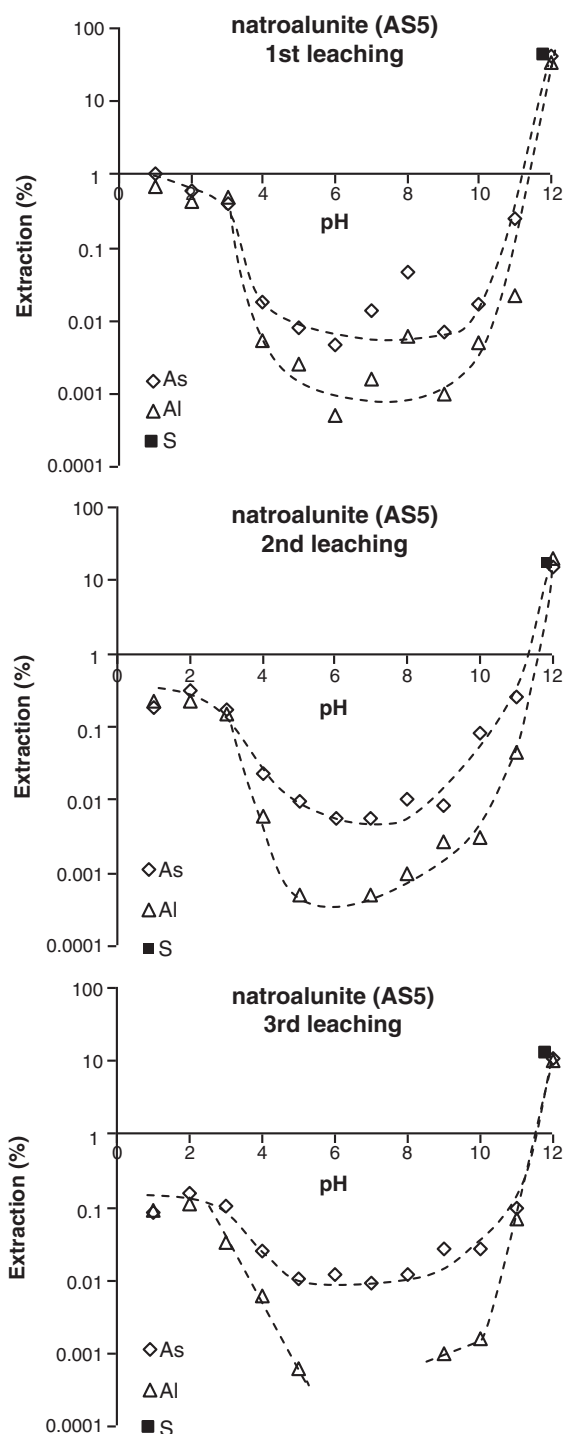
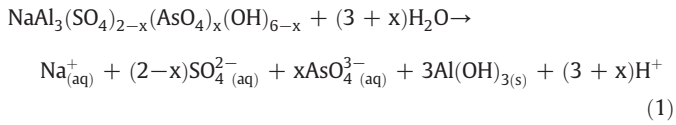


Fig. 6. Effect of pH on the Al and As extractions in arsenical natroalunite. (25 °C, 24 h).

Although the results of the 1st leaching are also reported, in order to minimize the effects of the poor washing and/or surface absorption, the discussion is focused mainly on the data of 2nd and 3rd leaching. At pH 1 to 3 the As and Al extractions had the same order, which was consistent by an essentially congruent dissolution of the crystal surfaces. This congruent behavior in acid medium also supported the incorporation of arsenate in the natroalunite structure, releasing As and Al according to its composition. Nevertheless, even at pH 1, the attack was small (0.2–0.3%) and the SEM-EDS studies of residual solids (Fig. 9A) did not detect appreciable changes.

For pH 4 to 11, the extractions of As were higher than those of Al, thereby indicating an incongruent dissolution of type:



However, this incongruent attack was still smaller (0.01–0.1%) and neither was a significant change found in the EDS spectra or in the

surface morphology (Fig. 9B). The maximum stability of natroalunite was between pH 5 to 8 pH with ~0.01% As and ~0.001% Al extractions in 24 h, respectively.

At pH 12, natroalunite attack was again congruent due to the formation of soluble aluminate species, as noted by the practically identical As, S and Al extractions. Under the conditions tested, the leaching tests showed a cumulative dissolution of 65% of natroalunite, and the residual crystals showed large etch pits (Fig. 9C).

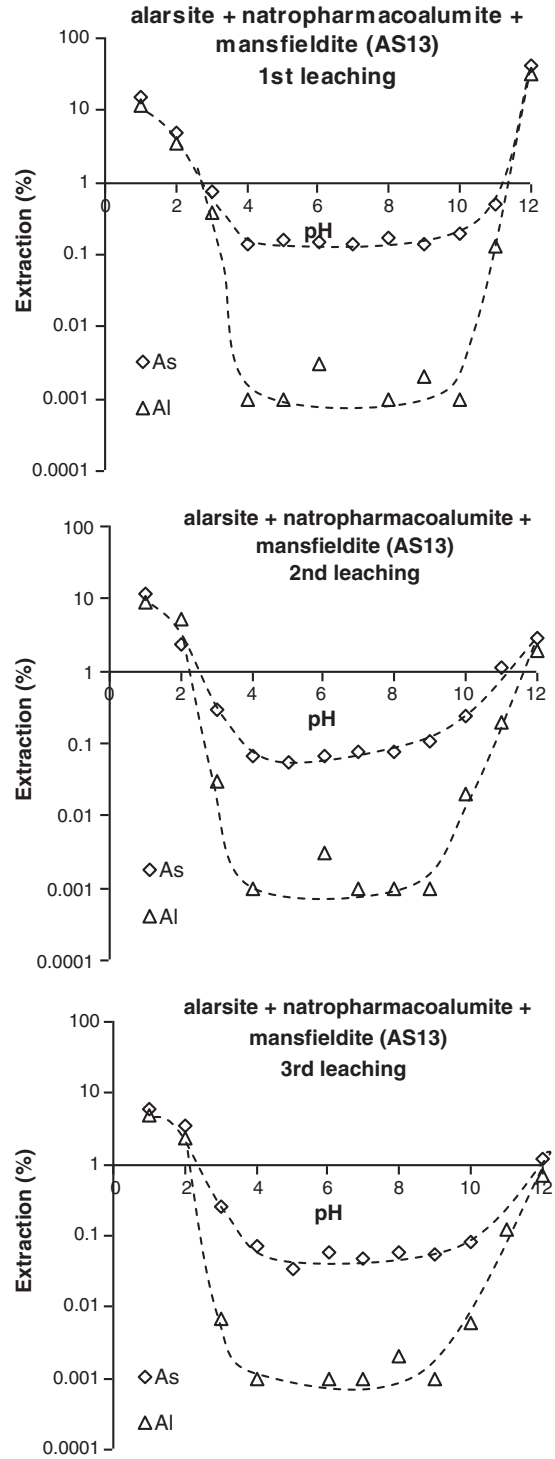
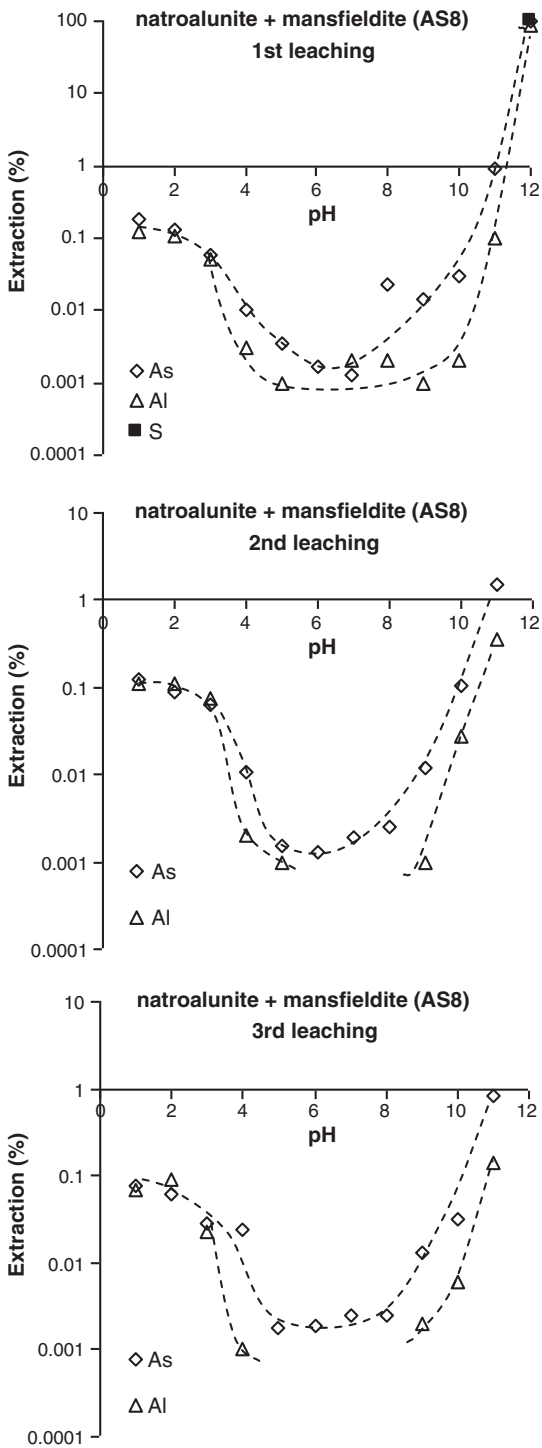


Fig. 7. Effect of pH on the Al and As extractions in mixture of arsenical natroalunite + mansfieldite (25 °C, 24 h).

Fig. 8. Effect of pH on the Al and As extractions in mixture of alarsite + natropharmacoalunite + mansfieldite (25 °C, 24 h).

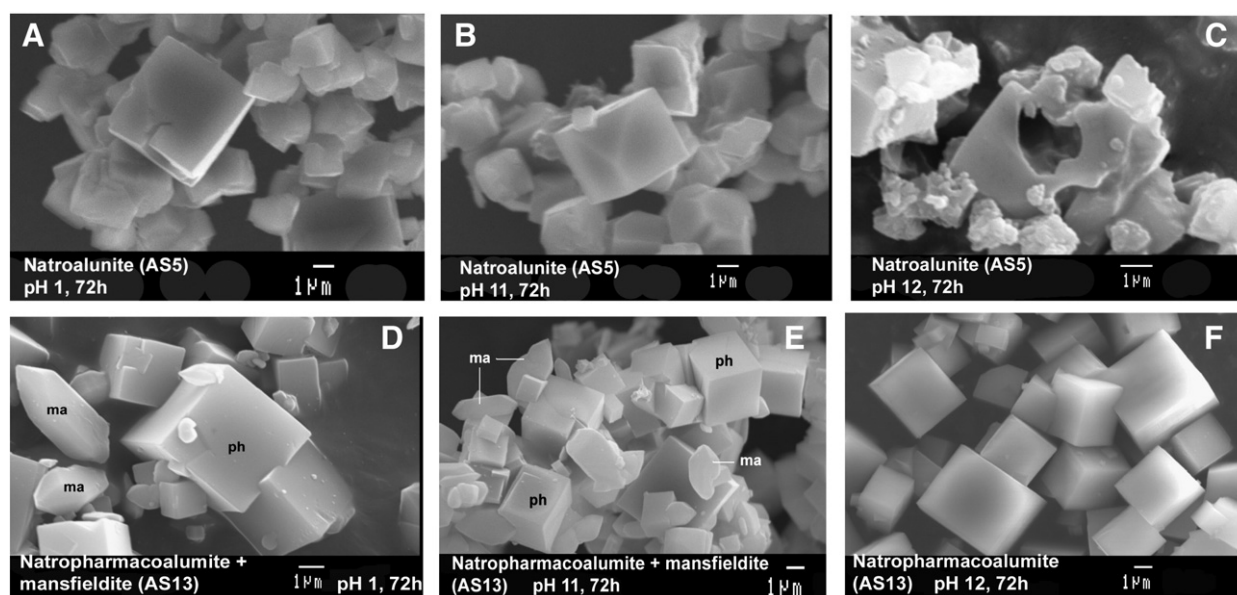


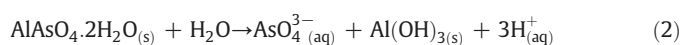
Fig. 9. A–C: Natroalunite treated at different pHs. D–F: Mixture of natropharmacoalumite and mansfieldite treated at different pHs. (SEM) (na: natroalunite; ma: mansfieldite; ph: natropharmacoalumite).

Fig. 7 shows the As and Al extractions for the sample containing natroalunite + mansfieldite. Like the sample containing only natroalunite, at pH 1 to 3 the As and Al extractions were practically identical. This also confirmed a 0.01–0.1% congruent dissolution. For pH 4 to 11, the attack was incongruent with minimum As extractions (0.01–0.001%) in the pH range 5 to 8.

At pH 11, the As extraction for the sample with natroalunite + mansfieldite was ~1%, one order of magnitude greater than that containing only natroalunite. Finally, at pH 12, natroalunite and mansfieldite were congruently and completely dissolved in the 1st leaching test.

All these leaching results indicated that the stability of natroalunite and mixtures natroalunite + mansfieldite in acid to neutral pH range was satisfactory in short-term tests. Nevertheless, the phase stability results obtained in these tests could be insufficient for evaluating the behavior of the arsenate phases for long-term storage.

The attack of mansfieldite in neutral or near neutral regions was reported by Le Berre et al. (2007a,b) as:



This incongruent leaching was very slow, reaching an apparent equilibrium in 5 weeks for As concentrations about 10 mg/L at pH 5 (Viñals et al., 2010). For pH 7, the equilibrium was not reached in 7 weeks, and As concentrations of 80 mg/L were released (Le Berre et al., 2007b).

In contrast to mansfieldite, long-term leaching tests at pH 5 (natural pH) in arsenical natroalunite published in Viñals et al. (2010) showed stabilized As concentrations of ~0.1 mg/L in three months, which can be considered satisfactory for arsenic disposal.

3.2.2.2. Alarsite. Alarsite was an arsenate phase obtained at 200 °C for high $(\text{AsO}_4^{3-}/\text{SO}_4^{2-})_{\text{aq}}$ ratios (>0.35). This phase already appeared partly re-dissolved at the final pH of the synthesis (~1) (Sunyer and Viñals, 2011-this issue). During the further leaching treatment, alarsite showed little stability and was responsible of the high As solubilization detected in sample AS13 (Fig. 5). SEM/EDS studies and XRD patterns of the solids after leaching treatment (Fig. 10) showed complete alarsite dissolution

at pH 1 and pH 12. On the other hand, the comparison of As and Al extractions in sample AS13 (Fig. 8) confirmed a congruent dissolution at $\text{pH} \leq 2$ and at pH 12, and incongruent attack at intermediate pH values. However, even in conditions of incongruent attack, the As extraction in alarsite was between one to two orders of magnitude greater than in natroalunite and mansfieldite.

3.2.2.3. Natropharmacoalumite. In contrast to alarsite, natropharmacoalumite was very stable. The XRD and SEM data showed insignificant damage to its basic structure during the treatment in the entire 1–12 pH interval, after the 72 h leaching (Figs. 9D–F and 10). Thus, natropharmacoalumite showed greater stability than natroalunite and mansfieldite in strong alkaline media (pH 12).

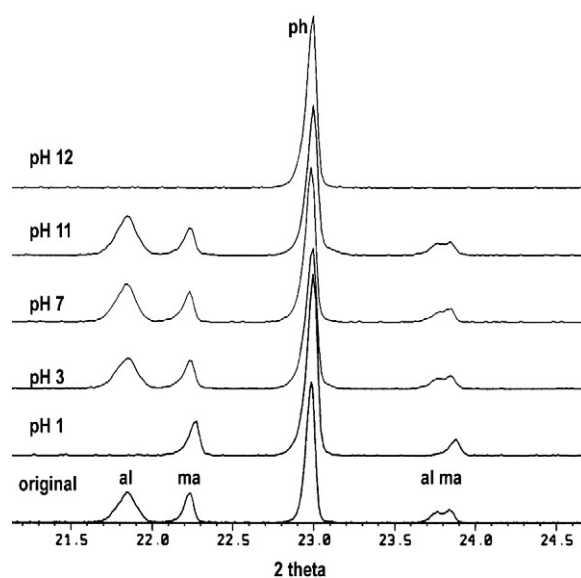


Fig. 10. Selected region of the XRD patterns of sample containing natropharmacoalumite (AS13) treated at different pHs (72 h). Note the complete leaching of alarsite at pH 1 and 12 and mansfieldite at pH 12. (ph: natropharmacoalumite; al: alarsite; ma: mansfieldite).

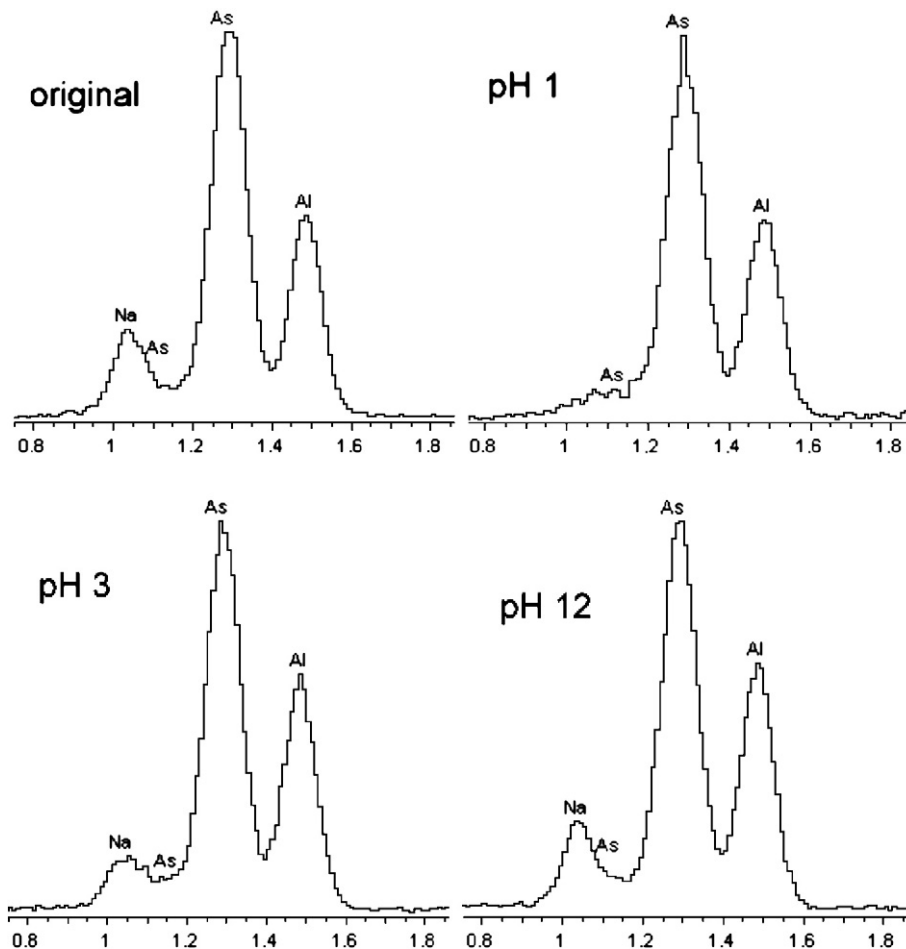
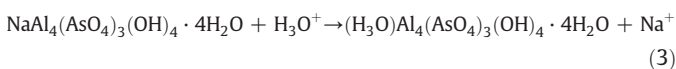


Fig. 11. EDS spectra of natropharmacoalumite treated at different pHs (72 h) (Scale in KeV).

On the other hand, in acid medium, natropharmacoalumite had a rapid H_3O^+ -for- Na^+ exchange (24 h) at ambient temperature:



This exchange (and buffering) effect was evidenced in the EDS spectra of the solids leached (Fig. 11) and through the Na^+ released in the leach solution (Fig. 12). Hydroniumpharmacoalumite is not yet known as a natural phase, but the Fe(III) analogous (hydroniumpharmacosiderite, $(\text{H}_3\text{O})\text{Fe}_4(\text{AsO}_4)_3(\text{OH})_4 \cdot 4\text{H}_2\text{O}$) was recently discovered (Mills et al., 2010). Moreover, the alkali-exchange properties of natropharmacoalumite should be related to the zeolite-type structure of the phases of the pharmacosiderite supergroup, which contains large channels occupied by alkaline cations and water molecules (Mutter et al., 1984; Rumsey et al., 2010). Consequently, the buffering effect of natropharmacoalumite could make it of interest for arsenic disposal purposes, especially when exist the possibility of a potential contact with acidic soils or acidic wastes, for instance those containing pyrite. Nevertheless it seems difficult to produce this phase from industrial wastes containing large $\text{SO}_4^{2-}/\text{AsO}_4^{3-}$ ratios, because synthesis conditions imply $\text{SO}_4^{2-}/\text{AsO}_4^{3-}$ aqueous molar ratios less than 1.5 and under these conditions unstable phases, such as alarsite, can co-precipitate (Sunyer and Viñals, 2011-this issue).

4. Conclusions

The Rietveld refinement of arsenical natroalunite confirmed the structural type R-3 m Z=3 of the alunite phases. The a unit-cell

parameter is practically independent of the AsO_4 and H_3O substitution. Substitutions of AsO_4 and H_3O produce an increase in the c unit-cell parameter. The increment in the latter in response to AsO_4 substitution is consistent with the expected cell expansion due to the differences between the As-O1 and S-O1 distances in the tetrahedral sites of the alunite-type structure.

The maximum stability of arsenical natroalunite is between pH 5 to 8, giving As solubilizations of 0.01–0.05 mg/L in 24 h. These low

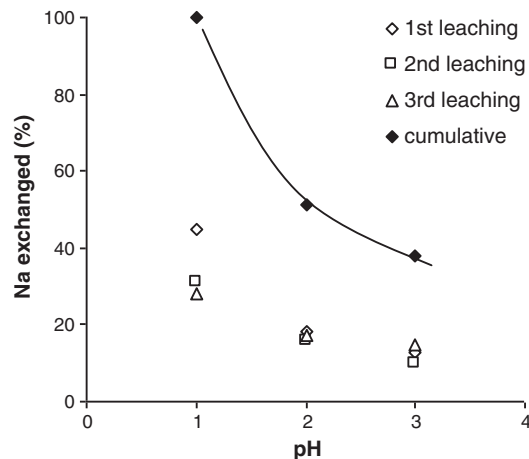


Fig. 12. Na exchanged as a function of pH in natropharmacoalumite.

rates of As release make this phase attractive for the inertization of wastes containing large $\text{SO}_4^{2-}/\text{AsO}_4^{3-}$ ratios.

Arsenical natroalunite undergoes congruent dissolution at $\text{pH} < 3$, an incongruent attack at $\text{pH} 4\text{--}11$ and again a congruent dissolution at $\text{pH} 12$. The congruent dissolution at $\text{pH} < 3$ is very small (0.1–1% in 24 h), but the attack at $\text{pH} 12$ is practically complete. The mixture of arsenical natroalunite and mansfieldite showed a similar behavior than arsenical natroalunite in short-term tests (24 h). However, precipitates containing alarsite or amorphous Al-arsenate presented As solubilization two or three orders of magnitude greater.

Natropharmacoalumite showed insignificant damage to its basic structure during the 72 h leaching in the pH range 1–12. In acid medium, natropharmacoalumite exchanged H_3O^+ for Na^+ . The stability and acid-exchange properties of this phase could make it potentially attractive for arsenic disposal, especially when exists the possibility of contact with soils or wastes of acidic nature.

Acknowledgements

The financial support of the Spanish *Ministerio de Ciencia e Innovación (DGI)* (Programa de Materiales, MAT 2007–61466) is gratefully acknowledged. We also thank Dr. X. Alcobé, *Serveis Científico-tècnics de la Universitat de Barcelona*, for his help with the structural study.

References

- Basciano, L.C., Peterson, R.C., 2008. Crystal Chemistry of the Natrojarosite-Jarosite and Natrojarosite-Hydronium Jarosite solid-solution series: A Synthetic Study with full Fe site Occupancy. *American Mineralogist* 93, 853–862.
- Basciano, L.C., Peterson, R.C., 2010. A crystallographic study of the incomplete solid-solution between plumbojarosite and jarosite. *Canadian Mineralogist* 48, 651–659.
- Bluteau, M.C., Demopoulos, G.P., 2007. The incongruent dissolution of scorodite – solubility, kinetics and mechanism. *Hydrometallurgy* 87, 163–177.
- Drouet, C., Navrotsky, A., 2003. Synthesis, characterization, and thermochemistry of K–Na–H₃O jarosites. *Geochimica et Cosmochimica Acta* 67 (11), 2063–2076.
- Fujita, T., Taguchi, R., Abumiya, M., Matsumoto, M., Shibata, E., Nakamura, T., 2009. Effect of pH on atmospheric scorodite synthesis by oxidation of ferrous ions: Physical properties and stability of scorodite. *Hydrometallurgy* 96, 189–198.
- Harrison, W.T.A., 2000. Synthetic mansfieldite, $\text{AlAsO}_4 \cdot 2\text{H}_2\text{O}$. *Acta Crystallographica*, Section C 56, e421.
- Hawthorne, F.C., Ferguson, R.B., 1975. Anhydrous sulphates. II. Refinement of the crystal structure of anhydrite. *The Canadian Mineralogist* 13, 289–292.
- Krause, E., Ettl, V.A., 1989. Solubilities and stabilities of ferric arsenate compounds. *Hydrometallurgy* 22, 311–337.
- Le Berre, J.F., Cheng, T.C., Gauvin, R., Demopoulos, G.P., 2007a. Hydrothermal synthesis and stability evaluation of mansfieldite in comparison to scorodite. *Canadian Metallurgical Quarterly* 46, 1–9.
- Le Berre, J.F., Cheng, T.C., Gauvin, R., Demopoulos, G.P., 2007b. Hydrothermal synthesis and stability evaluation of iron (III)-aluminum (III) arsenate solid solutions. *Metallurgical and Materials Transactions B* 38, 159–166.
- Li, G.J., Peacor, D.R., Essene, E.J., Brosnahan, D.R., Beane, R.E., 1992. Walthierite $\text{Ba}_{0.5}\text{Al}_3(\text{SO}_4)_2(\text{OH})_6$, and Huangite $\text{Ca}_{0.5}\text{Al}_3(\text{SO}_4)_2(\text{OH})_6$, 2 new minerals of the alunite group from the Coquimbo Region, Chile. *American Mineralogist* 77 (11–12), 1275–1284.
- Menchetti, S., Sabelly, C., 1976. Crystal chemistry of the alunite series: crystal structure refinement of alunite and synthetic jarosite. *Neues Jahrbuch für Mineralogie-Monatshefte*, 9, 407–417.
- Mills, S.J., Kampf, A.R., Williams, P.A., Leverett, P., Poirier, G., Raudsepp, M., Francis, C.A., 2010. Hydroniumpharmacosiderite, a new member of the pharmacosiderite supergroup from Cornwall, UK: structure and description. *Mineralogical Magazine* 74 (5), 863–869.
- Mutter, G., Eysel, W., Greis, O., Schmetzer, K., 1984. Crystal chemistry of natural and ion-exchanged pharmacosiderites. *Neues Jahrbuch für Mineralogie, Monatshefte* 183–192.
- Okada, K., Hirabayashi, J., Oosaka, J., 1982. Crystal structure of natroalunite and crystal chemistry of the alunite group. *Neues Jahrbuch für Mineralogie-Monatshefte* 12, 634–640.
- Paktunc, D., Dutrizac, J.E., 2003. Characterization of arsenate-for sulfate substitution in synthetic jarosite using X-ray diffraction and X-ray absorption spectroscopy. *Canadian mineralogist* 41, 905–919.
- Rietveld, H.M., 1967. Line profiles of neutron powder-diffraction peaks for structure refinement. *Acta Crystallographica* 22, 151–152.
- Rietveld, H.M., 1969. A profile refinement method for nuclear and magnetic structures. *Journal of Applied Crystallography* 2, 65–71.
- Rodríguez-Carvajal, J., 1990. FullProf: a program for Rietveld refinement and pattern matching analysis. Abstracts of the Satellite Meeting on Powder Diffraction of the XV Congress of the IUCr, 127, Toulouse, France.
- Rodríguez-Carvajal, J., 1997. Journées de la Diffusion Neutronique, Ecole Thematique Cristallographie et Neutrons, 12–13 mai 1997, Batz sur Mer (France).
- Rudolph, W.W., Mason, R., Schmidt, P., 2003. Synthetic alunites of the potassium-oxonium solid solution series and some other members of the group: synthesis, thermal and X-ray characterization. *European Journal of Mineralogy*, 15, 913–924.
- Rumsey, M.S., Mills, M.S., Spratt, J., 2010. Natropharmacoalumite, $\text{NaAl}_4(\text{OH})_4(\text{AsO}_4)_3 \cdot 4\text{H}_2\text{O}$, a new mineral of the pharmacosiderite supergroup and the renaming of aluminopharmacosiderite to pharmacoalumite. *Mineralogical Magazine* 74 (5), 929–936.
- Sato, E., Nakai, I., Miyawaki, R., Matsubara, S., 2009. Crystal structures of alunite family minerals: beaverite, corkite, alunite, natroalunite, jarosite, svanvergitte, and woodhouseite. *Neues Jahrbuch für Mineralogie-Abhandlungen* 185 (3), 313–322.
- Savage, K.S., Bird, D.K., O'Day, P.A., 2005. Arsenic speciation in synthetic jarosite. *Chemical Geology* 215 (81–4), 473–498.
- Schwab, R.G., Götze, C., Harold, H., De Oliveira, N.P., 1991. Compounds of the crandallite type: synthesis and properties of pure (Ca, Sr, Ba, Pb, La, Ce, to Eu)-arsenocrandallites. *Neues Jahrbuch für Mineralogie-Monatshefte* 3, 97–112.
- Schwab, R.G., Pimpl, T., Schukow, H., Stolle, A., Breiting, D.K., 2005. Compounds of the crandallite-type: Synthesis, properties and thermodynamic data of Ca–Sr–Ba–Pb-(arseno)-woodhouseites. *Neues Jahrbuch für Mineralogie-Abhandlungen*, 181 (3), 207–218.
- Shannon, R.D., 1976. Revised effective ionic radii and systematic studies of interatomic distances in halides and chalcogenides. *Acta Crystallographica A* 32, 751–767.
- Smith, A.M.L., Dubbin, W.E., Wright, K., Hudson-Edwards, K.A., 2006. Dissolution of lead- and lead-arsenic-jarosites at $\text{pH} 2$ and 8 and 20°C : Insights from batch experiments. *Chemical Geology* 229, 344–361.
- Sowa, H., 1991. The crystal structure of AlAsO_4 at high pressure. *Zeitschrift für Kristallographie* 194, 291.
- Sunyer, A., Viñals, J., 2011. Arsenate substitution in natroalunite: a potential method for arsenic immobilization. Part 1: synthesis and compositions. *Hydrometallurgy*, 109, 54–64 (this issue).
- Swash, P.M., Monhemius, A.J., Schaeckers, J.M., 2000. Solubilities of process residues from biological oxidation pretreatments of refractory gold ores. In: Young, C.A. (Ed.), *Minor Elements 2000*. SME, Littleton, CO, pp. 115–123.
- Szymanski, J.T., 1985. The crystal structure of plumbojarosite $\text{Pb}[\text{Fe}_3(\text{SO}_4)_2(\text{OH})_6]_2$. *Canadian Mineralogist* 23, 659–668.
- Viñals, J., Sunyer, A., Molera, P., Cruells, M., Llorca, N., 2010. Arsenic stabilization of calcium arsenate waste by hydrothermal precipitation of arsenical natroalunite. *Hydrometallurgy* 104, 247–259.

A.4 The behaviour of As(III) and As(V) during the precipitation of alunite at 98°C

A. Sunyer, J.E. Dutrizac, 2011, The Behaviour of As(III) and As(V) during the Precipitation of Alunite at 98°C, Waste Processing and Recycling in Mineral and Metallurgical Industries –VI Proceedings of the 50th Annual Conference of Metallurgists of CIM, Montreal, Canada, Edited by S.R. Rao, C.Q. Jia, C.A. Pickles, S. Brienne, V. Ramachandran, VI, 331-336. ISBN 978-1-926872-05-6

Resum en català

Els factors que afecten la precipitació de l'alunite sense arsènic ($\text{KAl}_3(\text{SO}_4)_2(\text{OH})_6$) van ser investigats per sèries en experiments de laboratori. Tot i que les quantitats de precipitació d'alunite van incrementar amb el temps de retenció, la temperatura, el pH de la solució i les concentracions de $\text{Al}(\text{SO}_4)_{1.5}$ o K_2SO_4 , la composició dels productes obtinguts va romandre quasi constant. Les condicions preferides identificades per a la precipitació d'alunites lliures d'arsènic van ser usades per assajar el comportament de l'As(III) i l'As(V) durant la precipitació d'alunite a 98°C. Un augment en les addicions d'As(III), com a NaAsO_2 o As_2O_3 , van donar un lleuger augment en la quantitat de precipitat format a pH 2.80. Tanmateix, l'anàlisi per difracció de raigs X va mostrar que tots els precipitats eren alunite, i en els productes es va detectar <0.2% d'As(III). En canvi, un augment en les addicions d'As(V), com a KH_2AsO_4 o As_2O_5 , van donar un augment significatiu dels precipitats formats a pH 2.80 o 3.00. A més a més, el contingut d'arseniat (AsO_4^{3-}) en els precipitats incrementa en un 15%, i el contingut de sulfat disminueix, tal i com la concentració d'As(V) en la solució de síntesis augmenta entre 0 i 9 g/L. La difracció de raigs X dels productes només detecta alunite, però hi ha una expansió progressiva en la cel·la de l'alunite amb l'increment del contingut d'arseniat. Això és conseqüència de la substitució del sulfat per arseniat a l'estructura. Les observacions preliminars de l'estabilitat en el medi ambient de l'alunite arsenical usant el protocol TCLP va donar solubilitats <0.4 mg/L en el precipitat que contenia un 8.5% d' AsO_4 i 7.8 mg/L del producte que conté un 19.5% d' AsO_4 . Així doncs, aparentment les alunites amb menys d'un ~10% d' AsO_4 serien acceptables per a l'eliminació de l'arsènic de solucions de processos hidrometal·lúrgics.

THE BEHAVIOUR OF As(III) AND As(V) DURING THE PRECIPITATION OF ALUNITE AT 98°C

*Alba Sunyer¹ and J.E. Dutrizac²

¹*University of Barcelona
Diagonal Sud, Facultats de Física i Química
C/ Martí i Franques 1
08028 Barcelona, Spain*

(*Corresponding author: asunyer@ub.edu)

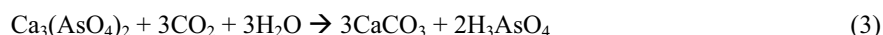
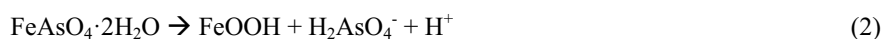
²*CANMET-MMSL
555 Booth Street
Ottawa, Canada K1A 0G1
jdutrizac@nrcan.gc.ca*

ABSTRACT

The factors affecting the precipitation of arsenic-free alunite ($\text{KAl}_3(\text{SO}_4)_2(\text{OH})_6$) were investigated in a series of laboratory experiments. Although the amount of alunite precipitated increased with increasing retention time, temperature, solution pH and the concentrations of $\text{Al}(\text{SO}_4)_{1.5}$ or K_2SO_4 , the composition of the products remained nearly constant. The preferred conditions identified for the precipitation of arsenic-free alunite were then used to assess the behaviour As(III) and As(V) during alunite precipitation at 98°C. Increasing additions of As(III), as NaAsO_2 or As_2O_3 , resulted in a slight increase in the amount of precipitate formed at pH 2.80. However, X-ray diffraction analysis showed all the precipitates to be alunite, and <0.2% As(III) was detected in the products. In contrast, increasing additions of As(V), as KH_2AsO_4 or As_2O_5 , resulted in significant increases in the amount of precipitate formed at pH 2.80 or 3.00. Furthermore, the arsenate (AsO_4^{3-}) contents of the precipitates increased up to 15%, and the sulphate contents decreased, as the As(V) concentration of the synthesis solution increased from 0 to 9 g/L. X-ray diffraction analysis of the products detected only alunite, but there was a progressive expansion of the alunite cell with increasing arsenate content. The implication is that arsenate substitutes for sulphate in the alunite structure. Preliminary observations on the environmental stability of the arsenate-bearing alunite using the TCLP protocol gave solubilities <0.4 mg/L from a precipitate containing 8.5% AsO_4 and 7.8 mg/L from a product containing 19.5% AsO_4 . Thus, it appears that alunites containing less than ~10% AsO_4 would be an acceptable vehicle for the disposal of arsenic from hydrometallurgical processing solutions.

INTRODUCTION

Arsenic is one of the contaminants commonly present in the ores used in the non-ferrous metallurgical industry. The arsenic creates problems in the recovery of the sought after metals and is hazardous for the environment. To solve the problems caused by the presence of dissolved, different methods of precipitation and stabilization have been developed. Usually, ferrihydrite ($\text{FeO}(\text{OH})(\text{H}_2\text{O})_{1+x}$), scorodite ($\text{FeAsO}_4 \cdot 2\text{H}_2\text{O}$) and calcium-arsenate ($\text{Ca}_3(\text{AsO}_4)_2$), are used to precipitate arsenic in the metallurgical industry [1, 2, 3]. Ferrihydrite can adsorb cations and anions such as AsO_3^{3-} and AsO_4^{3-} (Eq. 1) and the precipitation can be done at $<100^\circ\text{C}$. The arsenical ferrihydrite is precipitated at pH 2-3 and the neutralization is usually done with lime. Thus, if there is not sufficient Fe for the precipitation of arsenical ferrihydrite, calcium-arsenates will begin to precipitate. Although arsenical ferrihydrite yields low dissolved As concentrations in short term tests, its long term (many years) stability is in doubt because of its possible decomposition to goethite ($\alpha\text{-FeOOH}$) or hematite ($\alpha\text{-Fe}_2\text{O}_3$) and the consequent dissolution of the contained arsenic [1]. Scorodite can be readily synthesized at 150°C or by controlled neutralization at 95°C . It also exhibits good short term stability, but as was the situation for arsenical ferrihydrite, the scorodite can dissolve in contact with water during long term storage. It decomposes to goethite and a soluble arsenate species (Eq. 2) [4]. Calcium-arsenates are precipitated at pH 3-4 with the addition of lime. Calcium arsenate precipitation is an economical process, but the calcium arsenates are not stable during long term storage because calcium arsenate is carbonated in contact with CO_2 and water (Eq. 3). Consequently, the As is dissolved [1].



Other phases have also been studied for the precipitation and stabilization of dissolved arsenic. The alunite supergroup seems to be a possible option for sequestering arsenic. The general formula of alunite supergroup compounds is $\text{AB}_3(\text{TO}_4)_2(\text{OH})_6$, where A is Na^+ , K^+ , Ba^{2+} , Pb^{2+} , Tl^+ , NH_4^+ , H_3O^+ ; B is Fe^{3+} or Al^{3+} ; and TO_4 is SO_4^{2-} , AsO_4^{3-} or PO_4^{3-} . It is established that As(V), as AsO_4 , can substitute for part of the SO_4 in these compounds. For example, the incorporation of AsO_4 in jarosite-type compounds (e.g., $\text{KFe}_3(\text{SO}_4)_2(\text{OH})_6$) has been studied [5]. Jarosite-type compounds are used for iron removal in some metallurgical processes [6], and they offer the advantage that they can be synthesized at $<100^\circ\text{C}$ [6, 7]. Paktunc and Dutrizac [5] studied the incorporation of AsO_4 in jarosite-type compounds at 98°C and demonstrated an AsO_4 -for- SO_4 substitution of $\sim 17\%$. Jarosite-type compounds present good stability in short term tests, but the presence of contained ferric ions could make them unstable in reducing environments such as in anaerobic soils [1]. For this reason, the analogous alunite-type compounds, which contain Al(III) instead of Fe(III), offer advantages for arsenic stabilization because the Al(III) is not easily reduced. In this regard, the substitution of AsO_4 for SO_4 in natroalunite, $\text{NaAl}_3(\text{SO}_4)_2(\text{OH})_6$, was studied recently. Although natroalunite can be synthesized at 100°C , the precipitation rate is low and an amorphous phase is formed in the presence of As(V). However, at temperatures $>160^\circ\text{C}$, crystalline AsO_4 -bearing natroalunite can be readily synthesized [8]. The extent of substitution of AsO_4 -for- SO_4 in natroalunite is similar to the value found in synthetic sodium jarosite. Arsenic incorporation in both synthetic natroalunite and in natroalunite made using an industrial waste was studied, and in both cases, about 15% AsO_4 substitution for SO_4 was achieved in 2 h at 200°C . [8, 9, 10]. The environmental stability of natroalunite was also investigated in short term leaching tests (3 consecutive leaching stages each of 24 h duration) and in long term leaching tests (6 months). These tests gave low arsenic solubility values; the short term extractions were about 0.01-0.05 mg/L As at pH 5 to 8, and the long term extractions at pH 4-5 were about 0.1 mg/L As [8, 9, 10]. These values are lower than those found for scorodite dissolution [4].

Although AsO_4 -bearing natroalunite was extensively precipitated at 200°C , only 16% Al precipitation occurred after 72 h of reaction at 100°C , and the arsenic was precipitated as an amorphous phase [8]. It is well established that (potassium) jarosite is the most stable jarosite-type compound [7] and

it seems that (potassium) alunite is the favoured alunite-type compound [11]. It is known that both (potassium) jarosite and (potassium) alunite can be readily synthesized at temperatures $<100^{\circ}\text{C}$, and the advantages of operating an industrial precipitation process at ambient pressure are considerable. Accordingly, systematic series of experiments were undertaken to define the preferred conditions for the precipitation of alunite at 98°C and atmospheric pressure. The preferred conditions identified in those experiments were then used to evaluate the extent and nature of incorporation of As(III) and As(V) in alunite, where the As(III) was added as NaAsO_2 and As_2O_3 and the As(V) as KH_2AsO_4 and As_2O_5 . The results of the experimental program and a discussion of the nature of arsenic incorporation in alunite are summarized in this paper.

EXPERIMENTAL

Reagent grade chemicals were used for all the experiments. The experiments to synthesize alunite at $<100^{\circ}\text{C}$ were carried out in a 2-L reaction vessel, generally using a 24-h retention time and a 400 rpm stirring speed. To assess the effect of temperature on the precipitation reaction, a few experiments were also carried out at temperatures $>100^{\circ}\text{C}$ in a Parr 2-L autoclave fitted with a glass liner and titanium internal components. In all instances, known amounts of $\text{Al}_2(\text{SO}_4)_3 \cdot 18\text{H}_2\text{O}$ and K_2SO_4 were dissolved in 1-L of deionized water, and the pH was adjusted. Although the pH electrode was always calibrated at room temperature, the actual pH adjustment was made with MgCO_3 or H_2SO_4 at $45 - 46^{\circ}\text{C}$ or less commonly at $50 - 60^{\circ}\text{C}$. This procedure was necessary because some precipitation occurred at room temperature when concentrated solutions were prepared, and the precipitate was identified as alum, $\text{KAl}(\text{SO}_4)_2 \cdot 12\text{H}_2\text{O}$. Warming of the solution caused the alum to dissolve, such that the pH could be adjusted, and no precipitates were formed at the higher temperatures used to adjust the final pH regardless of the solution concentration. Initially, the solutions were heated to $50-60^{\circ}\text{C}$ before the pH was set, but the actual temperatures were not closely controlled and it was subsequently found that the product yield varied considerably over this pH-setting temperature range. This behaviour is illustrated in Table 1 which presents the product yields realized when the pH of 0.3 M $\text{Al}(\text{SO}_4)_{1.5} - 0.1$ M K_2SO_4 solutions was set at 2.80 at various temperatures, prior to heating the solution to 98°C for 24 h. The variation is due to the partial neutralization of the hydrolysis acid generated as the Al^{3+} ions are heated, and the variation increases as the pH-setting temperature increases. To minimize the variation in the product yields, the pH was set at $45-46^{\circ}\text{C}$ in all the subsequent experiments. Regardless of the temperature used to set the pH, the pH-adjusted solution was transferred to the appropriate reaction vessel which was then heated to the desired synthesis temperature. In those experiments designed to investigate the department of arsenic, the arsenic compound was first dissolved in warm water and, sometimes, with the addition of a small amount (<0.5 g) of KOH which facilitated the dissolution of the simple arsenic oxides. Once the arsenic compound dissolved, the appropriate amounts of $\text{Al}(\text{SO}_4)_{1.5}$ and K_2SO_4 were added and dissolved. The pH was then adjusted using the procedure outlined above. The As(III) was added as NaAsO_2 or As_2O_3 whereas the As(V) was added as KH_2AsO_4 or As_2O_5 . The product slurries from the atmospheric pressure tests were filtered while hot using a Buchner vacuum filter with No.3 Whatman paper. In the autoclave experiments, the final slurries were rapidly cooled (~ 15 min) in the autoclave, the autoclave was immediately opened, and the slurries were filtered using the Buchner vacuum filter. In both instances, the precipitates were washed with large amounts of water and finally dried at 110°C prior to chemical analysis and characterization.

The samples obtained were characterized by chemical analysis, X-ray diffraction analysis (XRD) and scanning electron microscopy (SEM). For the chemical analyses, the samples were dissolved in hot HCl; the samples which contained As were digested in sealed vessels in a microwave to minimize any As volatilization. The chemical analyses were performed using inductively coupled plasma (ICP) spectroscopy. The X-ray diffraction analyses were done using a Rigaku rotating anode diffractometer with $\text{CuK}\alpha_1$ radiation at 50 kV and 180 mA in a step scan of 0.02° and a scan rate of 4° per minute in 2θ . Some of the precipitates were examined by scanning electron microscopy with energy dispersive X-ray analysis (EDX) to characterize the phases present and to detect possible impurities. A few of the precipitates were also analyzed quantitatively using the wavelength dispersive analyzer of the electron microprobe

Table 1 - Variation of the Product Yield as a Function of the Temperature at which the pH was set at 2.80

Temperature of pH setting (°C)	Product Yield (g)	X-Ray diffraction results
30	3.3	Alunite
40	4.9	Alunite
45	5.7	Alunite
50	7.8	Alunite
60	15.2	Alunite
70	23.5	Alunite

RESULTS AND DISCUSSION

Effect of Retention Time and Synthesis Temperature

Figure 1 shows the amount of product formed after various periods of reaction when 0.3 M $\text{Al}(\text{SO}_4)_{1.5}$ - 0.2 M K_2SO_4 solutions at pH 3.00 were reacted at 98°C. The amount of precipitate increases in a nearly linear manner for the first 30 hours of reaction, but appears to level off for longer reaction times. Comparison with results obtained in the analogous jarosite precipitation system [12], indicates that alunite precipitation proceeds significantly more slowly than jarosite precipitation, under comparable conditions. Figure 2 illustrates the compositions of the precipitates formed after the various periods of reaction. Regardless of the amount of product formed as the retention time increases, the K, Al and SO_4 contents of the precipitates remain nearly constant. There is a suggestion that the K and SO_4 contents increase very slightly over the initial four or five hours of reaction, but the variations are within experimental/analytical error. Nevertheless, all instances the compositions approximate that of alunite. This observation is consistent with the X-ray diffraction results which detected only well crystallized alunite in all the samples. Thus, the precipitation of (potassium) alunite at 98°C yields a crystalline phase, even during the initial stages of reaction, whereas efforts to precipitate sodium alunite under similar conditions resulted in the formation of an amorphous phase [8]. Based on these results, a 24-h reaction period was selected for the remainder of the experimental program, as this retention time yielded a significant amount of product and was compatible with the schedule of the laboratory.

The effect of temperature on the alunite synthesis reaction was studied using 0.3 M $\text{Al}(\text{SO}_4)_{1.5}$ - 0.2 M K_2SO_4 solutions at pH 3.00, where the pH was adjusted at 45-46°C and at 50-60°C. Figure 3 shows the product yields obtained at temperatures between 70°C and 100°C for the experiments where the pH was set at 50-60°C, and at temperatures between 80 and 150°C for the tests where the pH was set at 45-46°C. The product yields obtained in both sets of experiments are similar, although there is an indication that slightly higher product yields are realized at the higher pH-setting temperature. The implication is that the pH-setting temperature in the experiments where the pH was set at 50-60°C was likely much closer to 50°C than 60°C. In both cases, however, the product yields increased significantly with increasing temperature. Regardless of the pH-setting temperature, only minor amounts of product formed at temperatures <85°C. As the temperature increased, the product yields increased significantly from about 4 g at 85°C to 15-20 g at 100°C and to over 45 g at temperatures above 130°C. Nearly constant product yields were realized at temperatures above 130°C and these product yields represent about 55% Al precipitation.

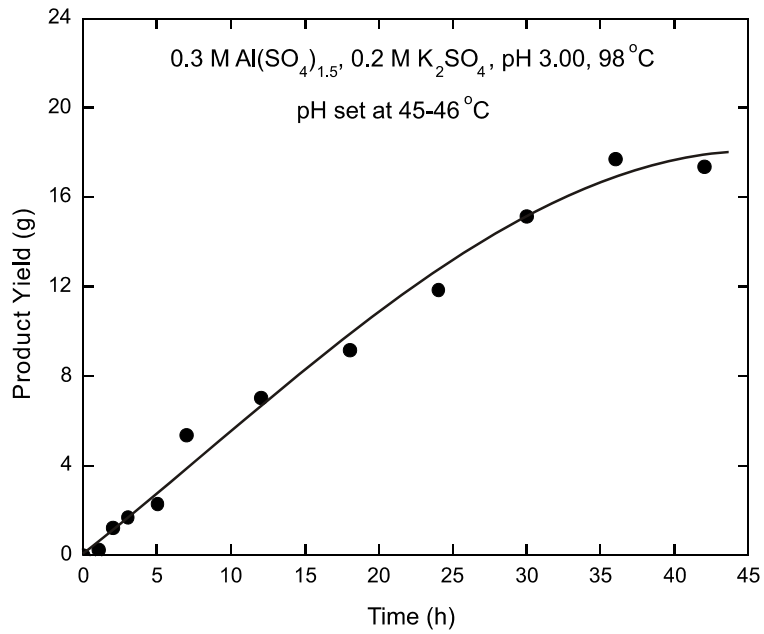


Figure 1 – Product yields realized when 0.3 M Al(SO₄)_{1.5} - 0.2 M K₂SO₄ solutions at pH 3.00 were reacted for various retention times at 98°C

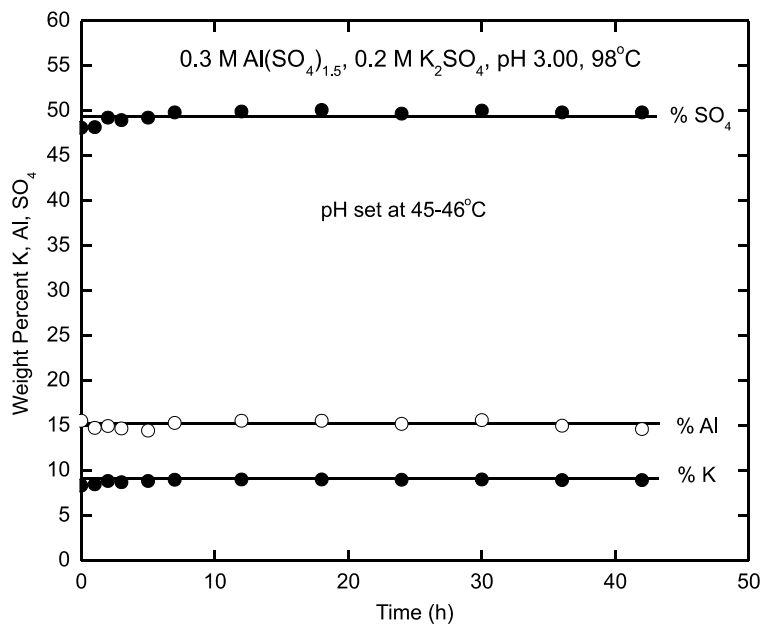


Figure 2 – Composition of the precipitates formed after various periods when 0.3 M Al(SO₄)_{1.5} – 0.2 M K₂SO₄ solutions at pH 3.00 were reacted at 98°C

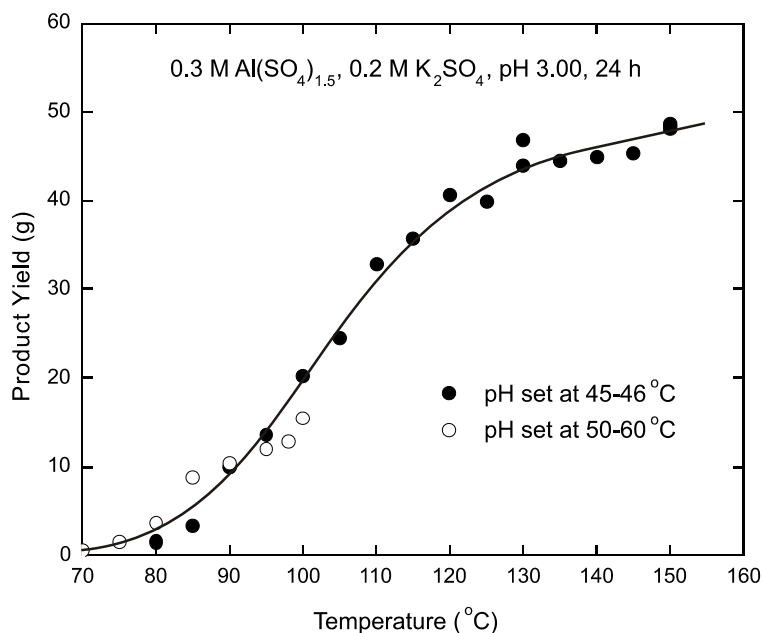


Figure 3 – Variation of the product yield when 0.3 M $\text{Al}(\text{SO}_4)_{1.5}$ - 0.2 M K_2SO_4 solutions at pH 3.00 were reacted for 24 h at various temperatures

Figure 4 presents the compositions of the precipitates formed at the different synthesis temperatures. Nearly identical compositions are detected in the precipitates formed at pH-setting temperatures of both 45-46°C and 50-60°C, and this observation is consistent with the similar product yields noted in Fig. 3. Regardless of the pH-setting temperature, the K, Al and SO_4 contents remain essentially constant at ~8.9%, ~15.3% and ~47.6%, respectively. There is, perhaps, an indication the SO_4 content increases slightly with increasing temperature in the 70 to 100°C range, but the variation is likely within the accuracy limits of the chemical analyses. End-member alunite has a composition of 9.44% K, 19.54% Al and 46.38% SO_4 . The slightly reduced K contents of the synthesized products indicate a modest degree of hydronium ion (H_3O^+) substitution for K^+ , and the slightly higher SO_4 contents are consistent with such a substitution. There is a more significant deficiency in the Al contents of the synthesized products that was confirmed by three independent chemical laboratories. Somewhat similar deficiencies were noted in the natroalunite products formed at >160°C [8, 10], but the mechanism of vacancy creation on the Al sub-lattice is not well understood. Nevertheless, the compositional data are consistent with the precipitation of alunite, and in fact, only well crystallized alunite was detected by X-ray diffraction analysis of the products formed in the entire temperature range from 70 to 150°C. The possible presence of an amorphous Al-sulphate species was carefully examined, but no amorphous species were detected in any of the X-ray diffraction patterns generated in this study. Thus, it is concluded that only alunite is precipitated and the composition of the alunite does not depend significantly on the synthesis temperature, or on the temperature at which the pH was initially set.

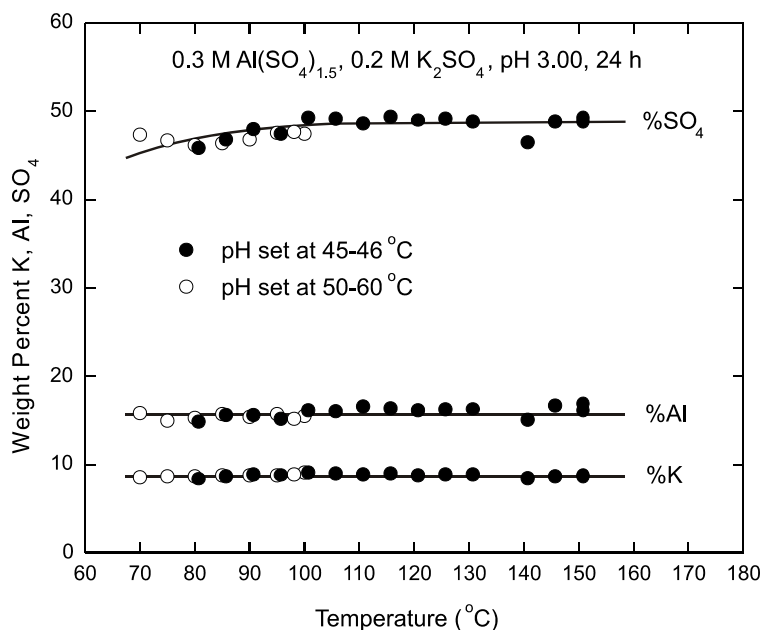


Figure 4 – Effect of the synthesis temperature on the composition of the precipitates formed when 0.3 M $\text{Al}(\text{SO}_4)_{1.5}$ - 0.2 M K_2SO_4 solutions at pH 3.00 were reacted for 24 h

Effect of the pH of the Synthesis Solution

The alunite precipitation reaction (Equation 4) generates significant amounts of hydrolysis acid, and thus, the pH of the synthesis solution is expected to be an important control parameter for alunite precipitation. In this regard, Figure 5 shows the variation of the product yield as a function of the initial pH of 0.3 M $\text{Al}(\text{SO}_4)_{1.5}$ - 0.2 M K_2SO_4 solutions which were reacted for 24 h at 98°C. The experiments were carried out using pH-setting temperatures of both 45-46°C and 50-60°C. Regardless of the pH-setting temperature, very similar product yields are obtained. Again, the implication is that the pH-setting temperature in the experiments where the pH was set at 50-60°C was likely close to 50°C. In both sets of experiments, the product yield increased progressively as then pH increased. Very little product forms at pH values <2.5, but the amount of precipitate increases significantly at higher pH values, and over 50 g of precipitate form at pH values >3.5. Although X-ray diffraction analysis of the precipitates formed at all the pH values detected only well crystallized alunite, it was observed that the products formed at pH values >3.4 were more difficult to filter. This behaviour seems to be a consequence of the finer particle sizes of the precipitates made at the higher pH values. For example, SEM examination of the precipitate made at pH 2.80 showed it to consist of spheroidal agglomerates 10-15 μm in diameter whereas the product formed at pH 3.6 consisted of loose masses of individual particles 1-2 μm in size.

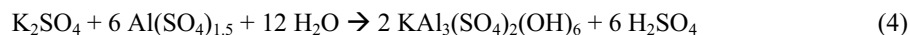


Figure 6 presents the compositions of the precipitates formed at the various pH values. Although the amount of product varies significantly as the pH increased, the composition of the precipitates remains essentially constant. Furthermore, virtually coincident compositional data are obtained for the products made using pH-setting temperatures of both 45-46°C and 50-60°C. The K, Al and SO_4 contents remain nearly constant at ~8.8%, ~15.0% and ~47.5%, respectively, as the pH increases from 0.7 to 3.7. EDX examination of the precipitate formed at pH 2.80 (Figure 7) showed the ~10 μm spheroidal particles to be porous but relatively uniform in composition. All the analyses detected K, Al, S and O, and the relative ratios of the elements seemed to be essentially constant; that is, the variations in the grey level simply reflect differences in the porosity of the particles. There was no indication of any Al-OH- SO_4 or other

impurity species. Overall, the compositional data are characteristic of that of precipitated alunite which was the only phase detected by X-ray diffraction analysis of these products. Based on these results, subsequent syntheses were carried out at pH 2.80 or 3.00, as these values generated adequate amounts of precipitate that were readily filterable.

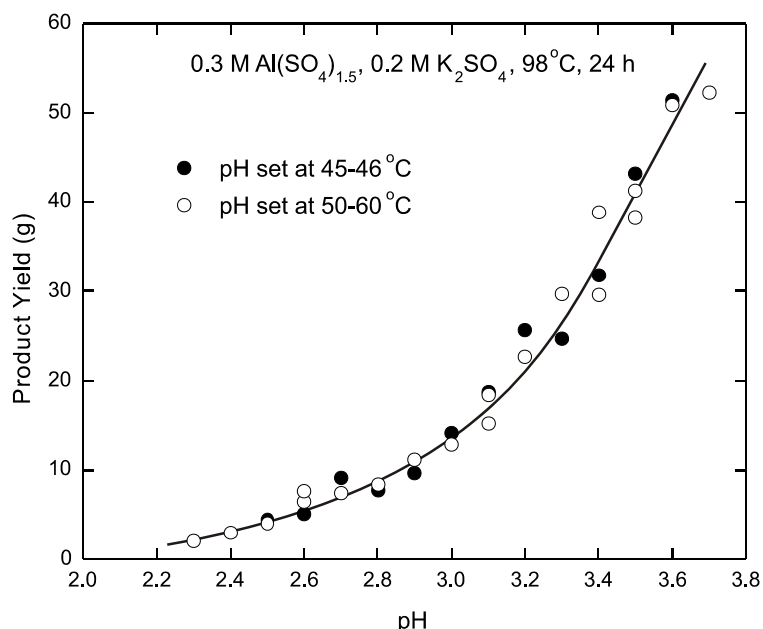


Figure 5 – Product yields realized when 0.3 M $\text{Al}(\text{SO}_4)_{1.5}$ - 0.2 M K_2SO_4 solutions at various initial pH values were reacted for 24 h at 98°C

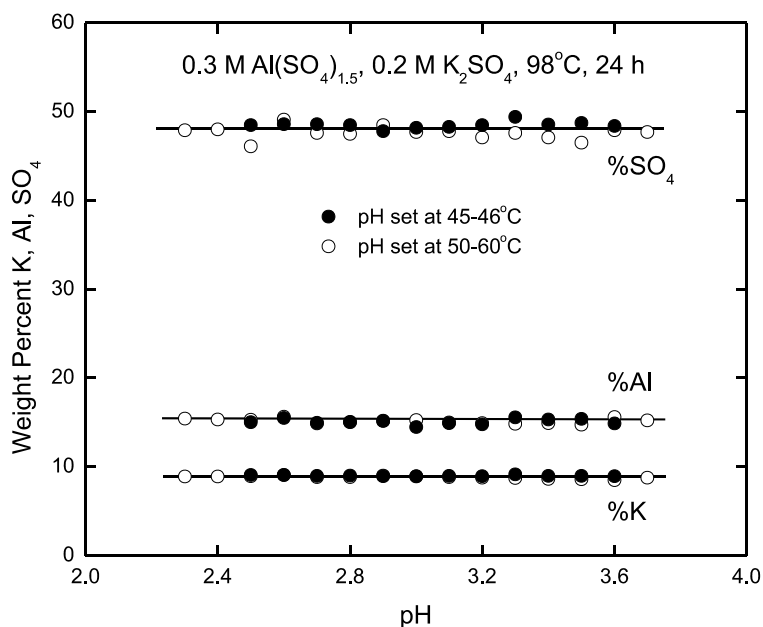


Figure 6 – Effect of the initial pH on the composition of the precipitates formed when 0.3 M $\text{Al}(\text{SO}_4)_{1.5}$ - 0.2 M K_2SO_4 solutions were reacted for 24 h at 98°C

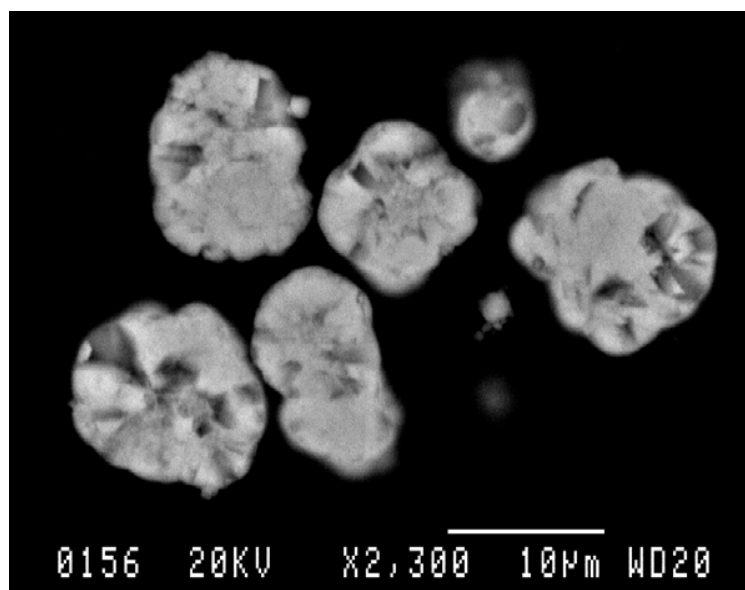


Figure 7 – Backscattered electron micrograph of the precipitate formed when 0.3 M $\text{Al}(\text{SO}_4)_{1.5}$ - 0.2 M K_2SO_4 solutions at pH 2.80 were reacted for 24 h at 98°C. Variations in the grey level reflect porosity differences, as all analyses detected K, Al, S and O. (polished cross-section)

Effect of the Concentration of K_2SO_4 and $\text{Al}(\text{SO}_4)_{1.5}$

Figure 8 illustrates the effect of the concentration of K_2SO_4 on the amount of product formed when 0.3 M $\text{Al}(\text{SO}_4)_{1.5}$ solutions at pH 3.00 were reacted for 24 h at 98°C. Results are presented for two similar series of experiments which were carried out where the pH was set at either 45-46°C or 50-60°C. In both series of experiments, the product yield increases rapidly as the K_2SO_4 concentration increases from 0.0 to about 0.1 M, but nearly constant product yields are achieved at higher K_2SO_4 concentrations. For the solutions used, the stoichiometric amount of K_2SO_4 to react with 0.3 M $\text{Al}(\text{SO}_4)_{1.5}$ is 0.05 M, and thus, a stoichiometric excess of a K_2SO_4 has little effect on the amount of precipitate formed. As shown in Figure 8, approximately twice as much precipitate formed in the tests where the pH-setting temperature was 50-60°C, and the implication is that actual pH-setting temperature of these tests was approximately 60°C (see Table 1). The differences in the results obtained at a pH-setting temperature of 50-60°C (likely about 60°C) and the analogous results obtained at a pH-setting temperature of 45-46°C confirm the importance of controlling the temperature at which the pH is set (Table 1).

The compositions of the precipitates made from the solutions containing various concentrations of K_2SO_4 are shown in Figure 9. As the concentration of K_2SO_4 increased from 0.01 to about 0.05 M, the K contents increased from 7.3 to ~8.3% and the SO_4 contents also increased slightly, from 47% to about 48%. In contrast, the Al contents decreased from 17.4% to ~16%. Further increases in the K_2SO_4 concentration have relatively little effect on the K, Al and SO_4 contents which remained nearly constant at 9.3%, 15.4% and 49%, respectively. Furthermore, essentially identical compositions were realized in the experiments where the pH was set at 45-46°C or at 50-60°C, despite the significant variations in the product yields realized at the two pH-setting temperatures. The compositions are generally characteristic of that of precipitated alunite. As noted above, the stoichiometric amount of K_2SO_4 to react with 0.3 M $\text{Al}(\text{SO}_4)_{1.5}$ is 0.05 M, and the modest compositional variations noted in Figure 9, especially the lower K contents, likely reflect an enhanced degree of hydronium ion (H_3O^+) substitution for K^+ in the precipitates formed from the more dilute K_2SO_4 solutions. However, despite the slightly elevated hydronium ion contents of some of the precipitates, X-ray diffraction analysis detected only (potassium) alunite. At the 98°C synthesis temperature, it is clear that sub-stoichiometric K_2SO_4 concentrations generate lesser amounts of

(potassium) alunite rather than precipitating larger quantities of hydronium-rich alunite, as was previously noted by Rudolph et al. [13].

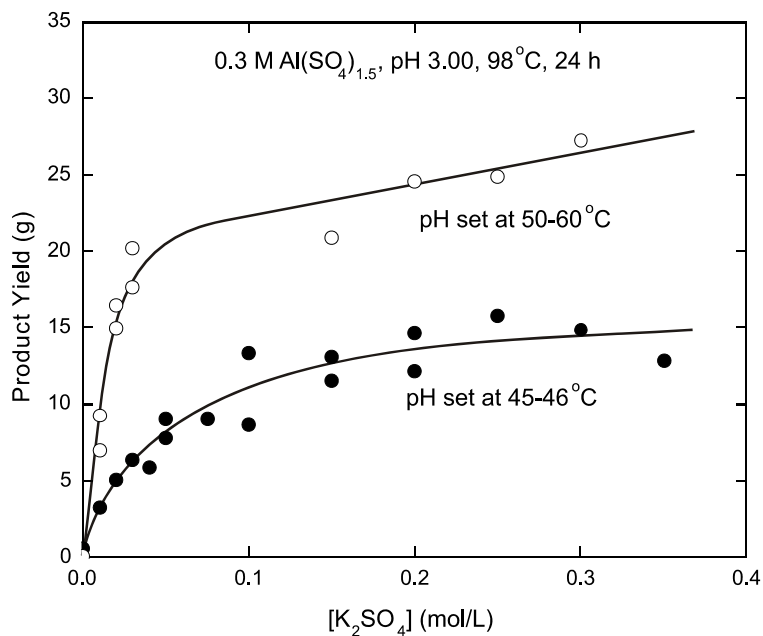


Figure 8 – Effect of the concentration of K_2SO_4 on amount of precipitate formed when 0.3 M $Al(SO_4)_{1.5}$ solutions at pH 3.00 were reacted for 24 h at 98°C. The product yields were significantly higher when the pH was set at 50-60°C rather than at 45-46°C

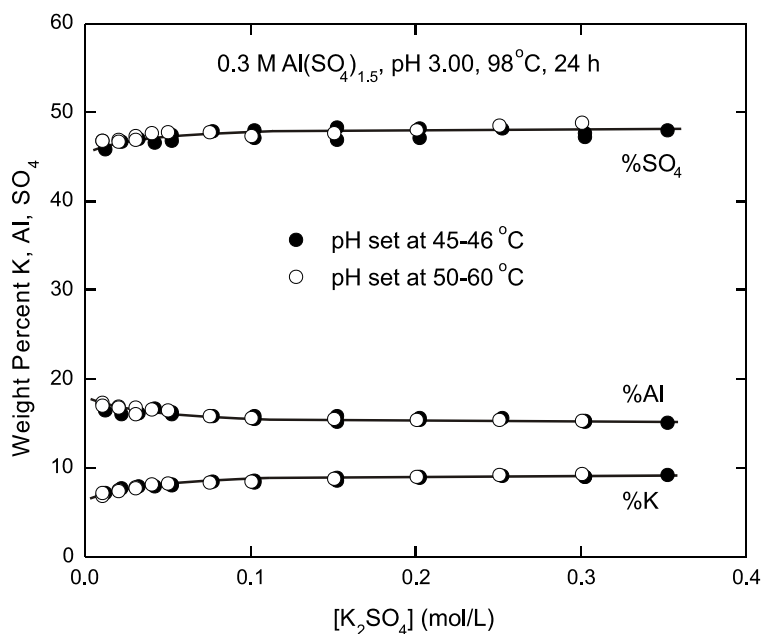


Figure 9 – Effect of the concentration of K_2SO_4 on the K, Al and SO_4 contents of the precipitates formed when 0.3 M $Al(SO_4)_{1.5}$ solutions at pH 3.00 were reacted for 24 h at 98°C

The effect of the concentration of $\text{Al}(\text{SO}_4)_{1.5}$ on the alunite precipitation reaction was studied at pH 3.00. The experiments were carried out for 24 h at 98°C using 0.1 M K_2SO_4 at pH 3.00, where the pH was set at $45\text{--}46^\circ\text{C}$. As shown in Figure 10, the product yield increases consistently as the concentration of $\text{Al}(\text{SO}_4)_{1.5}$ increases. Initially the product yield rises rapidly with increasing $\text{Al}(\text{SO}_4)_{1.5}$ concentration, but the rate of increase diminishes slightly for concentrations > 0.075 M. Thereafter, the product yield increases in a roughly linear manner as the $\text{Al}(\text{SO}_4)_{1.5}$ concentration increases from 0.10 to 0.35 M. For the range of $\text{Al}(\text{SO}_4)_{1.5}$ concentrations studied, a 0.1 M K_2SO_4 concentration represents a stoichiometric excess of K to Al, and under these conditions, an increase in the $\text{Al}(\text{SO}_4)_{1.5}$ concentration generates a corresponding increase in the amount of precipitate (Equation 4).

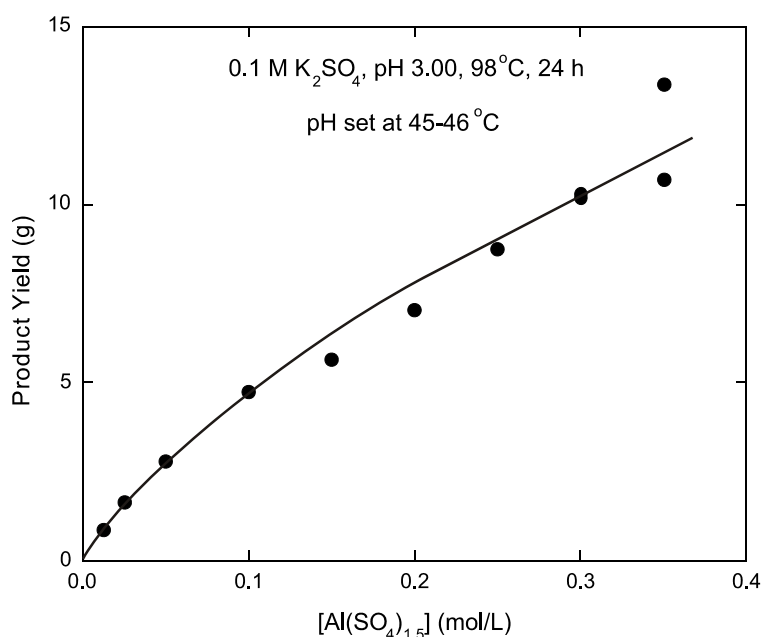


Figure 10 – Variation of the product yield with increasing $\text{Al}(\text{SO}_4)_{1.5}$ concentration when 0.1 M K_2SO_4 solutions at pH 3.00 were reacted for 24 h at 98°C

Figure 11 presents the compositions of the precipitates formed at the various $\text{Al}(\text{SO}_4)_{1.5}$ concentrations shown in Figure 10. The K, Al and SO_4 contents remain essentially constant at 9%, 15% and 48%, despite the relatively significant variation in the concentration of $\text{Al}(\text{SO}_4)_{1.5}$. The implication is that increasing $\text{Al}(\text{SO}_4)_{1.5}$ concentrations, in the presence of excess K_2SO_4 , generate more product but that the composition of the product remains nearly constant. Furthermore, the composition is typical of that of precipitated alunite, which was the only phase identified by X-ray diffraction analysis of these precipitates.

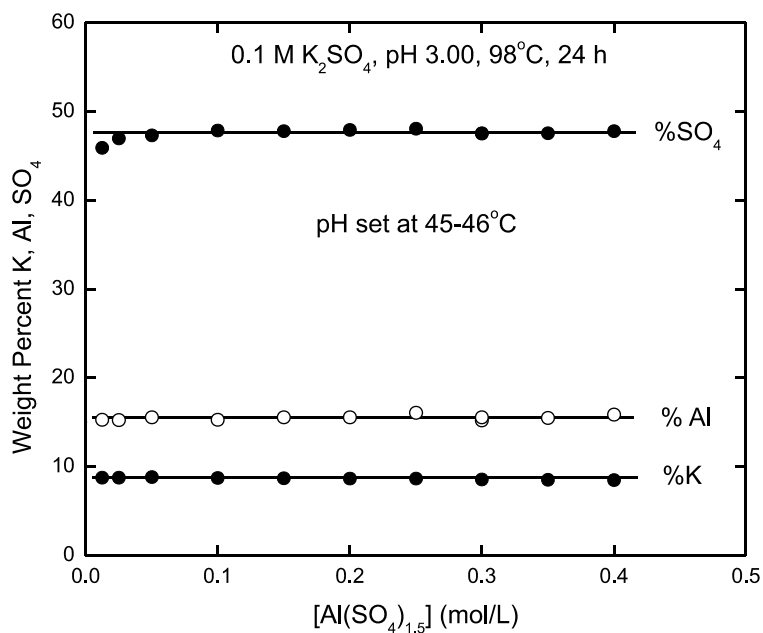


Figure 11 – Composition of the precipitates formed when 0.1 M K₂SO₄ solutions at pH 3.00, and containing various concentrations of Al(SO₄)_{1.5}, were reacted for 24 h at 98°C

Effect of the Concentration of As(III) and As(V)

Behaviour of As(III)

The behaviour of As(III) and As(V) was investigated under the preferred conditions identified above. In this regard, Figure 12 shows the variation of the product yield in a series of experiments where 0.3 M Al(SO₄)_{1.5} - 0.1 M K₂SO₄ solutions at pH 2.80 were reacted for 24 h at 98°C. The solutions also contained from 0.5 to 8 g/L of As(III) which was added as either NaAsO₂ or As₂O₃. Very similar product yields are realized regardless of whether the As(III) was added as NaAsO₂ or As₂O₃. In both sets of experiments, the product yield increased in a seemingly linear manner from about 6.5 g to 8.8 g as the concentration of As(III) increased from 0.5 to 8 g/L. The compositions of the precipitates made in the presence of various concentrations of As(III) are presented in Figure 13. No significant compositional differences were detected between the tests where the As(III) was added as NaAsO₂ or As₂O₃, and, consequently, the analytical results are treated as a single data set. Regardless of the concentration of As(III), the K, Al and SO₄ contents remain essentially constant at 7.8%, 15.0% and 47.5%, respectively. In the experiments where the As(III) was added as NaAsO₂, the products contained a small content of Na. However, the Na contents were always <0.23% and were generally <0.1% Na. This observation is consistent with the fact that (potassium) alunite is the most stable of all the alunite species [13], just as (potassium) jarosite is the most stable jarosite-type compound [6]. As shown in Figure 13, the As contents of the precipitates are reported as arsenite, AsO₃. Furthermore, the AsO₃ contents increase from 0.0 to only 0.26% as the concentration of As(III) increases from 0.5 to 8 g/L. In total, the compositions are consistent with that of precipitated alunite, and in fact, only (potassium) alunite was detected by X-ray diffraction analysis of these products. The implication of the data given in Figures 12 and 13 is that the presence of modest concentrations of As(III), or its chemical source, have relatively little effect on the alunite precipitation reaction.

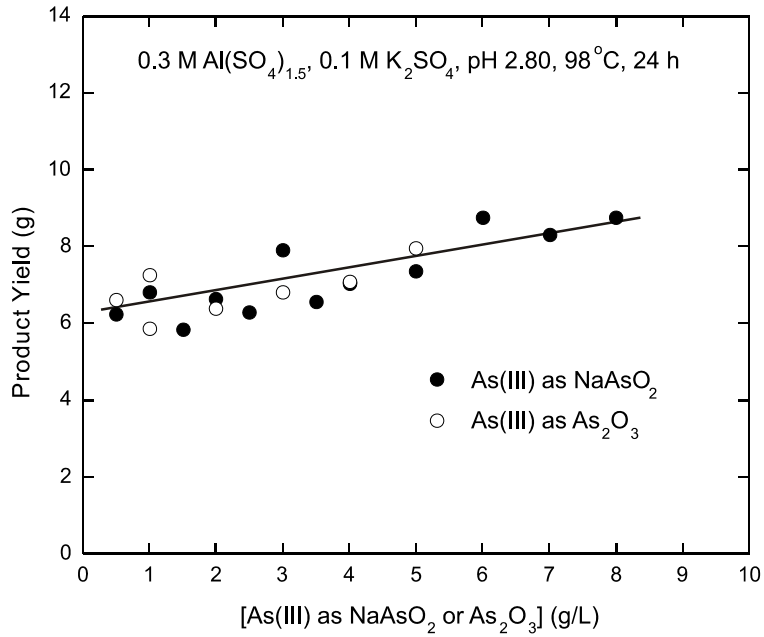


Figure 12 - Product yields realized when 0.3 M Al(SO₄)_{1.5}- 0.1 M K₂SO₄ solutions containing various concentrations of As(III) as NaAsO₂ or As₂O₃, at pH 2.80, were reacted for 24 at 98°C

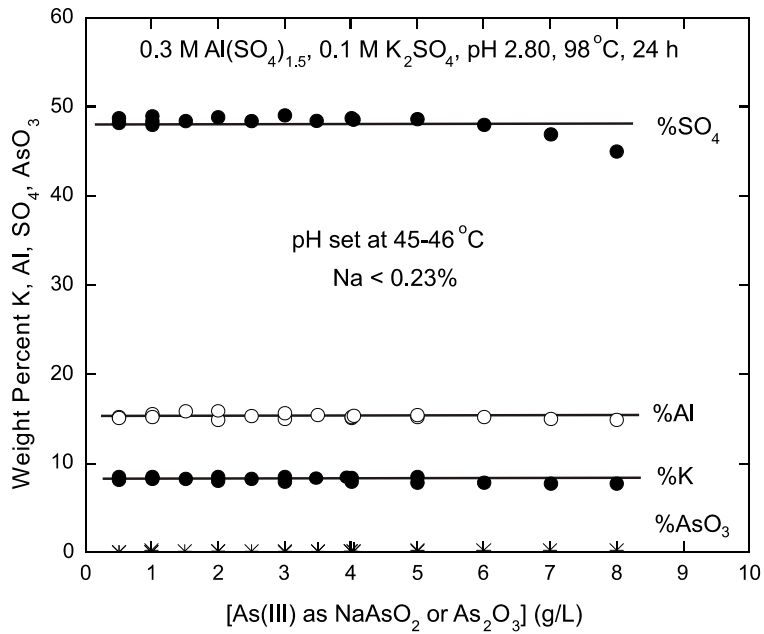


Figure 13 – Effect of the concentration of As(III) as NaAsO₂ or As₂O₃ on the composition of the precipitates formed when 0.3 M Al(SO₄)_{1.5}- 0.1 M K₂SO₄ solutions at pH 2.80 were reacted for 24 h at 98°C

Figure 14 is a backscattered electron micrograph of the precipitate made when a 0.3 M $\text{Al}(\text{SO}_4)_{1.5}$ -0.1 M K_2SO_4 solution containing 5 g/L of As(III) added as NaAsO_2 , at pH 2.80, was reacted for 24 h at 98°C. The bulk composition of this precipitate is 7.85% K, 0.23% Na, 15.2% Al, 47% SO_4 and 0.13% As which is reported as 0.21% AsO_3 . As was the situation for the As(III)-free product shown in Figure 7, the particles are spheroidal in shape and 10-15 μm in size. There is a considerable amount of porosity that results in variations in the grey level within the individual particles. Despite these variations, the EDX analyses of this precipitate detected only K, Al, S and O, and the ratios of the elements remained essentially constant from spot to spot within a given particle and among the different particles. Arsenic was not detected in any of the alunite particles, and this observation is consistent with the bulk As content of 0.13% which is below the minimum As detection limit of the instrument. Also, discrete As-rich phases were not detected. Although these results could be interpreted as showing a low level of AsO_3 (arsenite) incorporation in alunite, a different explanation is possible. As will be seen later, arsenate (AsO_4) is extensively incorporated in alunite, and the low As contents of the particles shown in Figure 14 could reflect the minor oxidation of As(III) to As(V) during the 24-h synthesis period and the incorporation of the resulting AsO_4 in the alunite structure. However, this possibility would require more detailed study.

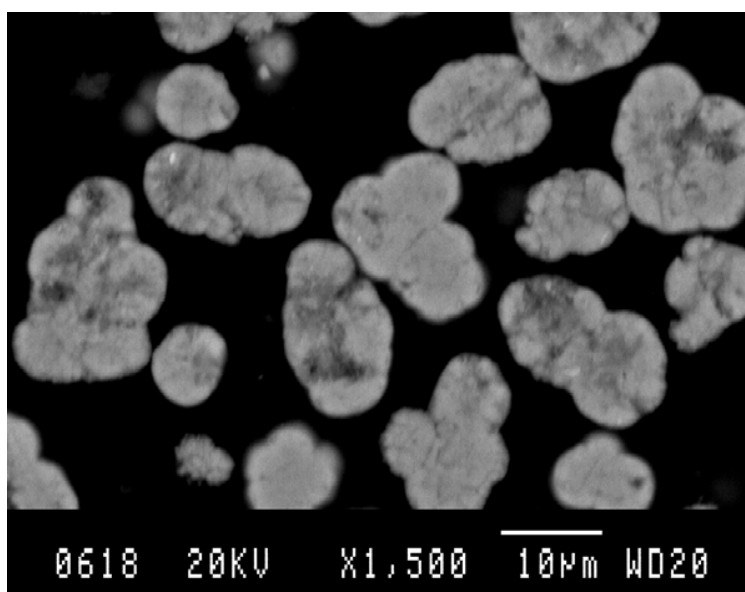


Figure 14 - Backscattered electron micrograph of the precipitate made when a 0.3 M $\text{Al}(\text{SO}_4)_{1.5}$ -0.1 M K_2SO_4 solution containing 5 g/L of As(III), at pH 2.80, was reacted for 24 h at 98°C. The precipitate contains 0.13% As (0.21% AsO_3). (polished cross-section)

Behaviour of As(V)

Figure 15 shows the effect of the concentration of As(V) on the product yields realized when 0.3 M $\text{Al}(\text{SO}_4)_{1.5}$ -0.1 M K_2SO_4 solutions at pH 2.80 were reacted for 24 h at 98°C. The initial pH was set at 45-46°C. The As(V) was added as either KH_2AsO_4 or As_2O_5 , and similar results were obtained regardless of the chemical form of the added As(V). A similar set of experiments was carried out using an initial pH of 3.00, also set at 45-46°C, and a similar trend was observed although those experiments yielded somewhat greater amounts of product. As shown in Figure 15, nearly constant product yields are realized for As(V) concentrations <2.0 g/L range. However, further increases in the concentration of As(V) clearly promote the extent of alunite precipitation, and the product yield increases from about 7 g for the

precipitate made in the presence of 2 g/L of As(V) to nearly 25 g in the precipitate made from solutions containing 7 g/L As(V). Thereafter, the product yield increased only slightly; for example, the product yield from the solution containing 9 g/L As(V) was just 26 g. The increase in the product yield with increasing As(V) concentration was also observed during the hydrothermal synthesis of natroalunite at temperatures between 160°C and 200°C [8]. In those experiments, part of the As(V) was initially precipitated as an amorphous As-phase that re-dissolved when the pH of the solution decreased because of the precipitation of Al(III) as natroalunite.

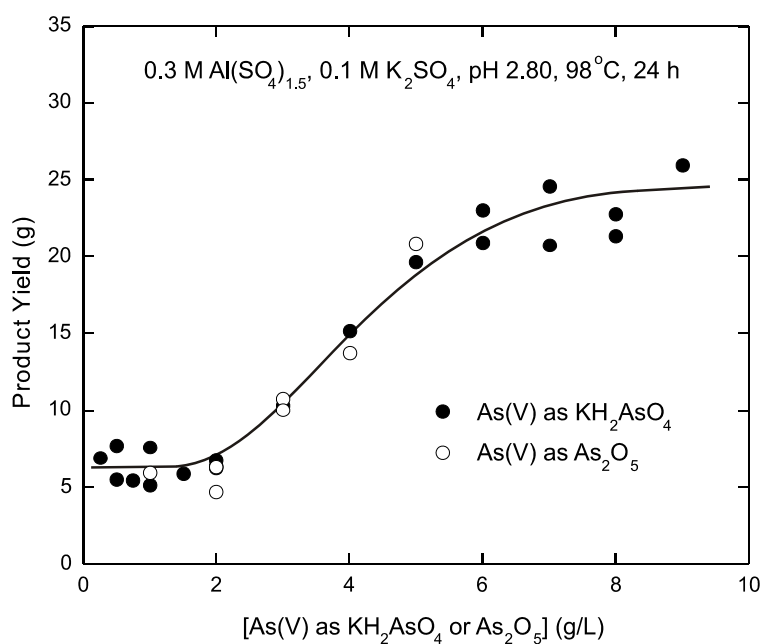


Figure 15 – Effect of increasing concentrations of As(V), added as either KH_2AsO_4 or As_2O_5 , on the amount of product formed when 0.3 M $\text{Al}(\text{SO}_4)_{1.5}$ - 0.1 M K_2SO_4 solutions at pH 2.80 were reacted for 24 h at 98°C

Figure 16 illustrates the effect of the As(V) concentration on the composition of the precipitates given in Figure 15. The compositions were essentially the same regardless of whether the As(V) was added as KH_2AsO_4 or As_2O_5 , and for this reason, the analyses are treated as a single data set. Although the Al contents remain nearly constant as the As(V) concentration increases from 0 to 9 g/L, the K contents seem to decrease slightly, from about 9 to 7 g/L. The SO_4 contents decrease significantly and most of the decrease occurs for As(V) concentrations in the 0 to 3-4 g/L range. Although there is some scatter of the data, the AsO_4 contents seem to increase in an inversely related manner, suggesting that AsO_4 substitutes for SO_4 in the alunite structure. X-ray diffraction analysis of the precipitates given in Figure 16 detected only alunite, although there were variations in the positions of the diffraction peaks as would occur if AsO_4 substituted for SO_4 in the alunite structure. In this regard, previous investigations concluded that AsO_4 substitutes for SO_4 in natroalunite [8, 9, 10] and in jarosite-type compounds [5].

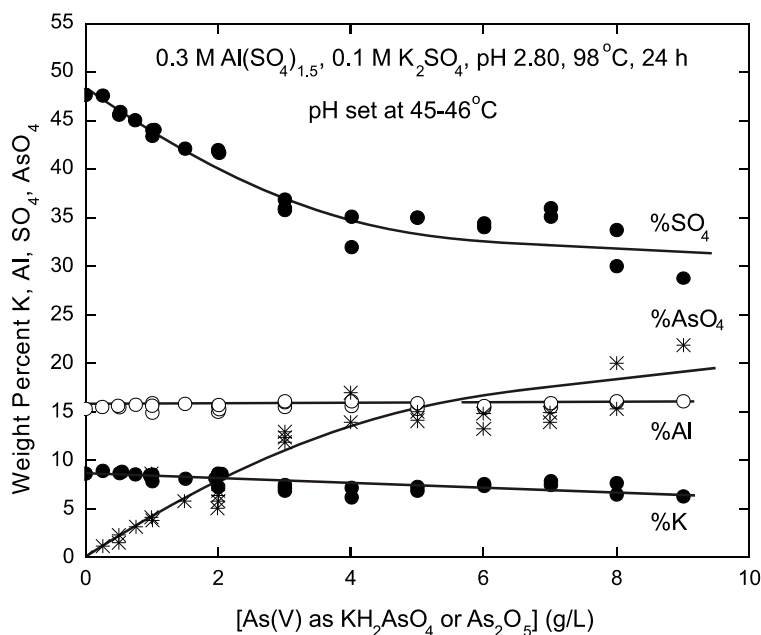


Figure 16 - Effect of the concentration of As(V), added as either KH_2AsO_4 or As_2O_5 , on the composition of the precipitates made when $0.3 \text{ M Al}(\text{SO}_4)_{1.5}$ - $0.1 \text{ M K}_2\text{SO}_4$ solutions at pH 2.80 were reacted for 24 h at 98°C

As noted above, similar experiments were carried out to determine the influence of the concentration of As(V) on the precipitation of alunite when $0.3 \text{ M Al}(\text{SO}_4)_{1.5}$ - $0.1 \text{ M K}_2\text{SO}_4$ solutions, at an initial pH of 3.00, were reacted for 24 h at 98°C . In those tests, the As(V) was added only as KH_2AsO_4 and the pH was set at $45\text{--}46^\circ\text{C}$. Figure 17 illustrates the compositions of the precipitates realized in that series of experiments. The data are very similar to those presented in Figure 16 for the experiments carried out at an initial pH of 2.80. That is, the K contents decrease slightly but the Al contents remain essentially constant at about 15.4% as the As(V) concentration rises from 1 to 8 g/L. The SO_4 contents decrease significantly with increasing As(V) concentration and the AsO_4 contents increase in an inversely related manner. The decreases in SO_4 and the increases in AsO_4 are slightly less pronounced for the experiments done using an initial pH of 3.00, rather than an initial pH of 2.80, but the differences are likely within the limits of error of the experimental/analytical procedures. In all instances, only alunite was detected by X-ray diffraction analysis of the precipitates made at pH 3.00.

Figure 18 illustrates the morphology of the alunite precipitate made when a $0.3 \text{ M Al}(\text{SO}_4)_{1.5}$ - $0.1 \text{ M K}_2\text{SO}_4$ solution at pH 2.80 was reacted for 24 h at 98°C in the presence of 2 g/L of As(V), added as KH_2AsO_4 . The sample analyzed 7.92% K, 15.76% Al, 39.2% SO_4 and 8.56% AsO_4 . The precipitate consists of spheroidal particles 10-15 μm in size that are very similar to those detected in the precipitates made in the absence of added arsenic (cf. Fig. 7). Although there is some porosity, which results in variations in the grey level within the individual particles, the precipitate seems to be single phase. Specifically, there is no indication of discrete As-rich or Al-rich species. That is, the arsenic content seems to be incorporated in the structure of the alunite. Electron microprobe analysis of 120 particles of this precipitate yielded an average AsO_4 content of 10.0%, with values ranging from 8.81% to 13.6%. The corresponding average K, Al and SO_4 contents were 5.8, 18.4 and 48.5%, respectively. Except for the value of K, the average analyses are somewhat higher than the bulk composition of the precipitate, and this seems to be a consequence of (1) problems associated with the electron microprobe analysis of small porous grains and (2) the difficulty of obtaining accurate K analyses in sulphate salts such as alunite and jarosite. In any event the relatively consistent AsO_4 contents detected by the electron microprobe support the conclusion that the arsenate content of this precipitate is incorporated in the alunite structure.

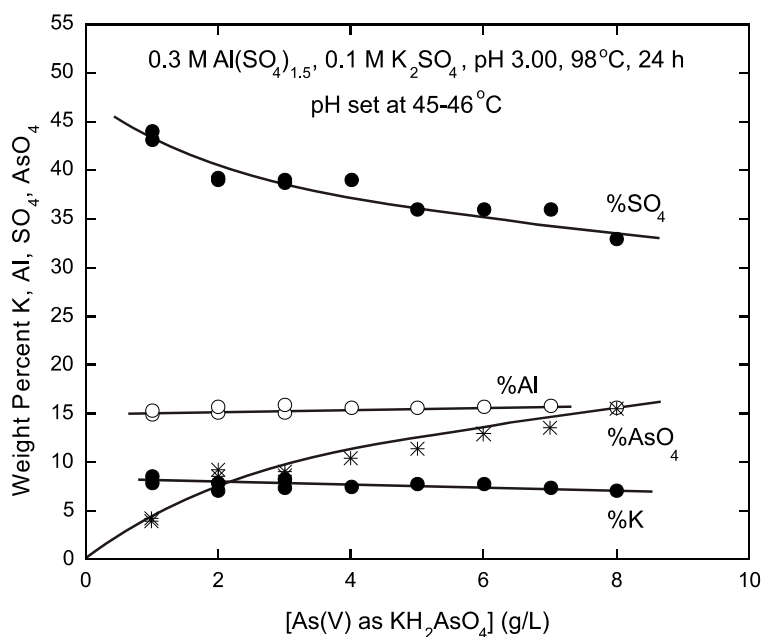


Figure 17 - Effect of the concentration of As(V), added as KH_2AsO_4 , on the composition of the precipitates made when 0.3 M $\text{Al}(\text{SO}_4)_{1.5}$ - 0.1 M K_2SO_4 solutions at pH 3.00 were reacted for 24 h at 98°C.

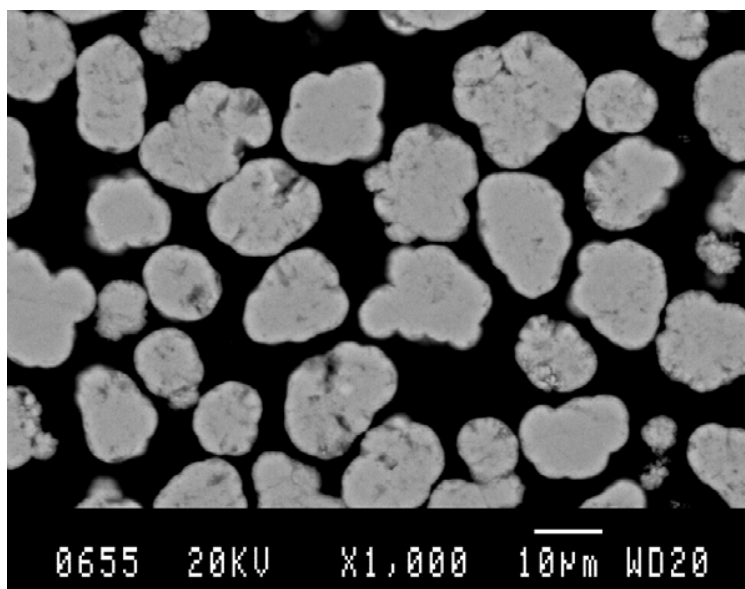


Figure 18 - Backscattered electron micrograph of the precipitate formed when a 0.3 M $\text{Al}(\text{SO}_4)_{1.5}$ - 0.2 M K_2SO_4 solution at pH 2.80 and containing 2 g/L of As(V) as KH_2AsO_4 was reacted for 24 h at 98°C. The precipitate has an average bulk AsO_4 content of 8.56%. (polished cross-section)

Figure 19 illustrates the morphology of the alunite precipitate made when a 0.3 M $\text{Al}(\text{SO}_4)_{1.5}$ - 0.1 M K_2SO_4 solution at pH 2.80 was reacted for 24 h at 98°C in the presence of 3 g/L of As(V), added as KH_2AsO_4 . This sample analyzed 6.90% K, 15.5% Al, 36.0% SO_4 and 12.9% AsO_4 . Unlike the precipitate illustrated in Figure 18, this product consists of irregular masses of 5-10 μm individual particles. Furthermore, it is apparent that this precipitate consists of two phases. SEM-EDX analysis indicated that both phases contain K, Al, SO_4 and AsO_4 , but the tiny core particles are really too fine for meaningful analysis and the elements detected may be influenced by the associated rims. Electron microprobe analyses of 22 of the particles in this precipitate were carried out. The darker appearing rims analyzed 10.6% K, 16.5% Al, 38.6% SO_4 and 14.6% AsO_4 (range 6.8-21.2%), and the average composition is generally compatible with that of arsenate-containing alunite. In contrast, the brighter-appearing cores were shown to contain 4.1% K, 15.5% Al, 23.7% SO_4 and 41.4% AsO_4 (range 37.2-46.0%). The elevated arsenate content of the core particles is notable, and the molar ratio of AsO_4 slightly exceeds that of SO_4 . The composition suggests the presence of a discrete As-bearing phase despite the fact that only alunite was detected by X-ray diffraction analysis of the bulk material.

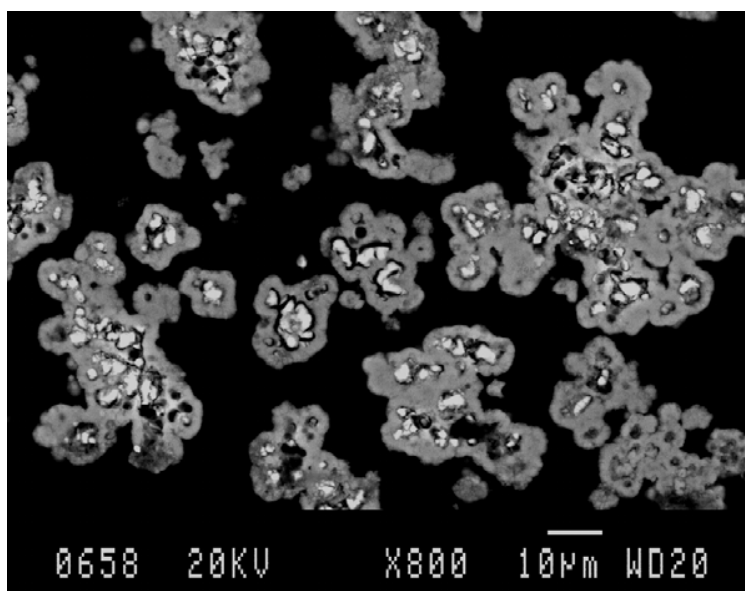


Figure 19 - Backscattered electron micrograph of the precipitate formed when a 0.3 M $\text{Al}(\text{SO}_4)_{1.5}$ - 0.2 M K_2SO_4 solution at pH 2.80 and containing 3 g/L of As(V) as KH_2AsO_4 was reacted for 24 h at 98°C. The precipitate has an average bulk AsO_4 content of 12.9%. (polished cross-section)

Similar two-phase morphologies were detected for all the precipitates having bulk AsO_4 contents greater than ~10%, and these products consisted of rims having a composition generally compatible with that of alunite, together with arsenate-rich cores. In this regard, Figure 20 is a field emission micrograph showing the detailed morphology of the precipitate made from a solution containing 5 g/L of As(V), added as KH_2AsO_4 and having a bulk composition of 6.89% K, 15.3% Al, 35.0% SO_4 and 15.0% AsO_4 . The sample consists of a rim enveloping a more extensive core. It is apparent that the interior of this particle consists of an agglomeration of numerous tiny crystals together with significant porosity. The structure may be that of the As-rich core or may simply reflect the interior surface of the rim. In many instances the tiny individual crystals are well formed, and their abundance and euhedral morphology suggest that their presence should be detectable by X-ray diffraction analysis. However, X-ray diffraction analysis of this material indicated only alunite. The patterns were "sharp" and there was no indication of line broadening or line splitting, as might be expected if two alunite compositions were present. There was also no

indication of the presence of an amorphous phase. These observations lead to the tentative conclusion that both phases are alunite, with cores of AsO_4 -rich alunite enveloped by lower- AsO_4 alunite rims, but further work will be required to elucidate the nature of the AsO_4 -rich phase.

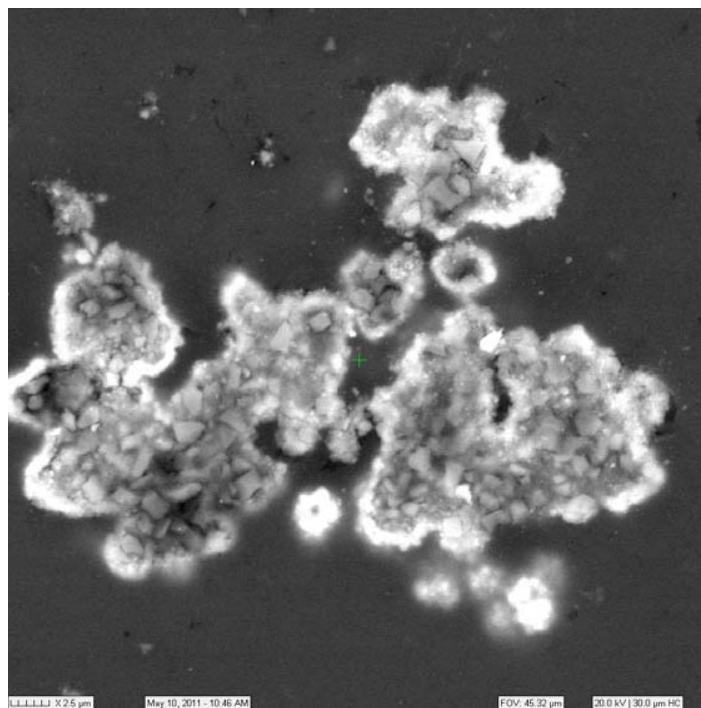


Figure 20 – Field emission SEM micrograph of a polished cross-section of the precipitate formed when a 0.3 M $\text{Al}(\text{SO}_4)_{1.5}$ - 0.2 M K_2SO_4 solution at pH 2.80 and containing 5 g/L of As(V) as KH_2AsO_4 was reacted for 24 h at 98°C. The precipitate has an average bulk AsO_4 content of 15.0%.
(image courtesy of Fibics Incorporated, Ottawa, Canada)

The above results suggest that several percent AsO_4 can be incorporated in alunite precipitates and that the AsO_4 substitutes for SO_4 in the alunite structure. To confirm this behaviour, X-ray diffraction patterns of several of the As(V)-containing products were obtained using 1-h exposure times and an internal Al_2O_3 standard. The patterns were indexed on the basis of the rhombohedral alunite cell, and the resulting a and c cell parameters are shown as a function of the mole fraction of $\text{AsO}_4/(\text{AsO}_4 + \text{SO}_4)$ in Figure 21. Clearly, the a cell parameter does not vary significantly as the mole fraction of $\text{AsO}_4/(\text{AsO}_4 + \text{SO}_4)$ increases from 0.0 to about 0.3. In contrast, the c cell parameter clearly increases progressively over the same compositional range. Although there is some scatter of the data that is partly a consequence of the fact that the more AsO_4 -rich precipitates are two-phase but yield only single diffraction peaks, the trend clearly indicates an expansion of the c cell parameter as the AsO_4 content increases. Such a trend is consistent with the substitution of the larger AsO_4 ion for SO_4 in the alunite structure.

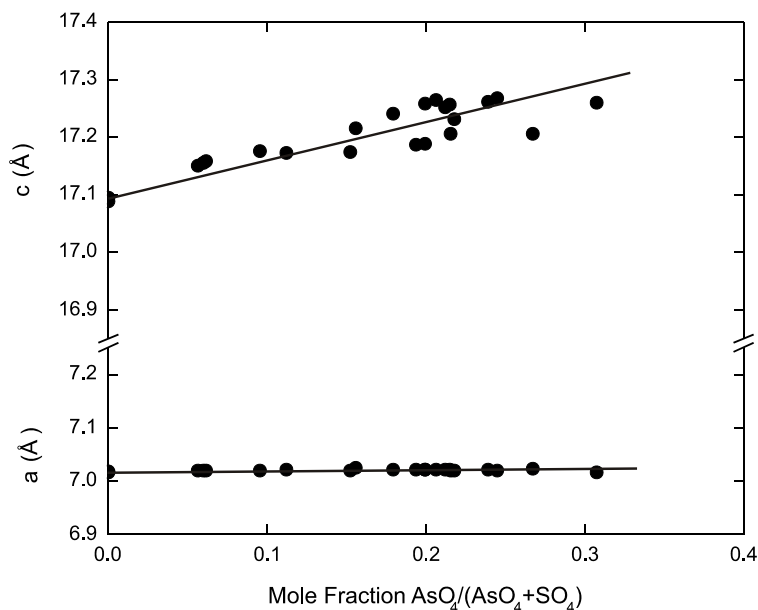


Figure 21 – Variation of the X-ray determined a and c cell parameters of the arsenate-containing alunite precipitates as a function of their mole fraction of $\text{AsO}_4/(\text{AsO}_4 + \text{SO}_4)$

Environmental Considerations

The TCLP leachate test was carried out on two alunite samples that contained 8.5% and 19.5% AsO_4 . These samples were re-pulped and washed several times with water prior to the leachate tests to eliminate any adsorbed or entrained arsenate. Two 100 g lots of the 8.5% AsO_4 alunite and one 100 g sample of the 19.5% AsO_4 alunite were bottle-rolled at room temperature in 1L of deionized water at pH 5 for 24 h. The resulting liquors were analyzed for As. The tests gave a low arsenic concentration of 0.37 mg/L for the samples containing 8.5% AsO_4 , and the final pH was 4.86. Thus, this As-bearing alunite passes the TCLP test. In contrast, the material containing 19.5% AsO_4 yielded a solution containing 7.8 mg/L As, and the final pH was 4.60. The latter As concentration is similar to the value found for arsenical natroalunite synthesized at 100°C [8], which also did not pass the TCLP test. This behaviour could be related to the presence of an As-rich phase in the more As-rich alunite precipitates. The implication seems to be that alunites synthesized at 98°C and containing less than ~10% AsO_4 (i.e., alunites precipitated from solutions containing less than 2-3 g/L As(V)) will pass the TCLP test, but that the more AsO_4 -rich precipitates will not.

The solubility of some of the As-bearing alunite samples was also tested at pH 1.0 and room temperature during three consecutive 24-h extractions using a 400 rpm stirring speed [9, 10, 14]. One-gram samples were stirred in 100 mL of H_2SO_4 solution, and the pH of the solution was controlled at 1.0. The samples used in this test were synthesized from solutions containing 1 and 5 g/L As(V), and analyzing 4% and 14% AsO_4 , respectively. The sample analyzing 4% AsO_4 gave solubilities of 4.7 to 5 mg/L As in the first two leaching stages, and a solubility of 9 mg/L As in the third stage. The alunite containing 14% AsO_4 gave higher As concentrations, about 36 mg/L, in the second and third leaching stages. These values are higher than those found for As-bearing natroalunite synthesized at 200°C, where As concentrations of <1 mg/L were observed [8, 9]. These comparatively high As concentrations suggest that the AsO_4 content of alunite synthesized at <100°C is not as strongly incorporated as it is in alunite-type compounds made at 200°C. The results also show that alunites containing more than ~10% AsO_4 are considerably less stable than alunites having a lower AsO_4 content.

CONCLUSIONS

The precipitation of alunite in the absence of dissolved arsenic depended on several factors, all of which had a direct impact on the product yield, but produced only minor variations in the composition of the products. For example, at 98°C, the product yield increased nearly linearly with increasing retention times up to 30 h, but the composition of the precipitates remained essentially constant. Little alunite formed at temperatures <80°C but the amount of product increased progressively as the synthesis temperatures increased up to 150-160°C. The product yield increased with increasing solution pH and higher pH values generated precipitates which were finer and consequently more difficult to filter. Furthermore, it was found that the temperature at which the initial pH was set also had a significant impact on the amount of product formed. Increasing K₂SO₄ concentrations up to 0.1 M resulted in significant increases in the product yield; furthermore, these precipitates had slightly lower K contents that reflected minor H₃O⁺ ion substitution for K⁺ in the alunite structure. However, K₂SO₄ concentrations higher than 0.1 M had little effect on either the amount of product or its composition. On the other hand, increasing Al(SO₄)_{1.5} concentrations increased the product yield, but had no significant effect on the composition of the alunite precipitates. Regardless of the synthesis conditions used, X-ray diffraction analysis showed all the products to be well crystallized alunite

The precipitation of the alunite in the presence of dissolved As(III), added as either NaAsO₂ or As₂O₃, had little effect on the alunite precipitation reaction at 98°C. The product yield increased slightly, and in a linear manner, as the concentration of As(III) increased up to 8 g/L, but the composition of the solids did not vary significantly. The K, Al and SO₄ contents were essentially constant and were similar to those found in the As-free alunites. The AsO₃ contents of the precipitates increased in a linear manner from 0.0 to only 0.26% as the As(III) concentration of the solution rose to 8 g/L, and similar compositions were realized regardless of the chemical form of the added As(III). Furthermore, the morphology of the precipitates was similar to that of the As-free alunites.

The precipitation of alunite at 98°C in the presence of dissolved As(V) was also investigated in series of experiments where the arsenic was added as KH₂AsO₄ or As₂O₅. The product yield varied only slightly as the As(V) concentration increased from 0 to 2 g/L but increased in a nearly linear manner as the concentration rose to 6 g/L As(V). Further increases in the As(V) concentration had little effect on the amount of product formed. The K and Al contents of the precipitates remained nearly constant for As(V) concentrations up to 9 g/L. In contrast, the SO₄ contents decreased from 48 to 30% and the AsO₄ contents increased in an inversely related manner, from 0 to 20%, as the As(V) concentration increased from 0 to 9 g/L, and virtually identical results were obtained regardless of the chemical form of the added arsenic. The precipitates containing less than ~10% AsO₄ were shown to consist of one phase, but the more AsO₄-rich precipitates consisted of a core of AsO₄-rich alunite rimmed by lower-AsO₄ alunite. X-ray diffraction analysis of the AsO₄-bearing alunites detected only alunite, and there was no indication of line splitting or line broadening. Although the *a* cell parameters of the precipitates remained essentially constant, the *c* cell parameters increased systematically as the AsO₄/(AsO₄+SO₄) molar ratio of the precipitates increased. In total, these observations suggest that AsO₄ substitutes the SO₄ in the alunite structure.

ACKNOWLEDGEMENTS

The authors wish to acknowledge the invaluable contributions provided by CANMET-MMSL staff members T.T. Chen with the characterization investigations, A. Kuiper with the experimental program and D. Smith with the X-ray diffraction analyses. A. Sunyer also wishes to thank the Spanish Ministerio de Ciencia e Innovación (Project MAT 2007-61466) for a grant for her doctoral studies which include the present investigation.

REFERENCES


1. P.A. Riveros, J.E. Dutrizac and P. Spencer, "Arsenic Disposal Practices in the Metallurgical Industry", *Canadian Metallurgical Quarterly*, Vol. 40(4), 2001, 395-420.
2. J.F. Le Berre, R. Gauvin and G.P. Demopoulos, "A Study of the Crystallization Kinetics of Scorodite via the Transformation of Poorly Crystalline Ferric Arsenate in Weakly Acidic Solution", *Colloids and Surfaces A: Physicochem. Eng. Aspects*, Vol. 315, 2008, 117-129.
3. T. Fujita, R. Taguchi, M. Abumiya, M. Matsumoto, E. Shibata and T. Nakamura, "Effect of pH on Atmospheric Scorodite Synthesis by Oxidation of Ferrous Ions: Physical Properties and Stability of the Scorodite", *Hydrometallurgy*, Vol. 96, 2009, 189-198.
4. M.C. Bluteau. and G.P. Demopoulos, "The Incongruent Dissolution of Scorodite — Solubility, Kinetics and Mechanism", *Hydrometallurgy*, Vol. 87, 2007, 163–177.
5. D. Paktunc and J.E. Dutrizac, "Characterization of Arsenate-for-Sulfate Substitution in Synthetic Jarosite using X-ray Diffraction and X-ray Absorption Spectroscopy", *The Canadian Mineralogist*, Vol. 41, 2003, 905-419.
6. J.E. Dutrizac and J.L. Jambor, "Jarosites and Their Application in Hydrometallurgy", *Sulfate Minerals – Crystallography, Geochemistry and Environmental Significance*, C.N. Alpers, J.L. Jambor and D.K. Nordstrom, Eds., Mineralogical Society of America, Washington, DC, U.S.A., 2000, 405-452.
7. C. Drouet. and A. Navrotsky, "Synthesis, Characterization, and Thermochemistry of K-Na-H₃O Jarosites", *Geochimica et Cosmochimica Acta*, Vol. 67(11), 2003, 2063-2076.
8. A. Sunyer and J. Viñals, "Arsenate Substitution in Natroalunite: A Potential Medium for Arsenic Immobilization. Part 1: Synthesis and Compositions; Part 2: Cell Parameters and Stability Tests", *Hydrometallurgy*, in press, 2011.
9. J. Viñals, A. Sunyer, P. Molera, M. Cruells and N. Llorca, "Arsenic Stabilization of Calcium Arsenate Waste by Hydrothermal Precipitation of Arsenical Natroalunite", *Hydrometallurgy*, Vol. 104, 2010, 247-259.
10. J. Viñals, A. Sunyer and E. Torres, "Arsenic Inertization from Copper Hydrometallurgy Through Phases of the Alunite Supergroup", *The World of Metallurgy - ERZMETALL*, Vol. 63(6), 2010, 5-13.
11. C. Palache, H. Berman and C. Frondel, *The System of Mineralogy, Volume II*, John Wiley and Sons, New York, NY, U.S.A., 1951.
12. J.E. Dutrizac, "Factors Affecting the Precipitation of Potassium Jarosite in Sulphate and Chloride Media", *Metallurgical and Materials Transactions*, Vol. 39B, 2008, 771-783.
13. W. Rudolph, R. Mason and P. Schmidt, "Synthetic Alunites of the Potassium-Oxonium Solid Solution Series and Some Other Members of the Group: Synthesis, Thermal and X-ray Characterization", *European J. Mineralogy*, Vol. 15, 2003, 913-924.
14. E. Krause and V.A. Ettel, "Solubilities and Stabilities of Ferric Arsenate Compounds". *Hydrometallurgy*, Vol. 22, 1989, 311-337.

A.5 Arsenic inertization from copper pyrometallurgy through phases of the alunite supergroup (Copper 2010)

J. Viñals, A. Sunyer, E. Torres, V. Beltran, N. Llorca, 2010, Arsenic Inertization from Copper Pyrometallurgy through Phases of the Alunite Supergroup, In: Harre, J., (Ed), Copper 2010, GDMB, Clausthal-zellerfeld, Germany, 5, 2071-2086. ISBN 978-3-940276-29-2

Resum en català

Residus d'arsènic incloent la pols de forn flash així com els arseniats càlcics procedents de la neteja de gasos de la indústria pirometal·lúrgica del coure van ser investigats. El procés d'inertització va consistir bàsicament en tres passos: 1) lixiviació de l'arsènic, 2) tractament de l'ozó per convertir espècies a As(V), i 3) precipitació hidrotermal en medi $\text{Na}^+/\text{Al}^{3+}/\text{SO}_4^{2-}/\text{AsO}_4^{3-}$ a 200°C, usant sulfats d'alumini i sodi com a reactius. Sota condicions òptimes, els precipitats consisteixen principalment en una natroalunita arsenical complexa amb, segons les condicions, traces o petites quantitats de mansfieldita o escorodita, depenent de la composició de la solució i de la temperatura. La precipitació és molt ràpida (≤ 15 min) i el major efecte en la composició de la fase i de la solubilitat d'arsènic dels precipitats va ser la relació molar en la solució inicial Al/As. Una solubilitat d'arsènic mínima es va obtenir en els precipitats que contenien natroalunita arsenical, lliure o amb traces de mansfieldita o d'escorodita. Això es va aconseguir per relacions $\text{Al}/\text{As} \geq 3$ en el líquid del medi, la solubilitat d'arsènic va ser de 0.01 a 0.02 mg/L a $\text{pH} \sim 7$, depenent de la composició de la fase.



Arsenic Inertization from Copper Pyrometallurgy through Phases of the Alunite Supergroup

J. Viñals, A. Sunyer, E. Torres, V. Beltran, N. Llorca

University of Barcelona

Department of Materials Science and Metallurgical Engineering

Martí i Franqués 1, 08028

Barcelona, Spain

Keywords: Arsenic, copper, waste, inertization, stabilization, alunite

Abstract

Arsenical wastes including flash smelting dusts as well as calcium arsenates produced from gas cleaning steps of the copper pyrometallurgy were investigated. The inertization process consists basically of three steps: 1) Arsenic leaching, 2) Ozone treatment to convert arsenic species into As^{V} , and 3) Hydrothermal precipitation in $\text{Na}^+ \text{-Al}^{3+} \text{-SO}_4^{2-} \text{-AsO}_4^{3-}$ media at ~ 200 °C, using aluminium and sodium sulfates as reactants. Under optimal conditions, the precipitates consist mainly of a complex arsenical natroalunite with - in some conditions - trace to minor amounts of mansfieldite or scorodite, depending on the solution composition and temperature. The precipitation rate is fast (≤ 15 min) and the major effect on phase composition and arsenic solubility of the precipitates was the initial Al/As molar ratio in the liquid. Minimum arsenic solubility was obtained with precipitates containing arsenical natroalunite, free or with only traces of mansfieldite or scorodite. This was achieved for $\text{Al/As} \geq 3$ in the liquid media, the arsenic solubility being 0.01-0.02 mg/L at pH ~ 7 , depending on the phase composition.

1 Introduction

Arsenic is one of the most common toxic impurities in raw materials and final wastes of base and precious metal industries. In copper pyrometallurgy, arsenic is mainly concentrated in wastes of gas cleaning steps as well as in electrolyte and anode slime of the electrorefining process [1]. Numerous methods for arsenic inertization were investigated such as the precipitation of calcium arsenates, ferrihydrite and scorodite [2]. Scorodite generation has been extensively studied [3-5], even at industrial scale [6], due to its relatively good stability. Scorodite precipitation can be verified hydrothermally and also at ~ 95 °C with precise control of supersaturation and seeding. Nevertheless, As-solubility in scorodite (typically 0.05-1 mg/L) [7, 8] may exceed the maximum permitted for inert wastes. For this reason, the research on other As-bearing phases could be interesting.



Phases of the alunite supergroup are common in the Earth's surface [9], where most of them were produced by weathering of polymetallic sulfide deposits and further natural precipitation [10]. These natural phases exhibit great stability in supergenic conditions, decomposing only in strong acid [11] or alkaline media [12]. They consist of structures $AB_2(TO_4)(OH)_6$, in which A can be monovalent (Na, K, Ag, H_3O etc.) or divalent (Pb, Sr, Ba, Ca), B is usually trivalent (Al, Fe, rare earth) and TO_4 is principally SO_4 , AsO_4 or PO_4 . These phases have also a great possibility of stoichiometric changes, such as the simultaneous substitution of an alkaline plus SO_4 by a divalent plus AsO_4 or PO_4 , or two alkaline by a divalent plus a vacancy, etc. For this reasons, phases of the alunite supergroup may be proposed as a host for stabilizing a variety of toxic heavy metals [13, 14].

Possibilities for arsenic inertization through alunite-type phases are, of course, evident. For instance, the co-inertization of As & Pb through beudantite ($PbFe_3(SO_4)(AsO_4)(OH)_6$) precipitation [13]. Another possibility could be the incorporation of the AsO_4 group in a diluted solid solution – with low thermodynamic activity – in simple alunites. Natroalunite ($NaAl_3(SO_4)_2(OH)_6$) was selected for the present laboratory-scale study.

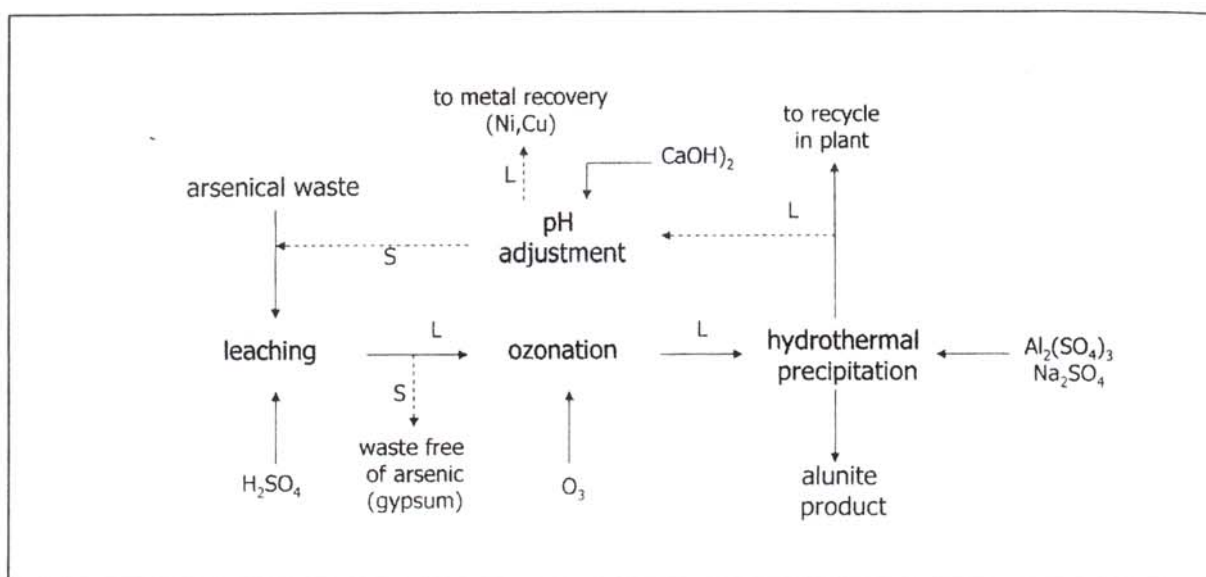


Figure 1: Schematic diagram of the inertization process.

Figure 1 shows a schema of the process. Waste is treated with H_2SO_4 in suitable conditions for As leaching. The resulting solution (or slurry) is ozonized to transform all arsenic species into As^V . Ozonation was preferred because it did not introduce new pollutants in the circuit. Hydrothermal precipitation is verified at ~ 200 °C using aluminium and sodium sulfates as reagents. After the treatment, the liquid can be recycled in a plant to recover the possible valuable elements (Cu, Ni, etc.) and finally, to the cleaning steps of the final effluent. Since hydrothermal precipitation in a single step does not eliminate all As from the liquid, an optional step of pH adjustment (to ~ 3.5) can be verified to recycle the remnant As & Al to the hydrothermal step.

Two kinds of wastes were tested in this study: A) "Calcium arsenate" obtained by lime precipitation of a final plant effluent from the electrolytic section of a pyrometallurgical plant and B) Flash



smelting dust. Since flash smelting dust contains large amounts of copper, a previous copper-leaching process followed by solution purification was studied. Hydrothermal precipitation was conducted from the waste of the solution purification, an intermediate amorphous ferric arsenate.

2 Experimental methods

Original wastes, intermediate products and all hydrothermal precipitates were studied by chemical analysis (ICP), X-ray diffraction (XRD) and scanning electron microscopy (SEM). Quantitative microanalysis of different phases was obtained by energy dispersive spectroscopy (EDS) at 20 kV, 0.6 nA, 30 s, through a JEOL JSM-840 instrument provided with an INCA-250 analyzer.

Leaching experiments on original wastes or intermediate products were conducted in a conventional thermostatic reactor coupled with magnetic stirring. The addition of leaching agent (H_2SO_4), ORP and pH were monitored. The degree of solubilization for selected elements was measured by sampling at different times and solution analysis (ICP). Particular conditions are described jointly with the experimental results. After leaching, the resulting solution or slurry was ozonized in the same reactor injecting an O_2/O_3 mixture through a fritted glass diffuser. Ozone was produced in a TRIOGEN generator at 0.75 L/min with an ozone mass flow of 3.36×10^{-2} g/min.

Hydrothermal experiments were performed in a PARR 4563 autoclave reactor, provided with temperature, pressure and stirring controllers. After the leaching and ozonation steps, the solution (or slurry) was placed into the reactor with the reagents (Al & Na sulfates). The system was heated to working temperature at a rate of 5 °C/min. Then the system was also cooled to room temperature at a rate of 5 °C/min. The hydrothermal product was filtered, washed and characterized as described. The conditions of each group of tests are reported with the corresponding results.

The solubility of hydrothermal products at different pH's was studied by stirring 0.50 g of solid into 50 mL solution at 25 °C during 24 h. These solutions were prepared by convenient dilution of H_2SO_4 or NaOH stock solutions. Eventual pH changes during these leaching tests were corrected by addition of small volumes of dilute H_2SO_4 or NaOH. Three consecutive leaching tests were performed for each pH. After each leaching the slurry was filtered and the solution was analyzed for As by ICP-MS.



3 Characterization of wastes

3.1 Calcium arsenate waste

The chemical composition is given in Table 1. XRD and SEM/EDS studies indicated that it mainly consists of gypsum, calcite and an amorphous precipitate containing As/Ca/Fe/Ni/Cu/Zn. Gypsum appeared as free, large (100-200 μm) crystals. The amorphous precipitate consisted of agglomerates of $\sim 1 \mu\text{m}$ spheroidal particles of variable composition with 15 % As mean content.

Although the waste was originally precipitated at pH 12, the pH of the As-received waste was about 9 and the As-solubility about 30 mg/L. This indicated that the usual process for arsenic removal from lime precipitation gives unstable calcium arsenates which decompose by atmospheric CO_2 generating soluble arsenic:



Table 1: Chemical composition of the studied wastes

	Calcium arsenate	Flash smelting dust	Intermediate ferric arsenate
As (%)	5.23	1.93	13.8
Ca (%)	22.80	0.24	0.07
Fe (%)	1.08	12.60	26.6
S (%)	11.37	6.50	2.30
Cu (%)	0.56	30.5	6.80
Zn (%)	0.95	3.66	0.04
Ni (%)	2.65	-	-
Mo (%)	-	0.18	1.80
Pb (%)	0.04	0.43	0.12
Bi (%)	0.02	0.13	-
SiO ₂ (%)	0.86	2.78	-

3.2 Flash smelting dust

The composition of flash smelting dust (Table 1) showed a high copper and relatively low arsenic content. XRD studies indicated that it mainly consists of soluble copper sulfates (CuSO_4 , $\text{CuSO}_4 \cdot \text{H}_2\text{O}$ and $\text{CuSO}_4 \cdot 5\text{H}_2\text{O}$), with cuprite (Cu_2O), tenorite (CuO), delafossite (CuFeO_2) and ferrite ($\text{M}^{2+}\text{M}^{3+}_2\text{O}_4$). Chemical phase analysis by selective leaching – confirmed by XRD – showed that 53 % of the total copper was present as soluble sulfates (25 °C, pH 4 leaching), 22 % as cuprite (25 °C, $\text{H}_2\text{SO}_4/\text{O}_2$ pH 1 leaching), 20 % as tenorite + delafossite (80 °C, H_2SO_4 0.5M/ O_2 leaching)

◆ *Arsenic Inertization from Copper Pyrometallurgy through Phases of the Alunite Soupergroup*

and the remaining 5 % as ferrite. SEM/EDS investigations (Figure 2) indicated that the main oxide phase was a zinc-rich ferrite, $Zn_xCu_yFe_{1-(x+y)}(Fe_7Al_{1-z})_2O_4$ (with ~7 % Cu), which appears as isometric 2-60 μm grains. Cuprite and tenorite were found as 1-20 μm rounded grains and delafossite as 10-50 μm lamellar crystals. As bearing phases were not clearly detected in SEM because they probably were of submicrometric size. However, a non identified arsenic product intergrowth with lead sulphate aggregates was occasionally found (Figure 2D). Solubility tests showed a pH of 4.5 and 5.5 mg/L As, with very high Cu solubilization (>10 g/L).

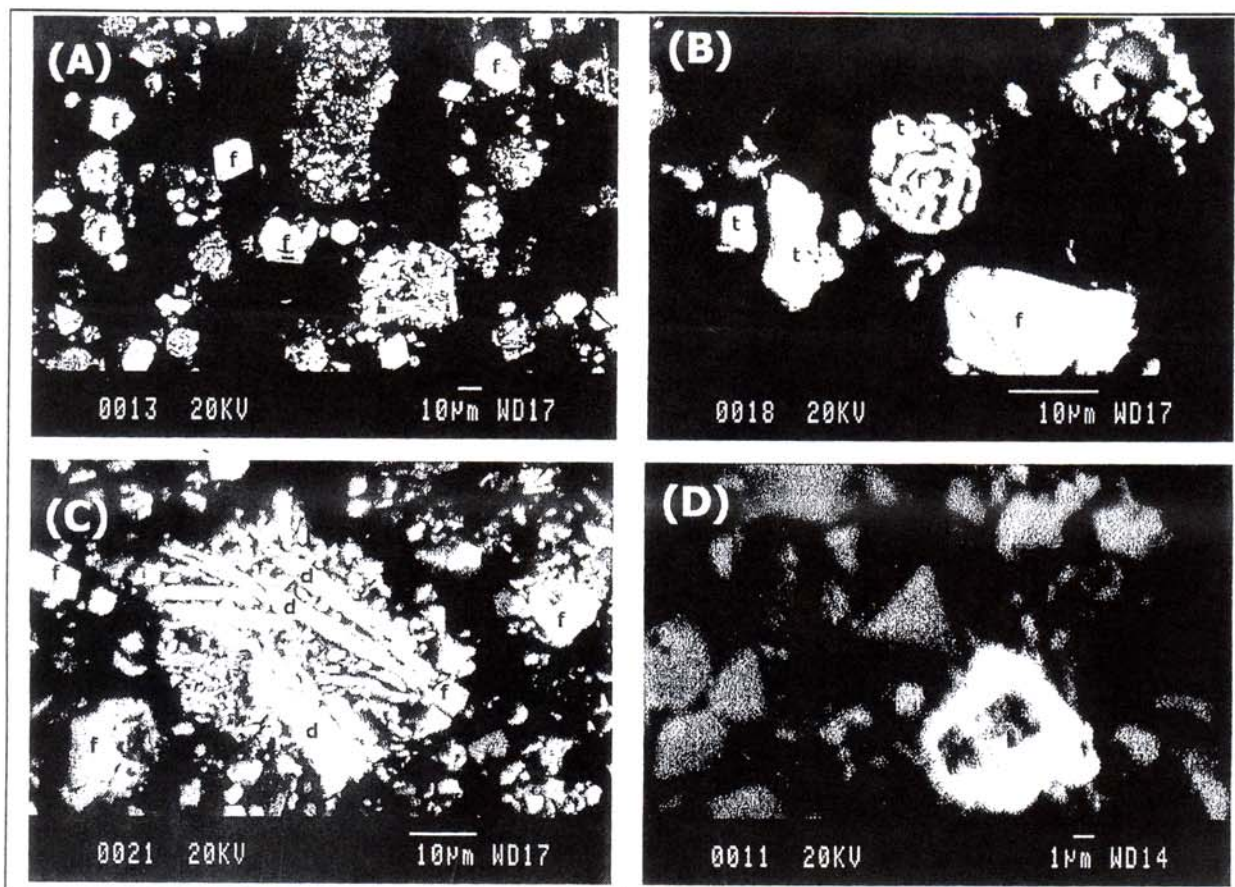


Figure 2: Flash smelting dust after removing soluble sulfates (SEM, cross sections): (A) General view showing abundant ferrite (f), (B) Tenorite particles (t), (C) Delafossite laths (d), (D) Aggregate of lead sulfate (white) containing arsenic.

4 Leaching

4.1 Calcium arsenate waste

The leaching behavior of calcium arsenate waste with H_2SO_4 was investigated by treating 2.00 g of solid in 200 ml solution at 25 °C, 600 rpm. Leaching was made through measured additions of H_2SO_4 1 M for reaching a selected pH. The extraction of different elements is shown in Figure 3.

According to the amorphous nature of the phases containing heavy metals, the reactivity of the waste was very high. After about 5 min of acid addition, the pH of the slurry was practically stabilized. Complete leaching of As, Fe, Ni, Cu and Zn was achieved at pH 1 in 5 min, with an acid consumption of 380 g H_2SO_4 /kg waste. The comparison of the extraction curves of As and Fe showed that about 75 % As were already leached at pH 4 without significant Fe solubilization, whereas the remaining 25 % As were only leached at pH 1 when all Fe was solubilized. Thus, it seems possible that these 25 % As were associated to amorphous ferric arsenates. The residue of the leaching treatment was nearly pure gypsum (> 99 %, Figure 5A). Gypsum could be eliminated or not prior alunite precipitation, depending on the potential commercial value. In the present study, these two options were tested in the section of hydrothermal treatment.

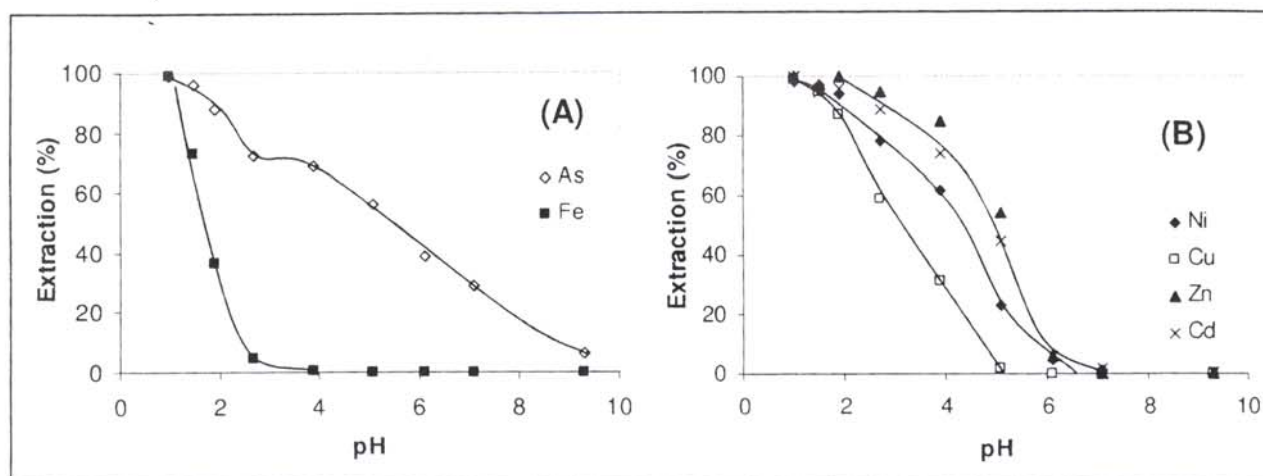


Figure 3: H_2SO_4 leaching of calcium arsenate waste as a function of pH (25 °C, 5 min): (A) As and Fe extraction, (B) Ni, Cu, Zn and Cd extraction.

Ozonation experiments on the slurry obtained after leaching at pH 1, showed a very effective oxidation method for converting As^{III} into As^V . The process can be easily followed through the ORP solution changes from ~400 mV to ~1200 mV (vs Ag/AgCl). Ozone consumption was 13 g O_3 /kg waste. According to the stoichiometry for $As(III)$ oxidation (Equation 2), the studied waste contained about 50 % of total arsenic as As^{III} .



4.2 Flash smelting dust

Main objectives for H₂SO₄ leaching of flash smelting dust were maximum arsenic extraction but also maximum copper recovery. The leaching behavior was however complex and only a brief summary is given here. At pH 1 and 25 °C, As & Cu extractions were only 65-70 %. Under these conditions, the copper phases which dissolved were sulfates and cuprite. An increase in copper extraction from tenorite and delafossite required an increase of acid concentration and temperature. Delafossite leaching was considered important not only for copper recovery but also for providing a sufficient amount of Fe³⁺ in the solution in order to co-precipitate As in a purification step.

Figure 4 shows the temperature effect on the leaching of 15 g dust in 150 ml 0.5 M H₂SO₄ in presence of O₂. According to the XRD data of leaching residues, only at T ≥ 80 °C all the copper phases, except ferrite, were leached. Under these conditions, copper recovery reached 95 % and the As extraction was nearly complete. Zn extraction (~40 %) was few sensitive to the temperature in the interval studied because ferrite remained practically unreacted. The H₂SO₄ consumption was 360 g H₂SO₄/kg flash smelting dust.

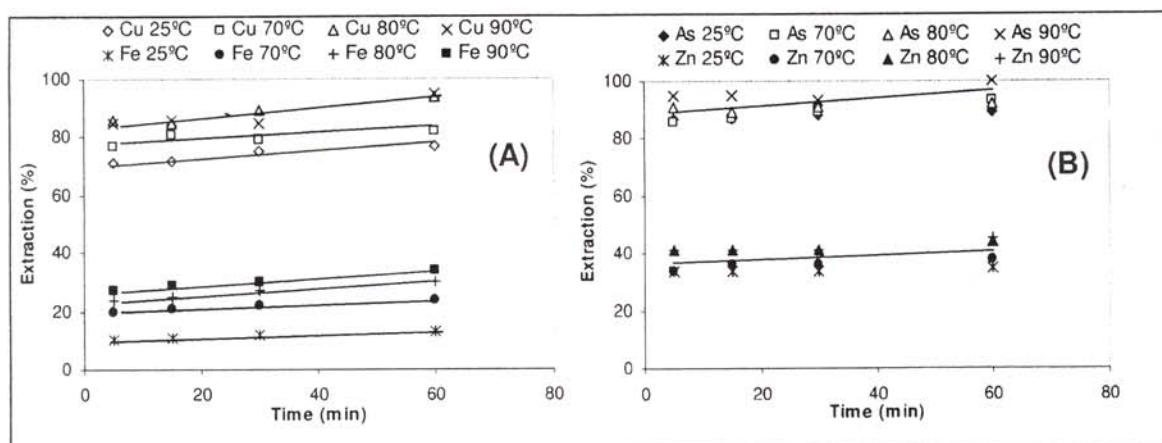


Figure 4: H₂SO₄ (0.5 M) leaching of flash smelting dust:
(A) Cu and Fe extraction, (B) As and Zn extraction.

The residue of the leaching treatment at 80 °C represents 220 g/kg dust. Solubility tests showed that it was inert with respect to As (< 0.05 mg/l) but not with respect to Pb (~1 mg/l). Probably this ferrite residue could be recycled in the flash smelting operation.

After leaching, the resulting solution was ozonized to ensure the complete oxidation of Fe and As. The ozone consumption was 60 g O₃/kg flash smelting dust. Depending on the solid/liquid ratio during the leaching, the composition of the solution varies from 20 to 50 g/l Cu, 1.1 to 2.8 g/l As, 2.1 to 5.3 g/l Fe, 1.1 to 2.8 g/l Zn, 0.1 to 0.3 g/l Mo and 0.01 to 0.02 g/l Sb. Solutions were treated with NaOH at pH 3.5-4 for removing Fe and As. The consumption was about 90 g NaOH/kg dust and the precipitate obtained was 130 g/kg dust. The purified solutions contained 0.012 g/l As, 0.003 g/l Mo, 0.001 g/l Sb and less than 0.001 g/l Fe. They were considered suitable for recycling to the electrolytic section of the pyrometallurgical plant.



The composition of the ferric arsenate obtained from the solution purification is given in Table 2. SEM examination showed that it consists of aggregates of submicron spheroids (Figure 5B), which highly suggests its amorphous nature. XRD confirmed this, because no ferrihydrite phases were detected. Probably, the presence of significant amounts of other metals precipitated jointly with Fe (Table 1) make the ferrihydrite ordering difficult. This intermediate ferric arsenate was used as raw material for the inertization of arsenic contained in the flash smelting dust.

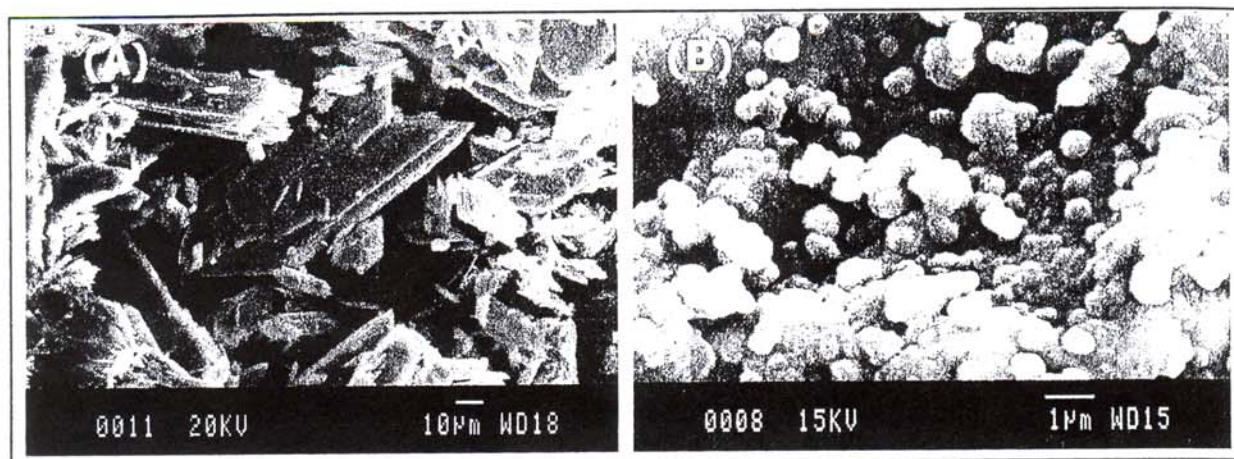


Figure 5: (A) Gypsum residue from calcium arsenate leaching, (B) Intermediate ferric arsenate from flash smelting dust.

5 Hydrothermal precipitation of As

5.1 Calcium arsenate waste

The effects of initial pH, Al/As molar ratio, As concentration at fixed Al/As ratio, reaction time, temperature and prior gypsum separation were investigated. Other possible effects, such as SO_4^{2-} and Na^+ concentration were not studied here, because the SO_4^{2-} concentration was basically fixed by the large SO_4^{2-} concentration of the leaching solution and, in all the experiments Na^+ was used in excess vs. Al^{3+} due to the stoichiometric requirements of the natroalunite precipitation, ideally:



Table 2: Experimental conditions used in the Al/As molar ratio effect

Test	Al ₂ (SO ₄) ₃ [g]	Na ₂ SO ₄ [g]	Initial molar ratios				Final pH
			Al/As	S/As	As/Ca	Na/Al	
T1	5.38	0.994	4.50	18	0.123	0.44	0.66
T2	3.58	0.994	3.00	12	0.123	0.66	0.65
T3	3.58	0.994	3.00	11	0.488	0.66	0.62
T4	2.69	0.994	2.25	16	0.123	0.89	0.68
T5	1.79	0.994	1.50	15	0.123	1.33	0.84

The effect of initial pH showed that production of fully crystalline precipitates required an initial pH ≤ 1 for this waste. These conditions ensure that Ni, Cu and Zn remain in the liquid phase which could facilitate further recovery.

5.1.1 Effect of Al/As molar ratio in the liquid phase

This was the most important effect on the phase composition. It was studied treating 10 g of leached and ozonized waste in 150 ml solution (pH 1) at 200 °C for 120 min. Reagents and initial molar ratios in the solution for this set of experiments are given in Table 2. Results can be summarized as follows:

- For an Al/As molar ratio of 4.5, arsenic precipitated practically only as arsenian natroalunite (~ (Na,Ca)(Al,Fe)₃((S,As,P)O₄)₂(OH)₆) (Figures 6 and 7). Decreasing the Al/As ratio, decreased the natroalunite precipitation and increased the formation of mansfieldite ((Al,Fe)(As,P)O₄·2H₂O). When Al/As was 1.5, As precipitated practically only as mansfieldite.
- Calcium present in the initial medium as gypsum transforms into anhydrite (Figures 6 and 7). The substitution of Ca in natroalunite was low at the studied conditions, 0.04-0.08 in formula (Table 3). The effect of prior gypsum separation was insignificant on the phase composition, except for the absence of anhydrite (Figures 7 and 8).
- The maximum As substitution in natroalunite was 0.14 in formula (Table 3). Natroalunite also incorporated Fe from the original waste because it substitutes Al in the alunite lattice. Fe coefficients in formula reached 0.12 when traces of mansfieldite were present, but decreased to 0.08 when a large amount of mansfieldite was precipitated. Traces of P, substituting in TO₄ group, were also incorporated into alunite (up to 0.02 in formula).

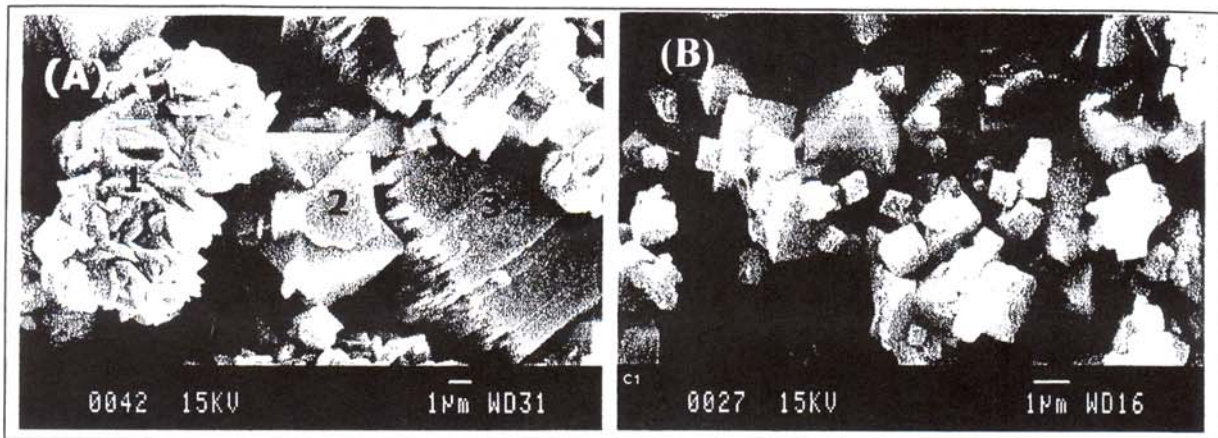


Figure 6: Typical phase morphology of the hydrothermal precipitates: (A) from calcium arsenate waste (1: As-natroalunite, 2: mansfieldite, 3: anhydrite), (B) from flash smelting dust (As-natroalunite).

- Mansfieldite also incorporates Fe. When mansfieldite was practically the only arsenic phase the substitution was extensive, 0.31 in formula (Table 3). This value decreases to 0.20 when the natroalunite precipitation increases. Phosphorous was also incorporated in mansfieldite, up to 0.05 in formula.
- If hydrothermal precipitation was performed in a single step, the arsenic precipitation yield was moderate (Figure 8A) and the liquid after precipitation had to be recirculated (Figure 1). The yield was maximal (~50 %) when mansfieldite was formed in large extension and minimal (~20 %) when natroalunite was the only phase. However, a yield of ~40 % can be achieved with formation of only small amounts of mansfieldite (~5 %).
- Al precipitation yields also depended on the Al/As ratio (Figure 8A). It was maximal (~60 %) when natroalunite precipitation was high and minimal (~20 %) when mansfieldite formation was extensive. Fe precipitation yield (80-90 %) was few sensitive to the phase composition, whereas Ni, Zn and Cu do not precipitate in significant amount.

Table 3: Effect of the Al/As ratio, 200 °C. Experimental formulas from EDS punctual analysis

From calcium arsenate waste		
Al/As	Natroalunite (normalized to S+As+P=2, OH from charge balance)	Mansfieldite (normalized to As+P =1)
4.50	$(\text{Na}_{0.98}\text{Ca}_{0.08})(\text{Al}_{2.70}\text{Fe}_{0.12})((\text{S}_{0.92}\text{As}_{0.07}\text{P}_{0.01})\text{O}_4)_2(\text{OH})_{5.44}$	-
3.00	$(\text{Na}_{0.96}\text{Ca}_{0.08})(\text{Al}_{2.69}\text{Fe}_{0.12})((\text{S}_{0.88}\text{As}_{0.11}\text{P}_{0.01})\text{O}_4)_2(\text{OH})_{5.33}$	$(\text{Al}_{0.78}\text{Fe}_{0.21})(\text{As}_{0.97}\text{P}_{0.03})\text{O}_4 \cdot 2\text{H}_2\text{O}$
3.00*	$(\text{Na}_{1.05})(\text{Al}_{2.82}\text{Fe}_{0.15})((\text{S}_{0.90}\text{As}_{0.10})\text{O}_4)_2(\text{OH})_{5.76}$	$(\text{Al}_{0.76}\text{Fe}_{0.24})(\text{As}_{0.96}\text{P}_{0.04})\text{O}_4 \cdot 2\text{H}_2\text{O}$
2.25	$(\text{Na}_{0.90}\text{Ca}_{0.04})(\text{Al}_{2.70}\text{Fe}_{0.08})((\text{S}_{0.84}\text{As}_{0.14}\text{P}_{0.02})\text{O}_4)_2(\text{OH})_{5.00}$	$(\text{Al}_{0.76}\text{Fe}_{0.24})(\text{As}_{0.99}\text{P}_{0.01})\text{O}_4 \cdot 2\text{H}_2\text{O}$
1.50	-	$(\text{Al}_{0.69}\text{Fe}_{0.31})(\text{As}_{0.95}\text{P}_{0.05})\text{O}_4 \cdot 2\text{H}_2\text{O}$
* In absence of gypsum		
From intermediate ferric arsenate obtained from flash smelting dust		
4.5	$(\text{Na}_{1.05})(\text{Al}_{1.76}\text{Fe}_{0.95})((\text{S}_{0.93}\text{As}_{0.07})\text{O}_4)_2(\text{OH})_{5.01}$	-
6.0	$(\text{Na}_{1.05})(\text{Al}_{1.97}\text{Fe}_{0.80})((\text{S}_{0.96}\text{As}_{0.04})\text{O}_4)_2(\text{OH})_{5.34}$	-
7.5	$(\text{Na}_{1.0})(\text{Al}_{2.03}\text{Fe}_{0.67})((\text{S}_{0.97}\text{As}_{0.03})\text{O}_4)_2(\text{OH})_{5.00}$	-
9.0	$(\text{Na}_{1.05})(\text{Al}_{2.23}\text{Fe}_{0.63})((\text{S}_{0.97}\text{As}_{0.03})\text{O}_4)_2(\text{OH})_{5.57}$	-

5.1.2 Other effects

The As concentration effect at fixed Al/As= 3.00 ratio was investigated in the range of 3.5 to 7 g/l at 200 °C. No significant effect on phase composition and precipitation yield was observed.

Previous research using synthetic reagents showed that incorporation of As in natroalunite was effective at $T \geq 180$ °C, because at lower temperatures intermediate amorphous arsenates were formed. Even at 180 °C, the formation of mansfieldite was preferential. This effect was confirmed for the calcium arsenate waste studied here. For Al/As = 3, 120 min, whereas at 200 °C the natroalunite/mansfieldite phase ratio was ~5, at 180 °C the same ratio decreased to ~2.5 (Figure 8B).

The effect of reaction time was studied at 200 °C, Al/As = 3, for 15, 30 and 120 min. No significant changes in precipitation yield and phase composition were observed (Figure 8). Consequently, at 200 °C hydrothermal precipitation can be verified at high rates (≤ 15 min). Bulk chemical compositions of representative hydrothermal precipitates are given in Table 4.

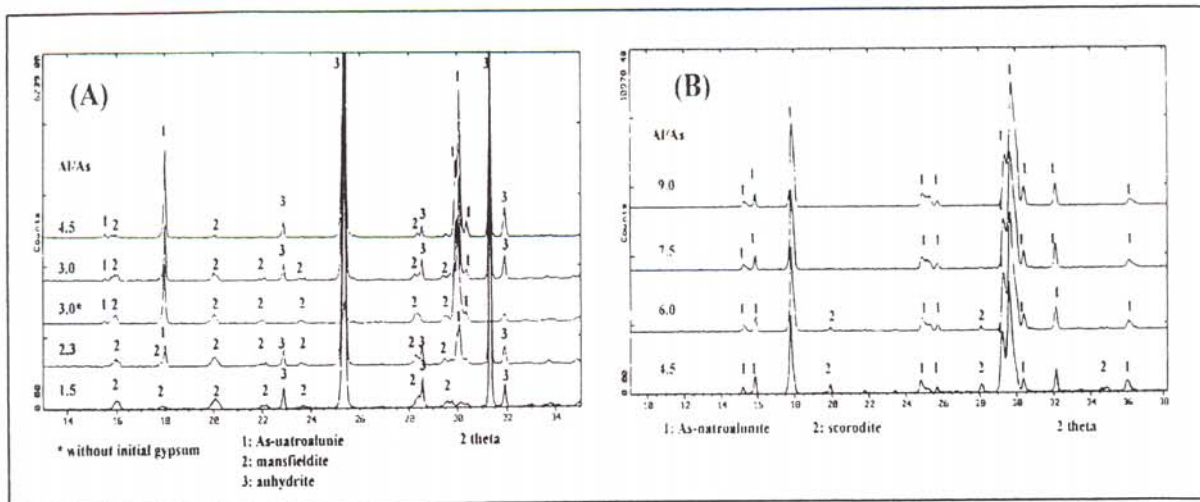


Figure 7: Effect of the Al/As molar ratio on phase composition: (A) from calcium arsenate waste, (B) from intermediate ferric arsenate of the treatment of flash smelting dust.

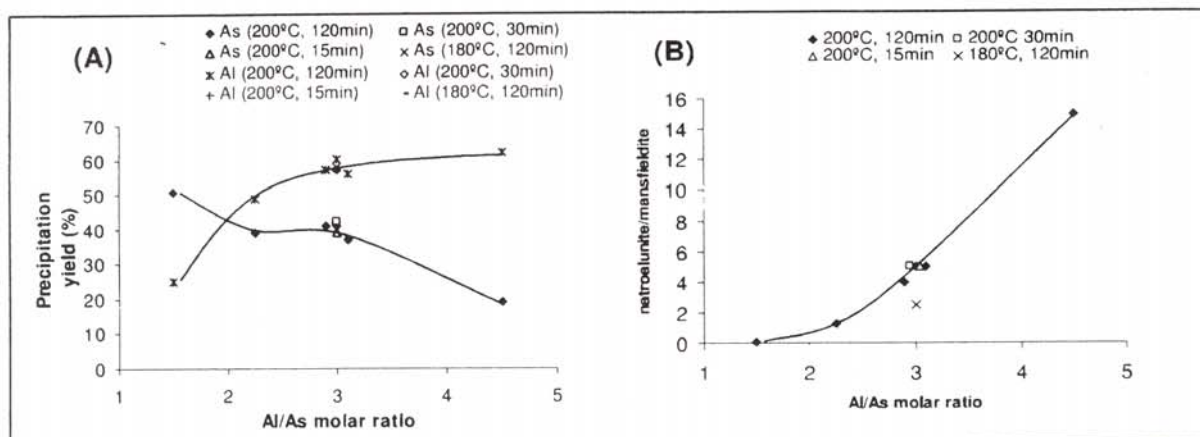


Figure 8: Effect of the Al/As molar ratio in the treatment of calcium arsenate waste. (A) As & Al precipitation yield, (B) Arsenic distribution.

◆ Arsenic Inertization from Copper Pyrometallurgy through Phases of the Alunite Soupergroup

Table 4: Representative bulk chemical composition of the hydrothermal precipitates (200 °C)

From calcium arsenate waste										
Al/As ratio	Time (min)	wt. %								
		Ca	S	As	Al	Na	Fe	Ni	Cu	Zn
4.50	120	18.4	19.4	1.10	5.98	1.60	0.94	0.01	0.05	0.01
3.00	15	22.1	21.0	2.41	4.04	1.10	1.10	0.01	0.02	0.02
3.00	30	21.6	20.4	2.58	4.01	1.05	1.15	0.01	0.04	0.02
3.00*	120	0.13	11.5	9.85	16.18	4.49	4.22	0.01	0.04	0.02
2.25	120	21.6	19.2	3.41	2.64	0.65	1.23	0.01	0.02	0.03
1.50	120	24.5	20.0	3.34	0.88	0.07	1.12	0.01	0.06	0.03

* Precipitated in absence of gypsum

From intermediate ferric arsenate obtained from flash smelting dust										
Al/As ratio	Time (min)	wt. %								
		S	Al	Na	As	Fe	Mo	Pb	Cu	Zn
9.0	15	14.4	13.2	4.48	0.71	9.39	0.38	-	0.06	0.02
7.5	15	15.6	13.6	4.78	0.94	12.0	0.59	0.06	0.05	0.01
6.0	15	14.5	12.0	4.41	1.61	12.8	0.57	0.05	0.08	0.01
4.5	15	12.6	9.60	4.41	2.72	14.4	0.53	0.07	0.10	0.01

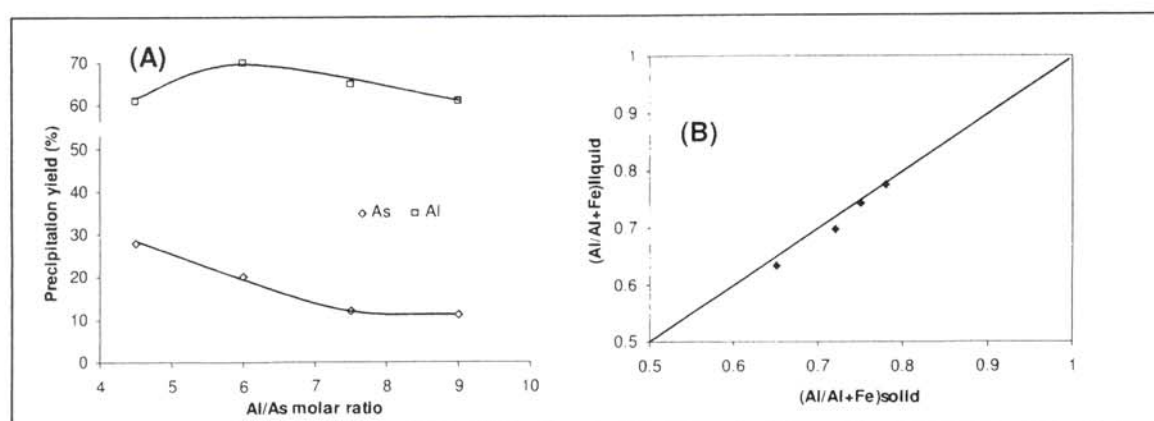


Figure 9: Effect of the Al/As molar ratio in the treatment of intermediate ferric arsenate from flash smelting dust: (A) As & Al precipitation yield, (B) Al & Fe distribution.



6 Intermediate ferric arsenate from flash smelting dust

Hydrothermal precipitation was studied by treating 3.8 g of intermediate ferric arsenate in 150 ml solution at pH 1 and 200 °C for 15min. Variable amounts of $\text{Al}_2(\text{SO}_4)_3$ were added, to give Al/As ratios in the liquid phase in the of range 4.5 to 9. Using these high Al/As ratios ensured no mansfieldite formation. Na_2SO_4 was also added to give Na/Al ratios in the interval of 0.5-0.6. Results can be summarized as follows:

- In the range investigated, arsenic precipitated practically as arsenian, highly ferroan natroalunite (Figures 6 and 7, Table 3). Trace (~0.5 %) to minor amounts of scorodite (~2 %) were only detected for 6.0 and 4.5 Al/As ratios, respectively.
- Maximum As substitution in natroalunite was 0.07 in formula (Table 3) for Al/As = 4.5. This was the same value as obtained from calcium arsenate waste, treated at the same Al/As conditions. Consistent with these data, As & Al precipitation yields (Figure 9A) were also similar at the same Al/As ratio.
- The main difference was the very high iron content in natroalunite as obvious consequence of the high iron content in the raw material (Table 4). Iron substitution in natroalunite increases proportionally to the decrease in the Al/Al+Fe ratio in the liquid phase (Figure 9B).
- As in calcium arsenate waste, Cu does not precipitate in significant amounts. However, Mo precipitates partially (Table 4), probably as minor substitution of MoO_4^{2-} in TO_4 group. However this was not confirmed by EDS punctual analyses because the Mo content was low.

6.1 Solubility of the precipitates

Results of solubility experiments for hydrothermal precipitates obtained from calcium arsenate waste are reported in Figure 10. Usually, at each pH, data of the first leaching were slightly higher than in the second leaching and these were slightly higher than in the third leaching. Nevertheless, differences were small, which suggests that the precipitates were easily washed. Moreover, solubilities in very acid medium (pH 1) were relatively small (0.5-2 mg/l), which also suggest the absence of amorphous As-phases.

Minimal solubility in all pH intervals corresponded to precipitates obtained at high Al/As ratio in the liquid (4.5) when the As phase was natroalunite. In contrast, maximal solubility could be observed at low Al/As ratio when mansfieldite was the only As-phase. In the neutral region, the As solubility of natroalunite was about 0.01 mg/l, whereas for mansfieldite it was ~0.1 mg/l. However, the most favorable conditions for this calcium arsenate waste probably were at Al/As = 3, when a mixture of natroalunite and minor mansfieldite was formed. The solubility in the neutral region is acceptable (~0.02 mg/l) and the arsenic precipitation yield in a single step (~40 %) was double compared to precipitates containing only natroalunite. An additional advantage can be the minor consumption of aluminium salt.

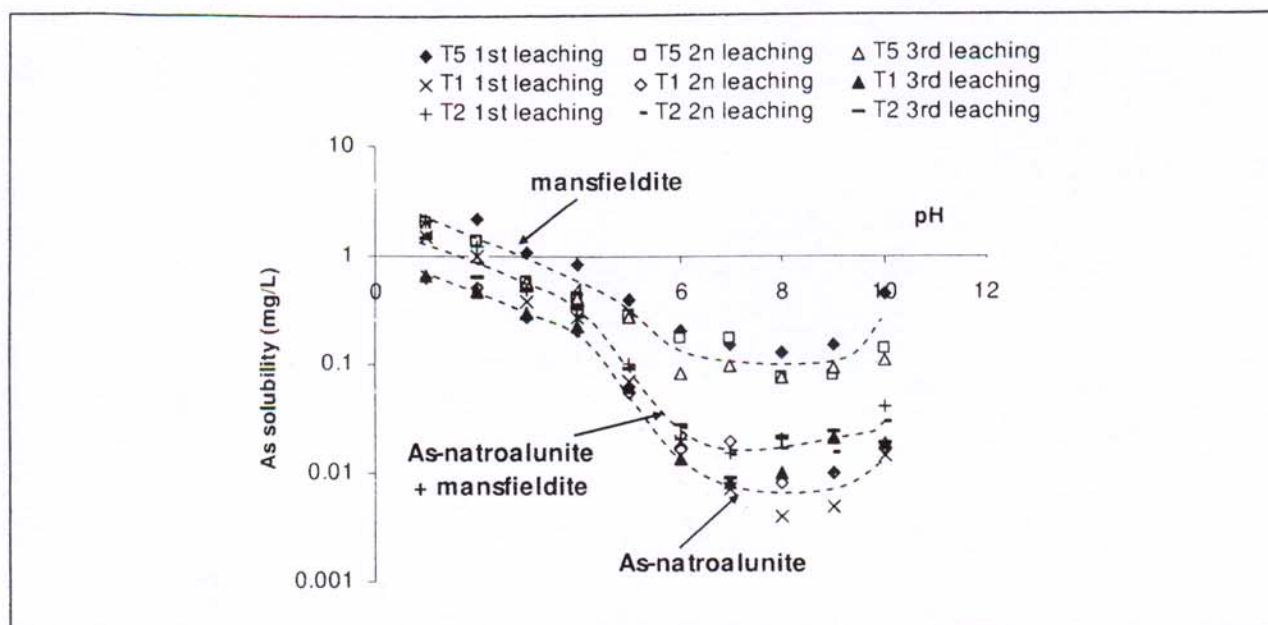


Figure 10: As solubility from hydrothermal precipitates obtained from calcium arsenate waste.

Solubility of natroalunites produced through intermediate ferric arsenate from flash smelting dust was only studied at pH 4.2-4.6, which was the natural pH, after 24 h. The results showed As solubilities in the range 0.005-0.01 mg/l for precipitates obtained at Al/As \geq 6. However, samples obtained at Al/As = 4.5 showed a higher solubility of 0.07 mg/l, probably as consequence of the scorodite content of ~2 % (Figure 7).

7 Conclusions

Hydrothermal precipitation of As(V) in acid $\text{Na}^+\text{-Al}^{3+}\text{-SO}_4^{2-}$ media at ~200 °C, using aluminium and sodium sulfates as reactants, may be an alternative for arsenic inertization from wastes of copper pyrometallurgy. Under optimal conditions, the precipitates consist mainly of a complex arsenical natroalunite. The precipitation rate is fast (\leq 15 min) and the major effect on phase composition and arsenic solubility of the precipitates was the Al/As molar ratio in the initial liquid. Minimum arsenic solubility was obtained with precipitates containing arsenical natroalunite free or with only traces of mansfieldite or scorodite. This was achieved for Al/As \geq 3 in the liquid media, the arsenic solubilities being 0.01-0.02 mg/l at pH ~7, depending on the phase composition.

Acknowledgements

The authors wish to thank the Spanish *Ministerio de Educación y Ciencia (DGI)* for the financial support of this research (*Programa de Materiales, MAT 2007-61466*). Thanks also to the *Serveis Científicotècnics de la Universitat de Barcelona* for their assistance in characterization studies.



References

- [1] PIRET, N.L. (1999): The removal and safe disposal of arsenic in copper processing, *JOM*, 51, pp. 16-17.
- [2] RIVEROS, P.A., DUTRIZAC, J.D. & SPENCER, P. (2001): Arsenic disposal practices in the metallurgical industry, *Canadian Metallurgical Quarterly*, 40, pp. 395-420.
- [3] DEMOPOULOS, G.P., LAGNO, F., WANG, Q. & SINGHANIA, S. (2003): The atmospheric scorodite process. *Copper 2003*, VI(2), Santiago, Chile, TMS, pp. 597-616.
- [4] MONHEMIUS, A. J. & SWASH, P.M. (1999): Removal and stabilizing As from copper refining circuits by hydrothermal processing, *JOM*, 51, pp. 30-33. .
- [5] SHINODA, K., TANNO, T., FUJITA, T. & SUZUKI, S. (2009): Coprecipitation of large scorodite particles from aqueous Fe(II) and As(V) solution by oxygen injection, *Materials Transactions*, 50, pp. 1196-1201.
- [6] ICHIMURA, R., TATEIWA, H., ALMENDARES, C. & SANCHEZ, G. (2007): Arsenic immobilization and metal recovery from El Teniente smelter dust. *Copper 2007*, IV(2), Toronto, Canada, CIM, pp. 597-616.
- [7] KRAUSE, E. & ETTTEL, V.A. (1989): Solubilities and stabilities of ferric arsenate compounds, *Hydrometallurgy*, 22, pp. 311-337.
- [8] BLUTEAU, M.C. & DEMOPOULOS, G.P. (2007): The incongruent dissolution of scorodite. Solubility, kinetics and mechanism, *Hydrometallurgy*, 87, pp. 163-177.
- [9] JAMBOR, J.L. (1999): Nomenclature of the alunite supergroup, *Canadian Mineralogist*, 37, pp. 1323-1341.
- [10] VIÑALS, J., ROCA, A., CRUELLS, M. & NÚÑEZ, C. (1995): Characterization and cyanidation of Rio Tinto gossan ores, *Canadian Metallurgical Quarterly*, 34, pp. 115-122.
- [11] VIÑALS, J. & NÚÑEZ, C. (1988): Kinetics of dissolution of argentian plumbojarosite from old tailings of sulfatizing roasting pyrites by HCl-CaCl₂ leaching, *Metallurgical Transactions B*, 19, pp. 365-373.
- [12] ROCA, A., VIÑALS, J., CALERO, J. & ARRANZ, M. (1999): Characterization and cyanidation of jarosite-beudantite phases from Rio Tinto gossan ores, *Canadian Metallurgical Quarterly*, 38, pp. 93-103.
- [13] ALCOVÉ, X., BASSAS, J., TARRUELLA, I., ROCA, A. & VIÑALS, J. (2001): Structural characterization of beudantite-type phases by Rietveld refinements, *Materials Science Forum*, 378, pp. 671-676.
- [14] KOLITSCH, U. & PRING, A. (2001): Crystal chemistry of the crandallite, beudantite and alunite groups: a review and evaluation of the suitability storage materials for toxic products, *Journal of Mineralogical and Petrological Sciences*, 96, pp. 67-78.

A.6 Arsenic inertization from copper pyrometallurgy through phases of the alunite supergroup (*Erzmetall*)

This article was published through invitaiton in *Erzmetall*.

J. Viñals, A. Sunyer, E. Torres, 2010, Arsenic Inertization from Copper Pyrometallurgy through Phases of the Alunite Supergroup, *Erzmetall*, 63, 6, 5-13.

Resum en català

Residus d'arsènic incloent la pols de forn flash així com els arseniats càlcics procedents de la neteja de gasos de la indústria pirometal·lúrgica del coure van ser investigats. El procés d'inertització va consistir bàsicament en tres passos: 1) lixiviació de l'arsènic, 2) tractament de l'ozó per convertir espècies a As(V), i 3) precipitació hidrotermal en medi $\text{Na}^+/\text{Al}^{3+}/\text{SO}_4^{2-}/\text{AsO}_4^{3-}$ a 200°C, usant sulfats d'alumini i sodi com a reactius. Sota condicions òptimes, els precipitats consisteixen principalment en una natroalunita arsenical complexa amb, segons les condicions, traces o petites quantitats de mansfieldita o escorodita, depenent de la composició de la solució i de la temperatura. La precipitació és molt ràpida (≤ 15 min) i el major efecte en la composició de la fase i de la solubilitat d'arsènic dels precipitats va ser la relació molar en la solució inicial Al/As. Una solubilitat d'arsènic mínima es va obtenir en els precipitats que contenien natroalunita arsenical, lliure o amb traces de mansfieldita o d'escorodita. Això es va aconseguir per relacions $\text{Al}/\text{As} \geq 3$ en el líquid del medi, la solubilitat d'arsènic va ser de 0.01 a 0.02 mg/L a $\text{pH} \sim 7$, depenent de la composició de la fase.

Your article at the Copper Conference 2010 - reprint at the journal World of Metallurgy - ERZMETALL

Redaktion GDMB, Jens Harre <Redaktion@gdmb.de>
Per a: asunyer@ub.edu

9 de setembre de 2010 9.55

Dear Alba Sunyer,

the Copper 2010 Conference is kept in mind as an outstanding successfully event this summer. Last but not least, the numerous brilliant papers were the key to success of this event and to the regard of the conference all over the world.

As a part of these papers of enormous interest our editorial office intends to publish your manuscript "Arsenic Inertization from Copper Pyrometallurgy Through Phases of the Alunite Supergroup" at our international journal World of Metallurgy - ERZMETALL (see <http://www.gdmb.de/world-of-metallurgy-en.php?>).

If you are interested in publishing your paper to our international readership we will appreciate your reply to our society by e-mail to Redaktion@gdmb.de . After your approach we will support you with the necessary details for the publication within our magazin. If you have any questions with regard to our query please do not hesitate to contact our editorials office.

With best regards,

Dipl.-Ing. Jens Harre

Editorial Staff
World of Metallurgy - ERZMETALL
World of Mining - Surface and Underground

GDMB-Informationsgesellschaft mbH
Paul-Ernst-Strasse 10
38678 Clausthal-Zellerfeld
Registergericht: Amtsgericht Braunschweig, HRB 110737
UST.-Nr. DE 155 158 950
Geschäftsführer: Dipl.-Ing. Jürgen Zuchowski

Telefon: 05323 / 937 20
Telefax: 05323 / 937 237

www.GDMB.de
Redaktion@GDMB.de

Sparkasse Goslar/Harz
Konto 20 024 (BLZ 268 500 01)
S.W.I.F.T.-BIC: NOLA DE 21 GSL
IBAN: DE36 2685 0001 0000 0200 24

Arsenic Inertization from Copper Pyrometallurgy through Phases of the Alunite Supergroup

Joan Viñals, Alba Sunyer, Elisabet Torres

Arsenical wastes including flash smelting dusts as well as calcium arsenates produced from gas cleaning steps of the copper pyrometallurgy were investigated. The inertization process consists basically of three steps: 1) arsenic leaching, 2) ozone treatment to convert arsenic species into As(V), and 3) hydrothermal precipitation in $\text{Na}^+ - \text{Al}^{3+} - \text{SO}_4^{2-} - \text{AsO}_4^{3-}$ media at $\sim 200^\circ\text{C}$, using aluminium and sodium sulfates as reactants. Under optimal conditions, the precipitates consist mainly of a complex arsenical natroalunite with – in some conditions – trace to minor amounts of mansfieldite or scorodite, depending on the solution composition and temperature. The precipitation rate is fast (≤ 15 minutes)

and the major effect on phase composition and arsenic solubility of the precipitates was the initial Al/As molar ratio in the liquid. Minimum arsenic solubility was obtained with precipitates containing arsenical natroalunite, free or with only traces of mansfieldite or scorodite. This was achieved for $\text{Al/As} \geq 3$ in the liquid media, the arsenic solubility being 0.01 to 0.02 mg/l at $\text{pH} \sim 7$, depending on the phase composition.

Keywords:

Arsenic – Copper – Waste – Inertization – Stabilization – Alunite

Arsen-Inertisierung bei der Pyrometallurgie des Kupfers durch Phasen der Alunitgruppe

Aus Abgasreinigungsstufen der Kupferpyrometallurgie wurden arsenhaltige Abfälle, die sowohl Stäube des Schwebeschmelzens als auch Kalziumarsenat enthielten, untersucht. Der Inertisierungsprozess besteht grundsätzlich aus drei Schritten: 1. Arsen-Laugung, 2. Ozonbehandlung zur Umwandlung von Arsenverbindungen in As(V), und 3. hydrothermale Ausfällung in $\text{Na}^+ - \text{Al}^{3+} - \text{SO}_4^{2-} - \text{AsO}_4^{3-}$ Medien bei $\sim 200^\circ\text{C}$ unter Einsatz von Aluminium- und Natriumsulfaten als Reaktionspartner. Unter optimalen Bedingungen bestehen die Ausscheidungsprodukte im Wesentlichen aus komplexem arsenhaltigen Natroalunit mit – unter bestimmten Bedingungen – Spuren bis kleinen Mengen von Mansfieldit oder Skorodit, abhängig von der Lösungszusammensetzung und Temperatur. Die Abschei-

dungsgeschwindigkeit ist hoch (≤ 15 Minuten) und die maßgebende Einflussgröße auf die Phasenzusammensetzung und Löslichkeit des Arsens war das anfänglich eingestellte Molverhältnis von Al/As in der Flüssigkeit. Die geringste Arsenlöslichkeit zeigten Präzipitate, die Arsen-Natroalunit enthielten, frei oder nur mit Spuren von Mansfieldit oder Skorodit. Dies wurde bei einem Al/As-Verhältnis von ≥ 3 im Flüssigmedium erzielt; die Arsenlöslichkeit bewegte sich in einem Bereich von 0,01 bis 0,02 mg/l bei einem pH-Wert von etwa 7, abhängig von der Phasenzusammensetzung.

Schlüsselwörter:

Arsen – Kupfer – Abfall – Inertisierung – Stabilisierung – Alunit

Inertisation arsénique de la pyrométallurgie de cuivre par l'intermédiaire des phases du supergroupe d'alunite

Inertización de arsénico de la pirometalurgia del cobre a través de fases del supergrupo de la alunita

Paper presented on the occasion of the Copper 2010 Conference held June 8 to 10, 2010 in Hamburg, Germany

1 Introduction

Arsenic is one of the most common toxic impurities in raw materials and final wastes of base and precious metal industries. In copper pyrometallurgy, arsenic is mainly concentrated in wastes of gas cleaning steps as well as in electrolyte and anode slime of the electrorefining process [1]. Numerous methods for arsenic inertization were investigated such as the precipitation of calcium arsenates,

ferrihydrate and scorodite [2]. Scorodite generation has been extensively studied [3-5], even at industrial scale [6], due to its relatively good stability. Scorodite precipitation can be verified hydrothermally and also at $\sim 95^\circ\text{C}$ with precise control of supersaturation and seeding. Nevertheless, As-solubility in scorodite (typically 0.05 to 1 mg/l) [7, 8] may exceed the maximum permitted for inert wastes. For this reason, the research on other As-bearing phases could be interesting.

Phases of the alunite supergroup are common in the Earth's surface [9], where most of them were produced by weathering of polymetallic sulfide deposits and further natural precipitation [10]. These natural phases exhibit great stability in supergenic conditions, decomposing only in strong acid [11] or alkaline media [12]. They consist of structures $AB_2(TO_4)(OH)_6$, in which A can be monovalent (Na, K, Ag, H_3O etc.) or divalent (Pb, Sr, Ba, Ca); B is usually trivalent (Al, Fe) and TO_4 is principally SO_4 , AsO_4 or PO_4 . These phases have also a great possibility of stoichiometric changes, such as the simultaneous substitution of an alkaline plus SO_4 by a divalent plus AsO_4 or PO_4 , or two alkaline by a divalent plus a vacancy, etc. For this reason, phases of the alunite supergroup may be proposed as a host for stabilizing a variety of toxic heavy metals [13, 14].

Possibilities for arsenic inertization through alunite-type phases are, of course, evident, for instance, the co-inertization of As and Pb through beudantite ($PbFe_3(SO_4)(AsO_4)(OH)_6$) precipitation [13]. Another possibility could be the incorporation of the AsO_4 group in a diluted solid solution – with low thermodynamic activity – in simple alunites. Natroalunite ($NaAl_3(SO_4)_2(OH)_6$) was selected for the present laboratory-scale study.

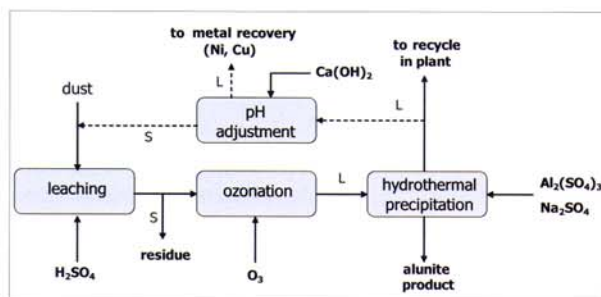


Fig. 1: Schematic diagram of the inertization process

Figure 1 shows a schema of the process. Waste is treated with H_2SO_4 in suitable conditions for As leaching. The resulting solution (or slurry) is ozonized to transform all arsenic species into As(V). Ozonation was preferred because it did not introduce new pollutants in the circuit. Hydrothermal precipitation is verified at $\sim 200^\circ C$ using aluminium and sodium sulfates as reagents. After the treatment, the liquid can be recycled in a plant to recover the possible valuable elements (Cu, Ni, etc.) and finally, to the cleaning steps of the final effluent. Since hydrothermal precipitation in a single step does not eliminate all As from the liquid, an optional step of pH adjustment (to ~ 3.5) can be verified to recycle the remnant As and Al to the hydrothermal step.

Two kinds of wastes were tested in this study: A) "Calcium arsenate" obtained by lime precipitation of a final plant effluent from the electrolytic section of a pyrometallurgical plant and B) flash smelting dust. Since flash smelting dust contains large amounts of copper, a previous copper-leaching process followed by solution purification was studied. Hydrothermal precipitation was conducted from the waste of the solution purification, an intermediate amorphous ferric arsenate.

2 Experimental methods

Original wastes, intermediate products and all hydrothermal precipitates were studied by chemical analysis (ICP), X-ray diffraction (XRD) and scanning electron microscopy (SEM). Quantitative microanalysis of different phases was obtained by energy dispersive spectroscopy (EDS) at 20 kV, 0.6 nA, 30 s, through a Jeol JSM-840 instrument provided with an Inca-250 analyzer.

Leaching experiments on original wastes or intermediate products were conducted in a conventional thermostatic reactor coupled with magnetic stirring. The addition of leaching agent (H_2SO_4), ORP and pH were monitored. The degree of solubilization for selected elements was measured by sampling at different times and solution analysis (ICP). Particular conditions are described jointly with the experimental results. After leaching, the resulting solution or slurry was ozonized in the same reactor injecting an O_2/O_3 mixture through a fritted glass diffuser. Ozone was produced in a Triogen generator at 0.75 l/min with an ozone mass flow of $3.36 \cdot 10^{-2}$ g/min.

Hydrothermal experiments were performed in a Parr 4563 autoclave reactor, provided with temperature, pressure and stirring controllers. After the leaching and ozonation steps, the solution (or slurry) was placed into the reactor with the reagents (Al and Na sulfates). The system was heated to working temperature at a rate of $5^\circ C/min$. Then the system was also cooled to room temperature at a rate of $5^\circ C/min$. The hydrothermal product was filtered, washed and characterized as described. The conditions of each group of tests are reported with the corresponding results.

The solubility of hydrothermal products at different pH's was studied by stirring 0.50 g of solid into 50 ml solution at $25^\circ C$ during 24 hours. These solutions were prepared by convenient dilution of H_2SO_4 or NaOH stock solutions. Eventual pH changes during these leaching tests were corrected by addition of small volumes of dilute H_2SO_4 or NaOH. Three consecutive leaching tests were performed for each pH. After each leaching the slurry was filtered and the solution was analyzed for As by ICP-MS.

3 Characterization of wastes

3.1 Calcium arsenate waste

The chemical composition is given in Table 1. XRD and SEM/EDS studies indicated that it mainly consists of gypsum, calcite and an amorphous precipitate containing As, Ca, Fe, Ni, Cu and Zn. Gypsum appeared as free, large (100 to 200 μm) crystals. The amorphous precipitate consisted of agglomerates of $\sim 1 \mu m$ spheroidal particles of variable composition with 15 % As mean content.

Although the waste was originally precipitated at pH 12, the pH of the As-received waste was about 9 and the As-solubility about 30 mg/l. This indicated that the usual process for arsenic removal from lime precipitation gives unstable calcium arsenates which decompose by atmospheric CO_2 generating soluble arsenic (Equation 1):

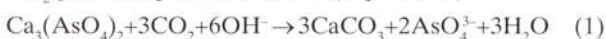


Table 1: Chemical composition of the studied wastes

[%]	Calcium arsenate	Flash smelting dust	Intermediate ferric arsenate
As	5.23	1.93	13.80
Ca	22.80	0.24	0.07
Fe	1.08	12.60	26.60
S	11.37	6.50	2.30
Cu	0.56	30.50	6.80
Zn	0.95	3.66	0.04
Ni	2.65	-	-
Mo	-	0.18	1.80
Pb	0.04	0.43	0.12
Bi	0.02	0.13	-
SiO ₂	0.86	2.78	-

3.2 Flash smelting dust

The composition of flash smelting dust (see Table 1) showed a high copper and relatively low arsenic content. XRD studies indicated that it mainly consists of soluble copper sulfates (CuSO_4 , $\text{CuSO}_4 \cdot \text{H}_2\text{O}$ and $\text{CuSO}_4 \cdot 5\text{H}_2\text{O}$), with cuprite (Cu_2O), tenorite (CuO), delafossite (CuFeO_2) and ferrite ($\text{M}^{2+}\text{M}^{3+}_2\text{O}_4$). Chemical phase analysis by selective leaching – confirmed by XRD – showed that 53 % of the total copper was present as soluble sulfates (25 °C, pH 4 leaching), 22 % as cuprite (25 °C, $\text{H}_2\text{SO}_4/\text{O}_2$, pH 1 leaching), 20 % as tenorite+delafossite (80 °C, H_2SO_4 , 0.5 M/ O_2 leaching) and the remaining 5 % as ferrite. SEM/EDS investigations (Figure 2) indicated that the main oxide phase was a zinc-rich ferrite, $\text{Zn}_x\text{Cu}_y\text{Fe}_{1-(x+y)}(\text{Fe}_z\text{Al}_{1-z})_2\text{O}_4$ (with ~7 % Cu), which appears as isometric 2 to 60 μm grains. Cuprite and tenorite were found as 1 to 20 μm rounded grains and delafossite as 10 to 50 μm lamellar crystals. As bearing phases were not clearly detected in SEM because they probably were of submicrometric size. However, a non

identified arsenic product intergrowth with lead sulphate aggregates was occasionally found (Figure 2D). Solubility tests showed a pH of 4.5 and 5.5 mg/l As, with very high Cu solubilization (>10 g/l).

4 Leaching

4.1 Calcium arsenate waste

The leaching behavior of calcium arsenate waste with H_2SO_4 was investigated by treating 2 g of solid in 200 ml solution at 25 °C, 600 rpm. Leaching was made through measured additions of 1 M H_2SO_4 for reaching a selected pH. The extraction of different elements is shown in Figure 3.

According to the amorphous nature of the phases containing heavy metals, the reactivity of the waste was very high. After about 5 min of acid addition, the pH of the slurry was practically stabilized. Complete leaching of As, Fe, Ni, Cu and Zn was achieved at pH 1 in 5 min, with an acid consumption of 380 g H_2SO_4 /kg waste. The comparison of the extraction curves of As and Fe showed that about 75 % As were already leached at pH 4 without significant Fe solubilization, whereas the remaining 25 % As were only leached at pH 1 when all Fe was solubilized. Thus, it seems possible that these 25 % As were associated to amorphous ferric arsenates. The residue of the leaching treatment was nearly pure gypsum (>99 %, see Figure 5A). Gypsum could be eliminated or not prior alunite precipitation, depending on the potential commercial value. In the present study, these two options were tested in the section of hydrothermal treatment.

Ozonation experiments on the slurry obtained after leaching at pH 1, showed a very effective oxidation method for converting As(III) into As(V). The process can be easily followed through the ORP solution changes from ~400 mV to ~1200 mV (vs. Ag/AgCl). Ozone consumption was 13 g O_3 /kg waste. According to the stoichiometry

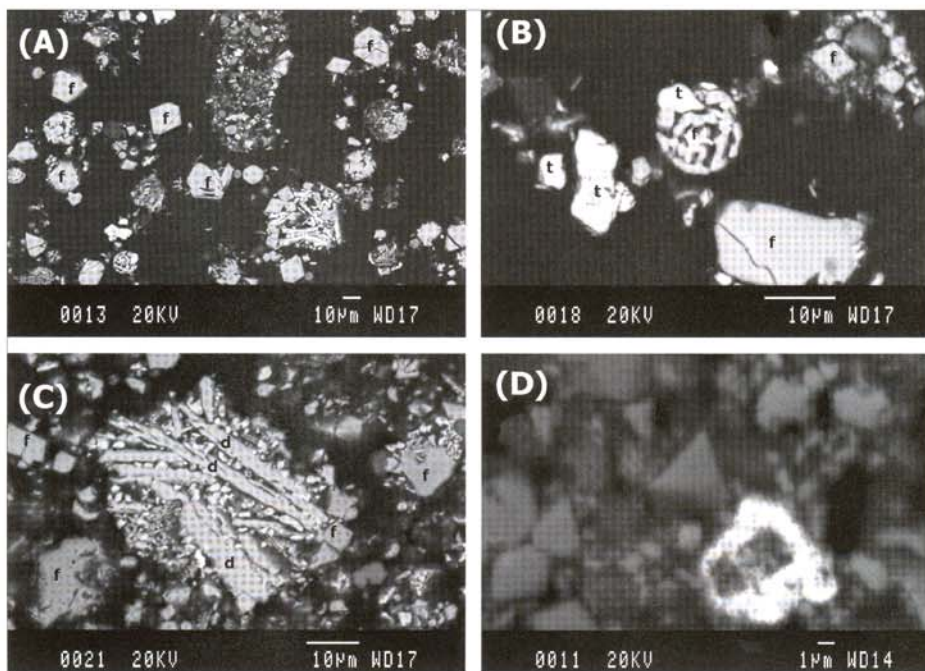


Fig. 2: Flash smelting dust after removing soluble sulfates (SEM, cross sections): (A) General view showing abundant ferrite "f", (B) tenorite particles "t", (C) delafossite laths "d", (D) aggregate of lead sulfate (white) containing arsenic

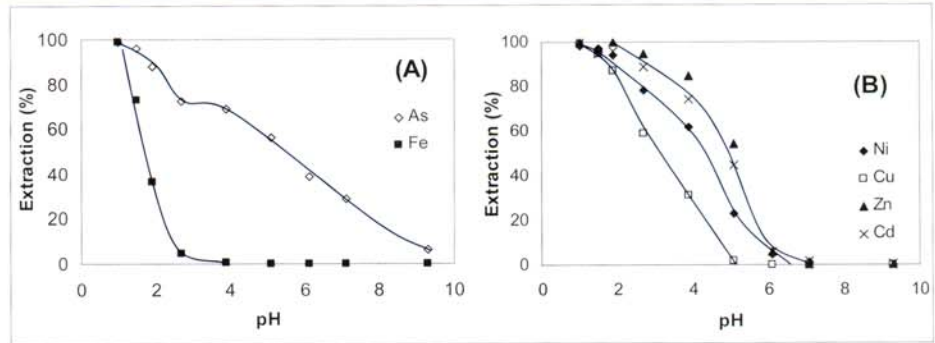


Fig. 3: H_2SO_4 leaching of calcium arsenate waste as a function of pH (25 °C, 5 min): (A) As and Fe extraction, (B) Ni, Cu, Zn and Cd extraction

for As(III) oxidation (Equation 2), the studied waste contained about 50 % of total arsenic as As(III).



4.2 Flash smelting dust

Main objectives for H_2SO_4 leaching of flash smelting dust were maximum arsenic extraction but also maximum copper recovery. The leaching behavior was, however, complex and only a brief summary is given here. At pH 1 and 25 °C, As and Cu extractions were only 65 to 70 %. Under these conditions, the copper phases which dissolved were sulfates and cuprite. An increase in copper extraction from tenorite and delafossite required an increase of acid concentration and temperature. Delafossite leaching was considered important not only for copper recovery but also for providing a sufficient amount of Fe^{3+} in the solution in order to coprecipitate As in a purification step.

Figure 4 shows the temperature effect on the leaching of 15 g dust in 150 ml 0.5 M H_2SO_4 in presence of O_2 . According to the XRD data of leaching residues, only at $T \geq 80$ °C all the copper phases, except ferrite, were leached. Under these conditions, copper recovery reached 95 % and the As extraction was nearly complete. Zn extraction (~40 %) was few sensitive to the temperature in the interval studied because ferrite remained practically unreacted. The H_2SO_4 consumption was 360 g H_2SO_4 /kg flash smelting dust.

The residue of the leaching treatment at 80 °C represents 220 g/kg dust. Solubility tests showed that it was inert with respect to As (<0.05 mg/l) but not with respect to Pb (~1 g/l). Probably, this ferrite residue could be recycled in the flash smelting operation.

After leaching, the resulting solution was ozonized to ensure the complete oxidation of Fe and As. The ozone consumption was 60 g O_3 /kg flash smelting dust. Depending on the solid/liquid ratio during the leaching, the composition of the solution varies from 20 to 50 g/l Cu, 1.1 to 2.8 g/l As, 2.1 to 5.3 g/l Fe, 1.1 to 2.8 g/l Zn, 0.1 to 0.3 g/l Mo and 0.01 to 0.02 g/l Sb. Solutions were treated with NaOH at pH 3.5 to 4 for removing Fe and As. The consumption was about 90 g NaOH/kg dust and the precipitate obtained was 130 g/kg dust. The purified solutions contained 0.012 g/l As, 0.003 g/l Mo, 0.001 g/l Sb and less than 0.001 g/l Fe. They were considered suitable for recycling to the electrolytic section of the pyrometallurgical plant.

The composition of the ferric arsenate obtained from the solution purification is given in Table 2. SEM examination showed that it consists of aggregates of submicron spheroids (Figure 5B), which highly suggests its amorphous nature. XRD confirmed this, because no ferrihydrite phases were detected. Probably, the presence of significant amounts of other metals precipitated jointly with Fe (see Table 1) make the ferrihydrite ordering difficult. This intermediate ferric arsenate was used as raw material for the inertization of arsenic contained in the flash smelting dust.

5 Hydrothermal precipitation of As

5.1 Calcium arsenate waste

The effects of initial pH, Al/As molar ratio, As concentration at fixed Al/As ratio, reaction time, temperature and prior gypsum separation were investigated. Other possible effects, such as SO_4^{2-} and Na^+ concentration were not studied here, because the SO_4^{2-} concentration was basically fixed by the large SO_4^{2-} concentration of the leaching solution

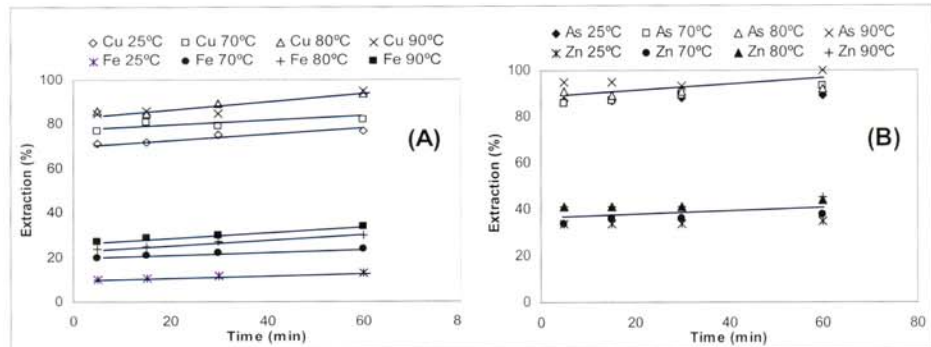


Fig. 4: H_2SO_4 (0.5 M) leaching of flash smelting dust: (A) Cu and Fe extraction, (B) As and Zn extraction

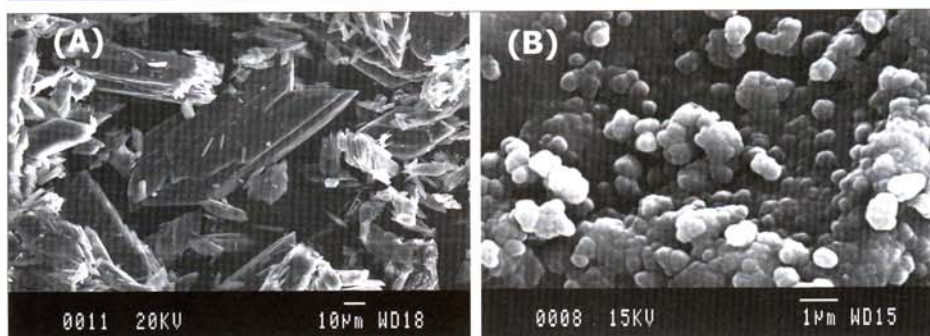
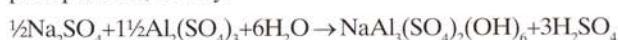


Fig. 5: (A) Gypsum residue from calcium arsenate leaching, (B) intermediate ferric arsenate from flash smelting dust

and, in all the experiments Na^+ was used in excess vs. Al^{3+} due to the stoichiometric requirements of the natroalunite precipitation, ideally:



The effect of initial pH showed that production of fully crystalline precipitates required an initial $\text{pH} \leq 1$ for this waste. These conditions ensure that Ni, Cu and Zn remain in the liquid phase which could facilitate further recovery.

5.1.1 Effect of Al/As molar ratio in the liquid phase

This was the most important effect on the phase composition. It was studied treating 10 g of leached and ozonized waste in 150 ml solution ($\text{pH} 1$) at 200°C for 120 min. Reagents and initial molar ratios in the solution for this set of experiments are given in Table 2. Results can be summarized as follows:

- For an Al/As molar ratio of 4.5, arsenic precipitated practically only as arsenic natroalunite ($\sim(\text{Na}, \text{Ca})(\text{Al}, \text{Fe})_3(\text{S}, \text{As}, \text{P})\text{O}_4 \cdot 2(\text{OH})_6$) (Figures 6 and 7). Decreasing the Al/As ratio, decreased the natroalunite precipitation and increased the formation of mansfieldite

Table 2: Experimental conditions used in the Al/As molar ratio effect

Test	Initial molar ratios						Final pH
	$\text{Al}_2(\text{SO}_4)_3$ [g]	Na_2SO_4 [g]	Al/As	S/As	As/Ca	Na/Al	
T1	5.38	0.994	4.50	18	0.123	0.44	0.66
T2	3.58	0.994	3.00	12	0.123	0.66	0.65
T3	3.58	0.994	3.00	11	0.488	0.66	0.62
T4	2.69	0.994	2.25	16	0.123	0.89	0.68
T5	1.79	0.994	1.50	15	0.123	1.33	0.84

($(\text{Al}, \text{Fe})(\text{As}, \text{P})\text{O}_4 \cdot 2\text{H}_2\text{O}$). When Al/As was 1.5, As precipitated practically only as mansfieldite.

- Calcium present in the initial medium as gypsum transforms into anhydrite (Figures 6 and 7). The substitution of Ca in natroalunite was low at the studied conditions, 0.04 to 0.08 in formula (Table 3). The effect of prior gypsum separation was insignificant on the phase composition, except for the absence of anhydrite (Figures 7 and 8).
- The maximum As substitution in natroalunite was 0.14 in formula (Table 3). Natroalunite also incorporated Fe from the original waste because it substitutes Al in the alunite lattice. Fe coefficients in formula reached 0.12 when traces of mansfieldite were present, but decreased to 0.08 when a large amount of mansfieldite was precipitated. Traces of P, substituting in TO_4 group, were also incorporated into alunite (up to 0.02 in formula).
- Mansfieldite also incorporates Fe. When mansfieldite was practically the only arsenic phase the substitution was extensive, 0.31 in formula (Table 3). This value decreases to 0.20 when the natroalunite precipitation increases. Phosphorous was also incorporated in mansfieldite, up to 0.05 in formula.
- If hydrothermal precipitation was performed in a single step, the arsenic precipitation yield was moderate (Figure 8A) and the liquid after precipitation had to be recirculated (see Figure 1). The yield was maximal ($\sim 50\%$) when mansfieldite was formed in large extension and minimal ($\sim 20\%$) when natroalunite was the only phase. However, a yield of $\sim 40\%$ can be achieved with formation of only small amounts of mansfieldite ($\sim 5\%$).

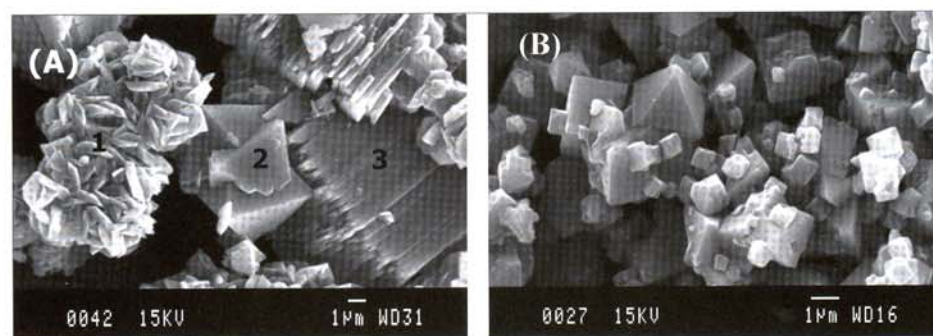


Fig. 6: Typical phase morphology of the hydrothermal precipitates: (A) from calcium arsenate waste (1: As-natroalunite, 2: mansfieldite, 3: anhydrite), (B) from flash smelting dust (As-natroalunite)

Table 3:
Effect of the Al/As ratio, 200 °C,
experimental formulas from EDS
punctual analysis

Al/As	From calcium arsenate waste	
	Natroalunite (normalized to S + As + P = 2, OH from charge balance)	Mansfieldite (normalized to As + P = 1)
4.50	$(\text{Na}_{0.98}\text{Ca}_{0.08})(\text{Al}_{2.70}\text{Fe}_{0.12})((\text{S}_{0.92}\text{As}_{0.07}\text{P}_{0.01})\text{O}_4)_2(\text{OH})_{5.44}$	–
3.00	$(\text{Na}_{0.96}\text{Ca}_{0.08})(\text{Al}_{2.69}\text{Fe}_{0.12})((\text{S}_{0.88}\text{As}_{0.11}\text{P}_{0.01})\text{O}_4)_2(\text{OH})_{5.33}$	$(\text{Al}_{0.78}\text{Fe}_{0.21})(\text{As}_{0.97}\text{P}_{0.03})\text{O}_4 \cdot 2\text{H}_2\text{O}$
3.00*	$(\text{Na}_{1.03})(\text{Al}_{2.82}\text{Fe}_{0.15})((\text{S}_{0.90}\text{As}_{0.10})\text{O}_4)_2(\text{OH})_{5.76}$	$(\text{Al}_{0.76}\text{Fe}_{0.24})(\text{As}_{0.96}\text{P}_{0.04})\text{O}_4 \cdot 2\text{H}_2\text{O}$
2.25	$(\text{Na}_{0.90}\text{Ca}_{0.04})(\text{Al}_{2.70}\text{Fe}_{0.08})((\text{S}_{0.84}\text{As}_{0.14}\text{P}_{0.02})\text{O}_4)_2(\text{OH})_{5.00}$	$(\text{Al}_{0.76}\text{Fe}_{0.24})(\text{As}_{0.99}\text{P}_{0.01})\text{O}_4 \cdot 2\text{H}_2\text{O}$
1.50	–	$(\text{Al}_{0.69}\text{Fe}_{0.31})(\text{As}_{0.95}\text{P}_{0.05})\text{O}_4 \cdot 2\text{H}_2\text{O}$
* In absence of gypsum		
From intermediate ferric arsenate obtained from flash smelting dust		
4.5	$(\text{Na}_{1.05})(\text{Al}_{1.76}\text{Fe}_{0.95})((\text{S}_{0.93}\text{As}_{0.07})\text{O}_4)_2(\text{OH})_{5.01}$	–
6.0	$(\text{Na}_{1.05})(\text{Al}_{1.97}\text{Fe}_{0.80})((\text{S}_{0.96}\text{As}_{0.04})\text{O}_4)_2(\text{OH})_{5.34}$	–
7.5	$(\text{Na}_{1.0})(\text{Al}_{2.03}\text{Fe}_{0.67})((\text{S}_{0.97}\text{As}_{0.03})\text{O}_4)_2(\text{OH})_{5.00}$	–
9.0	$(\text{Na}_{1.05})(\text{Al}_{2.23}\text{Fe}_{0.65})((\text{S}_{0.97}\text{As}_{0.03})\text{O}_4)_2(\text{OH})_{5.57}$	–

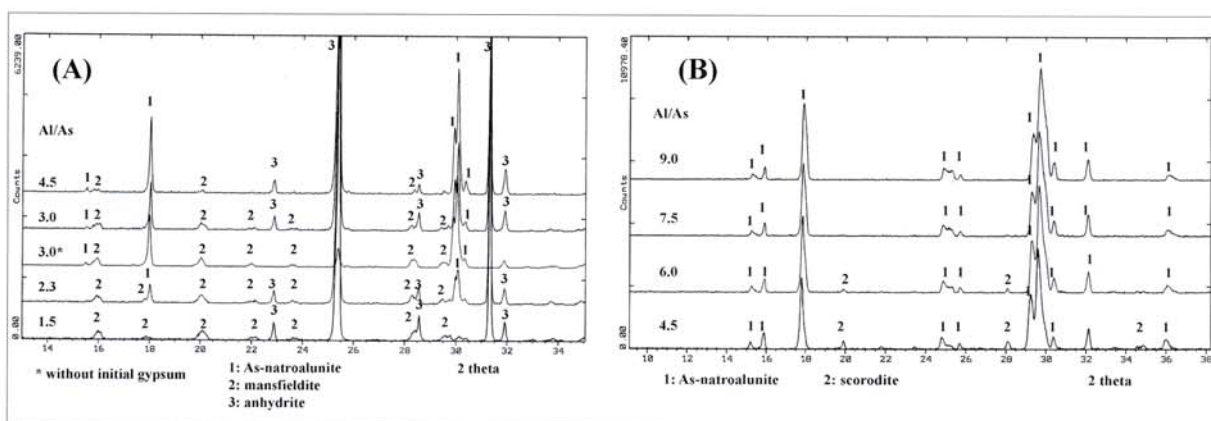


Fig. 7: Effect of the Al/As molar ratio on phase composition: (A) from calcium arsenate waste, (B) from intermediate ferric arsenate of the treatment of flash smelting dust

- Al precipitation yields also depended on the Al/As ratio (Figure 8A). It was maximal (~60 %) when natroalunite precipitation was high and minimal (~20 %) when mansfieldite formation was extensive. Fe precipitation yield (80 to 90 %) was few sensitive to the phase composition, whereas Ni, Zn and Cu do not precipitate in significant amount.

5.1.2 Other effects

The As concentration effect at fixed Al/As = 3.00 ratio was investigated in the range of 3.5 to 7 g/l at 200 °C. No significant effect on phase composition and precipitation yield was observed.

Previous research using synthetic reagents showed that incorporation of As in natroalunite was effective at $T \geq 180$ °C because at lower temperatures intermediate amorphous arsenates were formed. Even at 180 °C, the formation of mansfieldite was preferential. This effect was confirmed for the calcium arsenate waste studied here. For Al/As=3, 120 min, whereas at 200 °C the natroalunite/mansfieldite phase ratio was ~5, at 180 °C the same ratio decreased to ~2.5 (Figure 8B).

The effect of reaction time was studied at 200 °C, Al/As = 3, for 15, 30 and 120 min. No significant changes in precipitation yield and phase composition were observed (Figure 8). Consequently, at 200 °C hydrothermal precipitation can be verified at high rates (≤ 15 min). Bulk chemical compositions of representative hydrothermal precipitates are given in Table 4.

6 Intermediate ferric arsenate from flash smelting dust

Hydrothermal precipitation was studied by treating 3.8 g of intermediate ferric arsenate in 150 ml solution at pH 1 and 200 °C for 15 min. Variable amounts of $\text{Al}_2(\text{SO}_4)_3$ were added, to give Al/As ratios in the liquid phase in the of range of 4.5 to 9. Using these high Al/As ratios ensured no mansfieldite formation. Na_2SO_4 was also added to give Na/Al ratios in the interval of 0.5 to 0.6. Results can be summarized as follows:

- In the range investigated, arsenic precipitated practically as arsenic, highly ferrous natroalunite (see Figures 6 and 7, Table 3). Trace (~0.5 %) to minor amounts of scorodite (~2 %) were only detected for 6.0 and 4.5 Al/As ratios, respectively.

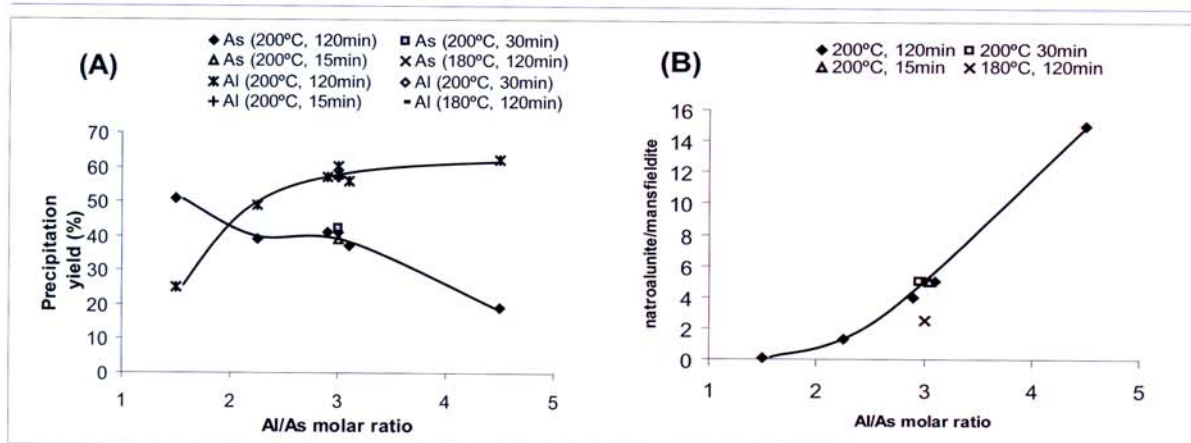


Fig. 8: Effect of the Al/As molar ratio in the treatment of calcium arsenate waste: (A) As and Al precipitation yield, (B) arsenic distribution

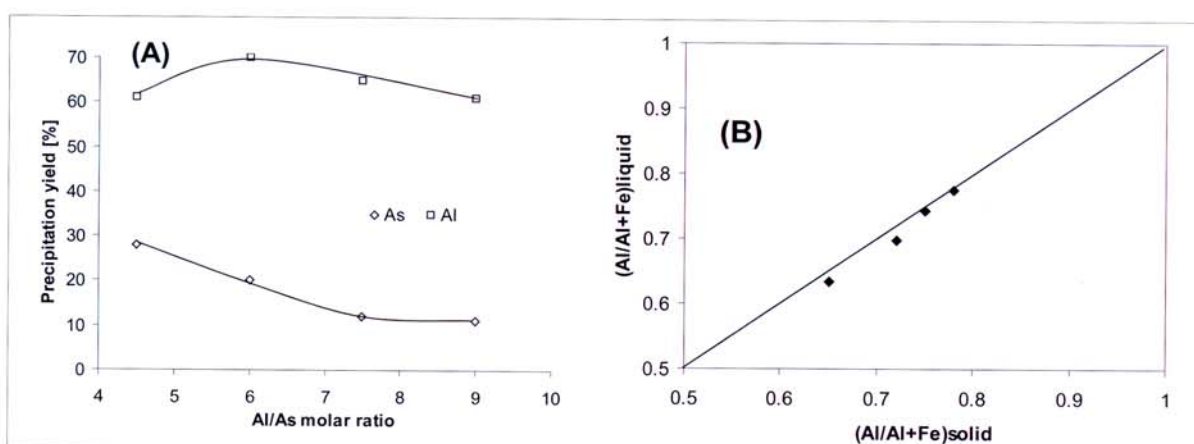


Fig. 9: Effect of the Al/As molar ratio in the treatment of intermediate ferric arsenate from flash smelting dust: (A) As and Al precipitation yield, (B) Al and Fe distribution

From calcium arsenate waste										
Al/As ratio	Time [min]	[wt. %]								
		Ca	S	As	Al	Na	Fe	Ni	Cu	Zn
4.50	120	18.4	19.4	1.10	5.98	1.60	0.94	0.01	0.05	0.01
3.00	15	22.1	21.0	2.41	4.04	1.10	1.10	0.01	0.02	0.02
3.00	30	21.6	20.4	2.58	4.01	1.05	1.15	0.01	0.04	0.02
3.00*	120	0.13	11.5	9.85	16.18	4.49	4.22	0.01	0.04	0.02
2.25	120	21.6	19.2	3.41	2.64	0.65	1.23	0.01	0.02	0.03
1.50	120	24.5	20.0	3.34	0.88	0.07	1.12	0.01	0.06	0.03
* Precipitated in absence of gypsum										
From intermediate ferric arsenate obtained from flash smelting dust										
Al/As ratio	Time [min]	[wt. %]								
		S	Al	Na	As	Fe	Mo	Pb	Cu	Zn
9.0	15	14.4	13.2	4.48	0.71	9.39	0.38	-	0.06	0.02
7.5	15	15.6	13.6	4.78	0.94	12.0	0.59	0.06	0.05	0.01
6.0	15	14.5	12.0	4.41	1.61	12.8	0.57	0.05	0.08	0.01
4.5	15	12.6	9.60	4.41	2.72	14.4	0.53	0.07	0.10	0.01

Table 4: Representative bulk chemical composition of the hydrothermal precipitates (200 °C)

- Maximum As substitution in natroalunite was 0.07 in formula (Table 3) for Al/As = 4.5. This was the same value as obtained from calcium arsenate waste, treated

at the same Al/As conditions. Consistent with these data, As and Al precipitation yields (Figure 9A) were also similar at the same Al/As ratio.

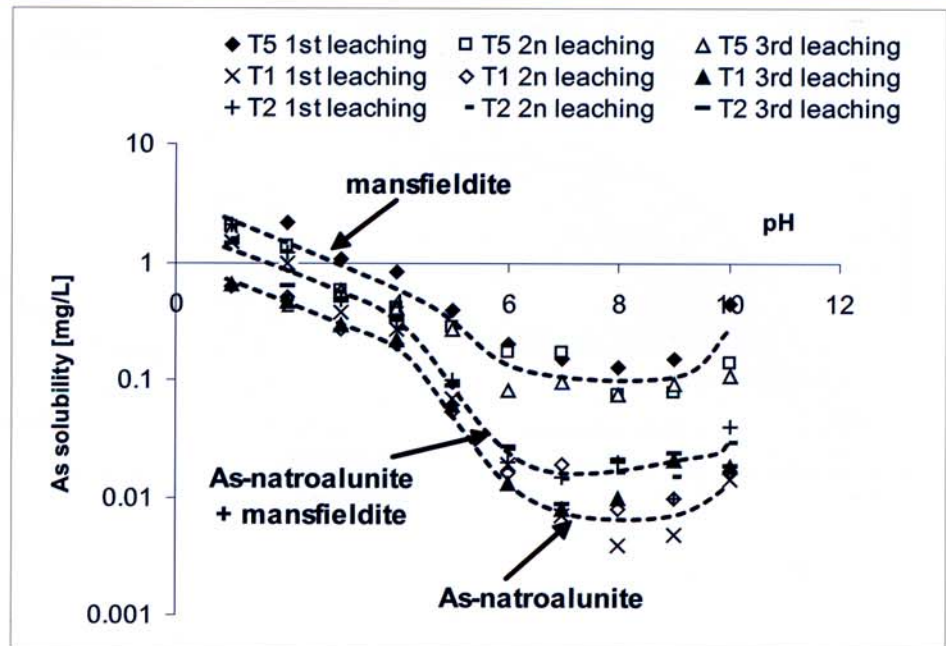


Fig. 10:
As solubility from hydrothermal precipitates obtained from calcium arsenate waste

- The main difference was the very high iron content in natroalunite as obvious consequence of the high iron content in the raw material (Table 4). Iron substitution in natroalunite increases proportionally to the decrease in the Al/Al+Fe ratio in the liquid phase (Figure 9B).
- As in calcium arsenate waste, Cu does not precipitate in significant amounts. However, Mo precipitates partially (Table 4), probably as minor substitution of MoO_4^{2-} in TO_4 group. However this was not confirmed by EDS punctual analyses because the Mo content was low.

6.1 Solubility of the precipitates

Results of solubility experiments for hydrothermal precipitates obtained from calcium arsenate waste are reported in Figure 10. Usually, at each pH data of the first leaching were slightly higher than in the second leaching and these were slightly higher than in the third leaching. Nevertheless, differences were small which suggests that the precipitates were easily washed. Moreover, solubilities in very acid medium (pH 1) were relatively small (0.5 to 2 mg/l), which also suggest the absence of amorphous As-phases.

Minimal solubility in all pH intervals corresponded to precipitates obtained at high Al/As ratio in the liquid (4.5) when the As phase was natroalunite. In contrast, maximal solubility could be observed at low Al/As ratio when mansfieldite was the only As-phase. In the neutral region, the As solubility of natroalunite was about 0.01 mg/l, whereas for mansfieldite it was ~0.1 mg/l. However, the most favorable conditions for this calcium arsenate waste probably were at Al/As = 3, when a mixture of natroalunite and minor mansfieldite was formed. The solubility in the neutral region is acceptable (~0.02 mg/l) and the arsenic precipitation yield in a single step (~40 %) was double compared to precipi-

tates containing only natroalunite. An additional advantage can be the minor consumption of aluminium salt.

Solubility of natroalunites produced by intermediate ferric arsenate from flash smelting dust was only studied at pH 4.2 to 4.6, which was the natural pH, after 24 hours. The results showed As solubilities in the range 0.005 to 0.01 mg/l for precipitates obtained at Al/As ≥ 6 . However, samples obtained at Al/As = 4.5 showed a higher solubility of 0.07 mg/l, probably as consequence of the scorodite content of ~2 % (Figure 7).

7 Conclusions

Hydrothermal precipitation of As(V) in acid $\text{Na}^+\text{-Al}_3^+\text{-SO}_4^{2-}$ media at ~200 °C, using aluminium and sodium sulfates as reactants, may be an alternative for arsenic inertization from wastes of copper pyrometallurgy. Under optimal conditions, the precipitates consist mainly of a complex arsenical natroalunite. The precipitation rate is fast (≤ 15 min) and the major effect on phase composition and arsenic solubility of the precipitates was the Al/As molar ratio in the initial liquid. Minimum arsenic solubility was obtained with precipitates containing arsenical natroalunite, free or with only traces of mansfieldite or scorodite. This was achieved for Al/As ≥ 3 in the liquid media, the arsenic solubilities ranged between being 0.01 to 0.02 mg/l at pH ~7, depending on the phase composition.

Acknowledgements

The authors wish to thank the Spanish Ministerio de Educación y Ciencia (DGI) for the financial support of this research (Programa de Materiales, MAT 2007-61466). Thanks also to the Serveis Científicotècnics de la Universitat de Barcelona for their assistance in characterization studies.

References

- [1] PIRET, N.L. (1999): The removal and safe disposal of arsenic in copper processing. – *JOM* **51**, 16-17.
- [2] RIVEROS, P.A., DUTRIZAC, J.D. & SPENCER, P. (2001): Arsenic disposal practices in the metallurgical industry. – *Canadian Metallurgical Quarterly* **40**, 395-420.
- [3] DEMOPOULOS, G.P. et al. (2003): The atmospheric scorodite process. – *Copper 2003*, VI (2), Santiago, Chile, TMS, 597-616.
- [4] MONHEMIUS, A. J. & SWASH, P.M. (1999): Removal and stabilizing As from copper refining circuits by hydrothermal processing. – *JOM* **51**, 30-33.
- [5] SHINODA, K. et al. (2009): Coprecipitation of large scorodite particles from aqueous Fe(II) and As(V) solution by oxygen injection. – *Materials Transactions* **50**, 1196-1201.
- [6] ICHIMURA, R. et al. (2007): Arsenic immobilization and metal recovery from El Teniente smelter dust. – *Copper 2007*, IV (2), Toronto, Canada, CIM, 597-616.
- [7] KRAUSE, E. & ETTTEL, V.A. (1989): Solubilities and stabilities of ferric arsenate compounds. – *Hydrometallurgy* **22**, 311-337.
- [8] BLUTEAU, M.C. & DEMOPOULOS, G.P. (2007): The incongruent dissolution of scorodite. Solubility, kinetics and mechanism. – *Hydrometallurgy* **87**, 163-177.
- [9] JAMBOR, J.L. (1999): Nomenclature of the alunite supergroup. – *Canadian Mineralogist* **37**, 1323-1341.
- [10] VIÑALS, J. et al. (1995): Characterization and cyanidation of Rio Tinto gossan ores. – *Canadian Metallurgical Quarterly* **34**, 115-122.
- [11] VIÑALS, J. & NÚÑEZ, C. (1988): Kinetics of dissolution of argentian plumbojarosite from old tailings of sulfatizing roasting pyrites by HCl-CaCl₂ leaching. – *Metallurgical Transactions B* **19**, 365-373.
- [12] ROCA, A. et al. (1999): Characterization and cyanidation of jarosite-beudantite phases from Rio Tinto gossan ores. – *Canadian Metallurgical Quarterly* **38**, 93-103.
- [13] ALCÓVE, X. et al. (2001): Structural characterization of beudantite-type phases by Rietveld refinements. – *Materials Science Forum* **378**, 671-676.
- [14] KOLITSCH, U. & PRING, A. (2001): Crystal chemistry of the crandallite, beudantite and alunite groups: a review and evaluation of the suitability storage materials for toxic products, *Journal of Mineralogical and Petrological Sciences* **96**, 67-78.

Dr. Joan Viñals
M.Sc. Alba Sunyer
Elisabet Torres
All:
University of Barcelona
Department of Materials Science and Metallurgical Engineering
Calle Martí i Fraqués 1
08028 Barcelona
Spain
e-mail:
jvinalsvinal@ub.edu
asunyer@ub.edu
etorregu@yahoo.es

A.7 Arsenic stabilization of calcium arsenate waste by hydrothermal precipitation of arsenical natroalunite

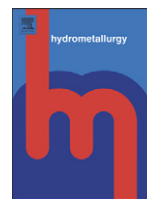
J. Viñals, A. Sunyer, P. Molera, M. Cruells, N. Llorca, 2010, Arsenic stabilization of calcium arsenate waste by hydrothermal precipitation of arsenical natroalunite, *Hydrometallurgy*, 104, 247- 259.

Resum en català

L'estabilització del residu d'arseniat càlcic procedent d'un forn de coure per precipitació de natroalunite arsenical ha estat investigada. Aquest procés pot solucionar el problema de la producció de guix arsenical perquè és transformat en anhidrita lliure d'arsènic. La precipitació de natroalunite va ser estudiada a 180-200°C a partir de la solució obtinguda després de la lixiviació amb H_2SO_4 i la ozonització del residu original, usant sulfats de sodi i alumini com a reactius. El residu d'arseniat càlcic i el precipitat final van ser caracteritzats per anàlisis químic (ICP), SEM-EDS i DRX. Els tests de solubilitat van ser fets amb el residu original i precipitats seleccionats.

Els efectes estudiats en el tractament hidrotermal van ser: pH inicial, relació molar Al/As, concentració d'As, temps de reacció i eliminació prèvia del guix. Per $(Al/As)_{aq}=4.5$, es va formar extensivament natroalunite complexa ($\sim(Na, Ca)(Al, Fe)_3((S, As, P)O_4)_2(OH)_6$). Sota aquestes condicions, la substitució d'arsènic en el TO_4 va ser del 7-8% molar. En $(Al/As)_{aq}$ decreixents, la substitució d'arsènic en la natroalunite va incrementar (fins a un $\sim 14\%$ molar) però la mansfieldita ($(Al, Fe)(As, P)O_4 \cdot 2H_2O$) va co-precipitar. Altres efectes com la concentració d'arsènic en un rang de 3.5-7.0 g/L i la separació prèvia del guix no va alterar significativament la relació de fases arsenicals ni la composició d'aquestes. Tanmateix, el tractament a 180°C va incrementar la precipitació de mansfieldita. La incorporació de calci a la natroalunite va ser petita (~ 0.04 en fórmula) i per un pH inicial 1, la precipitació de Cu, Ni i Zn va ser insignificant.

La natroalunite arsenical pot ser efectiva per a emmagatzematge a llarg termini. Al seu pH natural (4-5), la solubilitat d'arsènic va romandre estable a ~ 0.1 mg/L en 6 mesos. La mansfieldita no va ser estable sota les mateixes condicions amb una solubilitat de l'arsènic d'entre 5-10 mg/L. La major desavantatge de la natroalunite és la limitada partició d'arsènic entre fase sòlida i fase aquosa (~ 0.45 molar). Tanmateix, com que la velocitat de precipitació és elevada (< 15 min), sembla tècnicament factible millorar la precipitació d'arsènic amb una addició semicontinua dels reactius en una única operació hidrotermal. El cadmi s'incorpora a dins de l'estructura de l'anhidrita produint-se una dissolució dels lixiviat. Sembla que aquest problema només es pot solucionar treient prèviament el cadmi de l'effluent de planta.



Arsenic stabilization of calcium arsenate waste by hydrothermal precipitation of arsenical natroalunite

J. Viñals*, A. Sunyer, P. Molera, M. Cruells, N. Llorca

Department of Materials Science and Metallurgical Engineering, University of Barcelona, Martí i Franqués 1, 08028 Barcelona, Spain

ARTICLE INFO

Article history:

Received 15 February 2010
Received in revised form 14 June 2010
Accepted 22 June 2010
Available online 6 July 2010

Keywords:

Arsenic
Stabilization
Sodium alunite
Gypsum
Copper smelter waste

ABSTRACT

The stabilisation of calcium arsenate waste from a copper smelter by precipitation of arsenical natroalunite has been investigated. This procedure could solve the problem of arsenical gypsum production because it is transformed into arsenic-free anhydrite. Natroalunite precipitation was studied at 180–200 °C from the slurry obtained after H₂SO₄-leaching and ozonation of the original waste - using sodium and aluminum sulfates as reagents. Calcium arsenate waste and final precipitates were characterized by chemical analysis (ICP), SEM-EDS and XRD. Solubility tests were also performed on original waste and selected precipitates.

The effects studied in the hydrothermal treatment were: initial pH, Al/As molar ratio, As concentration, reaction time and prior gypsum removal. For (Al/As)_{aq} = 4.5, a complex natroalunite (~(Na,Ca)(Al,Fe)₃((S,As,P)O₄)₂(OH)₆) was extensively formed. Under these conditions, As-substitution in TO₄ was 7–8% molar. Decreasing (Al/As)_{aq} increased As-substitution in natroalunite (up to ~14% molar) but mansfieldite ((Al,Fe)(As,P)O₄·2H₂O) co-precipitated. Other effects such as the arsenic concentration in the range 3.5–7.0 g/L and prior gypsum removal did not significantly alter the arsenic phase ratio and the composition of the arsenic phases. However, treatment at 180 °C increased mansfieldite precipitation. Calcium incorporation in natroalunite was small (~0.04 in formula) and for initial pH = 1, precipitation of Cu, Ni and Zn was insignificant.

Arsenical natroalunite can be effective for long-term storage. At its natural pH (4–5), arsenic solubility remained stabilized at ~0.1 mg/L in 6 months. Mansfieldite was not stable under the same conditions with arsenic solubility between 5–10 mg/L. The major disadvantage of natroalunite is the limited arsenic partition between solid and aqueous phases (~0.45 molar). However, as the precipitation rate is fast (<15 min), it seems technically feasible to improve the arsenic precipitation yield by semi-continuous addition of reagents in a single hydrothermal operation. Cadmium incorporated into the anhydrite structure causes cadmium release in leachates. It seems that this problem can only be overcome through prior removal of cadmium from the plant effluent.

© 2010 Elsevier B.V. All rights reserved.

1. Introduction

Arsenic stabilization remains a significant challenge for the primary base-metal industry and particularly for copper pyrometallurgy (Piret, 1999; Riveros et al., 2001). Arsenic precipitation as scorodite (FeAsO₄·2H₂O) has been extensively studied as it is stable and has a high arsenic content (Demopoulos et al., 1995; Monhemius and Swash, 1999). Crystalline scorodite can be produced hydrothermally (>150 °C) and also at ~95 °C through precise supersaturation and seeding control (Demopoulos et al., 2003; Ichimura et al., 2007; Caetano et al., 2009). In a recently reported method, supersaturation conditions are controlled by slow oxidation of Fe(II) with air or O₂ (Fujita et al., 2008a,b, 2009a). The solubility of scorodite depends of pH and reaches minimum values of between 0.1 and 1 mg/L at pH ~5

(Krause and Ettel, 1989; Swash et al., 2000). However, Bluteau and Demopoulos (2007) and Bluteau et al. (2009) showed that scorodite suffers slow incongruent dissolution at neutral or near neutral pH, releasing arsenic (~5 mg/L at pH 7) which might not be appropriate for long-term storage.

Phases of the alunite supergroup are very common in nature, some of which appear to be very stable under a wide range of conditions and decompose only in strong acid or alkaline media (Viñals and Núñez, 1988; Roca et al., 1999; Viñals et al., 2003). They consist of structures AB₃(TO₄)₂(OH,H₂O)₆ (Jambor, 1999), in which the A (“alkali”) site can be occupied by a monovalent (Na, K, H₃O, etc) or a large divalent or trivalent (Ca, Ba, Pb, Bi, rare earth). The B site is usually occupied by Fe(III) or Al; and TO₄ is most often SO₄, AsO₄ or PO₄. Multiple substitutions are possible because charge balance can be compensated by cationic vacancies and/or protonation of OH groups (Paktunc and Dutrizac, 2003). Thus, these structures can be proposed for long-time storage of a variety of heavy metals (Kolitsch and Pring, 2001; Paktunc and Dutrizac, 2003). For instance, the co-inertization of

* Corresponding author. Tel.: +34 934021317; fax: +34 934039621.
E-mail address: jvinalsvinal@ub.edu (J. Viñals).

Table 1
Experimental conditions & reagents for the synthesis of arsenical natroalunite.

Fixed synthesis conditions: 150 mL; pH _i : 2.8–2.9; 200 °C; 120 min.				
Fixed reagent addition: Al ₂ (SO ₄) ₃ ·18H ₂ O: 6.33 g; Na ₂ SO ₄ : 0.45 g				
Test	Na ₂ HAsO ₄ ·7H ₂ O (g)	Molar ratios		
		(As/S + As) _{aq}	(Al/As) _{aq}	(Na/Al) _{aq}
S1	0	0	–	0.334
S2	0.89	0.083	6.66	0.634
S3	1.11	0.101	5.34	0.708
S4	1.27	0.114	4.67	0.762
S5	1.48	0.130	4.01	0.833
S6	1.78	0.152	3.33	0.934
S7*	1.98	0.170	3.00	0.668
S8	2.23	0.185	2.66	1.09
S9	2.97	0.231	2.00	1.34

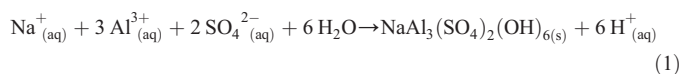
* : Addition 0.49 g CaSO₄·2H₂O.

As/Pb could be possible through beudantite (PbFe₃(SO₄)(AsO₄)(OH)₆) precipitation (Alcové et al. 2001). Other possibilities include the partial substitution of AsO₄³⁻ for SO₄²⁻ in simple alunites or jarosites (Dutrizac et al., 1987; Paktunc and Dutrizac, 2003; Savage et al., 2005). However, alunites might be more stable than jarosites or other Fe³⁺-bearing phases in contact with anaerobic soils, because Al³⁺ does not reduce under these conditions.

Basic studies in Al³⁺/SO₄²⁻/AsO₄³⁻ media, in the presence of Na⁺, Ca²⁺, Ba²⁺ or Pb²⁺ sulfates as the “alkali” carriers, are currently being undertaken by our research team. However, prior to finishing these studies, to check the potential application and detect unexpected effects, some research into real wastes appeared necessary. “Calcium arsenates” obtained from lime precipitation of plant effluents with a high SO₄²⁻/AsO₄³⁻ ratio, seem to be suitable for studying inertization processes based on SO₄²⁻/AsO₄³⁻ phases, such as alunite compounds. On the other hand, global inertization of such wastes should not generate intermediate gypsum, as it seems very difficult to obtain this compound with sufficiently low arsenic content for disposal (Fujita et al., 2009b). Precipitation in hydrothermal conditions could be suitable, since arsenical gypsum can be transformed into arsenic-free anhydrite. The concept of the treatment process would involve three basic steps (Viñals et al., 2009): 1) leaching of “calcium arsenate” with H₂SO₄ to solubilize the arsenic compounds, 2) ozonation of the resulting slurry to ensure that all the arsenic is in the form of As^V, and 3) hydrothermal precipitation using aluminium and “alkali” sulfates as reactants.

The present paper reports hydrothermal precipitation from real waste in a Na⁺/Ca²⁺/Al³⁺/SO₄²⁻/AsO₄³⁻ medium at ~200 °C, studying the composition and characteristics of the phases obtained and their solubility in short- and long-term experiments. The behavior of minor impurities such as cadmium was also studied, as it could establish preferential options. Experiments were designed to add the alumin-

ium salt as a stoichiometric limiting agent for natroalunite generation, ideally:



Some experiments on synthetic arsenical natroalunite are also included for comparison.

2. Materials and experimental methods

2.1. Materials

Synthetic arsenical natroalunite was prepared under the conditions shown in Table 1. The main aim was to obtain the ratio between aqueous solution composition and arsenic substitution in natroalunite, this is basically the correlation between the (AsO₄/SO₄ + AsO₄) ratio in the aqueous solution ((AsO₄/TO₄)_{aq}) and the same ratio in natroalunite ((AsO₄/TO₄)_s).

Calcium arsenate waste was obtained from an effluent from the gas cleaning steps of a large copper pyrometallurgical plant. This effluent was industrially treated with Ca(OH)₂ and Fe³⁺ until it reached pH 12. This treatment leads to the precipitation of gypsum and heavy metals such as arsenic. This original waste was characterized by chemical analysis (ICP), X-ray diffraction (XRD) and scanning electron microscopy coupled by energy dispersive spectroscopy (SEM-EDS). The solubility of minor elements at pH 9 (as received) and at pH 7, as well as leaching behavior in H₂SO₄ at different pH values, were also studied. These tests were performed by treating 2 g of waste in 200 mL solution at 25 °C, 600 rpm, 10 min. Solubility and extraction data for heavy metals were obtained from ICP solution analysis, except for very high extractions (>90%) which were determined by chemical analysis of residual gypsum.

Before the hydrothermal experiments were performed, the calcium arsenate waste was leached with H₂SO₄ and ozonized at 25 °C. Leaching was performed by stirring 10 or 20 g of waste in 150 mL of water with controlled additions of 1 M H₂SO₄ until the desired pH (1 or 2) was reached, and maintained for 10 min. H₂SO₄ consumption was approximately 170 and 430 g H₂SO₄/kg of waste at pH 2 and pH 1, respectively (Table 2). After leaching, the resulting slurry was ozonized to ensure all the arsenic was in the form of As(V). Ozone was produced by a TRIOGEN generator calibrated to a mass flow of 3.36 × 10⁻² g O₃/min. O₃ consumption was determined through the abrupt change in the ORP of the medium, from ~400 to ~1200 mV (vs Ag/AgCl).

Table 2
Experimental conditions for the hydrothermal treatment of calcium arsenate waste.

Leaching & ozonation					Hydrothermal conditions & reagents				
Test	Waste (g)	H ₂ SO ₄ (g)	O ₃ (g)	Initial pH	Temp (°C)	Time (min)	Al ₂ (SO ₄) ₃ ·18H ₂ O (g)	Na ₂ SO ₄ (g)	(Al/As) _{aq} molar ratio
P1	10	1.7	0.13	2.0	200	120	3.48	0.99	1.50
P2	10	4.6	0.10	1.0	200	120	3.48	0.99	1.50
P3	10	4.2	0.13	1.0	200	120	5.24	0.99	2.25
P4	10	4.4	0.13	1.0	200	120	6.97	0.99	3.00
P5	10	3.7	0.13	1.0	200	120	10.5	0.99	4.50
P6	20	6.7	0.27	1.0	200	120	13.9	1.99	3.00
P7	10	3.8	0.14	1.0	200	15	6.97	0.99	3.00
P8	10	3.9	0.10	1.0	200	30	6.97	0.99	3.00
P9	10	4.1	0.09	1.0	180	15	6.97	0.99	3.00
P10	10	3.9	0.11	1.0	180	30	6.97	0.99	3.00
P11	10	3.6	0.15	1.0	180	120	6.97	0.99	3.00
P12*	10	4.1	0.12	1.0	200	120	6.97	0.99	3.00

* Gypsum removal prior hydrothermal treatment.

Table 3
Bulk chemical composition (ICP) of synthetic natroalunite.

Test	(Al/As) _{aq}	pH _f	Bulk composition (weight %)					Phases
			S	Al	As	Na	Ca	
S1	0	1.0	15.07	17.95	–	4.05	–	natroalunite
S2	0.083	0.9	14.88	18.42	1.24	4.88	–	natroalunite
S3	0.101	1.0	13.94	17.18	1.32	4.52	–	natroalunite
S4	0.114	1.0	15.02	18.70	1.69	4.66	–	natroalunite
S5	0.130	1.0	13.53	16.96	1.94	4.59	–	natroalunite
S6	0.152	0.8	13.77	17.53	2.53	4.91	–	natroalunite
S7	0.167	0.9	16.14	20.36	2.60	4.75	1.07	natroalunite + anhydrite
S8	0.185	0.9	14.55	18.93	2.80	4.72	–	natroalunite
S9	0.231	1.0	10.46	17.92	13.0	3.68	–	natroalunite + mansfieldite

2.2. Hydrothermal experiments

Hydrothermal experiments were conducted in a PARR 4563 autoclave reactor equipped with temperature, pressure and stirring controls. The solutions or slurries containing the reactants were heated at 5 °C /min, then maintained at working temperature for a fixed, nominal time and finally cooled, also at 5 °C /min. The solution volume was 150 mL in all tests. For calcium arsenate waste, the experiments were performed with the slurry obtained after leaching and ozonation. Other conditions are summarized in Table 2. Most of the experiments were performed in presence of the insoluble gypsum, but one was made with prior to gypsum removal by filtration (test P12). After hydrothermal treatment, the precipitates were filtered and washed 5 times with 50 mL of distilled water (each time), dried for 5 days at ambient temperature and finally weighed.

2.3. Characterization of hydrothermal precipitates

Bulk chemical composition was determined by dissolving 0.1 g of the samples in 25 mL of 6 M HCl in a closed vessel that was stirred at 80 °C for 3–4 days. After proper dilution, the resulting solution was analyzed by ICP-OES in a Perkin Elmer Optima 3200RL apparatus. The phase composition was studied by XRD using Bragg-Brentano geometry in a Panalytical X'Pert PRO MDP Alpha 1. Using this method, ≥0.5% of the target phases, natroalunite and mansfieldite (ideally AlAsO₄·2H₂O), were detectable in studied precipitates.

SEM-EDS characterization was performed using a JEOL JSM-840 instrument. An approach of the coefficients of the components in the alunite and mansfieldite formulas was obtained by EDS, since the attempts to obtain these data by EPMA were unsatisfactory due to the large spot size this technique requires compared to the small crystal sizes. These coefficients were computed from the atomic percentage of each element obtained in the mean punctual analysis and assuming a structural basis of S + As + P = 2 in alunite-type compounds (Paktunc and Dutrizac, 2003) and As + P = 1 in the mansfieldite-scorodite series (Le Berre et al., 2007a,b). Samples were dispersed in water and a droplet was placed on a conductive bi-adhesive polymer film. Analyses were conducted from carbon coated mounts using a beam current of 0.6 nA and an acceleration voltage of 20 kV for 30 s

(spot size ~50 nm). The instrument was calibrated using the following standards: quartz (O K_α), albite (Na K_α), orthoclase (Al, K_α), pyrite (S, Fe K_α), apatite (P K_α), wollastonite (Ca K_α) and InAs (As L_α). The spectral results were processed through the INCA-250 software, normalizing to 100% atomic the sum of the amount of all the detected elements (except C). About 10 spots were processed for each sample. Care was taken to analyze individual crystals or clusters free of other phases than those of interest. In some precipitates from the calcium arsenate waste, mansfieldite crystals are very small and always intergrown with natroalunite; for this reason these results were not included. Previously, the single-phase samples of arsenical natroalunites obtained in similar hydrothermal conditions were also analyzed. Formula coefficients determined by EDS were close with those obtained by bulk chemical analysis (ICP) (Tables 3 and 4).

The percentages of anhydrite, natroalunite and mansfieldite in the precipitates from calcium arsenate waste were estimated from the results of the bulk chemical analysis. Anhydrite was calculated from the calcium content, because in conditions we used the degree of substitution of this element in the natroalunite lattice was very small. Natroalunite content was computed from the sodium content and assuming the natroalunite formula obtained by EDS. Mansfieldite content was estimated from the difference between total arsenic and that combined as natroalunite.

2.4. Leaching tests on hydrothermal precipitates

Short-term leaching of selected hydrothermal precipitates from industrial waste, containing natroalunite, natroalunite + mansfieldite and mansfieldite, was studied in the 1–10 pH range at room temperature. Tests were made by treating 0.5 g of precipitate in 50 mL solution placed in an erlenmeyer with magnetic stirring (250 rpm). Solutions of the desired pH were obtained from stock solutions of dilute H₂SO₄ or NaOH. Variations in pH were corrected. For pH < 7 these corrections were sporadic, but for pH > 7, the system required more correction due to a tendency to acidulation. In these tests at pH > 7, variations of 0.5 pH units were virtually inevitable. Three consecutive 24-h leaching tests were performed. After each leaching the precipitate was filtered and the solid underwent the subsequent leaching (without drying). Solutions and blanks were analyzed for As, Cd and occasionally for Al, by ICP-MS in a Perkin Elmer Elan-6000 spectrometer.

Long-term leaching (up to 6 months) was also studied for the same precipitates but only at their natural pH (pH 4–5). For comparison, a single phase sample of synthetic arsenical natroalunite (S6, Table 3) was also studied. Tests were performed with 2.5 g of precipitate in 250 mL of water in a closed erlenmeyer also with magnetic stirring (250 rpm). Samples of 3 mL of slurry were extracted at selected times and filtered. 1 mL of the filtered solution was diluted to 10 mL and finally analyzed for As by ICP-MS. The pH was also occasionally measured throughout the experiments. For all the samples, the pH decreased slightly, but this effect was not very significant.

Table 4
Formula coefficients for synthetic natroalunite samples. (Normalized to S + As = 2).

Test	(AsO ₄ /TO ₄) _{aq}	Bulk chemical analysis (ICP)				EDS				
		S	As	Al	Na	S	As	Al	Na	Ca
S1	0	2	0	2.83	0.75	2	0	2.88 ± 0.10	0.74 ± 0.08	0
S2	0.083	1.93	0.068	2.84	0.88	1.93 ± 0.02	0.074 ± 0.006	2.80 ± 0.10	0.80 ± 0.12	0
S3	0.101	1.92	0.078	2.82	0.87	1.92 ± 0.02	0.086 ± 0.006	2.80 ± 0.14	0.82 ± 0.16	0
S4	0.114	1.91	0.092	2.82	0.83	1.90 ± 0.02	0.100 ± 0.014	2.92 ± 0.08	0.88 ± 0.10	0
S5	0.130	1.88	0.120	2.80	0.89	1.88 ± 0.02	0.126 ± 0.010	2.82 ± 0.08	0.82 ± 0.12	0
S6	0.152	1.85	0.146	2.81	0.92	1.85 ± 0.02	0.152 ± 0.010	2.80 ± 0.08	0.94 ± 0.12	0
S7	0.167	not det., anhydrite present				1.84 ± 0.11	0.160 ± 0.010	2.99 ± 0.18	0.79 ± 0.07	0.04 ± 0.01
S8	0.185	1.85	0.151	2.86	0.84	1.84 ± 0.02	0.160 ± 0.018	2.84 ± 0.10	0.94 ± 0.10	0

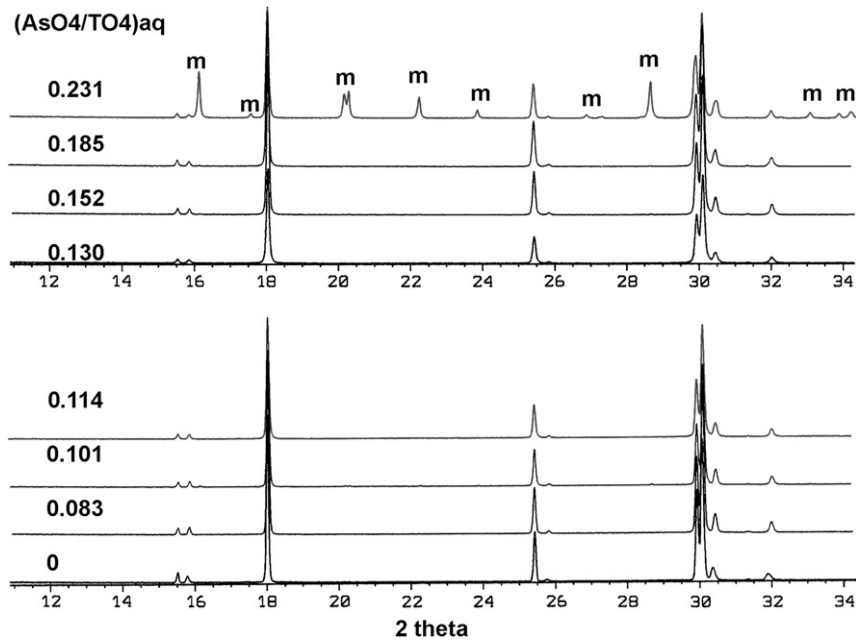


Fig. 1. X ray diffraction patterns for synthetic natroalunite from different $(\text{AsO}_4/\text{TO}_4)_{\text{aq}}$ (200 °C, 120 min. m: mansfieldite).

3. Results and discussion

3.1. Hydrothermal precipitation of synthetic arsenical natroalunite

Fig. 1 shows the X-ray patterns for samples obtained at different $(\text{AsO}_4/\text{TO}_4)_{\text{aq}}$. Below approximately 0.2 $(\text{AsO}_4/\text{TO}_4)_{\text{aq}}$ the only phase was natroalunite, but above this value mansfieldite formed. Precipitation of mansfieldite increased at 0.3 $(\text{AsO}_4/\text{TO}_4)_{\text{aq}}$ (not shown in the figure) and for 0.4 $(\text{AsO}_4/\text{TO}_4)_{\text{aq}}$ natroalunite was not obtained. Instead, mixtures of mansfieldite, alarsite (AlAsO_4) and the sodium analogue of alumpharmacosiderite ($\text{NaAl}_4(\text{AsO}_4)_3(\text{OH})_4 \cdot 7\text{H}_2\text{O}$) appeared (Fig. 2).

Bulk chemical composition (Table 3) showed a continuous arsenic increase in natroalunite as $(\text{AsO}_4/\text{TO}_4)_{\text{aq}}$ increased and abrupt growth when mansfieldite precipitated. Fig. 3 shows the degree of substitution of AsO_4 at the TO_4 site as a function of the molar fraction $(\text{AsO}_4/\text{TO}_4)_{\text{aq}}$ in the starting solution. The plotted interval corresponds to the formation of arsenical natroalunite as the only arsenic phase, which was also confirmed by the similar results from bulk and punctual

compositions (Table 4). $(\text{AsO}_4/\text{TO}_4)_s$ increased linearly with 2.2 as the slope as increased $(\text{AsO}_4/\text{TO}_4)_{\text{aq}}$. So, the results for synthetic natroalunite indicated that a significant arsenic substitution (up to approximately 8% molar) was possible without the generation of other arsenic phases such as mansfieldite. On the other hand, the presence of supersaturated CaSO_4 does not significantly alter the arsenic partition (Test S7).

3.2. Characterization of calcium arsenate waste

Table 5 shows the chemical composition. SEM-EDS characterization indicated that it consisted of 100–200 μm gypsum crystals (~77%) (Fig. 4A) and a precipitate (Fig. 4B) consisting of agglomerates of ~1 μm of spheroid grains. XRD characterization (Fig. 5A) confirmed the amorphous nature of the precipitate, since only gypsum and small amounts of calcite were detected as crystalline phases. The EDS spectra of the precipitate (Fig. 5B) showed Ca, S and As as the most abundant, with the heavy metals Fe, Ni, Cu, and Zn also present.

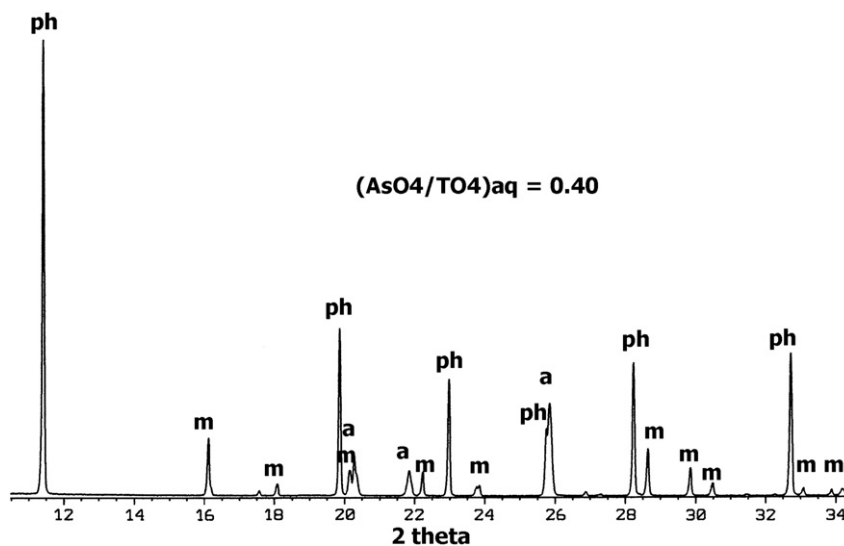


Fig. 2. X ray diffraction pattern of synthetic product at $(\text{AsO}_4/\text{TO}_4)_{\text{aq}} = 0.40$. (200 °C, 120 min. m: mansfieldite, a: alarsite, ph: Na-analogous of alumpharmacosiderite).

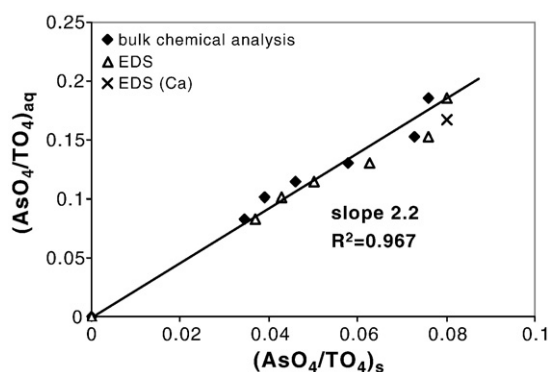


Fig. 3. Molar fraction of As in the starting solution vs molar fraction of As substituting in synthetic natroalunite. (200 °C, 120 min. Ca: In presence of supersaturated CaSO₄).

Cadmium was not well detected by EDS due to its low content. However, all cadmium in the original waste was present in the amorphous precipitate because it was completely solubilized during H₂SO₄ leaching (Table 5) and analysis of the insoluble gypsum showed insignificant cadmium content (<0.004%).

The arsenic solubility of the calcium arsenate waste was very high: at pH 9 (as received) it was 34 mg/L and at pH 7, 150 mg/L (Table 5). Leaching tests with H₂SO₄ (Table 5) showed that at pH 2 the dissolution of arsenic and iron was incomplete, 75% and 10%, respectively, but at pH 1 virtually complete leaching was achieved.

It is well known that arsenic volatilizes as As(III) during copper smelting processes and it can partially remain in this form in the effluents from gas cleaning steps (Vircikova et al., 1999). Oxidation of As(III) to As(V) with ozone in aqueous medium is a very fast process (Dodd et al., 2006) which occurs as:



Ozonation experiments on the waste studied showed an O₃ consumption of about 13 g O₃/kg of waste (Table 2). Because sulfite was not detected in the waste and iron comes from Fe(III) addition, this O₃ consumption was mainly attributed to the presence of As(III). In accordance with this consumption and the reaction stoichiometry (Eq. (2)), about 40% of the arsenic was in the form of As(III) in the original waste.

3.3. Hydrothermal precipitation from calcium arsenate waste

3.3.1. Effect of the initial pH

The effect of initial pH was studied at 200 °C, for 2 h and for a fixed Al/As molar ratio of 1.5 in the liquid phase. At pH 2, SEM/EDS

Table 5
Composition and leaching characteristics of the calcium arsenate waste.

Composition (weight %)										
Ca	S	As	Ni	Fe	Zn	Cu	Cd	Pb	Bi	SiO ₂
22.80	11.37	5.23	2.65	1.08	0.95	0.56	0.17	0.04	0.02	0.86
pH	Solubility (mg/L)									
	As	Ni	Zn	Cu	Cd	Fe				
9 (as received)	34	<0.10	<0.10	0.12	0.14	<0.10				
7	150	3.5	<0.10	0.10	0.31	<0.10				
H ₂ SO ₄ leaching pH	Extraction (%)									
	As	Ni	Zn	Cu	Cd	Fe				
4	69	62	85	31	74	<1				
3	72	78	95	59	89	4				
2	75	94	99	87	96	10				
1.5	96	97	99	95	95	73				
1	99	99	99	99	>99	>99				

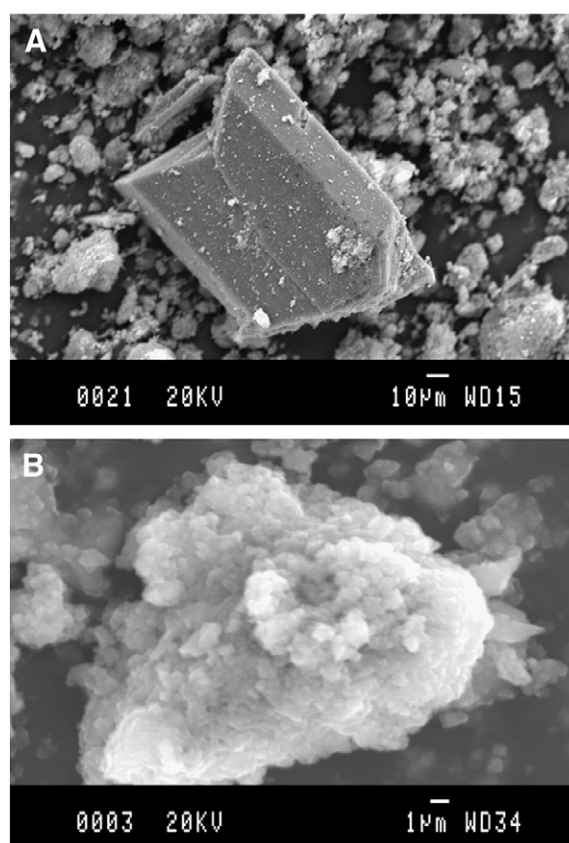


Fig. 4. Calcium arsenate waste: A) Gypsum crystal. B) Amorphous precipitate. (SEM).

observations indicated the formation of anhydrite, poorly crystalline mansfieldite – spherules (~5 µm) with crystals not resolved by SEM and an amorphous precipitate containing As/Fe/Ni/Cu/Zn (Fig. 6A). The results of the chemical composition (Table 6) at an initial pH 2 also showed a significant precipitation of minor elements such as Cu (30%), Zn (13%), Ni (6%) and Cd (63%). At pH 1, the precipitate was crystalline (Figs. 6B, 7), containing anhydrite, mansfieldite and a trace of natroalunite. On the other hand, the precipitation of minor elements – except cadmium – was practically insignificant (Table 6). Thus, for this waste, the production of crystalline precipitates required the prior solubilization of the initial phases containing heavy metals. So, an initial pH of 1 was selected for the subsequent study. This effect was the first difference observed in the behavior of a complex waste with respect to our research using synthetic soluble reagents (Tables 1 and 3), in which, for similar molar ratios, an initial pH < 3 ensured complete crystalline precipitates at 200 °C.

3.3.2. Effect of aluminium sulfate addition

This was studied at 200 °C, for 120 min to determine the effect of the (Al/As)_{aq} molar ratio of the initial solution (Table 2). Sodium concentration was fixed at 0.093 M, giving variable molar ratios Na/Al (from 1.33 to 0.45), but always in excess of the stoichiometric threshold for natroalunite precipitation (Na/Al = 0.333). The total amount of sulfate varied slightly (from 0.70 to 0.85 M), due to the use of aluminum as sulfate salt. However, most of the sulfate in the medium was fixed by its content in the original waste plus that produced in H₂SO₄ leaching. Initial S_{TOT}/As molar ratios only varied between 15 and 18.

Under these conditions, the (Al/As)_{aq} ratio was found to have an important effect on arsenic phase composition at 200 °C (Figs. 7 and 8). For (Al/As)_{aq} = 4.5, arsenic precipitated extensively as a complex natroalunite (~(Na,Ca)(Al,Fe)₃(S,As,P)O₄)₂(OH)₆) (Tables 6 and 7). Decreasing the Al/As ratio increased mansfieldite ((Al,Fe)(As,P)O₄)

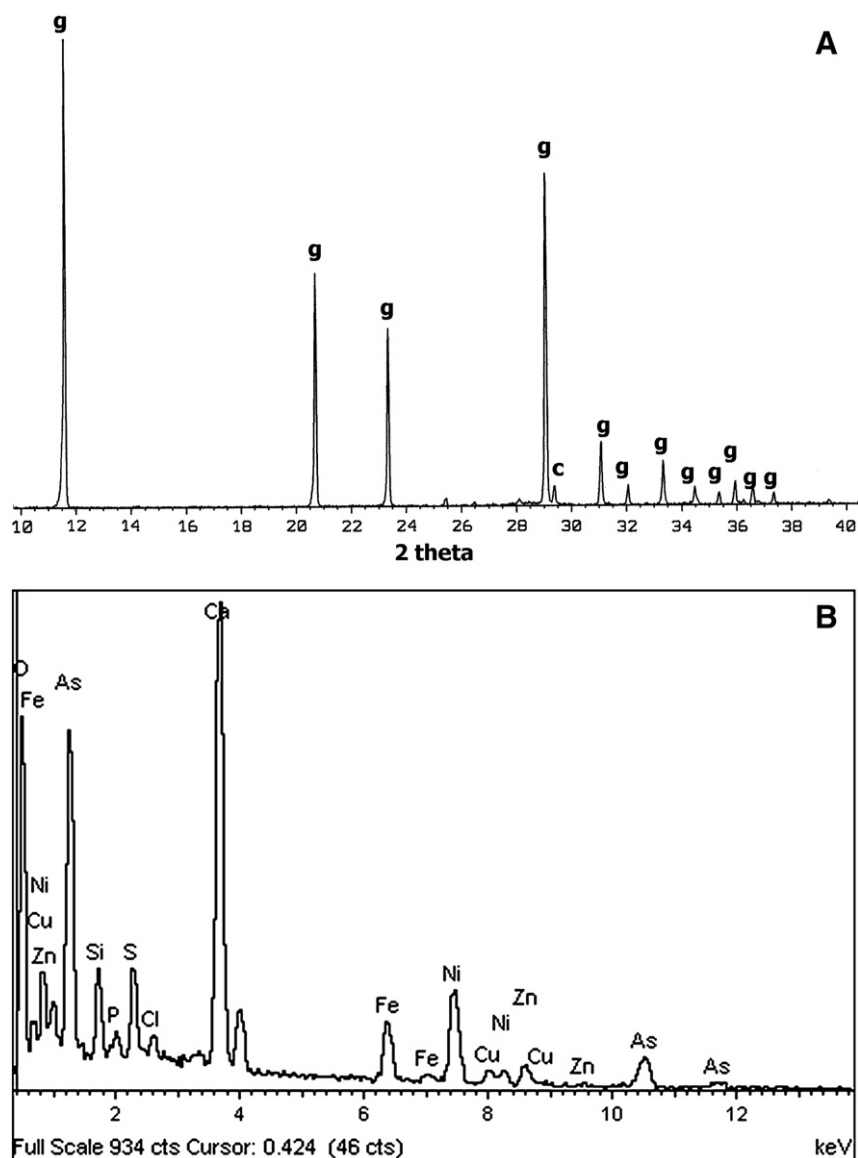


Fig. 5. Calcium arsenate waste: A) XRD pattern of the bulk product (g: gypsum, c: calcite). B) EDS spectrum of the amorphous precipitate.

precipitation. When the $(Al/As)_{aq}$ ratio was 1.5, arsenic precipitated almost exclusively as mansfieldite.

In all cases, the initial calcium from gypsum and arsenates was basically transformed into anhydrite which formed relatively large crystals (10–30 μm). Apparently, anhydrite crystallized fast during the heating stage because natroalunite and mansfieldite usually grow on anhydrite.

3.3.2.1. Natroalunite. Natroalunite appears as clusters of up to $\sim 50 \mu\text{m}$ size, formed by intergrowth of 1–4 μm crystals (Fig. 9A). Crystals were tabular due to the large development of the (001) face. For the waste studied, the size and shape of the natroalunite obtained at 200 °C was not essentially modified by changes in the $(Al/As)_{aq}$ value. However, arsenical natroalunite synthesized under similar conditions (including the presence of gypsum- but from pure reagents (Table 1, sample S7)), forms rhombohedral (pseudo-cubic) crystals (012) (Fig. 9C). The reason for such a difference in the crystal form is not known, but it could be attributable to the presence of impurities in the liquid medium or to minor element substitution (such as Fe).

For the waste studied, the arsenic substitution in natroalunite reached a maximum of about 14% molar in TO_4 (Table 7). This value is

relatively close to those reported for synthetic jarosite, maximum $\sim 17\%$ (Paktunc and Dutrizac, 2003; Savage et al., 2005), in which it is suggested that charge balance could be compensated by partial protonation of AsO_4 and SO_4 in the alunite structure. In the present study, arsenic substitution also depended of the $(Al/As)_{aq}$ ratio: when this ratio increased, arsenic substitution in natroalunite decreased and natroalunite/mansfieldite ratio in the precipitate increased (Fig. 8). For samples containing virtually only natroalunite the arsenic substitution was 7%. This situation was reached at a $(As/(S_{\text{TOT}} + As))_{aq}$ ratio of 0.13 which differs slightly from the same As-substitution in synthetic natroalunite (0.15, Fig. 3). Probably, the presence of small amounts of Fe(III) (or other impurities) from calcium arsenate waste may slightly alter the arsenic partition observed for synthetic samples.

The $(Al + Fe)$ coefficient in natroalunite was always deficient (2.8 ± 0.1 , Tables 4 and 7) both for synthetic and waste products. This trivalent deficit is also common in synthetic arsenical jarosites (Demopoulos et al., 2003; Savage et al., 2005). It has been suggested that this deficit could be related to arsenic substitution in the crystal structure, because the large AsO_4 group substituting in the tetrahedral SO_4 sites could be accommodated due to the deficiencies in the Fe-O(OH) octahedral sites. However, no clear correlation was

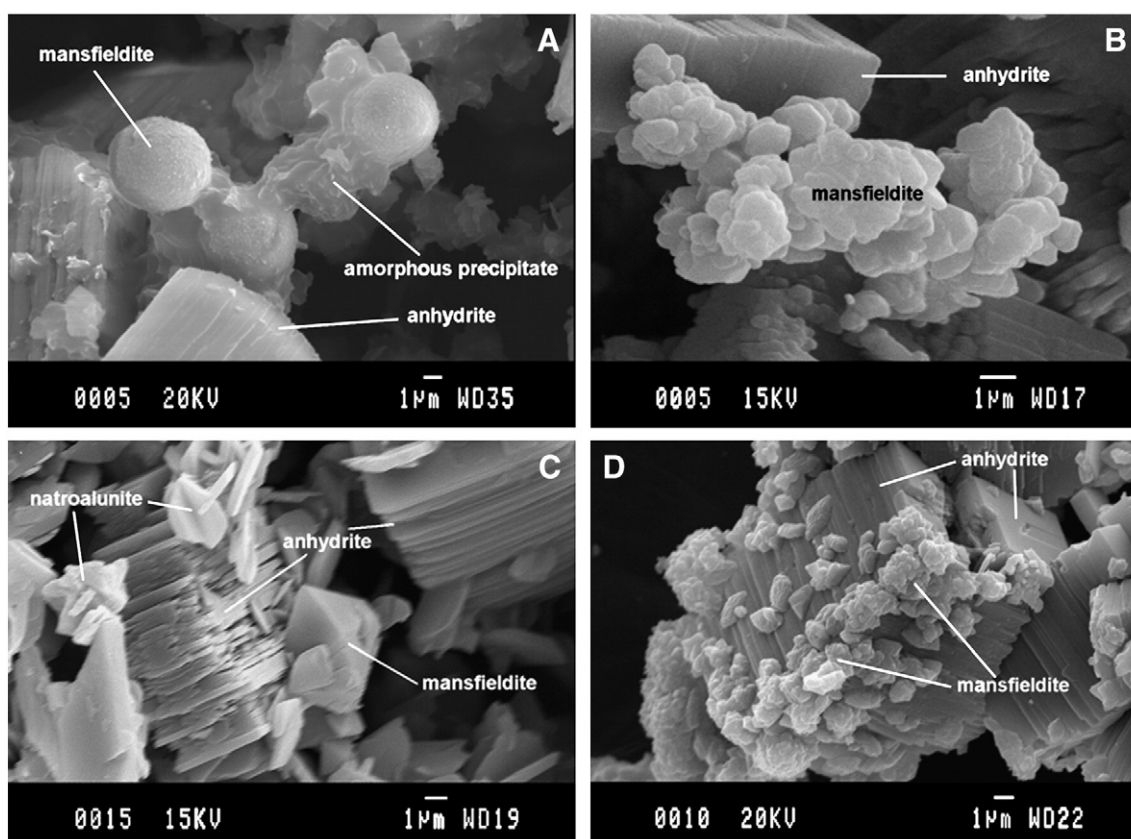


Fig. 6. Mansfieldite from hydrothermal treatment of the calcium arsenate waste (120 min): A) 200 °C, (Al/As)_{aq} = 1.5, pH_i 2. B) 200 °C, (Al/As)_{aq} = 1.5, pH_i 1. C) 200 °C, (Al/As)_{aq} = 3.0, pH_i 1. D) 180 °C, (Al/As)_{aq} = 3.0, pH_i 1. (SEM).

observed between the trivalent deficit and arsenic substitution in the present study for natroalunite.

Iron substitution for aluminium in natroalunite from waste was 0.12 in the formula, when this phase was virtually the exclusive arsenic compound, but it decreased to 0.08 when large amounts of mansfieldite precipitated. Small amounts of phosphorous present as traces in the initial waste also substitute to 1–2% molar in the TO₄ group. Recently, *Dutrizac and Chen (2010)* also reported small PO₄³⁻ substitution in sodium and potassium jarosites, but Cu, Ni, Zn and Cd were not detected by EDS in the natroalunite crystals.

In the conditions studied, calcium substitution in the natroalunite lattice was very limited (0.04–0.08 in formula, *Tables 4 and 7*),

compared to natural calcium-rich alunite (mineral minamiite (Na,Ca,K)Al₃(SO₄)₂(OH)₆), in which it can reach up to 0.3 (*Osaka et al, 1982*). On the other hand, Ca/As rich phases, such as slossmacherite ((H₃O,Ca)Al₃(AsO₄,SO₄)(OH)₆) or arsenocrandallite (CaAl₃(AsO₄)₂(OH)₅(H₂O)) were not formed under our conditions. Thus, the large excess of calcium in the system studied does not contribute significantly to the charge balance, or consequently to the increase in arsenic substitution in the alunite phase.

XRD patterns (*Figs. 1 and 7*) show narrow natroalunite peaks for all the samples. However, there was observed a slight peak displacement with respect to the standard natroalunite (PDF 41-1467) to smaller diffraction angles. This could indicate that the arsenic

Table 6

Bulk chemical composition (ICP) and approximate phase composition of precipitates from calcium arsenate waste (n: natroalunite; m: mansfieldite; a: anhydrite).

(Al/As) _{aq}	Temp (°C)	Time (min)	pH _i	pH _f	Bulk composition (weight %)										Phase composition (%)		
					S	As	Al	Fe	Ca	Na	Cd	Ni	Zn	Cu	n	m	a
1.50	200	120	2.0	1.6	19.0	3.77	2.66	1.34	22.5	0.26	0.15	0.22	0.18	0.24	–	~23*	~77
1.50	200	120	1.0	0.8	20.0	3.34	0.88	1.12	24.5	0.07	0.13	0.006	0.03	0.06	~1	~10	~85
2.25	200	120	1.0	0.7	19.2	3.41	2.64	1.23	21.6	0.65	0.13	0.01	0.03	0.02	~8	~12	~75
3.00	180	15	1.0	0.9	20.5	2.60	3.73	1.01	22.8	1.00	0.13	0.03	0.03	0.05	~18	~5	~77
3.00	180	30	1.0	0.8	20.4	3.05	3.85	1.05	21.7	1.09	0.12	0.05	0.04	0.04	~19	~6	~75
3.00	180	120	1.0	0.8	19.7	3.60	3.83	1.05	21.8	0.96	0.12	0.06	0.03	0.04	~17	~8	~75
3.00	200	15	1.0	0.7	21.0	2.41	4.04	1.10	22.1	1.10	0.13	0.008	0.02	0.02	~20	~5	~75
3.00	200	30	1.0	0.7	20.4	2.50	4.01	1.15	21.6	1.05	0.12	0.01	0.02	0.04	~20	~5	~75
3.00	200	120	1.0	0.7	19.7	2.67	4.20	1.16	20.6	1.15	0.12	0.008	0.02	0.04	~20	~5	~70
3.00**	200	120	1.0	0.5	19.3	2.45	3.69	1.07	22.4	1.11	0.12	0.009	0.03	0.03	~19	~5	~75
3.00***	200	120	1.0	0.5	11.5	9.85	16.2	4.22	0.13	4.49	0.004	0.008	0.02	0.04	~80	~20	–
4.50	200	120	1.0	0.7	19.4	1.10	5.98	0.94	18.4	1.60	0.09	<0.001	0.008	0.05	~30	~2	~65

* : mansfieldite + amorphous phase.

** : As concentration (7.0 g/L) double than in the rest of experiments.

*** : with prior gypsum removal.

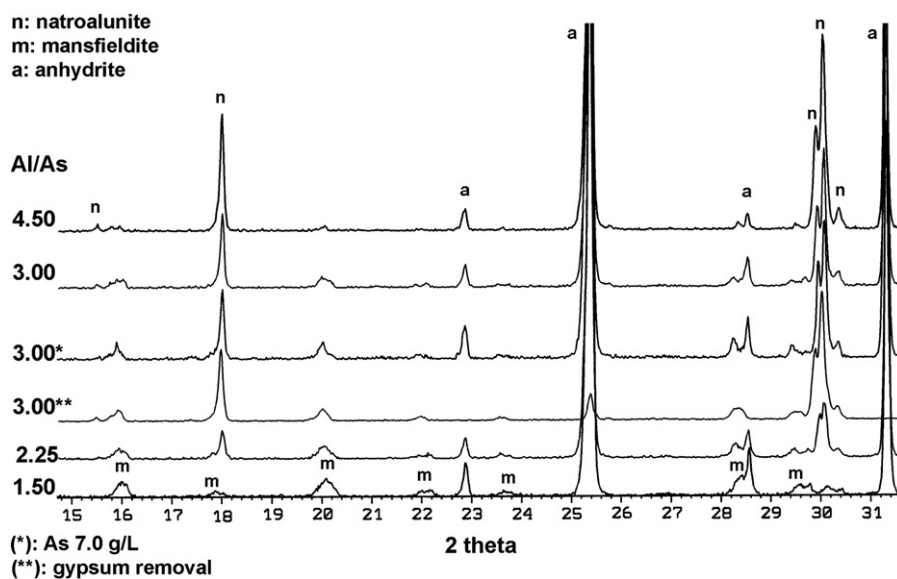


Fig. 7. XRD patterns of precipitates from calcium arsenate waste for different $(Al/As)_{aq}$ ratios (200 °C, 120 min, $pH_1 = 1$).

substitution increased alunite cell volume, as reported for arsenic substitution in jarosite (Paktunc and Dutrizac, 2003). However, our results were not conclusive, since the effect was not very pronounced (maximum ~ 0.05 Å in cell parameters) and other substitutions, such as Fe^{3+} in the trivalent site as well as Ca^{2+} and H_3O^+ in the alkali site, may also affect the cell dimensions. Structural research on arsenic substitution in complex natroalunites is currently underway.

3.3.2.2. Mansfieldite. Mansfieldite morphology changed as a function of its degree of precipitation. When it was formed in large amounts, mansfieldite appeared as relatively large clusters on anhydrite, but as very small, poorly developed crystals ($\leq 1 \mu m$, Fig. 6B). With decreasing mansfieldite precipitation, this phase tends to increase in crystal size (up to $\sim 4 \mu m$), usually appearing as isolated grains on anhydrite (Fig. 6C) or on natroalunite clusters. Under these conditions crystals were sharp pyramidal (111). Mansfieldite also incorporated iron from the original waste, because mansfieldite and scorodite form a solid solution series (Le Berre et al., 2007b). The observed substitution was between 24% and 34% (Table 7). Phosphorous also showed a small substitution (up to 5%), since phosphate analogous (variscite $(AlPO_4 \cdot 2H_2O)$) is isostructural. XRD patterns showed peaks for mansfieldite located at standard positions (PDF 23-0123). However, in contrast to natroalunite and synthetic mansfieldite (Figs. 1 and 2), mansfieldite peaks from the waste were very broad

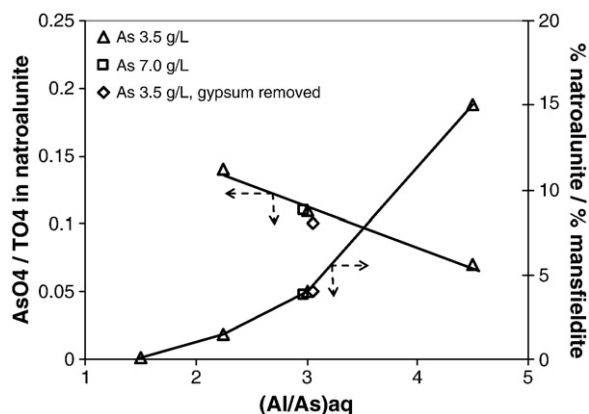


Fig. 8. Effect of $(Al/As)_{aq}$ on phase composition of precipitates from calcium arsenate waste (200 °C, 120 min).

(Figs. 7 and 11), suggesting multiple reflections caused by different compositional domains.

3.3.2.3. Precipitation yields. The effect of the $(Al/As)_{aq}$ molar ratio on precipitation yields at 200 °C, 120 min, is shown in Fig. 10, reflecting the discussed effect on phase composition. The sodium yield was negligible at $(Al/As)_{aq} = 1.5$, but increased continuously as natroalunite precipitation increased. The aluminium yield was low ($\sim 20\%$) at $(Al/As)_{aq} = 1.5$, because there was only mansfieldite as the Al phase, but also increased (up to 60%) due to the natroalunite precipitation. The arsenic yield was maximum ($\sim 50\%$) when mansfieldite precipitation was abundant and minimum ($\sim 20\%$) when natroalunite was practically the only arsenic phase precipitated. However, for $(As/Al)_{aq} = 3.0$, a moderate arsenic yield can be achieved ($\sim 40\%$) with the formation of only small amounts of mansfieldite ($\sim 5\%$). Iron precipitation yield was high (80–90%) as a consequence of apparent preferential precipitation of Fe vs Al on both mansfieldite and natroalunite. Le Berre et al. (2007a,b) reported a similar effect during the synthesis of the mansfieldite-scorodite solid solution series. Finally, cadmium precipitation yield (50–60%) was also independent of mansfieldite or natroalunite precipitation, suggesting that this minor element was associated to anhydrite (See 3.3.5).

3.3.3. Effect of arsenic concentration

The effect of arsenic concentration was only studied in the 3.5–7.0 g/L interval, fixing $(Al/As)_{aq} = 3.0$ at 200 °C, 120 min. This was achieved by dissolving double the amount of waste in 150 mL solution and adding double the amount of reagents (Test P6). No significant differences were observed in the arsenic phase relationship (Figs. 7 and 8), its size or morphology, nor in the precipitation yields (Fig. 10). Natroalunite composition was essentially the same, but it seems that an increase in iron concentration due to dissolving double the amount of waste slightly increased the iron content in mansfieldite (from 0.28 to 0.34).

3.3.4. Reaction time

This effect was studied for $(Al/As)_{aq} = 3.0$ at 180 °C and 200 °C. At 200 °C hydrothermal precipitation was very fast (< 15 min) because in the interval studied no significant effect was observed on the yield, phase ratio (Figs. 11 and 12), phase composition (Table 7) or morphology. At 180 °C, natroalunite precipitation was also very fast (< 15 min), maintaining similar arsenic substitution but slightly decreasing in crystal size to 1–3 μm . However, the most important effect at 180 °C was on mansfieldite precipitation which increased

Table 7
Formula coefficients of phases obtained from calcium arsenate waste (EDS).

(Al/As) _{aq}	Temp (°C)	Time (min)	Natroalunite (based on S + As + P = 2)							Mansfieldite (based on As + P = 1)			
			As	S	P	Al	Fe	Na	Ca	As	P	Al	Fe
1.50	200	120	Not determined (trace)										
2.25	200	120	0.28	1.68	0.04	2.70	0.08	0.90	0.04	0.95	0.05	0.69	0.31
3.00	180	15	0.26	1.70	0.04	2.78	0.10	0.94	0.07	Not determined (small grains)			
3.00	180	30	0.28	1.68	0.04	2.70	0.08	0.98	0.08	Not determined (small grains)			
3.00	180	120	0.28	1.70	0.02	2.74	0.08	0.98	0.07	Not determined (small grains)			
3.00	200	15	0.28	1.70	0.02	2.67	0.12	0.98	0.08	Not determined (small grains)			
3.00	200	30	0.24	1.72	0.04	2.63	0.09	0.96	0.07	Not determined (small grains)			
3.00	200	120	0.22	1.76	0.02	2.69	0.12	0.96	0.08	0.97	0.03	0.78	0.28
3.00*	200	120	0.22	1.74	0.04	2.65	0.09	1.00	0.08	0.98	0.02	0.66	0.34
3.00**	200	120	0.20	1.80	0.00	2.82	0.15	1.00	0.00	0.96	0.04	0.76	0.24
4.50	200	120	0.14	1.84	0.02	2.70	0.12	0.98	0.08	Not determined (trace)			

* As concentration (7.0 g/L) double that in the rest of experiments.

** With prior gypsum removal.

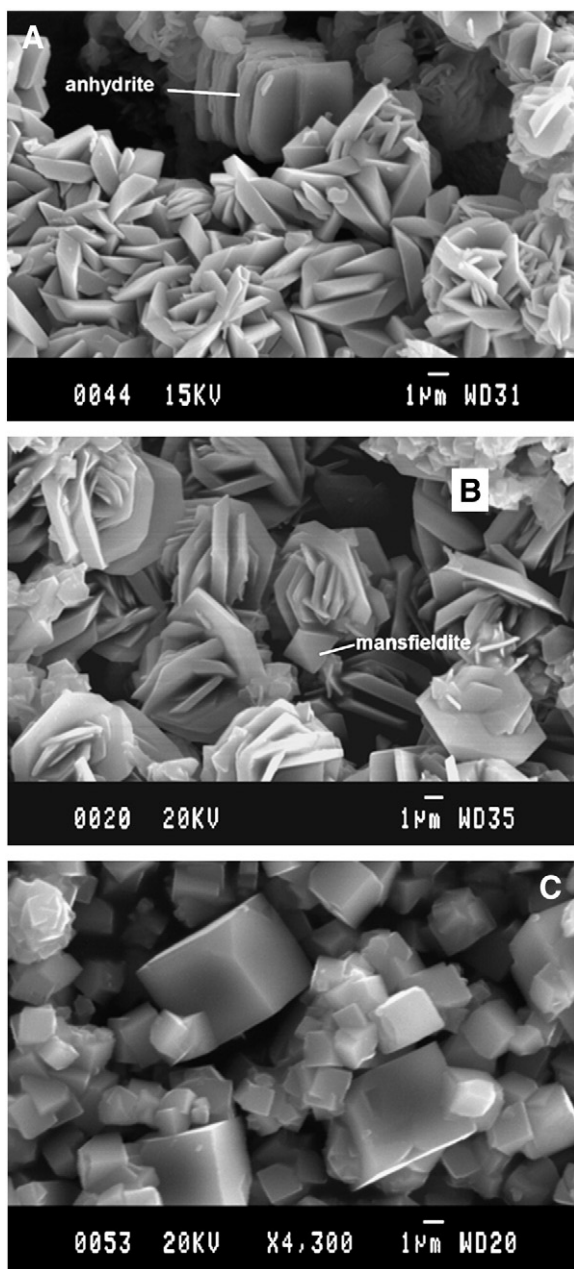


Fig. 9. Arsenical natroalunite: A) From calcium arsenate waste in presence of gypsum (test P5). B) Id. in absence of gypsum (test P12). C) Synthesized from pure reagents (test S7). (SEM).

with reaction time (Figs. 11 and 12). Under these conditions mansfieldite formed crusts of minute (<1 μm), rounded crystals on anhydrite (Fig. 6D), in contrast to the larger and sharper crystals obtained at 200 °C (Fig. 6C). Thus, our results suggest that in the strong acid medium generated by natroalunite precipitation (final pH ~0.6, Eq. (1)), poorly crystalline mansfieldite was unstable at 200 °C, and for this reason, temperatures <200 °C seem to be unfavorable for improving the chemical stability of precipitates.

3.3.5. Effect of gypsum removal

The effect of gypsum removal was studied at 200 °C, 120 min and for (Al/As)_{aq} = 3.0 (Test P12). In the absence of anhydrite, natroalunite

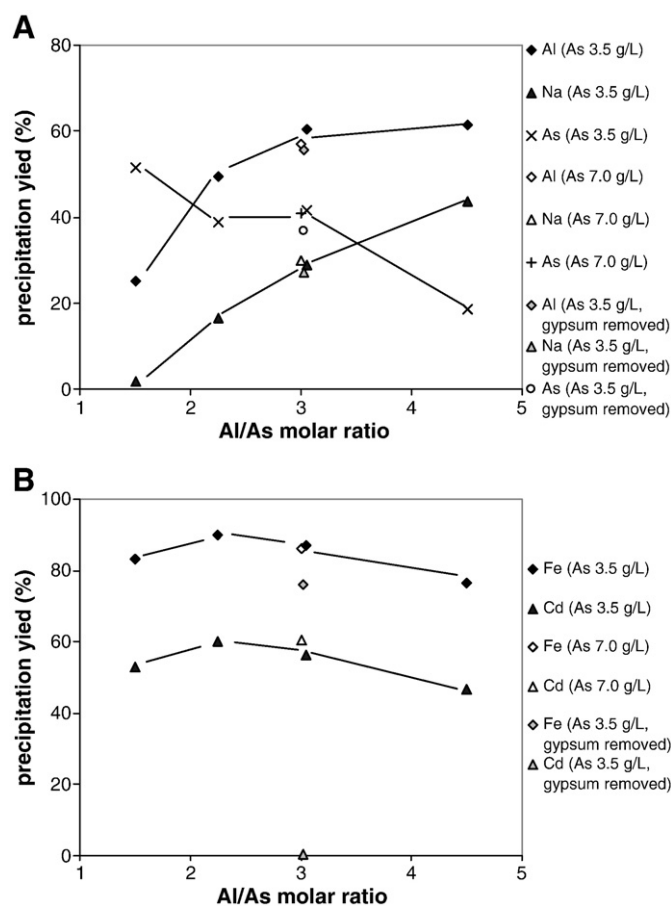


Fig. 10. Effect of (Al/As)_{aq} ratio on precipitation yields from calcium arsenate waste (200 °C, 120 min).

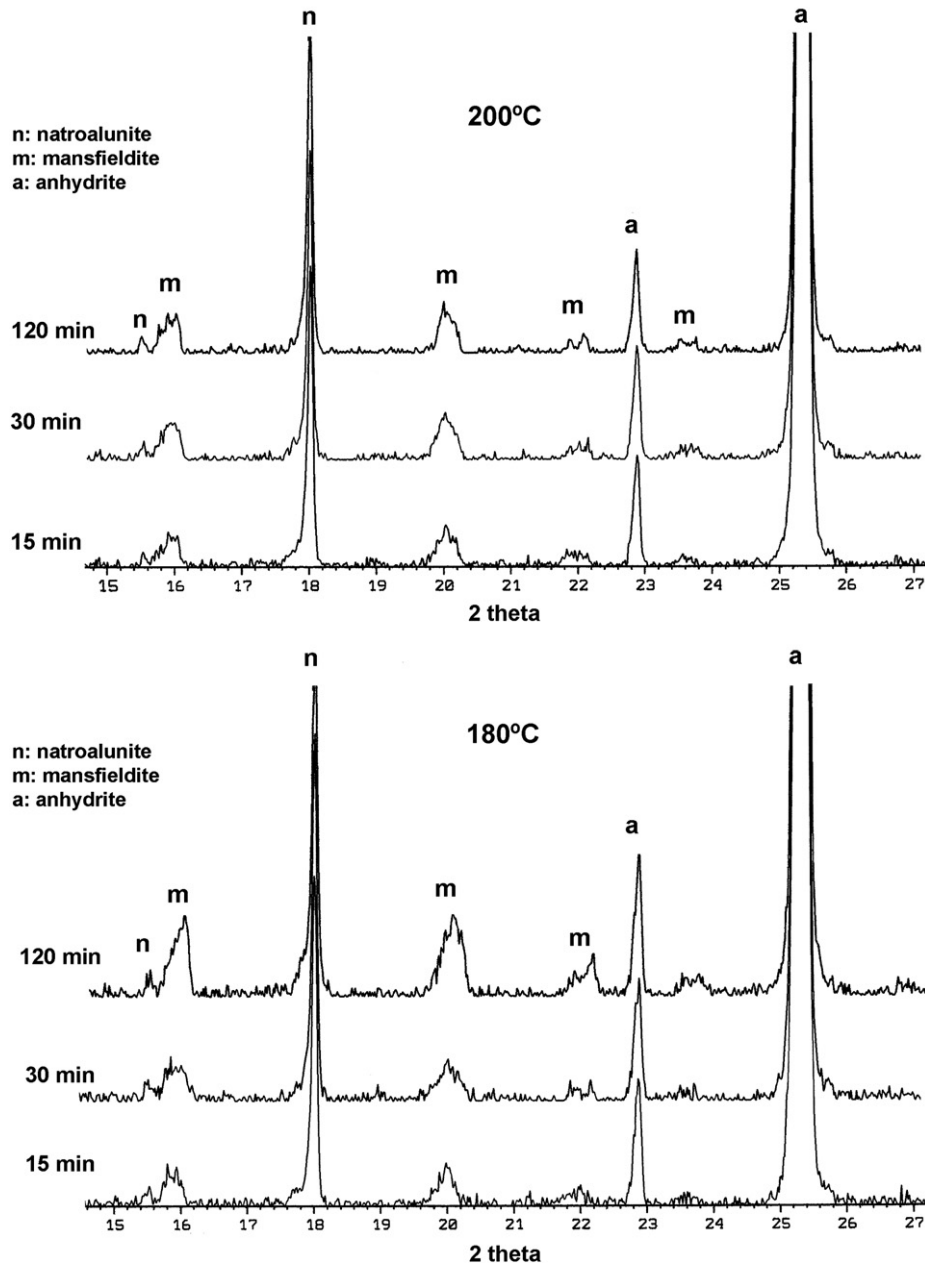


Fig. 11. XRD patterns showing the effect of the reaction time from calcium arsenate waste ($(Al/As)_{aq} = 3.0$).

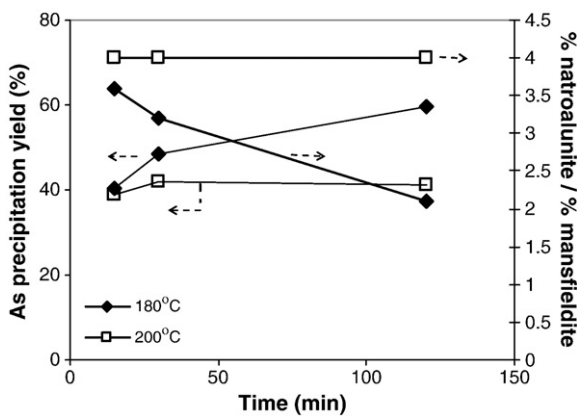


Fig. 12. Effect of the reaction time on As precipitation yield and phase ratio (Calcium arsenate waste ($(Al/As)_{aq} = 3.0$)).

crystals showed the same morphology but increased in size, up to about $8 \mu\text{m}$ (Fig. 9B). Probably, the absence of anhydrite makes natroalunite nucleation difficult, which favors its crystal growth. However, no significant changes were observed in the ratio of the arsenic phases, their composition (Fig. 8, Table 7) or the precipitation yield, except for cadmium (Fig. 10).

Thus, the major effect of gypsum removal was on the cadmium removal from hydrothermal precipitates (Table 6), indicating that this element was incorporated into the anhydrite structure. This substitution was cited by Van Der Sluis et al. (1986) and Kontrec et al. (2003), and is not surprising given the similarity of ionic radii (Ca^{2+} : 0.099 nm; Cd^{2+} : 0.097 nm), despite anhydrite (PDF 24-1035) and anhydrous cadmium sulfate (PDF 15-0084) not being isostructural. The content of cadmium in the anhydrite obtained in our experiments was estimated in about 0.2%. For this reason cadmium was not clearly detected by EDS analysis, but the content of cadmium correlates with the anhydrite content in the precipitates (Fig. 13).

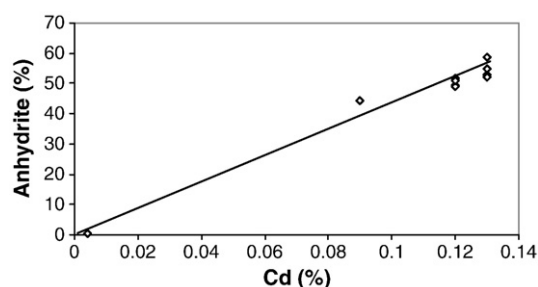


Fig. 13. Correlation between the anhydrite and cadmium contents in precipitates from calcium arsenate waste (200 °C, 120 min, various (Al/As)_{aq}).

3.4. Solubility of the hydrothermal precipitates

3.4.1. Arsenic solubility

3.4.1.1. Short-term leaching. Fig. 14 shows the results of three consecutive (24-h) leaching tests for selected samples. Except for sample P12, which was free from anhydrite, the solubilities do not correspond to pure water, but correspond to saturated calcium sulfate solutions. At each pH, in general terms, the results of the first leach are slightly higher than the second and third leach, which were practically identical. The first leach data may reflect adsorption of aqueous arsenic species, but it was especially relevant from a technical point of view, because it may show an approach to effectiveness of a conventional washing. In all cases, the first leaching at natural pH (~5) showed satisfactory values (<1 mg/L As) for EPA tests (Caetano et al., 2009).

Maximum solubilities for all the samples occurred at pH 1. In samples consisting of mansfieldite (P2) or containing minor mansfieldite (P4) these values are around 2 mg/L As in the three consecutive tests, whereas for natrolunite with very small amounts of mansfieldite (P5) the solubility falls to <1 mg/L in the 2nd and 3rd leach. In all samples, however, these low values at pH 1 are strongly indicative of the absence of amorphous arsenates. On the other hand, the stability of arsenian natrolunite and mansfieldite in the acid medium with respect to scorodite seems evident, because at pH 1 reported values for scorodite are 50–100 mg/L As (Krause and Ettel, 1989; Swash et al., 2000). A probably related effect was observed by Le Berre et al. (2007b) who indicated the difficulty of dissolving aluminum arsenate phases in strong acid media.

Also, for all samples, arsenic solubilities decreased when pH increased, reaching minimum values at pH 6–8. These were around 0.1 mg/L in mansfieldite (P2), 0.02 mg/L in natrolunite with minor mansfieldite (P4) and 0.01 mg/L in natrolunite with a trace of mansfieldite (P5). In sample P12, free from anhydrite, the solubility at pH 4.5 was similar to that of sample P4, which contained the same ratio of the arsenic phases - but in the presence of anhydrite. Thus, it was confirmed that anhydrite does not entrain significant arsenic.

The reported arsenic solubilities for scorodite obtained from pure As(V)/Fe(III) solutions, indicate minimum values of between 0.1 and 1 mg/L at pH ~5, increasing to 1–10 mg/L at pH ~7 (Krause and Ettel, 1989; Swash et al., 2000; Bluteau and Demopoulos, 2007). Recently, Fujita et al (2009a) showed that the solubility of scorodite obtained using their synthesis method also depends on crystal size and precipitation time. For small crystals and a short precipitation time (1 h) the reported solubility at pH ~5 was 1.5 mg/L. For 3 h it was ~0.5 mg/L and for 7 h <0.1 mg/L, when scorodite crystals reached 10 μm in size.

The results for arsenical natrolunite indicate that this phase is more stable than mansfieldite, as also confirmed through the aluminium extraction (Fig. 15). The major disadvantage could be the limited arsenic substitution which impeded a high yield in a single precipitation step. However, as natrolunite precipitation at 200 °C is

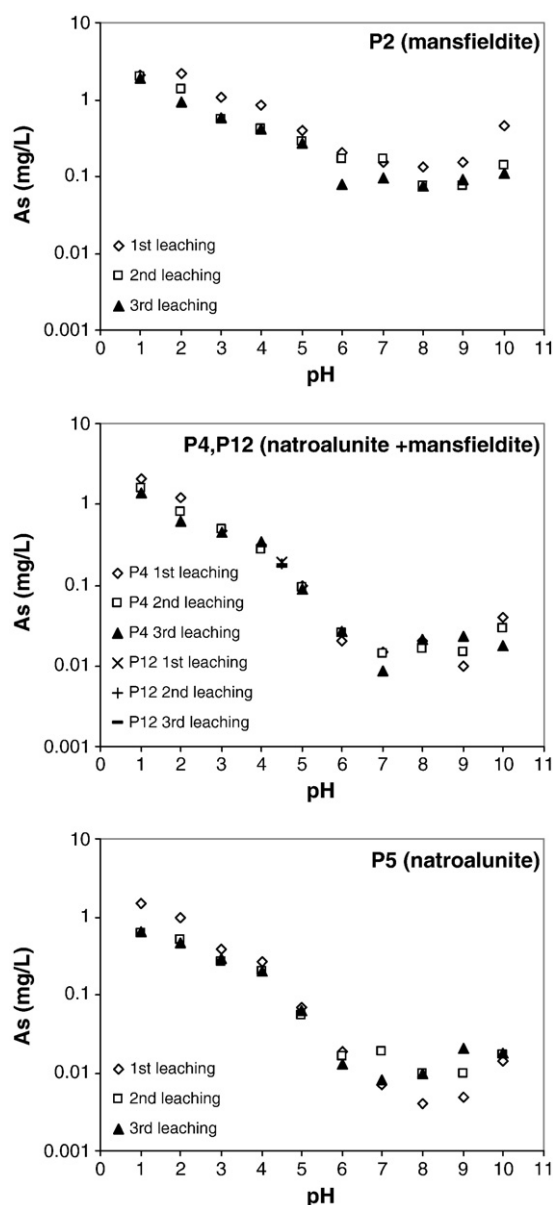


Fig. 14. Arsenic solubilities (24 h) for selected precipitates from calcium arsenate waste.

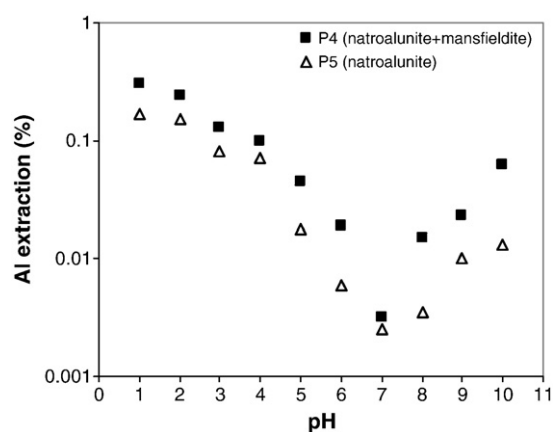
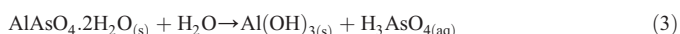


Fig. 15. Aluminium extraction for selected precipitates from calcium arsenate waste (24 h, data from 2nd leaching).

very fast, this yield could be significantly improved by semi-continuous addition of reagents (chiefly Al^{3+}) in a single hydrothermal operation. Mixtures of natroalunite with minor amounts of mansfieldite as large crystals (P4) showed very good arsenic solubility in short-term leaching (0.02 mg/L at pH 7), with the advantage that precipitation yield in a single step was doubled. However, Bluteau and Demopoulos (2007) and Le Berre et al. (2007a,b) showed that these short-term leaching results can be insufficient for evaluating the behavior in long-term storage of phases such as scorodite or mansfieldite, because slow incongruent dissolution processes may take place at neutral or near neutral pH's.

3.4.1.2. Long-term leaching. Long-term solubility was studied for the same samples used in previous short-term tests, as well as for a sample of synthetic arsenical natroalunite (Table 3, S6). Samples were not previous washed, except after hydrothermal precipitation. Fig. 16 shows arsenic concentration as a function of time at natural pH (4–5). In all cases, arsenic concentration increased with leaching time up to about 5 weeks, after which it was observed that mansfieldite had a very slow leaching rate and that for natroalunite an apparent equilibrium was reached. Samples containing virtually only natroalunite (P5) and the synthetic sample (S6) exhibit near identical long-term behavior, stabilizing arsenic concentration at ~0.1 mg/L, which can be considered a very good value for a complex precipitate obtained from real waste. Bluteau and Demopoulos (2007) reported a stabilized value of ~0.5 mg/L As for pure, previously equilibrated, scorodite at this pH. XRD patterns of the leach products are identical to those of the initial samples except for the transformation of anhydrite to gypsum in sample P5.

In contrast to natroalunite, samples containing significant amounts of mansfieldite exhibited high long-term solubility, reaching arsenic concentrations of 5–10 mg/L in 6 months. These results are in accordance with the studies of Le Berre et al. (2007a,b) which indicate that synthetic mansfieldite was more reactive than scorodite in long-term leaching at neutral or near neutral pH. For this reason and despite their acceptable short-term leachability, precipitates with significant amounts of mansfieldite seem to be ineffective as carriers for long-term arsenic stabilization. Decomposition of mansfieldite probably occurs via incongruent dissolution forming aluminium hydroxide and releasing soluble arsenate species (Le Berre et al., 2007b):



However, in our studies, no crystalline $\text{Al}(\text{OH})_3$ was observed by XRD in leached residues of P2 and P4 samples.

3.4.2. Cadmium solubility

The (24-h) solubility of cadmium in precipitates containing anhydrite was practically independent of the other phase composition (Fig. 17). On the other hand, the solubility (~4 mg/L) was also

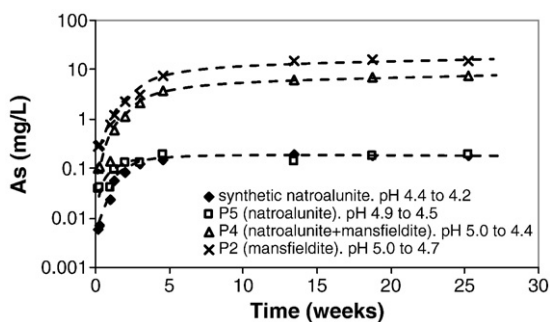


Fig. 16. As concentration as a function of time from different precipitates from calcium arsenate waste and from synthetic natroalunite (S6).

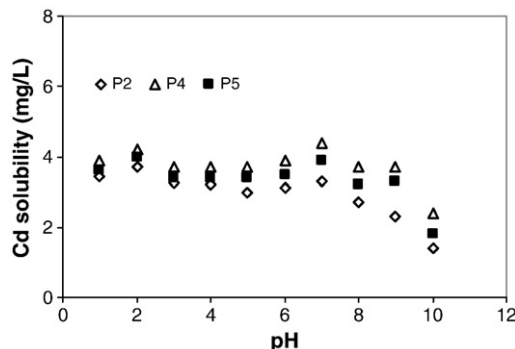


Fig. 17. Cadmium solubilities in precipitates from calcium arsenate waste (24 h, 1st leaching tests).

practically independent of pH in the 1–9 range, decreasing to approximately 2 mg/L at pH 10. This was consistent with the assumption that cadmium substitutes in the anhydrite lattice and consequently, cadmium solubility depends chiefly on the anhydrite solubilization. Fig. 18 correlates the solubilities of cadmium and calcium obtained in all the leaching tests. The solubility of cadmium in precipitates free from anhydrite (test P12) was studied at pH 4.5. The solubility was <0.01 mg/L in the three consecutive leachings, confirming that the prior gypsum separation solved the problem of cadmium release in the hydrothermal precipitates.

However, prior gypsum separation probably results in a major problem such as the generation of large amounts of arsenic contaminated gypsum. Gypsum obtained after leaching the studied waste at pH 1 and conventionally washed did not contain significant cadmium (<0.004%), but contained some arsenic (0.11%). Leaching tests (24 h) showed only 0.06 mg/L Cd, but 2.8 mg/L As. It is probable that a more efficient washing treatment would reduce these arsenic levels but, as suggested by Fujita et al. (2009b), not to satisfactory arsenic values for gypsum commercialization or disposal. For this reason, it seems that the cadmium problem can only be solved by prior removal of this element from the initial plant effluent.

4. Conclusions

Natroalunite precipitation at 200 °C from synthetic reagents reached up to ~8% molar substitution of As in the TO_4 group, without co-precipitation of other arsenic phases. This was achieved for solutions containing ~80% molar ($\text{SO}_4/(\text{SO}_4 + \text{AsO}_4)$), offering an alternative for arsenic stabilization from wastes with similarly large (SO_4/AsO_4) ratios, such as “calcium arsenates” from effluent cleaning in copper metallurgy. The procedure may solve the problem of production of intermediate arsenical gypsum because it is

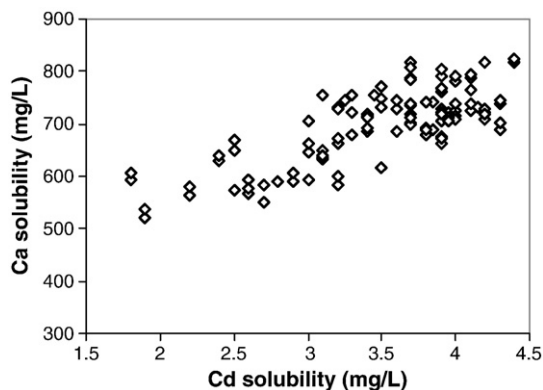


Fig. 18. Correlation between Ca & Cd solubilities for precipitates from calcium arsenate waste containing anhydrite. (1–10 pH range in consecutive tests).

transformed into arsenic-free anhydrite. The precipitation rate at 200 °C is very fast (<15 min).

Natroalunite, precipitated from calcium arsenate waste, is a complex phase in which Fe, Ca and P were also substituted in small amounts. However, under the conditions studied, Ca substitution was very low (~0.04 in the formula) and it did not significantly improve the charge balance for the arsenic substitution. For $\text{pH}_i \leq 1$, Ni, Cu and Zn do not precipitate in appreciable amounts.

Natroalunite composition and the natroalunite/mansfieldite ratio in precipitates at 200 °C depend chiefly on the $(\text{Al}/\text{As})_{\text{aq}}$ molar ratio. For $(\text{Al}/\text{As})_{\text{aq}} = 4.5$, natroalunite was virtually the only arsenic phase. Decreasing the $(\text{Al}/\text{As})_{\text{aq}}$ ratio increased arsenic substitution in natroalunite (up to ~14%) but mansfieldite co-precipitated. Other effects such as reaction time (in the interval 15–120 min.), arsenic concentration in the range 3.5–7.0 g/L and prior gypsum removal did not significantly alter the arsenic phase ratio or composition of the arsenic phases. However, treatment at 180 °C increased mansfieldite content in the precipitates.

The stability of arsenical natroalunite and mixtures with small amounts of mansfieldite in short-term leaching (24 h) was good over a wide range of pH, reaching minimum values for As of 0.01–0.02 mg/L at pH ~7. Arsenical natroalunite obtained from the waste studied also seems suitable for long-term storage. At its natural pH (4–5), arsenic solubility remained stabilized at ~0.1 mg/L for 6 months. However, mansfieldite was not stable in long-term leaching, giving arsenic concentrations of 5–10 mg/L under the same conditions. One major disadvantage for arsenic stabilization as natroalunite was the limited arsenic precipitation yield caused by the low arsenic partition between the solid and aqueous phases. Technically however, as the precipitation rate is very fast, these yields could be significantly improved by semi-continuous addition of reagents in a single hydrothermal operation. Another disadvantage was the incorporation of cadmium into the anhydrite structure which caused cadmium release in the leachates. This problem only seems to be overcome by prior removal of this element from the plant effluent.

Acknowledgements

The financial support of the Spanish *Ministerio de Ciencia e Innovación (DGI) (Programa de Materiales, MAT 2007-61466)* is gratefully acknowledged. We also thank the *Serveis Científicotècnics de la Universitat de Barcelona* for their assistance with instrumentation for the characterization studies.

References

Alcové, X., Bassas, J., Tarruella, I., Roca, A., Viñals, J., 2001. Structural characterization of beudantite-type phases by Rietveld refinements. *Materials Science Forum* 378, 671–676.

Bluteau, M.C., Demopoulos, G.P., 2007. The incongruent dissolution of scorodite – Solubility, kinetics and mechanism. *Hydrometallurgy* 87, 163–177.

Bluteau, M.C., Becze, L., Demopoulos, G.P., 2009. The dissolution of scorodite in gypsum-saturated waters: Evidence of Ca-Fe-AsO₄ mineral formation and its impact on arsenic retention. *Hydrometallurgy* 97, 221–227.

Caetano, M., Ciminelli, V., Rocha, S., Spitale, M., Caldeira, C., 2009. Batch and continuous precipitation of scorodite from dilute industrial solutions. *Hydrometallurgy* 95, 44–52.

Demopoulos, G., Droppert, D., Van Weert, G., 1995. Precipitation of crystalline scorodite from chloride solutions. *Hydrometallurgy* 38, 245–261.

Demopoulos, G.P., Lagno, F., Wang, Q., Singhana, S., 2003. The atmospheric scorodite process. In: Riveros, P., Dixon, D., Dreisinger, D., Menacho, J. (Eds.), *Proceedings Copper 2003*, Santiago, Chile: TMS, Warrendale, vol. VI(2), pp. 597–616.

Dodd, M.C., Vu, N.D., Ammann, A., Le, V.C., Kissner, R., Pham, H.V., Cao, T.H., Berg, M., Von Gunten, U., 2006. Kinetics and mechanistic aspects of As(III) oxidation by aqueous chlorine, chloramines and ozone: Relevance to drinking water treatment. *Environmental Science and Technology* 40 (10), 3285–3292.

Dutrizac, J.E., Chen, T.T., 2010. The behaviour of phosphate during jarosite precipitation. *Hydrometallurgy* 102, 55–65.

Dutrizac, J.E., Jambor, J.L., Chen, T.T., 1987. Behaviour of arsenic during jarosite precipitation: Reactions at 150 °C and the mechanism of arsenic precipitation. *Canadian Metallurgical Quarterly* 26 (2), 103–115.

Fujita, T., Taguchi, R., Abumiya, M., Matsumoto, M., Shibata, E., Nakamura, T., 2008a. Novel atmospheric scorodite synthesis by oxidation of ferrous sulfate solution. Part I. *Hydrometallurgy* 90, 92–102.

Fujita, T., Taguchi, R., Abumiya, M., Matsumoto, M., Shibata, E., Nakamura, T., 2008b. Novel atmospheric scorodite synthesis by oxidation of ferrous sulfate solution. Part II. Effect of temperature and air. *Hydrometallurgy* 90, 85–91.

Fujita, T., Taguchi, R., Abumiya, M., Matsumoto, M., Shibata, E., Nakamura, T., 2009a. Effect of pH on atmospheric scorodite synthesis by oxidation of ferrous ions: Physical properties and stability of scorodite. *Hydrometallurgy* 96, 189–198.

Fujita, T., Taguchi, R., Shibata, E., Nakamura, T., 2009b. Preparation of an As(V) solution for scorodite synthesis and a proposal for an integrated As fixation process in a Zn refinery. *Hydrometallurgy* 96, 300–312.

Ichimura, R., Tateiwa, H., Almendares, C., Sanchez, G., 2007. Arsenic immobilization and metal recovery from El Teniente smelter dust. In: Riveros, P.A., Dixon, D.G., Dreisinger, D.B., Collins, M.J. (Eds.), *Proceedings Copper 2007*, Toronto: CIM, Montreal, vol. IV(2), pp. 191–203.

Jambor, J.L., 1999. Nomenclature of the alunite supergroup. *Canadian Mineralogist* 37, 1323–1341.

Kolitsch, U., Pring, A., 2001. Crystal chemistry of the crandallite, beudantite and alunite groups: a review and evaluation of the suitability storage materials for toxic products. *Journal of Mineralogical and Petrological Sciences* 96, 67–78.

Kontrec, J., Kralj, D., Brecevic, L., 2003. Cadmium removal from calcium sulphate suspension by liquid membrane extraction during recrystallization of calcium sulphate anhydrite. *Colloids and Surfaces A: Physicochemical and Engineering Aspects* 223 (1–3), 239–249.

Krause, E., Ettel, V.A., 1989. Solubilities and stabilities of ferric arsenate compounds. *Hydrometallurgy* 22, 311–337.

Le Berre, J.F., Cheng, T.C., Gauvin, R., Demopoulos, G.P., 2007a. Hydrothermal synthesis and stability evaluation of mansfieldite in comparison to scorodite. *Canadian Metallurgical Quarterly* 46, 1–9.

Le Berre, J.F., Cheng, T.C., Gauvin, R., Demopoulos, G.P., 2007b. Hydrothermal synthesis and stability evaluation of iron(III)-aluminum(III) arsenate solid solutions. *Metallurgical and Materials Transactions B* 38, 159–166.

Monhemius, A.J., Swash, P.M., 1999. Removal and stabilizing As from copper refining circuits by hydrothermal processing. *JOM* 51, 30–33.

Osaka, J., Hirabayashi, J., Okada, K., Kobayashi, R., Hayashi, T., 1982. Crystal structure of minamiite, a new mineral of the alunite group. *American Mineralogist* 67, 114–119.

Paktunc, D., Dutrizac, J.E., 2003. Characterization of arsenate-for sulfate substitution in synthetic jarosite using X-ray diffraction and X-ray absorption spectroscopy. *Canadian Mineralogist* 41, 905–919.

Piret, N.L., 1999. The removal and safe disposal of arsenic in copper processing. *JOM* 51, 16–17.

Riveros, P.A., Dutrizac, J.E., Spencer, P., 2001. Arsenic disposal practices in the metallurgical industry. *Canadian Metallurgical Quarterly* 40, 395–420.

Roca, A., Viñals, J., Calero, J., Arranz, M., 1999. Characterization and cyanidation of jarosite-beudantite phases from Rio Tinto gossan ores. *Canadian Metallurgical Quarterly* 38, 93–103.

Savage, K.S., Bird, D.K., O'Day, P.A., 2005. Arsenic speciation in synthetic jarosite. *Chemical Geology* 215 (1–4), 473–498.

Swash, P.M., Monhemius, A.J., Schaeckers, J.M., 2000. Solubilities of process residues from biological oxidation pretreatments of refractory gold ores. In: Young, C.A. (Ed.), *Minor Elements 2000*. SME, Littleton, CO, pp. 115–123.

van der Sluis, S., Witkamp, G.J., Van Rosmalen, G.M., 1986. Crystallization of calcium sulfate in concentrated phosphoric acid. *Journal of Crystal Growth* 79 (1–3), 620–629.

Viñals, J., Núñez, C., 1988. Kinetics of dissolution of argentine plumbogjarosite from old tailings of sulfatizing roasting pyrites by HCl-CaCl₂ leaching. *Metallurgical Transactions B* 19B, 365–373.

Viñals, J., Roca, A., Arranz, M., 2003. Autoclave alkaline decomposition and cyanidation of jarosite-beudantite phases from Rio Tinto gossan ores. *Canadian Metallurgical Quarterly* 42 (1), 29–40.

Viñals, J., Cruells, M., Sunyer, A., Garcia, L., Beltrán, V., 2009. Arsenic stabilization by hydrothermal synthesis of alunite-type phases. Application to the copper metallurgy. In: Domic, E., Casas, J. (Eds.), *Proceedings HydroCopper 2009*, Antofagasta, Chile. Gecamin Ltd., pp. 37–46.

Vircikova, E., Molnar, L., Palfy, P., 1999. Methods of arsenic waste treatment and disposal- Case studies. In: Gaballah, I., Hager, J., Solozábal, R. (Eds.), *Proceedings Rewas '99*, San Sebastian, Spain. TMS, INASMET, pp. 65–73.

A.8 Arsenic stabilization by hydrothermal synthesis of alunite-type phases. application to the copper metallurgy.

J. Viñals, M. Cruells, A. Sunyer, L. Garcia, V. Beltrán, 2009, Arsenic Stabilization by Hydrothermal Synthesis of Alunite-type Phases. Application to the Copper Metallurgy. Proceedings of the HydroCopper 2009. P. 37-46. E. Domic & J. Casas Eds. .Gecamin Ltd. Santiago, Chile. ISBN 978-956-8504-21-2

Resum en català

Un procés nou per a l'estabilització d'arsènic a partir de residus sòlids o aquosos de la metal·lúrgia del coure s'ha estudiat. El procés va consistir en tres passos: 1) lixiviació (en cas de ser necessària). 2) Ozonització per tal de convertir tot l'arsènic a As^{V} . 3) Precipitació hidrotermal de l'arsènic en medi àcid (pH inicial ~ 1) $\text{Na}^+/\text{Al}^{3+}/\text{Ca}^{2+}/\text{SO}_4^{2-}$ a $\sim 200^\circ\text{C}$ (~ 15 bar), usant sulfats de sodi i alumini com a reactius. Sota aquestes condicions l'arsènic es va estabilitzar com a natroalunita arsenical juntament amb traces o petites quantitats de mansfieldita. La precipitació es va aconseguir amb un pH final fortament àcid (0.6). Així doncs, la precipitació va ser lliure de fases amorfes o poc cristal·lines, exhibint una baixa solubilitat. A $\sim 200^\circ\text{C}$, pH 1, i amb excés de SO_4^{2-} , Ca^{2+} i Na^+ en la solució inicial, el major efecte en la composició i la solubilitat dels precipitats va ser la relació molar Al/As en el medi aquós. Per la relació Al/As = 0.15, la única fase d'arsènic va ser la mansfieldita ferrosa. Per relacions Al/As=4.5 la única fase d'arsènic va ser una natroalunita amb arsènic calci i ferro. Per relacions Al/As intermedies, es va obtenir una mescla de natroalunita i mansfieldita, incrementant el contingut de mansfieldita amb la disminució de la relació Al/As a la solució inicial. Els residus de la metal·lúrgia del coure, consistien en mescles amorfes d'arseniats calci/ferro i guix que es poden convertir en fases cristal·lines, principalment anhidrita i natroalunita arsenical. La solubilitat de l'arsènic a pH ~ 7 va ser de 150 mg/L en el residu original i sobre 0.01-0.02 mg/L en els precipitats estabilitzats, depenent de la composició de la fase.

ARSENIC STABILIZATION BY HYDROTHERMAL SYNTHESIS OF ALUNITE-TYPE PHASES. APPLICATION TO THE COPPER METALLURGY

Joan Viñals, Montserrat Cruells, Alba Sunyer,
Laura García & Victoria Beltran

Department of Materials Science and Metallurgical Engineering,
University of Barcelona, Spain

ABSTRACT

A novel process for arsenic stabilization from solid or aqueous wastes of copper metallurgy was studied. The process consists of three steps: 1) Leaching (if necessary). 2) Ozonation to convert all arsenic compound into As^V . 3) Hydrothermal precipitation of arsenic in an acid (initial pH ~ 1) $Na^+ - Al^{3+} - Ca^{2+} - SO_4^{2-}$ medium at ~ 200°C (~15 bar), using sodium and aluminium sulfates as reactants. Under these conditions arsenic is stabilized as arsenian natroalunite together with trace to minor amounts of mansfieldite. The precipitation was achieved at a strong acid final pH (0.6). So, the precipitate was free of amorphous or poorly crystalline phases, exhibiting a very slow solubility. At ~ 200°C, pH 1, and for an excess of SO_4^{2-} , Ca^{2+} and Na^+ in the initial slurry, the major effect on phase composition and solubility of the precipitates was the Al/As molar ratio in the aqueous medium. For Al/As ratio 0.15, the unique arsenic phase was ferroan mansfieldite. For Al/As ratio 4.5 the arsenic phase was arsenian-calcian-ferroan natroalunite. For intermediate Al/As ratios, a mixture of natroalunite and mansfieldite was obtained, increasing the mansfieldite content as decrease the Al/As ratio in the initial slurry. Wastes from copper metallurgy, consisting of a mixture of amorphous calcium/iron arsenates and gypsum can be converted into crystalline phases, mainly anhydrite and arsenian natroalunite. The solubility of arsenic at pH ~ 7 was about 150 mg/L in the original waste and about 0.01 – 0.02 mg/L in the stabilized precipitates, depending of phase composition.

INTRODUCTION

Arsenic stabilization of wastes from base metal industry and particularly, from copper metallurgy is a well known problem [1]. Different methods have been investigated, among others, the precipitation of calcium arsenates, ferrihydrite and scorodite [2]. Due the superior stability of scorodite, the precipitation of such phase has been extensively studied [3, 4], even at industrial scale [5]. Scorodite generation can be verified hydrothermally (~ 150°C) or at ~ 95°C but through precise supersaturation and seeding control. However, As solubility of scorodite in neutral region (0.1-1 mg/L) [6], falls near the legal limits of advanced countries for disposal of hazardous wastes. On the

other hand, scorodite examined in long term leaching [7], suffers incongruent dissolution at neutral pH, giving As solubility of about 5 mg/L. Taking into account the more and more restrictive tendency in legal limits, it seems reasonable to research also other As-host phases.

Minerals of the alunite supergroup [8] are very common in Earth surface, exhibiting very low solubility. These phases consist of structures $AB_2(XO_4)_2(OH,H_2O)_6$ where A can be a monovalent (Na, K, H₃O, Ag, etc) or a divalent (Pb, Sr, Ba, Ca), B is usually a trivalent (Al, Fe, etc) and XO_4 can be principally SO_4 , AsO_4 and PO_4 . The lattice of such phases has a great possibility of stoichiometric changes due to formation of cation vacancies and substitution of OH for H₂O. For instance, it is typical the substitution of two alkaline sites by a divalent plus a vacancy, or the simultaneous substitution of an alkaline plus SO_4^{2-} by a divalent plus PO_4^{3-} or AsO_4^{3-} . Thus, it is possible to synthesize alunite-type phases with the AsO_4^{3-} group in diluted solid solution, so, with low thermodynamic activity.

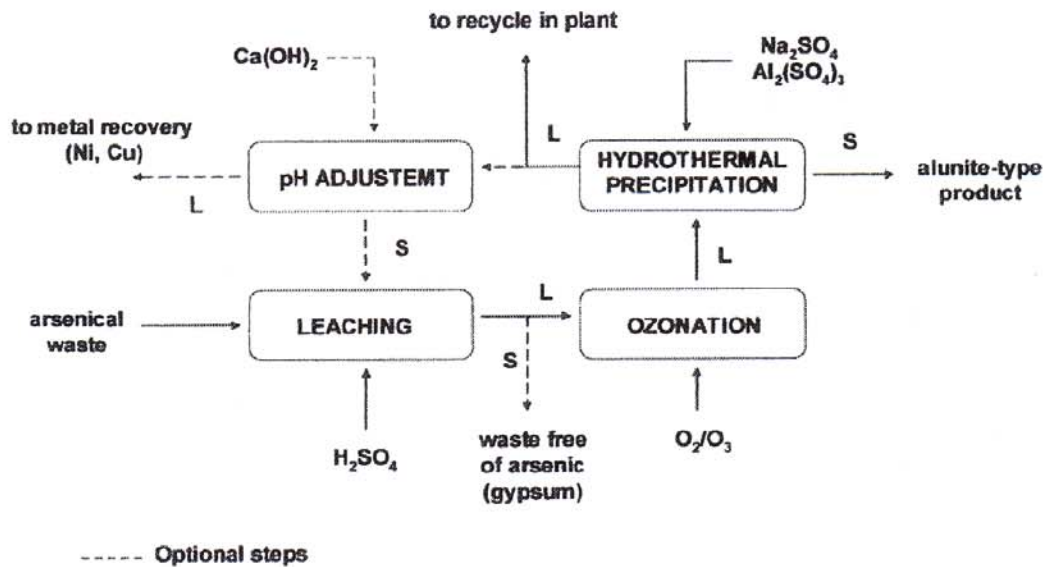


Figure 1: Concept of the process

The concept of this process is shown in Figure 1. Arsenical waste is leached usually with H_2SO_4 , in appropriate conditions for As leaching. The resulting slurry or solution is ozonized to transform any As compound to $As(V)$. Ozonation is preferred because it does not introduce new chemicals to the circuit. The leached and ozonized slurry is conducted to hydrothermal ($\sim 200^\circ C$) precipitation, using sodium and aluminium sulfates as reactants. After treatment, the liquid can be recycled in plant for potential recovery of valuable metals (Ni, Cu, etc) and to cleaning steps of final effluent. Since hydrothermal precipitation in a single step does not remove all As from the liquid, an optional step of pH adjustment (to ~ 3.5) can be performed. This permit to recycle the remnant As & Al to the leaching and hydrothermal steps.

The selection of a $Na^+/Ca^{2+}/Al^{3+}/SO_4^{2-}/AsO_4^{3-}$ medium as a system to generate alunite-type phases was due to the following considerations: a) Low solubility of natural analogous phases. b) SO_4^{2-} and Ca^{2+} are very common in metallurgical circuits, because $Ca(OH)_2$ is largely used as a precipitant. c) Na^+ is the most economic alkaline. d) Al^{3+} is a very common cation in soils. This could produce a long term nucleation and growth (cover) of other natural alunite-type phases. In addition, in contrast to Fe^{3+} , Al^{3+} is not reducible in anaerobic conditions.

METHODOLOGY

The original waste, some intermediate products and all hydrothermal precipitates were characterized by wet chemical analysis (ICP or ICP-MS), X-ray diffraction (XRD) and scanning electron microscopy (SEM) in a JEOL JSM-840 instrument. Quantitative microanalysis of different phases was obtained by energy dispersive spectroscopy (EDS) at 20kV, 0.6nA, 30s, through an INCA-250 analyzer.

Leaching experiments of the original waste were conducted in a conventional thermostatic reactor coupled with a magnetic stirring. The addition of reagent (H_2SO_4), pH, ORP and stirring speed were monitored. The solubilization of different elements was obtained by sampling and solution analysis (ICP). After leaching, the slurries were ozonized in the same reactor by injecting a mixture of O_2/O_3 through a fritted-glass diffuser. Ozone was produced in TRIOGEN generator. The gas flow was 0.75 L/min and the ozone mass flow 3.36×10^{-2} g/min. The process was followed through the change in the ORP of the medium.

Autoclave experiments were made in a PARR 4563 reactor provided of temperature, pressure and stirring controllers. After the steps of leaching and ozonation, the slurry was placed into reactor with the additives, sodium and aluminium sulfates, in the amounts required in each test. The system was heated until the working temperature (usually 200°C) at rate of 5°C/min. Then the system was maintained at constant temperature for a fixed time and then was also cooled at the rate of 5°C/min. The hydrothermal precipitate was filtered, washed and characterized as described. Particular conditions of the experiments are reported together with the corresponding results.

The solubility of the hydrothermal precipitates was investigated at 25°C by stirring 0.50g of solids into 50 mL of solutions of different pH, during 24h. These solutions were made by convenient dilution of stock H_2SO_4 or NaOH solutions. Eventual pH changes during these tests were corrected by addition of small volumes of dilute H_2SO_4 or NaOH. Three consecutive leaching tests were performed at each pH. After each leaching, slurry was filtered and the solution was analyzed for As by ICP-MS.

RESULTS AND DISCUSSION

Waste Characterization

The chemical composition of the initial waste is shown in table 1. The characterization by XRD and SEM/EDS indicated that it mainly consisted of gypsum (~ 77%) and an amorphous precipitate containing basically As/Ca/Fe/Ni/Cu/Zn. Gypsum appeared as free, relatively large (100-200µm) crystals. No significant impurities were detected in gypsum by EDS analysis. The amorphous precipitate consisted in agglomerates of very small individual particles (0.1-1µm) of variable composition; with a mean content of ~15% As. Precipitate's pH was about 9. This should be a consequence of a natural carbonation process, because the waste was originally precipitated at pH 12. The presence of a small amount of $CaCO_3$ was clearly showed in the obtained XRD patterns.

Table 1: Original waste. Chemical composition

Element	wt %	element	wt %	element	wt %
Ca	20.01	Fe	1.07	Si	0.40
S	11.37	Zn	0.88	Pb	0.04
As	5.23	Mg	0.53	Sb	0.03
Ni	2.32	Cu	0.49	Bi	0.02

Leaching with H₂SO₄ and Ozonation

Leaching characteristics of the original waste with H₂SO₄ were studied by treating 2.00g of solid in 200 mL solution at 25°C, 600 rpm. Acid was added through controlled volumes of H₂SO₄ 1M for reaching a specified pH. According to fine grain size and amorphous nature of the components containing the heavy metals, the reactivity of the waste was very high. After about 5 min. of acid addition, pH of the slurry was practically stabilized. Results of the solubility of heavy metals as a function of pH are given in Fig. 2. Arsenic was the most soluble heavy metal, 34 mg/L, at the initial pH 9.3 (without H₂SO₄ addition). This is clearly due because the process of As-precipitation by Ca(OH)₂ at pH 12 gives unstable calcium arsenates, which decompose by atmospheric CO₂ generating soluble arsenic acid:

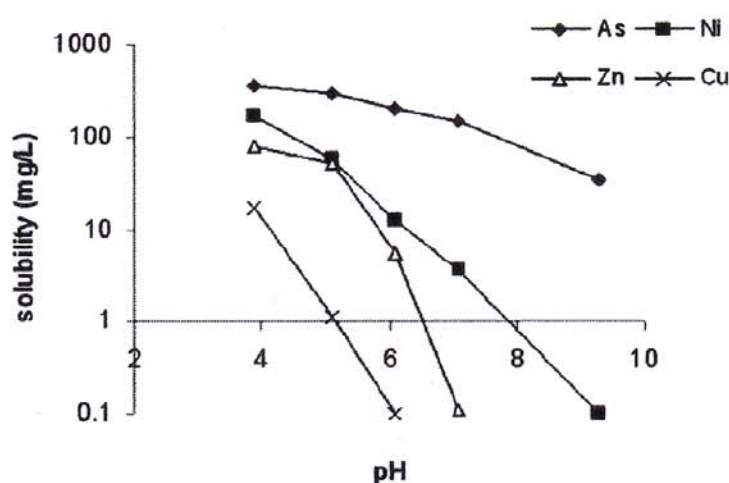
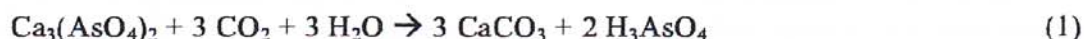


Figure 2: Solubility of heavy metals as a function of pH

The extraction of different elements as a function of pH is shown in Fig. 3. Complete leaching of As, Ni, Fe, Zn and Cu was achieved at pH 1 in 5 min, with an acid consumption of 380 gH₂SO₄/Kg waste. The comparison of the leaching curves of As and Fe indicated that about 75% As was already leached at pH 4 without significant Fe solubilization, whereas the remaining 25% As was only leached at pH 1 when all Fe was solubilized. Thus, it seems probable that in the investigated waste, this 25% As was associated to amorphous ferric arsenates. The residue of the leaching treatment at pH 1 was only insoluble gypsum.

Preliminary ozonation experiments conducted with pure H₃AsO₃ showed that the stoichiometry for As(III) oxidation was:



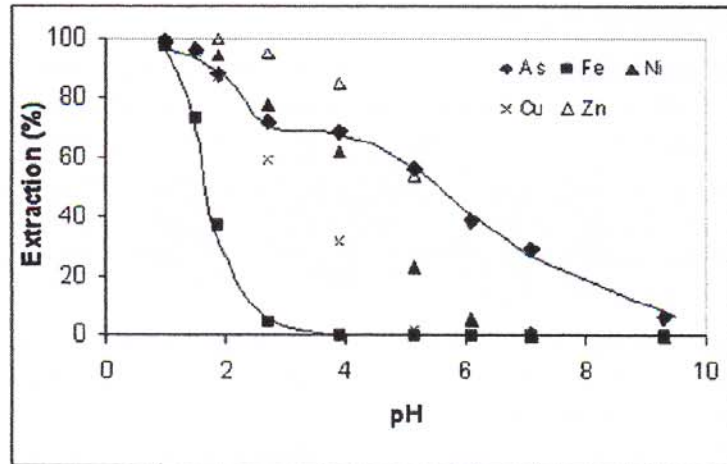


Figure 3: Extraction of heavy metals as a function of pH (25°C, 5 min)

The reaction was very fast. In the used reactor, process exhibited pseudo zero-order kinetics. All O_3 injected reacts in the gas-liquid interface, as a consequence, the process can be easily followed through ORP changes, from ~ 400 mV to ~ 1200 mV (vs Ag/AgCl). For the studied waste, ozone consumption was 13 g O_3 /Kg waste. According with the stoichiometry of As(III) oxidation and O_3 consumption, the waste contained about 50% of the total arsenic as As(III).

Hydrothermal Precipitation

Variables studied in hydrothermal precipitation were: a) initial pH, b) As/Al molar ratio, c) As concentration at fixed As/Al ratio, d) reaction time and c) temperature. Other potential effects such as SO_4^{2-} and Na^+ concentration were not studied because SO_4^{2-} concentration was basically determined by the large SO_4^{2-} content in the waste and, in all experiments, Na^+ was used in excess vs Al^{3+} for the stoichiometric requirements of natroalunite precipitation:

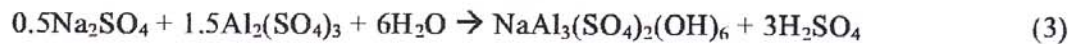


Table 2: Experimental conditions used in the effect of As/Al molar ratio

Test	molar ratios						final pH
	$Al_2(SO_4)_3$ (g)	Na_2SO_4 (g)	Al/As	S/As	As/Ca	Na/Al	
H2	1.79	0.994	1.50	15	0.123	1.33	0.84
H5	2.69	0.994	2.25	16	0.123	0.89	0.68
H4	3.58	0.994	3.00	12	0.123	0.66	0.65
H3	5.38	0.994	4.50	18	0.123	0.44	0.66

The effect of initial pH was studied in a set of preliminary experiments. For the used waste, production of fully crystalline precipitates (natroalunite and/or mansfieldite) required an initial pH ≤ 1 . This ensures an extensive precipitation of As, S, Ca and Fe. Under these conditions, Ni, Cu and Zn remain in the liquid phase which could facilitate their further recovery.

Effect of the As/Al Molar Ratio in the Liquid

The most important effect on precipitates phase composition was the As/Al molar ratio in the liquid. The effect was studied treating 10 g of leached and ozonized slurry (pH 1) at 200°C, 120 min. Reagent additions and initial molar ratios are shown in Table 2. Results indicated:

- The only phases obtained were natroalunite ($\sim(\text{Na,Ca})(\text{Al,Fe})_3((\text{S,As,P})\text{O}_4)_2(\text{OH})_6$), mansfieldite ($(\text{Al,Fe})(\text{As,P})\text{O}_4 \cdot 2\text{H}_2\text{O}$) and anhydrite (CaS O_4) (Figures. 4 and 5). Calcium, which becomes from gypsum and calcium arsenates, was transformed basically into anhydrite. The substitution of Ca in natroalunite is low, 0.04-0.08 in formula.
- For Al/As molar ratio in liquid 1.5, arsenic precipitated practically only as *mansfieldite*. Increasing Al/As ratio increased natroalunite precipitation (Figure 6). When Al/As was 4.5, As precipitated practically only as natroalunite.
- The maximum substitution of As in natroalunite phase was 0.11-0.14 in formula (Table 3). Natroalunite also incorporates Fe of the original waste because it substitutes Al in the alunite lattice. Fe coefficients in formula reached 0.12 when only trace of mansfieldite was formed, but decreasing to 0.08 when large amounts of mansfieldite were precipitated. Trace of P, substituting in TO_4 group, was also incorporated in alunite (up to 0.02 in formula).

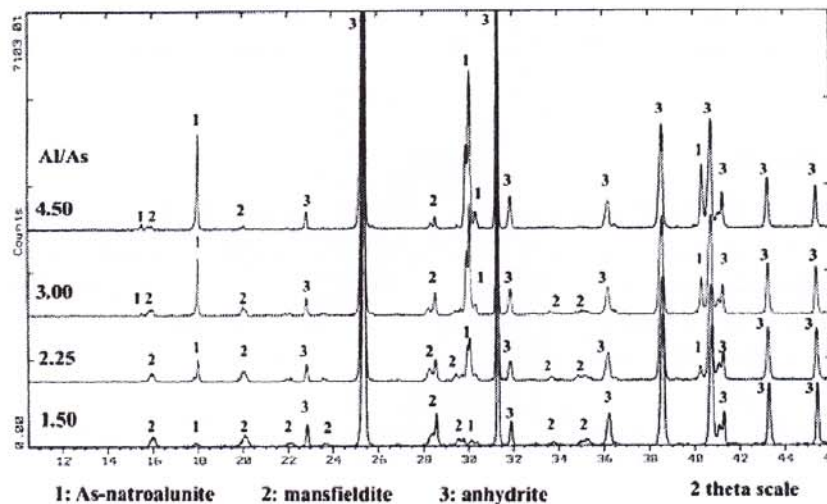


Figure 4: Effect of the As/Al molar ratio on phase composition

- Mansfieldite also incorporates Fe of the original waste (Table 3). When mansfieldite is practically the only arsenic phase, substitution was extensive, 0.31 in formula. This value decreases to 0.20 when increase the formation of As-natroalunite. Phosphorous was also incorporated in mansfieldite, up to 0.05 in formula.
- When hydrothermal precipitation was performed in only one step, the yield of arsenic precipitation is moderate (Figure 7), so the liquid must be recirculated. The yield is maximum ($\sim 50\%$) when mansfieldite was formed in large extension and minimum ($\sim 20\%$) when natroalunite was practically the only phase. However, it can be reaching a yield of $\sim 40\%$ with formation of only small amounts of mansfieldite ($\sim 5\%$).

Table 3: Experimental formulas from EDS punctual analysis (mean values)

Al/As ratio	Natroalunite (normalized to S+As+P = 2, OH from charge balance)	Mansfieldite (normalized to As+P = 1)
1.50	-	$(Al_{0.69}Fe_{0.31})(As_{0.95}P_{0.05})O_4 \cdot 2H_2O$
2.25	$(Na_{0.90}Ca_{0.04})(Al_{2.70}Fe_{0.08})((S_{0.84}As_{0.14}P_{0.02})O_4)_2(OH)_{5.00}$	$(Al_{0.76}Fe_{0.24})(As_{0.99}P_{0.01})O_4 \cdot 2H_2O$
3.00	$(Na_{0.96}Ca_{0.08})(Al_{2.69}Fe_{0.12})((S_{0.88}As_{0.11}P_{0.01})O_4)_2(OH)_{5.33}$	$(Al_{0.78}Fe_{0.21})(As_{0.97}P_{0.03})O_4 \cdot 2H_2O$
4.50	$(Na_{0.98}Ca_{0.08})(Al_{2.70}Fe_{0.12})((S_{0.92}As_{0.07}P_{0.01})O_4)_2(OH)_{5.44}$	-

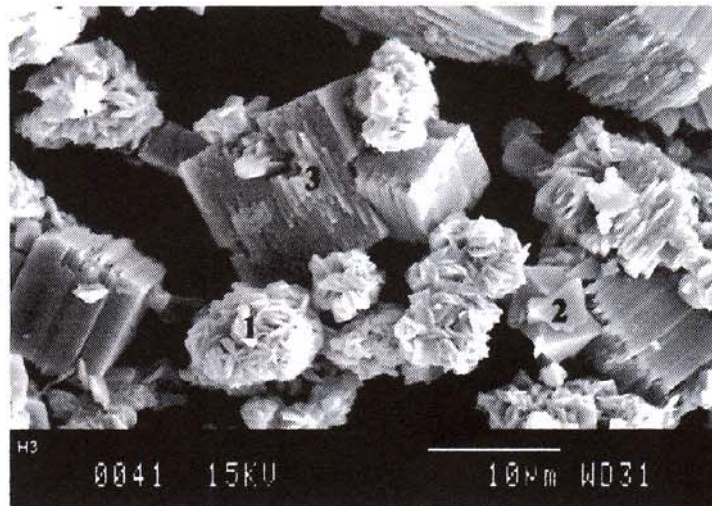


Figure 5: Typical phase morphology of the hydrothermal precipitates (1: As-natroalunite; 2: mansfieldite; 3: anhydrite)

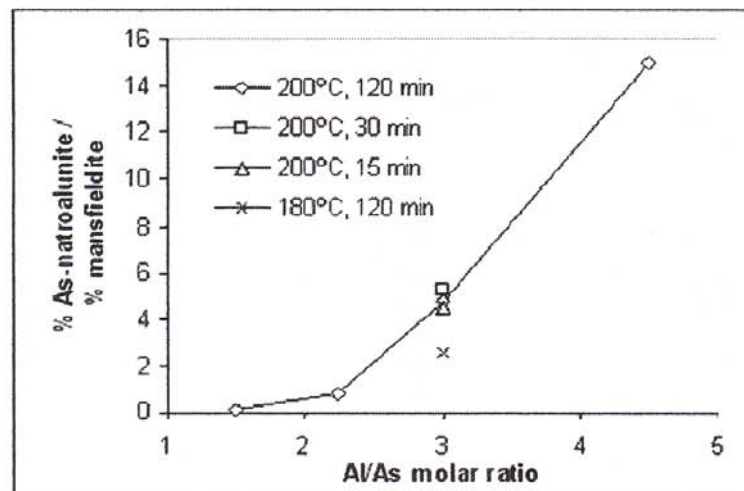


Figure 6: Effect of As/Al molar ratio on arsenic distribution

- Al precipitation yield also depends of the Al/As ratio (Figure 7). It was maximum (~ 60%) when natroalunite formation was high and minimum (~ 25%) when mansfieldite formation was extensive. This was clearly due to the different stoichiometry of both precipitation reactions.

However, Fe precipitation yield (~ 90%) was few sensitive to phase composition, whereas Ni, Zn and Cu do not precipitated in significant amounts.

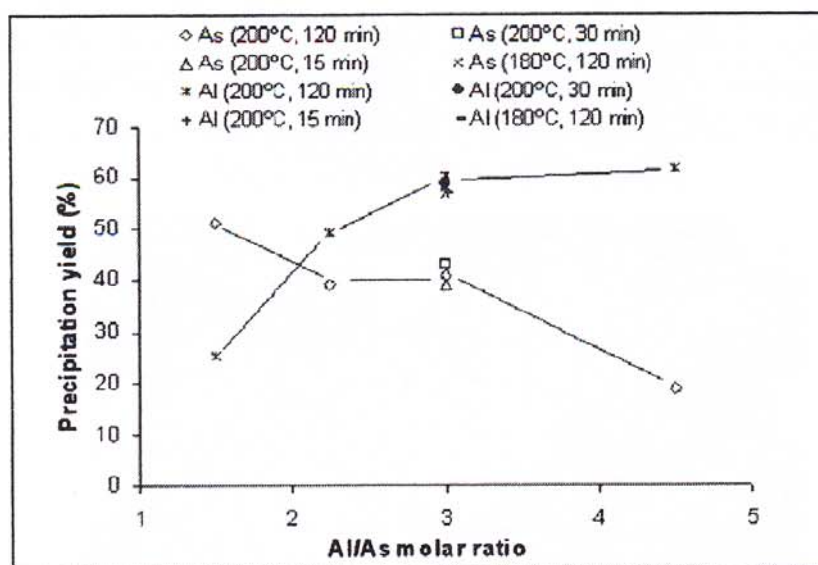


Figure 7: As & Al precipitation yield as a function of Al/As molar ratio in the liquid

Other Effects

Effect of As concentration at fixed Al/As molar ratio was studied at 200°C, 120 min, by using 10 and 20 g of leached and ozonized waste in 150 mL solution and fixing reagents to Al/As = 3.00 and Na/Al = 0.66. In the range of As concentration studied (3.5-7 g/L), no significant change on phase composition and precipitation yields were observed.

Table 4: Composition of hydrothermal precipitates (Initial pH: 1. Initial solution: 150 cm³)

waste (g)	Al/As ratio	temp (°C)	time (min)	Precipitate composition (wt %)								
				Ca	S	Al	As	Na	Fe	Ni	Cu	Zn
10	1.50	200	120	24.5	20.0	0.88	3.34	0.07	1.12	0.01	0.06	0.03
10	2.25	200	120	21.6	19.2	2.64	3.41	0.65	1.23	0.01	0.02	0.03
10	3.00	200	120	20.6	19.7	4.20	2.67	1.15	1.16	0.01	0.04	0.02
10	3.00	200	30	21.6	20.4	4.01	2.58	1.05	1.15	0.01	0.04	0.02
10	3.00	200	15	22.1	21.0	4.05	2.41	1.10	1.10	0.01	0.02	0.02
20	3.00	180	120	20.4	19.3	3.69	2.45	1.01	1.07	0.01	0.03	0.03
10	4.50	200	120	18.4	19.4	5.98	1.10	1.60	0.94	0.01	0.05	0.01

Temperature effect was studied in previous research using synthetic reagents. Although natroalunite can be precipitated at >100°C, the rate was low until ≥160°C. Moreover, As incorporation in natroalunite was effective at ≥180°C because at lower temperature, intermediate amorphous arsenates are formed. However, even at 180°C the formation of mansfieldite was preferential. This fact was confirmed in the present study on the selected waste. For Al/As = 3, 120 min, whereas at 200°C the ratio natroalunite/ mansfieldite was ~ 5, at 180°C the same ratio decreased at ~ 2.5 (Figure 6). For this reason, selected temperature was 200°C in the proposed process.

Effect of reaction time was studied at 200°C, Al/As molar ratio 3, for 15, 30 and 120 min (conditions as test H4 in table 2). The results obtained indicated no significant changes in phase composition (Figure 6) and precipitation yield (Figure. 7). Thus, at 200°C, hydrothermal precipitation process can be verified at small residence times (~ 15 min). Chemical composition of representative hydrothermal precipitates is shown in Table 4.

Solubility

Results of the solubility tests are reported in Figure 8. Generally, at each pH, data of the first leaching was slightly higher than in second leaching and these slightly higher than in third leaching. However, differences were small, which suggests absence of significant amounts of aqueous arsenic species adsorbed on crystal surfaces and that the washing of precipitates was effective. On the other hand, arsenic solubility in a very acid medium, pH 1, was relatively small (1-2 mg/L), which indicates absence of significant amounts of amorphous As-phases.

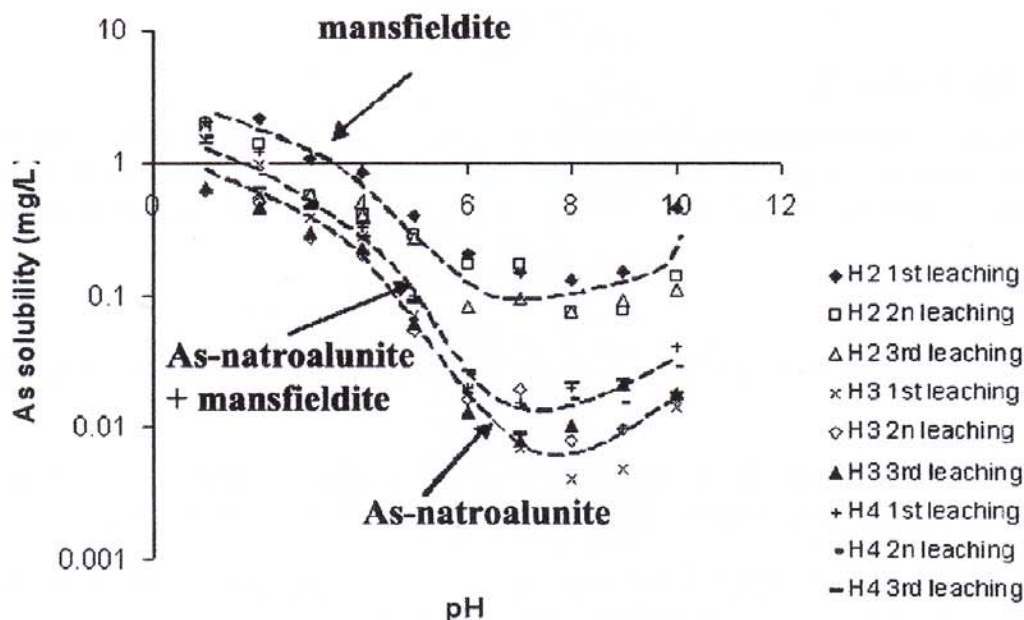


Figure 8: As solubility as a function of pH (24 h)

In all pH interval, the minimal solubility corresponds to precipitates obtained at high Al/As ratio in the liquid (4.5), when the As phase was natroalunite. The maximum is for low Al/As ratio (1.5), when mansfieldite was the only As phase. In neutral zone, As solubility of natroalunite is ~ 0.01 mg/L, whereas for mansfieldite is ~ 0.1 mg/L. However, in the waste studied, the most favorable conditions correspond to precipitates obtained at Al/As ratio 3, when a mixture of natroalunite with minor mansfieldite was formed. The As solubility is very acceptable (0.02 mg/L) and the precipitation yield in a single step (~ 40%) is double respect to the precipitates containing only natroalunite. Other advantage is the minor consumption of aluminium salt.

CONCLUSIONS

Hydrothermal precipitation of arsenic(V) in an acid (initial pH ~ 1) Na^+ - Al^{3+} - Ca^{2+} - SO_4^{2-} medium at ~ 200°C (~15 bar), using sodium and aluminium sulfates as reactants, offers an alternative for arsenic stabilization. The precipitation achieves a strong acid final pH (0.6), which produces products free of amorphous or poorly crystalline phases. At ~ 200°C, pH 1, and for an excess of SO_4^{2-} , Ca^{2+} and Na^+ in the initial slurry, the major effect on phase composition and solubility of the precipitates is the Al/As molar ratio in aqueous medium. For Al/As ratio 0.15, the unique arsenic phase is mansfieldite. For Al/As ratio 4.5, arsenic phase is arsenian natroalunite. For intermediate Al/As ratios, a mixture of natroalunite and mansfieldite is obtained, increasing the mansfieldite content as decrease the Al/As ratio in the initial slurry. Hydrothermal process at 200°C is very fast (~ 15 min) and practically independent of the arsenic concentration in the range of ~ 1-10 g/L at fixed Al/As ratio. Wastes from copper metallurgy, consisting of a mixture of amorphous calcium/iron arsenates and gypsum can be converted into crystalline phases, mainly anhydrite and arsenian natroalunite. The solubility of arsenic at pH ~ 7 is about 150 mg/L in the original waste and about 0.01 – 0.02 mg/L in the stabilized precipitates, depending of phase composition.

ACKNOWLEDGEMENTS

The authors wish to thank the Spanish *Ministerio de Educación y Ciencia (DGI)* for the financial support of this research (*Programa de Materiales, MAT 2007-61466*). Thanks also to the *Serveis Científicotècnics de la Universitat de Barcelona* for their assistance in characterization studies.

REFERENCES

- Piret, N.L. (1999). *The removal and safe disposal of arsenic in copper processing*. JOM 51(9), p.p. 16-17. [1]
- Riveros, P. A., Dutrizac, J. E. & Spencer, P. (2001). *Arsenic disposal practices in the metallurgical industry*. Canadian Metallurgical Quarterly 40, p.p. 395-420. [2]
- Demopoulos, G., Droppert D. & G., Van Weert, G. (1995). *Precipitation of Crystalline Scorodite from Chloride Solutions*. Hydrometallurgy 38, p.p. 245-261. [3]
- Monhemius, A. J. & Swash, P.M. (1999). "Removing and Stabilizing As from Copper Refining Circuits by Hydrothermal Processing". JOM 51(9), pp. 30-33. [4]
- Ichimura, R., Tateiwa, H., Almendares C. & Sánchez, G. (2007). *Arsenic Immobilization and Metal Recovery from El Teniente Smelter Dust*. Copper 2007 Conference, CIM, Montreal, Canada, August 25-30. [5]
- Krause, E. & V. A., Ettel, V. A. (1989). *Solubilities and stabilities of ferric arsenate compounds*. Hydrometallurgy 22, pp. 311-337.[6]
- Bluteau, M. C. & Demopoulos, G. P. (2007). *The incongruent Dissolution of Scorodite. Solubility, Kinetics and Mechanism*. Hydrometallurgy, 87, p.p. 163-177. [7]
- Jambor, J. L. (1999). *Nomenclature of the Alunite supergroup*. Canadian Mineralogist 37, p.p. 1323-1341.[8]

B.1 Arsenic immobilization as alunite-type phases: The arsenate substitution in alunite and hydronium alunite.

A. Sunyer, M. Currubí, J. Viñals, Arsenic immobilization as alunite-type phases: The arsenate substitution in alunite and hydronium alunite, *Journal of Hazardous Materials*, in review.

In review at *Journal of Hazardous Materials*.

Resum en català

La substitució d'AsO₄ per SO₄ en alunita (KAl₃(SO₄)₂(OH)₆) i alunita d'hidroni ((H₃O)Al₃(SO₄)₂(OH)₆) ha estat investigada per precipitació hidrotermal a 200°C. L'alunita arsenical va presentar un bon rendiment de precipitació i una substitució significativa d'AsO₄ (de fins a un 15% molar). El grau de substitució depèn de la composició de la solució. Aquest va incrementar (AsO₄/(SO₄ + AsO₄))_{alunite} ≈ 0.5 (AsO₄/(SO₄ + AsO₄))_L. Per (AsO₄/(SO₄ + AsO₄))_L < 0.26, L'alunita arsenical va ser la única fase i, per sobre d'aquesta relació, la mansfieldita (AlAsO₄ · 2 H₂O) va co-precipitar. El paràmetre de cel·la *a* és pràcticament independent a la substitució d'AsO₄, però el paràmetre de cel·la *c* van incrementar congruentment amb les diferències entre les distàncies As-O1 i S-O1 dels llocs tetraèdrics de l'estructura. La màxima estabilitat de l'alunita arsenical en tests a curt termini és entre pH 5-8, amb una solubilització de l'arsènic de 0.01-0.03 mg/L en 24 h. Els tests a mitjà termini es van fer en algunes de les mostres sintetitzades a pH natural. L'alunita arsenical es va estabilitzar a 0.3 mg/L d'As dissolt en 2.5 setmanes. Aquests valors van ser similars als obtinguts en escorodita natural pura i cristal·lina (0.4 mg/L As dissolt), però menors als obtinguts en escorodita sintètica (1.3 mg/L As dissolt). Així doncs, l'alunita arsenical pot ser efectiva en la immobilització de l'arsènic, especialment per efluent o residus que contenen una relació SO₄/AsO₄ elevada. L'alunita d'hidroni presenta un rendiment de precipitació baix i una incorporació d'arseniat baixa (d'un 1% molar). Això pot estar relacionat amb la dificultat de substituir grups protonats d'HAsO₄²⁻ per SO₄²⁻ o H₂O per OH⁻, degut a la localització dels ponts d'hidrogen a l'estructura. Aquestes característiques fan que l'alunita d'hidroni no serveixi per a la immobilització d'arsènic.

1 Arsenic immobilization as alunite-type phases: The arsenate substitution in alunite and
2 hydronium alunite.

3 Alba Sunyer¹, Marta Currubí², Joan Viñals³

4 ¹²³Department of Materials Science and Metallurgical Engineering, University of
5 Barcelona

6 ¹²³Martí i Franquès 1, 08028 Barcelona, SPAIN

7 ¹²³Tel: +34934021317, fax: +34934021291

8 ¹asunyer@ub.edu

9 ²mcurruvi7@alumnes.ub.edu

10 ³jvinalsvinal@ub.edu

11

12 ABSTRACT

13

14 AsO₄-for-SO₄ substitution in alunite (KAl₃(SO₄)₂(OH)₆) and hydronium alunite
15 ((H₃O)Al₃(SO₄)₂(OH)₆) has been investigated by hydrothermal precipitation at 200°C.
16 Arsenical alunite presented a good precipitation yield and a significant AsO₄
17 substitution (up to 15% molar). The degree of arsenate substitution depends on the
18 solution composition. It increased as $(\text{AsO}_4/(\text{AsO}_4+\text{SO}_4))_{\text{alunite}} \cong 0.5$
19 $(\text{AsO}_4/(\text{AsO}_4+\text{SO}_4))_{\text{L}}$. For $(\text{AsO}_4/(\text{AsO}_4+\text{SO}_4))_{\text{L}} < 0.26$, arsenical alunite was the unique
20 phase and, above this ratio, mansfieldite (AlAsO₄·2H₂O) co-precipitated. The *a* unit
21 cell parameter is practically independent of the AsO₄ substitution, but the *c* unit cell
22 parameter increased consistently with the differences between the As-O1 and S-O1
23 distances in tetrahedral sites of the structure. The maximum stability of arsenical alunite
24 in short-term tests is between pH 5-8, with an As-solubilization of 0.01-0.03 mg/L in 24
25 h. Medium-term tests were performed at some synthesized samples at its natural pH.
26 Arsenical alunite was stabilized at 0.3 mg/L released As in 2.5 weeks. These values
27 were similar to those obtained in pure and largely crystalline natural scorodite (0.4
28 mg/L released As), but lower than the obtained for synthetic scorodite (1.3 mg/L

29 released As). Thus, arsenical alunite could be effective for arsenic immobilization,
30 especially for effluents or wastes containing large SO_4/AsO_4 ratio. Hydronium alunite
31 presents a low precipitation yield and a very low arsenate incorporation (up to 1%
32 molar). This may be related by the difficulty of substituting protonated HAsO_4^{2-} -for-
33 SO_4^{2-} or H_2O -for- OH^- groups, due to the location of the H- bridges of the H_3O in the
34 structure. These characteristics make hydronium alunite unsuitable for arsenic
35 immobilization.

36

37

38 1. Introduction:

39

40 Arsenic is a common element in non-ferrous metallurgies wastes, particularly copper
41 pyrometallurgy. Lots of studies have searched the way to remove and stabilize it. The
42 most used industrial method is the precipitation with calcium hydroxide, which gives
43 calcium arsenate products. Nevertheless, these products are unstable in contact with
44 water and, the arsenic is released [1]. Some other phases such as scorodite
45 ($\text{FeAsO}_4 \cdot 2\text{H}_2\text{O}$) [2, 3] have been proposed for arsenic precipitation and storage.
46 Scorodite presents a great stability in short-term solubility tests (As: ~ 0.1 mg/L at pH
47 5). However, it suffers a slow incongruent dissolution at neutral pHs (As: ~ 5 mg/L at
48 pH 7) [4, 5, 6, 7]. Other crystalline arsenate phases synthesized in sulfate media present
49 similar or better stability than scorodite. The most stable is BFAS ($\text{Fe}(\text{AsO}_4)_{1-x}$ -
50 $(\text{SO}_4)_x(\text{OH})_x \cdot (1-x)\text{H}_2\text{O}$) [8], also named type-2 [9] and phase 3 [10]). Swash and
51 Monhemius [9] considered that BFAS/type-2/phase 3 present an stability similar to
52 scorodite's (0.34 mg/L As released). And Gomez et al. [8] reported that BFAS/type-
53 2/phase 3 presented better values in short and in long-term leaching studies than
54 scorodite's (<1 mg/L (1st contact) to 0.1 mg/L As at pH 5 in short-term leaching and 0.1
55 mg/L As at pH 5 and long-term leaching).

56 Arsenic precipitation as sulfate-type compounds -with arsenate in diluted solid solution-
57 can be of interest, especially for effluents, which contain moderate to high $\text{SO}_4^{2-}/\text{AsO}_4^{3-}$
58 ratios [11, 12, 13, 14]. Recently, some studies focused on the AsO_4 incorporation in
59 natroalunite (ideally, $\text{NaAl}_3(\text{SO}_4)_2(\text{OH})_6$). Natroalunite belongs to alunite supergroup,

60 $AB_3(TO_4)_2(OH)_6$, where A is a monovalent or a divalent such as Na, K, Ba, Pb, H_3O ,
61 etc; B is a trivalent such as Fe or Al; and T is S, As or P. The compounds of the alunite
62 supergroup have good stability in environmental conditions, so they have been proposed
63 for the immobilization of toxic metals [15, 16]. These phases exhibit multiple
64 substitutions in the different sites because charge balance can be achieved by coupled
65 substitutions, vacancies or protonation of OH or TO_4 groups. In arsenical natroalunite,
66 the AsO_4 -for- SO_4 substitution can be up to 15% molar in the TO_4 site and low arsenic
67 dissolution was found in short leaching tests (As: 0.01-0.05 mg/L at pH 5-8) [11, 12,
68 14]. Results of long term leaching showed an equilibrated solubility of ~ 0.1 mg/L in 6
69 months at its natural pH (~ 5) [11, 12].

70

71 Some studies synthesized and compared the behavior of the incorporation of other
72 elements in alunite structure. Rudolph et al. [17] studied the alunites with different
73 elements in the A site. In this study, an increase in the A ionic radius correlates with the
74 *c* cell parameter: $Na < H_3O < K < NH_4 < Rb$. Sunyer and Viñals [13], also determined the
75 effect of the incorporation of arsenate in the natroalunite structure and found that the *c*
76 cell parameter increased in a linear manner, as consequence of the differences between
77 As-O and S-O distances of the TO_4 site. Similar dependence on cell expansion was
78 previously found for the AsO_4 -for- SO_4 substitution in jarosite ($KFe_3(SO_4)_2(OH)_6$) [12].

79

80 The As incorporation in the Al-members of the alunite group have been only tested in
81 natroalunite. For this reason, the study of AsO_4 -for- SO_4 substitution in alunite
82 ($KAl_3(SO_4)_2(OH)_6$) and hydronium alunite ($(H_3O)Al_3(SO_4)_2(OH)_6$) was of interest.
83 Additionally, their larger cells can facilitate the incorporation of the large arsenate
84 group in the structure. The objective of this paper is the study of AsO_4 -for- SO_4
85 substitution in alunite and hydronium alunite. Short-term leaching tests in a pH range 1-
86 12 are also reported, as well as a comparative medium-term leaching test in arsenical
87 alunite and natural and synthetic scorodite at its natural pH in pure water.

88

89 2. Experimental:

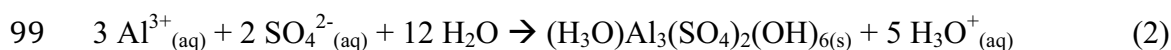
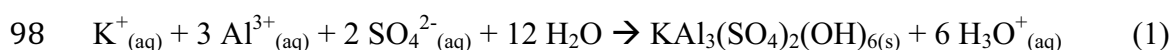
90

91 2.1. Hydrothermal synthesis of arsenical alunite and hydronium-alunite

92

93 Experiments were performed in similar way than in previous papers [11-14]. A pressure
94 reactor PARR 4843; equipped with stirring, pressure and temperature control was
95 employed. The reagents used are reported in Table 1. For alunite, a molar ratio Al/K= 3
96 was used, according to the stoichiometry of the synthesis reactions:

97



100

101 All reagents were previously dissolved with deionized water up to 150 mL and the pH
102 was adjusted to 1.0 with the addition of small amounts of H₂SO₄. The experiments were
103 carried out at 200°C during 1 h and then were cooled. The precipitates were filtered and
104 washed 3 times with 50 mL deionized water and finally dried at room temperature.

105 Table 1. Synthesis conditions (pH_{initial}=1).

test	Al ₂ (SO ₄) ₃ .1 8H ₂ O (g)	H ₃ AsO ₄ (g)	K ₂ SO ₄ (g)	initial solution molar ratio (AsO ₄ /(SO ₄ + AsO ₄)) _L	wt precipitate (g)	pH _{final}
alunite						
K0	6.332	0	0.552	0	2.0391	0.2
K0.5	6.332	0.450	0.552	0.091	1.8571	0.3
K1	6.332	0.900	0.552	0.167	2.3241	0.2
K1.5	6.332	1.350	0.552	0.231	1.9557	0.4
K2	6.332	1.804	0.552	0.290	2.2583	0.4
K2.5	6.333	2.243	0.551	0.333	2.1729	0.2
hydronium alunite						
H0	6.333	0	-	0	0.6733	0.5
H0.25	6.331	0.227	-	0.053	0.4122	0.5
H0.5	6.331	0.455	-	0.101	0.2349	0.7
H0.75	6.331	0.667	-	0.142	0.2509	0.6
H1	6.330	0.894	-	0.181	0.1455	0.7
H1.5	6.330	1.349	-	0.250	0.0339	0.8

106

107

108 2.2. Characterization of precipitates

109

110 All samples have been analyzed using chemical analysis by inductively coupled plasma
111 (ICP-OES), scanning electron microscopy (SEM-EDS), and X-Ray diffraction (XRD).

112

113 ICP-OES was used to know the bulk chemical composition of the samples. These were
114 prepared by digestion of 0.1 g with 10 mL of concentrated HCl and diluted to 50 mL
115 before the analysis. For these analyses was used a Perkin Elmer Optima 3200 RL.

116

117 SEM-EDS study was performed using a Jeol JSM-840 equipped with an INCA 250-
118 analyzer. Samples were coated with carbon and analyzed at a beam current of 0.6 nA at
119 20 kV for 30 s for minimizing the spot size (about 50 nm in these conditions). The EDS
120 was calibrated with the following standards: quartz (O K α), orthoclase (K K α), alumina
121 (Al K α), pyrite (S K α), and InAs (As L α). The data were normalized to 100% atomic of
122 all detected elements excluding the C. The compound formulae were obtained from the

123 mean atomic percentage of 10 spot analyses as it was done in previous studies [11, 12,
124 13], assuming the structural basis of $S + As = 2$. The H_3O content in formula was
125 obtained by difference, considering full occupancy in the A site. Previous studies
126 proved that the formula coefficients obtained under these conditions were similar to that
127 obtained using bulk chemical analyses [11] (Table 3).

128

129 X-ray diffraction was done using PANalytical X'Pert PRO MDP Alpha'1 equipment
130 with Bragg Brentano geometry and 240 mm radius. Data was collected from 10° to 120°
131 2θ with a monochromatic radiation $Cu-K_{\alpha 1}$ 1.5406, with a step size of 0.017 using a
132 step counting time of 200 s. Under these conditions the detection limit of the target
133 phases is about 0.5%. The X-ray diffraction was used to identify the different crystalline
134 phases in the samples and to determine the cell parameters and the phase composition
135 using Rietveld refinement. Rietveld refinement was performed with FullProf program,
136 as in Sunyer and Viñals [13] for natroalunite samples. The modified Thomson-Cox-
137 Hasting pseudo-Voigt function was used for the calculated profile. The starting atomic
138 parameters for alunite were taken from Menchetti and Sabelli [21] and for hydronium
139 alunite were taken natroalunite initial parameters from Okada et al. [22] in which was
140 changed sodium and potassium ionic radii for H_3O radius (1.52 Å) [25, 26]. The initial
141 cell parameters for both alunite and hydronium alunite were taken from Rudolph et al.
142 [17]. The starting atomic parameters for mansfieldite were taken from Harrison [27].
143 The starting site occupancies for the different alunites were changed depending on the
144 formula obtained by EDS analyses. The refined parameters were the background, the
145 scale factors, the unit cell parameters, the profile and the asymmetry. All the parameters
146 were adjusted to minimum values.

147

148 2.3. Leaching tests

149

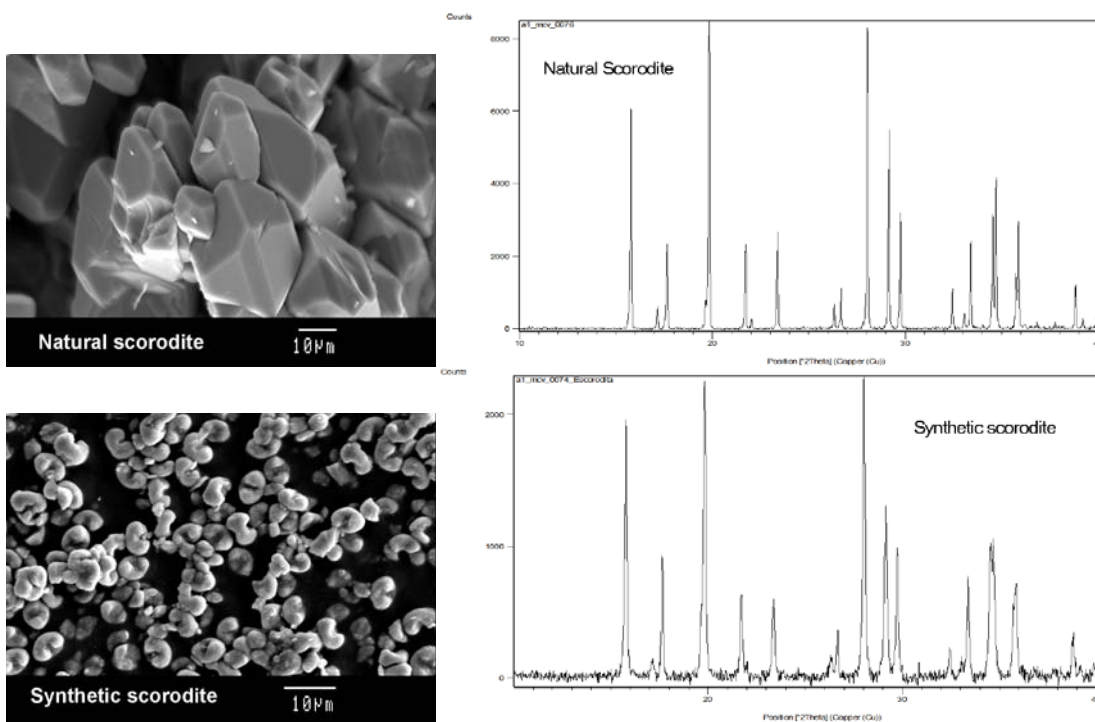
150 Short-term (24 hour) leaching tests at pH between 1 and 12 were performed for a
151 selected arsenical alunite sample (K1) as detailed in Sunyer and Viñals [13]. Solutions
152 were made from diluted H_2SO_4 or NaOH. The tests consisted in three 24-h consecutive
153 leaching in a plastic erlenmeyer with magnetic stirring at 250 rpm. It was performed
154 with 0.5 g of sample in 50-mL solution. The pH was monitored during all 24-h
155 leaching, and it was adjusted in case of variations. After the leaching, the solid was

156 filtrated and leached again at the same pH. All leaching liquids and blanks were
157 analyzed by ICP-OES and for low concentrations (<1 mg/L) by ICP-MS.

158

159 Medium-term stability was evaluated for the same arsenical alunite sample (K1), a
160 natural scorodite sample and a synthetic scorodite sample. The natural scorodite was
161 extracted from a museum grade specimen from Ojuela mine (Durango, Mexico), which
162 consisted of intergrown crystals of 10-50 μm in size (Fig.1). The extracted crystal
163 clusters were carefully examined by SEM/EDS and XRD (Fig. 1), which confirmed the
164 purity of the sample. Prior the leaching treatment, the sample was milled to <10 μm and
165 finally washed with deionized water. Synthetic scorodite was prepared by hydrothermal
166 reaction of ferric nitrate and arsenic acid at 160°C and 24 h, as described by Dutrizac
167 and Jambor [28]. It consisted in microcrystalline aggregates which formed spheroidal
168 particles of $\sim 5 \mu\text{m}$ (Fig. 1). The purity of the sample was confirmed by SEM/EDS and
169 XRD (Fig. 1).

170



171

172 Fig. 1. SEM images and XRD patterns of the natural and synthetic scorodite samples.

173

174 These tests were performed using 2.5 g of sample with 250 mL of deionized water in a
175 plastic Erlenmeyer with magnetic stirring (300 rpm) for a period of 5 weeks at its
176 natural pH. Samples were taken during this period and analyzed by ICP-MS.

177

178 3. Results and Discussion

179

180 3.1. Synthesis of arsenical alunite and arsenical hydronium alunite

181

182 3.1.1. Arsenical alunite

183

184 Table 2 shows the bulk chemical composition, the precipitation yield and the phase
185 composition as observed by XRD (Fig. 2) and SEM-EDS (Fig. 3). The alunite
186 precipitation yield – computed through the Al data – reached about 70-80% under these
187 conditions. These values were similar to the obtained in the arsenical natroalunite
188 synthesis [11, 13, 14]. The phases formed under these conditions were arsenical alunite
189 for a molar ratio of $\text{AsO}_4/(\text{SO}_4+\text{AsO}_4) < 0.29$ in the liquid phase and a mixture of
190 arsenical alunite and mansfieldite ($\text{AlAsO}_4 \cdot 2\text{H}_2\text{O}$) for $\text{AsO}_4/(\text{SO}_4+\text{AsO}_4) \geq 0.29$. The As
191 yield was 10-13% when arsenical alunite was the unique phase, and it increased when
192 mansfieldite co-precipitated. Then, in K or Na alunites, a limited but significant
193 incorporation of arsenic in the structure is possible.

194

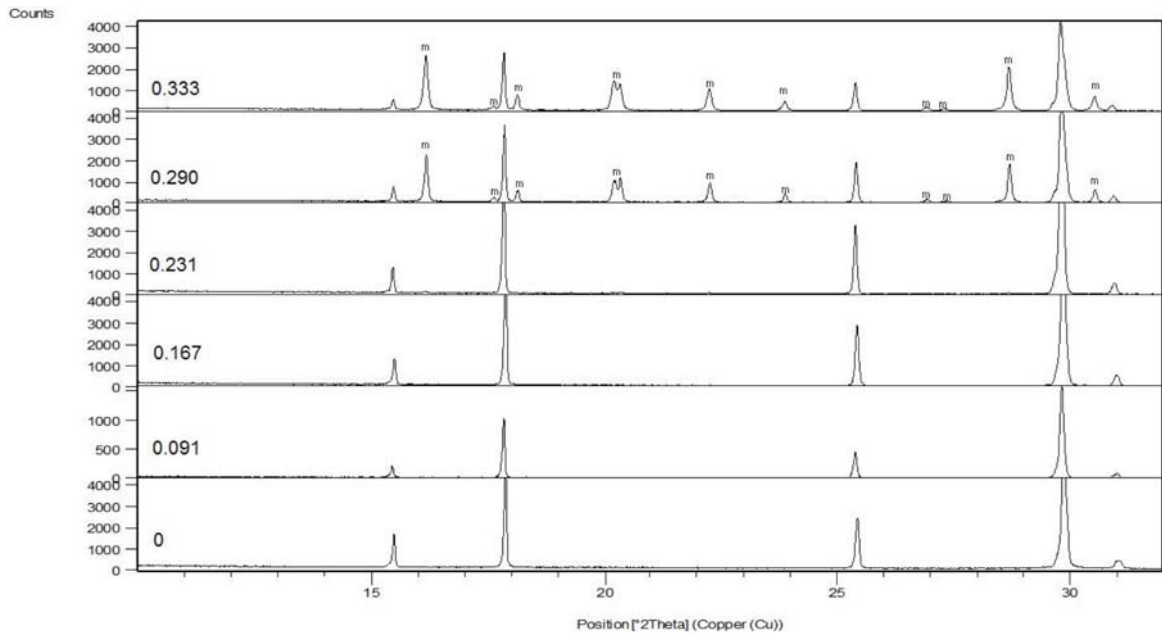
195 The alunite crystals showed the same size (1-10 μm) and shape, independently of the
196 AsO_4 -for- SO_4 substitution (Fig. 3). The shape was rhombohedric (pseudo-cubic) with
197 (012) dominant and (001) subordinate faces, in the same way as the observed in
198 natroalunite synthesis [13].

199 Table 2. Bulk chemical composition, precipitation yield and phase composition of
 200 precipitates.

(AsO ₄ / (SO ₄ + AsO ₄)) _L	bulk chemical composition (%)				precipitation yield (%)		phases (XRD and SEM/EDS)
	Al	S	K	As	Al	As	
alunite synthesis							
0	18.72	15.21	6.31	0.00	75	-	alunite
0.091	18.90	14.37	6.07	1.63	69	13	alunite
0.167	18.55	14.01	5.94	2.30	84	11	alunite
0.231	17.36	12.55	5.41	3.61	67	10	alunite
0.290	15.98	8.96	5.26	13.00	70	31	alunite (66%) + mansfieldite (34%)
0.333	16.00	7.10	4.32	17.24	68	32	alunite (51%) + mansfieldite (49%)
hydronium alunite synthesis							
0	20.60	15.91	-	0	27	-	H ₃ O-alunite
0.053	20.21	16.01	-	0.167	16	0.6	H ₃ O-alunite (trace mansfieldite)
0.101	20.81	16.13	-	0.056	10	0.05	H ₃ O-alunite
0.142	20.66	15.93	-	0.034	10	0.02	H ₃ O-alunite
0.181	21.00	16.28	-	0.082	6	0.03	H ₃ O-alunite + amorphous phase
0.250	19.28	12.44	-	10.89	1	0.5	H ₃ O-alunite + mansfieldite + amorphous phase

201

202



203 Fig. 2. XRD patterns of the alunite synthesis at different $\text{AsO}_4/(\text{SO}_4/\text{AsO}_4)$ molar ratios
 204 in the liquid phase. m: mansfieldite. The rest of peaks correspond to alunite.
 205

206

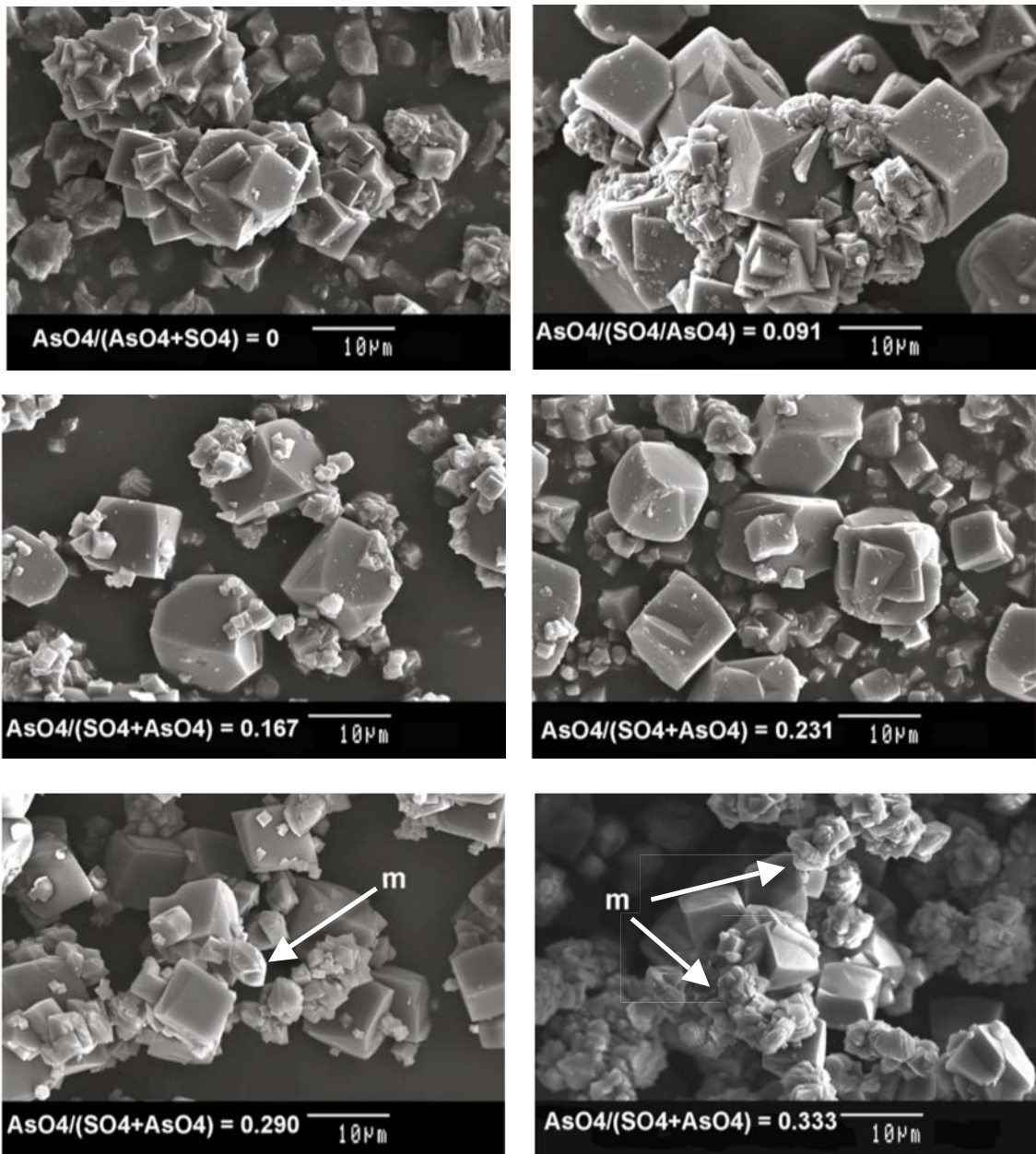
207 The formula coefficients of the alunite phase are shown in table 3. They showed a small
 208 deficit in Al-site and a significant H_3O -for-K substitution in the alkali site, common also
 209 in the synthesis of natroalunites and jarosites [13, 18]. The incorporation of arsenic in
 210 alunite reached 0.32 moles per formula unit, a value also similar to the obtained in
 211 natroalunite [7]. However, in natroalunite the incorporation was up to 0.15 moles per
 212 formula unit before mansfieldite formation, whereas the incorporation of arsenic in
 213 alunite was up to 0.24 moles per formula unit before the formation of this second phase.

214

215 Mansfieldite formed at high $\text{AsO}_4/(\text{SO}_4+\text{AsO}_4)$ ratio appeared as smaller orthorhombic
 216 crystals (up to $5\mu\text{m}$) on the alunite crystal clusters. However, samples with mansfieldite
 217 were not studied in leaching tests of the present study. According to Le Berre et al. [19,
 218 20], mansfieldite was more reactive than scorodite at neutral or near neutral pH, and
 219 previous studies on arsenical-natroalunite also showed that samples which contained
 220 mansfieldite were more reactive [11]. For this reason, mansfieldite appears to be
 221 unsuitable for arsenical immobilization.

222

223



224

225

226

227

228

Fig. 3. Morphology of the alunite precipitates obtained at different $\text{AsO}_4/(\text{SO}_4+\text{AsO}_4)$ molar ratios in the liquid phase. m: mansfieldite (SEM/SE).

228 Table 3. Formula coefficients normalized to S+As=2. BCA from bulk chemical
 229 analysis, and EDS: from spot analysis by EDS; H₃O: assuming full occupancy in A site)

$(\text{AsO}_4/(\text{SO}_4+\text{AsO}_4))_L$	BCA					EDS				
	S	As	Al	K	H ₃ O	S	As	Al	K	H ₃ O
alunite										
0	2.00	0.00	2.93	0.68	0.32	2.00	0.00	2.92	0.65	0.35
0.091	1.91	0.093	2.98	0.66	0.34	1.88	0.12	2.93	0.63	0.37
0.167	1.87	0.13	2.93	0.65	0.35	1.84	0.16	2.89	0.62	0.38
0.231	1.78	0.22	2.93	0.63	0.37	1.76	0.24	2.92	0.63	0.37
0.290	Not det. (phase mixture)					1.72	0.28	2.94	0.60	0.40
0.333	Not det. (phase mixture)					1.67	0.32	2.91	0.62	0.38
hydronium alunite										
0	2.00	0.00	3.08	-	1.00	2.00	0.00	2.94	-	1.00
0.053	1.99	0.009	2.99	-	1.00	1.99	0.011	2.91	-	1.00
0.101	2.00	0.003	3.06	-	1.00	1.99	0.009	2.96	-	1.00
0.142	2.00	0.002	3.08	-	1.00	1.99	0.008	2.90	-	1.00
0.181	Not deter. (phase mixture)					1.98	0.019	2.98	-	1.00
0.250	Not deter. (phase mixture)					Not deter. (extremely fine intergrowth)				

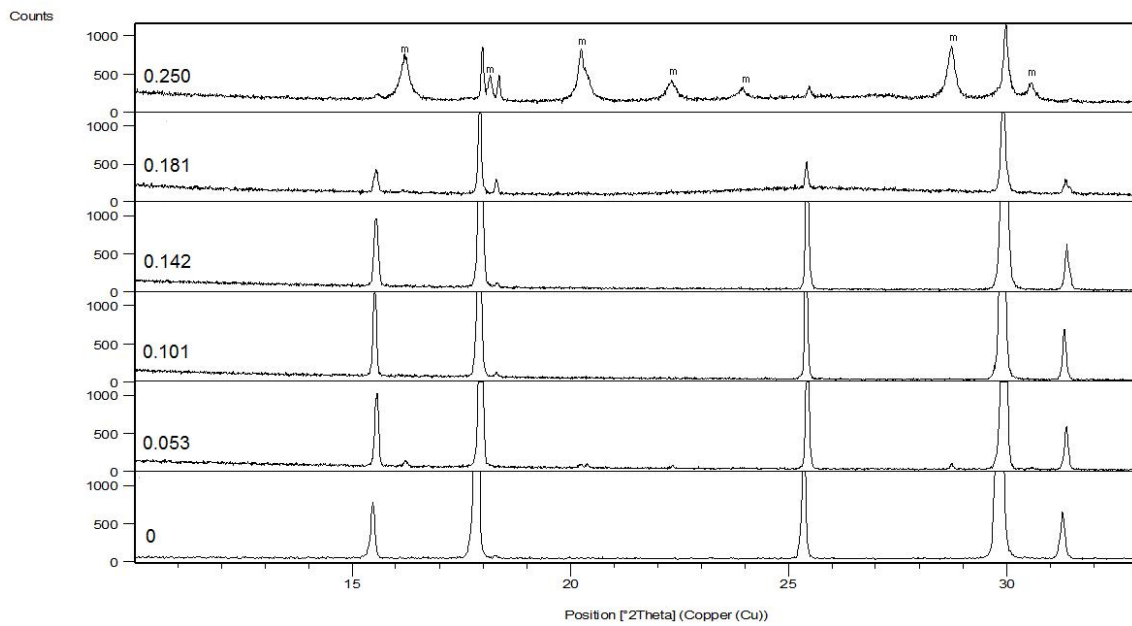
230

231 3.1.2. Arsenical hydronium alunite

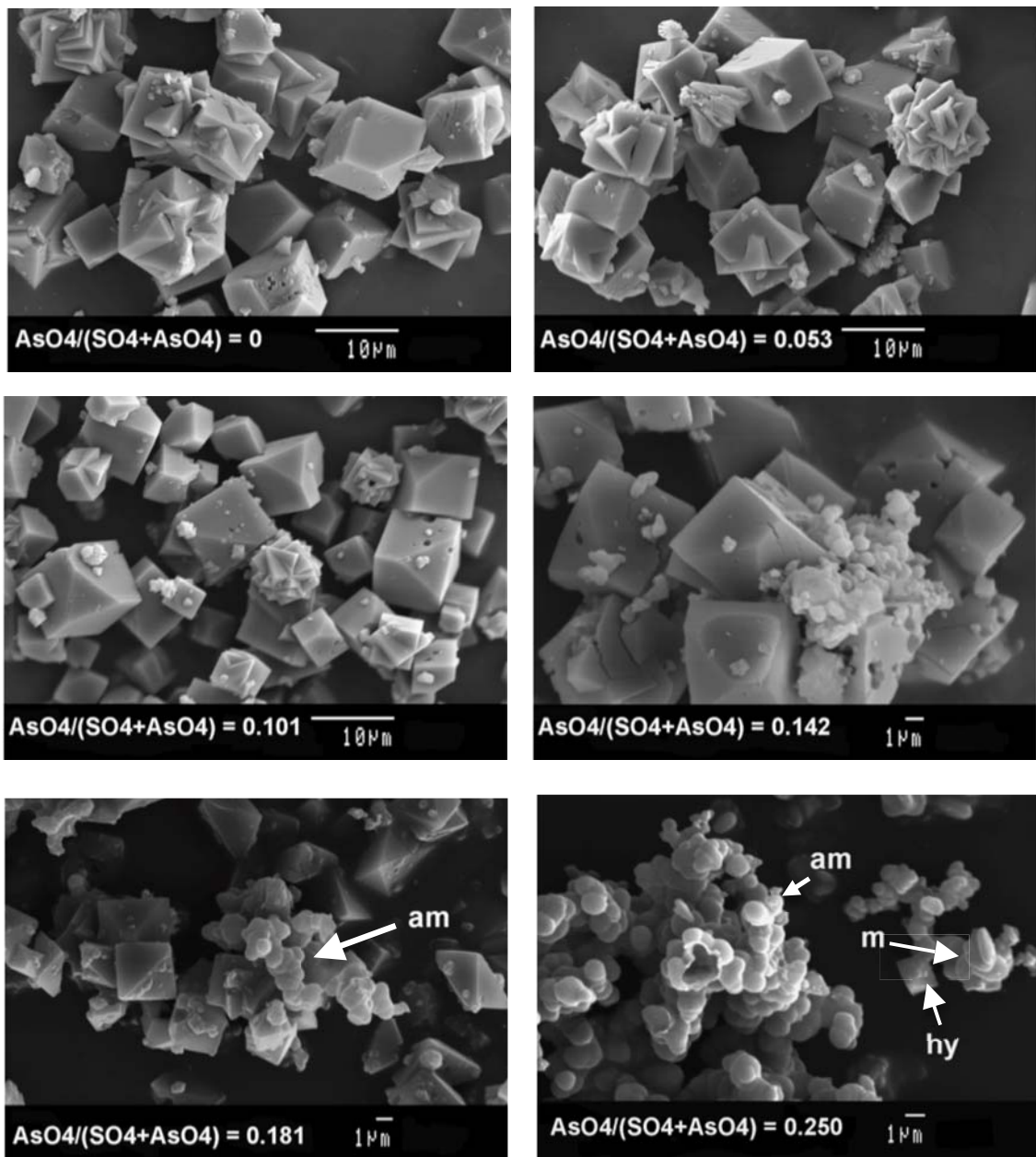
232

233 Table 2 shows the bulk chemical composition, the precipitation yield and the phase
 234 composition as observed by XRD (Fig. 4) and SEM-EDS (Fig. 5). In contrast of alunite
 235 and natroalunite, hydronium alunite had a low precipitation yield in all experiments.
 236 These results agree by those found by Rudolph et al. [17], which obtained similar
 237 precipitation yields in As-free hydronium alunite. Furthermore, the arsenic addition in
 238 the aqueous medium caused a decrease in the precipitation yield when the arsenic
 239 concentration increased, that was very small to practically negligible for
 240 $(\text{AsO}_4/(\text{SO}_4+\text{AsO}_4))_L > 0.18$, in which an amorphous Al-arsenate-sulfate phase (Figs. 5
 241 and 6) and mansfieldite precipitated. In addition, the AsO₄-for-SO₄ substitution in the
 242 hydronium alunite phase (Table 3) was extremely small (~ 0.01-0.02 in formula) and

243 this effect was practically independent of the As-concentration in the aqueous media.
244 Thus, hydronium alunite is clearly unsuitable for arsenic immobilization.
245



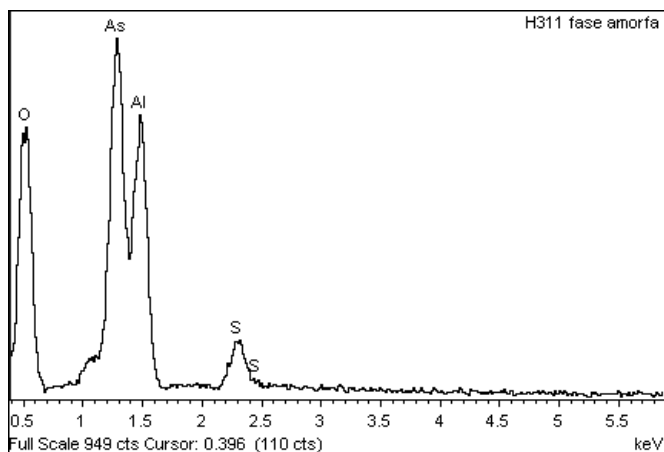
246 Fig. 4. XRD patterns of the hydronium alunite synthesis at different $\text{AsO}_4/(\text{SO}_4/\text{AsO}_4)$
247 molar ratios in the liquid phase. m: mansfieldite. The rest of peaks correspond to
248 hydronium alunite.
249
250



251

252 Fig. 5. Morphology of the hydronium alunite precipitates obtained at different
 253 $\text{AsO}_4/(\text{SO}_4+\text{AsO}_4)$ molar ratios in the liquid phase. m: mansfieldite, am: amorphous
 254 phase, hy: hydronium alunite (SEM/SE).

255



256

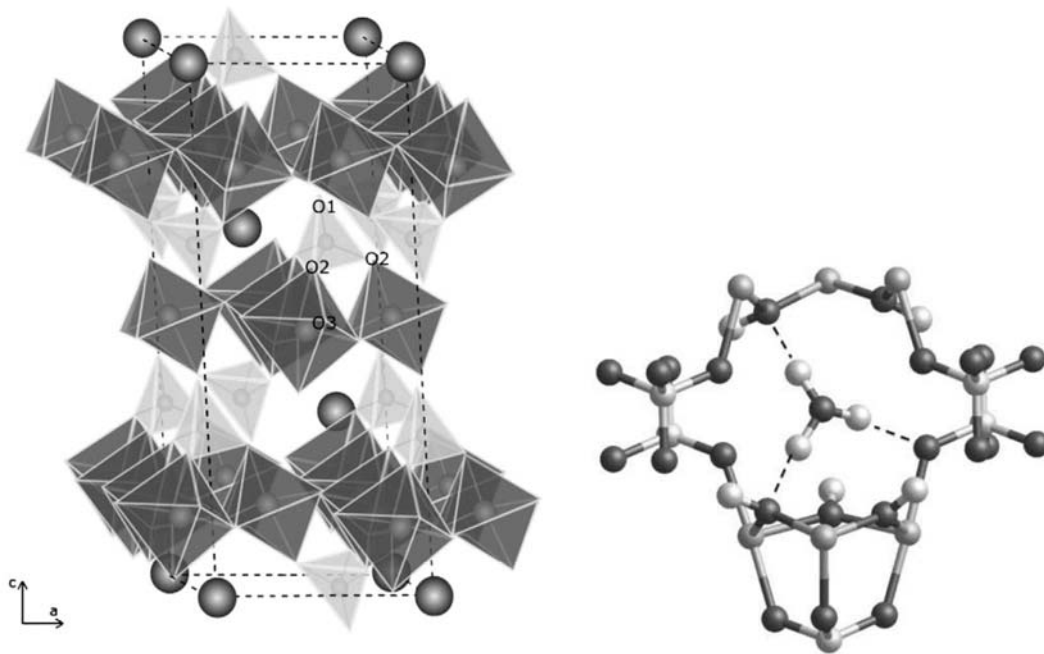
257 Fig. 6. EDS spectrum of the amorphous Al-arsenate-sulfate obtained at
 258 $\text{AsO}_4/(\text{SO}_4+\text{AsO}_4) > 0.14$.

259

260 The precedent results indicated that the cell dimension in simple alunites (Na, K and
 261 H_3O -alunites) do not significantly affect the AsO_4 -for- SO_4 substitution. Natroalunite,
 262 which has a small cell ($c \sim 16.7 \text{ \AA}$ [22]), incorporated similar AsO_4 than alunite ($c \sim$
 263 17.4 \AA [22]) and much more than hydronium alunite, which have a larger cell ($c \sim 17.1$
 264 \AA).

265

266 Thus, it is reasonable that the extension of the AsO_4 -for- SO_4 substitution in simple
 267 alunites can be limited by charge balance considerations. In simple alunites (or
 268 jarosites), the substitution of SO_4^{2-} for AsO_4^{3-} requires a charge compensation. Paktunc
 269 and Dutrizac [18] suggested that it might occur via protonation of AsO_4^{3-} to HAsO_4^{2-} .
 270 HAsO_4^{2-} group was found in alunite-type structures such as in dussertite
 271 ($\text{BaFe}_3(\text{AsO}_4)_2(\text{OH})_5$) [23]. Another possibility is the protonation of OH^- to H_2O . In this
 272 line, H_2O molecules were also found in alunite-type structures such as hidalgoite
 273 ($\text{PbAl}_3(\text{AsO}_4)(\text{SO}_4)(\text{OH})_6$) [24]. In alunite, natroalunite and jarosite the maximum
 274 observed substitution was $\sim 15\%$ molar (~ 0.3 in formula). Then, the low precipitation
 275 yield and the extremely low incorporation of arsenic in the hydronium alunite can be
 276 related by the difficulty of coupling these protonated groups with the position of the
 277 H_3O in the structure, and vice versa. Recently, Gale et al. [29], proposed a structure of
 278 the hydronium alunite where the H_3O^+ hydrogen bonded with the O of the $\text{Al-O}_2(\text{OH})_4$
 279 octahedra and the O of the SO_4 tetrahedra (Fig. 7). In hydronium alunite, the
 280 substitution of SO_4^{2-} by HAsO_4^{2-} or OH^- by H_2O implies an additional H, which can
 281 deprive H_3O^+ to make the hydrogen bridge.



282

283 Fig. 7. Left: Schema of the structure of simple alunites [12]. The dashed lines show the
 284 unit cell. TO_4 groups (SO_4 , AsO_4) are the light colored tetrahedra, $\text{Al-O}_2(\text{OH})_4$
 285 octahedra are dark grey and the large spheres represent A atom (Na, K, H_3O). The TO_4
 286 group is triply coordinated with $\text{Al-O}_2(\text{OH})_4$ octahedra through the O2 atom, whereas
 287 the O1 (apical) atom is not coordinated. The O3 atom is linked as OH group (H atoms
 288 are not shown). Right: Detailed location of H_3O with the c axis being vertical as shown,
 289 according to Gale et al. [29]. The hydronium cation forms two hydrogen bonds to O
 290 atoms of hydroxyl groups that bridge aluminum atoms (on left-hand side of figure) and
 291 one hydrogen bond to an O atom of a sulfate group coordinated to another aluminum
 292 atom (right-hand side).

293

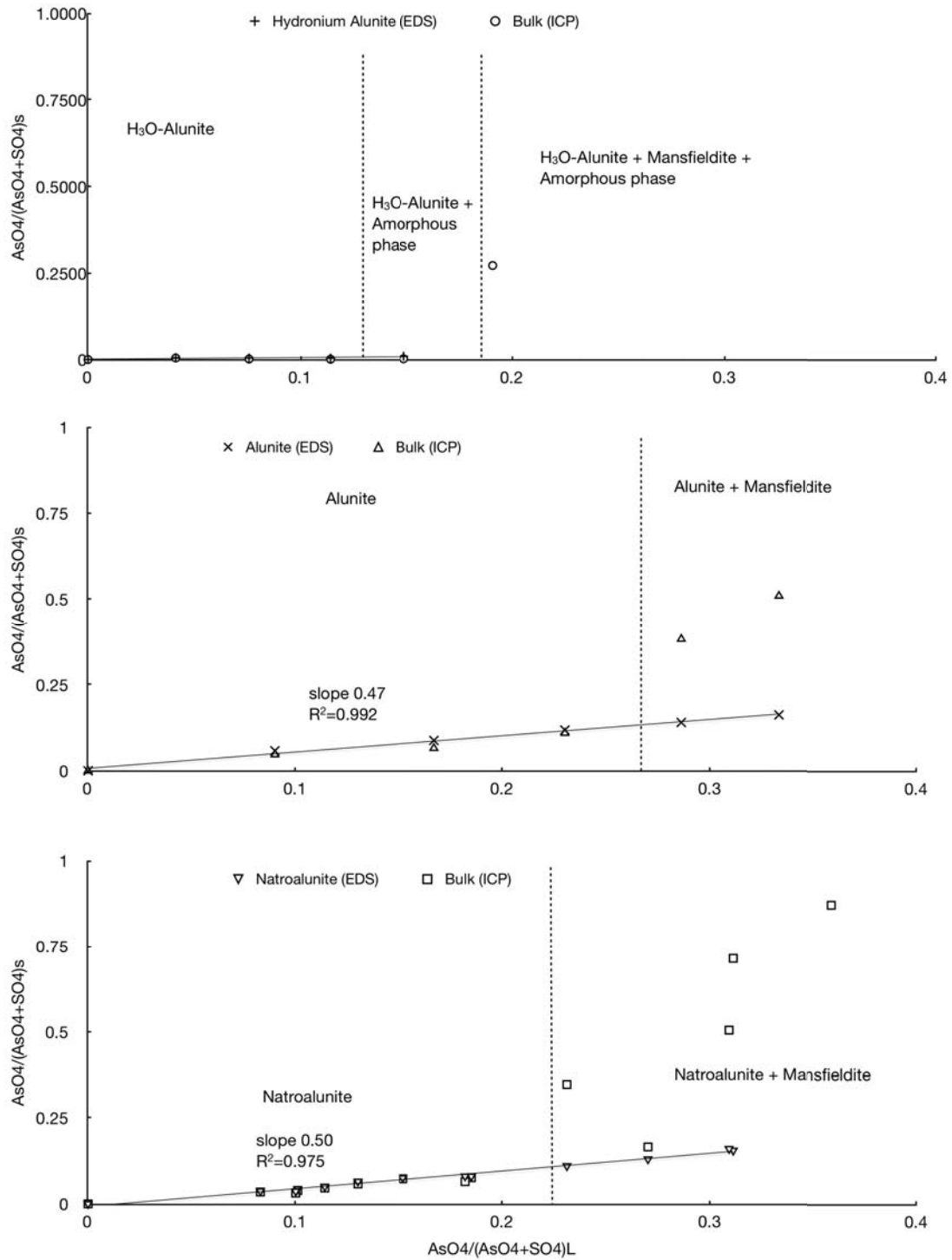
294

295 3.2. Arsenic partition during the synthesis of K, Na and H_3O alunites

296

297 The arsenic partition during the synthesis of simple alunites is summarized in Fig. 8. In
 298 the regions of the formation of a single alunite phase, the results for
 299 $(\text{AsO}_4/(\text{SO}_4+\text{AsO}_4))_{\text{alunite phase}}$ - obtained by spot EDS analysis - and the bulk chemical
 300 analysis $((\text{AsO}_4/(\text{SO}_4+\text{AsO}_4))_{\text{bulk}})$ (obtained by ICP) were coincident. When a second
 301 arsenate-rich phase (amorphous or mansfieldite) was formed, the
 302 $(\text{AsO}_4/(\text{SO}_4+\text{AsO}_4))_{\text{bulk}}$ were obviously higher than the observed in the spot analysis of
 303 the alunite crystals. For hydronium alunite, an increase in $\text{AsO}_4/(\text{SO}_4+\text{AsO}_4)$ molar ratio

304 in the liquid phase, increased very slightly the As-substitution. Other As-bearing phases
305 (amorphous Al-arsenate-sulfate and mansfieldite) appeared rapidly at
306 $(\text{AsO}_4/(\text{SO}_4+\text{AsO}_4))_{\text{L}} > 0.14$. For natroalunite and alunite, an increase in
307 $(\text{AsO}_4/(\text{SO}_4+\text{AsO}_4))_{\text{L}}$, implied a linear increase in AsO_4 -for- SO_4 substitution according
308 to: $(\text{AsO}_4/(\text{SO}_4+\text{AsO}_4))_{\text{alunite phase}} \cong 0.5(\text{AsO}_4/(\text{SO}_4+\text{AsO}_4))_{\text{L}}$. The second phase for
309 alunite and natroalunite synthesis was mansfieldite, appearing at $(\text{AsO}_4/(\text{SO}_4+\text{AsO}_4))_{\text{L}} >$
310 0.2 in natroalunite and $(\text{AsO}_4/(\text{SO}_4+\text{AsO}_4))_{\text{L}} > 0.25$ in alunite.



311

312 Fig. 8. Effect of solution composition ($\text{AsO}_4/(\text{SO}_4+\text{AsO}_4)_L$) on the arsenic distribution
 313 in the bulk precipitate ($\text{AsO}_4/(\text{SO}_4+\text{AsO}_4)_S$) and in alunite-type phase at 200°C. (Data of
 314 natroalunite from Sunyer and Viñals [13])

315

316 3.3. Effect of arsenate substitution in cell parameters

317

318 Cell parameters and the structure refinement details obtained by the Rietveld method
319 are shown in table 4. Most of the crystallographic R_F parameters are less than 10%,
320 indicating that the structural model for alunite-type phases [30] was satisfactory,
321 independently of the AsO_4 -for- SO_4 substitution. The goodness of fitting (S) was also
322 satisfactory, especially for alunite samples.

323

324 The obtained a cell parameters for alunite and hydronium alunite were very close (\sim
325 7.01 Å) and similar to those obtained in previous works (6.983 Å and 7.008 Å [17],
326 respectively). This is consistent with the topology of the alunite-type structure (Fig. 7),
327 where a cell parameter depends practically only on B-O2 distance, in this case Al-O2
328 distance (2.81 Å [30]).

329

330 Otherwise, c cell parameter depends on both, A cation size and T-O1 distance. Thus, it
331 reflects the contribution of the substitutions in the alkali site (H_3O -for-K substitution)
332 and the AsO_4 -for- SO_4 substitution. However, the overlapped effect of the H_3O -for-K
333 substitution can be corrected as $c_{\text{cor}} = c + 0.1945X_{\text{H}_3\text{O}}$ (Å), according to the data of
334 Rudolf et al. [17] on the effect of the H_3O -occupancy ($X_{\text{H}_3\text{O}}$) in the K- H_3O alunite
335 series.

336

337 For hydronium alunite, the variation in c cell parameter was insignificant (Table 4), and
338 confirmed the negligible substitution of the AsO_4 in the structure. The value of c (17.13
339 Å) was similar to those reported in previous works (17.136 Å [17]).

340

341 The variation of the c cell parameter in alunite with the AsO_4 -for- SO_4 substitution is
342 given in Fig. 9. The c cell parameter increased with an slope of 0.577, very similar to
343 those found in natroalunite (0.588-0.591[12]) and, relatively similar in arsenical jarosite
344 (0.44 [18]). As discussed in a previous paper [12], this cell expansion can be directly
345 related with the difference in the As-O1 and S-O1 apical distances (0.12 Å [30]). Thus,
346 these results confirm the AsO_4 -for- SO_4 substitution in the tetrahedral sites of the alunite
347 structure.

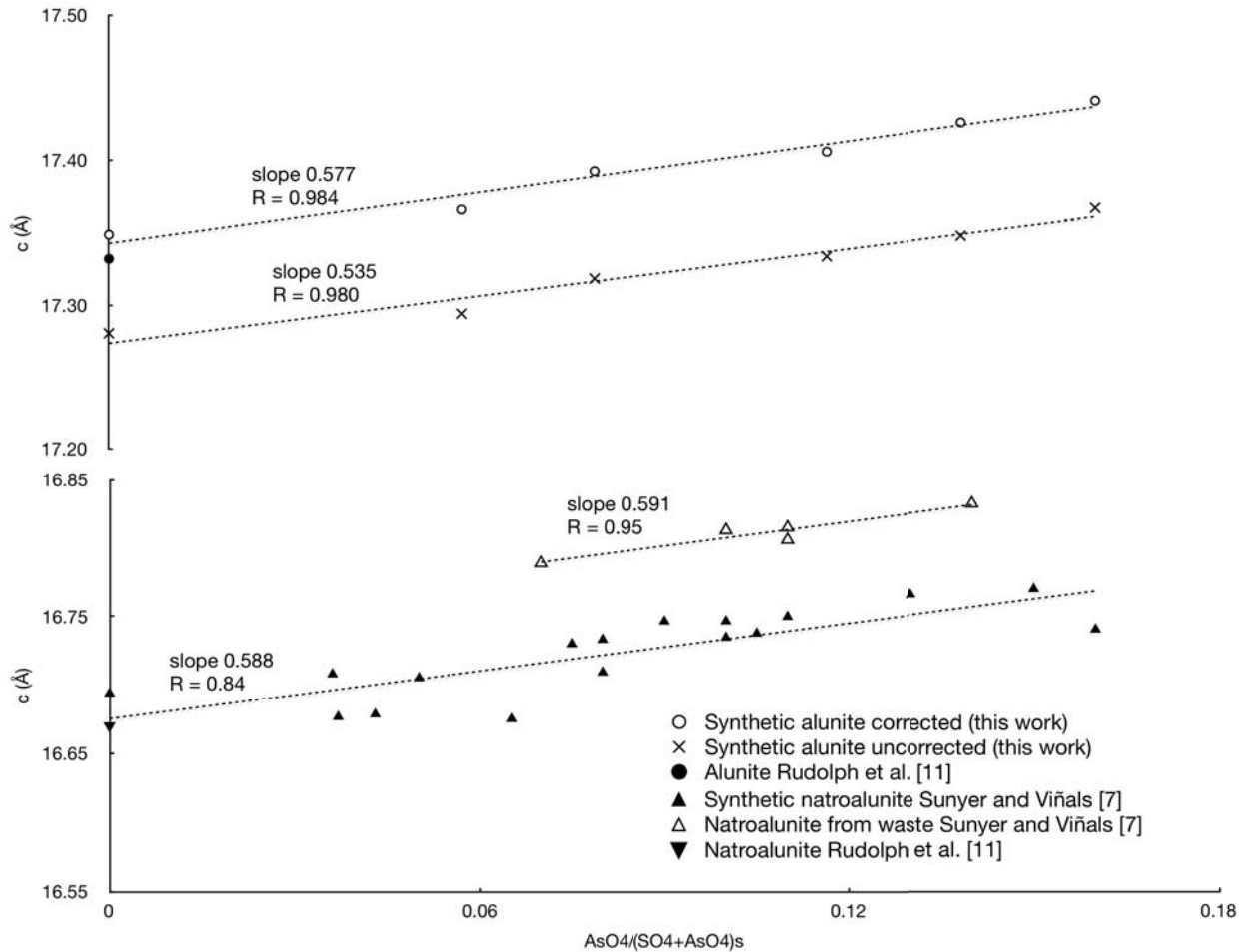
348

349 Table 4. Cell parameters and structure refinement details ($X_{As} = (AsO_4/(SO_4+AsO_4))_S$).

hydronium alunite										
sample	X_{As}	X_{H3O}	a (Å)	c (Å)	V (Å ³)	R_p	R_{wp}	R_{exp}	S	R_F
H0	0.00	1.00	7.014(9)	17.133(5)	730.1(6)	15.4	21.3	11.53	1.85	9.63
H0.25	0.005	1.00	7.014(0)	17.137(8)	730.1(6)	13.8	19.4	8.60	2.26	10.40
H0.5	0.005	1.00	7.012(3)	17.136(3)	729.7(4)	13.2	18.7	8.53	2.19	13.40
H0.75	0.004	1.00	7.013(2)	17.138(3)	730.0(2)	13.3	18.6	8.72	2.13	9.17
H1	0.01	1.00	7.012(8)	17.137(6)	729.9(0)	13.1	18.4	8.69	2.12	8.68
alunite										
sample	X_{As}	X_{H3O}	a (Å)	c (Å)	V (Å ³)	R_p	R_{wp}	R_{exp}	S	R_F
K0	0.00	0.35	6.998(1)	17.280(5)	732.9(2)	14.7	19.0	11.63	1.63	6.74
K0.5	0.06	0.37	7.005(5)	17.294(0)	735.0(3)	12.7	17.0	11.74	1.45	6.91
K1	0.08	0.38	7.008(4)	17.318(3)	736.6(7)	12.6	17.1	11.62	1.47	6.72
K1.5	0.12	0.37	7.011(6)	17.333(7)	738.0(1)	13.5	18.4	11.49	1.60	7.49
K2	0.14	0.40	7.012(7)	17.347(6)	738.8(4)	16.1	20.1	15.47	1.30	5.08
K2..5	0.16	0.38	7.014(7)	17.366(6)	740.0(6)	10.3	14.0	11.16	1.25	4.61

350 X : Occupancies; R_p : R-pattern; R_{wp} : weighted pattern; R_{exp} : R-expected; $S = R_{wp}/R_{exp}$:
 351 goodness of fitting; R_F : crystallographic R-factor for the alunite phase

352



353 Fig. 9. Effect of the AsO_4 -for- SO_4 substitution in the c cell parameter for alunite and
 354
 355 natroalunite
 356

357 3.4. Leaching study

358

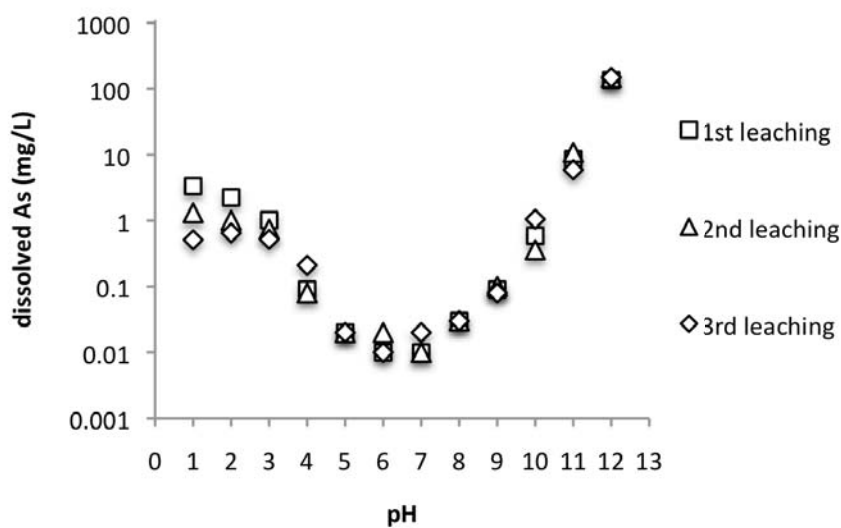
359 3.4.1. Short-term tests

360

361 The leached arsenic (24 h) from arsenical alunite in a wide range of pHs is shown in
 362 Fig. 10. Between moderate to strong acid media ($\text{pH} \leq 3$), first leaching gives some
 363 higher values than the second and third leaching. This fact was attributed to surface
 364 adsorption of aqueous arsenic species from the synthesis media. Nevertheless, the
 365 results confirmed a great stability of the arsenical alunite in acid medium. For $\text{pH}=1$, the
 366 arsenic leached was about 1 mg/L, in contrast with the reported values from scorodite
 367 (50-100 mg/L [5, 31]). The stability of the arsenical alunite increased at neutral pHs.
 368 The minimum arsenic release was found at pHs between 5 and 8, when only between

369 0.01 and 0.03 mg/L of arsenic were dissolved (Fig. 10). The arsenic releasing of alunite
370 (As leaching > 1mg/L) increased at $\text{pH} \geq 10$, and extensive alunite dissolution occurred
371 at pH 12. These results were very similar to those found in arsenical natroalunite, which
372 at pHs between 5 and 8 were dissolved between 0.01 and 0.05 mg/L of arsenic [11, 12].
373 The low arsenic dissolution in short-term stability tests in acid to moderate alkaline
374 media ($\text{pH} \leq 10$) indicated a good As inertization capacity of the phases of alunite
375 supergroup.

376



377

378 Figure 10: Arsenic leaching at different pHs (24 h).

379 3.4.2. Medium-term tests

380

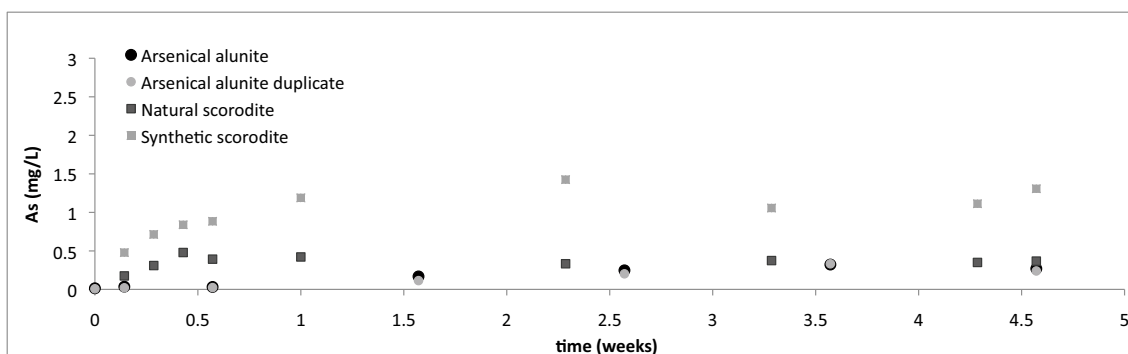
381 Medium-term leaching of arsenical alunite was done by duplicate at its natural pH 6.6-
382 5.2. The dissolved arsenic equilibrated in about 2.5 weeks at about 0.3 mg/L in both
383 tests (Fig. 11). Synthetic scorodite at its natural pH (4.8 to 4.5) was equilibrated in
384 about 1 week at 1.3 mg/L As, and natural scorodite (pH 5.8-5.6) at about 0.4 mg/L As.
385 However, Bluteau and Demopoulos [4] and Fujita et al [3] showed that the solubility of
386 scorodite involves complex phenomena such as dependence on the crystal size and the
387 presence of other phases –such as goethite- which acts as adsorbent of dissolved
388 arsenic. Despite Paktunc and Bruggemann [7] reported that nanocrystalline scorodite
389 solubility was similar to its crystalline counterparts, recent studies (Fujita et al [3])
390 reported that in absence of a second phase, the arsenic dissolved in scorodite at its

391 natural pH (5.8-3.9) increased exponentially on decreasing the crystal size, and reached
 392 values > 5 mg/L for crystals of < 1µm in size. Values of about 0.5 mg/L were only
 393 achieved for crystals > 10 µm. The differences between the values can be due because if
 394 this process is chemically controlled, the amount of arsenic released depends on the
 395 surface area of each sample. This could explain the difference obtained in the present
 396 work between synthetic (microcrystalline) and natural (largely crystalline) scorodite. In
 397 any case, arsenical alunite presents similar leached arsenic that the best reported values
 398 obtained for scorodite in absence of goethite.

399

400 However, arsenical alunite showed some more arsenic leaching than arsenical
 401 natroalunite, which was equilibrated at about 0.1 mg/L As at its natural pH (4.4 -4.2)
 402 [11]. The cause of this behavior was not clear, because the reported thermodynamic
 403 properties for alunite and natroalunite were very similar [32], even though the solubility
 404 product for alunite ($pK_{sp}= 85.4$) is slightly smaller than natroalunite's ($pK_{sp}= 79.7$).

405



406

407 Figure 11: Medium-term arsenic leaching of arsenical alunite and natural and synthetic
 408 scorodite

409

410 4. Conclusions:

411

412 Alunite presented a good precipitation yield and significant AsO_4 -for- SO_4 substitution
 413 (up to 15% molar) at 200°C. The degree of arsenate substitution depends on the solution
 414 composition, increasing as: $(AsO_4/(AsO_4+SO_4))_{alunite} \cong 0.5 (AsO_4/(AsO_4+SO_4))_L$. For
 415 $(AsO_4/(AsO_4+SO_4))_L < 0.26$, arsenical alunite was the unique phase and, above this
 416 ratio mansfieldite co-precipitated. The Rietveld refinement of the arsenical alunite

417 confirmed the structural type R-3 m Z=3 of the alunite phases. The *a* unit cell parameter
418 is practically independent of the AsO₄-for-SO₄ substitution. However, the *c* unit cell
419 parameter increases with the AsO₄ substitution, in consistency with the difference
420 between the AsO1 and SO1 distances in the tetrahedral sites of the structure. These
421 characteristics for arsenical alunite are very similar to those found in previous studies on
422 arsenical natroalunite.

423

424 Arsenical alunite presents good stability in a wide range of pHs. The maximum stability
425 in short-term tests is between pH 5-8, with an As-solubilization of 0.01-0.03 mg/L in 24
426 h. Medium-term tests at its natural pH (~5) showed an equilibrated solubility of 0.3
427 mg/L As in 2.5 weeks. These values are smaller than most of reported data for synthetic
428 scorodite and comparable -in medium-term leaching- to the results in pure and largely
429 crystalline (natural) scorodite. Thus, arsenical alunite could be effective for arsenic
430 immobilization, especially for effluents or wastes with large SO₄/AsO₄ ratio, in the
431 same way than the observed in previous studies on arsenical natroalunite.

432

433 Hydronium alunite presents a low precipitation yield and very low arsenate
434 incorporation (up to 1% molar). This may be related to the difficulty of substituting
435 protonated HAsO₄²⁻-for-SO₄²⁻ or H₂O-for-OH⁻ groups due to the location of the H-
436 bridges of the H₃O in the structure. Precipitation in Al³⁺/SO₄²⁻/AsO₄³⁻ aqueous media
437 produces mainly an amorphous Al-AsO₄-SO₄ phase and mansfieldite. These
438 characteristics make hydronium alunite unsuitable for arsenic precipitation and
439 immobilization.

440

441 Acknowledgements

442 The financial support of the Spanish Ministerio de Ciencia e Innovación (DGI)
443 (Programa de Materiales, MAT 2007-61466) is gratefully acknowledged. As well as the
444 University of Barcelona for the fellowship APIF conceded. We also thank the Serveis
445 Científico-Tècnics of the University of Barcelona for their help with the
446 characterization studies.

447

448 5. References:

449

- 450 [1] P.A, Riveros, J.E. Dutrizac, P. Spencer, Arsenic Disposal Practices in the
451 Metallurgical Industry, *Can. Metall. Q.*, 40(4) (2001) 395-420.
- 452 [2] G.P. Demopoulos, F. Lagno, Q. Wang, S. Singhana, 2003. The atmospheric
453 scorodite process. In: P. Riveros, D. Dicon, D. Dreisinger, J. Menacho (Eds.), *Copper*
454 2003, IIMCH-MET SOC Canada, Santiago, Chile, TMS, VI(2), 597-616.
- 455 [3] T. Fujita, S. Fujieda, K. Shinoda, S. Suzuki. Environmental leaching characteristics
456 of scorodite synthesized with Fe(II) ions. *Hydrometallurgy*, 111-112 (2012) 87-102.
- 457 [4] M.C. Bluteau, G.P. Demopoulos, The incongruent dissolution of scorodite -
458 Solubility, kinetics and mechanism, *Hydrometallurgy*, 87 (2007) 163-177.
- 459 [5] E. Krause, V.A, Ettel, Solubilities and stabilities of ferric arsenate compounds.
460 *Hydrometallurgy*, 22 (1989) 311–337.
- 461 [6] R.G. Robins, Solubility and stability of scorodite, $\text{FeAsO}_4 \cdot 2\text{H}_2\text{O}$: Discussion.
462 *American Mineralogist*, 72 (1987) 842-844.
- 463 [7] D. Paktunc, and K. Bruggeman, Solubility of nanocrystalline scorodite and
464 amorphous ferric arsenate: Implications for stabilization of arsenic in mine wastes.
465 *Applied Geochemistry*, 25(5) (2010) 674–683.
- 466 [8] M. A. Gomez, L. Becze, J. N. Cutler, and G. P. Demopoulos, Hydrothermal reaction
467 chemistry and characterization of ferric arsenate phases precipitated from $\text{Fe}_2(\text{SO}_4)_3$ -
468 As_2O_5 - H_2SO_4 solutions. *Hydrometallurgy*, 107(3-4) (2011) 74–90.
- 469 [9] P. M. Swash, A. J. Monhemius, Hydrothermal precipitation from aqueous solutions
470 containing iron(III), arsenate and sulphate. In *Proceedings Hydrometallurgy'94* (eds.
471 Chapman & Hall). New York, N.Y., pp. 177–190.
- 472 [10] J. E. Dutrizac and J. L. Jambor, Characterization of the iron arsenate-sulphate
473 compounds precipitated at elevated temperatures. *Hydrometallurgy*, 86(3-4) (2007)
474 147–163.
- 475 [11] J. Viñals, A. Sunyer, P. Molera, M. Cruells, N. Llorca, Arsenic stabilization of
476 calcium arsenate waste by hydrothermal precipitation of arsenical natroalunite,
477 *Hydrometallurgy*, 104 (2010) 247-259.

- 478 [12] A. Sunyer, J. Viñals, Arsenate substitution in natroalunite: A potential medium for
479 arsenic immobilization. Part 2: Cell parameters and stability tests, *Hydrometallurgy*,
480 109 (2011) 106-115.
- 481 [13] A. Sunyer, J. Viñals, Arsenate substitution in natroalunite: A potential medium for
482 arsenic immobilization. Part 1: Synthesis and compositions, *Hydrometallurgy*, 109
483 (2011) 54-64.
- 484 [14] J. Viñals, A. Sunyer, E. Torres, V. Beltran, Arsenic inertization from copper
485 pyrometallurgy through phases of the alunite supergroup, *Erzmetall*, 63(6) (2010) 5-13.
- 486 [15] X. Alcobé, J. Bassas, I. Tarruella, A. Roca, J. Viñals, Structural Characterization of
487 Synthetic Beudantite-Type Phases by Rietveld Refinement, *Materials Science Forum*,
488 378 (2001) 671-676.
- 489 [16] U. Kolitsch, A. Pring, Crystal chemistry of the crandallite, beudantite and alunite
490 groups: a review and evaluation of the suitability as storage materials for toxic metals, *J.*
491 *Miner. Petrol. Sci.*, 96(2) (2001) 67-78.
- 492 [17] W.W. Rudolph, R. Mason, P. Schmidt, Synthetic alunites of the potassium-
493 oxonium solid solution series and some other members of the group: synthesis, thermal
494 and X-ray characterization, *Eur. J. Mineral.*, 15 (2003) 913-924.
- 495 [18] D. Paktunc, J.E. Dutrizac, Characterization of arsenate-for-sulfate substitution in
496 synthetic jarosite using X-ray diffraction and X-ray absorption spectroscopy, *Can.*
497 *Mineral.*, 41 (2003) 905-919.
- 498 [19] J.F. Le Berre, T.C. Cheng, R. Gauvin, G.P. Demopoulos, Hydrothermal synthesis
499 and stability evaluation of mansfieldite in comparison to scorodite. *Canadian*
500 *Metallurgical Quarterly* 46 (2007) 1-9.
- 501 [20] J.F. Le Berre, T.C. Cheng, R. Gauvin, G.P. Demopoulos, Hydrothermal synthesis
502 and stability evaluation of iron(III)-aluminum(III) arsenate solid solutions.
503 *Metallurgical and Materials Transactions B* 38 (2007) 159-166.
- 504 [21] S. Menchetti, C. Sabelli, Crystal chemistry of the alunite series: crystal structure
505 refinement of alunite and synthetic jarosite, *Neues Jahrb. Mineral.-Monatsh.* 9 (1976)
506 406-417.

- 507 [22] K. Okada, J. Hirabayashi, J. Ossaka, Crystal structure of natroalunite and crystal
508 chemistry of the alunite group, *Neues Jahrb. Mineral.-Monatsh.* 12 (1982) 634-640.
- 509 [23] R. L. Frost, S. Bahfenne, J. Čejka, J. Sejkora, J. Plášil, S. J. Palmer, E.C. Keeffe
510 and I. Nemeč, Dussertite $\text{BaFe}_3\text{+3(AsO}_4\text{)}_2\text{(OH)}_5$ - a Raman spectroscopic study of a
511 hydroxy-arsenate mineral. *Journal of Raman Spectroscopy*, 42(1) (2011) 56–61.
- 512 [24] R. L. Frost, S. J. Palmer, and Y. Xi, The molecular structure of the multianion
513 mineral hidalgoite $\text{PbAl}_3\text{(AsO}_4\text{)}\text{(SO}_4\text{)}\text{(OH)}_6$ – Implications for arsenic removal from
514 soils. *Journal of Molecular Structure*, 1005(1-3) (2011) 214–219.
- 515 [25] L.C.Basciano, R.C. Peterson, Crystal chemistry of the natrojarosite-jarosite and
516 natrojarosite-hydronium jarosite solid-solution series: A synthetic study with full Fe site
517 occupancy, *Am. Miner.*, 93 (2008) 853-862.
- 518 [26] R.D. Shannon, Revised Effective Ionic Radii and Systematic Studies of Interatomic
519 Distances in Halides and Chalcogenides, *Acta Cryst.*, A32 (1976) 751.
- 520 [27] W.T.A. Harrison, Synthetic mansfieldite, $\text{AlAsO}_4\cdot 2\text{H}_2\text{O}$, *Acta Cryst.*, C56 (2000)
521 e421.
- 522 [28] J.E. Dutrizac, J.L. Jambor, The Synthesis of Crystalline Scorodite, $\text{FeAsO}_4\cdot 2\text{H}_2\text{O}$.
523 *Hydrometallurgy*, 19 (1988) 377-384.
- 524 [29] J.D. Gale, K.Wright, K.A. Hudson-Edward, A first-principles determination of the
525 orientation of H_3O^+ in hydronium alunite, *Am. Miner.*, 95 (2010) 1109-1112.
- 526 [30] E. Sato, I. Nakai, R. Miyawaki, S. Matsubara, Crystal structures of alunite family
527 minerals: beaverite, corkite, alunite, natroalunite, jarosite, svanbergite, and
528 woodhouseite, *Neues Jahrb. Mineral.-Monatsh.*, 185/3 (2009) 313-322.
- 529 [31] P.M. Swash, A.J. Monhemius, J.M. Schaekers, Solubilities of process residues
530 from biological oxidation pretreatments of refractory gold ores. In: Young, C.A. (Ed.),
531 *Minor Elements 2000*. SME, Littleton, CO, (2000) 115–123.
- 532 [32] J. Pietzel, B. Mayer, Isotopic fractionation of basaluminite, alunite and
533 natroalunite. *Chem. Geol.*, 215 (2005), 525-535.

C.1 Copper and zinc recoveries and arsenic stabilization from copper smelter flue dusts

A. Morales, M. Cruells, A. Roca, A. Sunyer, J. Viñals, 2011, Copper and Zinc Recoveries and Arsenic Stabilization from Copper Smelter Flue Dusts. Proceedings of the 6th International Seminar on Copper Hydrometallurgy, Viña del Mar, Chile, Edited by Jesús M. Casas, Cleve Lightfoot, Gustavo Tapia, 38-39. ISBN 978-956-8504-49-6.

Resum en català

Un procés pel tractament de la pols de forn de coure per a extraccions de coure i zinc i l'estabilització de l'arsènic s'ha establert. Per pols contenant residus de sulfur d'un forn continu, el procés va consistir a lixiviar en àcid sulfúric diluït (dissolució del coure, l'arsènic i el zinc) i hidrociclonant el residu corresponent. Després d'això, la fracció grossa es pot reciclar al forn i la fracció fina es pot mesclar amb el fang obtingut d'una paperera (procés de co-inertització) per abocaments. Per pols sense residus de sulfurs d'un forn flash, el procés proposat va consistir en la lixiviació amb àcid sulfúric diluït i barrejant el residu obtingut amb el fang, tal i com s'ha descrit anteriorment. En ambdós casos, el procés es va fer a temperatura ambient. En ambdós processos es va obtenir un líquid lixiviat amb coure (de 10 g/L a 28 g/L), zinc (de 2 g/L a 5 g/L) i arsènic (2.5 g/L a 3.0 g/L). En el present article, l'aplicació de tècniques com la cementació, l'electròlisis i la precipitació es van aplicar per a la recuperació de coure i zinc, així com per a l'estabilització de l'arsènic en un residu compacte i inert. Els millors resultats es van obtenir de la següent manera: oxidació d'As(III) a As(V), i precipitació d'aquest element com a alunita arsenical. Després d'això, es va dur a terme una electròlisis per a la recuperació del coure. Els líquids de l'electròlisis es poden reciclar en la lixiviació amb àcid sulfúric. Aquest líquid es pot escórrer i la pols de zinc es pot afegir per recuperar el coure restant. Finalment el zinc es pot recuperar per electròlisis o per precipitació. L'aplicació de processos hidrometal·lúrgics com aquest fa possible la recuperació d'elements valuosos de pols de forn de coure i la inertització de l'arsènic que contenen.

Copper and zinc recoveries and arsenic stabilisation from copper smelter flue dusts

Alejandro Morales

Universidad Católica del Norte, Chile

Montserrat Cruells, Antonio Roca, Alba Sunyer and Joan Viñals

Universitat de Barcelona, Spain

ABSTRACT

A process for the treatment of copper smelter flue dusts for copper and zinc extractions and arsenic stabilisation was established. For dusts containing residual sulphides from a continuous furnace, the process consists of leaching with dilute sulphuric acid (dissolution of copper, arsenic and zinc) and hydrocycloning the corresponding residue. After this, the coarse fraction can be recycled to the furnace and the fine fraction can be mixed with sludge from a paper factory (co-inertisation process) for landfills. For dusts without residual sulphides from a flash furnace, the proposed process consists of leaching with dilute sulphuric acid and mixing the obtained residue with the sludge, as previously described. In both cases, the process is developed at room temperature. In both processes, a leaching liquor containing copper (10 g/L to 28 g/L), zinc (2 g/L to 5 g/L) and arsenic (2.5 g/L to 3.0 g/L) is obtained. For the present paper, the application of techniques such as cementation, electrolysis and precipitation were applied for copper and zinc recovery, as well as arsenic stabilisation in a compact and inert residue. The best results were obtained as follows: oxidation of As(III) to As(V), and precipitation of this element as arsenical alunite. After this, electrolysis for copper recovery can be carried out. Liquids from electrolysis can be recycled to the sulphuric acid leaching step. This liquid can drain off and zinc powder can be added for recovering the remaining copper. Then zinc can be recovered by electrolysis or precipitation. The application of hydrometallurgical processes such as those described makes it possible to recover the valuable elements of copper smelter flue dusts and the inertisation of the arsenic content.

INTRODUCTION

In copper pyrometallurgy, numerous by-products and residues are generated during copper production. By-products are recycled according to their chemical and mineralogical composition and residues must be treated to recover the valuable elements contained and then detoxified previous to dumping them for environmental purposes. In the last decades, many studies have been carried out to develop this activity including treatments of roasting and leaching; smelting and leaching; roasting; smelting or leaching [1-6].

In previous works, our research team has developed some processes for copper and zinc recovery and arsenic stabilisation from copper smelter flue dusts materials at laboratory scale [7-9]. The proposed processes are based on the following items:

- Hydrometallurgical process using dilute reagents
- Operating at room temperature and atmospheric pressure
- Few unit operations and low energy costs
- Generation of final compact and inert residue for landfill

According to the considerations described above, the leaching processes can be carried out leaching with water or dilute sulphuric acid (high amounts of copper are present in the dusts as copper sulphate and basic sulphate). The residue obtained after leaching can be hydro-cycloned (if residual sulphides are present) being the coarse fraction (including sulphides and ferrites), recycled to the furnace and the fine fraction (arsenic-rich fraction), should be mixed with wastewater sludge from a paper factory, to make both residues inert before to send them to the landfill. When residual sulphides are not present (dusts from flash furnace), the residue obtained after leaching with sulphuric acid is subjected to the same treatment as the arsenic-rich fraction described above.

The objective of the present work is the description of two possible routes for the treatment of copper smelter flue dust samples, including the study of copper and zinc recovery from the leaching liquors using processes such as cementation and electrolysis in the presence of arsenic in solution.

MATERIALS AND EXPERIMENTAL PROCEDURE

The original materials used in all the investigation were samples generated in continuous furnace and in flash furnace of copper pyrometallurgy. The main characterisation studies have been included in previous papers [8, 9]. Complementary characterisation studies are included in this work, using X-ray fluorescence (XRF), X-ray diffraction (XRD), scanning electron microscopy in conjunction with energy dispersive microanalysis (SEM-EDS), electron microprobe (EPMA) and emission spectrometry from inductively coupled plasma (ICP).

In this study, a sample from flash furnace was leached with sulphuric acid (0.1 M) at a solid-liquid ratio of 1/5 (w/v) and at room temperature. Dissolved elements were determined using ICP. After leaching, a first possibility for copper recovery was its precipitation by cementation. Iron powder of >95% purity was used in this study and the concentration of the elements Cu, Fe, Zn, As, Mo, Cd and Pb were determined by ICP. Solids obtained were characterised by SEM-EDS.

Another possibility after leaching was conducted such as follows: the liquor from leaching with sulphuric acid was ozonised and then heated at 80°C to promote the precipitation of arsenic as iron arsenate. The solids obtained were mixed with $Al_2(SO_4)_3 \cdot 18H_2O$ and Na_2SO_4 at a ratio (in weight) of

1.8 / 7 / 1 and introduced in a vessel pressure in a solid/liquid ratio of 1/15, and pH 1 adjusted by sulphuric acid. The experimental conditions were: 200 °C, 14 bar and 1 hour reaction time. The pH after this process was 0.28. Solids obtained were characterised by ICP and XRD. Liquids obtained after precipitation of iron arsenate were electrolysed for copper recovery at a voltage of 2 V, and current densities used are indicated in the item Results and Discussion. The cathode was made of stainless steel and the anode of lead. Liquids were characterised by ICP and solids by SEM-EDS.

RESULTS AND DISCUSSION

Characterisation of copper smelter flue dusts

Table 1 shows the chemical composition of the copper smelter flue dusts samples from continuous furnace and from flash furnace obtained by XRF [7-9].

Table 1 Chemical composition (range) of copper smelter flue dusts

Element	wt%	Element	wt%
Cu	26 - 37	Si	1.1 - 1.7
Fe	11 - 14	Cd	0.12 - 0.66
As	3.8 - 13	Pb	0.43 - 5.1
Zn	4.5 - 5.8	Mo	0.40 - 0.64
S	5.6 - 6.5	Bi	0.13 - 1.1

The main phases detected by XRD [7-9] are: spinel phases (from magnetite to cupro-spinel), copper sulphate (chalcocianite), copper basic sulphate (dolerofanite), zinc sulphate (zinkosite) and in some cases arsenic oxides (claudetite and arsenolite). As minor phases copper oxides (cuprite and tenorite) and a copper iron oxide (delafossite) were detected. Samples from continuous furnaces present appreciable amounts of copper sulphides and sulpho-arsenides: digenite, anilite, bornite, cubanite and enargite.

As example of particles of copper smelter flue dusts detected by SEM-EDS, Figure 1 is a general SEM image (SE-secondary electrons) of a zone of one of the characterised samples. Its white zones correspond to an anhydrous copper sulphate and/or basic sulphates of this element. Spherical-shaped particles and other irregular ones, ranging in size from tens of micrometers to one-tenth of a micrometer, can also be seen.

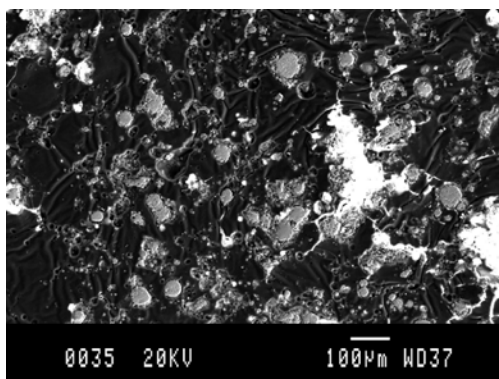


Figure 1 SEM-SE image of a copper smelter flue dust sample

Figure 2 gives SEM images that show a complex particle detected ($\cong 30 \mu\text{m}$ size); image (A) was obtained with secondary electrons (SEM-SE); and image (B), with back-scattered electrons (SEM-BSE). Figure 3 shows EDS diagrams of zones 1 and 2 in Figure 2. It can be deduced that sulphate or basic copper sulphate surrounds the particle, which essentially consists of cupro-spinel crystals.

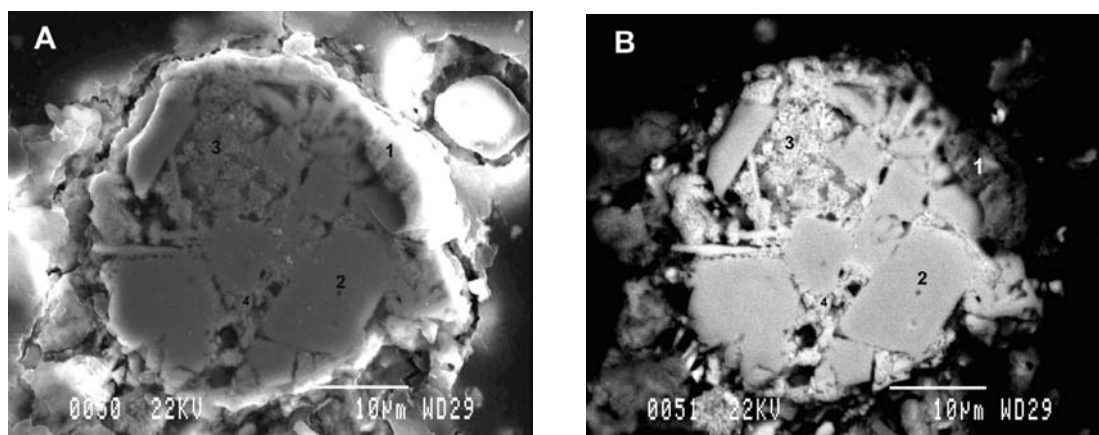


Figure 2 Images of a complex particle (A, SEM-SE; B, SEM-BSE)

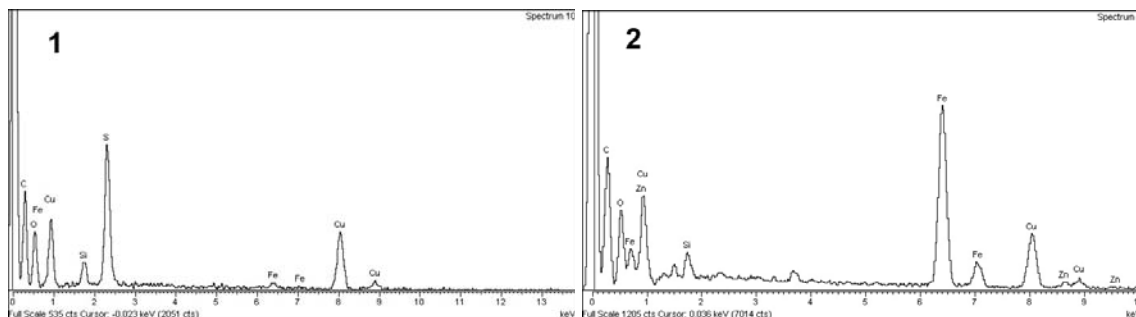


Figure 3 EDS diagrams of a copper sulphate (1) and a cupro-spinel phase (2)

Figure 4 shows EDS diagrams of zones 3 and 4 in Figure 2. In zone 3, a mixture of copper and arsenic oxides was detected. In zone 4, the particle is copper oxide.

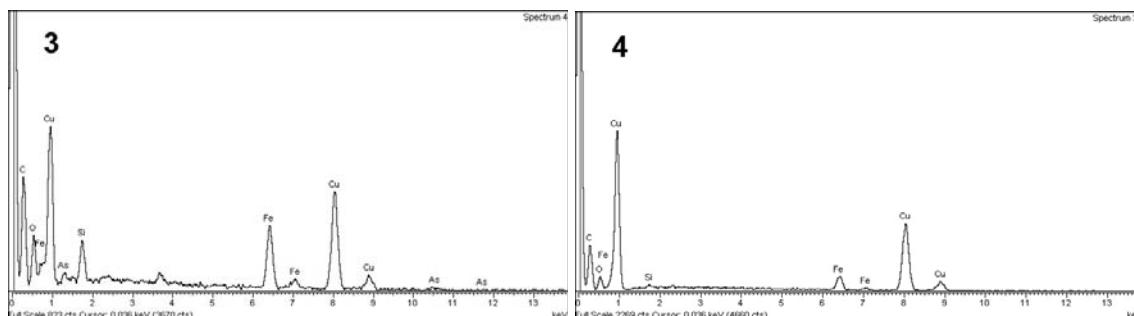


Figure 4 EDS diagrams of oxides of copper and arsenic (3) and oxide of copper (4)

Leaching of copper smelter flue dusts with sulphuric acid solutions

A sample of copper smelter flue dusts was leached with a sulphuric acid solution (0.1 M), at room temperature, with an initial pH of 1.3 and the end pH of 1.40. After solid-liquid separation, ozone was injected to the filtrate to oxidise the remaining arsenic (III) to As (V) and then was heated at 80 °C to promote the precipitation of arsenic as iron arsenate. The pH of liquids after precipitation was 1.35. Analysis carried out by EDS indicated that the main elements of this precipitate were arsenic and iron; copper and cadmium as minor elements were also detected. XRD of this precipitate indicates that this precipitate was amorphous in nature. Solid obtained was analysed by EPMA and the chemical composition obtained was 20% to 22% Fe, 29% As, 1.5% to 3% Cu, and 0.25% to 0.40% S. The ratio As/Fe obtained is similar to that of the iron arsenate. Table 2 includes the chemical composition of the leach solution after separation of iron arsenate.

Table 2 Chemical composition of leach solution after iron arsenate separation

Element	Cu g/L	Zn g/L	S g/L	Fe mg/L	As mg/L	Cd mg/L	Mo mg/L	Ca mg/L
	12.6	1.1	8.3	350	550	33	41	163

In a previous work [7], it was determined that other elements such as Bi, Mo, Cd and Pb remain in the leaching residue and appears inertised after pelletising previous to landfill.

Transformation of iron arsenate precipitates to an arsenical natro-alunite

Amorphous or crystalline iron arsenate may exceed the maximum permitted solubilisation level when these materials are subjected to leaching tests from the environmental point of view. An alternative process to obtain a good stabilisation of arsenic is a hydrothermal precipitation as a complex arsenical natro-alunite; this process has been extensively studied [10-12]. Using the best conditions obtained in the indicated works, iron arsenate precipitated after leaching copper smelter flue dusts was mixed with aluminium sulphate and sodium sulphate and introduced into a pressure vessel. XRD of the obtained product (Figure 5) confirms that an arsenical natro-alunite has been obtained. Chemical analysis obtained by ICP indicates that this product is formed by: 9.4% Al,

8.8% Fe, 9.1% S, 11% As, 2.84% Na. XRD indicates that solids obtained are a mixture of ferrical natro-alunite with amounts of scorodite. With adequate Al/As ratio it is possible to obtain a natro-alunite with minor amounts of scorodite [11].

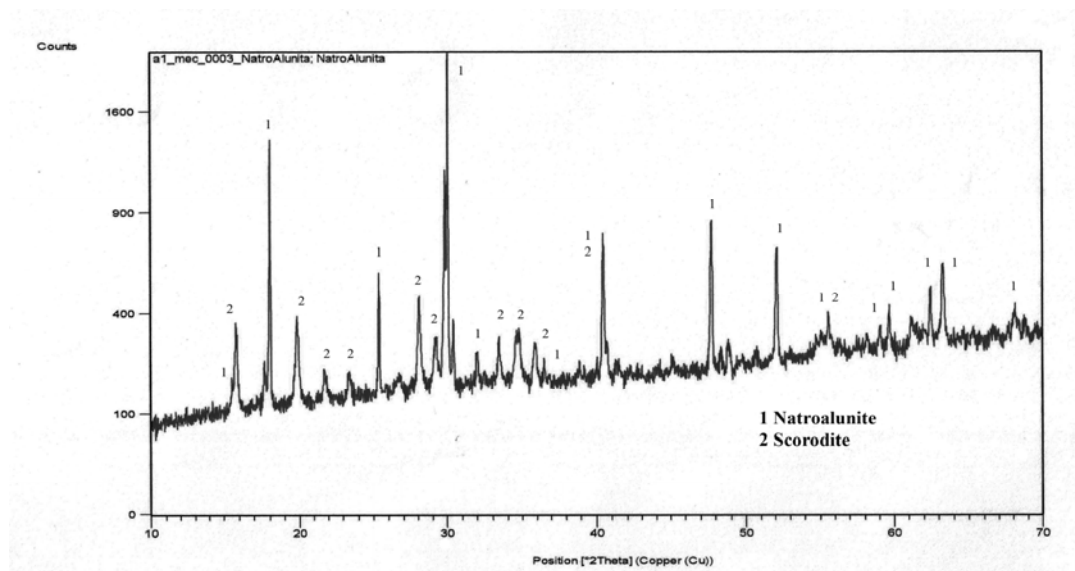


Figure 5 XRD diffractogram of arsenical natroalunite

Copper recovery from the leaching liquid

For cementation experiments, an iron powder of >95% Fe was used. An amount of 16 g/L Fe was added and the behaviour of the elements Cu, Fe, Zn, As, Mo, and Cd was determined at different cementation times (Table 3). The initial pH of the system was 1.50, and after 30 minutes of cementation the pH was 1.65.

Table 3 Liquid composition after copper cementation at different times (ICP)

Time (min) / Element (mg/L)	7.5	15	30	60	120	1440
Cu	400	140	6.8	2.7	6.6	9.7
Fe	11300	11900	11800	12200	12300	13600
Zn	1060	1080	1030	1050	1010	1090
As	560	520	445	390	300	190
Mo	34	36	26	21	20	11
Cd	27	27	26	26	25	26

Copper concentration sharply decreased from 12.6 g/L (original dissolution) to 0.4 g/L in 7.5 min cementation time; iron sharply increased from 0.35 g/L to 11.3 g/L at the same time, whereas Zn, Mo and Cd maintained their concentration. Arsenic diminished its concentration from 15 min cementation time. Figure 6 is a SEM image of cemented copper, which is formed by aggregates of tenths of micrometer. Figure 7 is a SEM image of an iron particle surrounded by cemented copper.

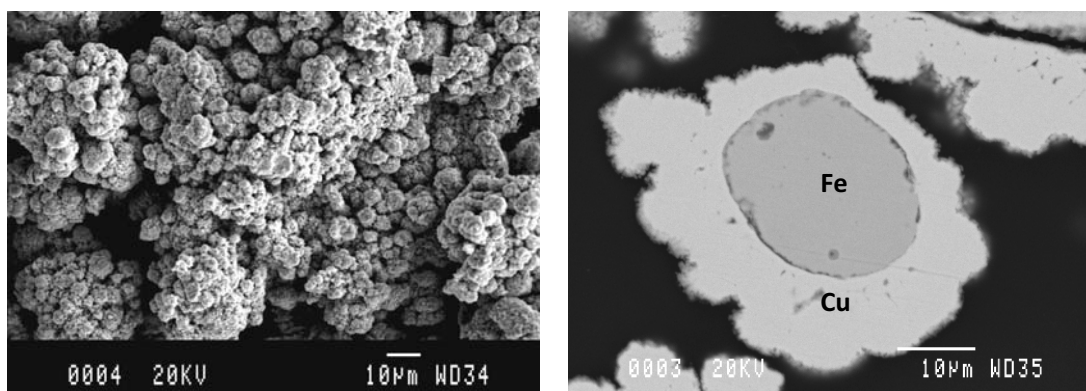


Figure 6 and Figure 7 SEM images of cemented copper using iron

The main problem for the application of the cementation process for copper recovery is the introduction of high amounts of iron into the solution (see Table 3), but it is also necessary to take into account the possible generation of arsine due to the presence of some amounts of arsenic in the system. Consequently, an alternative study for the production of copper by electrolysis is carried out.

Electrolysis was carried out at 2 V and with a current density of 1.2 A dm⁻². Purity of the copper obtained was higher than 99% (SEM-EDS). The progress of the electrolytic process was determined by weighing the cathode at different times and results obtained are presented in Figure 8. The end pH after electrolysis was 0.70. Copper concentration decreased from 12.6 g/L to 1.0 g/L in 8 hours in the experimental conditions employed and the current yield was of 90%.

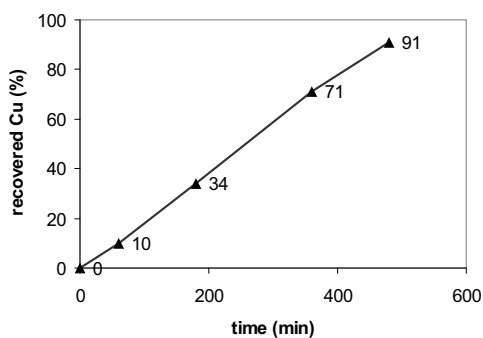


Figure 8 Percent recovery of copper vs. time during the electrolytic process

Acid liquids obtained after electrolysis can be recycled to the leaching step to increase zinc concentration. After a complete cycle is accomplished, the circuit can be drained in a percentage that can be determined in a pilot plant studies to recover zinc by electrolysis or by chemical precipitation.

PROCESS FOR THE TREATMENT OF COPPER SMELTER FLUE DUSTS

Figure 9 is a diagram of the proposed process for copper and zinc recovery and arsenic stabilisation from copper smelter flue dusts.

The dusts are leached with sulphuric acid that proceeds from recycling liquids after copper recovery by direct electrolysis. From the solutions generated, and after ozone injection and heating, arsenic precipitates as an amorphous iron arsenate and is separated from the filtrate. Copper is recovered by electrolysis and from the drain off; zinc can be recovered by electrolysis or chemical precipitation (the percent liquid drained from the circuit should be determined at the pilot plant level). Iron arsenate separated from the filtrate is introduced into a pressure vessel with simultaneous addition of the adequate amounts of aluminium sulphate and sodium sulphate, and arsenic is well stabilised by forming an inert arsenical natro-alunite that can be dumped without any environmental problems. Only a few amounts of ozone are needed previously to iron arsenate precipitation. The consumption of aluminium sulphate can be of $\cong 1$ kg and of sodium sulphate can be of 0.2 kg per kg of copper smelter flue dusts.

The residue from sulphuric acid leaching of copper smelter flue dusts from continuous furnaces (these materials could contain certain amounts of residual sulphides) could be hydro-cycloned with a cut size of 12 μm , recycling the coarse fraction to the furnace (fraction formed by residual sulphides and ferrites), and mixing the fine fraction with sludge from a paper factory before pelletising and landfill. An example of the composition of the coarse fraction is: 46% Cu, 22% Fe, 0.19% Zn, 0.06% As and the fine fraction is: 17% Cu, 25% Fe, 1.4% Zn, 11% As. The residue from sulphuric acid leaching of copper smelter flue dusts from flash furnaces could be directly mixed with sludge from a paper factory before pelletising and landfill.

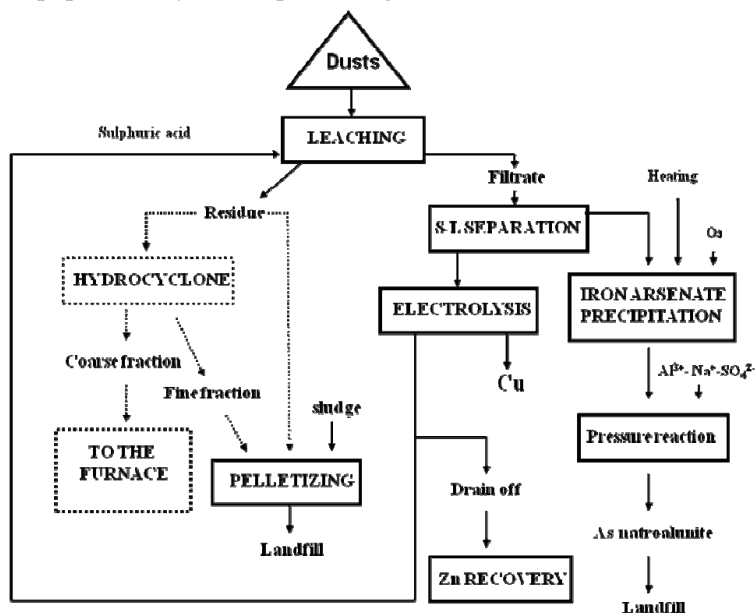


Figure 9 Conceptual process diagram proposed for the treatment of copper smelter flue dusts materials

CONCLUSIONS

Copper smelter flue dusts containing residual sulphides can be leached with the sulphuric acid solution from copper electrolysis. The leaching residue can be hydrocycloned. The coarse fraction can be recycled to the furnace and the fine fraction mixed with sludge from a paper factory previously to landfill.

Copper smelter flue dusts without residual sulphides can also be leached with the same solution. Leaching residue is directly inertised by mixing it with sludge previously to landfill.

In both cases, iron arsenate precipitates from leaching liquids, and this precipitate is mixed with aluminium sulphate and sodium sulphate and introduced into an autoclave for obtaining an inert arsenical natroalunite.

Copper in solution is recovered by direct electrolysis and from the drain off; zinc can be recovered by electrolysis or chemical precipitation.

ACKNOWLEDGEMENTS

We are grateful to the “Serveis Científicotècnics de la Universitat de Barcelona” for their assistance in the characterisation studies developed in this work. Thanks are also due to Ms. Paola Armengol and Shellah P. Cáceres for their collaboration in this work.

REFERENCES

- Gorai, B., Jana, R.K., & Khan, Z.H. (2002). *Electrorefining Electrolyte from Copper Plant Dust*. Materials Transactions 43 (3), pp. 532-536. [1]
- Zhang, Z., Lu, W., & Zheng, F. (1992). *Separation and Recovery of Copper and Zinc from Flue Dust*. Huanjing Kexue 11 (6), pp. 1012-1016. [2]
- Fu, Y., Jiang, L., & Wang, D. (2000). *Removal of Arsenic from Copper Smelter Flue Dust by Calcinations*. Yelian Bufen 6, pp. 14-16. [3]
- Núñez, C., Espiell, F., & Roca, A. (1985). *Recovery of Copper, Silver and Zinc from Huelva (Spain) Copper Smelter Flue Dust by a Chloride Leach Process*. Hydrometallurgy 14 (1), pp. 93-103. [4]
- Ke, J., & Qin, R. (2000). *Arsenic Removal and Bismuth Recovery from Copper Smelter Flue Dust*. Symposium Minor Elements 2000: Processing and Environmental Aspects of Arsenic, Antimony, Selenium, Tellurium and Bismuth. Society for Mining, Metallurgy and Exploration, USA, pp. 293-298. [5]
- Vircikova, E., & Havlik, M. (1999). *Removing Arsenic from Converter Dust by a Hydrometallurgical Method*. JOM 51 (9), pp. 20-23. [6]
- Morales, A. (2006). *Caracterización de polvos de fundición de cobre y establecimiento de rutas de procesado*. PhD Thesis. Universitat de Barcelona, Barcelona, Spain. [7]
- Morales, A., Cruells, M., Roca, A., & Bergó, R. (2007) *Characterization of flue dusts from a copper smelter furnace, copper recovery and arsenic stabilization*. The John E. Dutrizac Symp. on Copper Hydrometallurgy 4, book 2, Montreal, QC, Canada: The Canadian Institute of Mining, Metallurgy and Petroleum, pp. 177-189. [8]
- Morales, A., Cruells, M., Roca, A., & Bergó, R. (2010) *Treatment of copper flash smelter flue dusts for copper and zinc extraction and arsenic stabilization*. Hydrometallurgy, 105 (1-2), pp. 148-154. [9]

- Viñals, J., Sunyer, A., Molera, P., Cruells, M., & Llorca, N. (2010) *Arsenic stabilization of calcium arsenate waste by hydrothermal precipitation of arsenical natroalunite*. *Hydrometallurgy*, 104 (2), pp. 247-259. [10]
- Viñals, J., Sunyer, A., & Torres E. (2010) *Arsenic inertization from copper hydrometallurgy through phases of the alunite supergroup*. *Erzmetall*, 63 (6), pp. 301-309. [11]
- Viñals, J., Cruells, M., Sunyer, A., García, L., & Beltran, V. (2009) *Arsenic stabilization by hydrothermal synthesis of alunite-type phases. Application to the copper metallurgy*. *HydroCopper 2009*, Antofagasta, Chile, Gecamin Ltd., pp. 37-46. [12]

C.2 New process for treating slag furnace (SCF) flue dust at Atlantic Copper

G. Rios, C. Arbizu, A. Sunyer, J. Viñals, 2012, New Process for Treating Slag Furnace (SCF) Flue Dust at Atlantic Copper, Proceedings of T.T. Chen Honorary Symposium. Edited by S. Wang, J.E. Dutrizac, M.L. Free, J.Y. Hwang and D. Kim, 177-190. John Wiley & Sons, Hoboken, New Jersey, USA. ISBN 978-1-11829-123-8.

Resum en català

Atlantic Copper és una de les productores de coure més gran d'Europa. Les seves instal·lacions de producció estan localitzades a Huelva (Espanya) i compten amb un forn d'aproximadament un milió de tones per any de concentrats per produir uns 260 quilos de tones per any de càtodes i 900 quilos de tones per any d'àcid sulfúric. Durant la fundició de concentrat de coure, l'escòria provinent del forn flash i dels convertidors PS són tractats en un forn elèctric de neteja d'escòria. Com a resultat del tractament dels gasos d'aquest forn, es produeixen aproximadament 2000 tones per any d'un tortó de filtració ric en zinc i s'envien a gestors de residus autoritzats. Aquest article descriu la caracterització del material i els resultats preliminars d'un nou procés de recuperació de zinc com a hidroxicarbonat de zinc pur mentre el plom es recupera com a un producte d'anglesita ric en indi. El comportament de les impureses (Cd, As, Tl, Sn, Sb, Bi, Cu, Se, Te) en el lixiviat, la purificació de la solució i els passos de precipitació també estan explicats.

NEW PROCESS FOR TREATING SLAG CLEANING FURNACE (SCF) FLUE DUST AT ATLANTIC COPPER

Guillermo Rios¹, Cristina Arbizu¹, Alba Sunyer² and Joan Viñals²

¹Atlantic Copper (Subsidiary of Freeport McMoRan Copper & Gold)
Av. Francisco Montenegro, s/n 21001 Huelva, Spain

²University of Barcelona. Department of Materials Science and Metallurgical Engineering
Martí i Franquès, 1 08028 Barcelona, Spain

Keywords: Flue Dust, Zinc Recovery, Indium Leaching

Abstract

Atlantic Copper is one of the largest copper producers in Europe. Its production facilities are located in Huelva (Spain) and account for the smelting of over one million tpy of concentrates to produce up to 260 ktpy cathodes and 900 ktpy of sulphuric acid. During copper concentrate smelting, the slag coming from the flash furnace and PS converters are treated in an electrical slag cleaning furnace. As a result of the treatment of the off gases from this furnace, approximately 2,000 tpy of a Zn-rich filter cake are produced and are sent to authorized waste managers. This paper describes the characterization of this material and the preliminary results of a new process to recover zinc as a pure zinc hydroxycarbonate while lead is collected as an indium-rich anglesite product. The behavior of impurities (Cd, As, Tl, Sn, Sb, Bi, Cu, Se, Te) in the leaching, solution purification and precipitation steps is also reported.

Introduction

The Atlantic Copper Metallurgical Complex in Huelva (Spain) was commissioned in 1970 with a capacity of 40,000 tpy of copper from concentrate. In 1975, the old blast furnaces were replaced by Outokumpu flash smelting furnace (FSF) technology, and the copper refinery capacity was increased to 108,000 tpy. Between 1994 and 1996, an expansion project was carried out to increase the copper from concentrate and cathodes to 250,000 tpy and 215,000 tpy, respectively. This expansion basically consisted of a new sulphuric acid plant, replacement of the anode furnaces by two 400 t units, redesign of the slag cleaning furnace (SCF), an increase in the electrolytic cells to 1,120 and implementation of ISA permanent cathode technology. Furthermore, a debottlenecking project has led to a capacity of 1,000,000 tpy of fresh concentrate since 1997. Meanwhile between 1995 and 1998, a cathode production rate of 260,000 tpy was reached as a result of a progressive increase in the current density in the refinery.

During copper concentrate smelting, the slag coming from the flash furnace and the PS converters is treated in an electrical slag cleaning furnace where the matte droplets entrapped in the slag are settled under a reducing atmosphere. These working conditions allow most of the Zn content in the copper concentrates to be collected as a Zn fume in the off gases from the slag cleaning furnace (SCF). Figure 1 shows a schematic flowsheet of the Huelva Smelter.

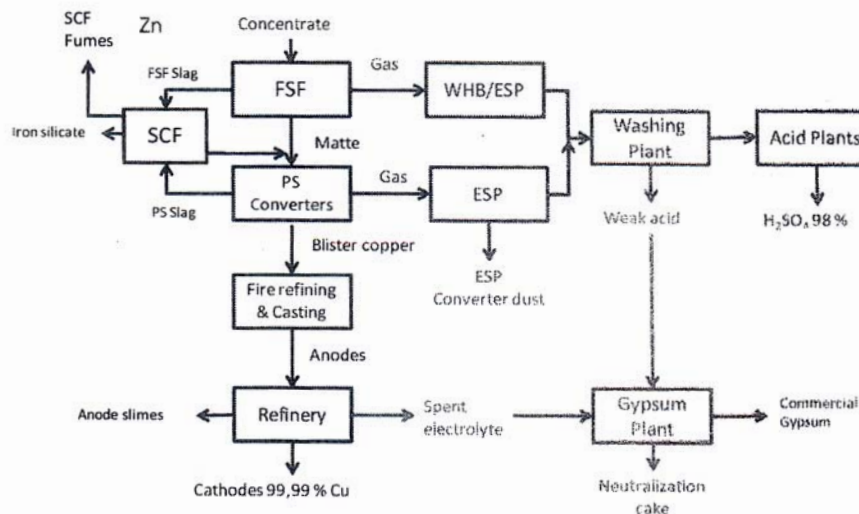


Figure 1. Atlantic Copper flowsheet

As a result of the scrubbing treatment of the off gases from this furnace, approximately 2,000 tpy of a Zn-rich filter cake are produced. Currently this material, which contains 40-50 % Zn and 10-15 % Pb, is sent to authorized waste managers as it is considered to be hazardous waste according to Spanish environmental regulations.

There is substantial R&D in the literature on metal recovery from Zn-bearing smelter dusts, especially from EAF dusts and Waelz oxides. The treatment processes depend on the phase composition, Zn grade and impurities. Hydrometallurgical processes are usually based on H₂SO₄ leaching [1,2,3], HCl leaching [4,5] or NaOH leaching [6,7]. Recovery of zinc from the leach solution can be performed by solution purification and electrolysis [8] or by precipitation, such as hydroxycarbonate [9]. However, our SCF differs from EAF dust in the virtual absence of ferrite and from Waelz oxides [10] in the large amount of impurities, such as As, Tl, Cu, Cd, etc, as well as in its high In grade. Consequently, a specific research project has been carried out in collaboration with the University of Barcelona to recover the Zn content and obtain an In-rich concentrate from this waste. This paper describes the results of this project, which involved:

- The characterization of this material to select the best Zn recovery treatment.
- The evaluation of two treatment processes based on leaching of the Zn and its subsequent precipitation as a zinc hydroxycarbonate while lead is collected as an indium-rich anglesite product. The main difference between the two processes was the purity of the Zn product.
- A study of the leaching of indium from the lead residue.

Zn Filter Cake Characterization

As has been stated, the Zn fumes carried over with the SCF off gases are collected in a scrubber during the treatment of this stream. The scrubbing slurry is filtered, and the Zn waste is collected as a filter cake. Samples of this cake were chemically assayed and studied by XRD and SEM-EDS. The chemical composition is shown in Table I.

Table I. Zn filter cake chemical composition

Element	Dried sample (100°C)	Element	Dried sample (100°C)
Zn (%)	52.73	Fe (%)	0.61
Pb (%)	9.51	Mo (g/t)	700
As (%)	2.96	In (g/t)	496
S (%)	2.08	Se (g/t)	264
Na (%)	0.62	Te (g/t)	6.8
Ca (%)	0.36	Mn (g/t)	40
Mg (%)	0.32	Tl (g/t)	58
Sn (%)	0.58	Ag (g/t)	12
Sb (%)	0.29	Ge (g/t)	15
Cd (%)	0.32	Insoluble (%)	1.24
Bi (%)	0.17	Soluble Si (%)	0.41
Cu (%)	0.32	Original moisture (%)	44.6

An X-ray diffractogram of this material is shown in Figure 2, the main phases being zincite (ZnO) and hydrocerussite ($Pb_3(CO_3)_2(OH)_2$). Minimal amounts of the zinc ferrite phase have been detected, and this suggests that Zn could easily be leached from this material.

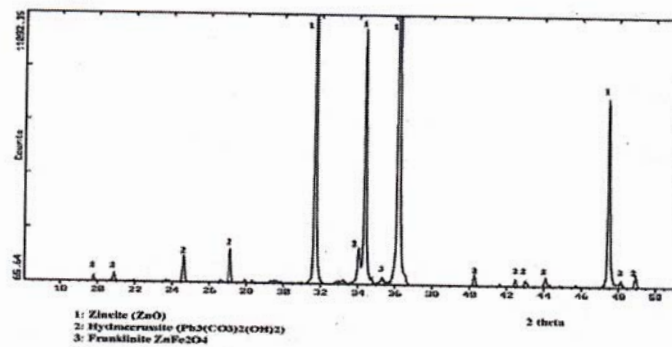


Figure 2. X-ray diffractogram of the zinc cake

Figure 3 shows an SEM image and its EDS spectrum. It was observed that this material consists of very small spheroidal particles ($< 2\mu\text{m}$) in which the Zn and Pb phases are intermixed, so the separation of Zn from Pb by mechanical procedures (such as size classification) is not feasible.

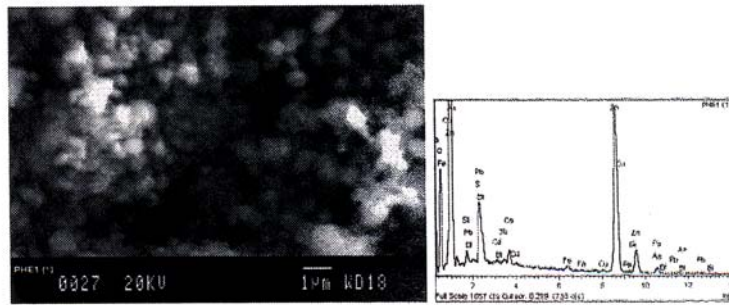


Figure 3. Zn cake SEM/EDS analysis

Zn Recovery Process

The characterization of this material led us to conclude that the most suitable treatment process would be the selective leaching of Zn and its subsequent precipitation as hydrocarbonate (hydrozincite). Two treatments have been studied based on this leaching approach; the main differences relate to the purification of the leach liquor and, hence, the purity of the final Zn product.

- Treatment 1: As removal prior to Zn precipitation
- Treatment 2: As, Cu and Cd removal prior to Zn precipitation

Zn Leaching Study

A study was made of Zn leaching in H_2SO_4 media. Figure 4 shows the acid consumption vs. pH. Acid consumption increases as the pH increases from 6.5 to 3.5 as a result of ZnO solubilization. A minor increase is observed below pH 1 mainly due to Fe leaching. Figure 5 depicts the extraction of the different elements present in the Zn filter cake vs. pH. It can be seen that 90 % of the Zn is leached at pH 2 but that the leach liquor is clearly contaminated with other elements such as As, Cd and Cu.

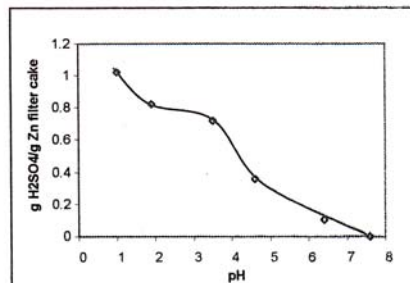


Figure 4. Zn leaching as indicated by H_2SO_4 consumption vs. pH

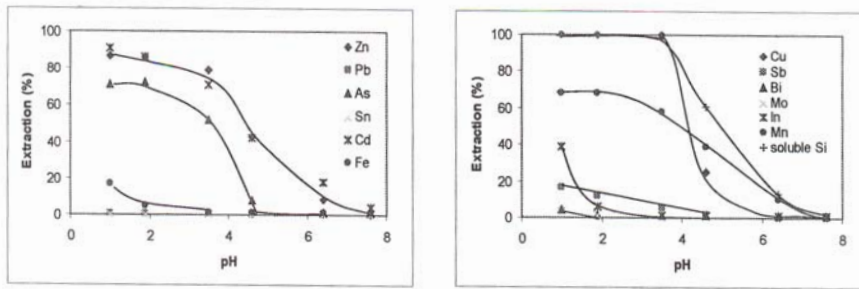
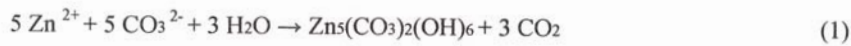


Figure 5. Zn leaching and metal extractions vs. pH

Consequently, it was concluded that the optimum leaching pH would be 2, with the H₂SO₄ consumption of about 0.8 kg/kg dry cake. Furthermore, the optimum S/L ratio during the leaching to reach a suitable Zn concentration, which would lead to a filterable material when the Zn was precipitated with soda ash (Na₂CO₃) according to the Equation 1, was determined:



This precipitation was studied using synthetic Zn solutions having concentrations ranging from 133 g/L to 35 g/L at different temperatures. The main conclusion was that to reach a filterable product at room temperature, the Zn concentration should be lower than 65 g/L. Accordingly, the selected optimum S/L ratio was between 1/10 and 1/15.

The kinetics of the leaching process were also studied with the aforementioned S/L ratio at a pH of 2-3. As seen in Figure 6, 90 % of the Zn is leached within the first 30 minutes. Table II shows the composition of the resulting leach liquor.

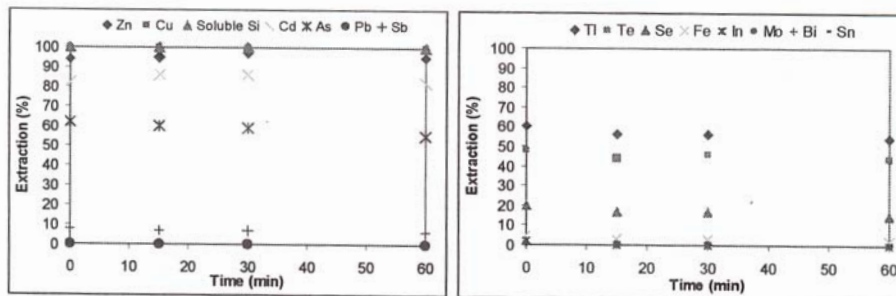


Figure 6. Zn leaching and metal extractions as a function of time (pH 2-3, S/L 1/12)

Table II. Zn leach liquor composition (pH 2-3, S/L 1/12) prior to and after As removal

	Leach solution (pH 2-3, S/L 1/12)	Purified solution with Fe(III) and soda ash (pH 4)
Zn (g/L)	42.0	43.0
S (g/L)	27.3	24.2
As (g/L)	1.4	< 0.003
Si (g/L)	0.29	0.29
Cu (g/L)	0.34	0.35
Cd (g/L)	0.22	0.17
Fe (ppm)	14	4.7
Sb (ppm)	16	1.8
Tl (ppm)	2.6	1.1
Pb (ppm)	9	7.1
Te (ppm)	0.25	<0.05
Bi (ppm)	<0.1	<0.1
Hg (ppm)	<0.1	<0.1
Sn (ppm)	<1	<1
In (ppm)	<0.05	<0.05
Ag (ppm)	<0.05	0.06
Ge (ppm)	9	0.69
Se (ppm)	3.2	3.9
Mn (ppm)	2.8	11
Ga (ppm)	<0.1	<0.1
Ni (ppm)	0.9	1.6
Co (ppm)	0.4	0.53
Mo (ppm)	0.22	0.1

Leach Liquor Purification and Zn Recovery

Treatment 1: As Removal and Hydrozincite Precipitation

As Removal It is proposed that As be removed by co-precipitation with Fe^{3+} . This removal will be carried out in the same leaching reactor before the filtration stage. After As removal, Zn will be recovered as a hydroxycarbonate. Figure 7 shows a flowsheet for this Zn recovery process.

In order to perform this purification, the ORP of the solution has to be increased from 180 mV (vs. Ag/AgCl) to 420 mV to ensure that all metals (mainly As) are fully oxidized. This is achieved by the addition of H_2O_2 . It has been determined that the H_2O_2 consumption is 4.75 g/kg dry Zn cake. Then, a solution of $Fe_2(SO_4)_3$ is added at an Fe/As molar ratio of 3/1. After that, the pH of the solution is increased to pH 4 using soda ash. The estimated soda ash consumption is 115 g/kg dry cake. Table II summarizes the chemical analysis of the leach liquor before and after As removal; as can be seen, Cu and Cd remain in solution.

The use of Zn filter cake instead of soda ash to raise the pH was also assessed but this alternative was discarded as it was observed that a layer of $Fe(OH)_3$ deposited on the Zn particles resulting in a high consumption of filter cake, and up to 35 % of the added Zn was lost with the leach solid residue. Figure 8 shows the XRD diffractograms of the leach residue that compare the use of soda ash and Zn filter cake.

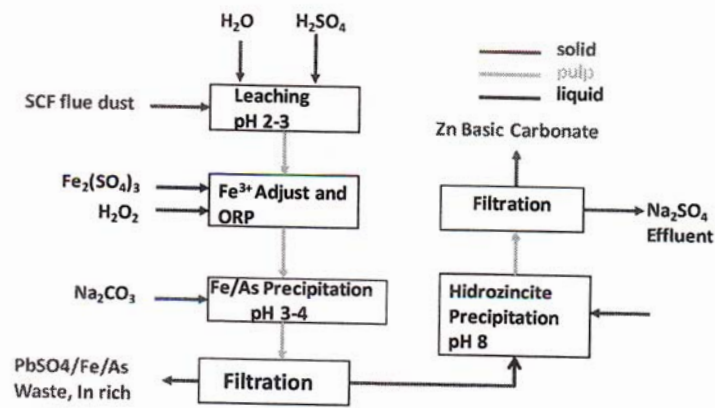


Figure 7. Zn Recovery process flowsheet with As removal

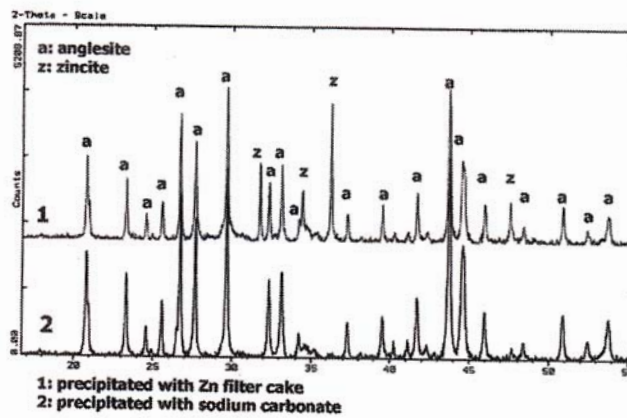


Figure 8. X-ray diffractograms of the leach residue from the As removal process.

As has been mentioned, the leach liquor residue will also collect the As that has been removed. It has been determined that 383 g of residue per kg of dry cake will be produced. The chemical composition of this residue is shown in Table III. Figure 7 shows that this residue is essentially anglesite. The high In content of this product (0.12% wt) should also be noted.

Zn Precipitation As previously explained, Zn is precipitated from the leach liquor at ambient temperature using Na_2CO_3 . The precipitation process can be easily monitored by pH measurements as Zn precipitates within a pH range of 6 to 8. During the precipitation tests a specific Na_2CO_3 consumption of 1.8 kg/kg Zn was discovered. It is higher than the theoretical value (1.6) because of the precipitation of impurities. A 99 % Zn recovery rate was achieved, yielding an hydroxycarbonate containing up to 55 % of Zn, as shown in Table IV. This

precipitate is composed of a hydrozincite phase, as observed in the XRD diffractograms in Figure 9.

Table III. Chemical composition of the leach residue after As removal

	Wt %		Wt %
Pb	24.81	In	0.12
Zn	2.77	Mg	0.03
Fe	13.11	Se	0.07
As	5.56	Ba	0.02
S	4.72	Tl	0.009
Sn	1.22	Sr	0.008
Cu	0.05	Mn	0.005
Sb	0.70	Ag	0.004
Bi	0.32	Ga	0.002
Mo	0.26	Te	0.002
Ca	0.14	Co	0.13
Al	0.14	Ni	0.081
Cd	0.04	Hg	n. detec.
Si (soluble)	0.21	Insoluble	2.8

Table IV. Chemical analysis of the hydrozincite from the first treatment option (As removal).

Zn (%)	54.9	Bi (g/t)	2.2
Na (%)	0.48	Mo (g/t)	6.7
S (%)	0.31	In (g/t)	n. detec.
Cu (%)	0.40	Se (g/t)	n. detec.
Cd (%)	0.22	Ag (g/t)	4.4
Ca (%)	0.18	Te (g/t)	6.7
Si soluble (%)	0.13	Hg (g/t)	n. detec.
Fe (%)	0.008	Ni (g/t)	n. detec.
Mn (%)	0.011	Co (g/t)	n. detec.
Pb (%)	0.014	Ga (g/t)	n. detec.
As (g/t)	11	Tl (g/t)	6.7
Sn (g/t)	4.3	Moisture (%)	80.8
Sb (g/t)	24		

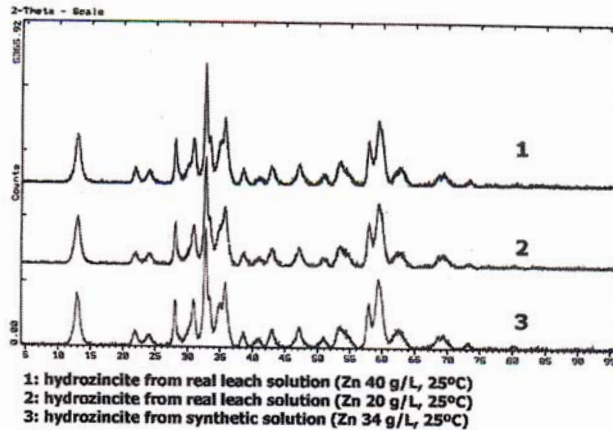


Figure 9. X-ray diffractograms of the hydrozincite precipitates

The final effluent from this filtration stage is a Na_2SO_4 solution (70-100 g/l) with a low metal content. It has been estimated that the effluent generated would be 10-15 m³/t filter cake. A mass balance of this Zn recovery process is summarized in Table V.

Table V. mass balance for As removal and hydrozincite precipitation

		Zn filter cake	Hydrozincite	Solid residue	Final effluent
Mass (dry)		1 Tm	940 kg	359 kg	10-15 m ³
Moisture (%)		45	80	59	
Consumption					
H_2SO_4	H_2O_2	Fe^{3+}	Na_2CO_3 for As removal	Na_2CO_3 for hydrozincite	Total Na_2CO_3
885 kg	19 kg	41 kg	122 kg	930 kg	1052 kg

Treatment 2: As, Cu and Cd Removal and Zn Precipitation

As explained before, As, Cu and Cd are the main impurities in the Zn-rich leach liquor. A specific Cu and Cd removal stage is now under consideration to produce pure zinc hydroxycarbonate. Figure 10 shows a flowsheet for this recovery treatment.

Although Zn metal dust was initially considered as a Cu and Cd cementation reagent, some re-dissolution of the cemented metals was observed. Precipitation with Na_2S was finally selected to remove Cu and Cd as sulfides, as they react with ZnS , which is immediately formed when Na_2S is added to the leach liquor at pH 4. No H_2S evolution was observed. All Cu and 97 % of the Cd were removed. Nevertheless it should be noted that 5 % of the Zn in the solution is lost with the Cu/Cd sulfide residue. Tables VI and VII show the results of the Cu/Cd removal step and the

chemical analysis of the hydrozincite recovered afterwards. A mass balance of this Zn recovery process is summarized in Table VIII.

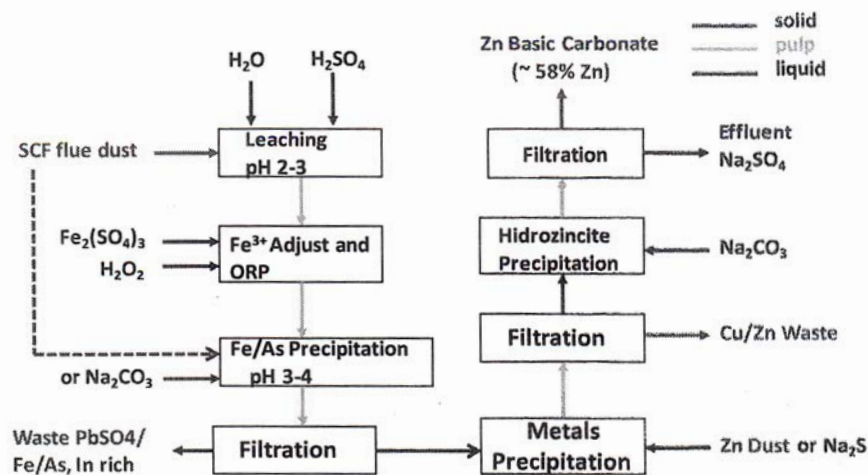


Figure 10. Flowsheet of the Zn recovery process with As, Cu and Cd removal

Table VI. Solution composition after Cu and Cd removal ($\text{Na}_2\text{S}\cdot 8\text{H}_2\text{O}$ dosing 3.4 g/L)

Zn (g/L)	39.3	Fe (ppm)	11.2
Na (g/L)	23.4	Se (ppm)	n. detect.
S (g/L)	22.2	Sb (ppm)	1.36
Mg (g/L)	0.14	Ni (ppm)	1.2
Si (g/L)	0.15	Tl (ppm)	0.11
Ca (g/L)	0.13	Ge (ppm)	0.42
Cu (ppm)	n. detect.	Co (ppm)	0.49
Cd (ppm)	12.9	Mo (ppm)	n. detect.
As (ppm)	n. detect	In (ppm)	n. detect.
K (ppm)	46	Bi (ppm)	n. detect.
Al (ppm)	13	Hg (ppm)	n. detect.
Mn (ppm)	10	Te (ppm)	n. detect.
Pb (ppm)	0.37	pH	3.0

Table VII. Chemical analysis of the hydrozincite after a Cu/Cd removal step

Zn (%)	57.7	Sb (g/t)	22
Na (%)	0.14	Bi (g/t)	n. detect.
S (%)	0.28	Mo (g/t)	n. detect.
Cu (%)	0.0008	In (g/t)	n. detect.
Cd (%)	0.0013	Se (g/t)	n. detect.
Ca (%)	0.079	Ag (g/t)	n. detect.
Mg (%)	0.018	Te (g/t)	n. detect.
Soluble Si (%)	0.084	Hg (g/t)	n. detect.
Fe (%)	0.019	Ni (g/t)	n. detect.
Mn (%)	0.011	Co (g/t)	n. detect.
Pb (%)	0.0082	Ge (g/t)	n. detect.
As (g/t)	n. detect.	Tl (g/t)	n. detect.
Sn (g/t)	n. detect.	Moisture (%)	80

Table VIII. As, Cu and Cd removal and hydrozincite precipitation mass balance

		Zn filter cake	Hydrozincite				Solid residue (In rich)	Final effluent	
Mass (dry)		1 Tm	915 kg				359 kg		
Moisture (%)		45	80				59	10-15 m ³	
Residual sulfide									
Mass (dry)	Moisture	Cu(%)	Cd(%)	Pb(%)	Se(%)	Tl(%)	Sb(%)	Zn (%) balance	
63 kg	70%	10	5	0.2	0.12	0.03	0.02	~38	
Consumption									
H ₂ SO ₄	H ₂ O ₂	Fe ³⁺	Na ₂ CO ₃ for As removal		Na ₂ CO ₃ for hydrozincite		Na ₂ CO ₃ total	Na ₂ S	
885 kg	19 kg	41 kg	122 kg		905 kg		1027 kg	20 kg	

Indium Leaching from the Residual Anglesite

The anglesite product resulting from the Zn leaching and As precipitation step contains up to 1450 g/t of In. A preliminary study of In leaching in 10 % media H₂SO₄ has been carried out in order to determine if this residue can be marketed as an In concentrate. It was found that 90 % of In was leached at 60 °C, as shown in Figure 11.

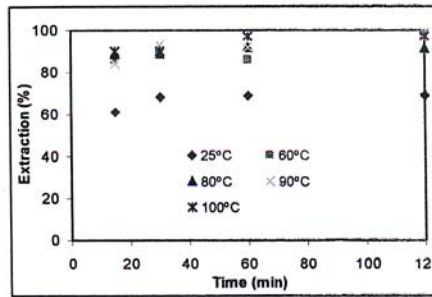


Figure 11. In leaching vs. time and temperature in 10 % H₂SO₄. S/L ratio 1/5

The main impurities, such as As, Fe, Bi and Sn, are partly dissolved under these leaching conditions, as shown in Figure 12.

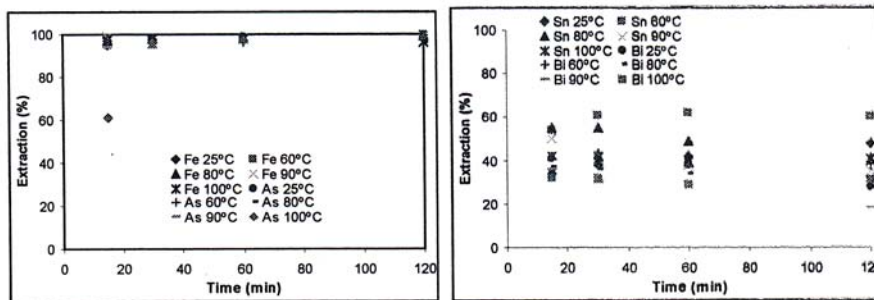


Figure 12. Behavior of impurities during In leaching in 10 % H₂SO₄. S/L ratio 1/5

It has to be noted that most of the As and Fe is dissolved, reaching relatively high concentrations in the leach liquor (50 and 100 g/L, respectively). This could hinder the recovery of In from the leachate. In order to avoid this detrimental effect, a preliminary leaching and removal of Fe and As at pH 1-2 at room temperature is recommended; this pre-treatment would also remove Sn and Bi.

Conclusions

The Zn filter cake from the treatment of the SCF off gases consists of micro-particles (< 2µm), with the main components being zincite (ZnO) and hydrocerusite (Pb₃(CO₃)₂(OH)₂).

Zinc recovery from this material, based on its selective leaching in acid media and its later precipitation with soda ash, has been studied, and the main conclusions are:

- Zinc leaching at pH 2-3 in H₂SO₄ media and As removal from the leach liquor by precipitation with Fe(III) at pH 4 can be carried out in the same reactor in two different stages.
- Zinc can be recovered as As-free hydrozincite (55 % Zn) containing up to 0.3 % Cd and 0.4 % Cu. This Cu and Cd content would not be a problem if the product could be sold to electrolytic zinc producers. Moreover a Cu/Cd removal step using Na₂S has been studied and optimised; it yield pure hydrozincite.
- The leach residue is mainly anglesite, which collects the precipitated As and Fe and has a relatively high In (0.12 %) content which can be easily leached in 10 % H₂SO₄. So, this residue could be sold as an In concentrate.

Acknowledgements

The authors wish to thank Atlantic Copper for permission to publish this paper and the *Serveis Científicotècnics de la Universitat de Barcelona* for its support of the characterization studies.

References

1. M. Cruells, A. Roca and C. Nunez, "Electric arc furnace flue dusts: characterization and leaching with sulfuric acid," *Hydrometallurgy*, 31(3), (1992), 213-231.
2. T. Havlik, B. Friedrich and S. Stopic, "Pressure leaching of EAF dust with sulphuric acid," *World of Metallurgy-Erzmetall*, 57(2), (2004), 83-90.
3. T. Havlik et al., "Atmospheric leaching of EAF dust with diluted sulphuric acid," *Hydrometallurgy*, 77(1-2), (2005), 41-50.
4. H.I. Lee, D.S. Baik and H.B. Jo, "Acidic leaching with HCl of electric-arc furnace dust for zinc recovery and electrowinning," U.S. Patent (2002), US 6338748 B1 20020115.
5. D.S. Baik and D.J. Fray, "Recovery of zinc from electric-arc furnace dust by leaching with aqueous hydrochloric acid, plating of zinc and regeneration of electrolyte," *Transactions of the Institution of Mining and Metallurgy, Section C: Mineral Processing and Extractive Metallurgy*, 109, (2000), C121-C128.
6. G. Orhan, "Leaching and cementation of heavy metals from electric arc furnace dust in alkaline medium," *Hydrometallurgy*, 78(3-4), (2005), 236-245.
7. A.J. Dutra, P.R. Paiva and L.M. Tavares, "Alkaline leaching of zinc from electric arc furnace steel dust," *Minerals Engineering*, 19(5), (2006), 478-485.
8. R. Vega and D. Correa, "Alkaline electro-hydrometallurgical process for Zn extraction from electric arc furnace dust," Eur. Patent (2008), EP 1878806 A2 20080116.

9. R. Solozabal et al., "In situ recovery of metals from EAFD by means of the INTECT process in laboratory and pilot plant experiments," *Afinidad*, 62(519), (2005), 373-382.
10. T.T. Chen, J.E. Dutrizac and G. Poirier, "Mineralogical characterization of Waelz kiln products" (Paper presented at the International Symposium on Waste Processing and Recycling in Mineral and Metallurgical Industries, Hamilton, ON, Canada. 22 August 2004), 681-696.

ANNEX D

DATABASE PETITIONS

D.1 ICSD database

Invitation to include into ICSD (Inorganic crystal structure database) the data published in *Hydrometallurgy*, 109(2011) p. 106-115. Title: Arsenate substitution in natrolunite: A potential medium for arsenic immobilization. Part 2: Cell parameters and stability tests.

FIZ-Karlsruhe is the producer of ICSD database.

We would like to include the structure that you published in Hydrometallurgy, 109(2011) p. 106-115

Title: Arsenate substitution in natrolunite: A potential medium for arsenic immobilization.

Pt. 2: Cell parameters and stability tests

into our ICSD database.

We would appreciate if you could send us a cif file or a free format table of atomic parameters.

We strongly prefer cif.

Thank you for your help.

With best regards

Ralph D. Graupner

ICSD Team

FIZ Karlsruhe

Hermann-von-Helmholtz-Platz 1

D-76344 Eggenstein-Leopoldshafen

crysdata@fiz-karlsruhe.de

Please have a look on our website

<http://www.fiz-karlsruhe.de/icsd.html>

 **FIZ Karlsruhe**
Leibniz-Institut für Informationsinfrastruktur

Avui en dia, l'arsènic és un dels principals problemes mediambientals que existeix. La precipitació d'arsènic ha estat molt estudiada en fases com l'escorodita ($\text{FeAsO}_4 \cdot 2\text{H}_2\text{O}$) i la ferrihidrita. No obstant, aquestes fases permeten la precipitació d'arsènic, però en llarg termini acaben descomponent-se a goethita (FeOOH), i goethita + hematita (Fe_2O_3) respectivament. A més a més, aquestes fases contenen ferro, el qual pot ser fàcilment reduït en sòls reductors. Aquest fet pot afectar l'estabilitat de fases amb ferro i produir l'alliberament de l'arsènic.

Aquesta tesi ha estat escrita com a compendi d'articles i s'ha estructurat en les següents parts:

- Introducció.
- Resultats i discussió:
 - Síntesis de fases tipus alunita: Na, K, H_3O , Ba i Pb.
 - Síntesis de natroalunites arsenicals generades a partir de residus industrials.
 - Tests d'estabilitat (curt/mig/llarg termini).
 - Estudi d'estructura.
- Conclusions

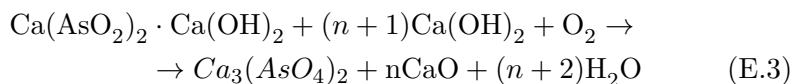
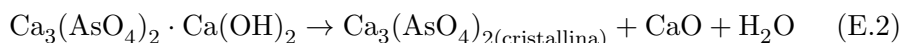
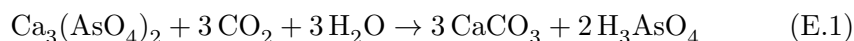
Com que algunes de les parts dels articles s'han agrupat per tal de fer la tesi més consistent i fàcil de seguir, tots els articles s'han adjuntat com a annexes.

Breu introducció

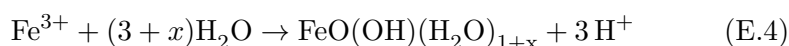
L'arsènic és un element tòxic trobat a menes de metalls no ferrosos. A països del centre i sud Amèrica, així com alguns països asiàtics, tenen elevades concentracions d'arsènic a l'aigua que afecten la salut de la població. La creixent demanda d'alguns metalls, com el coure, fan incrementar la contaminació d'arsènic dels freàtics en alguns països. Les menes de coure cada vegada contenen més arsènic degut a l'esgotament de les menes amb menys contingut d'arsènic. Aquesta situació a induït en la recerca de nous mètodes de precipitació d'arsènic.

Actualment, els principals mètodes de precipitació d'arsènic usats en la indústria són:

- Arseniat càlcic: És el mètode més econòmic, però l'arsènic d'aquest precipitat es dissol fàcilment per l'acció del CO_2 present a l'atmosfera (Eq. E.1). Alguns estudis revelen que l'arsènic d'aquest precipitat es pot estabilitzar amb una calcinació a 700°C (Eq. E.2 i E.3). Aquesta calcinació s'usa a les metal·lúrgies de Xile, a on el clima sec ajuda a l'estabilitat d'aquesta fase.



- Co-precipitació d'arsènic amb ions fèrrics: Aquest mètode utilitza Fe(III) per precipitar As(V). Bàsicament l'As(V) es quimiadsorbeix a la ferrihidrita formada. Aquesta reacció es dona a 80°C de temperatura en medi àcid i incrementant el pH a 2-3 per precipitar el ferro (III) com a ferrihidrita (Eq. E.4) i que l'arsènic present en el medi s'hi adsorbeixi (Eq. E.5). Finalment, la solució es neutralitza amb calç per assegurar que l'arsènic es precipiti. El precipitat obtingut és voluminós i difícil de filtrar. A períodes a llarg termini aquesta fase descompon en goethita i hematita. Tot i la poca estabilitat, el gran volum i la dificultat de filtració d'aquesta fase, aquest mètode és molt utilitzat al Canadà.



- Escorodita ($\text{FeAsO}_4 \cdot 2 \text{H}_2\text{O}$): Aquesta fase ha estat extensament estudiada. L'escorodita pot ser sintetitzada per diferents vies (enumerades més avall). Tots els processos de síntesis d'escorodita descrits a sota permeten obtenir escorodita cristal·lina. Per això mateix, aquesta fase és fàcilment filtrable i ocupa un volum més reduït comparat amb les fases descrites més amunt. L'escorodita, però, també pot descompondre a goethita en un temps a llarg termini.

1. Síntesi hidrotermal: A més de 125°C de temperatura, en solucions equimolars (0.3 M As(V) i 0.3 M Fe(III)) (Eq. E.6). L'escorodita sintetitzada està ben cristal·litzada. Els estudis d'estabilitat realitzats a les escorodites hidrotermals necessitaven molts rentats degut a la presència d'una fase amorfa.



2. Síntesi a menys de 100°C: Per reduir el cost econòmic de l'escorodita, la síntesi a baixa temperatura ha estat estudiada. La síntesi a aquestes temperatures es pot fer bàsicament per dues vies:
 - (a) Síntesi a partir de ferro (III), controlada per la saturació dels reactius en el medi. Aquest tipus de síntesi s'ha fet tan en medis clorurs com en medis amb sulfats. Aquesta última és important donat que la majoria d'effluents amb arsènic són rics en sulfats. La presència de sulfats produeix un efecte inhibitori que disminueix o impossibilita la formació d'escorodita.
 - (b) A través de l'oxidació controlada de ferro (II) a ferro (III). El procés consisteix en la oxidació de Fe(II) amb l'aire o l'oxigen en presència d'As(V). A temperatures d'entre 70 i 95°C i un temps de retenció d'entre 1 i 7 h, suficient per permetre l'oxidació del Fe(II), es formen escorodites cristal·lines (figura E.1)

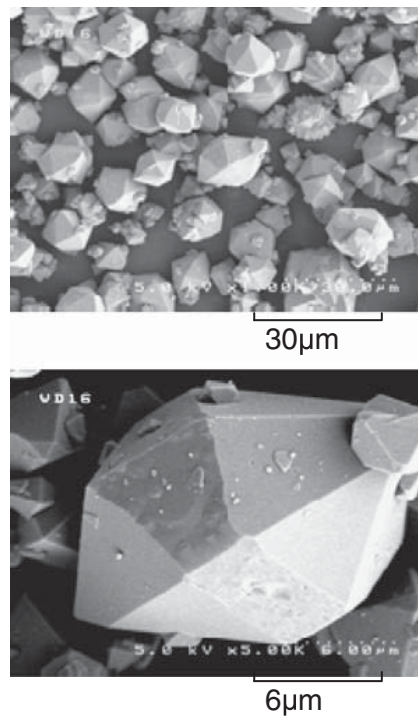


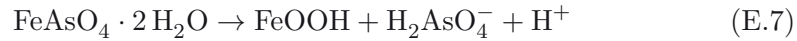
Figura E.1: Micrografia SEM d'escorodita sintètica [Fujita et al., 2011].

3. Síntesi bioquímica: L'ús de varis microorganismes termofílics (que suporten temperatures de més de 60°C), com l'*Acidianus Sulfidivorans* i l'*Acidithiobacillus Ferrooxidans*, permeten una oxidació lenta de ferro (II) a ferro (III) per produir escorodita tal i com es fa a la síntesi a menys de 100°C controlada per l'oxidació del Fe(II).

Així doncs, l'escorodita presenta l'avantatge de ser un precipitat fàcilment filtrable. El volum de l'escorodita és petit comparat amb el de la ferrihidrita i

que els arseniats càlcics. A més a més, permet la precipitació de grans quantitats d'arsènic, ja que la relació Fe:As és 1:1.

L'escorodita, però, s'ha demostrat que és metastable en condicions atmosfèriques normals, produint-se una transformació lenta de l'escorodita a goethita que permet la dissolució de l'arsènic (Eq. E.7)



En aquesta tesi les fases estudiades per a la immobilització de l'arsènic són del tipus alunita. A diferència de les fases explicades anteriorment, en aquesta tesi no s'han estudiat fases amb ferro, sinó fases d'aquest supergrup que contenen alumini a l'estructura. El fet d'estudiar les fases amb alumini en comptes de ferro és que aquest últim és fàcilment reduïble en sòls reductors, mentre que l'alumini no es pot reduir.

El supergrup de minerals tipus alunita tenen una estructura tipus $\text{AB}_3(\text{TO}_4)_2(\text{OH})_6$, a on A és un monovalent o un divalent (Na, K, Ba, etc.), B és un trivalent (Fe, Al, etc.) i TO_4 pot ser SO_4 , PO_4 , o AsO_4 . A la natura, unes de les alunites més trobades són les alunites ($\text{KAl}_3(\text{SO}_4)_2(\text{OH})_6$) i les natroalunites ($\text{NaAl}_3(\text{SO}_4)_2(\text{OH})_6$) (figura E.2).

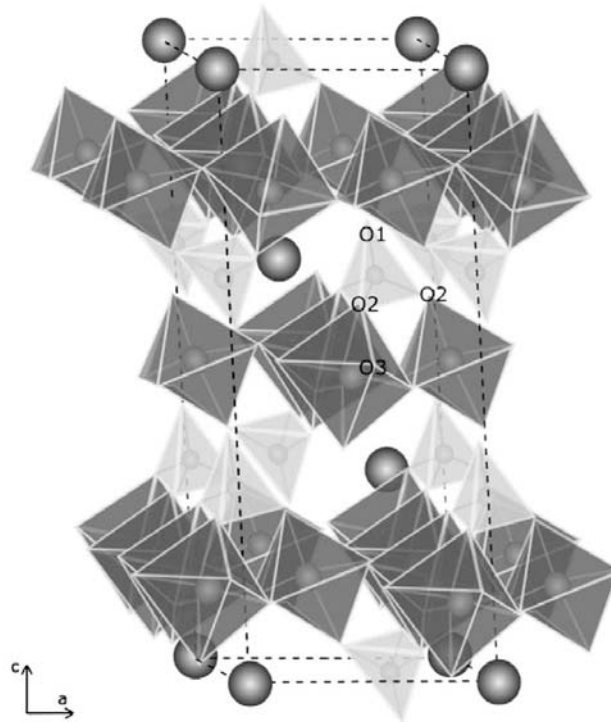


Figura E.2: Estructura tipus alunita [Sunyer i Viñals, 2011].

L'ús de les fases tipus alunites com a fases a on incorporar arsènic ve donat per a la possibilitat de la substitució parcial del SO_4 per AsO_4 .

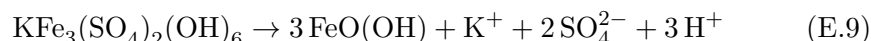
La substitució dels llocs A, B i TO_4 afecten els paràmetres de xarxa de l'estructura. L'efecte sobre els paràmetres de cel·la ve determinat pel lloc substituït

i pel radi iònic dels elements (el substituït i el substitut). En el nostre cas, la substitució de SO_4 per AsO_4 afectarà el paràmetre de cel·la c , el qual incrementarà amb la incorporació d'arsènic a l'estructura. No obstant, el paràmetre de cel·la c també es pot modificar canviant el lloc A.

La fase tipus alunita més estudiada per a la incorporació d'arsènic és la jarosita ($\text{KFe}_3(\text{SO}_4)_2(\text{OH})_6$). Les jarosites, en particular les jarosites de sodi i d'amoni, són àmpliament usades en la hidrometal·lúrgia, especialment en la indústria del zinc. El seu ús principal és el control d'impureses com el ferro i els sulfats alcalins (Eq. E.8). La principal propietat d'aquesta fase és que els metalls divalents com el coure, el zinc i el níquel no precipiten. Les jarosites són, a més, fàcilment filtrables i es poden sintetitzar en condicions àcides.



Les jarosites es poden sintetitzar a baixa temperatura (menys de 100°C). Les jarosites arsenicals poden ser sintetitzades a 98°C , obtenint una precipitació d'arsènic d'un 9.91 % abans que l'escorodita comenci a precipitar. Com les fases ferroses explicades anteriorment, les jarosites poden descomponer a goethita a llarg termini (Eq. E.9). Aquesta descomposició podria provocar la dissolució de l'arsènic en jarosites arsenicals.

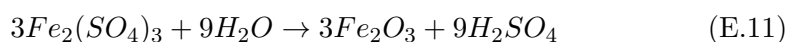


Les jarosites no poden ser usades com a subproducte, a més a més, tenen el problema de ser voluminoses. Per aquesta raó la formació d'hematita a partir de jarosita pot ser d'interès. L'hematita és un precipitat filtrable que ocupa un volum petit i que a més, s'usa com a subproducte a les indústries cimenteres. El procés de síntesis de les hematites és molt car degut a la necessària oxidació del ferro. Com que les jarosites contenen ferro (III), llavors, la temperatura del procés de síntesis d'hematita es pot reduir per l'ús de la jarosita en la síntesis d'hematita.

La transformació de la jarosita a hematita es pot fer a partir de dos passos:

1. Concentració del ferro a través de la precipitació de la jarosita.
2. Transformació de la jarosita a hematita.

Les reaccions que es produeixen durant el procés de conversió són les Eq. E.10, E.11 i E.12.



La concentració prèvia del ferro a través de la precipitació de la jarosita permet una reducció econòmica en el procés perquè el ferro ja va ser oxidat en la precipitació de la jarosita i a més a més està concentrat.

Excepte les jarosites, les fases tipus alunites no s'usen en la indústria. Per aquesta raó les alunites no han estat molt estudiades. La gran majoria d'investigacions han estat enfocades en l'estudi d'estructura. En aquests estudis

la síntesis d'alunita s'ha fet hidrotermalment, a temperatures d'entre 190°C i 205°C. La reacció de síntesis que té lloc és la de l'equació E.13, a on A és l'alcalí.



Tot i que les alunites no han estat mai estudiades com a fases per a la incorporació d'arsènic, en fases anàlogues com les jarosites s'ha demostrat que poden incorporar arsènic en la seva estructura. Les fases amb ferro presenten desavantatges com la possible inestabilitat en sòls reductors degut a la fàcil reducció del ferro. D'altra banda, l'alumini no pot ser reduït en condicions reductores. Aquesta característica fa que les fases alunites siguin atractives com a fases per a l'estabilització d'arsènic.

Objectius de la tesi

El principal objectiu d'aquesta tesi és la inertització d'arsènic a través de fases tipus alunita, l'estabilitat d'aquestes fases a llarg termini i l'aplicació en residus de la pirometal·lúrgia del coure en relacions sulfat/arseniat altes. Per això s'han marcat els següents objectius:

1. Síntesi de natroalunites arsenicals: optimització del procés i estabilitat de l'arsènic.
2. Aplicació de la natroalunita arsenical en residus arsenicals de la pirometal·lúrgia del coure.
3. Efecte de la incorporació d'arsènic en estructures tipus alunita: Síntesis d'altres fases d'alunites arsenicals com l'alunita de potassi, la d'hidroni, la de bari o la de plom.
4. Avaluació de l'estabilitat de les alunites arsenicals (de potassi) a mitjà termini. Per completar l'estudi els tests a mig termini també es van fer en escorodita natural i escorodita sintètica.

Resultats i discussió

Natroalunites arsenicals sintètiques

La síntesi de natroalunites arsenicals ha estat estudiada en diferents condicions. En els següents punts es troben resumits els resultats obtinguts. A les taules E.1 i E.2 es poden trobar els resultats obtinguts en la síntesis de les natroalunites arsenicals en cada una de les condicions.

- Efecte de la temperatura de síntesis: Tots els experiments van ser realitzats amb un temps de retenció de 2 h.
 - En absència d'arsènic la precipitació va incrementar linealment entre 140°C i 200°C. A 200°C el rendiment de precipitació va ser del 55%.
 - En presència d'arsènic ($\text{AsO}_4/(\text{SO}_4 + \text{AsO}_4) = 0.185$): a 160°C/180°C va precipitar una mescla de natroalunita arsenical i de mansfieldita ($\text{AlAsO}_4 \cdot 2\text{H}_2\text{O}$). A 200°C només va precipitar natroalunita arsenical.
- Efecte del temps de retenció: Aquest efecte va ser avaluat a diferents temperatures i a diferents relacions molars $\text{AsO}_4/(\text{SO}_4 + \text{AsO}_4)$. Els resultats obtinguts van ser els següents:

- $\text{AsO}_4/(\text{SO}_4 + \text{AsO}_4) = 0.185$:
 - * A 15 min: A 160°C / 180°C van precipitar fases arsenicals amorfes i natroalunita arsenical.
 - * A 30 min: A 160°C van aparèixer fases amorfes i la precipitació de natroalunita arsenical va incrementar. A 180°C van precipitar natroalunita arsenical i mansfieldita.
 - * A 2 h: A 160°C va precipitar natroalunita arsenical. A 180°C van precipitar natroalunita arsenical i mansfieldita.
 - * A 4 h: A $160^\circ\text{C}/180^\circ\text{C}$ van precipitar natroalunita arsenical i mansfieldita.
 - * A 5 min o més: A 200°C va precipitar natroalunita arsenical.
- $\text{AsO}_4/(\text{SO}_4 + \text{AsO}_4) = 0.083$:
 - * A 2 h i 180°C va precipitar natroalunita arsenical.
 - * A 5 min o més a 200°C va precipitar natroalunita arsenical.
- Efecte de la concentració d'arsènic.
 - $0 < \text{AsO}_4/(\text{SO}_4 + \text{AsO}_4) < 0.2$: Van precipitar natroalunita/natroalunita arsenical.
 - $0.2 < \text{AsO}_4/(\text{SO}_4 + \text{AsO}_4) < 0.4$: Van co-precipitar natroalunita i mansfieldita.
 - $\text{AsO}_4/(\text{SO}_4 + \text{AsO}_4) \sim 0.421$: Van precipitar alarsita (AlAsO_4) i una mica de mansfieldita.
 - $\text{AsO}_4/(\text{SO}_4 + \text{AsO}_4) \sim 0.474$: Van precipitar natrofarmacoalunita ($\text{NaAl}_4(\text{AsO}_4)_3(\text{OH})_4 \cdot 4\text{H}_2\text{O}$) i mansfieldita.
 - Es va determinar que la incorporació d'arsènic a 200°C seguia (figura E.3):

$$(\text{AsO}_4/(\text{SO}_4 + \text{AsO}_4))_{nat} \approx 0.5 (\text{AsO}_4/(\text{SO}_4 + \text{AsO}_4))_{aq}$$
- Síntesis amb calci: El calci no va afectar la síntesis de la natroalunita arsenical. Una petita part de calci es va incorporar a l'estructura de la natroalunita arsenical. La resta del calci va precipitar com a anhidrita.
- La síntesis amb calci i absència de sodi: L'objectiu era la precipitació de schlossmacherita ($(\text{H}_3\text{O}, \text{Ca})\text{Al}_3(\text{SO}_4, \text{AsO}_4)_2(\text{OH})_6$) o arsenocrandellita ($\text{CaAl}_3(\text{AsO}_4)_2(\text{OH})_6(\text{H}_2\text{O})$). No obstant, cap de les dues fases es va poder precipitar.

Taula E.1: Composició bulk (ICP) i fases (Rietveld) del precipitat hidrotermal (na: natroalunita; am: fase amorfa; ma: mansfieldita; al: alarsita; ph: natrofarmacoalunita).

Temperature (°C)	Time (h)	(As/(S + As)) _{aq}	Chemical composition (%)				Phases (XRD and SEM/EDS)
			Na	Al	S	As	
<i>Na⁺/Al³⁺/SO₄²⁻</i>							
100	2	0	–	–	–	–	no precipitate
100	72	0	not det.	–	–	–	na (16% yield)
100	72	0	3.84	20.08	16.64	0.00	na (29% yield)
120	2	0	–	–	–	–	no precipitate
140	2	0	not det.	–	–	–	na (1% yield)
160	2	0	not det.	–	–	–	na (16% yield)
180	2	0	not det.	–	–	–	na (37% yield)
200	2	0	4.05	17.95	15.07	0.00	na (55% yield)
<i>Na⁺/Al³⁺/SO₄²⁻/AsO₄³⁻</i>							
100	72	0.185	3.49	18.48	11.91	7.22	na (74% ^a) + am (26% ^b)
160	0.083	0.185	1.63	15.45	6.14	14.72	na (33% ^a) + am (67% ^b)
160	0.5	0.185	3.77	17.43	11.77	7.26	na (75% ^a) + am (25% ^b)
160	2	0.185	5.10	20.02	15.12	2.95	na
160	4	0.185	4.16	18.25	12.52	8.51	na (85%) + ma (15%)
180	0.083	0.185	3.63	17.92	11.96	7.42	na (73% ^a) + am (27% ^b)
180	0.5	0.185	3.83	18.40	12.45	7.29	na (87%) + ma (13%)
180	2	0.185	4.98	18.97	13.67	7.53	na (91%) + ma (9%)
180	4	0.185	4.00	18.87	12.93	8.59	na (82%) + ma (18%)
200	0.083	0.185	5.18	19.13	15.07	3.43	na
200	0.5	0.185	4.57	18.40	14.87	3.00	na
160	0.083	0.083	1.75	19.05	7.74	8.46	na (35% ^a) + am (65% ^b)
160	2	0.083	5.08	18.92	14.99	1.45	na
160	4	0.083	4.73	18.38	17.62	3.09	na (95%) + ma (5%)
180	2	0.083	5.18	18.90	16.46	1.43	na
200	0.083	0.083	4.87	18.63	14.86	1.52	na
200	0.5	0.083	4.98	18.36	14.91	1.28	na
200	2	0.083	4.88	18.42	14.88	1.24	na
200	2	0.101	4.52	17.18	13.94	1.32	na
200	2	0.114	4.66	18.70	15.02	1.69	na
200	2	0.130	4.59	16.96	13.53	1.94	na
200	2	0.152	4.91	17.53	13.77	2.53	na
200	2	0.185	4.72	18.93	14.55	2.80	na
200	2	0.231	3.68	17.92	10.46	12.97	na (71%) + ma (29%)
200	2	0.270	5.26	19.27	12.91	5.98	na (95%) + ma (3%) + al (2%)
200	2	0.311	1.79	15.41	4.41	25.71	na (32%) + ma (68%)
200	2	0.359	0.87	14.24	2.00	30.09	na (16%) + ma (85%)
200	2	0.421	0.18	16.46	0.06	41.99	al (98%) + ma (2%)
200	2	0.474	2.17	14.96	0.08	32.52	ph (65% ^a) + (al + ma) (35% ^b)

^a Determined from the Na content in the bulk product.

^b By difference.

Taula E.2: Composició química i fases obtingudes en presència de calci.

Temperature (°C)	Time (h)	(As/ ((S-Ca) + As)) _{aq}	Chemical composition (%)					Phases (XRD and SEM/EDS)
			Na	Ca	Al	S	As	
<i>Na⁺/Ca²⁺/Al³⁺/SO₄²⁻/AsO₄³⁻</i>								
200	2	0.100	4.20	1.03	21.00	17.91	1.35	na (98%) + an (2%)
200	2	0.182	4.75	1.07	20.37	16.14	2.60	na (98%) + an (2%)
200	0.5	0.182	4.26	1.55	18.44	14.93	3.46	na (97%) + ma (1%) + an (2%)
200	0.25	0.182	4.50	1.98	18.09	14.87	3.38	na (97%) + ma (1%) + an (2%)
180	2	0.182	4.11	1.53	17.34	13.03	6.62	na (89%) + ma (9%) + an (2%)
180	0.5	0.182	4.07	1.56	18.33	14.08	4.15	na (92%) + am (6%) + an (2%) ^a
180	0.25	0.182	4.42	1.49	17.24	14.24	3.60	na (94%) + am (4%) + an (2%) ^a
200	2	0.309	1.79	3.60	15.51	9.25	22.05	na (36%) + ma (51%) + an (11%)
200	2	0.309	1.57	7.90	13.52	10.33	18.69	na (31%) + ma (43%) + an (26%)
<i>Ca²⁺/Al³⁺/SO₄²⁻/AsO₄³⁻</i>								
200	2	0.182	0.00	17.97	9.71	14.88	9.33	hy (3%) + am (37%) + an (60%) ^b
200	2	0.309	0.00	1.20	15.20	3.55	34.40	ma (96%) + an (4%)
200	2	0.309	0.00	9.27	10.09	8.47	26.61	ma (68%) + an (32%)

^a Natroalunite and anhydrite from the Na and Ca contents. Amorphous by difference.

^b Anhydrite from Ca content. Hydronium alunite from the ratio hydronium alunite/anhydrite from Rietveld. Amorphous by difference.

Síntesis d'alunita arsenical

L'alunita arsenical es va sintetitzar a 200°C i a 100°C. L'objectiu era obtenir més substitució d'AsO₄ que en les natroalunites arsenicals. Aquest objectiu estava basat en el major paràmetre de cel·la *c* de les alunites arsenicals.

Les alunites arsenicals sintetitzades a 200°C i amb un temps de retenció d'1 h van ser estudiades a diferents relacions molars AsO₄/(SO₄ + AsO₄). La conclusió principal va ser que la incorporació d'arsènic va ser similar al trobat en les natroalunites arsenicals. Així que la substitució d'AsO₄ per SO₄ va ser determinada per (figura E.3):

$$(AsO_4/(SO_4 + AsO_4))_{nat} \approx 0.5 (AsO_4/(SO_4 + AsO_4))_{aq}$$

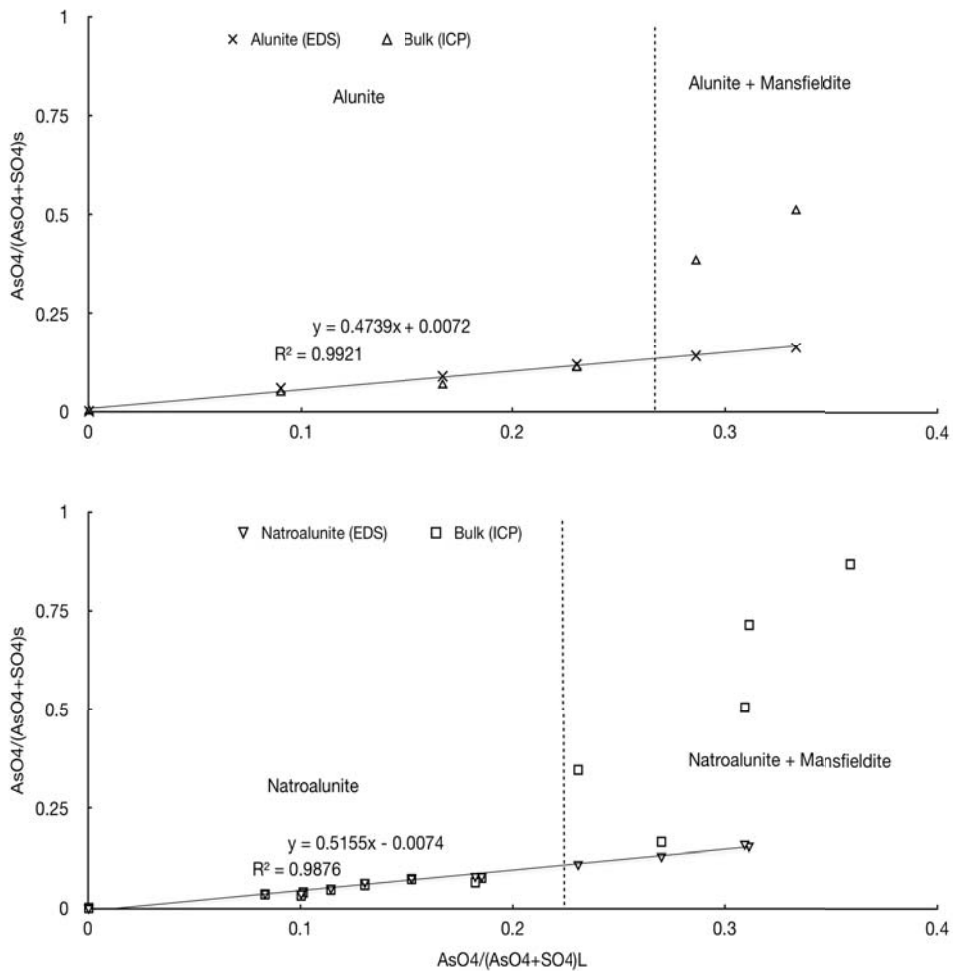


Figura E.3: Comparació entre natroalunites arsenical i alunites arsenicals a diferents $AsO_4/(SO_4 + AsO_4)_s$ (en el bulk in en As-alunita/As-natroalunita) i $AsO_4/(SO_4 + AsO_4)_{aq}$.

Les alunites sintetitzades a 98°C van ser estudiades amb i sense la presència d'arsènic al medi, a diferents temperatures de síntesi, a diferents temps de retenció, a diferents concentracions de reactius, i en presència d'arsènic (III) i d'arsènic (V).

- Efecte del temps de retenció i de temperatura de síntesi: A baixa tem-

peratura el rendiment de precipitació depèn del temps de retenció. Un increment amb el temps de retenció significa un increment en el rendiment de precipitació. El rendiment de precipitació també depèn de la temperatura de síntesis. A més altes temperatures, més rendiment de precipitació s'obté.

- Efecte de la concentració de reactius: Baixes concentracions d'un dels reactius afecte el rendiment de precipitació de l'alunita. Aquest efecte és important per tal d'optimitzar la síntesis de l'alunita.
- Efecte de l'As (III) i l'As (V): L'arsènic (III) pràcticament no es va incorporar a l'estructura. No obstant, la seva presència en el medi va fer incrementar el rendiment de precipitació de l'alunita. L'arsènic (V) es va incorporar a les alunites. Com l'arsènic (III), el rendiment de precipitació també va incrementar en presència d'arsènic (V). Els precipitats amb menys arseniat (8.5 %) van passar els tests de toxicitat TCLP, mentre que els precipitats amb més alt contingut d'arsènic (19.5 %) no van passar els tests de toxicitat TCLP.

Síntesis d'alunites de hidroni, bari, plom

L'alunita d'hidroni es va poder sintetitzar en absència d'arsènic, però en presència d'arsènic el rendiment de precipitació va disminuir i l'alunita d'hidroni pràcticament no va precipitar. Les petites quantitats obtingudes en presència d'arsènic no van incorporar arsenic. A més a més, van precipitar fases arsenicals amorfes i mansfieldita (taula E.3).

Es va intentar sintetitzar les alunites de bari i plom en diferents condicions. Malgrat tot, la insolubilitat del sulfat de bari i del sulfat de plom no van fer possible la síntesis d'aquestes fases.

Natroalunites arsenicals generades a partir de residus industrials

Per la generació de natroalunites arsenicals es va usar dos residus diferents procedents de la indústria pirometal·lúrgica del coure: Un arseniat càlcic a partir de l'effluent final de la secció electrolítica, i pols de forn flash.

Els precipitats van ser caracteritzats. La prioritat va ser recuperar els metalls valuosos presents en els residus i la precipitació d'arsènic a través de la síntesis de natroalunites-arsenicals.

Per a la síntesis de la natroalunita arsenical es van seguir els següents passos:

1. Lixiviació (a pH 1 amb H_2SO_4): Per tal de dissoldre completament tots els metalls presents en el residu.
2. Ozonització: Per tal d'oxidar l'arsènic (III) a arsènic (V), i en cas de presència de ferro, per oxidar el ferro (II) a ferro (III).
3. Precipitació hidrotermal: Amb l'addició d' $\text{Al}_2(\text{SO}_4)_3$ i Na_2SO_4 per obtenir natroalunita arsenical. La síntesi de natroalunita arsenical no va precipitar metalls divalents com el Ni o el Cu. Així doncs, es pot fer abans de la recuperació de metalls valuosos.

Taula E.3: Condicions inicials i resultats de síntesis de les hidroni-alunites.

	$\text{Al}_2(\text{SO}_4)_3 \cdot 18\text{H}_2\text{O}$ (g)	As (g) as H_3AsO_4	$\frac{\text{AsO}_4}{(\text{SO}_4 + \text{AsO}_4)}$	V (mL)	T (°C)	t (h)	pH ₀	pH _f	Wt (g)	XRD	SEM
H0	6.3329	0	0	150	200	1	3.2	1.0	0.6733	H ₃ O-alunite	H ₃ O-alunite
H0.25	6.3309	0.12	0.0413	150	200	1	0.95	0.5	0.4122	H ₃ O-alunite	H ₃ O-alunite
H0.5	6.331	0.24	0.0757	150	200	1	0.95	0.67	0.2349	H ₃ O-alunite	H ₃ O-alunite
H0.75	6.3311	0.352	0.1141	150	200	1	0.97	0.64	0.2509	H ₃ O-alunite	H ₃ O-alunite
H1	6.3300	0.472	0.1489	150	200	1	0.98	0.75	0.1455	H ₃ O-alunite	H ₃ O-alunite
H1.5	6.3301	0.712	0.1908	150	200	1	0.99	0.78	0.0339	Mansfieldite (48.13%) + H ₃ O- alunite (51.87%)	Mansfieldite + H ₃ O-alunite

Taula E.4: Condicions inicials, composicions bulk i composició de fases de la síntesis de natroalunites arsenicals a partir de residus industrials.

(Al/As) _{aq}	Temp (°C)	Time (min)	pH _i	pH _f	Bulk composition (weight %)										Phase composition (%)		
					S	As	Al	Fe	Ca	Na	Cd	Ni	Zn	Cu	n	m	a
1.50	200	120	2.0	1.6	19.0	3.77	2.66	1.34	22.5	0.26	0.15	0.22	0.18	0.24	-	~23*	~77
1.50	200	120	1.0	0.8	20.0	3.34	0.88	1.12	24.5	0.07	0.13	0.036	0.03	0.06	-1	~10	~85
2.25	200	120	1.0	0.7	19.2	3.41	2.64	1.23	21.6	0.65	0.13	0.01	0.03	0.02	~8	~12	~75
3.00	180	15	1.0	0.9	20.5	2.60	3.73	1.01	22.8	1.00	0.13	0.03	0.03	0.05	~18	~5	~77
3.00	180	30	1.0	0.8	20.4	3.05	3.85	1.05	21.7	1.09	0.12	0.05	0.04	0.04	~19	~6	~75
3.00	180	120	1.0	0.8	19.7	3.60	3.83	1.05	21.8	0.96	0.12	0.05	0.03	0.04	~17	~8	~75
3.00	200	15	1.0	0.7	21.0	2.41	4.04	1.10	22.1	1.10	0.13	0.038	0.02	0.02	~20	~5	~75
3.00	200	30	1.0	0.7	20.4	2.50	4.01	1.15	21.6	1.05	0.12	0.01	0.02	0.04	~20	~5	~75
3.00	200	120	1.0	0.7	19.7	2.67	4.20	1.16	20.6	1.15	0.12	0.038	0.02	0.04	~20	~5	~70
3.00**	200	120	1.0	0.5	19.3	2.45	3.69	1.07	22.4	1.11	0.12	0.039	0.03	0.03	~19	~5	~75
3.00***	200	120	1.0	0.5	11.5	9.85	16.2	4.22	0.13	4.49	0.004	0.038	0.02	0.04	~80	~20	-
4.50	200	120	1.0	0.7	19.4	1.10	5.98	0.94	18.4	1.60	0.09	<0.031	0.008	0.05	~30	~2	~65

* : mansfieldite + amorphous phase.

** : As concentration (7.0 g/L) double than in the rest of experiments.

*** : with prior gypsum removal.

4. Els metalls valuosos es poden recuperar a partir de l'effluent final.

Les condicions de síntesis, la composició bulk dels resultats i les fases obtingudes es mostren a la taula E.4.

El calci present als residus va ser transformat a anhidrita (CaSO_4). No obstant, l'eliminació del guix abans del tractament hidrotermal és aconsellable degut a què la incorporació de cadmi a l'anhidrita pot causar problemes mediambientals.

Altes concentracions de ferro presents en els residus es poden usar com a intermedis per a la precipitació d'arsènic ajustant el pH. El precipitat obtingut es pot usar com a intermedi en el tractament hidrotermal per obtenir la precipitació de natroalunita arsenical.

Tests d'estabilitat

Els tests a curt termini es van realitzar en mostres de natroalunites arsenicals (sintètiques i de residus) i d'alunites arsenicals. En les natroalunites arsenicals i en les alunites arsenicals els valors obtinguts van ser bons, amb un mínim de dissolució d'arsènic a pH's entre 5 i 8 de 0.01-0.03 mg As/L (figures E.4 i E.5). Altres fases com la mansfieldita, l'alarsita i fases amorfes van presentar valors 2 i 3 ordres de magnitud superiors que les natroalunites arsenicals i les alunites arsenicals. La natrofarmacoalunita no va presentar cap dany en el rang de pH's d'entre 1 i 12. Aquesta fase va presentar un intercanvi iònic a pH's àcids, a on Na^+ va ser substituït per H_3O^+ (figura E.6).

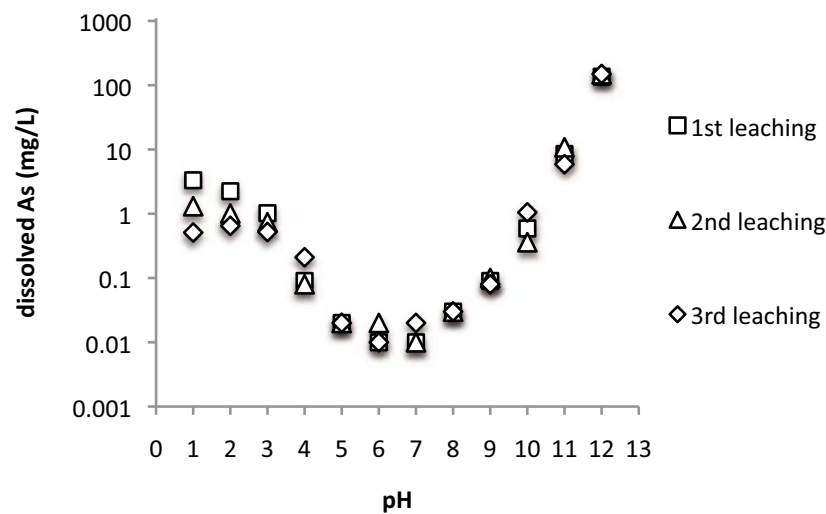


Figura E.4: Arsènic solubilitzat en alunita arsenical (24 h).

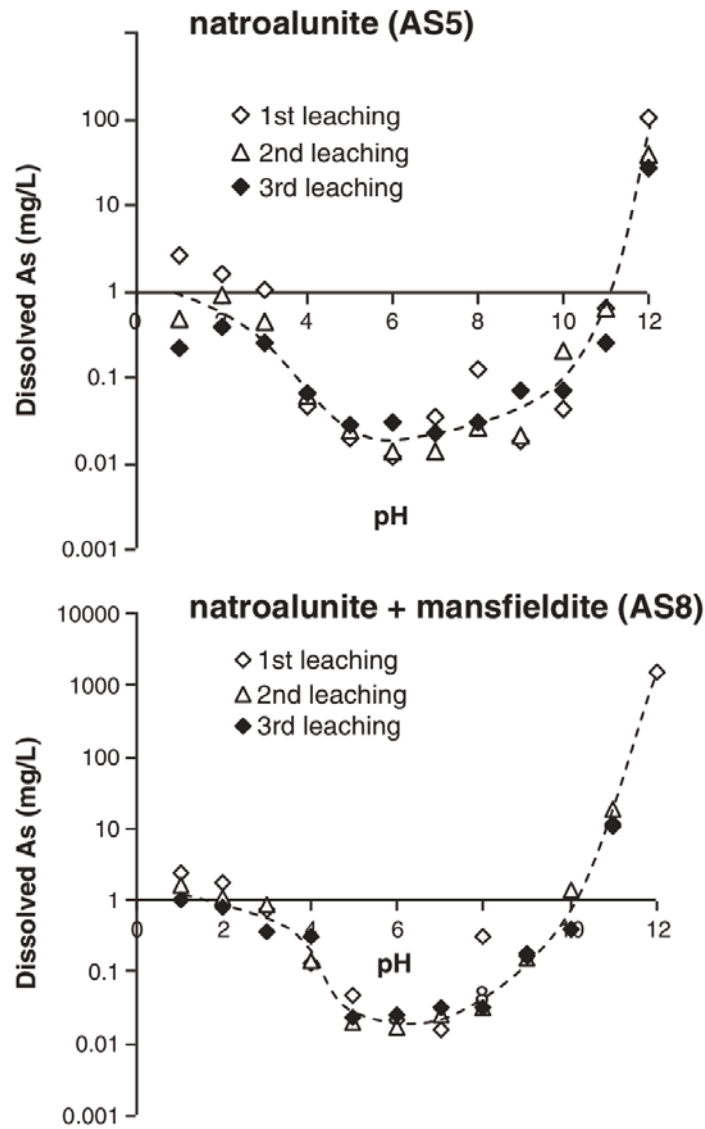


Figura E.5: Arsènic solubilitzat en natroalunites arsenicals sintètiques i mescles de natroalunita arsenical i mansfieldita.

En tests a llarg termini (6 mesos) les natroalunites arsenicals van donar valors baixos, de 0.1 mg As/L (figura E.7). Els tests de mig termini (5 setmanes) es van fer a les alunites arsenicals, les quals van donar valors, també baixos però no tan bons com els de la natroalunita arsenical, de 0.3 mg As/L. L'escorodita natural va donar uns valors similars a l'alunita arsenical, de 0.4 mg/L. L'escorodita sintètica va donar uns valors molt alts de dissolució d'arsènic, de 1.3 mg As/L (figura E.8).

Estudi d'estructura

L'estudi per Rietveld va confirmar que les natroalunites arsenicals i les alunites arsenicals tenen una estructura tipus R-3m i Z=3. L'expansió de la cel·la experimentada en ambdós casos amb la incorporació d'arsènic va ser la mateixa: ~ 0.58 . Aquest increment és consistent amb l'expansió esperada de cel·la degut a la diferència amb les distàncies As-O1 i S-O1 (figura E.9).

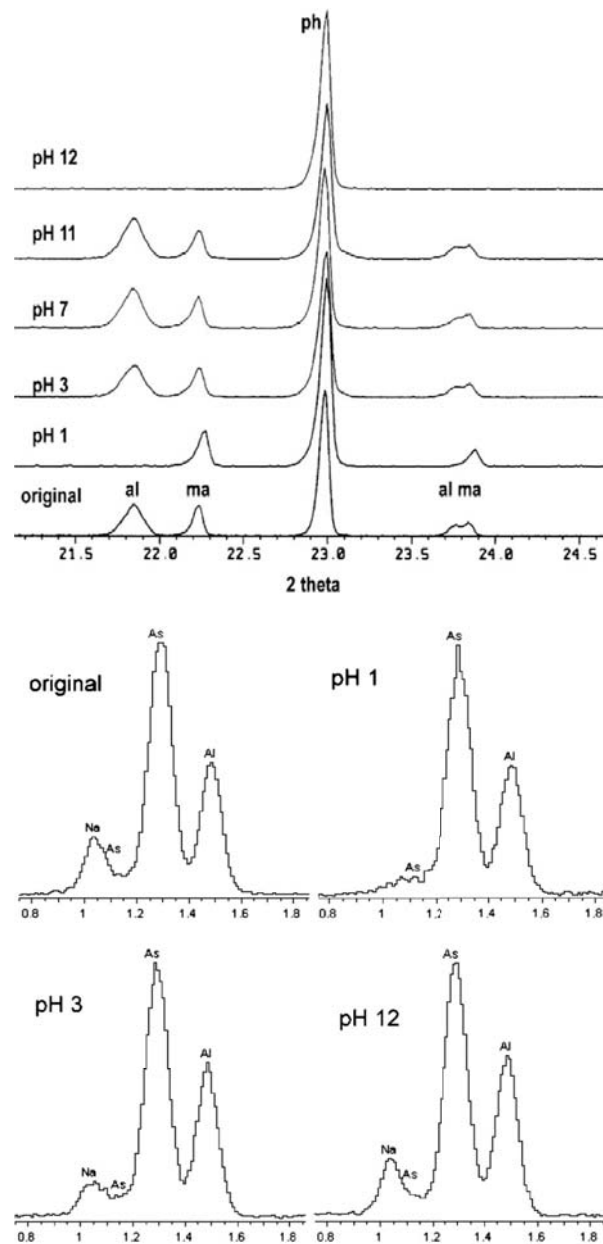


Figura E.6: A dalt) DRX de la mostra original i de les mostres després dels tests de lixiviació a diferents pH's de natrofarmacoalumita. A sota) Anàlisi SEM-EDS de la natrofarmacoalumita: mostra original i de les mostres després dels tests de lixiviació a diferents pH's .

L'estudi per Rietveld també es va realitzar a les alunites d'hidroni. En aquesta fase no es va incorporar arsènic de manera significativa, com queda demostrat en els paràmetres de cel·la trobats per aquesta fase. La incorporació d'arseniat en aquesta fase pot veure's afectada per la protonació de $(\text{AsO}_4)^{3-}$ com a $(\text{HAsO}_4)^{2-}$ o la protonació de OH^- com a H_2O . Aquestes espècies poden afectar el lloc de l' H_3O en l'estructura de l'hidroni alunita degut als ponts d'hidrogen que té amb els oxígens possiblement protonats.

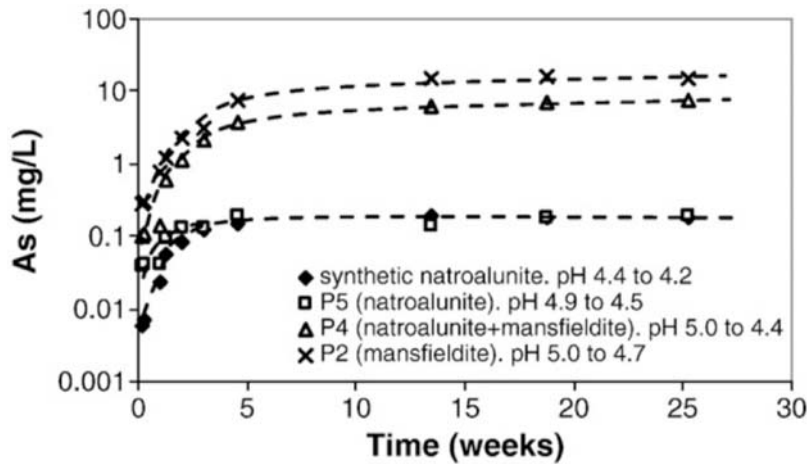


Figura E.7: Tests de llarg termini de natroalunita arsenical, natroalunita arsenical més mansfieldita, i natroalunita arsenical del residu d'arseniat càlcic.

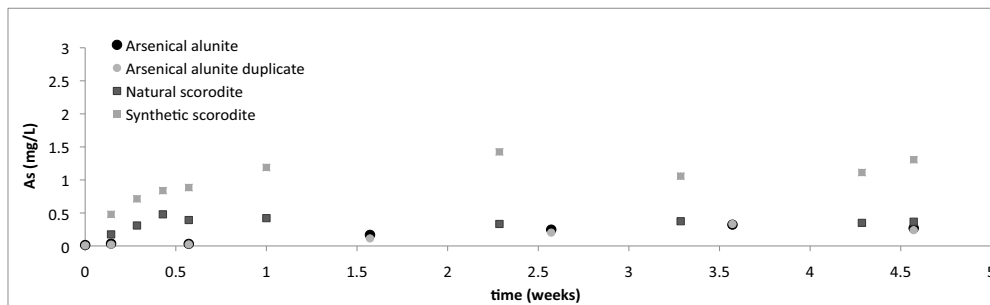


Figura E.8: Tests a mitjà termini de alunita arsenical, escorodita sintètica i escorodita natural.

Conclusions

Les principals conclusions són:

- Les alunites i natroalunites arsenicals sintètiques es poden fer en menys de 5 min a 200°C. A aquesta temperatura el temps de retenció no afecta el producte final.
- La incorporació d'arsènic en alunites/natroalunites a 200°C ve determinada per:

$$(AsO_4/(SO_4 + AsO_4))_{nat} \approx 0.5 (AsO_4/(SO_4 + AsO_4))_{aq}$$
- Les alunites d'hidroni no incorporen arsènic a l'estructura, i en presència d'arsènic pràcticament no es formen.
- Les natroalunites arsenicals es poden generar a partir de residus industrials. Com en les natroalunites sintètiques, la precipitació és molt ràpida, menys de 15 min. La incorporació d'arsènic és similar a la trobada en sintètic. Els metalls divalents com el Ni, el Cu o el Zn no precipiten durant la síntesis de natroalunita arsenical, permetent la recuperació d'aquests metalls a partir de l'efluent final.

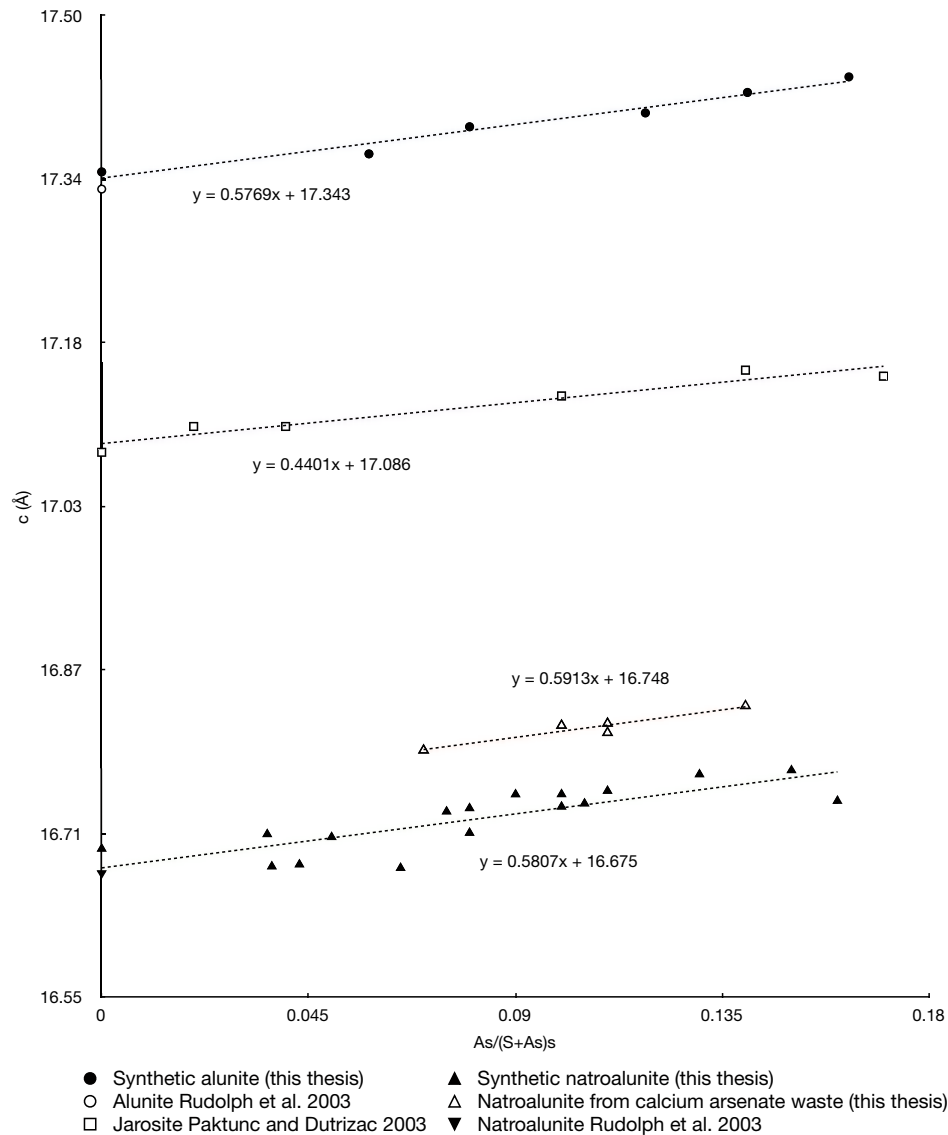


Figura E.9: El paràmetre de cel·la c vs la relació molar $\text{AsO}_4/(\text{SO}_4 + \text{AsO}_4)$ en natroalunita arsenical (de reactius sintètics i de residus industrials), alunita arsenical i jarosita arsenical.

- Els tests a curt termini indiquen una bona estabilitat de les natroalunites i les alunites arsenicals amb mínims de dissolució d'arsènic de 0.01-0.03 mg/L a pH's entre 5 i 8. La mansfieldita, l'alarsita i les fases amorfes presenten valors alts de dissolució d'arsènic, de 2 o 3 ordres de magnitud més elevats que la natroalunita i l'alunita arsenical. La natrofarmacoalunita no pateix danys en un rang de pH's entre 1 i 12.
- Els tests a llarg termini (6 mesos) en natroalunites arsenicals presenten bons resultats, de només 0.1 mg As/L. Els tests a mig termini (5 setmanes) en alunites arsenicals donen també bons resultats, 0.3 mg As/L, tot i que, la dissolució d'arsènic és superior a la trobada en natroalunites arsenicals.

- Els estudis d'estructura de les natroalunites arsenicals i les alunites van confirmar que tenen estructures $R\bar{3}m$ i $Z=3$. L'expansió de la cel·la és igual en ambdós fases: el paràmetre de cel·la a no varia, mentre que el paràmetre de cel·la c incrementa amb una pendent de ~ 0.58 .